A STUDY OF FLEXIBLE SPACE STRUCTURES: DYNAMICS AND CONTROL

ANANT KIRAN SINGH GREWAL

B.A.Sc.(Honours), University of British Columbia, 1985
M.S., University of Minnesota, 1987

A THESIS SUBMITTED IN PARTIAL FULFILMENT OF
THE REQUIREMENTS FOR THE DEGREE OF

DOCTOR OF PHILOSOPHY

in

The Faculty of Graduate Studies
Department of Mechanical Engineering

We accept this thesis as conforming
to the required standard

THE UNIVERSITY OF BRITISH COLUMBIA

September 1994

In presenting this thesis in partial fulfilment of the requirements for an advanced degree at the University of British Columbia, I agree that the Library shall make it freely available for reference and study. I further agree that permission for extensive copying of this thesis for scholarly purposes may be granted by the head of my department or by his or her representatives. It is understood that copying or publication of this thesis for financial gain shall not be allowed without my written permission.

(Signature)

Department of MECHANICAL ENGINEERING

The University of British Columbia
Vancouver, Canada

Date 28 SEPTEMBER 1994

ABSTRACT

A relatively general formulation for studying dynamics of flexible multibody orbiting systems in a tree topology is developed. It is applicable to a large class of present and future spacecraft, and readily amenable to simulation of closed loop systems as well as control system synthesis. Some of the distinctive features of the formulation include:

(a) its ability to simulate an arbitrary number of rigid, plate and beam–type structural members, each free to undergo translational and rotational maneuvers, as well as an arbitrary number of force and moment actuators on each member;

(b) the modelling of orbital perturbations through consideration of the trajectory radius and true anomaly as generalized coordinates;

(c) inclusion of structural damping, the foreshortening effect, and quasi–comparison functions for the improved discretization of flexibility;

(d) development of a compact set of nonlinear, nonautonomous, coupled governing equations by exploiting the cancellation of terms in the equations;

(e) determination of a linear model, indispensable for the controller design, through computation of the Jacobian matrices by finite differences;

(f) ability to include a dynamic compensator model which allows for the simulation of the closed loop system consisting of a nonlinear plant and a linear controller.

After presenting a brief introduction to the subject and a review of the relevant literature in the areas of multibody dynamics and control, the Lagrangian formulation of interconnected flexible systems is introduced. Issues pertaining to the numerical

implementation of the formulation and its validation are discussed next. The latter is accomplished through verification of energy conservation as well as comparisons with particular cases reported by other investigators. An approximate, closed–form, analytical treatment of the problem, developed in Chapter 4, is applicable to a general set of n second order nonlinear differential equations. The approach proves to be quite accurate promising considerable savings in computational time and effort. It is particularly suitable during the preliminary design stage.

Now, the attention is directed towards application of the formulation to study dynamics of several flexible systems of contemporary interest, exposed to a variety of disturbances, thus illustrating versatility of the approach. It also helps explain the foreshortening effect and the improved matching of boundary conditions through the use of quasi–comparison functions. The results clearly establish a need for active control of the Space Station. Finally, attitude control of the First Element Launch (FEL) of the Station, and simultaneous attitude and vibration control for the Permanently Manned Configuration (PMC) are studied, in the presence of realistic disturbances, using three linear methods: the Linear Quadratic Regulator (LQR), Linear Quadratic Gaussian/ Loop Transfer Recovery (LQG/LTR), and H_∞. The controller design is substantiated, in each case, through its application to the complete nonlinear system. The results suggest all the three approaches to be effective, however, the H_∞ controller shows better performance but at a cost of a larger compensator.

The thesis concludes with a summary of significant results and recommendations for future investigations.

TABLE OF CONTENTS

LIST OF TABLES

LIST OF FIGURES

LIST OF SYMBOLS

$\vec{d}_i, \vec{d}_{i,j}$	position vectors from $\mathcal{O}_c$ to $\mathcal{O}_i$ and $\mathcal{O}_i$ to $\mathcal{O}_{i,j}$, respectively
$dm_c, dm_i, dm_{i,j}$	elemental mass in body B_c, B_i, and $B_{i,j}$, respectively
h	orbital angular momentum per unit mass of spacecraft
i	orbit inclination with respect to the ecliptic plane
$\hat{i}_k, \hat{j}_k, \hat{k}_k,$	unit vectors in the directions of X_k, Y_k, and Z_k axes, respectively; $k = c$, i, (i,j), o, p or s
$\vec{\ell}$	direction cosine vector of $\vec{R}_{cm}$ with respect to $\mathcal{F}_p$
l_b, l_p	beam and plate lengths, respectively
$m_c, m_i, m_{i,j}$	mass of the bodies B_c, B_i, and $B_{i,j}$, respectively
$\vec{q}$	vector of system generalized coordinates
q_k	flexibility generalized coordinates; $k = c$, i or (i,j)
t	time
$\mathbf{u}$	control input vector
u, v, w	transverse vibration of a member in its X, Y and Z directions, respectively
v_k^b, w_k^b	transverse vibration of a beam in its Y and Z directions, respectively; $k = c$, i or (i,j)
w_k^p	transverse vibration of the plate in its Z direction; $k = i$ or (i,j)
$\mathbf{x}$	state vector
$\mathbf{y}$	output (measurement) vector
A_{p_k}	plan area of the plate; $k = i$ or (i,j)

$\mathbf{C_i^c}$,$\mathbf{C_{i,j}^i}$	transformation matrices defining orientation of $\mathcal{F}_i$ with respect to $\mathcal{F}_c$, and $\mathcal{F}_{i,j}$ with respect to $\mathcal{F}_i$, respectively
$\vec{C}_{cm}$	position vector from $\mathcal{O}_c$ to the instantaneous center of mass of the spacecraft
C_f	center of mass of the spacecraft
D	flexural rigidity of the plate
$\mathbf{E}$	identity matrix
EI_{yy}, EI_{zz}	flexural rigidity of a beam about its Y and Z axes, respectively
$\mathcal{F}_k$	body fixed reference frame for B_c, B_i and $B_{i,j}$, respectively; $k = c, i$ or (i, j)
$\mathcal{F}_o$	inertial reference frame located at earth's center
$\mathcal{F}_p$	reference frame with origin at C_f and parallel to $\mathcal{F}_c$
$\mathcal{F}_s$	orbital reference frame
$H_k^{s,t}$	generalized coordinate associated with the s^{th} and t^{th} shape functions in its X and Y directions, respectively, for a plate undergoing transverse vibrations; $k = i$ or (i, j)
$\vec{H}$	angular momentum of spacecraft with respect to $\mathcal{F}_c$
$\mathbf{I}$	identity matrix
$\mathbf{I_{sys}}$	inertia matrix of spacecraft with respect to $\mathcal{F}_c$
I_{xx}, I_{yy}, I_{zz}	principal mass moments of inertia
M	total mass of the spacecraft
$\mathcal{O}_k$	origin of the coordinate axes reference frame $\mathcal{F}_k$; $k = c$, i, (i, j), o, p or s

P_k^r, Q_k^r	generalized coordinates associated with the r^{th} transverse vibration mode of a beam in its Y and Z directions, respectively; $k = c, i$ or (i, j)
$\vec{R}_{cm}$	position vector from the earth's center to C_f
$\vec{R}_c, \vec{R}_i, \vec{R}_{i,j}$	position vectors of the mass elements dm_c, dm_i, and $dm_{i,j}$, respectively with respect to the earth's center
$R_{cm}, R_c, R_i, R_{i,j}$	magnitudes of $\vec{R}_{cm}$, $\vec{R}_c$, $\vec{R}_i$, and $\vec{R}_{i,j}$, respectively
T	total kinetic energy of spacecraft
U	potential energy of spacecraft; $U_e + U_g$
U_e	strain energy of spacecraft
U_g	gravitational potential energy of the spacecraft
X_k, Y_k, Z_k	coordinate axes associated with reference frame $\mathcal{F}_k$; $k = c$, i, (i, j), o, p or s
$\alpha^s_{\ell_i}$	joint angles for B_i; $\ell = 1, 2, 3$
$\alpha^s_{\ell_{i,j}}$	joint angles for $B_{i,j}$; $\ell = 1, 2, 3$
$\vec{\delta}_c, \vec{\delta}_i, \vec{\delta}_{i,j}$	vectors representing transverse vibration of dm_c, dm_i, and $dm_{i,j}$, respectively
δ_k^y, δ_k^z	tip deflection of a beam element in the Y_k and Z_k directions, respectively; $k = c$, i, or (i, j)
ϵ	eccentricity
ϵ_k^z	end deflection of a plate centerline in the Z_k direction; $k = i$ or (i, j)
θ	true anomaly
λ	yaw, rotation about the local vertical direction

$\lambda_i[\mathbf{A}]$	eigenvalues of $\mathbf{A}$
μ_e	gravitational constant for earth
ρ	longitude of the ascending node
$\vec{\rho}_c, \vec{\rho}_i, \vec{\rho}_{i,j}$	vectors denoting positions of dm_c, dm_i, and $dm_{i,j}$, respectively, in the undeformed configuration of the spacecraft
$\sigma_i[\mathbf{A}]$	singular values of $\mathbf{A}$
ϕ	roll, rotation about the local horizontal direction
$\mathbf{\Phi}$	matrix of admissible functions
ψ	pitch, rotation about the orbit normal
ω	argument of the perigee point
$\vec{\omega}$, $\vec{\omega}^{p/o}$	librational angular velocity vector of spacecraft

ABBREVIATIONS

ACES	Advanced Control Evaluation for Structures
AF	Admissible Function
c.m.	center of mass
CMG	Control Moment Gyro
COFS	Control of Flexible Structures
CSI	Control Structure Interaction
DISCOS	Dynamics Interaction Simulation of COntrol Structures
d.o.f.	degree of freedom
DVFB	Direct Velocity FeedBack
EOS	Earth Observation System

ESA	European Space Agency
FEL	First Element Launch
HAC	High Authority Controller
JPL	Jet Propulsion Laboratory
LAC	Low Authority Controller
LEO	Low Earth Orbit
LQG	Linear Quadratic Gaussian
LQR	Linear Quadratic Regulator
LSAT	Large SATellite System
LTR	Loop Transfer Recovery
ONLH	Orbit Normal–Local Horizontal
ONLV	Orbit Normal–Local Vertical
PMC	Permanently Manned Configuration
PV	PhotoVoltaic
QCF	Quasi–Comparison Function
RCS	Reaction Control System
RMS	Remote Manipulator System
SCOLE	Structural COntrol Laboratory Experiment
SFU	Space Flyer Unit
TEA	Torque Equilibrium Attitude
TPBVP	Two Point Boundary Value Problem
LU	Lower–Upper Decomposition

Dot ($\dot{}$) represents differentiation with respect to time t. Subscripts o and e indicate initial and equilibrium conditions, respectively. Unless otherwise stated arrows ($\vec{}$) and lower case **boldfaced** symbols represent vectors, and upper case **BOLDFACED** symbols, matrices. (^{T}) denotes the transpose of a vector or matrix.

ACKNOWLEDGEMENTS

I would like to express my appreciation to Prof. V.J. Modi for his guidance throughout my doctoral studies and for his inspiring instruction.

I also wish to acknowledge my colleagues, notably Dr. Fakhreddine Karray, Dr. Alfred Ng, Dr. Itshak Marom and Mr. Satyabratha Pradhan who contributed to my work through numerous discussions and suggestions.

A special note of appeciation is due to my family; my parents and sister for their lifelong encouragement and support, and my wife for her understanding and sacrifice.

This investigation was supported by the Natural Sciences and Engineering Research Council of Canada, Grant No. A–2181, and the Networks of Centers of Excellence Program, Institute of Robotics and Intelligent Systems, Grant No. C–8/5–55380.

1. INTRODUCTION

1.1 Preliminary Remarks

The first earth orbiting satellite Sputnik was launched by the Soviet Union in 1957. The early spacecraft carried their own source of power to accomplish the desired mission objectives. Typically it was either chemical or electrochemical [1]. The missions, mostly scientific, were of relatively short duration and therefore these sources proved to be adequate. The advent of satellites for communication, remote sensing, weather forecasting, etc. created the need for a longer lasting supply of power. A logical source was the sun, and as satellite technology matured during the sixties and seventies, satellites were designed with solar arrays for photovoltaic power generation. This coupled with more demanding mission requirements, which were beginning to include meteorology and surveillance, resulted in an increase in the size of satellites. The high cost of delivering payloads to space necessitated that the mass and pre-deployed volume of satellites remain low. These seemingly conflicting demands were satisfied by developing satellites with flexible, light solar arrays and, in some cases, antennae which are deployed once the spacecraft had attained their final orientation. Thus, the early artificial satellites can be characterized as being essentially rigid bodies, while current ones are represented by flexible, multibody systems.

Of course this is a convenient generalization. Even the early, so–called, rigid satellites were often greatly influenced by flexibility effects. An example of this was the first American probe, *Explorer I*. Stability analysis of a rigid body in the absence of energy dissipation shows that it can be stabilized by imparting spin about either the

major or the minor inertia axes. However, in the presence of energy dissipation only the configuration with spin about the major axis of inertia is stable [2]. Unfortunately, *Explorer I* was spun about its minor axis. Furthermore, it was equipped with small, flexible antennae which were a source of energy dissipation, rendering its librational behaviour unstable. Within ninety minutes of orbit injection it was tumbling to the dismay of engineers at the Jet Propulsion Laboratory (JPL) [3]. The flexible character of modern spacecraft is much more pronounced as illustrated by a few examples of contemporary interest:

(i) The Japanese Space Flyer Unit (SFU), an unmanned, reusable, free-flying platform for multipurpose use, is scheduled for launch by the H-II rocket in 1995. It consists of an octogonally shaped central body of about 5 m in width, with two solar arrays each approximately 10 m in length.

(ii) The European Space Agency's (ESA) L–SAT (Large SATellite system, *Olympus-I*) was launched in 1989. It is an advanced multipurpose communications platform with two solar arrays extending to 25 m, tip–to–tip. A follow-up to *Olympus-I* is proposed with solar panels that extend beyond 35 m.

(iii) The Earth Observing System (EOS) is aimed at remote sensing of global environmental changes. Comprising of a system of around 50-90 satellites in Low Earth Orbit (LEO), it is aimed at monitoring phenomena such as global warming, carbon dioxide and methane concentrations, loss of vegetation, etc. A typical EOS spacecraft has a asymmetric geometry, with a single solar panel extending from the satellite's main body.

(iv) The proposed Space Station, a permanently manned platform being developed collaboratively by the United States, ESA, Japan, Canada and the recently added

partner Russia. The principle objective of the program is the utilization of space for scientific research and technology development. The proposed space station has undergone numerous configurational changes since its inception, and will likely undergo more modification before it becomes a reality by the turn of the century. The current design of the station consists of a 110 m long central truss-like structure called the Power Boom (Figure 1-1). Attached to both ends of the Boom are plate-like solar arrays, each extending to 33 m.

The inability to effectively simulate, on earth, the space environment with its unique features has, thus far, precluded a comprehensive experimental approach to the dynamical response and control studies required for flexible spacecraft design. Mathematical analyses, aided in great part by numerical methods, became the principal tool as the complexity of spacecraft increased in the 1960's. With the ever increasing speed and decreasing cost of computing, numerical simulation of the dynamics and control of flexible, multibody spacecraft continues to be a major tool in their design. It is only recently that planned experiments such as the Space Shuttle based Structural COntrol Laboratory Experiment (SCOLE) and Control Structure Interaction (CSI) have been proposed.

From the point of view of applicability to a large class of spacecraft and space platforms, the development of a relatively general dynamical formulation and associated computer code appears quite attractive. The reward for the greater complexity and demand on time in such development is the availability of a powerful tool that is versatile.This approach allows a potential user to predict a spacecraft's dynamical behaviour and necessary control for desired operation without engaging in the arduous task of derivation and programming of the equations of motion.

A number of computer codes are available which offer this approach. They include

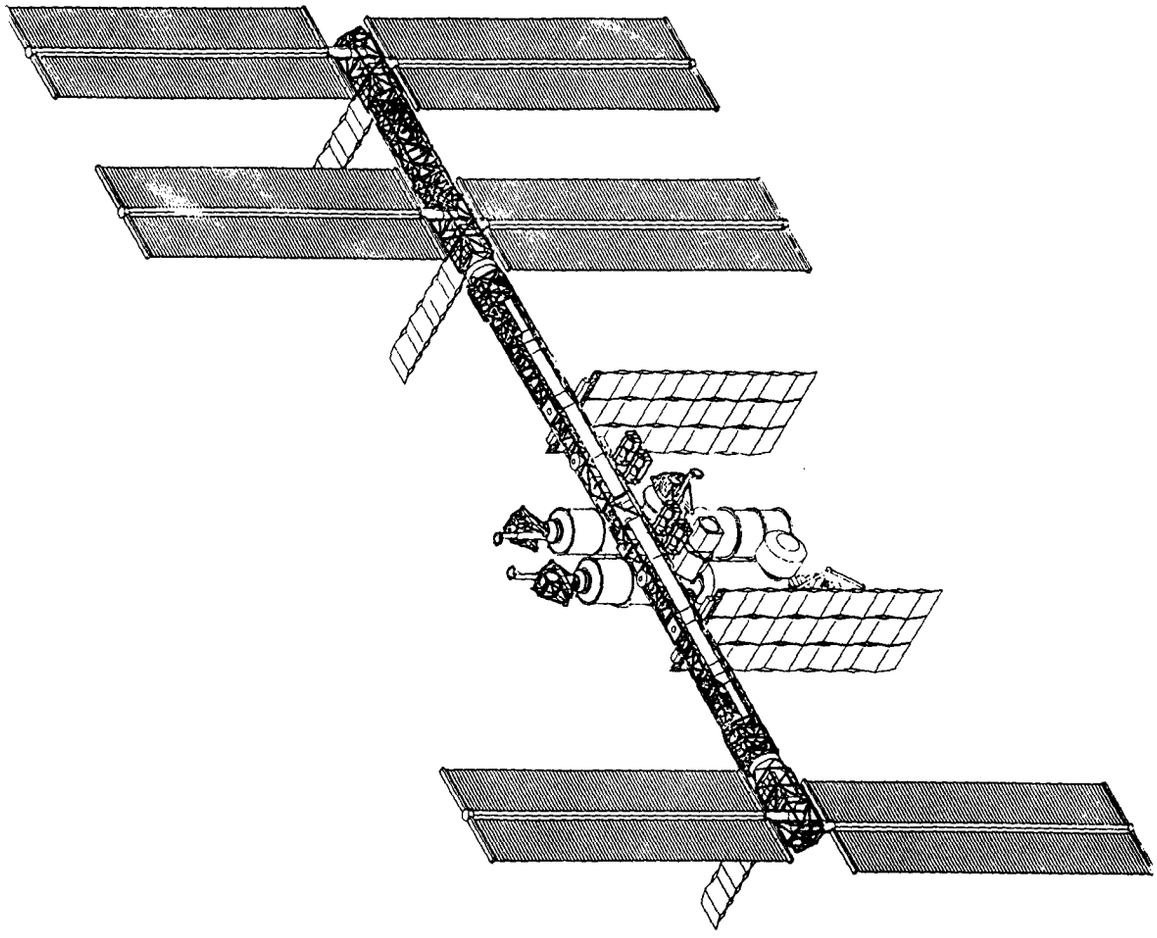

Figure 1-1 The proposed geometry of the Space Station as of January 1994. It has undergone configurational changes.

ALLFLEX, *Treetops*, DISCOS and others. ALLFLEX, developed by Ho and Herber [4], simulates the dynamics and control of large flexible multibody systems where the neighbouring bodies are connected by gimballed hinges with torsional springs and dampers. Time varying boundary conditions are accounted for by treating the quasi–static and homogeneous parts separately, and modal functions are generated by structural dynamics programs. The nominal behaviour of the idealized rigid system is represented by nonlinear equations of motion, while the behaviour of the perturbed motion due to structural flexibility is characterized by linearized equations. The direct path method [5] is used to transform the dynamic variables of individual bodies into the system dynamic variables. Both the Lagrangian and the Newton–Euler approaches may be followed to derive the governing equations of motion.

Singh et al. [6] developed a program called *Treetops*. The features of this package include the ability to model a system of interconnected rigid and flexible bodies in a tree-type topology. The hinge-points between adjacent bodies are capable of translation and rotation, and the equations of motion are generated by employing Kane's method, resulting in a system of minimum dimensions. The user is able to specify a controller by either supplying the controller equations in the form of a linear, block diagram, or as a subroutine. Furthermore, the user is able to choose from a set of seven sensors and four actuators.

A third example is represented by Dynamics Interaction Simulation of Controls and Structures (DISCOS), a public domain package developed by NASA, which is featured as an industry-standard software [7]. Its capabilities include an ability to handle tree-type topologies and the so–called order–N dynamical formulation, where the number of computations necessary for simulation are proportional to the number of bodies present.

The availability of multibody computer programs such as the ones described above may satisfy the needs of many users. However, a major impediment to their use as a research tool is often their proprietary nature whereby vital detailed information about the formulation, program architecture, source code, etc. are witheld from the user. This is particularly true with ALLFLEX and *Treetops*. When details are available, the amount of time and effort required to achieve a thorough understanding is substantial. Obviously, computational techniques employed by the developers of software are the result of experience gained during the development process. Any modifications of parts of the program to suit one's specific objectives are difficult if not impossible. Even when such modifications are possible to introduce, their effect on other parts of the program are often unpredictable. Furthermore, the understanding gained through the formulation and programming of the equations of motion is invaluable and cannot be substituted by the use of the proverbial 'black boxes.' Hence, the independent development of simulation software even at the cost of time and effort is often pursued. That is the approach followed in this thesis, with the objective of studying the dynamics and control of flexible, multibody orbiting systems.

Challenges in the area of spacecraft control include simultaneous libration and vibration control, presence of a closely packed frequency spectrum, overlap between the controller bandwidth and the vibrational natural frequencies, need to ensure performance and stability robustness in the presence of parameter uncertainty and unmodeled dynamics, sensor and actuator placement, to mention a few. Also, there is a desire to base the control design on a system model which is of relatively small-order and yet accurately represents the dynamical characteristics of the system. These issues are further complicated by the presence of operational disturbances caused by the Solar Array tracking, manipulators maneuvers and crew activities.

1.2 A Brief Review of the Relevant Literature

Despite being a relatively young field, the area of spacecraft dynamics and control has generated a vast body of literature over the past thirty five years. Broadly speaking, focus has been on four areas: multibody formulation; dynamics and control; environmental effects; and, most recently, experimental validation. The present investigation pertains to the first two areas, and hence only literature relevant to these fields are reviewed here. Also, there have also been several review papers published over the years which have summarized the developments at some length. An early paper by Shrivastava et al. [8] concentrated on the literature related to passive stabilization using gravity gradient torque. Modi later reviewed material in the area of attitude dynamics of satellites with flexible appendages [9]. An overview of developments in the field of spacecraft attitude control was presented by Roberson in 1979 [10] while a survey of literature in the area of satellite attitude dynamics and control in the presence of environmental torques was conducted by Modi and Shrivastava [11] in 1983. Likins [3] provides an insight into the field of satellite attitude dynamics and control from the point of view of his personal involvements, particularly during the early period. More recently, the literature, particularly in the areas of multibody formulation and dynamics, has been reviewed by Suleman [12], Ng [13] and Ibrahim [14] in their respective doctoral dissertations. Here, more important aspects of the relevant literature in the area of multibody dynamics are reviewed first, followed by that in the area of control theory as applied to rigid and flexible spacecraft systems.

As previously mentioned, multibody dynamics had its genesis in the 1960's during the early days of the space program. Hooker and Marguiles [15] developed the equations of motion governing the dynamics of an assemblage of n rigid bodies in a tree topology, placed in Earth's gravitational field. In their formulation, bodies

were capable of undergoing rotation, but not translation, relative to neighbouring members. The joints could be elastic and dissipative, and the equations were derived using the Newton-Euler procedure. Roberson and Wittenburg [16] extended the work of Hooker and Marguiles with the goal of making the formulation amenable to digital computer implementation. This was achieved by exploiting the concept of system graphs and incidence matrices to uniquely define the system topology. Later Roberson [17] applied this methodology to the study of a non-rigid tree-type topology.

Hooker [18] presented a formulation based on the Newton-Euler approach which avoided explicit appearance of constraint forces and moments in the final equations of motion. The bodies were taken to be rigid and interconnected in an arbitrary fashion. The author extended his work to include systems where the terminal bodies were allowed to be flexible [19]. In 1978, Jerkovsky [20] introduced the concept of path and reference matrices for defining the configuration of the system and developed a formalism for the governing equations of motion for an assemblage of rigid bodies.

The linearized equations of motion for a chain of flexible bodies with rigid end members were developed by Hughes [21] employing the Newton-Euler approach. The equations are particularly suited for control system design. The study was motivated by the Canadian Remote Manipulator System (RMS) for the Space Shuttle program; hence the selection of rigid end bodies, representing the shuttle at one end and a rigid payload at the other. Kane and Levinson [22] examined several different methods employed in practice to formulate equations of motion for multibody systems, including the use of momentum principles (commonly referred to as the Newton-Euler approach), D'Alembert's principle, Lagrangian procedure and Hamilton's canonical equations. They also described a 'new procedure' developed by Kane in 1965 which is commonly referred to as "Kane's method." Not surprisingly, the authors concluded

that their method is the simplest for formulating equations of motion for complex spacecraft.

Modi and Ibrahim [23] presented a formulation applicable to a large class of spacecraft with deploying, flexible members. The formulation, which employed the Lagrangian procedure, was extremely versatile and accounted for a shifting system centre of mass, variable mass density, flexural rigidity and cross-sectional area, vibrational motion and appendage offset. Meirovitch and Quinn [24] developed the equations of motion for a flexible spacecraft undergoing large rigid-body maneuvers. Elastic deformation was assumed to be small, resulting in a set of linear differential equations with time-varying coefficients which described the perturbed behaviour for the elastic motion. However, the equations governing the rigid body motion were nonlinear. The Lagrangian method was employed, along with component-mode or substructure synthesis for the modeling of the vibration of elastic members.

Vu-Quoc and Simo [25] adopted an approach which is applicable to flexible space structures undergoing large deformations by employing "geometrically-exact structural theories" and referring the dynamics of the system directly to an inertial frame. This results in the equations of motion which are simpler than those obtained by using rotating intermediate reference frames. To avoid the numerical ill–conditioning that would arise due to the disparity between the small structural deformation and the large earth-satellite distance, both of which are expressed in an inertial reference frame, the authors propose the use of a "parallel translate of the inertial frame." This refers to a frame which is parallel to the true inertial frame, but whose location is coincident with the instantaneous centre of mass.

Much of the recent literature on multibody dynamics focuses on the development of so–called order–N formulations. Here the number of computations required per

integration time–step is proportional to the number of generalized coordinates employed. By this convention, most formulations are of order N^3. The majority of order–N formulations rely on a sequential rather than a simultaneous formation of each component of the vector equations of motion. Keat [26] presented one such method using the Newton–Euler approach. Bodies, which may be rigid or flexible, were allowed to form an open-chain, closed-loop or tree-type topology, and joints were permitted to have upto six degrees of freedom (i.e. translation and rotation). Constraint forces were calculated only at joints in a closed-loop where a cut was introduced. Constraint terms at other joints were avoided through the use of a "Velocity Transform". Jain [27] presented an order–N formulation for a system of rigid bodies connected serially. Jain and Rodriguez [28] employed spatial operators and recursive algorithms to develop the equations of motion for serial, flexible multibody systems, and discussed extensions to more complicated topologies.

Banerjee [29] presented a block–diagonal matrix formulation of the equations of motion for a flexible multibody system undergoing large rotation and translation. Both tree and closed–loop topologies were accounted for in this recursive formulation. Kane's equations were employed. Kurdila et al. [30] studied a nonrecursive order–N formulation for multibody systems. The authors considered their method preferable to the recursive, sequential order–N approaches, particularly for systems with many degrees of freedom, because of its nonassembling nature. Furthermore, the authors state that it is amenable to parallel, multiprocessor implementation.

The area of spacecraft control is an extremely wide one, with specialties such as maneuvering control, attitude control and momentum management, vibration control of flexible structures, and others. The first two areas can be further subdivided into cases where only the rigid motion is controlled, and situations where simultane-

ous vibration as well as maneuvering or attitude control are required. Furthermore, the control methodology employed in each case may be either linear or nonlinear. For spacecraft undergoing significant parameter changes adaptive control and system identification may be used. The field of attitude control is reviewed by Roberson [10], while the area of flexible space structure control has been surveyed by Balas [31], and Meirovitch et al. [32,33]. In a recent survey paper, Van Woerkom [34] summarizes a number of recently developed techniques for the control of large, flexible structures. These include the Linear Quadratic Gaussian, Loop Transfer Recovery (LQG/LTR); H_∞; μ; and positivity synthesis approaches.

Yet another approach that has received some attention is that of the Modal–Space Control. Here the flexible structure dynamics, which is governed by a set of partial differential differential equations, is discretized by the eigenmodes of the system. The generalized coordinates associated with the modes are used as the states of the system for the controller design. Balas [35] has shown that a desired performance can be assured provided the retained modes are controllable and observable, the truncated modes are unobservable, and the control spillover satisfies a bound determined by the desired performance. The term 'control spillover' refers to the excitation of the truncated modes by the actuators. Meirovitch and Öz [36] proposed the Independent-Modal Control, where a system is transformed to the Jordan form after discretization, in conjunction with a reduced–order observer for the control of a distributed gyroscopic system. In a related study, the authors have investigated optimal control for the same type of systems [37].

A number of investigators have approached the problem of attitude control of large space platforms by incorporating the concept of momentum management. The integrated approach provides an implementable strategy that prevents saturation of

the momentum-based torque actuators, such as the Control Moment Gyros (CMG). Saturation of the CMG's is avoided by the use of the natural forces (gravity-gradient, aerodynamic, magnetic, etc.), or through desaturation effectors such as the reaction control system (RCS) [38]. Under certain situations, the latter is not favoured due to undesirable disturbances, propellant expenditure, the possibility of contamination, and damage due to plume impingement. Woo et al. [38] have presented an approach which utilizes the Linear Quadratic Regulator (LQR) technique to maintain attitude control of the Space Station about a Torque Equilibrium Attitude (TEA), which need not be known *a priori*. A rigid model of the Space Station was considered in the investigation, and natural forces were used in the momentum management system. Chu et al. [39] applied Bode-type techniques, together with a graphical model reduction method, to design the attitude control system of a Space Station model. The model used included both CMG's and thrusters to maintain attitude control during normal station operation in the presence of crew induced disturbances, orbit reboost maneuvers, and shuttle docking. It also included flexibility effects although no consideration was given to vibration control. Sunkel and Shieh [40] presented a scheme which combined optimal (LQR) control and pole placement for the design of a momentum management controller for a rigid Space Station model. A digital redesign of this continuous time controller was also conducted [41] and a matrix sign algorithm was applied to decompose the Space Station's equations of motion into two decoupled subsystems [42]. The optimal pole placement technique used in their previous work [40] was then used to design controllers for each of the subsystems.

Vadali and Oh [43] developed a nonlinear control strategy based on Lyapunov's second method to design an attitude control and momentum management system for the proposed Space Station. The investigation was based on a rigid model of the

Station, and revealed that momentum management, in most cases, can be achieved by using the gravity gradient torque. The use of gain scheduling was avoided because a nonlinear approach was employed.

Harduvel [44] utilized disturbance rejection filters to design a momentum management system for the coupled, 3-axis, rigid body dynamics of a spacecraft. The investigation also developed an approximate closed-form expression for the TEA in the presence of an aerodynamic environment. An application of H_∞ control theory to the design of an attitude and momentum control system of the Space Station was explored by Byun et al. [45]. The rigid model accounted for parameter uncertainty.

Control of flexible spacecraft undergoing maneuvers has also attracted considerable interest. Bainum and Li [46] investigated optimal three–dimensional large angle slew of flexible spacecraft using Pontryagin's Maximum Principle. A quasilinearization technique was used to solve the resulting nonlinear Two-Point Boundary-Value Problem (TPBVP). Sharony and Meirovitch [47] studied the near-minimum time single-axis slewing of a flexible spacecraft, modeled as a rigid hub and a single flexible appendage, employing a perturbation method. The problem was approached by first solving the minimum-time maneuver of a rigid spacecraft model. The resulting nonlinear TPBVP was solved using a bang-bang control strategy giving the zero-order solution. The first order equations incorporating the elastic degrees of freedom as well as the perturbed rigid degrees of freedom, which are time-varying because of the zero-order maneuver, were then controlled using a reduced-order optimal compensator. A related problem, where the disturbances created by the optimal slewing maneuvers of multiple flexible appendages are controlled, was investigated by Meirovitch and Kwak [48].

Singh and Vadali [49] considered the three-dimensional maneuvers of a space-

craft modeled as a rigid hub with flexible beam–like appendages. A rigid model was used to derive the optimal (minimum time) bang–bang controller with five–switches. A time–delay prefilter shaped the torque to minimize vibratory motion of the appendages. Using a method based on the Lyapunov stability criteria, which does not require discretization of the partial differential equations governing the flexible motion, Junkins et al. [50] developed tracking control laws for a flexible spacecraft model which suppressed the departure of the actual trajectory from the reference target trajectory defined *a priori*. Experimental results validated the approach taken in the analytical work. Li and Bainum [51] derived a control law, which relies on momentum exchange between the flexible and rigid body motions, to suppress vibrations of a flexible spacecraft during both stationkeeping and large angle maneuvers. The stability of the scheme was proven using the Lyapunov direct method. Junkins and Bang [52] utilized Lyapunov stability theory to develop generalized procedures for maneuver and vibration control of flexible systems. The method used system energy derived from a PDE model of the system to guarantee robustness of the control law, and is particularly useful for hybrid discrete/distributed parameter systems. Hecht and Junkins [53] developed a near–minimum time control law for a flexible, two–link manipulator system by generating a reference bang–bang minimum–time control law for a rigid system and smoothing the control torque given by the reference control law to ensure acceptable vibratory response. A second term was also added to the control law to cancel the nonlinear dynamics resulting from the maneuver. This basic approach was applied to three–dimensional maneuvers and near–minimum–fuel control of flexible spacecraft by Bell and Junkins [54].

Parlos and Sunkel [55] presented an attitude and momentum management system for large angle maneuvers of rigid spacecraft using the LQR pole placement method

in conjunction with gain scheduling. On the other hand, Zhao et al. [56] explored the design of a self–tuning adaptive controller to the same end. A rigid model was used with optimal regional pole placement, and the controller was implemented via a digital redesign step.

Garcia and Inman [57] studied effects of the slewing control servomechanism of a flexible beam on the boundary conditions at the actuated end. Detailed modeling of the servo system, including the motor and the gearbox, was undertaken. A similar detailed modeling of a slewing servo system, for the sun tracking control of the proposed Space Station's solar arrays, is reported by Kumar et al. [58].

Literature in the area of active control of space structures has been reviewed by Hyland et al. [59] Balas [60,61] studied the effect of noncolocated sensors and actuators on the control and observation spillover problem due to the residual modes. The resulting instability was alleviated by the use of a phase-locked loop prefilter. The numerical results presented were for the case of a simply supported Euler-Bernoulli beam. Balas also presented the conditions under which Direct Velocity FeedBack (DVFB) control is possible [62]. Here vibration velocities of a structure at a number of finite locations are fedback, after appropriate multiplication by a gain matrix, to force actuators, which are colocated with the sensors. The approach minimizes the spillover and guarantees stability.

The problem of the sensitivity to parameter variations was studied by Yedavalli [63]. In particular, the parameters critical for achievement of a given performance level in a Linear Quadratic Gaussian (LQG) regulator problem were identified.

The potential of piezoelectric actuators and sensors to improve structural damping characteristics was explored by Goh and Caughney [64]. The benefits of such

actuators over conventional reaction-type devices were also discussed.

Sundararajan et al. [65] applied the LQG/LTR design procedure to the pointing control of a flexible space antenna. Although vibration control was not achieved, the flexibility of the structure was incorporated in the model to achieve the required stability robustness of the closed–loop system. Wie [66] applied classical transfer function techniques to design a controller for the shuttle–based Control of Flexible Structural (COFS) experiment. Active vibration control synthesis, which is robust to both parameter uncertainty and unmodeled dynamics, was investigated by Heise et al. [67]. Both the LQG performance index and the H_∞ norm of a disturbance transfer matrix were optimized simultaneously.

Williams and Juang [68] applied state feedback to render as many vibration modes as possible *unobservable* at critical points in a structure. These, typically, correspond to locations where sensors or fragile components are present. The authors developed a strategy for complete pole–zero cancellation while minimizing the norm of the control gain matrix.

Hanagud et al. [69] have presented optimal control laws based on quadratic performance indeces which are applicable to beam–type structures. Colocated piezoceramic sensors and actuators were employed and static output feedback in conjunction with signal conditioning was used.

Reddy et al. [70] applied several techniques, including pole–placement and LQR, for the control of a large flexible orbiting platform, which was modeled as a plate. For the study, point force actuators were employed for simultaneous vibration and attitude control. The H_∞ approach was applied by Safonov et al. [71] in the synthesis of a controller for a ground–based laboratory model of a flexible space structure. The

structural damping characteristics of the model were first enhanced through rate output feedback achieved by employing colocated sensors and actuators. Subsequently, the H_∞ procedure was applied to control the two 'tilt' modes of the structure.

Although many features of flexible spacecraft and the space environment are unique, there has been some interest in the use of ground–based experiments to validate control laws derived using mathematical models. The ground–based structures are designed in such a way that they share some important characteristics of the flexible spacecraft under study, including low and closely spaced frequency spectra that overlap the controller bandwidth, and very light damping. Lessons learned in implementing control strategies on such ground–based flexible structures can then be applied in the design of control systems for the prototype flexible spacecraft.

A survey of both recent ground–based experiments and test facilities related to large flexible structures was conducted by Sparks and Juang [72]. The review also includes some space–based experimental work. Wie [73] describes investigations conducted at the Advanced Control Evaluation for Structures (ACES) testbed at the NASA Marshall Space Flight Center. The testbed consists of a 13-m deployable beam-like structure with a mass of 2.27-kg. The objective is to understand the problems of control–structure interaction, and investigate the effects of simplifying assumptions in the controller design on the resulting behaviour of a complex structure with the controller in place. An experimental assessment of three robust linear control techniques (LQG/LTR, H_∞, and μ synthesis) for the vibration suppression of a ten bay vertical truss structure situated at the NASA Langley Research Center was made by Dunn [74]. The LQG/LTR controller was found to give the most favorable results. Buddie et al. [75] applied the H_∞ procedure for vibration suppression to two ground–based experimental testbeds involving: a flexible antenna at the Jet Propulsion Laboratory

(JPL); and a cantilever truss at the Wright–Patterson Air Force. Also, for the former testbed, Ih et al. have implemented adaptive control strategies to achieve vibration suppression [76,77].

1.3 Scope of the Investigation

The thesis focuses on an approach to study the dynamics and control of large space structures, a topic of considerable contemporary interest. Although primarily motivated by the proposed Space Station, it has direct relevance to the analysis and design of a wide spectrum of spacecraft currently under consideration. The problem is approached in several stages: a relatively general formulation is the fundamental requirement together with an efficient numerical code for its implementation. Both the formulation and the numerical algorithm represent significant contributions to the field. Next, versatility of the formulation is demonstrated through the dynamical study of several systems of contemporary interest. Finally, the effectiveness of several linear control strategies is assessed through application to two evolving configurations of the proposed Space Station (Figure 1-2). Such a global approach – formulation, numerical code, validation, dynamic, and code – is indeed rare and provides a powerful tool for tackling contemporary problems as well as tomorrow's challenges.

The formulation follows the Lagrangian direct path approach where kinematic quantities are expressed with respect to the central body of the multibody system, which is taken to form a tree–type topology. The distinctive features of the formulation include:

(i) An ability to simulate the dynamics of a system with an arbitrary combination of interconnected flexible and rigid bodies. When the central body is flexible, it is taken to be a beam–like structure, while other flexible bodies are modeled

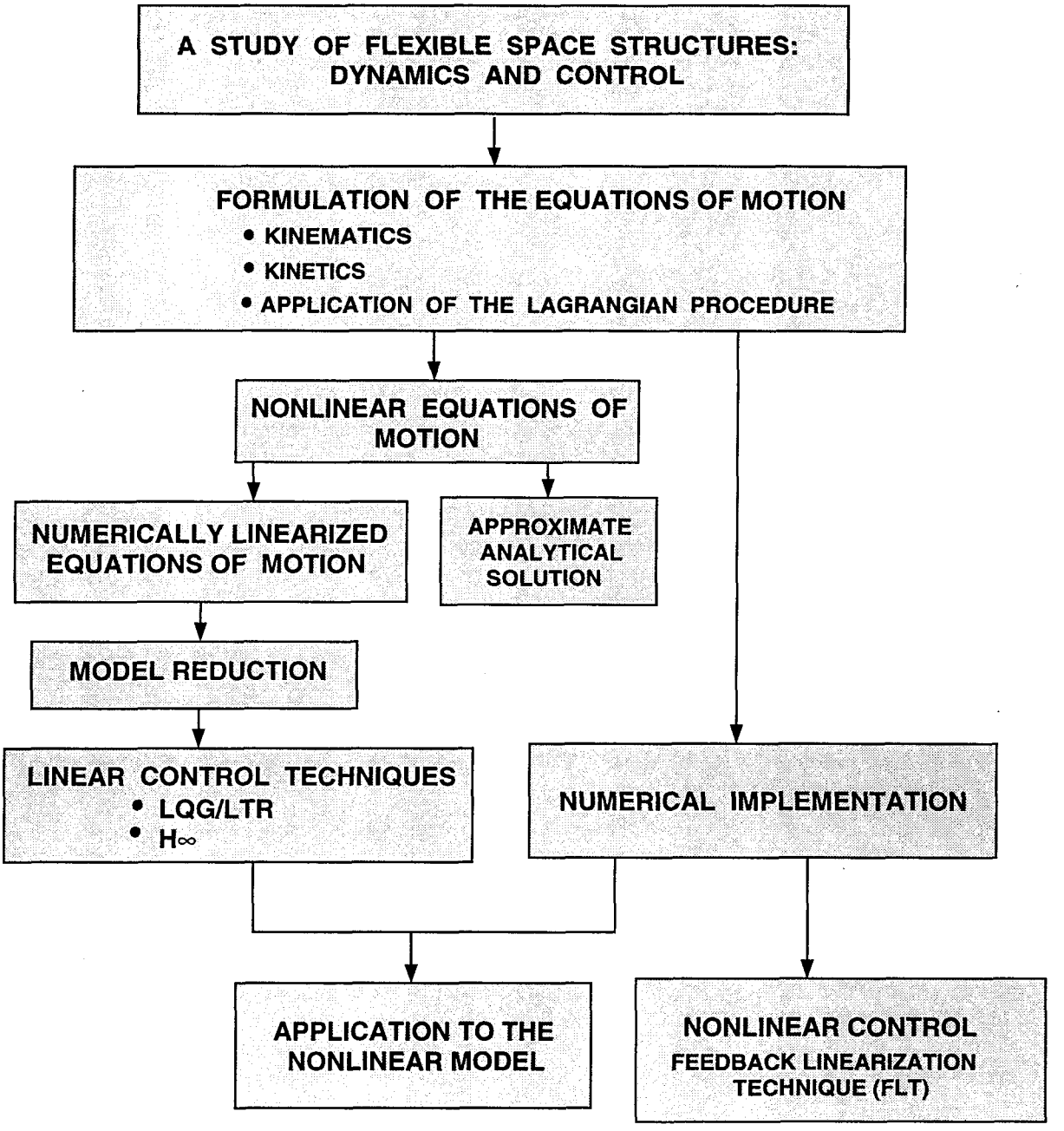

Figure 1-2 An outline of the proposed investigation.

as beams and/or plates. The system is in an arbitrary elliptic orbit.

(ii) The relative slewing and translation of bodies is permitted. The angular rotation between adjacent bodies can be treated as either specified or generalized coordinates.

(iii) The shift in the center of mass due to flexibility effects as well as slewing and translational maneuvers is accounted for. The formulation also considers the foreshortening effect.

(iv) Structural damping of flexible bodies is incorporated.

(v) Coupling between orbital, librational and vibrational motions is included, i.e. orbital parameters are treated as generalized coordinates.

(vi) Quasi-comparison functions are introduced to improve the discretization of flexibility.

(vii) By exploiting significant cancellation of terms in the equations of motion, a compact set of equations are obtained, resulting in an efficient computer program.

To begin with, the approach used in representing the kinematics of a flexible, multibody, systems is outlined together with a discussion on the modeling of structural deformations. Determination of the system kinetic and potential energies follows leading to the governing equations of motion using the Lagrangian procedure. Judicious grouping of terms leads to their cancellation at places resulting in a significant simplification of the extremely lengthy (even in matrix notation), nonlinear, nonautonomous and coupled equations of motion. Such a simplified form of the equations has not been reported before and, as can be expected, results in considerable savings of computational time and effort.

As can be anticipated, in general, the nonlinear character of the governing equations of motion does not admit any closed form analysis of the system. However, by judicious simplification, one can capture the essential character of the system dynamics with sufficient accuracy to assist during the preliminary design. This is illustrated in Chapter 4 where a closed–form solution is obtained, using an extension of the Butenin method, for a simplified, yet nonlinear approximation of the system.

Of course, the main objective is to establish a versatile and efficient algorithm that would assist in the dynamical analysis and controller design for a large class of flexible multibody systems. This is pursued in the two subsequent chapters. The uncontrolled dynamics of the two milestone stages of the proposed Space Station, the First Element Launch (FEL) and Permanently Manned Configuration (PMC), is studied in Chapter 5. The intent here is not to obtain a vast amount of response data to a wide variety of disturbances through an extensive parametric analysis. Of course, a design engineer can use the computer code developed here to that end. The focus is on illustrating the versatility of the formulation and its ability to analyse dynamically complex situations. In the process, it also demonstrates the foreshortening effect and improved accuracy through the use of quasi–comparison functions for flexibility discretization

Finally, the controlled behaviour of the aforementioned stages of the Space Station is investigated employing the LQR, LQG/LTR and H_∞ techniques. Here, a comprehensive approach is followed where issues such as model linearization and reduction, robust controller design and its verification, nonlinear plant model, etc. are addressed. The controller design is verified, in each case, through its application to the nonlinear plant model.

A summary of the salient results are presented in the concluding chapter, along

with some suggestions for future research in this field.

2. FORMULATION OF THE PROBLEM

2.1 Preliminary Remarks

There are a number of widely accepted approaches to the formulation of the equations of motion for flexible multibody systems. These include the Newton–Euler, Lagrangian and Hamiltonian methods, as well as Kane's procedure. The equivalence of these methods is often underemphasized. It should be noted that both Lagrange's and Kane's equation can be derived from Newton's second law for simple dynamical systems [78]. Notwithstanding this, the Newton–Euler approach is commonly referred to as momentum based, while the Lagrangian method relies on system energy. This is because the derivation of the governing equations of motion reduces to mathematical manipulations of the linear and angular momenta in the case of the Newton–Euler formulation, and of the kinetic and potential energies in the case of the Lagrangian method. Kane's procedure involves manipulations of abstract quantities called the *generalized speeds*, which are related to the generalized velocities of the system, and *partial velocities* which are the partial derivatives of the actual velocities with respect to the generalized speeds.

The advantages of employing the Lagrangian approach in formulating the governing equations of motion for a flexible, multibody, orbiting system are discussed by Ng in his doctoral dissertation [13]. To summarize, the Lagrangian method is favoured over the Newton–Euler one as it does not involve introduction of joint constraint forces and moments, which have to be subsequently eliminated by algebraic manipulation of the equations. Furthermore, the Newton–Euler method requires that the angular momentum of the system be expressed about the system center of mass. For a system with a shifting center of mass this is not a trivial task. The use of the

energy based Lagrangian approach permits the verification of energy conservation for nondissipative systems. Of course, this is also possible with the Newton–Euler method, although determination of the system energy would involve additional effort as it is not directly involved in the derivation. In general, the Newton–Euler approach leads to a relatively compact set of governing equations.

It is well recognized that the Lagrangian method leads to lengthy expressions arising primarily through the square of the velocity terms and their derivatives. Hence, derivation of the equations of motion demands considerable time and effort. However, since the equations are applicable to a large class of systems, the additional time and effort is deemed acceptable. Furthermore, the cancellation of terms, which was exploited in this investigation, results in a relatively compact set of equations.

In this chapter, the kinematics of the system is discussed first, followed by the modeling of the structural vibrations, translation vectors, system kinetics and structural damping. Finally, the derivation of the governing equations of motion using the Lagrangian procedure is presented.

2.2 Kinematics

2.2.1 System Geometry

As mentioned earlier, one objective of this thesis is to develop a methodology for studying the dynamics of flexible multibody systems. It is important, then, that the model chosen be versatile enough to encompass a large class of present, as well as future spacecraft and space platforms. A multibody system in a tree–like topology is a logical configuration when one is interested in spacecraft dynamics. On the other hand, the chain–type geometry would be more appropriate for an investigation of manipulator dynamics. Note, the closed–loop geometry would require consideration

of appropriate constraint relations. An illustration of the common system topologies encountered in the area of multibody dynamics is shown in Figure 2-1 .

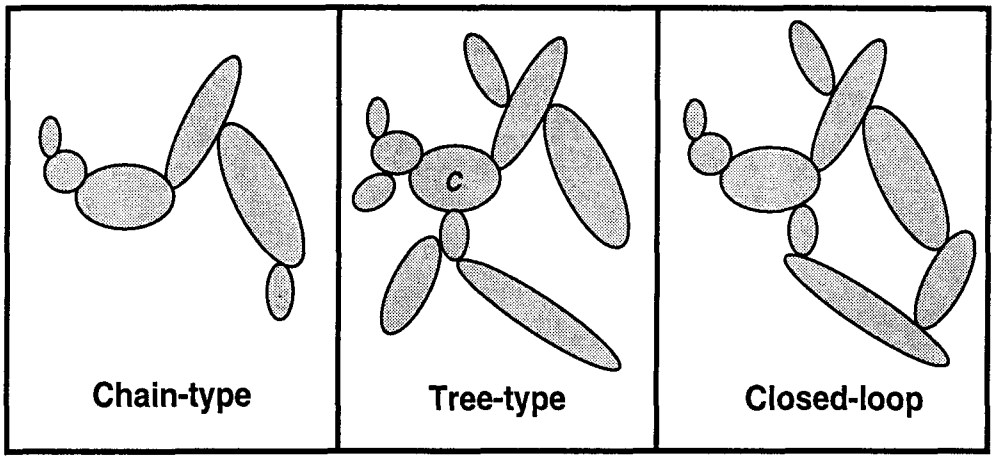

Figure 2-1 Common topologies for multibody systems.

The model considered for this study (Figure 2-2) consists of a central body, B_c connected to B_i bodies ($i = 1, \ldots, N$). Each B_i body is, in turn, connected to $B_{i,j}$ bodies ($j = 1, \ldots, N_i$). The number of B_i and $B_{i,j}$ bodies is kept completely arbitrary in order to facilitate the simulation of a large class of flexible, orbiting structures. The selection of a structural member to act as the central body is strictly speaking general although, in most spacecraft, the choice becomes obvious when criteria such as mass and inertia are employed.

This model has 3 levels of bodies, or equivalently 2 levels of branches. Obviously, the number of levels of bodies for a completely general tree–type topology can be arbitrarily large. However, most spacecraft can be adequately represented by the present model. For example, for the proposed Space Station, the Power Boom or the main truss may act as the central body (B_c). The remaining elements, such as the solar arrays, solar and station radiators, stinger and remote manipulator (Figure

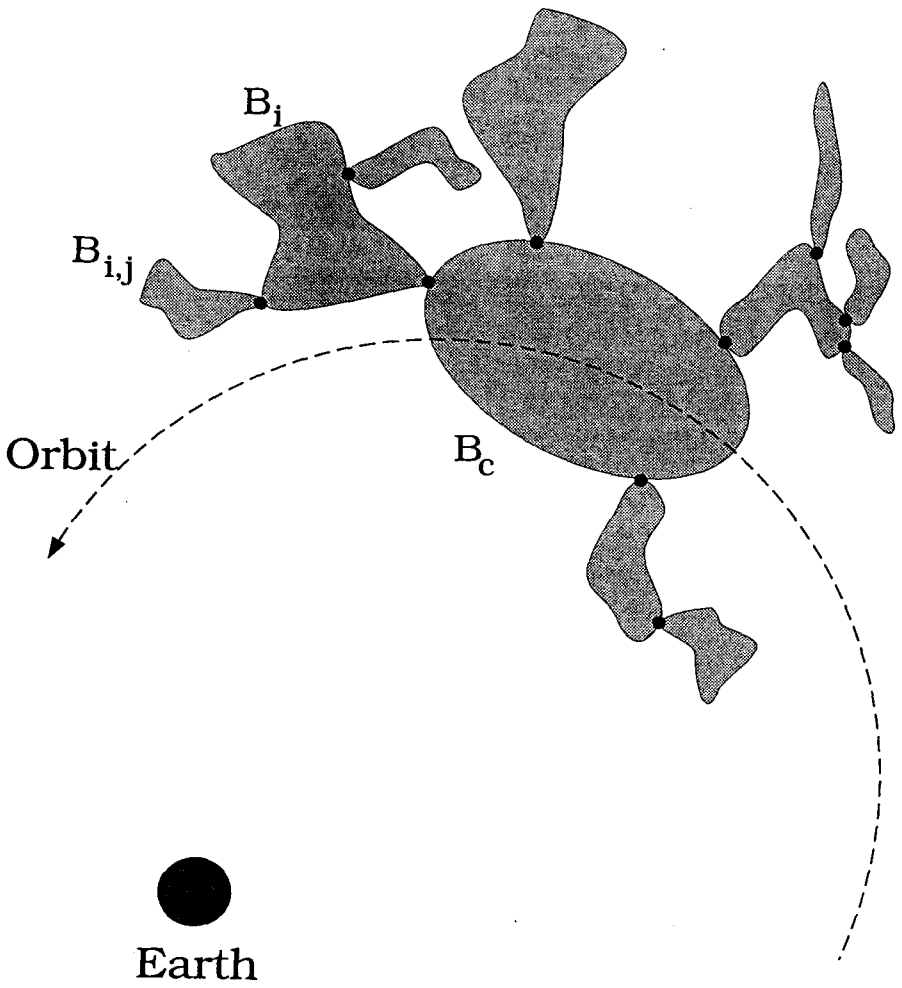

Figure 2-2 A schematic diagram of the multibody model used in the study.

1-1), can be represented by the B_i bodies. Alternatively, if greater accuracy in the modeling of the manipulator is desired, it can be represented by a B_i and a single $B_{i,j}$ body.

2.2.2 Reference Frames

The presence of a number of structural members, each capable of rotation relative to neighboring ones, necessitates that position, deformation, and velocity of a given body be expressed in local, body–fixed reference frames. Coordinate transformation matrices, then, allow for vectors in local frames to be expressed in a single, common reference frame. The actual number of reference frames employed would, of course, depend on the number of bodies encountered in a particular problem. However, for this study six *types* of reference frames are employed (Figure 2-3). These are:

(i) The inertial reference frame, $\mathcal{F}_o$, taken to be fixed at the earth's center.

(ii) The first of the noninertial reference frames, referred to as the orbital frame, is denoted by $\mathcal{F}_s$. Its origin, $\mathcal{O}_s$, is located at the instantaneous center of mass of the system, C_f.

(iii) The central body frame, which is a body-fixed reference frame, is denoted as $\mathcal{F}_c$. The location of this frame on the central body, in general, is arbitrary. However, it is often convenient to take its origin at either the geometric center or the mass center of the central body.

(iv) The so–called "system" reference frame, $\mathcal{F}_p$, with its axes oriented parallel to the axes of the central body frame, $\mathcal{F}_c$, and its origin, $\mathcal{O}_c$ located at the instantaneous system center of mass.

(v) The body–fixed reference frame for B_i, denoted $\mathcal{F}_i$, whose origin $\mathcal{O}_i$ is located at the interface between the bodies B_c and B_i.

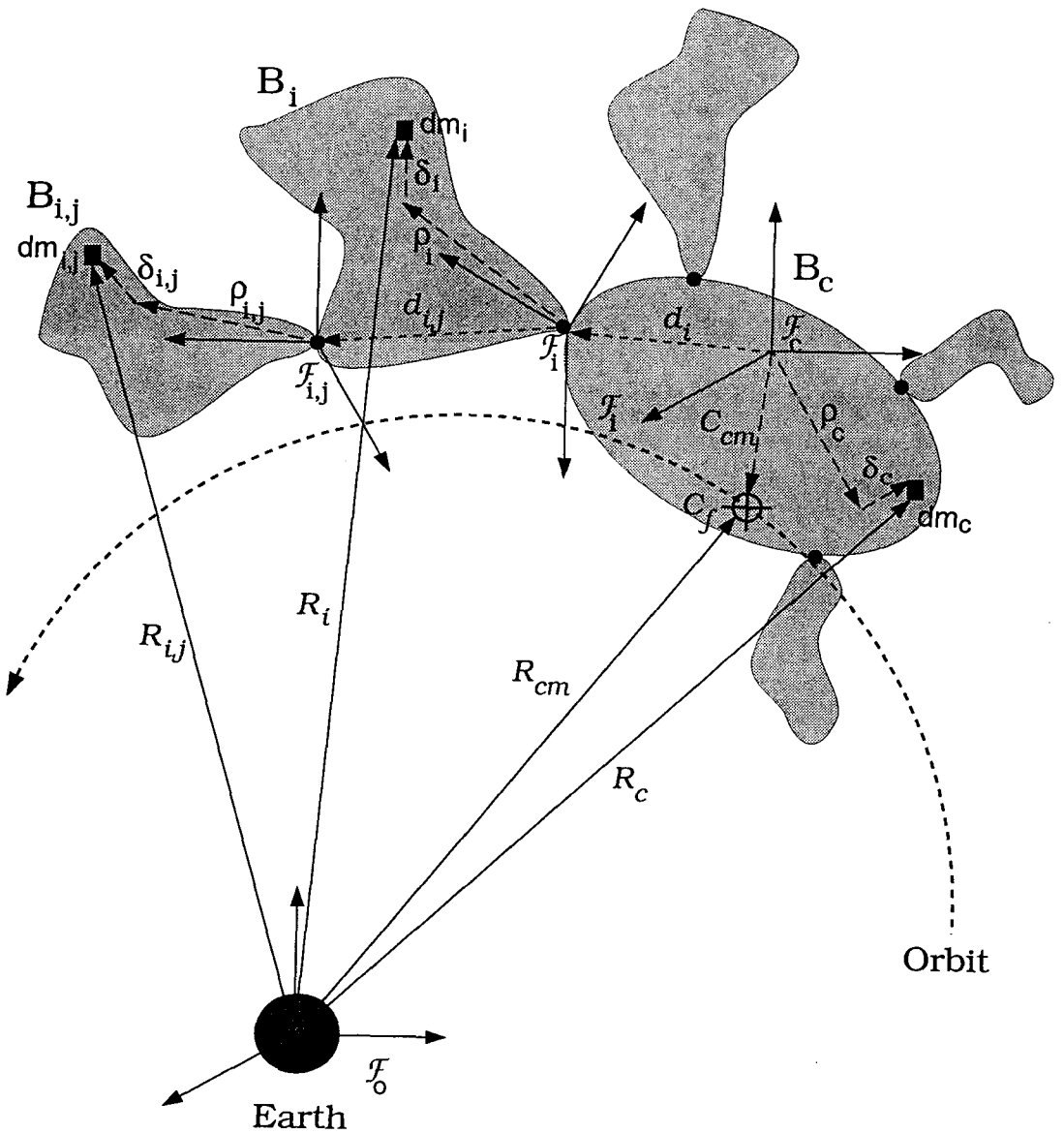

Figure 2-3 Reference frames used in the formulation of the problem.

(vi) The body–fixed reference frame for members $B_{i,j}$, denoted as $\mathcal{F}_{i,j}$, with the origin, $\mathcal{O}_{i,j}$, located at the interface between the bodies B_i and $B_{i,j}$.

2.2.3 Position Vectors of Elemental Masses

In order to develop expressions for the kinetic and potential energies of the system, the position, displacement and velocity vectors of mass elements in bodies B_c, B_i and $B_{i,j}$ must be expressed with respect to the inertial reference frame $\mathcal{F}_o$. This is achieved by establishing a path to the central body, and then extending it to the secondary (B_i) and tertiary $(B_{i,j})$ bodies. The position vector of a mass element dm_c in body B_c is expressed with respect to $\mathcal{O}_c$ by the vector $\vec{\rho}_c$. $\mathcal{O}_c$ is, in turn, defined with respect to $\mathcal{F}_o$ by the vectors $\vec{R}_{cm}$ and $\vec{C}_{cm}$. $\vec{R}_{cm}$ is the position vector of the instantaneous system center of mass (C_f) while $\vec{C}_{cm}$ defines the position of C_f with respect to $\mathcal{O}_c$. The displacement of the mass element dm_c from its undeformed position is given by $\vec{\delta}_c$.

In an analogous fashion, the position of a mass element in body B_i, denoted dm_i, is defined with respect to $\mathcal{O}_c$ by first referring the origin $\mathcal{O}_i$ of the frame $\mathcal{F}_i$ by the vector $\vec{d}_i$. The mass element is then referred to $\mathcal{O}_i$ by the position vector $\vec{\rho}_i$ and the displacement vector $\vec{\delta}_i$. Note that $\vec{d}_i$ includes both the position and the displacement of $\mathcal{O}_i$. By extension, a mass element in body $B_{i,j}$, denoted $dm_{i,j}$, is referred to $\mathcal{O}_c$ by $\vec{d}_i$, $\vec{d}_{i,j}$, $\vec{\rho}_{i,j}$ and $\vec{\delta}_{i,j}$. $\vec{d}_{i,j}$ is the vector which defines $\mathcal{O}_{i,j}$, the origin of the frame $\mathcal{F}_{i,j}$, with respect to $\mathcal{O}_i$, the origin of the frame $\mathcal{F}_i$.

Orientation of the reference frame $\mathcal{F}_i$ relative to the frame $\mathcal{F}_c$ is defined by the 3×3 coordinate transformation or rotation matrix $\mathbf{C}_{\mathbf{i}}^{\mathbf{c}}$. Similarly, orientation of the frame $\mathcal{F}_{i,j}$ relative to $\mathcal{F}_i$ is defined by the matrix $\mathbf{C}_{\mathbf{i,j}}^{\mathbf{i}}$.

The transformation matrix $\mathbf{C}_{\mathbf{i}}^{\mathbf{c}}$ is defined as the rotation matrix which, when pre-

multiplied by a vector projected onto frame $\mathcal{F}_i$, results in the vector being projected onto frame $\mathcal{F}_c$,

$$\vec{\alpha}_c = \mathbf{C}_{\mathbf{i}}^{\mathbf{c}} \vec{\alpha}_i. \tag{2.1}$$

In general, the relative rotation of body B_i with respect to body B_c can be decomposed into three successive rotations: due to flexure of the body B_c, denoted by $\mathbf{C}_{\mathbf{i,v}}^{\mathbf{c}}$; caused by rigid body orientation, written as $\mathbf{C}_{\mathbf{i,r}}^{\mathbf{c}}$; and finally, the slewing motion of B_i with respect to B_c given by $\mathbf{C}_{\mathbf{i,s}}^{\mathbf{c}}$,

$$\mathbf{C}_{\mathbf{i}}^{\mathbf{c}} = \mathbf{C}_{\mathbf{i,v}}^{\mathbf{c}} \mathbf{C}_{\mathbf{i,r}}^{\mathbf{c}} \mathbf{C}_{\mathbf{i,s}}^{\mathbf{c}}. \tag{2.2}$$

Furthermore, in each of the three rotations above, a specific Euler angle sequence is adopted, whereby a rotation α_1 is first performed about the y axis, followed by α_2 about the resulting x axis, and finally α_3 about the resulting z axis,

$$\mathbf{C}_{\mathbf{i},\zeta}^{\mathbf{c}} = \mathbf{C_2}(\alpha_1)\mathbf{C_1}(\alpha_2)\mathbf{C_3}(\alpha_3), \qquad \zeta = v, r, s. \tag{2.3}$$

In the above expression, the subscript for the "primitive" rotation matrix, $\mathbf{C}$, signifies the axis about which the rotation takes place (i.e. $1 = x$, $2 = y$, $3 = z$), and the subscript for α represents the order in which the rotations take place. The primitive rotation matrices are defined as:

$$\mathbf{C_2}(\alpha_1) = \begin{bmatrix} \cos\alpha_1 & 0 & \sin\alpha_1 \\ 0 & 1 & 0 \\ -\sin\alpha_1 & 0 & \cos\alpha_1 \end{bmatrix}; \tag{2.4a}$$

$$\mathbf{C_1}(\alpha_2) = \begin{bmatrix} 1 & 0 & 0 \\ 0 & \cos\alpha_2 & -\sin\alpha_2 \\ 0 & \sin\alpha_2 & \cos\alpha_2 \end{bmatrix}; \tag{2.4b}$$

$$\mathbf{C_3}(\alpha_3) = \begin{bmatrix} \cos\alpha_3 & -\sin\alpha_3 & 0 \\ \sin\alpha_3 & \cos\alpha_3 & 0 \\ 0 & 0 & 1 \end{bmatrix}. \tag{2.4c}$$

The Euler angles for a fixed orientation, denoted by the superscript r (α_1^r, α_2^r, α_3^r)

remain, of course, constant. However, when a slewing maneuver is present, either prescribed (specified), or as a motion governed by the joint dynamics (joint angles are degrees of freedom), the Euler angles for slewing motion, denoted by the superscript s (α_1^s, α_2^s, α_3^s), are not constant with time. Furthermore, when the central body is flexible, the angles in the transformation matrix due to flexibility, denoted by the superscript v (α_1^v, α_2^v, α_3^v), are functions of the flexibility generalized coordinates of the central body.

In the case of joint motion, the angles in the transformation matrix are identically those as either prescribed or the generalized coordinates. However, in the case of rotation due to flexibility, the Euler angles must be related to the flexibility generalized coordinates. Since the plate members are confined to be terminal bodies, the relationships for only beam rotation are required.

Consider a beam element, located at x^*, to deflect by δ_y and δ_z in the y and z directions, respectively (Figure 2-4). In addition, let the beam element rotate due to flexure by γ in the negative y direction, and by β in the z direction. Note, γ is the angle between the tangent of the projection of the beam element on the x-z plane and the x axis. Similarly, β is the angle between the tangent of the projection of the beam element on the x-y plane and the x axis. Because these rotations take place simultaneously in both the directions, β and γ do not equate exactly to the Euler angles, α_1^v and α_3^v, respectively. Also, when torsional motion is not included, $\alpha_2^v = 0$

The equations relating β and γ can be shown to be:

$$\beta = -\alpha_1^v; \tag{2.5a}$$

$$\gamma = \arctan\left(\frac{\tan\alpha_3^v}{\cos\alpha_1^v}\right). \tag{2.5b}$$

It can be seen that to the first order approximation $\beta = -\alpha_1^v$ and $\gamma = \alpha_3^v$. The

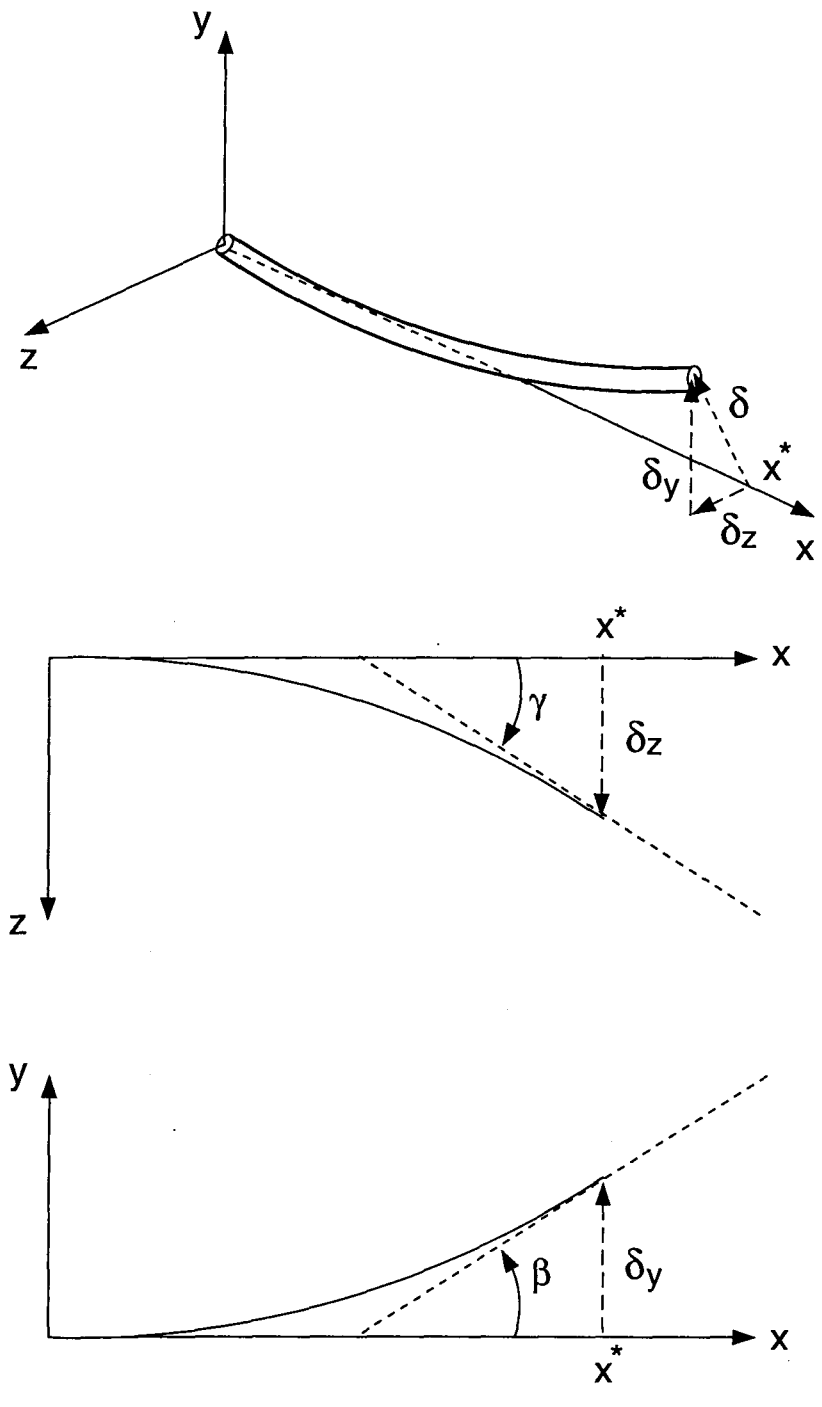

Figure 2-4 Deflection and rotations of a beam element.

relationships between β, γ and the flexibility generalized coordinates are:

$$\tan\beta = \left.\frac{\partial \delta_y}{\partial x}\right|_{x=x^*} = \sum_{\ell=1}^{n} \left.\frac{d\psi_y^\ell}{dx}\right|_{x=x^*} P^\ell(t); \tag{2.6a}$$

$$\tan\gamma = \left.\frac{\partial \delta_z}{\partial x}\right|_{x=x^*} = \sum_{\ell=1}^{n} \left.\frac{d\psi_z^\ell}{dx}\right|_{x=x^*} Q^\ell(t); \tag{2.6b}$$

where $\psi_y(x)$ and $\psi_z(x)$, are the shape functions for beam deflections in the y and z directions, respectively, and $P^\ell(t)$ and $Q^\ell(t)$ are the corresponding generalized coordinates used in the assumed modes method. Expressions for the first and second time derivatives of the transformation matrix $\mathbf{C_i^c}$, as well as its derivatives with respect to the flexibility generalized coordinates P^ℓ and Q^ℓ, can be developed from the above equations in a rather straightforward manner. In addition to the orientation of a body, it is also necessary to define its position relative to the adjacent one. The position vector for the body B_i relative to the body B_c is denoted $\vec{d}_i$. Similarly, $\vec{d}_{i,j}$ denotes the location of $B_{i,j}$ relative to B_i. As with the transformation matrices, the position vector $\vec{d}_i$, in general, consists of three unique contributions: from the rigid position, denoted by $\vec{d}_i^r$; the flexure of the central body, $\vec{d}_i^v$; and the translation of body B_i, given by $\vec{d}_i^t$,

$$\vec{d}_i = \vec{d}_i^r + \vec{d}_i^v + \vec{d}_i^t. \tag{2.7}$$

The first two contributions can be further expressed as:

$$\vec{d}_i^r = \vec{\rho}_c(\mathcal{O}_i) = \left\{ \begin{array}{c} x^* \\ 0 \\ 0 \end{array} \right\}; \tag{2.8a}$$

$$\vec{d}_i^v = \vec{\delta}_c(\mathcal{O}_i) = \left\{ \begin{array}{c} 0 \\ \sum_{\ell=1}^{n} \psi_{y,c}^\ell(x^*) P_c^\ell(t) \\ \sum_{\ell=1}^{n} \psi_{z,c}^\ell(x^*) Q_c^\ell(t) \end{array} \right\}; \tag{2.8b}$$

while the third is considered to be prescribed, i.e. its time history is specified as a particular function of time. The derivatives of $\vec{d}_i$ with respect to both time and the

flexibility generalized coordinates can be evaluated readily.

2.2.4 Spacecraft Position and Orientation in Space

In terms of orbital mechanics, the proposed problem can be posed as that of a spacecraft with its center of mass at C_f following an arbitrary trajectory under the influence of a central force due to the gravitational attraction of a spherical, homogeneous earth. The position of C_f is given by six orbital elements: $\rho, i, \omega, \epsilon, R_{cm}$ and θ (Figure 2-5). These elements are defined below:

- ρ longitude of the ascending node ;
- i inclination of the orbit ;
- ω argument of the perigee point ;
- ϵ orbit eccentricity ;
- R_{cm} instantaneous orbit radius (distance to the c.m.) ;
- θ true anomaly .

The first three parameters define the orbital plane and the orientation of the axis of the orbit, while the fourth determines the shape of the orbit. These parameters are fixed for a given problem. The last two elements are functions of time. Note that the inclination of the orbit, i, is defined as the angle between the orbital plane and the ecliptic plane, i.e. the plane of the earth's orbit about the sun. These six orbital elements are sufficient to describe the motion of the center of mass of an orbiting body. However, for a body with finite dimensions, its orientation needs to be specified. At least three additional angular parameters are required to specify the orientation of an object in orbit. In some cases, use of a fourth parameter avoids the problem of a singularity in the transformation that arises for certain combinations of spacecraft orientation and rotation sequence [2]. These angular parameters are not unique, and

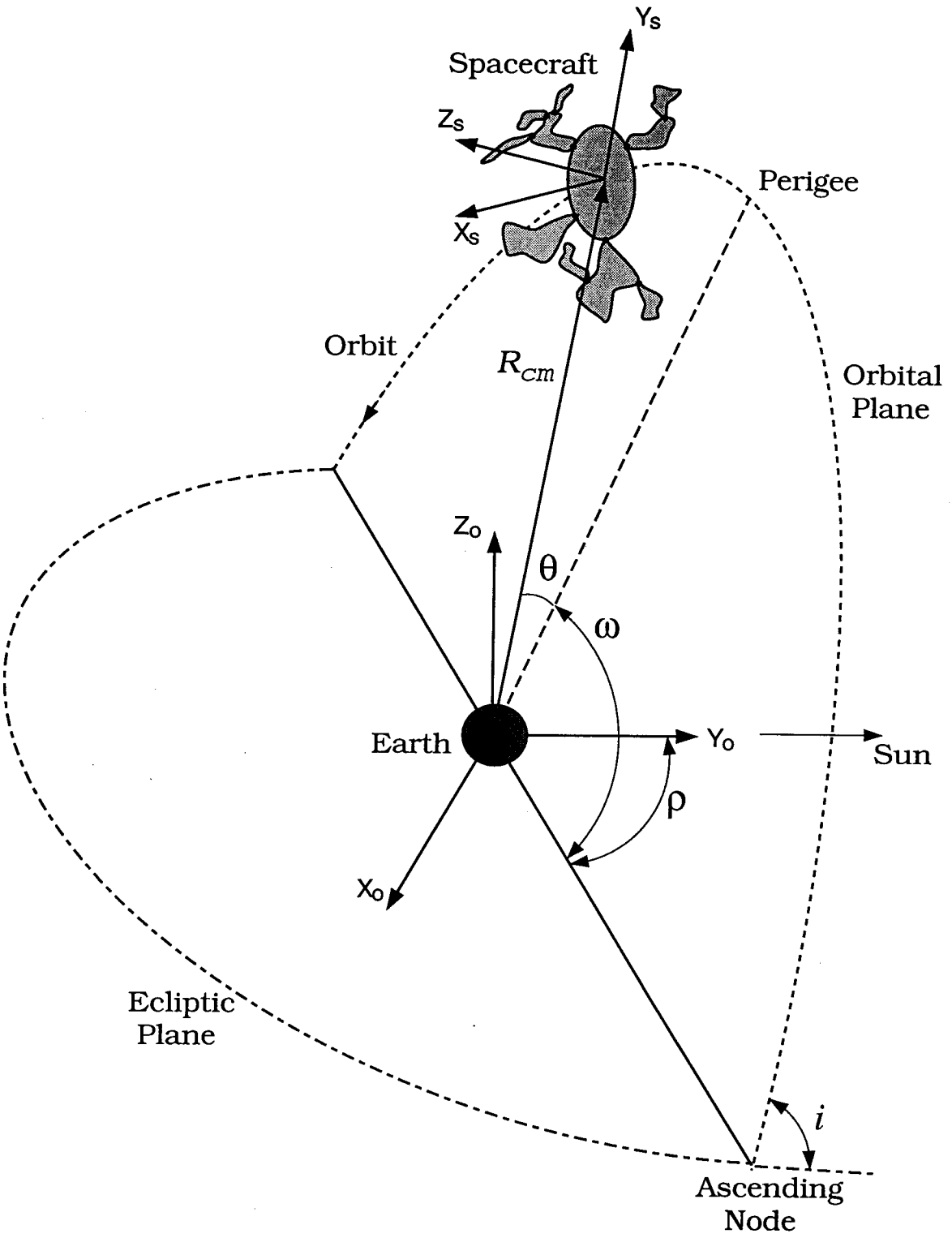

Figure 2-5 Orbital position of the spacecraft model.

may be chosen to satisfy the specific needs of the problem at hand.

The combination of θ, ρ, i and ω completely specify the orientation of the orbital reference frame ($\mathcal{F}_s$) at any instant in time. Two unique configurations of the orbital reference frame are employed in this study to avoid the problem of singularities inherent when three angular parameters are used to specify the relative rotation between the system ($\mathcal{F}_p$) and orbital frames ($\mathcal{F}_s$). In the first case (configuration A), the axes X_s, Y_s and Z_s are oriented along the orbit normal, local vertical, and local horizontal, respectively. In the second case (configuration B), however, the X_s, Y_s and Z_s axes are aligned with the local vertical, local horizontal, and orbit normal directions, respectively.

The orientation of the system reference frame ($\mathcal{F}_p$) relative to the orbital frame ($\mathcal{F}_s$) is defined by a set of modified Eulerian rotations, which are a sequence of three successive rotations. For configuration A, these are defined as follows: pitch, denoted by ψ, a rotation about the X_s axis; roll, denoted by ϕ, a rotation about the resulting Z axis; and finally, yaw, denoted by λ, a rotation about the resulting Y axis. For configuration B, the order of rotation, and the Euler angle notations with respect to the local vertical, local horizontal, and orbit normal directions are preserved employing the following sequence: pitch rotation (ψ), about the Z_s axis; roll rotation (ϕ) about the resulting Y axis; and finally, a yaw rotation (λ) about the resulting X axis.

The librational angular velocity, which is the angular velocity of the system reference frame ($\mathcal{F}_p$) relative to the inertial reference frame ($\mathcal{F}_o$), is denoted $\vec{\omega}^{p/o}$, and can, for configuration A, be shown to be,

$$\begin{aligned}\vec{\omega}^{p/o} = \vec{\omega} =&[(\dot{\psi}+\dot{\theta})\cos\phi\cos\lambda - \dot{\phi}\sin\lambda]\hat{i}_p + [-(\dot{\psi}+\dot{\theta})\sin\phi + \dot{\lambda}]\hat{j}_p \\ &+[(\dot{\psi}+\dot{\theta})\cos\phi\sin\lambda + \dot{\phi}\cos\lambda]\hat{k}_p. \qquad (2.9)\end{aligned}$$

The corresponding expression for the configuration B has the form,

$$\begin{aligned}\vec{\omega} =&[\dot{\lambda} - (\dot{\psi} + \dot{\theta})\sin\phi]\hat{i}_p + [(\dot{\psi} + \dot{\theta})\cos\phi\sin\lambda + \dot{\phi}\cos\lambda]\hat{j}_p \\ &+[(\dot{\psi} + \dot{\theta})\cos\phi\cos\lambda - \dot{\phi}\sin\lambda]\hat{k}_p. \end{aligned} \tag{2.10}$$

2.2.5 Position and Velocity Vectors of Elemental Masses

For an assemblage of bodies which are allowed to translate and rotate relative to one another, the kinetic energy of the system is best obtained by summing the kinetic energies of the individual bodies. Furthermore, if one or more of the bodies are flexible, then the kinetic energy of those members may be defined in a differential form and subsequently integrated over the individual body. Therefore, the velocity "field" over the domain of the body must be developed. With this in mind, the position vectors of elemental masses in each of bodies B_c, B_i and $B_{i,j}$, from the center of the earth, are first defined. With respect to the system reference frame $\mathcal{F}_p$, they can be expressed as:

$$\vec{R}_c = \vec{R}_{cm} - \vec{C}_{cm} + \vec{\rho}_c + \vec{\delta}_c; \tag{2.11}$$

$$\vec{R}_i = \vec{R}_{cm} - \vec{C}_{cm} + \vec{d}_i + \mathbf{C}_{\mathbf{i}}^{\mathbf{c}}(\vec{\rho}_i + \vec{\delta}_i); \tag{2.12}$$

$$\vec{R}_{i,j} = \vec{R}_{cm} - \vec{C}_{cm} + \vec{d}_i + \mathbf{C}_{\mathbf{i}}^{\mathbf{c}}\vec{d}_{i,j} + \mathbf{C}_{\mathbf{i}}^{\mathbf{c}}\mathbf{C}_{\mathbf{i,j}}^{\mathbf{i}}(\vec{\rho}_{i,j} + \vec{\delta}_{i,j}). \tag{2.13}$$

Furthermore, the position vector of the instantaneous system c.m., also from the earth center, denoted $\vec{R}_{cm}$, can be defined with respect to the same reference frame ($\mathcal{F}_p$) as

$$\vec{R}_{cm} = \frac{1}{M}\left\{\int_{m_c}\vec{R}_c dm_c + \sum_{i=1}^{N}\left[\int_{m_i}\vec{R}_i dm_i + \sum_{j=1}^{N_i}\int_{m_{i,j}}\vec{R}_{i,j}dm_{i,j}\right]\right\}, \tag{2.14}$$

where

$$M = m_c + \sum_{i=1}^{N} \left[m_i + \sum_{j=1}^{N_i} m_{i,j} \right] \tag{2.15}$$

is the total mass of the assemblage of bodies.

Substituting equations (2.11) to (2.13) into equation (2.14), yields an expression for the shift in the system center of mass, $\vec{C}_{cm}$, as measured from the center of the central body frame ($\mathcal{F}_c$),

$$\begin{aligned} \vec{C}_{cm} = \frac{1}{M} \Bigg\{ & \int_{m_c} (\vec{\rho}_c + \vec{\delta}_c) dm_c + \sum_{i=1}^{N} \Bigg[\int_{m_i} (\vec{d}_i + \mathbf{C}_{\mathbf{i}}^{\mathbf{c}} (\vec{\rho}_i + \vec{\delta}_i)) dm_i \\ & + \sum_{j=1}^{N_i} \int_{m_{i,j}} (\vec{d}_i + \mathbf{C}_{\mathbf{i}}^{\mathbf{c}} \vec{d}_{i,j} + \mathbf{C}_{\mathbf{i}}^{\mathbf{c}} \mathbf{C}_{\mathbf{i,j}}^{\mathbf{i}} (\vec{\rho}_{i,j} + \vec{\delta}_{i,j})) dm_{i,j} \Bigg] \Bigg\}. \end{aligned} \tag{2.16}$$

Next equations (2.11), (2.12), (2.13) and (2.16) are differentiated to obtain the expressions for velocities of mass elements in bodies B_c, B_i and $B_{i,j}$, as well as the shift in the system c.m. Note, although the position and velocity vectors are measured relative to $\mathcal{O}_o$, the origin of the inertial reference frame, they are projected onto reference frame $\mathcal{F}_p$:

$$\dot{\vec{R}}_c = \dot{\vec{R}}_{cm} - \dot{\vec{C}}_{cm} + \dot{\vec{\delta}}_c + \vec{\omega}^{p/o} \times (-\vec{C}_{cm} + \vec{\rho}_c + \vec{\delta}_c); \tag{2.17}$$

$$\begin{aligned} \dot{\vec{R}}_i = & \dot{\vec{R}}_{cm} - \dot{\vec{C}}_{cm} + \dot{\vec{d}}_i + \dot{\mathbf{C}}_{\mathbf{i}}^{\mathbf{c}} (\vec{\rho}_i + \vec{\delta}_i) + \mathbf{C}_{\mathbf{i}}^{\mathbf{c}} \dot{\vec{\delta}}_i \\ & + \vec{\omega}^{p/o} \times (-\vec{C}_{cm} + \vec{d}_i + \mathbf{C}_{\mathbf{i}}^{\mathbf{c}} (\vec{\rho}_i + \vec{\delta}_i)); \end{aligned} \tag{2.18}$$

$$\begin{aligned} \dot{\vec{R}}_{i,j} = & \dot{\vec{R}}_{cm} - \dot{\vec{C}}_{cm} + \dot{\vec{d}}_i + \dot{\mathbf{C}}_{\mathbf{i}}^{\mathbf{c}} \vec{d}_{i,j} + \mathbf{C}_{\mathbf{i}}^{\mathbf{c}} \dot{\vec{d}}_{i,j} + \dot{\mathbf{C}}_{\mathbf{i}}^{\mathbf{c}} \mathbf{C}_{\mathbf{i,j}}^{\mathbf{i}} (\vec{\rho}_{i,j} + \vec{\delta}_{i,j}) \\ & + \mathbf{C}_{\mathbf{i}}^{\mathbf{c}} \dot{\mathbf{C}}_{\mathbf{i,j}}^{\mathbf{i}} (\vec{\rho}_{i,j} + \vec{\delta}_{i,j}) + \mathbf{C}_{\mathbf{i}}^{\mathbf{c}} \mathbf{C}_{\mathbf{i,j}}^{\mathbf{i}} \dot{\vec{\delta}}_{i,j} \\ & + \vec{\omega}^{p/o} \times (-\vec{C}_{cm} + \vec{d}_i + \mathbf{C}_{\mathbf{i}}^{\mathbf{c}} \vec{d}_{i,j} + \mathbf{C}_{\mathbf{i}}^{\mathbf{c}} \mathbf{C}_{\mathbf{i,j}}^{\mathbf{i}} (\vec{\rho}_{i,j} + \vec{\delta}_{i,j})); \end{aligned} \tag{2.19}$$

$$\dot{\vec{C}}_{cm} = \frac{1}{M}\Bigg\{ \int_{m_c} \dot{\vec{\delta}}_c dm_c + \sum_{i=1}^{N} \Bigg[\dot{\vec{d}}_i m_i + \int_{m_i} \left[\dot{\mathbf{C}}_{\mathbf{i}}^{\mathbf{c}} (\vec{\rho}_i + \vec{\delta}_i) + \mathbf{C}_{\mathbf{i}}^{\mathbf{c}} \dot{\vec{\delta}}_i \right] dm_i$$
$$+ \sum_{j=1}^{N_i} \Bigg[(\dot{\vec{d}}_i + \dot{\mathbf{C}}_{\mathbf{i}}^{\mathbf{c}} \vec{d}_{i,j} + \mathbf{C}_{\mathbf{i}}^{\mathbf{c}} \dot{\vec{d}}_{i,j}) m_{i,j} + \int_{m_{i,j}} \left[\dot{\mathbf{C}}_{\mathbf{i}}^{\mathbf{c}} \mathbf{C}_{\mathbf{i,j}}^{\mathbf{i}} (\vec{\rho}_{i,j} + \vec{\delta}_{i,j}) \right.$$
$$\left. + \mathbf{C}_{\mathbf{i}}^{\mathbf{c}} \dot{\mathbf{C}}_{\mathbf{i,j}}^{\mathbf{i}} (\vec{\rho}_{i,j} + \vec{\delta}_{i,j}) + \mathbf{C}_{\mathbf{i}}^{\mathbf{c}} \mathbf{C}_{\mathbf{i,j}}^{\mathbf{i}} \dot{\vec{\delta}}_{i,j} \right] dm_{i,j} \Bigg] \Bigg] \Bigg\}. \tag{2.20}$$

Here $\dot{\vec{R}}_c$, $\dot{\vec{R}}_i$ and $\dot{\vec{R}}_{i,j}$ are time derivatives relative to the inertial reference frame $\mathcal{F}_o$, while <u>all</u> other time derivatives are w.r.t. the non–inertial reference frame $\mathcal{F}_c$.

2.3 Modeling of Structural Vibrations

2.3.1 Discretization of Flexible Motion

The dynamics of multibody flexible space structures includes attitude motion (libration), joint motion, as well as elastic deformations. The dynamics governing attitude and joint motion is expressed in terms of Ordinary Differential Equations (ODE), which are generally coupled and nonlinear. On the other hand, the time dependent elastic deformations of a distributed parameter system require Partial Differential Equations (PDE) for their description. Thus a multibody flexible system is characterized by a set of hybrid or mixed ordinary–partial differential equations. While each librational degree of freedom contributes one generalized coordinate, the vibration of even a simple distributed parameter system leads to an infinite set. Fortunately, by expressing the elastic deformations as a product of a finite number of mode shapes or admissible functions and generalized coordinates, one is able to represent the system dynamics with a reasonable engineering accuracy [79]. The manner in which this is accomplished is, of course, critical to the level of accuracy achieved in the resulting model. The discretization process can be introduced either after the

hybrid governing equations have been derived, or after the expressions for the system energies are obtained (i.e. before the equations of motion are actually derived). In this study the latter approach is taken.

Several popular procedures have been proposed for discretizing the flexible character of a structure, including the use of the finite element, Rayleigh–Ritz, and substructuring methods. The objective is to approximate the continuous displacement variable(s), which gives rise to a differential eigenvalue problem, by a set of discrete variables, leading to an algebraic eigenvalue problem. It is important to note that, generally speaking, the differential eigenvalue problem is not solvable, while the algebraic one is [80].

2.3.2 Discretization via Finite Element Method

Application of the *finite element method*, also referred to as the *system modes approach*, to the solution of a general boundary–value problem involves [81] the development of the variational or weak form of the governing differential equations and the determination of its approximate solution through the use of finite elements. The term "finite element" refers to the division of the problem domain into grids or meshes. The approximate equations are solved at the finite element or subdomain level after the continuous variable is represented as a number of discrete ones through the use of element level shape functions. As the mesh size used to discretize the structure is made sufficiently fine (depending on the complexity of the structure, among other factors), the solution to the approximate problem converges to that of the "real problem." However, for a complex problem, this generally requires a large number of nodal coordinates corresponding to the fine mesh used. Obviously, the numerical solution to such a problem would be not only time consuming and memory intensive, but also subject to inaccuracies inherent in many numerical algorithms employed for

large dimensional systems. This is especially true of algorithms related to matrix computations.

The use of the finite element method for discretization is fairly common in the study of flexible spacecraft models with a fixed geometry, that is, for spacecraft without any deployment, translation or slewing maneuvers [65,71]. Suleman [12] extended this approach to study the dynamics of spacecraft with a varying geometry due to translating and slewing members. In employing this method, the actual nodal degrees of freedom may be used directly, although it is not desirable because this introduces far too many degrees of freedom. Instead, the use of the natural modes of the system as computed from the finite element analysis of the structure are preferred for discretization.

2.3.3 Rayleigh–Ritz Discretization

In the *Rayleigh–Ritz* approach, a number of shape or admissible functions, defined over the entire structure, are used for discretization. These functions have to satisfy all geometric boundary conditions present in the system. On the other hand, comparison functions satisfy both the natural and the geometric boundary conditions [82]. Neither of these functions, in general, exactly satisfy the governing equations. The advantage is the reduction of the system to a smaller order, with adequate accuracy, compared to that obtained using the finite element method. Conversely, for a system characterized by complicated boundary conditions, the selection of appropriate admissible functions is a difficult task. As such the method is not particularly suited to systems characterized by interconnected flexible bodies.

2.3.4 Discretization via Substructuring

This approach is particularly suited to flexible multibody systems and is com-

monly referred to as *substructuring* or *component modes synthesis.* It has elements of the two methods described earlier. The structure is first decomposed into a number of constituent components or substructures, for which admissible functions are more readily obtained. These functions or "component modes" usually include rigid body, normal or displacement, static deflection, and constraint modes [83], and may also contain experimentally obtained shape functions [80]. Although the shape functions for the individual components are first considered separately, compatibility conditions are eventually imposed in the form of constraint equations. They ensure that the assemblage of bodies indeed represents a single structure rather than a collection of disjointed bodies. These conditions are typically related to the matching of displacements, and slopes or rotations of adjacent bodies at their interfaces. Although the approach is an extension of the Rayleigh–Ritz method to a multibody system, it can also be viewed as a special case of the finite element method where each component represents a single finite element [80].

One advantage of discretization through substructuring over the finite element method is the fact that, in many cases, it is compatible with the real engineering and system integration issues inherent in space related projects. Typically, different contractors or subcontractors are responsible for different substructures of a system, employing different methods of analyses, software, etc. The integration of the information required for discretization is made much simpler if each responsible organization or agency simply provides the modal characteristics of its component, rather than the structural parameters, from which a new finite element model can be developed to analyze the entire system. Furthermore, any modification to a given component can now be incorporated with greater ease.

Much of the research in the area has concentrated on the issues of the choice of

substructure modes and the efficient application of the geometric compatibility conditions. The approach taken by Hurty [84], and by Craig and Bampton [85], relies on the use of component modes obtained while treating all interfaces of a specific component as being fixed. This is repeated in sequence for all the components of the system. These modes, referred to as "fixed interface modes", are augmented by "constraint modes", obtained through sequentially imposing a unit deflection at each of the interface coordinates of the system, and computing the deformation shape. The resulting shape functions or modes are *statically complete*, meaning that any combination of force loading at the interfaces can be correctly represented by some combination of the constraint modes. It should be pointed out that Craig and Bampton employed a lumped mass model in their study. On the other hand, Benfield and Hruda [86] employed "free interface" component modes which were modified by including the mass and stiffness effects of the adjoining components. While this procedure can result in a much improved mode set as the presence of the adjoining of bodies is at least partially incorporated, the computational complexity increases greatly when a large number of bodies are present. Furthermore, modification of any one component would require that each component mode set be recomputed. MacNeal [87] and Rubin [88] used a set of free interface modes along with "residual modes" to account for the effect of the neglected higher modes. MacNeal accounted only for their static contributions, while Rubin's study also considered inertial and dissipative effects.

Spanos and Tsuha [89] applied the Craig–Bampton, Benfield–Hruda and MacNeal–Rubin approaches of component modes synthesis to study the low frequency system dynamics of *Galileo*, a dual–spin spacecraft. It consists of a rotor and a stator, both flexible, and a rigid platform. The component modes were computed using the NASTRAN finite element package. All three methods were found to work equally well.

2.3.5 Discretization by the Assumed Modes Method

Yet another procedure to spatial discretization, which may be considered to be a special case of substructuring, is the method of *assumed modes.* Here, a finite number of component level shape functions, which are taken to be admissible functions, are used in conjunction with the Lagrangian approach to develop the equations of motion. These admissible functions must be from a complete set, meaning that the mean square error between the continuous variable and its discretized version, can be made arbitrarily small by increasing the number of admissible functions used in representing the discretized variable. For a multibody system, the formulation may be developed in such a way that the geometric compatibility conditions, which ensure the integrity of the multibody assemblage, are incorporated directly in the systems kinematics. This is in contrast to the component modes synthesis method where constraint conditions are applied after the equations of motion, for generalized coordinates governing individual bodies, are obtained to eliminate the redundant degrees of freedom. The shape functions, which satisfy only the geometric boundary conditions, do not, in general, satisfy the governing hybrid differential equations. If they did indeed solve them, the shape functions would be the system eigenvectors or eigenfunctions [90]. It is desirable that the linear combination of the chosen shape functions approximate the system eigenvectors, and therefore render the *Rayleigh quotient* essentially stationary [90]. Rayleigh's quotient, $\mathcal{R}$, is given by

$$\mathcal{R}(\vec{u}) = \omega^2 = \lambda = \frac{\vec{u}^{\,T}[\mathbf{K}]\vec{u}}{\vec{u}^{\,T}[\mathbf{M}]\vec{u}}, \tag{2.21}$$

where $\mathbf{K}$, $\mathbf{M}$ and $\vec{u}$ are the system stiffness matrix, mass matrix, and shape function vector, respectively. For a shape function different from a system eigenfunction $\vec{u}_r$ by

a small amount, say ϵ,

$$\vec{u} = \vec{u}_r + \vec{\epsilon}, \tag{2.22}$$

Rayleigh's quotient gives an upper bound to the corresponding system eigenvalue or natural frequency,

$$\omega^2 = \omega_r^2 + \mathcal{O}(\vec{\epsilon}^T\vec{\epsilon}). \tag{2.23}$$

As alluded to earlier, the assumed shape functions need only satisfy the geometric boundary conditions. Therefore, it is possible to use a variety of shape functions including low–order polynomials. The use of polynomials has a number of advantages including the relative computational ease, and the fact that their determination is not based on the mass and stiffness properties of the components. They are also, of course, more plentiful than the eigenfunctions of a component [91, 92]. However, it has been demonstrated that in some cases, a large number of polynomial shape functions may be required when a fewer number of component eigenfunctions would have sufficed as admissible functions [80].

The method of assumed modes is particularly attractive when one is able to identify a set of admissible functions which approximate the system eigenfunctions. While there is no possible way of being sure of the closeness of the admissible functions to the resulting eigenfunctions or normal modes *a priori*, engineering judgement can be helpful. For example, Meirovitch [82] discusses how the admissible functions of a given system can be taken as the actual eigenfunctions of a related system with a simpler eigenvalue problem, but with identical geometric boundary conditions. As an example, he discusses the use of the natural modes of a simple cantilever beam as the admissible functions for a rotating cantilever beam.

2.3.6 Discretization via Quasi–Comparison Functions

In the Rayleigh–Ritz method, and indeed in the method of substructuring, the convergence of the approximate solution to the exact one is guaranteed as long as the admissible functions used are from a complete set. This in itself is an encouraging result because the admissible functions do not have to satisfy the natural boundary conditions or the differential equations. However, the rate of convergence, which is not addressed by the Rayleigh–Ritz theorem, can depend greatly on the set of admissible functions employed [93]. In theory, a complete set will guarantee convergence, although it is often very slow. This can be traced to the fact that a finite set of admissible functions frequently does not satisfy the natural boundary conditions. Therefore, the concept of completeness, while mathematically rigorous, attains reduced importance when practical computational factors, such as retaining as few degrees of freedom as necessary, are considered. The problem would then appear to be solvable if comparison functions, which satisfy all the boundary conditions, natural as well as geometric, are used. However, for complex systems with interconnected members, this is not feasible, as the natural boundary conditions would be dependent on the dynamics of the adjacent members. Therefore, the effort involved in determining the comparison functions would be prohibitive.

It is important to note that each comparison function would have to satisfy all the natural boundary conditions. Meirovitch and Kwak [93–95] have shown that the use of certain classes of admissible functions, capable of satisfying the natural boundary conditions in finite linear combination, can greatly improve convergence. These functions, named quasi–comparison functions, taken individually behave as admissible functions and collectively as comparison functions. Furthermore, besides being complete in energy, they can also be considered to be complete in boundary condi-

tions. Interestingly, it has been shown that in some cases the use of quasi–comparison functions yields better results than those obtained with comparison functions [93].

2.3.7 Modeling of Transverse Vibrations

In the present study, the approach taken in formulating the governing equations of motion is a general one. Therefore, the expressions for the system kinetic and gravitational potential energies, as well as their contributions to the Lagrange equations of motion, are developed in a fashion which does not limit the flexible bodies to be of a particular type. Furthermore, the nature of the elastic deformations experienced by the structural members is kept arbitrary. Hence, the equations of motion are applicable to a wide variety of flexible multibody systems. Of course, for a numerical implementation to study the dynamics of a specific system, the nature of the flexible bodies and their deformations will have to be specified. However, the general approach to the problem makes it a powerful tool. The procedure is represented schematically in Figure 2-6 . It shows the specific implementation of the formulation adopted in this study (shaded ellipse), as well as other possible applications.

The advantage of the general approach used in formulating the kinetic and gravitational potential energy expressions is illustrated by the following example. Consider a system consisting of interconnected beams undergoing torsional vibrations. Following the approach described above, one has only to equate the deflection terms in the final governing equations to expressions unique for beams undergoing torsional vibrations. This methodology obviates the need for rederiving the governing equations of motion for different systems of interest. Obviously, the savings in time and effort is significant as will become apparent in a later section when details of the governing equations are discussed.

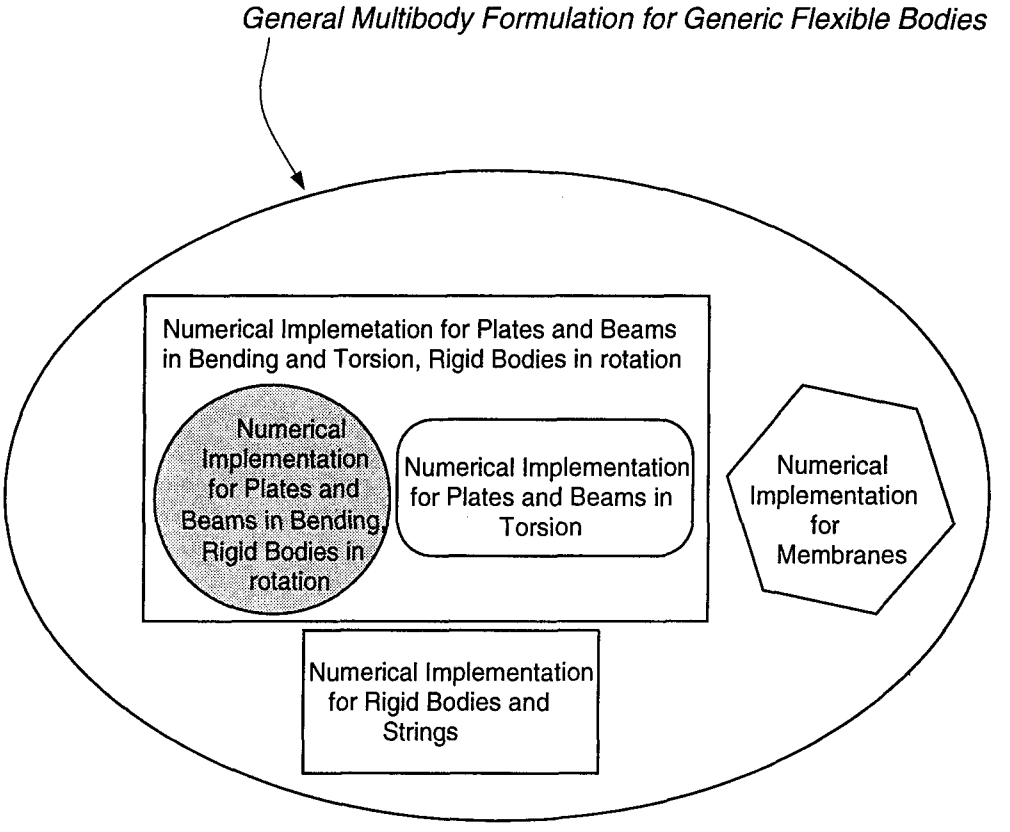

Figure 2-6 Schematic representation showing potential of the formulation and its implementation in the present thesis.

For the elastic strain energy, the expressions are dependent on the type of the flexible body (e.g. string, beam, plate, shell, membrane) and the nature of vibration (longitudinal, transverse, torsional). Fortunately, as shown later, the expressions for strain energy as well as its contribution to the governing equations of motion are much simpler than those for kinetic or gravitational potential energy contributions.

The class of systems considered for the numerical implementation is comprised of beams and plates, which are taken to vibrate transversely. The central body (B_c) is

assumed to be a beam–type structure or an arbitrary rigid body. B_i and $B_{i,j}$ bodies may be rigid, beam or plate–like structural members, the latter as terminal bodies. In other words, a plate–type B_i body may not have any $B_{i,j}$ member attached to it. This modeling choice is motivated by the design and layout of existing and future spacecraft in which plate–like solar arrays, heat rejection radiators and antennae are never intermediate bodies in a "branch" of the tree topology.

The position vector of a mass element in a body (rigid or flexible) is given in terms of a cartesian coordinate system, that is with x, y and z representing the components of the vector. For generic flexible bodies, components u, v and w are used to represent the deformations of the mass element in the x, y and z directions, respectively, i.e.

$$\vec{\delta} = \left\{ \begin{array}{c} u \\ v \\ w \end{array} \right\}. \tag{2.24}$$

When a rigid body is considered, orientation of its body fixed coordinate frame may be entirely arbitrary, provided that the first and second mass moments of inertia are consistently expressed with respect to the chosen orientation of the coordinate frame. However, for flexible bodies, a specific convention is adopted in order to make the formulation more efficient. For beam–type bodies, the beam axis is taken to be in the x direction, and the transverse vibrations are permitted in both the y and z directions. This convention is adopted for all beam–type structures, be they B_c, B_i or $B_{i,j}$ level bodies. Therefore, the position, $\vec{\rho}$, and deformation, $\vec{\delta}$, vectors of an element of mass in a beam–type body are given by:

$$\vec{\rho} = \left\{ \begin{array}{c} x \\ 0 \\ 0 \end{array} \right\}; \tag{2.25}$$

$$\vec{\delta} = \mathbf{\Phi} \cdot \vec{q} = \left\{ \begin{array}{c} 0 \\ \sum_{\ell=1}^{n} \psi_y^\ell(x) P^\ell(t) \\ \sum_{\ell=1}^{n} \psi_z^\ell(x) Q^\ell(t) \end{array} \right\}; \tag{2.26}$$

where $\mathbf{\Phi}$ and $\vec{q}$ are the matrix of admissible functions and vector of associated generalized coordinates used in discretizing the body, respectively. In terms of scalar quantities, the ℓ-th admissible function in the y and z directions are given by ψ_y^ℓ and ψ_z^ℓ, respectively, while the associated generalized coordinates are P^ℓ and Q^ℓ.

For bodies modeled as rectangular plates, the y direction is aligned along the fixed edge of the plate (i.e. the edge which is connected to the neighbouring body), the x coordinate is taken to be perpendicular to the fixed edge and in the plane of the plate, while the z direction in which the plate is assumed to vibrate, is normal the plate. The position, $\vec{\rho}$, and deformation, $\vec{\delta}$, vectors of an element of mass in a plate are given by:

$$\vec{\rho} = \left\{ \begin{array}{c} x \\ y \\ 0 \end{array} \right\}; \tag{2.27}$$

$$\vec{\delta} = \mathbf{\Phi} \cdot \vec{q} = \left\{ \begin{array}{c} 0 \\ 0 \\ \sum_{\ell=1}^{n} H^\ell(t)\eta^\ell(x,y) \end{array} \right\}. \tag{2.28}$$

Here, the admissible functions, which are defined over the x, y–domain, are represented by $\eta^\ell(x,y)$, and the corresponding generalized coordinated by $H^\ell(t)$.

Many satellites and space structures can be modeled essentially as rigid bodies to which are attached beam and plate–type appendages. The rigid body may represent the satellite bus while the beams and plates the antennae and solar arrays, respectively. The satellite bus is usually the most massive, often more than a hundred times in weight than any other part of the satellite (e.g. INdian communications SATellite INSAT, Japanese Space Flyer Unit SFU). In these cases, the flexible components are best modeled as cantilevered beams and plates. Therefore, the logical choice for admissible functions is the family of corresponding eigenfunctions. This results in a set of admissible functions completely satisfying the geometric boundary conditions (i.e.

zero slope and deflection) at the clamped end, and the natural boundary conditions (i.e. zero moment and shear force) at the free end.

In some cases, best illustrated by the proposed Space Station, the central body (power boom) itself is flexible. Now, the modeling of the flexible character requires more attention. Furthermore, the Power Boom weighs approximately $150,000\ kg$, while the second most massive structure, the station radiator, has a mass of around $1,400\ kg$. Therefore, the central body can be approximated as a free–free beam while other flexible members can be modeled as cantilevered or clamped–free beams and plates.

2.3.8 Modeling of Beam Vibration

For beam–type bodies, the Euler–Bernoulli beam theory, which does not model the effects of shear deformation and rotatory inertia, is employed in the formulation. The partial differential equation governing this type of beam flexure, in the absence of external loading, is given [96]

$$\frac{\partial^2}{\partial x^2}\left(EI_{zz}\frac{\partial^2 v}{\partial x^2}\right) + \bar{m}_b\frac{\partial^2 v}{\partial t^2} = 0. \tag{2.29}$$

Hence, $\bar{m}_b$ represents the beam mass per unit length, and EI_{zz} the flexural rigidity in the y direction. An analogous expression can be written for beam deflections in the z direction. The boundary conditions can be of four types: related to the shear force, bending moment, deflection and rotation experienced by the beam at the boundaries. The former two are referred to as natural boundary conditions, while the latter two as geometric boundary conditions. The natural boundary conditions can be represented as:

$$\mathcal{V}_y^b(x) = -EI_{zz}\frac{\partial^3 v}{\partial x^3};$$

$$\mathcal{M}_z^b(x) = EI_{zz}\frac{\partial^2 v}{\partial x^2}; \tag{2.30}$$

where $\mathcal{V}_y^b$ and $\mathcal{M}_z^b$ denote the beam shear force and bending moments, respectively, in the directions indicated by the subscripts. Corresponding expressions can be written for flexure in the z direction.

Equation (2.29) can be solved exactly by taking the beam deflection $v(x,t)$ to be a function of both time, $Y(t)$, and the spatial domain, $\phi(x)$ as

$$v(x,t) = \phi(x)Y(t). \tag{2.31}$$

Of particular interest is the solution for $\phi(x)$, because the family of shape functions under various loading conditions will be used subsequently as admissible and quasi–comparison functions. These shape functions are excellent candidates as admissible functions as, in a number of cases, the boundary conditions experienced by individual bodies in a multibody system approximate the fundamental loading conditions for which the exact shape functions can be found readily (e.g. free–free, clamped–free). Furthermore, shape functions for other loading conditions (e.g. clamped–clamped) can be used in conjunction with the admissible functions to form the set of quasi–comparison functions. The general form for ϕ is [96]

$$\phi(x) = A_1 \sin ax + A_2 \cos ax + A_3 \sinh ax + A_4 \cosh ax, \tag{2.32}$$

where: $a = \lambda/L$; $A_1, \ldots, A_4$ are constants which depend on the boundary conditions; λ, a multi–valued frequency parameter given by a transcendental equation, which depends on the boundary conditions; and L denotes the beam length. For several boundary conditions, these relations are summarized in Table 2-1 [97].

Table 2-1 Euler–Bernoulli beam shape function parameters

Boundary Condition	Equation for λ	Formula for A_1
Free–Free	$\cos\lambda\cosh\lambda - 1 = 0$	$\frac{\cos\lambda-\cosh\lambda}{\sinh\lambda-\sin\lambda}$
Clamped–Free	$\cos\lambda\cosh\lambda + 1 = 0$	$\frac{\sinh\lambda-\sin\lambda}{\cosh\lambda+\cos\lambda}$
Clamped–Clamped	$\cos\lambda\cosh\lambda - 1 = 0$	$\frac{\cosh\lambda-\cos\lambda}{\sinh\lambda-\sin\lambda}$

The coefficients have the value:

$$A_3 = A_1, \quad A_2 = A_4 = 1, \qquad \text{free–free beam;}$$

$$A_3 = -A_1, \quad A_2 = -A_4 = -1, \qquad \text{clamped–free beam;}$$

$$A_3 = -A_1, \quad A_2 = -A_4 = -1, \qquad \text{clamped–clamped beam.}$$

2.3.9 Modeling of Plate Vibration

The governing equations of motion for a rectangular plate, developed under the classical assumptions (thin plate and small deflections, plane sections remain plane) is given by [98]

$$\frac{\partial^4 w}{\partial x^4} + 2\frac{\partial^4 w}{\partial x^2 y^2} + \frac{\partial^4 w}{\partial y^4} + \frac{\bar{m}_p}{D}\frac{\partial^2 w}{\partial t^2} = 0, \tag{2.33}$$

where: $\bar{m}_p$ is the plate mass per unit area; and D, the flexural rigidity of the plate, is expressed as

$$D = \frac{Eh^3}{12(1-\nu^2)}. \tag{2.34}$$

Here, E and ν refer to Young's modulus and Poisson's ratio for the plate material, respectively, while h is the plate thickness.

The geometric boundary conditions for displacement and slopes, w, $\partial w/\partial x$ and $\partial w/\partial y$, can be evaluated easily for various loading conditions. The expressions relat-

ing the moments and the shear forces are [99]:

$$\mathcal{V}_x^p(x,y) = -D\frac{\partial}{\partial x}\left(\frac{\partial^2 w}{\partial x^2} + \frac{\partial^2 w}{\partial y^2}\right); \tag{2.35a}$$

$$\mathcal{V}_y^p(x,y) = -D\frac{\partial}{\partial y}\left(\frac{\partial^2 w}{\partial x^2} + \frac{\partial^2 w}{\partial y^2}\right); \tag{2.35b}$$

$$\mathcal{M}_x^p(x,y) = -D\left(\frac{\partial^2 w}{\partial x^2} + \nu\frac{\partial^2 w}{\partial y^2}\right); \tag{2.35c}$$

$$\mathcal{M}_y^p(x,y) = -D\left(\frac{\partial^2 w}{\partial y^2} + \nu\frac{\partial^2 w}{\partial x^2}\right); \tag{2.35d}$$

$$\mathcal{M}_{xy}^p(x,y) = -\mathcal{M}_{yx}^p(x,y) = D(1-\nu)\frac{\partial^2 w}{\partial x \partial y}. \tag{2.35e}$$

The convention adopted for the shear forces and bending moments is illustrated in Figure 2-7 .

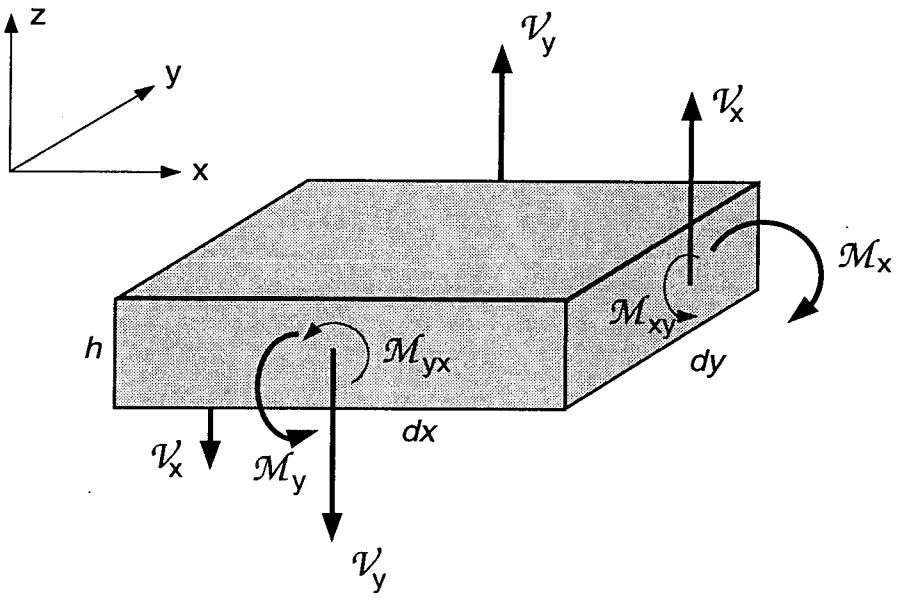

Figure 2-7 Shear forces and bending moments for plates.

In addition to the bending moments and shear forces, there also exist a pair of twisting moments as shown in Figure 2-7. The boundary conditions can be applied

directly from equations (2.35a-e).

As in the case of the beam, what is of particular interest is the family of eigenfunctions with various boundary conditions. If such eigenfunctions are available, they can then be used as admissible functions for plate elements in the multibody system. Considering the three fundamental types of boundary conditions, namely free, simply supported and clamped, 21 unique cases exist. Exact eigenfunctions can be obtained for the six cases when two opposite edges of a plate are simply supported [98, 100]. However, for the remaining 15 cases, only approximate eigenfunctions are available. An excellent set of admissible functions can be obtained by forming a product of the beam eigenfunctions with the appropriate boundary conditions [97, 98, 100]. Therefore, the deformation of a plate mass element as given in equation (2.28) can be rewritten as,

$$\vec{\delta} = \begin{Bmatrix} 0 \\ 0 \\ \sum_{s=1}^{m} \sum_{t=1}^{n} H^{s,t}(t) \psi^s(x) \phi^t(y) \end{Bmatrix}, \tag{2.36}$$

where $\psi^s(x)$ and $\phi^t(y)$ are appropriate beam eigenfunctions satisfying the boundary conditions at $x = 0$, l_p, and $y = -w_p/2$, $w_p/2$, respectively. It should be reiterated that these eigenfunctions, when used to form the plate admissible functions, satisfy the boundary conditions completely when a clamped or simply supported edge is encountered, but only approximately for a free edge. Nevertheless, this approach is found to give results that are quite accurate and is employed in the present study for modeling plate vibrations.

2.4 Kinetic Energy

The kinetic energy, T, for the general system considered in this study, can be

determined by evaluating the following expression,

$$T = \frac{1}{2}\Bigg\{ \int_{m_c} (\dot{\vec{R}}_c \cdot \dot{\vec{R}}_c)\, dm_c + \sum_{i=1}^{N} \Bigg[\int_{m_i} (\dot{\vec{R}}_i \cdot \dot{\vec{R}}_i)\, dm_i + \sum_{j=1}^{N_i} \int_{m_{i,j}} (\dot{\vec{R}}_{i,j} \cdot \dot{\vec{R}}_{i,j})\, dm_{i,j} \Bigg] \Bigg\}, \tag{2.37}$$

where $\dot{\vec{R}}_c$, $\dot{\vec{R}}_i$ and $\dot{\vec{R}}_{i,j}$ are given by equations (2.17–2.19). After a considerable amount of cancellation, and grouping together of identical terms (Appendix I), the system kinetic energy can be written as

$$\begin{aligned} T =& T_{orb} + T_{cm} + T_h + T_v + T_s + T_{h,s} + T_{h,v} + T_{s,v} \\ &+ \frac{1}{2}\vec{\omega}^{\,T}\mathbf{I_{sys}}\,\vec{\omega} + \vec{\omega}^{\,T}\vec{H}, \end{aligned} \tag{2.38}$$

where: $\vec{\omega}$ is the system angular velocity vector; $\mathbf{I_{sys}}$, the system inertia matrix; and $\vec{H}$, the system angular momentum vector about the central body reference frame, $\mathcal{F}_c$. The contributions from various sources are reflected in equation (2.38), with $\frac{1}{2}\vec{\omega}^{\,T}\mathbf{I_{sys}}\,\vec{\omega}$ representing the effect of librational motion and $\vec{\omega}^{\,T}\vec{H}$ due to the coupling between librational, translational, slewing and spacecraft flexibility. Other contributions are denoted by the following subscripts:

orb	orbital motion;
cm	shift in the center of mass motion;
h	translation motion (due to both specified translation and flexibility) between B_c and B_i as well as B_i and $B_{i,j}$ bodies;
v	vibration;
s	rotation (due to both slewing and flexibility) between B_c, B_i, and B_i, $B_{i,j}$ bodies;
h, s	coupling between translation and rotation;

h, v coupling between translation and vibration;

s, v coupling between rotation and vibration.

The system inertia matrix can also be written as a sum of its components, each representing the contributions of the above effects,

$$\mathbf{I_{sys}} = \mathbf{I_{cm}} + \mathbf{I_r} + \mathbf{I_h} + \mathbf{I_v} + \mathbf{I_{h,r}} + \mathbf{I_{h,v}} + \mathbf{I_{r,v}}. \tag{2.39}$$

The new subscript, r, denotes the rigid body contribution. Likewise, the system angular momentum vector, $\vec{H}$ can also be written as

$$\vec{H} = \vec{H}_{cm} + \vec{H}_h + \vec{H}_v + \vec{H}_{h,r} + \vec{H}_{h,v} + \vec{H}_{r,v} + \vec{H}_{r,s} + \vec{H}_{v,s} + \vec{H}_{h,s}. \tag{2.40}$$

The details are presented in Appendix I. It must be emphasized that these expressions for the system kinetic energy are completely general, and in their present form can be applied to any flexible multibody system. No assumption regarding the geometry (i.e. beam, plate, membrane, string) or the nature of the deformation (i.e. torsional, bending, longitudinal vibrations) of the individual bodies of the system has yet been made.

2.5 Potential Energy

There are two sources of contributions to the potential energy, U, of the spacecraft model under consideration: the gravitational energy, U_g; and the strain energy due to elastic deformations, U_e.

2.5.1 Gravitational Potential Energy

The potential energy of the multibody model due to Earth's gravitation field can

be expressed exactly as

$$U_g = -\mu_e \left\{ \int_{m_c} \frac{dm_c}{R_c} + \sum_{i=1}^{N} \left[\int_{m_i} \frac{dm_i}{R_i} + \sum_{j=1}^{N_i} \left[\int_{m_{i,j}} \frac{dm_{i,j}}{R_{i,j}} \right] \right] \right\}. \tag{2.41}$$

Substituting for $\vec{R}_c, \vec{R}_i$ and $\vec{R}_{i,j}$ (eqs. 2.11-2.13) into the above equation, expanding and neglecting terms of order ${R_{cm}}^{-4}$ and higher, U_g can be written as [14]:

$$U_g = -\frac{\mu_e M}{R_{cm}} - \frac{\mu_e}{2{R_{cm}}^3}\text{trace}[\mathbf{I_{sys}}] + \frac{3\mu_e}{2{R_{cm}}^3}\vec{\ell}^T\mathbf{I_{sys}}\vec{\ell}, \tag{2.42}$$

where $\vec{\ell}$ is the direction cosine vector of $\vec{R}_{cm}$ with respect to the coordinate frame $\mathcal{F}_p$. $\vec{\ell}$ is given by the following expression,

$$\begin{aligned}\vec{\ell} =& (\cos\psi \sin\phi \cos\lambda + \sin\psi \sin\lambda)\hat{i}_c + (\cos\psi \cos\phi)\hat{j}_c \\ &+ (\cos\psi \sin\phi \sin\lambda - \sin\psi \cos\lambda)\hat{k}_c.\end{aligned} \tag{2.43}$$

2.5.2 Strain Energy

In the development of a general formulation, it is desirable to specify the nature of the flexible structural elements as late as possible. As far as the kinetic and gravitational potential energies are concerned, this is feasible after obtaining the Lagrange equations of motion. However, this is not so with the strain energy. This is because a general expression for the strain energy applicable to an arbitrary elastic body is not available. Knowledge of the geometry of the flexible member, and character and nature of the deformation (bending, torsion, shear, etc.) is necessary. In the present study, focus is on beam and plate–type structural members.

The strain energy of a beam in flexure in both transverse directions is given by

[101],

$$U_{e,beam} = \frac{1}{2}\int_{l_b}\left[EI_{yy}\left(\frac{\partial^2 w}{\partial x^2}\right)^2 + EI_{zz}\left(\frac{\partial^2 v}{\partial x^2}\right)^2\right]dx, \tag{2.44}$$

and the corresponding expression for a plate is [101]

$$\begin{aligned} U_{e,plate} = \frac{1}{2}\int_{A_p} D\Bigg[&\left(\frac{\partial^2 w}{\partial x^2}\right)^2 + 2\nu\left(\frac{\partial^2 w}{\partial x^2}\right)\left(\frac{\partial^2 w}{\partial y^2}\right) \\ &+ \left(\frac{\partial^2 w}{\partial y^2}\right)^2 + 2(1-\nu)\left(\frac{\partial^2 w}{\partial x \partial y}\right)^2\Bigg] dA_p. \end{aligned} \tag{2.45}$$

For the multibody system topology described in sections 2.2.1 and 2.3.7 , the following convention is adopted in developing the generalized expression for the system strain energy. The central body, if flexible, is taken to be a beam element. The first N_b of the B_i bodies (i.e. B_1, B_2,... ,B_{N_b}) are taken to be beam elements while the remaining $(N - N_b)$ members (B_{N_b+1}, B_{N_b+2},... , B_N) are considered to be plate elements. The N_b bodies that are modeled as beams may have either beam or plate–type appendages attached to them. For each B_i body ($i = 1, \ldots, N_b$), the first N_{b_i} of the $B_{i,j}$ bodies are taken to be beam elements, while the remaining $(N_i - N_{b_i})$ are plate–type members. The flexural strain energy for such a system can be written as

$$\begin{aligned} U_e =& \frac{1}{2}\int_{l_c}\left[E_c I_{cyy}\left(\frac{\partial^2 w_c^b}{\partial x_c^2}\right)^2 + E_c I_{czz}\left(\frac{\partial^2 v_c^b}{\partial x_c^2}\right)^2\right]dx_c \\ &+ \frac{1}{2}\sum_{i=1}^{N_b}\int_{l_i}\left[E_i I_{iyy}\left(\frac{\partial^2 w_i^b}{\partial x_i^2}\right)^2 + E_i I_{izz}\left(\frac{\partial^2 v_i^b}{\partial x_i^2}\right)^2\right]dx_i \\ &+ \frac{1}{2}\sum_{i=N_b+1}^{N}\int_{A_{p_i}} D_i\Bigg[\left(\frac{\partial^2 w_i^p}{\partial x_i^2}\right)^2 + 2\nu_i\left(\frac{\partial^2 w_i^p}{\partial x_i^2}\right)\left(\frac{\partial^2 w_i^p}{\partial y_i^2}\right) \\ &+ \left(\frac{\partial^2 w_i^p}{\partial y_i^2}\right)^2 + 2(1-\nu_i)\left(\frac{\partial^2 w_i^p}{\partial x_i \partial y_i}\right)^2\Bigg] dA_{p_i} \end{aligned}$$

$$+\frac{1}{2}\sum_{i=1}^{N_b}\sum_{j=1}^{N_{b_i}}\int_{l_{i,j}}\left[E_{i,j}I_{i,j_{yy}}\left(\frac{\partial^2 w_{i,j}^b}{\partial x_{i,j}^2}\right)^2+E_{i,j}I_{i,j_{zz}}\left(\frac{\partial^2 v_{i,j}^b}{\partial x_{i,j}^2}\right)^2\right]dx_{i,j}$$
$$+\frac{1}{2}\sum_{i=1}^{N_b}\sum_{j=N_{b_i}+1}^{N_i}\int_{A_{p_{i,j}}}D_{i,j}\left[\left(\frac{\partial^2 w_{i,j}^p}{\partial x_{i,j}^2}\right)^2+2\nu_{i,j}\left(\frac{\partial^2 w_{i,j}^p}{\partial x_{i,j}^2}\right)\left(\frac{\partial^2 w_{i,j}^p}{\partial y_{i,j}^2}\right)\right.$$
$$\left.+\left(\frac{\partial^2 w_{i,j}^p}{\partial y_{i,j}^2}\right)^2+2(1-\nu_{i,j})\left(\frac{\partial^2 w_{i,j}^p}{\partial x_{i,j}\partial y_{i,j}}\right)^2\right]dA_{p_{i,j}}. \tag{2.46}$$

2.6 Structural Damping

The effects of dissipation, such as structural damping, can be incorporated into the governing equations as nonconservative generalized forces, or, for viscous structural damping, through Rayleigh's dissipation function, $\mathcal{R}^d$. This is defined as one–half of the instantaneous rate of mechanical energy dissipation occurring in the system [102]. The latter approach is employed here. The only dissipative effect considered is that due to the structural damping. Determination of a precise model for the structural damping is an area of research in itself. Here, the objective is to capture its overall effect on the system response. To that end, an equivalent viscous damping term is added to the conventional elastic stress–strain relationship (Hooke's Law) [96],

$$\sigma(t) = E\varepsilon(t) + C_s\dot{\varepsilon}(t), \tag{2.47}$$

where: σ is the uniaxial stress; ε, the strain; and C_s, the damping modulus. By isolating the contribution of the viscous effects, the dissipation function for a beam, $\mathcal{R}_b^d$, and plate, $\mathcal{R}_p^d$, can be obtained:

$$\mathcal{R}_b^d = \frac{1}{2}\int_{l_b}\left[C_s I_{yy}\left(\frac{\partial^2 \dot{w}}{\partial x^2}\right)^2+C_s I_{zz}\left(\frac{\partial^2 \dot{v}}{\partial x^2}\right)^2\right]dx; \tag{2.48}$$

$$\mathcal{R}_p^d = \frac{1}{2}\int_{A_p} F\left[\left(\frac{\partial^2 \dot{w}}{\partial x^2}\right)^2 + 2\nu\left(\frac{\partial^2 \dot{w}}{\partial x^2}\right)\left(\frac{\partial^2 \dot{w}}{\partial y^2}\right) + \left(\frac{\partial^2 \dot{w}}{\partial y^2}\right)^2 + 2(1-\nu)\left(\frac{\partial^2 \dot{w}}{\partial x \partial y}\right)^2\right] dA_p; \tag{2.49}$$

where

$$F = \frac{C_s h^3}{12(1-\nu^2)}. \tag{2.50}$$

The similarity between these expressions, and those for the corresponding strain energies given by equations (2.44, 2.45) is obvious. In fact, Lagrange's equation, clearly showed contributions from elastic strain energy and viscous dissipation to have a similar form.

2.7 Lagrange's Equations

The governing equations of motion are obtained through application of the Lagrangian principle,

$$\frac{d}{dt}\left(\frac{\partial T}{\partial \dot{\xi}_i}\right) - \frac{\partial T}{\partial \xi_i} + \frac{\partial U}{\partial \xi_i} + \frac{\partial \mathcal{R}^d}{\partial \dot{\xi}_i} = Q_i, \qquad i = 1, \ldots, n_g, \tag{2.51}$$

where: T and U are the kinetic and potential energies, respectively; ξ_i, the generalized coordinate; Q_i is the non–conservative generalized force associated with ξ_i; and $\mathcal{R}^d$ is Rayleigh's dissipation function. This represents a set of n_g second order nonlinear differential equations, where n_g is the total number of generalized coordinates. The presence of actuators, such as Control Moment Gyros (CMG) and thrusters, will contribute to the generalized forces.

The set of generalized coordinates include: the orbital degrees–of–freedom, R_{cm} and θ; the librational degrees–of–freedom, ψ, ϕ and λ; the flexibility generalized coordinates, denoted as q_c, q_i and $q_{i,j}$ for the flexible B_c, B_i and $B_{i,j}$ bodies, respectively;

and the joint degrees of freedom $\alpha^s_{\ell_i}$ $(\ell = 1, \ldots, 3)$ for the B_i bodies and $\alpha^s_{\ell_{i,j}}$ for the $B_{i,j}$ bodies. Of course, not all the generalized coordinates are required for the different cases of interest.

The orbital coordinates, R_{cm} and θ, are treated as generalized coordinates in this study. Alternately, the orbit may be assumed to be Keplerian, in which case R_{cm} and θ are given by the following relations [103]:

$$\begin{aligned} R_{cm} &= \frac{h^2}{\mu_e(1 + \epsilon \cos\theta)}; \\ R^2_{cm}\dot{\theta} &= h; \end{aligned} \tag{2.52}$$

where h is the orbital angular momentum. These relations are developed under the assumption that the satellite is a point mass. When the finite dimensions and flexibility of the spacecraft are taken into account, the assumption of a Keplerian orbit is no longer strictly true. One can consider satellite inertia and flexibility, as well as translation and slewing, as having perturbing effects on the orbital radius and true anomaly. These perturbations are usually very small and normally of little significance unless the satellite dimensions are comparable to that of the orbital radius [104]. However, the system energy is quite sensitive to these small orbital perturbations, because the orbital contribution to the kinetic and potential energies is significantly higher than that due to the elastic or the librational motions. Hence, with the Keplerian motion, the total energy may not remain constant even for a conservative system. To avoid this situation, the equations governing orbital motion are also derived, and may be used in place of the Keplerian relations, to define the time histories of R_{cm} and θ. These equations are given in Appendix II.

The equations governing the librational motion, and the vibration of the B_c, B_i and $B_{i,j}$ bodies also appear in Appendix II. Furthermore, the equations governing

the joint degrees of freedom $\alpha^s_{\ell_i}$ $(\ell = 1, \ldots, 3)$ for the B_i bodies and $\alpha^s_{\ell_{i,j}}$ for the $B_{i,j}$ bodies are given in the same appendix. Appendices III-VI contain details of terms in the governing equations which involve various derivatives of the system angular velocity vector, direction cosine vector, angular momentum vector, and inertia matrix.

As mentioned earlier, the presence of a significant amount of cancellation and combination of terms (termed simplification, however there is no approximation involved) was taken advantage of before evaluating the kinetic energy contributions, from flexibility and joint generalized coordinates, to the final equations of motion (Appendix II). The kinetic energy component of the equations of motion was developed separately for each different contribution to the energy (i.e. orbital, shift in the center of mass, hinge motion, vibration, joint rotation, and the coupling effects). It is between these contributions that the simplification through cancellation occurs. The extent of reduction in terms is indicated in Tables 2-2 and 2-3 .

Table 2-2 Simplification in the equations of motion governing vibrations

Expression	Number of Terms	
	Before Simplification	After Simplification
$d/dt(\partial T_a/\partial \dot{q}_{c_m}) - \partial T_a/\partial q_{c_m}$	129	69
$d/dt(\partial \vec{H}/\partial \dot{q}_{c_m}) - \partial \vec{H}/\partial q_{c_m}$	99	47
$d/dt(\partial T_a/\partial \dot{q}_{i_n}) - \partial T_a/\partial q_{i_n}$	90	44
$d/dt(\partial \vec{H}/\partial \dot{q}_{i_n}) - \partial \vec{H}/\partial q_{i_n}$	70	29
$d/dt(\partial T_a/\partial \dot{q}_{i,j_p}) - \partial T_a/\partial q_{i,j_p}$	40	14
$d/dt(\partial \vec{H}/\partial \dot{q}_{i,j_p}) - \partial \vec{H}/\partial q_{i,j_p}$	30	9

* (where $a = cm, h, v, s, hs, hv, sv$)

The equations are written in a compact form in terms of matrix and vector quantities, and operators. Here, the phrase "number of terms" refers to the terms involving

Table 2-3 Simplification in the equations of motion governing joint rotations

Expression	Number of Terms	
	Before Simplification	After Simplification
$d/dt(\partial T_a/\partial \dot{\alpha}_i) - \partial T_a/\partial \alpha_i$	106	50
$d/dt(\partial \vec{H}/\partial \dot{\alpha}_i) - \partial \vec{H}/\partial \alpha_i$	80	33
$d/dt(\partial T_a/\partial \dot{\alpha}_{i,j}) - \partial T_a/\partial \alpha_{i,j}$	60	27
$d/dt(\partial \vec{H}/\partial \dot{\alpha}_{i,j}) - \partial \vec{H}/\partial \alpha_{i,j}$	37	17

* (where $a = cm, h, v, s, hs, hv, sv$)

matrix/vector operations. Obviously, the reduction in scalar terms would be significantly higher depending on the number of bodies and the number of modes used to discretize the vibration of each body. To illustrate the simplification procedure, several examples are presented in Appendix VII. For the sake of brevity, simple cases are purposely chosen.

The resulting equations have the following structure,

$$\mathbf{M}(\vec{\xi}, t)\ddot{\vec{\xi}} + \vec{C}(\vec{\xi}, \dot{\vec{\xi}}, t) + \vec{K}(\vec{\xi}, t) = \vec{Q}(t), \tag{2.53}$$

where the mass matrix $\mathbf{M}$ can be written as

$$\begin{bmatrix} [\mathbf{M_o}] & [\mathbf{M_{o,l}}] & [\mathbf{M_{o,v}}] \\ [\mathbf{M_{o,l}}]^T & [\mathbf{M_l}] & [\mathbf{M_{l,v}}] \\ [\mathbf{M_{o,v}}]^T & [\mathbf{M_{l,v}}]^T & [\mathbf{M_v}] \end{bmatrix}, \tag{2.54}$$

and the vector of generalized coordinates, $\vec{\xi}$, as

$$\begin{Bmatrix} R_{cm} \\ \theta \\ \psi \\ \phi \\ \lambda \\ \vec{q}_f \end{Bmatrix}, \tag{2.55}$$

with $\vec{q}_f$ representing to the vector of flexibility generalized coordinates. The mass matrix is symmetric, nonsingular, nonlinear in the generalized coordinates, and contains terms only from the $d/dt(\partial T/\partial \dot{\xi})$ expression. Due to specified slewing or translation of bodies, the system mass matrix will, in general, be time varying. The vector $\vec{C}(\vec{\xi}, \dot{\vec{\xi}}, t)$, in general nonlinear and time varying, contains gyroscopic terms that arise from $d/dt(\partial T/\partial \dot{\xi})$ and $\partial T/\partial \xi$, and damping terms from $\partial \mathcal{R}^d/\partial \dot{\xi}$. The vector $\vec{K}(\vec{\xi}, t)$, representing the stiffness of the system is also nonlinear and time varying, and contains terms entirely from the $\partial U/\partial \xi$ expression.

2.7.1 Non–conservative Generalized Forces

The nonconservative generalized forces, Q_i, are derived from the virtual work consideration, i.e.

$$\delta W = \sum_{i=1}^{n_g} Q_i \, \delta \xi_i, \tag{2.56}$$

where δW is the virtual work and $\delta \xi_i$ the virtual displacement. For the system under study, the generalized forces arise from the CMG's, which are essentially torque actuators, and from thrusters, which are force actuators. The spacecraft model includes an arbitrary number of force and torque actuators on an individual body, each capable of producing torque or force in the x, y, or z (local) direction. The procedure for evaluating Q_i is quite well established. The resulting expressions being lengthy are

purposely not presented here. As an illustration, the virtual work done by the n_{cam} moment actuators $\vec{M}_c^i$ $(i = 1, \ldots, n_{cam})$ on the flexible central beam–type body is considered,

$$\begin{aligned}
\delta W = & \left(M_{cx}^t \cos\lambda \cos\phi - M_{cy}^t \sin\phi + M_{cz}^t \sin\lambda \cos\phi\right) \delta\theta \\
& + \left(M_{cx}^t \cos\lambda \cos\phi - M_{cy}^t \sin\phi + M_{cz}^t \sin\lambda \cos\phi\right) \delta\psi \\
& + \left(M_{cz}^t \cos\lambda - M_{cx}^t \sin\lambda\right) \delta\phi + M_{cy}^t \, \delta\lambda \\
& + \sum_{i=1}^{n_{cam}} \left(M_{cz}^i \left(\sum_{\ell=1}^{M_{mc}} \delta P_c^\ell(t) \frac{d\psi_{cy}^\ell}{dx_c}\Big|_{x_c = x_{cm}^i} \right) \right. \\
& \left. - M_{cy}^i \left(\sum_{\ell=1}^{M_{mc}} \delta Q_c^\ell(t) \frac{d\psi_{cz}^\ell}{dx_c}\Big|_{x_c = x_{cm}^i} \right) \right),
\end{aligned} \tag{2.57}$$

where:

$$\begin{aligned}
\vec{M}_c^i &= M_{cx}^i \hat{i}_c + M_{cy}^i \hat{j}_c + M_{cz}^i \hat{j}_c; \\
M_{cx}^t &= \sum_{i=1}^{n_{cam}} M_{cx}^i; \\
M_{cy}^t &= \sum_{i=1}^{n_{cam}} M_{cy}^i; \\
M_{cz}^t &= \sum_{i=1}^{n_{cam}} M_{cz}^i.
\end{aligned} \tag{2.58}$$

2.8 Orbital Equations

When an elliptical Keplerian orbit is assumed, the spacecraft position vector R_{cm}, and first and second time derivatives of the true anomaly, $\dot{\theta}$ and $\ddot{\theta}$, must be known as functions of time. The other approach would be to consider the true anomaly θ as an independent variable [13]. Such a change in the independent variable can be carried

out readily:

$$\frac{d}{dt} = \dot{\theta}\frac{d}{d\theta};$$
$$\frac{d^2}{dt^2} = \dot{\theta}^2\left(\frac{d^2}{d\theta^2} - \frac{2\epsilon\sin\theta}{1+\epsilon\cos\theta}\frac{d}{d\theta}\right).$$

The disadvantage of this approach is that the number of terms in the equations increase. An alternative to this, which is the approach followed in this study, is to solve for R_{cm}, $\dot{\theta}$, and $\ddot{\theta}$ as functions of time independently. If the orbital perturbations are modeled, that is when R_{cm} and θ are taken to be generalized coordinates, the problem does not arise because R_{cm}, $\dot{\theta}$, and $\ddot{\theta}$ are part of the set of variables which are solved for directly.

For the case when the orbit is assumed to be Keplerian, R_{cm}, $\dot{\theta}$, and $\ddot{\theta}$ are computed at each time step as follows. First, the *eccentric* anomaly, α is defined as follows [103]:

$$\tan\frac{\alpha}{2} = \sqrt{\frac{1-\epsilon}{1+\epsilon}}\tan\frac{\theta}{2}. \tag{2.59}$$

The eccentric anomaly is related to the orbital radius, R_{cm}, and a, the semi–major axis of the orbit by the expression

$$a\epsilon\cos\alpha = a - R_{cm}. \tag{2.60}$$

From the above equations, and from those of the conservation of angular momentum and total energy, the following equation relating the eccentric anomaly α to time, t, can be obtained,

$$\sqrt{\frac{\mu_e}{a^3}}t = \alpha - \epsilon\sin\alpha. \tag{2.61}$$

At each instant of interest, the above transcendental equation can be solved numerically for α. Next, using eq. (2.60), one obtains R_{cm}. $\dot{\theta}$ can be evaluated once R_{cm} is

known using the expression for orbital angular momentum,

$$R_{cm}^2\dot{\theta} = h = \sqrt{\mu_e a(1-\epsilon^2)}. \tag{2.62}$$

To obtain $\ddot{\theta}$, eq. (2.62) is first differentiated w.r.t. time and the terms are rearranged to yield

$$\ddot{\theta} = -\frac{2\dot{R}_{cm}\dot{\theta}}{R_{cm}}. \tag{2.63}$$

Next, eq. (2.60) is differentiated once w.r.t. time giving

$$\dot{R}_{cm} = a\epsilon \sin\alpha\dot{\alpha}. \tag{2.64}$$

Similarly, from eq. (2.61),

$$\dot{\alpha} = \frac{1}{1-\epsilon\cos\alpha}\sqrt{\frac{\mu_e}{a^3}}. \tag{2.65}$$

Finally, eqs. (2.64) and (2.65) are substituted into eq. (2.63) to give

$$\ddot{\theta} = -\frac{2a\epsilon\sin\alpha\dot{\theta}}{R_{cm}(1-\epsilon\cos\alpha)}\sqrt{\frac{\mu_e}{a^3}}. \tag{2.66}$$

2.9 Summary

In this chapter, formulation of the kinematics and dynamics of a flexible, multi-body spacecraft was presented. To begin with, the system geometry, reference frames employed, and the position and orientation of the model in space were described, followed by the development of position and velocity vectors for mass elements and shift in the system center of mass. Next, modeling of the transverse vibrations of the beam and plate–type flexible elements was undertaken and discretization of the flexible motion explained. With this, the stage was set to evaluate the kinetic and potential energies of the system, with the lengthy mathematical expressions presented

in Appendix I. Finally, the governing equations of motion were obtained, with details provided in Appendices II–VII. The process of the cancellation of terms in the governing equations was also explained with details given in Appendix VII.

3. COMPUTER IMPLEMENTATION

3.1 Preliminary Remarks

It is quite apparent from the preceding chapter that the governing equations of motion are nonlinear, nonautonomous and coupled. Furthermore, the equations are extremely lengthy despite the fact that a considerable degree of simplification was achieved through cancellation and combination of terms. Obviously, the computer implementation of the formulation would represent a challenging task. Important factors which should be considered during the planning and development stage of the simulation code include:

(i) the programming architecture employed ensuring efficiency, ease of debugging, as well as code management issues related to program modifications and enhancements;

(ii) the numerical subroutines used for tasks such as matrix inversion, numerical integration, and integration of the differential equations.

The methodology used in this study incorporates features which address the above issues. In particular, the code is written in a modular fashion, evaluating various contributing parameters (e.g. angular momentum, moment of inertia, potential and strain energies) separately. The approach facilitated debugging and management of the code.

In this chapter, the structure of the computer code is discussed first, followed by a description of the major subprograms. A brief overview of stiff systems is presented next, as well as a discussion on the numerical linearization. The linearized equations are particularly useful in the control investigation pursued later. Finally, validation of the code was established by comparing the results for particular cases with those

obtained by other researchers, and through conservation of the total energy for an undamped system.

3.2 Program Structure

The uncontrolled as well as controlled response of spacecraft to disturbances is of interest to researchers as well as design engineers. The disturbances may be environmentally induced (solar heating, micrometeorite impacts, free–molecular forces, etc.) and operational (Space Shuttle docking, crew activity, solar panel tracking, manipulator maneuvers, etc.) in character. This study focuses on response to operational disturbances. Effects of micrometeorite collisions and free–molecular forces can be modeled quite readily and incorporated as generalized forces. Alternately, their influence can be assessed through the introduction of appropriate initial conditions to the appropriate generalized coordinates. Ng [13] studied the effect of solar heating using the latter approach.

The simulation code implements the flexible multibody formulation as described in the previous chapter, with two exceptions: (i) a two–level tree–type multibody configuration with rigid tip–masses is simulated, rather than the three–level model for which the governing equations were developed; (ii) joint rotations are treated as specified as opposed to generalized coordinates. Even with these simplifications, the resulting code is quite lengthy, consisting of approximately 16,000 lines of FORTRAN source code, excluding the ODE solver and numerical integration routines.

Mathematically, the present problem is one of numerically solving the initial value problem for a set of nonlinear, nonautonomous, coupled, ordinary differential equations. Furthermore, because of control forces and moments, the problem is also a nonhomogeneous one. A numerical solution can be obtained by casting the problem as a set of first order differential equations, with initial conditions and marching in

time:

$$\dot{\vec{z}} = \vec{g}(\vec{z}, \vec{u}, t);$$
$$\vec{z}(0) = \vec{z}^{\,o}; \tag{3.1}$$

where $\vec{u}$ is the vector of generalized forces and $\vec{z}$, the state vector, is formed by augmenting the generalized coordinates $\vec{x}$ with the generalized velocities $\dot{\vec{x}}$ i.e.

$$\vec{z} = \begin{Bmatrix} \vec{x} \\ \dot{\vec{x}} \end{Bmatrix}. \tag{3.2}$$

The governing equations can be written as

$$\mathbf{M}(\vec{x}, t)\, \ddot{\vec{x}} = \vec{f}(\dot{\vec{x}}, \vec{x}, \vec{u}, t), \tag{3.3}$$

where $\mathbf{M}(\vec{x}, t)$ is the system mass matrix. All the stiffness, damping, gyroscopic, and generalized force terms, which are in general nonlinear and time varying, are incorporated in the vector denoted $\vec{f}(\dot{\vec{x}}, \vec{x}, \vec{u}, t)$. In terms of the original generalized coordinates and velocities, and the system mass matrix, eq. (3.1) can be written as

$$\begin{Bmatrix} \dot{\vec{x}} \\ \ddot{\vec{x}} \end{Bmatrix} = \begin{Bmatrix} \dot{\vec{x}} \\ \mathbf{M}^{-1}(\vec{x}, t)\, \vec{f}(\dot{\vec{x}}, \vec{x}, \vec{u}, t) \end{Bmatrix}. \tag{3.4}$$

An appropriate ODE solver would require initial values of the states (i.e. generalized coordinates and velocities), the system mass matrix $\mathbf{M}(\vec{x}, t)$, and the right hand side vector $\vec{f}(\dot{\vec{x}}, \vec{x}, \vec{u}, t)$ in order to generate the time history of the generalized coordinates and velocities. This rather simplistic description of the numerical methodology belies the complexity associated with actually forming the mass matrix and the right hand side vector. In particular, generation of $\mathbf{M}(\vec{x}, t)$ requires greater care because each element of the matrix must be computed.

The architecture of the simulation code is shown schematically in Figure 3-1 . The

first two subroutines called by the main program, *ReadIn1* and *ReadIn2*, introduce the data related to the system configuration, physical parameters, initial conditions, shape functions, and integration parameters from the input file.

When controlled motion is to be simulated, the user supplied linear compensator model is read in by the subroutine *ReadCon*. Subsequently, two subroutines, *ModInt* and *ModInt2*, compute the beam and plate modal integrals required by the governing equations of motion. The numerical computation of the various modal integrals is accomplished by the *DCADRE:* IMSL quadrature integration routine, which uses the Romberg method along with adaptive integration intervals. Next, the subroutine *TotMass* computes the total system mass, as well as the masses of all the beams, plates and rigid members, while *RhoInteg* evaluates the first mass moment of each body in the system. Both these quantities serve as building blocks at several other places in the simulation code. To facilitate verification of the data introduced into the code, most of the input file is reprinted as two output files by subroutines *Echodat1* and *Echodat2*. The computed modal integrals are also printed, along with the first mass moments of the individual bodies.

Next, if specified by the user in the input file, the subroutine *LinCont* computes a linearized model of the governing equations at a specified state. A linear model is desirable from the controller design point of view. Despite recent developments in nonlinear control theory, linear control remains the favoured approach from practical design considerations such as robustness to model uncertainty and ease of implementation. Furthermore, nonlinearities in the governing equations for many flexible spacecraft, in the absence of large maneuvers, often tend to be relatively small.

Consider the nonlinear governing equation (3.1). The system is assumed to be following some nominal trajectory denoted as $\mathbf{z^o}$ due to some nominal control input

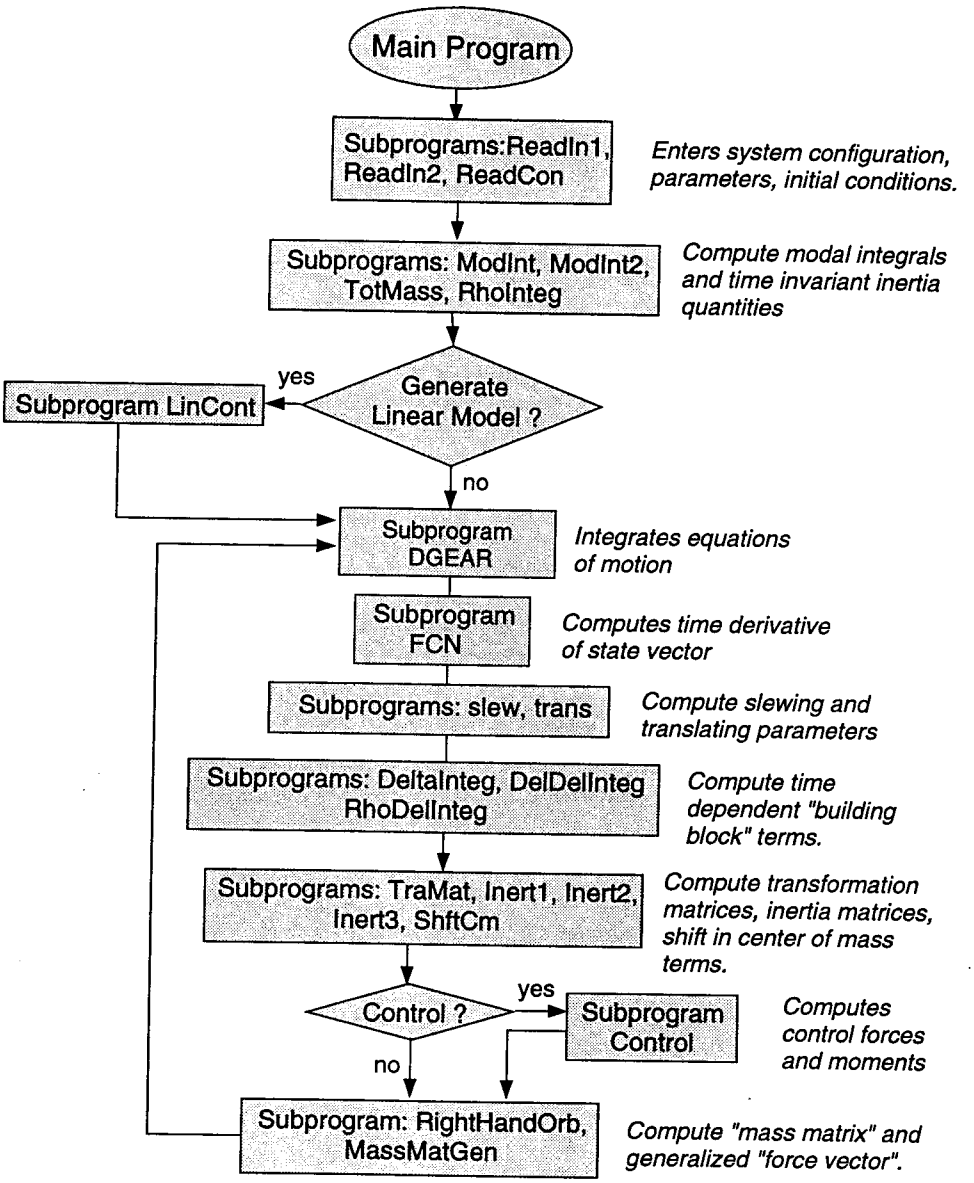

Figure 3-1 Flowchart for the simulation program.

$\mathbf{u^o}$. Note that the standard vector notation ($\vec{\cdot}$) is dispensed with. The departure of the state and input from the nominal values are denoted $\tilde{\mathbf{z}}$ and $\tilde{\mathbf{u}}$, repectively:

$$\begin{aligned} \mathbf{u} &= \mathbf{u^o} + \tilde{\mathbf{u}}; \\ \mathbf{z} &= \mathbf{z^o} + \tilde{\mathbf{z}}. \end{aligned} \tag{3.5}$$

The nominal trajectory $\mathbf{z^o}$ satisfies the equation

$$\dot{\mathbf{z}}^{\mathbf{o}} = \mathbf{g}(\mathbf{z^o}, \mathbf{u^o}, t). \tag{3.6}$$

Now, assuming that the actual trajectory deviates from the nominal trajectory by a small amount, eq. (3.5) is substituted into eq. (3.1) and expanded in Taylor series to give [105]:

$$\dot{\mathbf{z}}^{\mathbf{o}} + \dot{\tilde{\mathbf{z}}} = \mathbf{g}(\mathbf{z^o}, \mathbf{u^o}, t) + \left[\frac{\partial \mathbf{g}}{\partial \mathbf{z}}\right](\mathbf{z^o}, \mathbf{u^o})\tilde{\mathbf{z}} + \left[\frac{\partial \mathbf{g}}{\partial \mathbf{u}}\right](\mathbf{z^o}, \mathbf{u^o})\tilde{\mathbf{u}} + \tilde{\mathbf{h}}(t); \tag{3.7}$$

where $\left[\frac{\partial \mathbf{g}}{\partial \mathbf{z}}\right](\mathbf{z^o}, \mathbf{u^o})$ and $\left[\frac{\partial \mathbf{g}}{\partial \mathbf{u}}\right](\mathbf{z^o}, \mathbf{u^o})$ are the Jacobian matrices of the nonlinear system w.r.t. the state and control vectors, respectively, and $\tilde{\mathbf{h}}(t)$ represents higher order terms which are small compared to the linear terms. Subtracting the nominal solution given by eq. (3.6) from eq. (3.7), and neglecting the higher order terms, yields the linear set of ODE's governing the departure of the state from its nominal value,

$$\dot{\tilde{\mathbf{z}}}(t) = \mathbf{A}(t)\,\tilde{\mathbf{z}}(t) + \mathbf{B}(t)\,\tilde{\mathbf{u}}(t), \tag{3.8}$$

where:

$$\begin{aligned} \mathbf{A}(t) &= \left[\frac{\partial \mathbf{g}}{\partial \mathbf{z}}\right](\mathbf{z^o}, \mathbf{u^o}); \\ \mathbf{B}(t) &= \left[\frac{\partial \mathbf{g}}{\partial \mathbf{u}}\right](\mathbf{z^o}, \mathbf{u^o}). \end{aligned} \tag{3.9}$$

Note that, in general, the matrices **A** and **B** are functions of time, because the system is linearized about a trajectory rather than an equilibrium or stationary state. If, however, linearization is performed about an equilibrium state, the matrices would be time invariant.

Given the size of the equations of motion, the analytical derivation of the Jacobian matrices would be a prohibitive task. However, a numerical computation of **A** and **B** is possible by approximating the partial derivatives of the nonlinear vector function, $\mathbf{g}(\mathbf{z}, \mathbf{u}, t)$, by the finite differences equations:

$$\begin{aligned}
\left(\frac{\partial g_i}{\partial z_j}\right)\Big|_{\mathbf{z^o},\mathbf{u^o}} &\approx \left(\frac{g_i(\mathbf{z^o} + \Delta\mathbf{z_j}, \mathbf{u^o}, t) - g_i(\mathbf{z^o}, \mathbf{u^o}, t)}{\Delta z_j}\right); \\
\left(\frac{\partial g_i}{\partial u_j}\right)\Big|_{\mathbf{z^o},\mathbf{u^o}} &\approx \left(\frac{g_i(\mathbf{z^o}, \mathbf{u^o} + \Delta\mathbf{u_j}, t) - g_i(\mathbf{z^o}, \mathbf{u^o}, t)}{\Delta u_j}\right);
\end{aligned} \tag{3.10}$$

where g_i is the i–th element of vector $\mathbf{g}$, z_j the j–th element of the state vector, and $\Delta\mathbf{z_j}$ and $\Delta\mathbf{u_j}$ are vectors with zeros except for the j–th element. Of course, in the limit as $\Delta\mathbf{z_j}$ and $\Delta\mathbf{u_j}$ tend to zero, the approximations become equalities. However, this result is of no value when the Jacobians are computed numerically because one is limited by the finite floating point precision of the computer. An optimal choice of $|\Delta\mathbf{z_j}|$ and $|\Delta\mathbf{u_j}|$ for computing the Jacobians can be obtained by minimizing the sum of the round–off and truncation errors [106]. The optimum value of the step–size, h, is given by

$$h = |\Delta\mathbf{z_j}| = |\Delta\mathbf{u_j}| \sim \sqrt{\epsilon_m}, \tag{3.11}$$

where ϵ_m is the machine accuracy, typically around 10^{-16} for most FORTRAN compilers working in double precision. By ensuring that h is an exactly representable number, a sufficiently accurate linear model may be obtained. Given the inaccuracies inherent in modeling flexible systems, those introduced by the aforementioned numer-

ical approximation are quite modest. The method is implemented in the subroutine *LinCont*. Furthermore, the user has the option of using the linearized equations for the numerical simulation.

The subprograms described above are called only once after the program execution begins because they are responsible for either inputting the data or computing the time invariant quantities. The subprograms described below, however, are called at every integration time step. Next, the ODE integration routine *DGEAR* is called. *DGEAR* is an IMSL developed program with a number of attractive features which makes it particularly suited to the present problem. Its features include [107]:

(i) A choice of using either the implicit Adams method (up to order twelve) for nonstiff applications, or the Backward Differentiation Formula (BDF) for stiff equations. The latter is also called Gear's stiff method. Both procedures employ the implicit linear multistep method of the Predictor–Corrector, type.

(ii) The automatic selection of the integration step–size based on the user specified relative error bound.

(iii) The possibility of a user provided function for the evaluation of the Jacobian matrix of $\mathbf{g}(\mathbf{z}, \mathbf{u}, t)$. Alternatively, a numerical computation of the Jacobian, or functional iteration, which does not require any information about the Jacobian, is also possible.

In the one step methods, such as the Runge–Kutta approach, only the previous solution, i.e. $\mathbf{z}_{n-1}$, is used to determine the next one, i.e. $\mathbf{z}_n$. In multistep methods, a number of previous solutions, e.g. $\mathbf{z}_{n-k}, \ldots, \mathbf{z}_{n-1}$, are used to obtain $\mathbf{z}_n$. The Predictor–Corrector methods form a subset of the multistep methods, and can rely on either functional iteration or Newton's method to generate a preliminary value of $\mathbf{z}_n^o$ in the prediction step, which is essentially an extrapolation. This is denoted as $\mathcal{P}$. Next,

in the evaluation phase, denoted $\mathcal{E}$, the derivative $\mathbf{z}'_n$ is computed from the differential equation. A corrector step, $\mathcal{C}$, uses $\mathbf{z}'_n$ to obtain a refined value for $\mathbf{z}_n$. Steps $\mathcal{E}$ and $\mathcal{C}$ can be repeated to improve the solution until acceptable convergence is achieved. Alternately, the integration step size may be reduced to improve convergence [106].

As the systems under consideration are often stiff, a brief discussion concerning their numerical solution would be appropriate.

The term "stiff" refers to the situation when there are two or more widely differing time scales on which the states are changing. This condition is manifested by a wide range of natural frequencies present in the system. Flexible, orbiting structures are inherently stiff. The librational natural frequencies are approximately of the order of the orbital period (around 100 minutes for a satellite in a Low Earth Orbit, LOE; approximately 10^{-4} Hz). On the other hand, the fundamental natural frequencies in flexure range from 0.1 Hz to a few Hz for the proposed Space Station.

Integration schemes are classified as being explicit, implicit or semi–implicit. In an explicit scheme, expressions for the dependent variable at the new interval are specified in terms of the corresponding values at the previous interval and the derivative of the dependent variable also at the previous interval. For a forward Euler scheme, the expression is

$$\mathbf{z}_{n+1} = \mathbf{z}_n + h\,\mathbf{z}'_n. \tag{3.12}$$

When the system is linear, time–invariant and stable, the relationship between $\mathbf{z}$ and $\mathbf{z}'$ is simply

$$\mathbf{z}' = \mathbf{A}\mathbf{z}. \tag{3.13}$$

Applying eq. (3.13) to eq. (3.12) gives

$$\mathbf{z}_{n+1} = (\mathbf{I} + h\mathbf{A})\mathbf{z}_n. \tag{3.14}$$

The difference equation given by eq. (3.14), and hence the integration scheme, is stable only if the largest eigenvalue of $(\mathbf{I} + h\mathbf{A})$ lies within the unit circle in the complex plane, i.e.

$$\max_i \left|\lambda_i(\mathbf{I} + h\mathbf{A})\right| \leq 1, \tag{3.15}$$

which can be rewritten as

$$\max_i \left|h\lambda_i(\mathbf{A}) + 1\right| \leq 1. \tag{3.16}$$

Assuming that $\mathbf{A}$ has real eigenvalues, eq. (3.16) can be manipulated to yield

$$h \leq \frac{2}{-\lambda_{min}}, \tag{3.17}$$

where λ_{min} is the smallest eigenvalue (i.e. the most negative) of $\mathbf{A}$. Note, it corresponds to the fastest mode of the system. The equation defines the largest possible step–size for the integration scheme to remain stable. Clearly for stiff systems, the maximum integration step–size is dictated by the fastest eigenvalue present in the system.

In an implicit integration scheme employing the backward Euler formula,

$$\mathbf{z}_{n+1} = \mathbf{z}_n + h\,\mathbf{z}'_{n+1}. \tag{3.18}$$

Again, for a linear, stable, time–invariant system given by eq. (3.13), it can be shown that [106]

$$\mathbf{z}_{n+1} = (\mathbf{I} - h\mathbf{A})^{-1}\mathbf{z}_n. \tag{3.19}$$

The eigenvalues of eq. (3.19) are simply

$$\mathbf{eig}\left[(\mathbf{I}-h\mathbf{A})^{-1}\right]=\frac{1}{1-h\lambda_i}, \tag{3.20}$$

where λ_i are the eigenvalues of $\mathbf{A}$. Since λ_i are all negative, it can be seen that the implicit integration scheme is stable for any step–size.

The dynamical system used in the above analysis was purposely chosen to be simple (i.e. linear, time–invariant) to illustrate the differences between implicit and explicit integration schemes. Furthermore, the rather simple Euler procedure was used. Nevertheless, it does help focus on the characteristic feature of the explicit integration scheme: the time–step must be much smaller than the time–constant of the fastest mode present even though, in many instances, it may settle down early in the integration. When an implicit scheme is used, although stability is preserved regardless of the time–step chosen, matrix inversion at every step is necessary, even for a linear time invariant system, if adaptive step–sizing is employed. Semi–implicit methods are used when the system is nonlinear or time–varying, in which case, the Jacobian of the nonlinear function is used. The schemes are not guaranteed to be globally stable, although in most cases they are. This is because the behaviour of the nonlinear system in the neighbourhood of each time–step approaches that of a linear time–invariant system. Hence an implicit or a semi–implicit procedure is favoured for the numerical solution of stiff ODE's.

The structure of the *DGEAR* routine makes it readily amenable for use in simulation programs. The user only has to specify integration parameters such as the number of differential equations (in the first order form) to be simulated, the initial and final values of the independent variable, the initial integration step–size (subsequent step–sizes are chosen automatically), the required relative error bound, and parameters related to the method to be employed (Adams or Gear, Jacobian used,

etc.). In addition to this, the user supplies a function called *FCN* which computes the right hand side vector of the ODE. Essentially, besides reading in the correct parameters and initial conditions, and controlling the simulation output, the code's principal function is to compute this vector (acceleration) at each time–step. An analytically evaluated Jacobian of the right hand side vector can be employed in the integration process through the function *FCNJ*. Except in rare instances when rigorous debugging is necessary, the user normally does not have to concern himself with the approximately 4000 lines of source code in the *DGEAR* routine.

Function *FCN* assembles the right hand vector by calling a number of subroutines which compute various terms in the governing equations. Note, both *FCN* and the subprograms it executes are called a number of time per integration time–step until convergence is attained. Subroutine *Slew* calculates the rotations, as well as the angular velocities and accelerations of bodies, which slew. The user can choose between four common maneuver profiles: the sine–ramp; cubic; parabolic and linear. Furthermore, any other desired profile can be specified by writing an algorithm for it. Similarly, specified translation is computed through the subroutine *Trans* in an analogous fashion. The subroutine *DeeFlex* determines displacements and velocities of the attachment points of B_i bodies due to the flexure of the central body. In addition, *DeeFlex* determines the central body shape functions, as well as their first spatial derivatives at the attachment points.

The foreshortening effect in beams is modeled in the code by specifying a variable in the input file. The effect is incorporated through the subroutine *ForShor* and is described in detail in a subsequent chapter. Briefly, the foreshortening effect pertains to the preservation of the beam arclength in its mathematical model. In the conventional linear theory, the projection of the displaced beam along its undeformed axis

is assumed to be constant, which is strictly speaking not true. However, this assumption is of little consequence unless the beam is extremely flexible or fast rotational maneuvers are executed. Consistent with the general approach taken in this study, combinations of high rotational rates and flexible beam type structures are considered in the formulation as well as the simulation code.

Most of the terms computed by the subroutines are used repeatly in the program. In particular, the subroutines *DeltaInteg*, *DelDelInteg* and *RhoDelInteg* evaluate terms which are required by many of the subsequently described subprograms. *DeltaInteg* computes the following vector quantities (for all flexible bodies):

$$\begin{aligned} &\int_m \vec{\delta}\, dm; \\ &\int_m \dot{\vec{\delta}}\, dm. \end{aligned} \tag{3.21}$$

The subroutine *DelDelInteg*, meanwhile, evaluates the matrix quantities:

$$\begin{aligned} &\int_m \vec{\delta}\,\vec{\delta}^{\,T} dm; \\ &\int_m \vec{\delta}\,\dot{\vec{\delta}}^{\,T} dm, \end{aligned} \tag{3.22}$$

while *RhoDelInteg*, gives the matrix quantities:

$$\begin{aligned} &\int_m \vec{\rho}\,\vec{\delta}^{\,T} dm; \\ &\int_m \vec{\rho}\,\dot{\vec{\delta}}^{\,T} dm. \end{aligned} \tag{3.23}$$

The subroutine *TraMat* assembles the transformation matrices $\mathbf{C_i^c}$ for the B_i bodies, as well as the first derivatives of the matrices with respect to both time and the flexibility generalized coordinates of the central body. Furthermore, the portion of the second time derivatives of the matrices which do not contribute to the system mass matrix are also evaluated. These are the terms which do not contain the second

time derivatives of the flexibility generalized coordinates.

The shift in the system center of mass, $\vec{C}_{cm}$, as well as its first derivatives with respect to time and the flexibility generalized coordinates are evaluated by the subroutine *ShftCM*. The portion of the second time derivative which does not contribute to the mass matrix (i.e. the terms which do not contain second time derivatives of the flexibility generalized coordinates) are also evaluated by this subroutine.

The subroutine *Inert1* computes the system inertia matrix and its first time derivative. Derivatives of the inertia matrix with respect to the flexibility generalized coordinates of the central body and the B_i bodies, meanwhile, are evaluated by the subroutines *Inert2* and *Inert3*, respectively.

If the user indicates in the data input file that a controlled simulation is desired, the subroutine *Control* evaluates the control input variables based on the specified linear controller model which has the following structure:

$$\begin{aligned} \dot{\mathbf{x}}_\mathbf{c} &= \mathbf{A_c x_c} + \mathbf{B_c}(\mathbf{r} - \mathbf{y}); \\ \mathbf{u} &= \mathbf{C_c x_c}; \end{aligned} \tag{3.24}$$

where $\mathbf{x_c}$ is the vector of compensator states; $\mathbf{y}$, the plant output vector; $\mathbf{r}$, the reference control input; and $\mathbf{u}$, the plant input vector. $\mathbf{A_c}$, $\mathbf{B_c}$ and $\mathbf{C_c}$ are the user supplied matrices, obtained after a suitable control system synthesis. For the control option, the system generalized coordinates and velocities are augmented by the compensator states, and simulated together as a single state vector.

The system mass matrix, which is formed by the coefficients of the second derivatives of the generalized coordinates, is evaluated by the subroutine *MassMatGen*. The right hand vector, $\vec{f}(\dot{\vec{x}}, \vec{x}, \vec{u}, t)$, is computed by the subroutine *RightHandOrb* by calling a number of subroutines including the following:

(i) *DirCos*, which determines the direction cosine vector as well as its derivatives with respect to the librational generalized coordinates;

(ii) *Orbit* determines the orbital radius, radial velocity vector, true anomaly, angular velocity and angular acceleration, based on the satellite height at perigee, elapsed time and the orbit eccentricity. The subroutine is employed only if a Keplerian orbit is assumed (i.e. when the orbital coordinates are not degrees of freedom);

(iii) *Omega*, which computes the angular velocity and acceleration vectors, as well as the various derivatives of the angular velocity with respect to the librational generalized coordinates and velocities (Appendix III);

(iv) *AngMom1*, which evaluates the system angular momentum vector, $\vec{H}$, and the portion of its time derivative which does not contribute to the system mass matrix;

(v) *AngMom2* and *AngMom3* compute the various derivatives of $\vec{H}$ with respect to the flexibility generalized coordinates of B_c and B_i, respectively (Appendix V).

Once $\vec{f}(\dot{\vec{x}}, \vec{x}, \vec{u}, t)$ is assembled by *FCN*, the system of equations is cast in the first order form by solving eq. (3.3) for $\ddot{\vec{x}}$. This is accomplished by employing an algorithm which uses the LU decomposition directly, without relying on matrix inversion, thereby reducing the total number of floating point operations. The result is a lower round–off error as well as a saving in the overall execution time. At each time–step, the total, kinetic, gravitational potential and strain energies are evaluated if so desired by the subroutine *EneChkOrb*.

3.3 Verification of the Computer Code

The development of a model and computer code as complex as the one described must be validated before it can be used in any predictive capacity. Basically, there are two different sources of errors; those introduced during the mathematical modeling;

and those introduced in the algorithm development and coding stages.

With the size of the governing equations, not to mention the number of operations required to derive them, the introduction of errors is a possibility. To some extent, their presence can be sensed by observing characteristic "patterns" in the equations. However, this may serve only as an indicator and did prove helpful for spotting obvious mistakes. Some programming errors which lead to "compile" or "link" errors have to be detected prior to successful program compilation. However, most modeling and programming errors often tend to be elusive and hence require precise checks.

Several avenues are available to this end. These include: (i) comparisons with data collected from real spacecraft; (ii) matching of simulation results for particular cases obtained by other researchers; (iii) conservation of total system energy and angular momentum under specific situations; etc. For example, a system in the absence of energy dissipation or input should maintain its total energy constant.

The first method of verification is of little help in the present situation due to the lack of relevant data. Most measured information pertains to the librational and orbital motions. Several dynamical and control experiments with flexible systems are in the planning stage and may provide, in the future, a viable option for verification. Comparisons with results obtained by other researchers, for specific configurations, is feasible as there is considerable data available from other studies. In particular, there is a degree of overlap in the general model studied here and the models of Chan [108] as well as Ng [13]. Of course, the third option, perhaps the most effective, is always available.

3.3.1 Comparisons with Particular Cases

Results reported by Chan [108] are used to validate the modeling of maneuvers,

consisting of both translation and slewing of appendages. Chan's formulation includes both the structural flexibility of appendages and joint stiffness. The central body, however, is considered rigid and oriented in the gravity gradient configuration. The model is restrictive as the appendages are taken to be beam–type with librational and vibrational motions confined to the plane of the orbit, considered circular. Though limited in many aspects, Chan's formulation proves useful in the validation process.

Rigid Platform and Manipulator

To begin with, a comparison with a case involving a rigid manipulator is made. The model considered consists of the platform, and a manipulator (without payload), both taken to be rigid cylinders with a uniform mass distribution. The platform has a total mass of 214,000 kg, and a length of 115 m. The manipulator's mass and length are 3200 kg and 15 m, respectively. Both the platform and the manipulator have axial to transverse inertia ratios of 0.003. The system is in a circular orbit with a period of 100 minutes. As mentioned above, the long axis of the platform is nominally aligned with the local vertical direction. The manipulator, located at the center of the platform, slews through 180° (relative to the platform) as shown in Figure 3-2 .

The slewing maneuver is executed at various speeds, represented by the ratio, τ, of the duration of the maneuver to the orbital period. A sine–on ramp maneuver profile is assumed, where the slew angle, α, is given by

$$\alpha = \left(\frac{\alpha_f}{t_f}\right)\left[t - \left(\frac{t_f}{2\pi}\right)\sin\left(\frac{2\pi t}{t_f}\right)\right]. \tag{3.25}$$

The quantities with the subscript 'f' refer to values at the termination of the maneuver. The results given by the code developed in this study are compared with those obtained by Chan [108] in Figure 3-3 . The pitch response, ψ, given by the code is in excellent agreement with that reported by Chan. They show the expected trends.

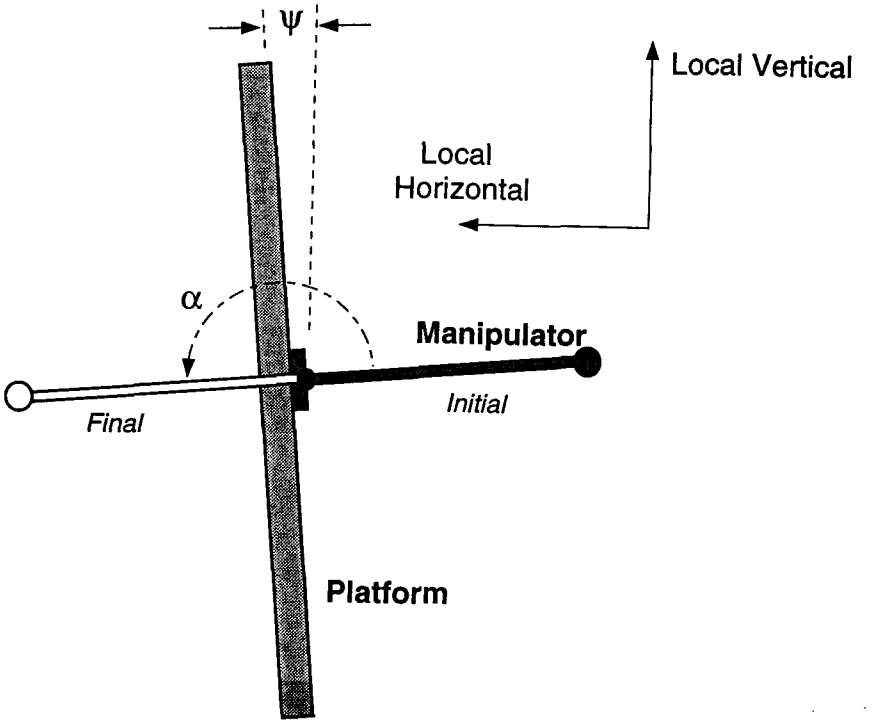

Figure 3-2 Schematic of rigid orbiting platform with a manipulator executing a slewing maneuver through 180°.

A faster maneuver results in a greater pitch disturbance. Note, the counterclockwise maneuver leads to an initial response that is negative (i.e. clockwise). The oscillations are at the pitch natural frequency.

Next, the effect of payload mass on the librational response is examined. Now, the manipulator executes a general maneuver which combines a translational maneuver through 30 m with a clockwise slew through 90° (Figure 3-4). Both the maneuver profiles are of the sine–on ramp type and are completed in 0.01 orbit (1 minute). The pitch response results for payload to manipulator mass ratios (i.e. m_p) of 0, 1, 2, 5

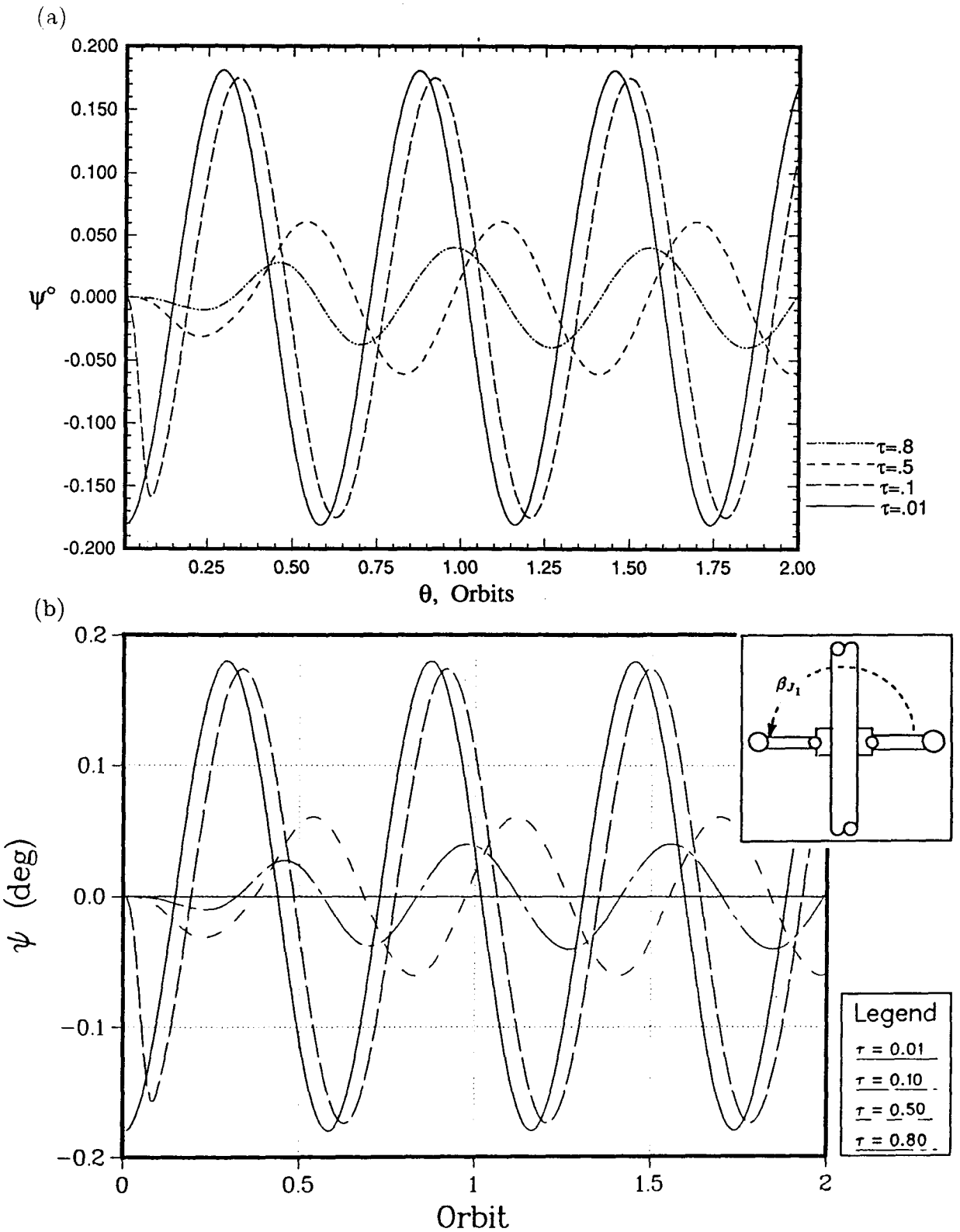

Figure 3-3 Librational response due to a slewing maneuver of a rigid manipulator with varying maneuver periods: (a) results from the present multibody code ; (b) results obtained by Chan.

and 10 are presented in Figure 3-5 . Again, the results are in excellent agreement with those reported by Chan. The trends established by the results are as expected: the larger the payload mass for a given maneuver, the greater the pitch excitation.

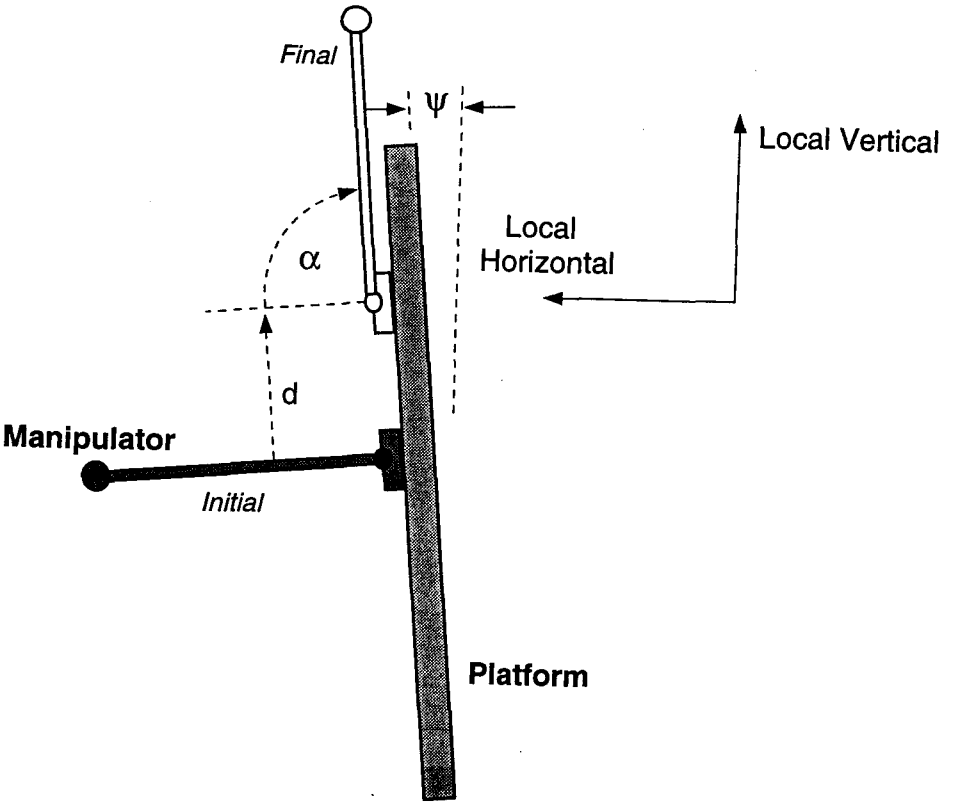

Figure 3-4 A schematic diagram showing a rigid orbiting platform with a manipulator executing combined slew and translation maneuvers.

Rigid Platform with Flexible Manipulator

The next logical step is to verify results accounting for the flexible character of the manipulator. The combined translation–slew maneuver as before is used. A large payload mass of 32,000 kg, i.e. $m_p = 10$, is considered with several values of the manipulator bending stiffness corresponding to fundamental frequency, ω_1, of 1.0, 1.2,

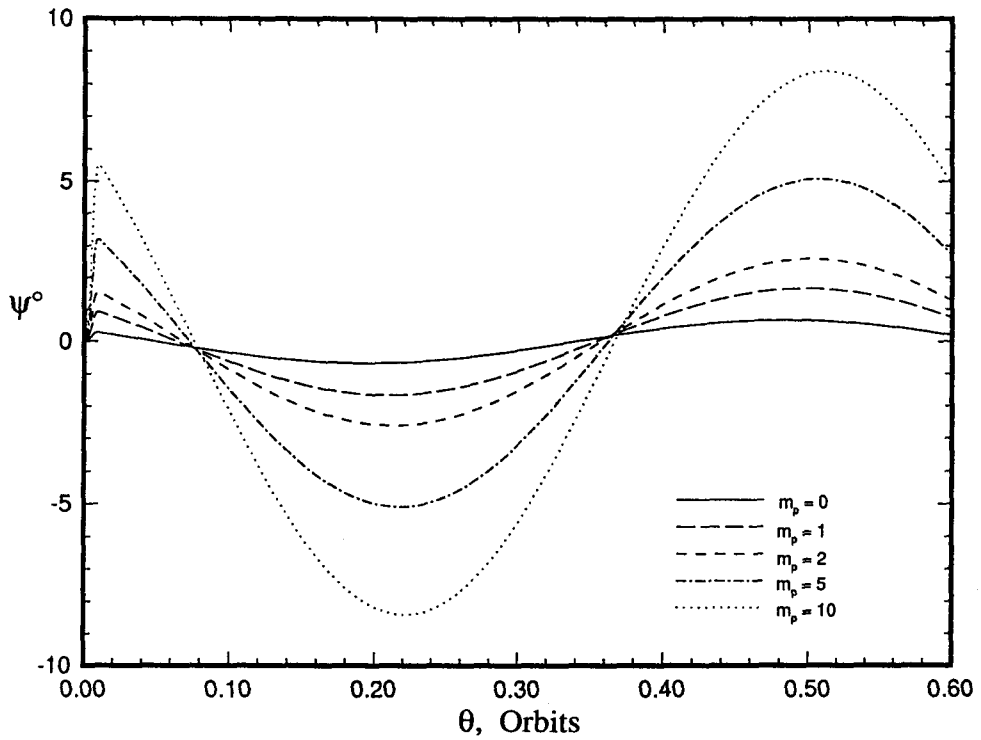

Figure 3-5 Librational response due to combined slew and translation maneuvers of a rigid manipulator as affected by the payload mass ratio.

1.5, 2.0 and 5.0 rad/s. The response for the rigid case ($\omega_1 = \infty$) is also considered. Only the first cantilever beam mode is simulated. The resulting time histories of pitch, ψ, and manipulator tip deflection, δ_t, are shown in Figure 3-6. Again, the results compared rather well with those reported by Chan. Note, the effect of flexibility, modulates the response about the rigid manipulator results. The modulation amplitude varies from $\pm 1.5°$ for a manipulator with a fundamental bending frequency of 1.0 rad/s, to less than $\pm 0.4°$ for a frequency of 1.5 rad/s. For the manipulator bending frequency greater than 5.0 rad/s, the effect of flexibility on the librational response

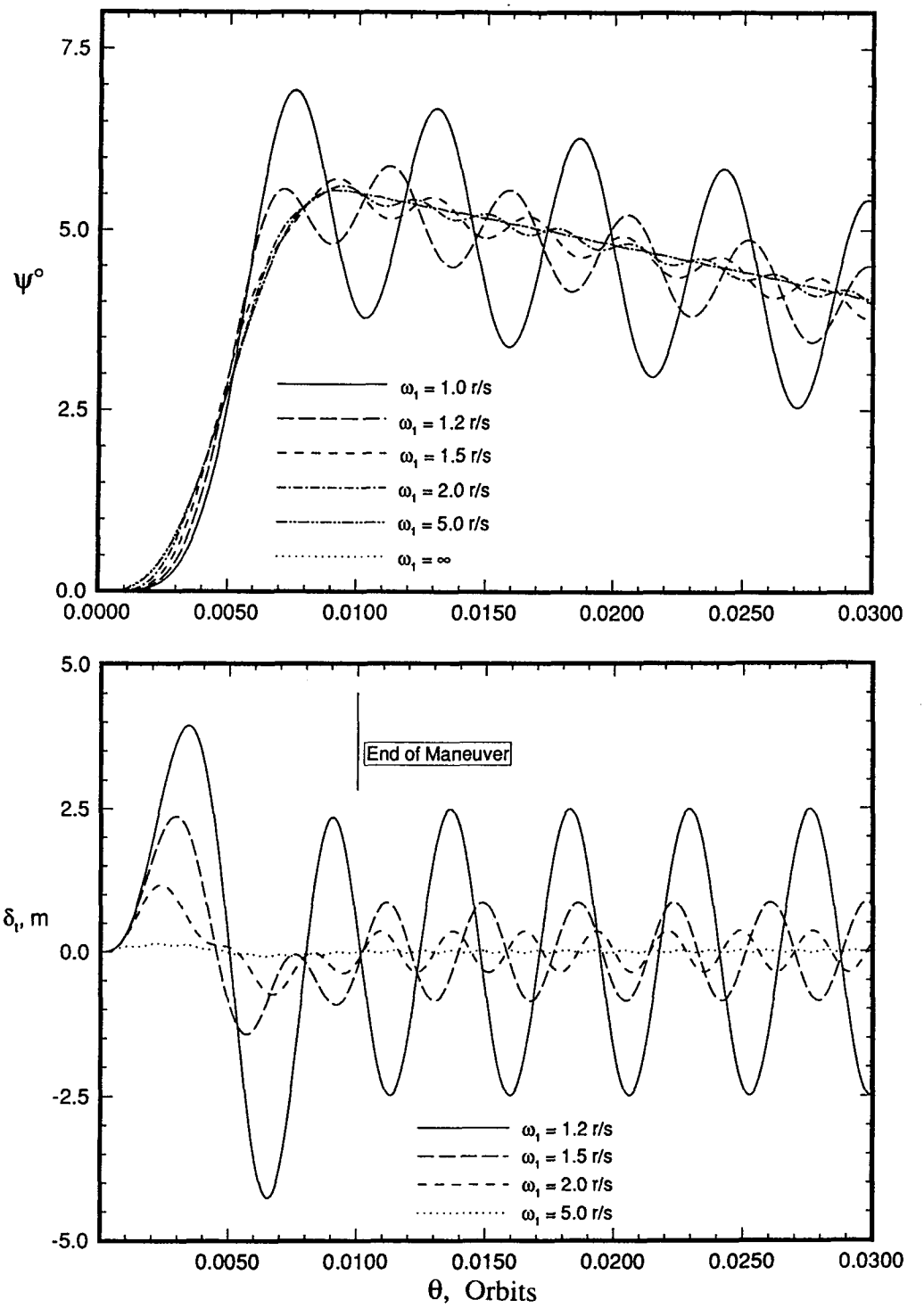

Figure 3-6 Pitch and manipulator tip deflection time histories due to a combined slewing and translation maneuver of a flexible manipulator with varying bending stiffness.

is virtually negligible. From a longer duration time history, the 'mean' librational response is observed to be at the pitch natural frequency. The maximum manipulator tip deflection varies from approximately ± 4 m for a fundamental bending frequency of 1.2 rad/s, to approximately ± 1 m for a bending frequency of 2.0 rad/s. Note, the maximum deflection occurs during the maneuver, and reduces somewhat during the post–maneuver phase. In the absence of any form of damping, the oscillations in both tip deflection and pitch angle continue without attenuation.

For the system described above, the effects of both the number of shape functions used in the discretization and the type of maneuver profile were also investigated, for $m_p = 10$ and $\omega_1 = 2$ rad/s. The combined slew–translation maneuver was completed in 1 minute. Four distinct cases were investigated corresponding to sine–on ramp and cubic maneuver profiles with 1 and 3 cantilever beam shape functions. As the name suggests, for the case of the cubic maneuver profile the slew angle has a cubic dependence on time. Compared to the sine–on ramp profile, the cubic case is less smooth, because the acceleration at the start and end of the maneuver is not zero as in the case of the sine–on ramp. Therefore, as can be expected, the modulations in the pitch and the manipulator tip deflection are greater when a cubic maneuver profile is employed (Figures 3-7 , 3-8). In particular, the post–maneuver tip deflection is approximately twice as large with the cubic profile. The effect of increasing the number of shape functions from 1 to 3 results in a slightly lower frequency of oscillation in both the cubic and sinusoid maneuver cases. Furthermore, in the case of the cubic profile, the post–maneuver tip amplitude is slightly greater. These results, again, were found to be in agreement with those reported by Chan.

Flexible Space Station Model with 3-D Dynamics

In the next stage of the model and program validation, three dimensional attitude

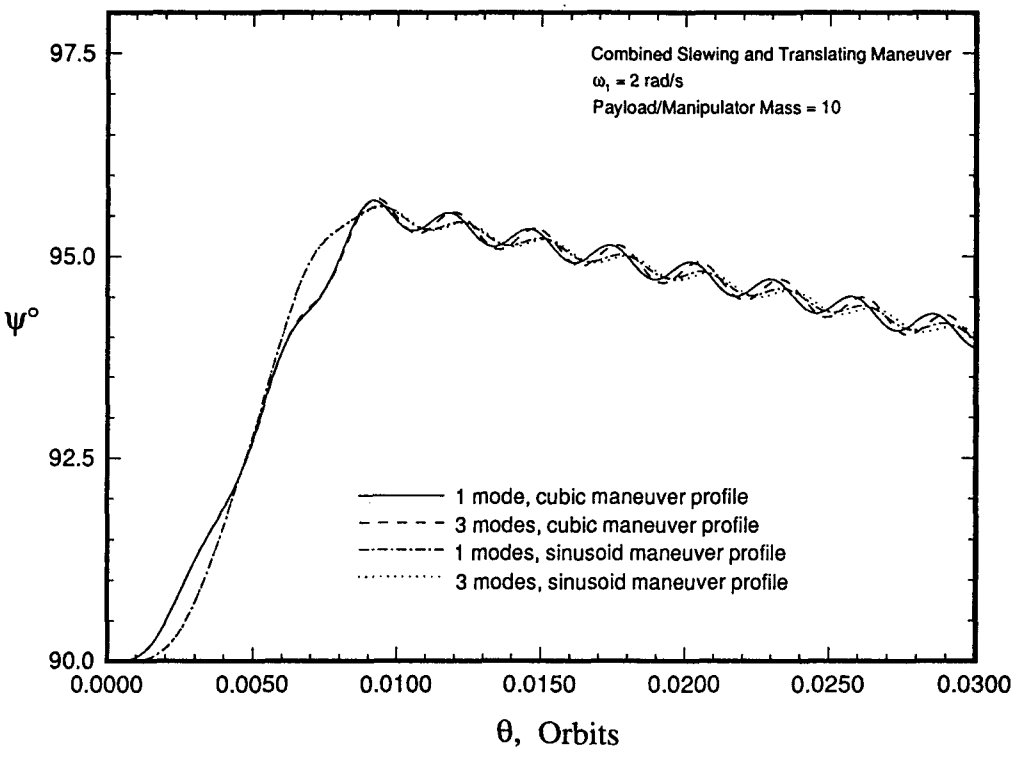

Figure 3-7 Pitch response due to a combined slew-translation maneuver of a flexible manipulator as affected by the maneuver profiles and number of modes.

motion, as well as more detailed modeling of flexibility is introduced. The results given by the code are compared with those reported by Ng [13] in his doctoral dissertation. The model used for this part of the study is representative of the First Element Launch (FEL) configuration once proposed for the Space Station. The Space Station is still evolving and hence its final configuration has still not been finalized. Fortunately, the general character of this formulation is ideally suited to tackle such uncertainty. The model is taken to be in a circular orbit at a height of 400 km. The principal component of the FEL is the central truss–like structure called the power boom. Attached to

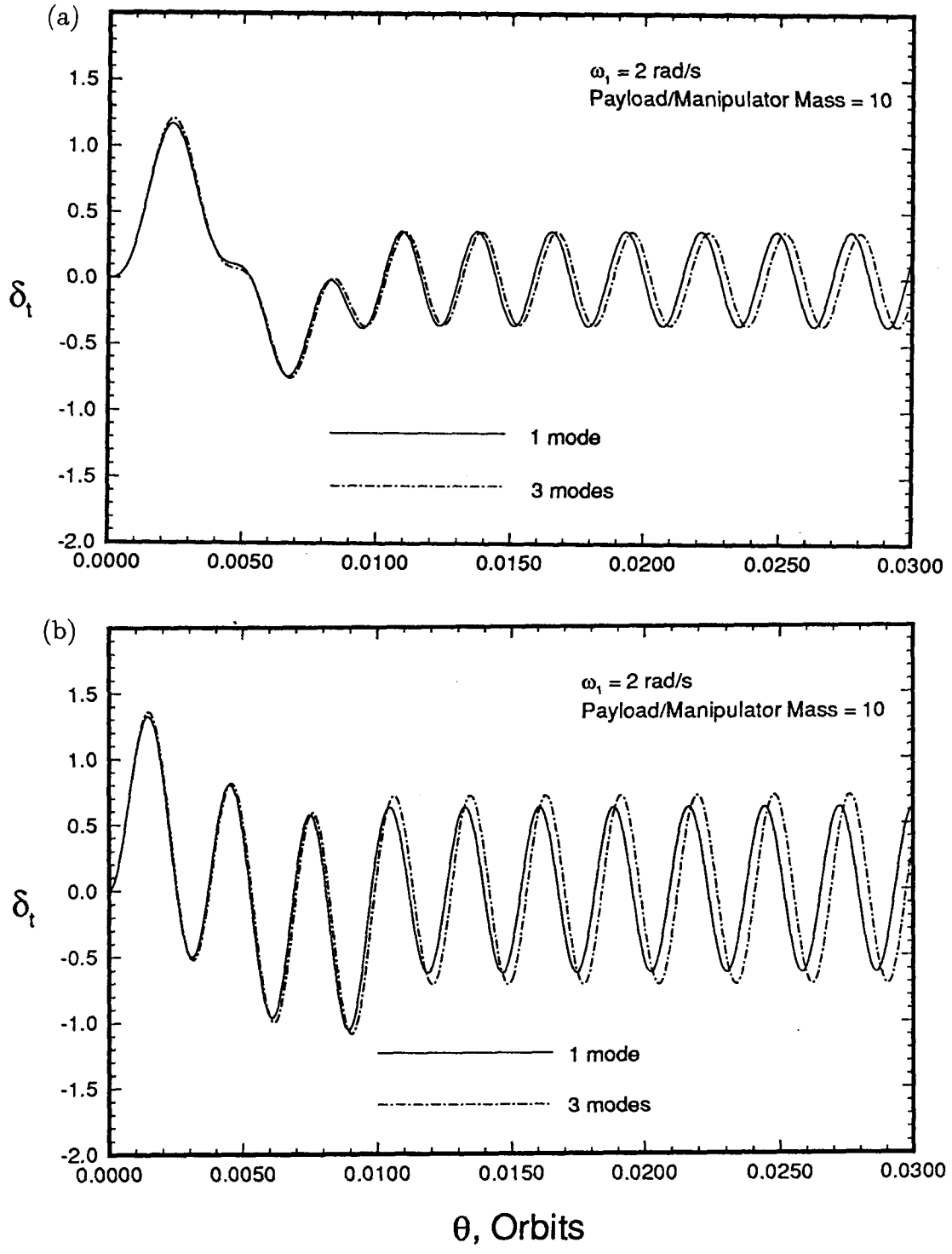

Figure 3-8 Effect of number of modes and maneuver profile on the tip deflection response to a combined slewing and translation maneuver: (a) sinusoid maneuver; (b) cubic maneuver.

the power boom at approximately its center are the various modules required for experimentation, habitation, logistics, etc. (Figure 3-9). Other prominent elements of the FEL are a pair of solar arrays situated approximately at one end of the power boom, and a solar radiator which is located inboard of the solar arrays. The function of the radiator is the rejection of excess heat. A stinger is also located at the other end of the power boom. It carries a resistojet at its free end for waste disposal. In his study, Ng modeled the Space Station as an interconnected system of beams and plates representing its different components. The power boom is modeled as a free–free beam, the stinger–resistojet assembly as a cantilever beam, while the solar arrays and radiator are treated as cantilever plates. The principal physical characteristics of the FEL are given in Table 3-1 .

Table 3-1 Physical characteristics of the FEL model

Body	Length (m)	Mass (kg)	ω_1* (rad/s)	I_{xx} (kg-m^2)	I_{yy} (kg-m^2)	I_{zz} (kg-m^2)
Power Boom	60	15,840	12.164	1.5×10^5	4.37×10^6	4.28×10^6
Stinger	26.7	270	3.1415	10	64,160	64,160
PV Radiator	11.5	450	0.628	50	19,837	19,887
PV Array	33	444	0.628	1,332	161,172	162,504

* ω_1 is the fundamental bending natural frequency

As pointed out by Ng, the proposed orientation of the FEL (Figure 3-9) is neither in equilibrium nor stable. Ng studied the responses of the FEL to various librational and vibrational disturbances. For the purpose of verification, two of the cases considered by Ng were simulated using the present code: the response to initial tip deflections of 1 cm in the z transverse direction given to the power boom or the stinger. One shape function for each body, corresponding to the fundamental bend-

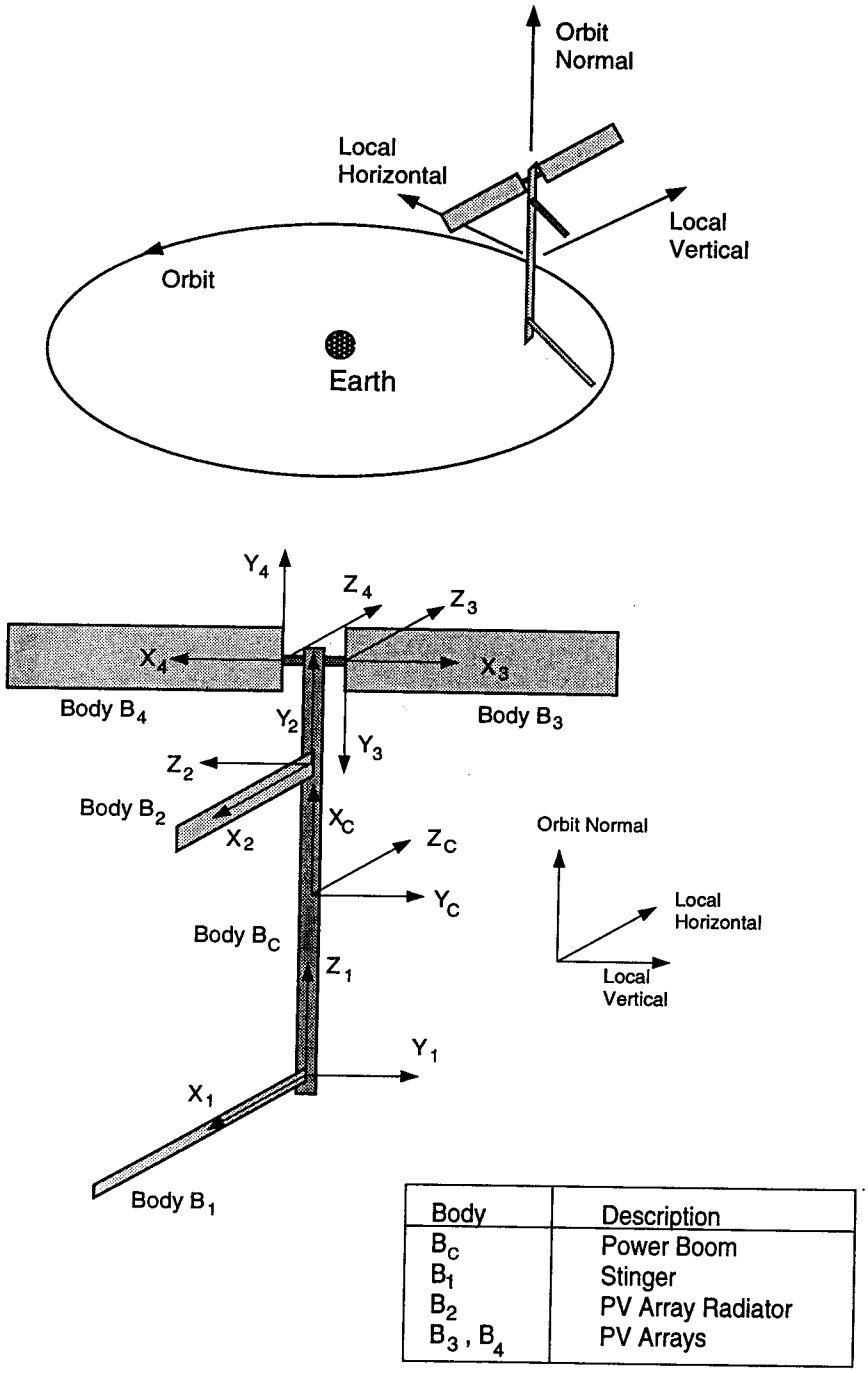

Body	Description
B_C	Power Boom
B_1	Stinger
B_2	PV Array Radiator
B_3 , B_4	PV Arrays

Figure 3-9 Schematic diagram of the FEL configuration of the proposed Space Station.

ing mode, was used for the discretization of the flexibility. Furthermore, the orbital elements, R_{cm} and θ are treated as generalized coordinates. As a result, the system has 12 degrees of freedom: 2 for the orbital motion; 3 for the librational motion; 2 each for the power boom and stinger vibrations, and 1 each for the 2 solar arrays and the radiator. The system response given by the present code for a tip deflection to the power boom of 1 cm ($\delta_c^z = 1$ cm) is presented in Figure 3-10 . It may be pointed out that the period of the orbit is approximately 93 minutes, while the results are presented for only 0.02 orbit to limit the computational time. These results compared extremely well with those reported by Ng [13]. Similarly, the response to the stinger tip excitation of $\delta_1^z = 1$ cm is shown in Figure 3-11 . Again, the agreement between the two sets of results was found to be excellent.

In fact, all the simulation results for the FEL presented by Ng were verified using the present code with excellent correlation throughout. Not only did it provide a measure of confidence in the present formulation and the code, but it also showed its efficiency in terms of the computation time. As an example, for the case of zero initial conditions, the execution time using the new code was approximately 16 minutes, compared to around 55 minutes with Ng's program. For this comparison, a SUN Sparc 2 computer was used, and the programs were compiled with the best code optimization option available for the SUN FORTRAN compiler. A reduction in the computational time can be directly traced to the simplification of the governing equations (however keeping them exact) exploited in this study as discussed before. With a reduction in the total number of terms by approximately a factor of two, the number of floating point operations are also reduced, thus contributing to a shorter execution time.

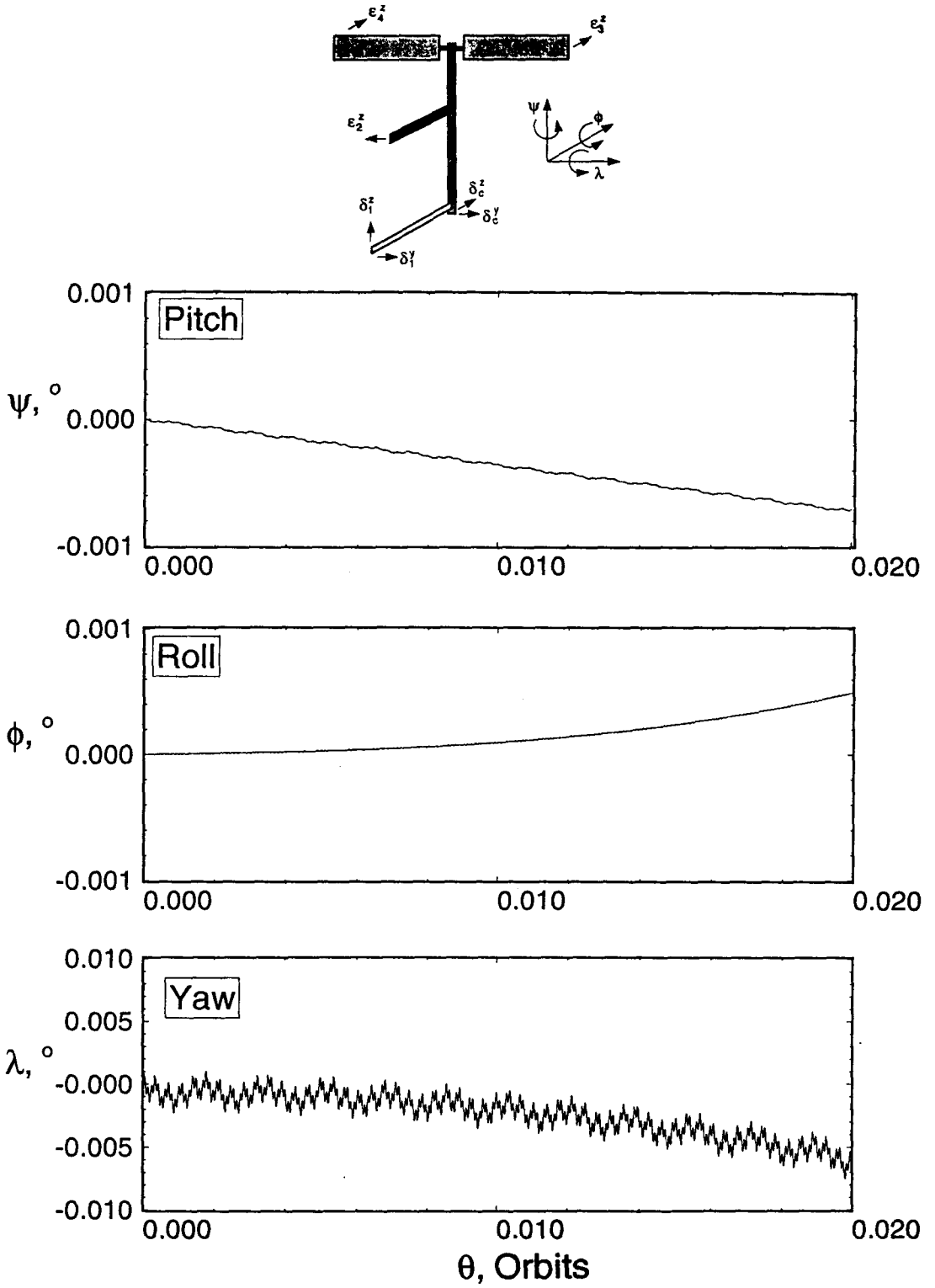

Figure 3-10 Response of the FEL to power boom initial tip deflection $\delta_c^z(0) = 1$ cm : (a) librational time histories.

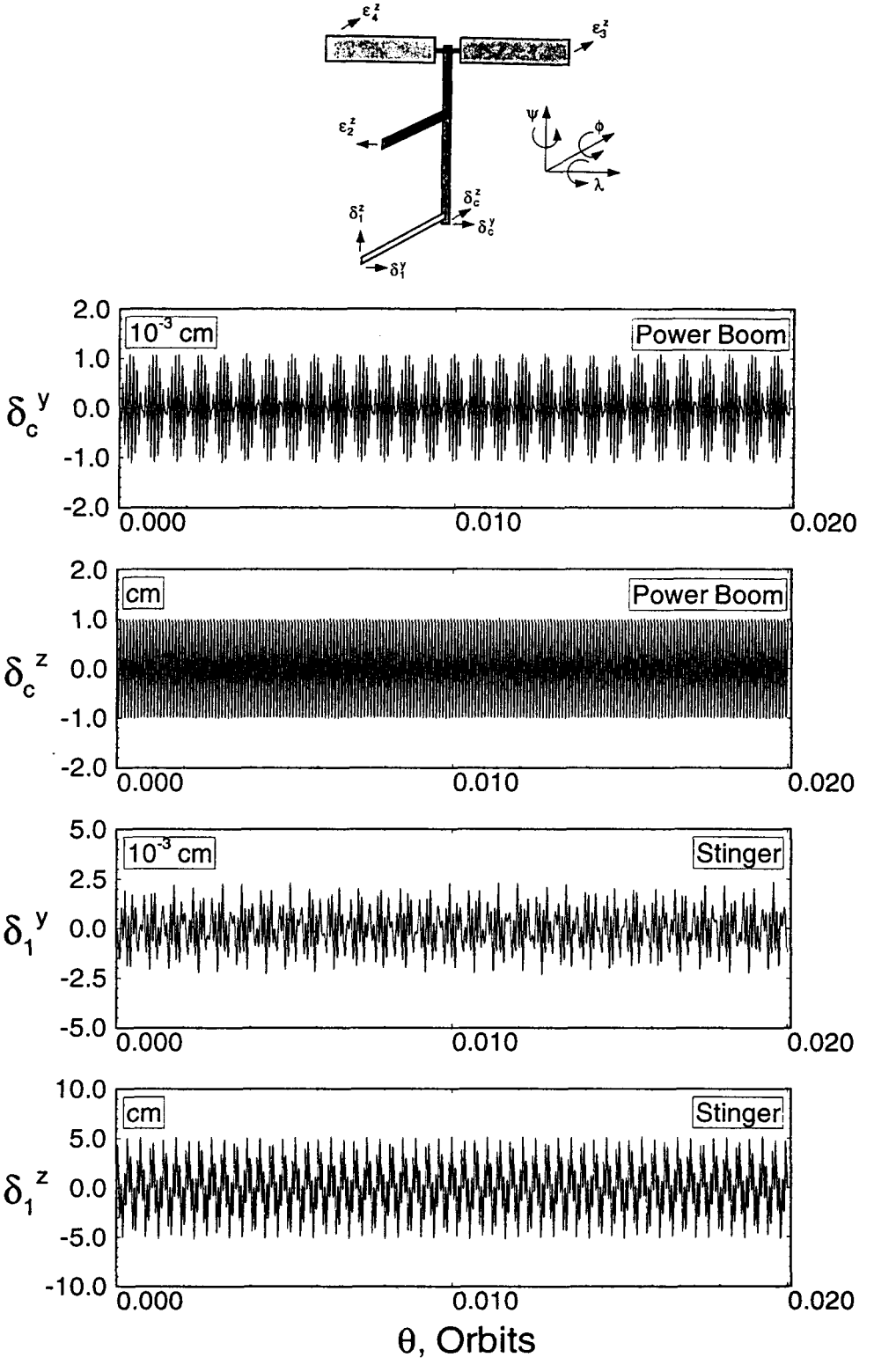

Figure 3-10 Response of the FEL to power boom initial tip deflection $\delta_c^z(0) = 1$ cm : (b) power boom and stinger vibrational time histories.

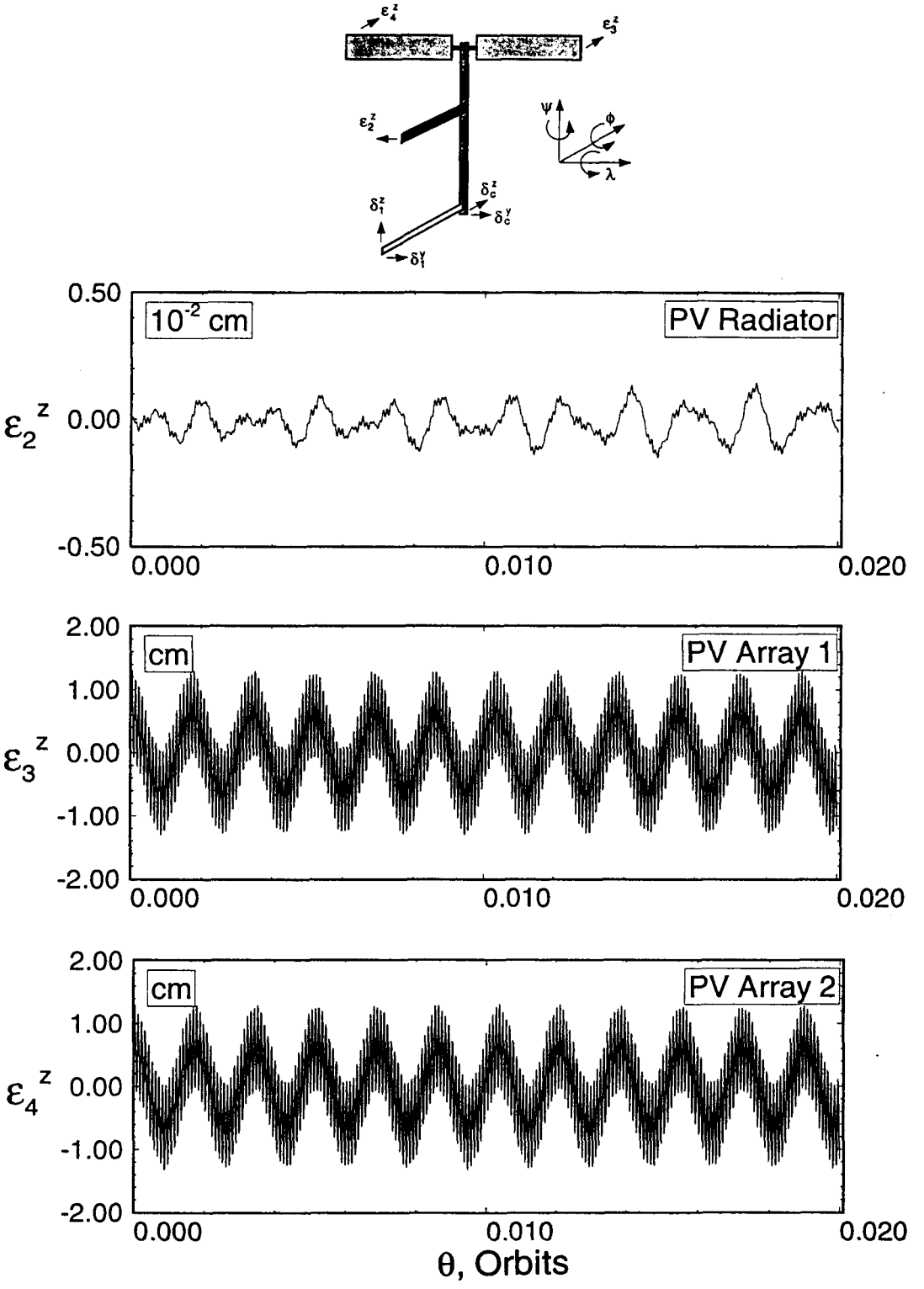

Figure 3-10 Response of the FEL to power boom initial tip deflection $\delta_c^z(0) = 1$ cm : (c) solar arrays and radiator vibrational time histories.

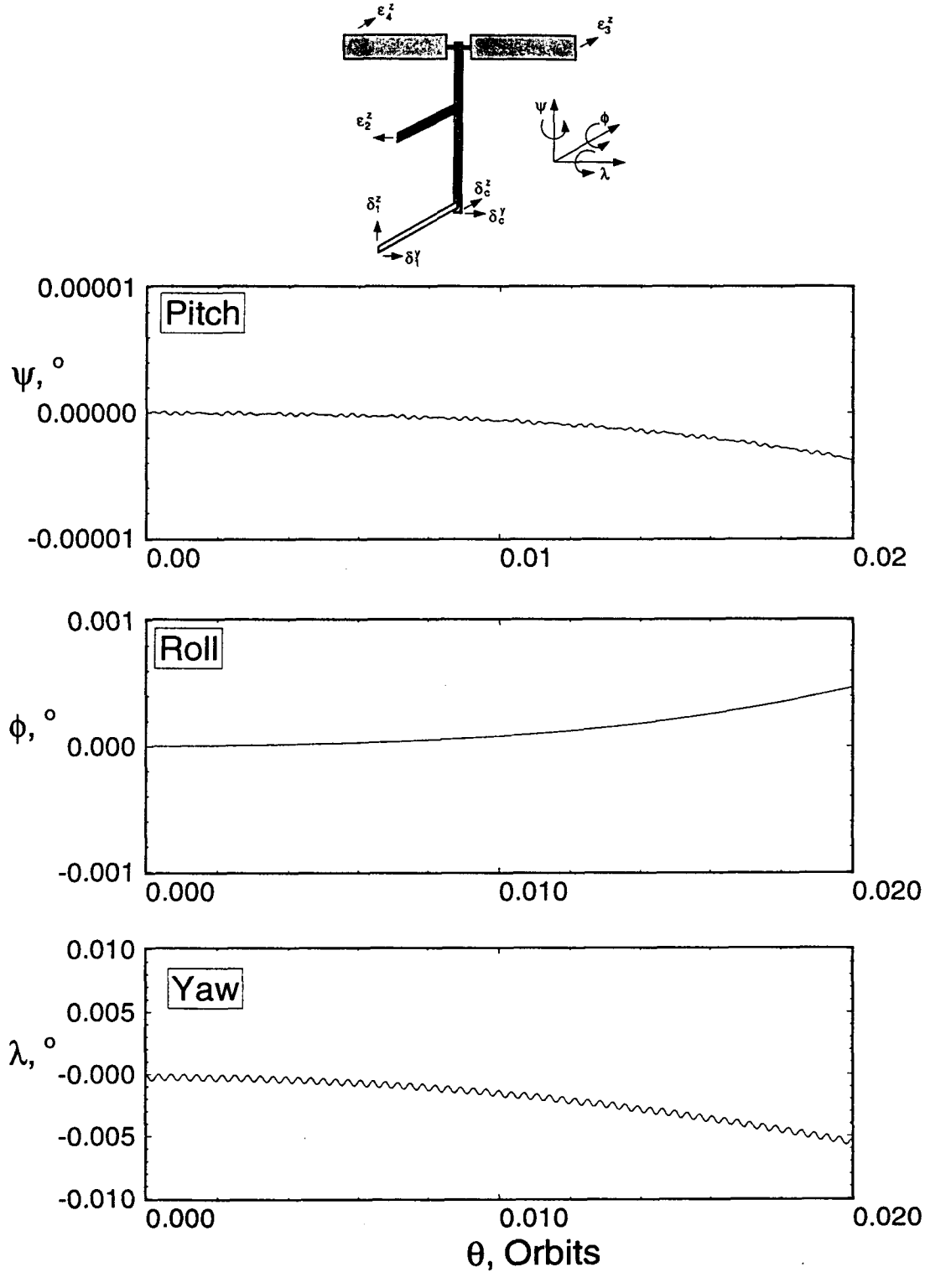

Figure 3-11 Response of the FEL to stinger initial tip deflection $\delta_1^z(0) = 1$ cm : (a) librational time histories.

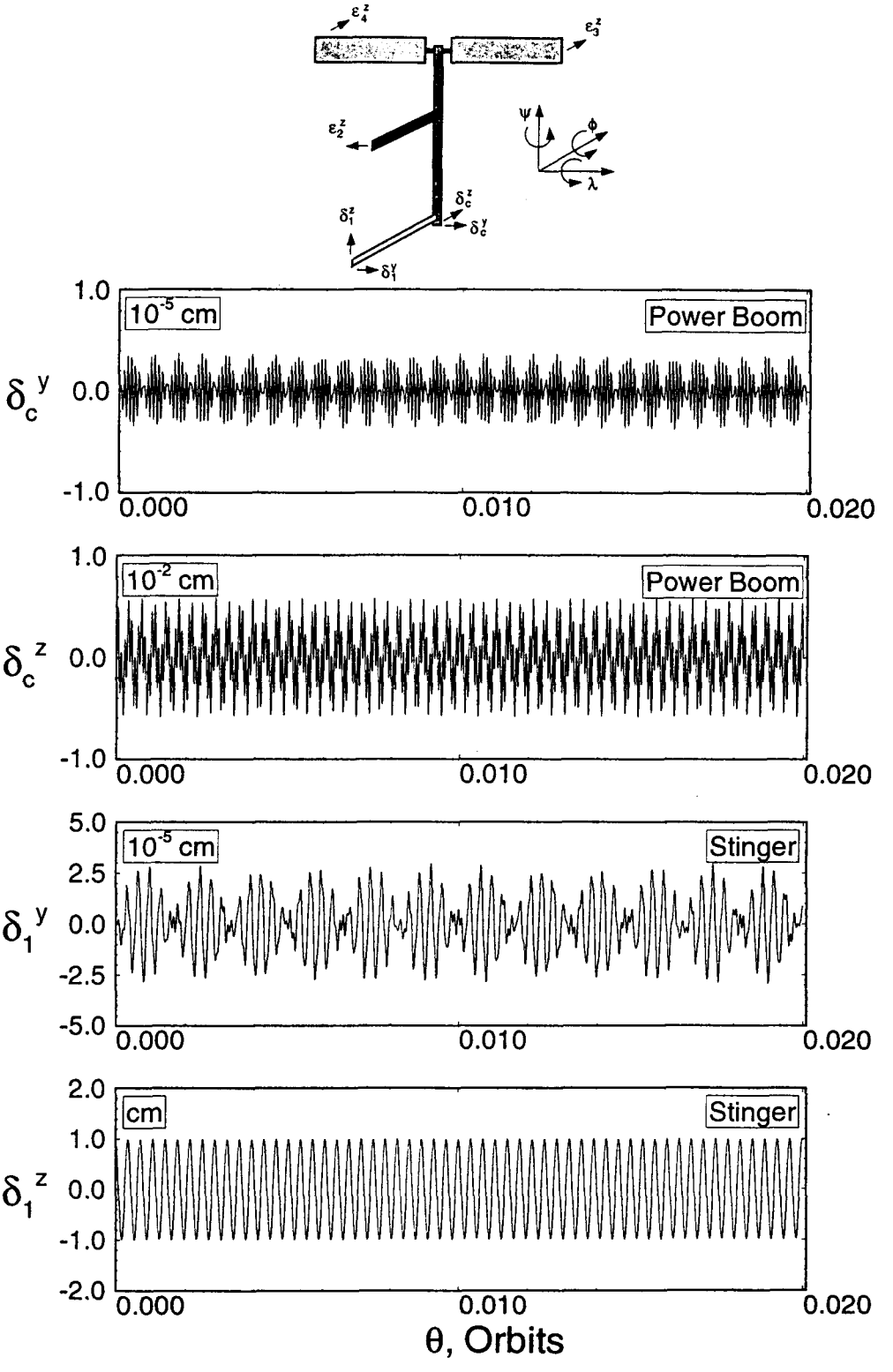

Figure 3-11 Response of the FEL to stinger initial tip deflection $\delta_1^z(0) = 1$ cm : (b) power boom and stinger vibrational time histories.

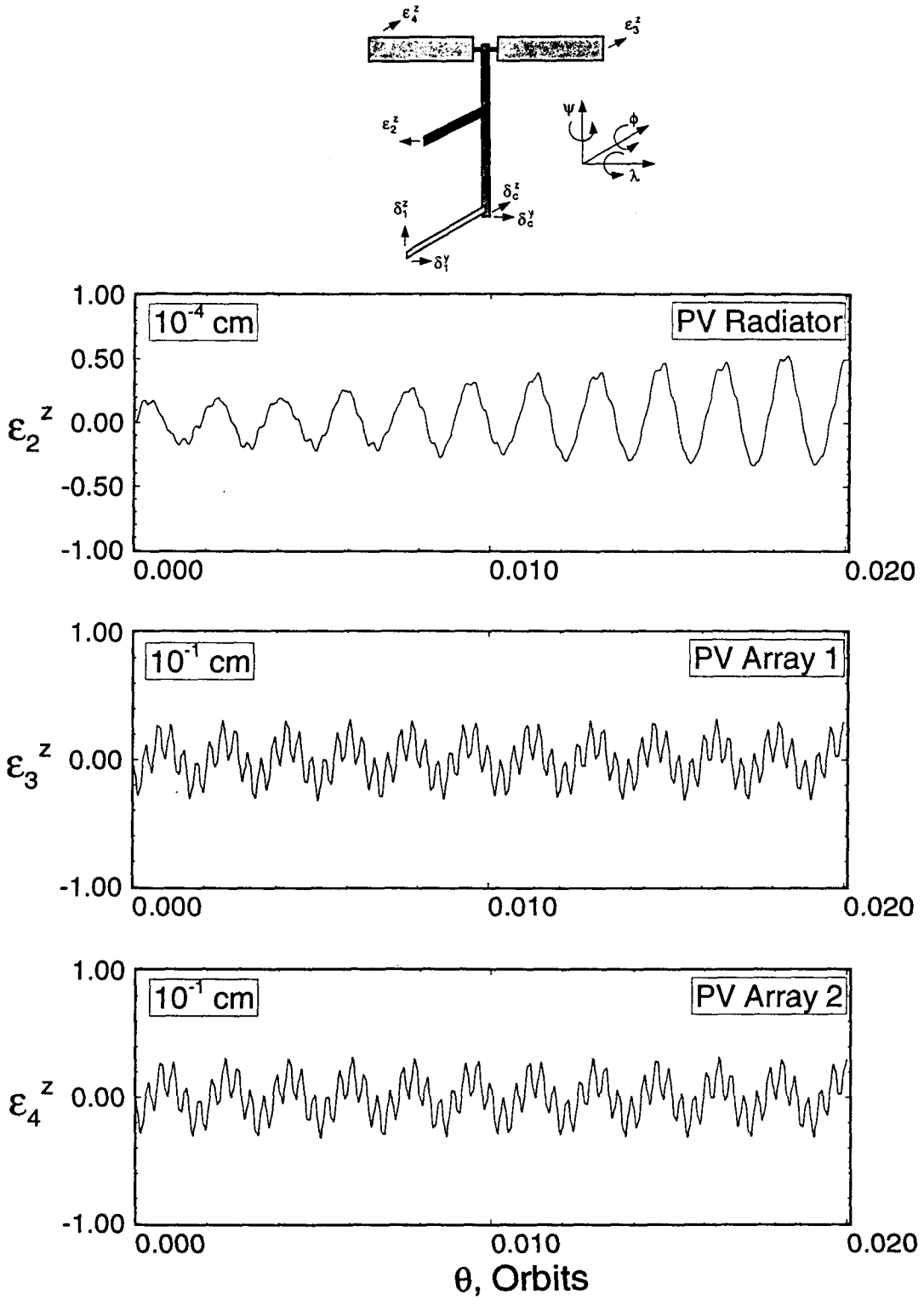

Figure 3-11 Response of the FEL to stinger initial tip deflection $\delta_1^z(0) = 1$ cm : (c) solar arrays and radiator vibrational time histories.

3.3.2 Conservation of Energy

In the absence of energy dissipation or input, such as structural damping, aerodynamic forces, thrusters, CMG's, etc., the total system energy should be conserved. In his investigation, Ng [13] attempted to verify this, but was not quite successful because the model did not allow for orbital perturbations (assumed a Keplerian orbit). However, when $\dot{\theta}$ was constrained to be zero, the system energy was conserved. Nevertheless, conservation of energy for the 'true' system could only be surmised by considering the fictitious system, but could not be shown conclusively. Ng also observed that fluctuations in the total energy were small compared to the orbital kinetic and potential energies. However, the fluctuations in total energy were significant when compared to the *fluctuations* in the kinetic and potential energies.

The orbital coordinates R_{cm} (radius) and θ (true anomaly) can be taken to be either generalized coordinates or specified coordinates. The latter amounts to the assumption of a Keplerian orbit. On the other hand, in the former case, orbital perturbations are modeled, allowing for a proper verification of the energy conservation. The kinetic energy of a flexible, multibody system was given in eq. (2.38) with details provided in Appendix I. The gravitational potential energy, meanwhile, was given by eq. (2.42), and the strain energy by eq. (2.46). In the computer program developed, the user is able to specify whether or not the conservation of energy is to be verified. If it is, any deviations between the initial and instantaneous values of the total, kinetic, gravitational potential and strain energies are computed at each integration time step and written into a file by the subroutine *EneChkOrb*.

Flexible Space Station Model with 3-D Dynamics

For the FEL model considered in the previous subsection, the conservation of energy was verified. In the first simulation, an initial tip deflection of 1 cm was given to

the power boom in the z transverse direction. The energy plots are presented in Figure 3-12 . The results, shown over a period of 0.002 orbit, clearly illustrate the exchange between the strain and kinetic energies. Although there is approximately a 30 N-m energy exchange, variation in the total energy remains negligible. Since, the vibrational degrees of freedom are the ones primarily excited in this case, the variation in gravitational potential energy is, expectedly, negligible. Similar results were also obtained for the case when an initial tip deflection of 1 cm was given to the stinger in the z direction (Figure 3-13). Again the dominant exchange between strain and kinetic energies is apparent, albeit at a lower frequency owing to the lower natural frequency of the stinger. Note, that the results are presented over 0.02 orbit for this case. The maximum fluctuation in the total energy is approximately 1×10^{-5} N-m, while the variation in strain and kinetic energy is approximately 0.03 N-m, which amounts to a minute error (i.e. $\frac{\Delta E}{\Delta T}$) of about 0.03%.

Satellite with rigid central body, flexible appendages

Ng and Modi [109] studied the dynamics of a satellite modeled by a rigid central body with two long, flexible appendages. The simulation results obtained for this model were used by Ng to validate his code. The physical parameters of the satellite are shown in Table 3-2 and a schematic of the satellite in Figure 3-14 .

Table 3-2 Physical characteristics of the satellite with rigid central body and flexible appendages studied by Ng and Modi [109].

Body	Length (m)	Mass (kg)	ω_1* (rad/s)	I_{xx} (kg-m^2)	I_{yy} (kg-m^2)	I_{zz} (kg-m^2)
Central Body	10	42,000	rigid	1.0×10^5	4.0×10^5	4.0×10^5
Appendages	100	10	0.01885	≈ 0	33,333	33,333

* ω_1 is the fundamental bending natural frequency

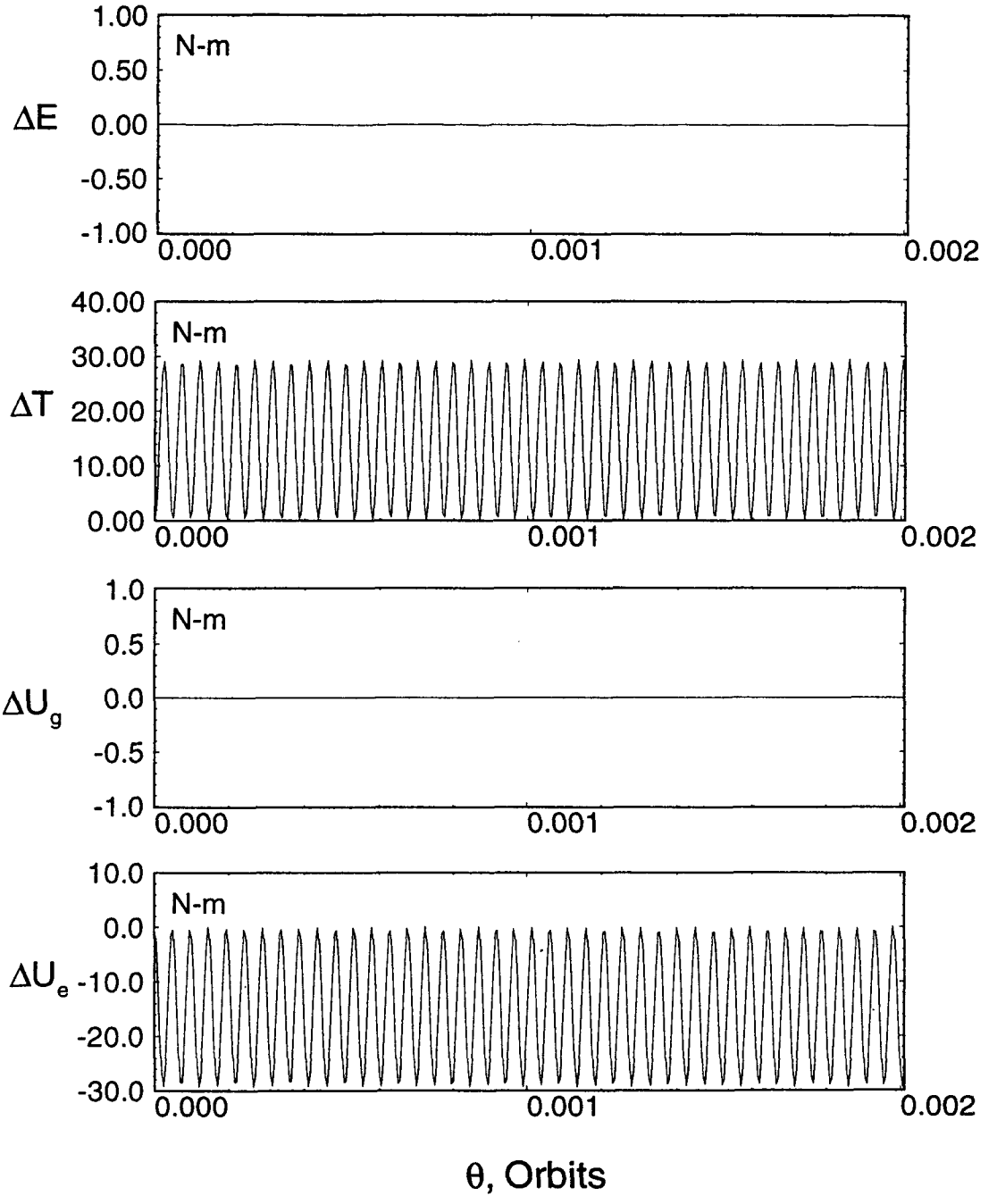

Figure 3-12 Energy variations of the FEL configuration: power boom initial tip deflection $\delta_c^z(0) = 1$ cm.

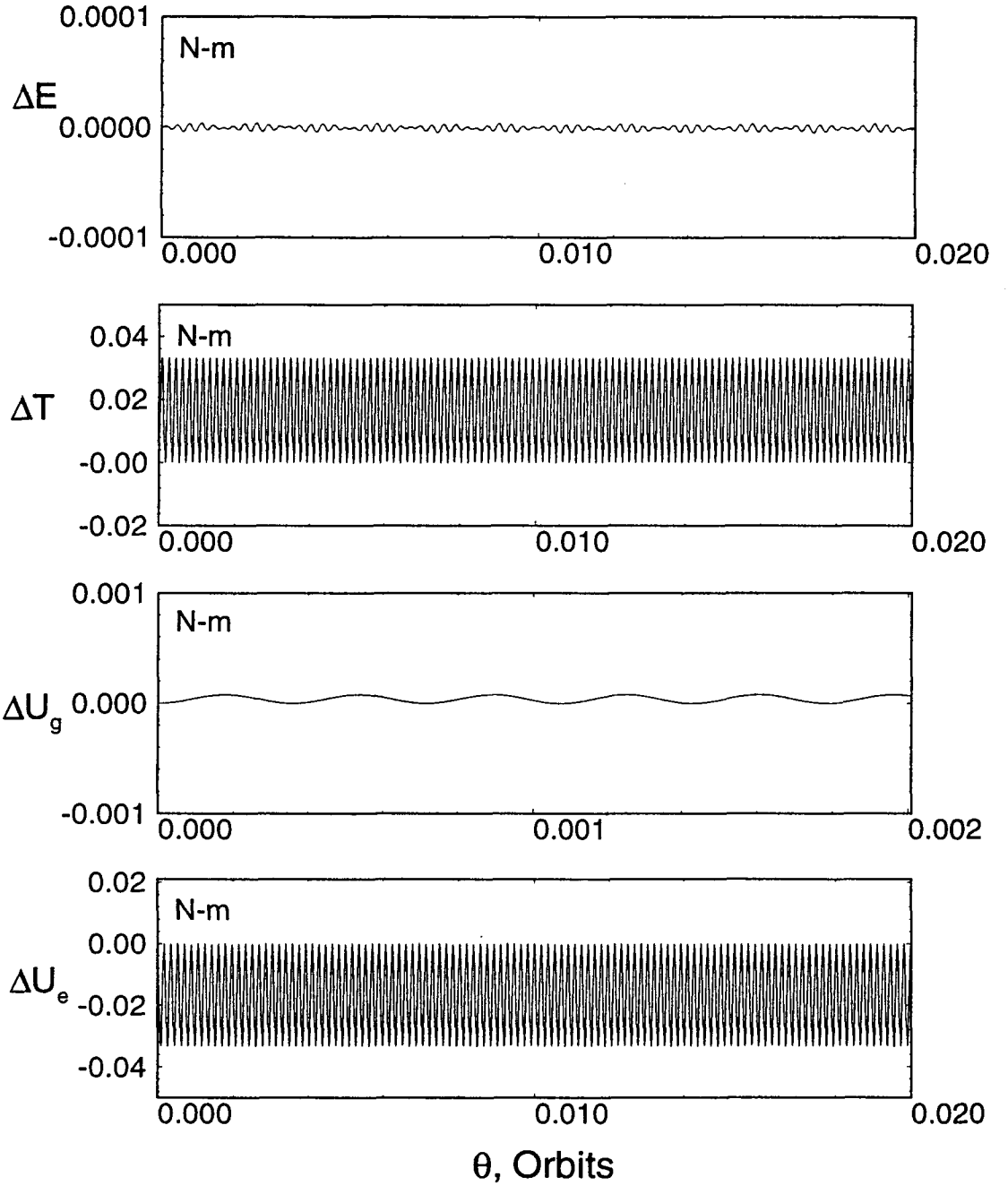

Figure 3-13 Energy variations of the FEL configuration: stinger initial tip deflection $\delta_1^z(0) = 1$ cm.

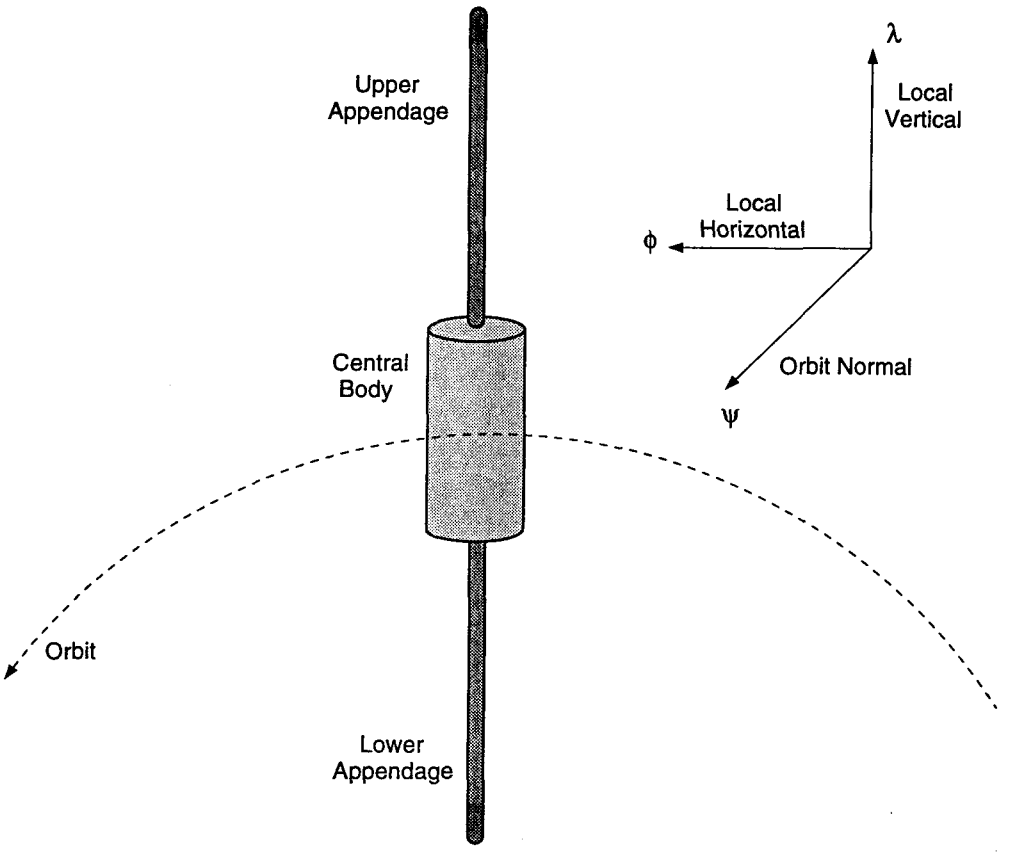

Figure 3-14 Schematic of the satellite with a rigid central body and flexible beam–type appendages studied by Ng and Modi [109].

Responses for various orbit eccentricities and initial conditions were investigated. However, only the results for $\epsilon = 0.2$ and an inplane tip deflection of 10 m to the lower appendage are given here. The investigation included both the Keplerian orbit as well as their perturbations. These results, consisting of time histories of the pitch angle, the flexibility generalized coordinates, and variations of the energies are given in Figure 3-15 . Part (a) of the figure shows the results for the Keplerian orbit model, and (b) for the case when the orbital elements are treated as generalized coordinates. There is virtually no difference between the time histories of the generalized coordinates in parts (a) and (b). However, there are significant differences in the energy results. In part (a), the conservation of energy cannot be inferred. Note, here varia-

tion in the total energy is of the same order as fluctuations in the constituent energies. In part (b), however, energy conservation is clearly demonstrated. Note, the variation in the total energy (including orbital components) is of the order of 0.1 N-m, while the changes in the kinetic and potential energies are of the order of 10^{12} N-m. The high value of energy exchange is attributed to the elliptical orbit. It is quite clear that when a Keplerian orbit is considered, in general, no useful information can be derived by examining the energy contribution to the system from different sources. Orbital perturbations have to be modeled in order to verify energy conservation. However, because the differences between the time histories of the generalized coordinates given by the two orbital models are insignificant, one can deduce that the Keplerian orbit assumption is a valid one as far as the system dynamics is concerned.

The actual perturbations in the orbital coordinates are shown in Figure 3-16 . Instead of perturbations in the true anomaly, $\Delta\theta$, variations in the orbital rate $\Delta\dot{\theta}$ are presented. The average orbital rate is 0.001163 rad/s, while the mean orbital radius is approximately 6,650 km. The orbital perturbations are about 0.01 mm in R_{cm} and 6×10^{-15} rad/s in $\dot{\theta}$. These small perturbations, however, are sufficient to ensure that the total system energy remains in equilibrium.

3.3.3 Comparison of Linear and Nonlinear Solutions

Earlier in this chapter, the numerical linearization of the governing equations through the use of a finite difference algorithm was described. The linearized equations are useful for the design of linear control systems which are invariably required to stabilize as well as enhance the dynamic characteristics of spacecraft. The user of the simulation program now has the option of utilizing the linear model for the dynamic simulation if considered adequate.

The use of double precision variables, floating point functions and operations,

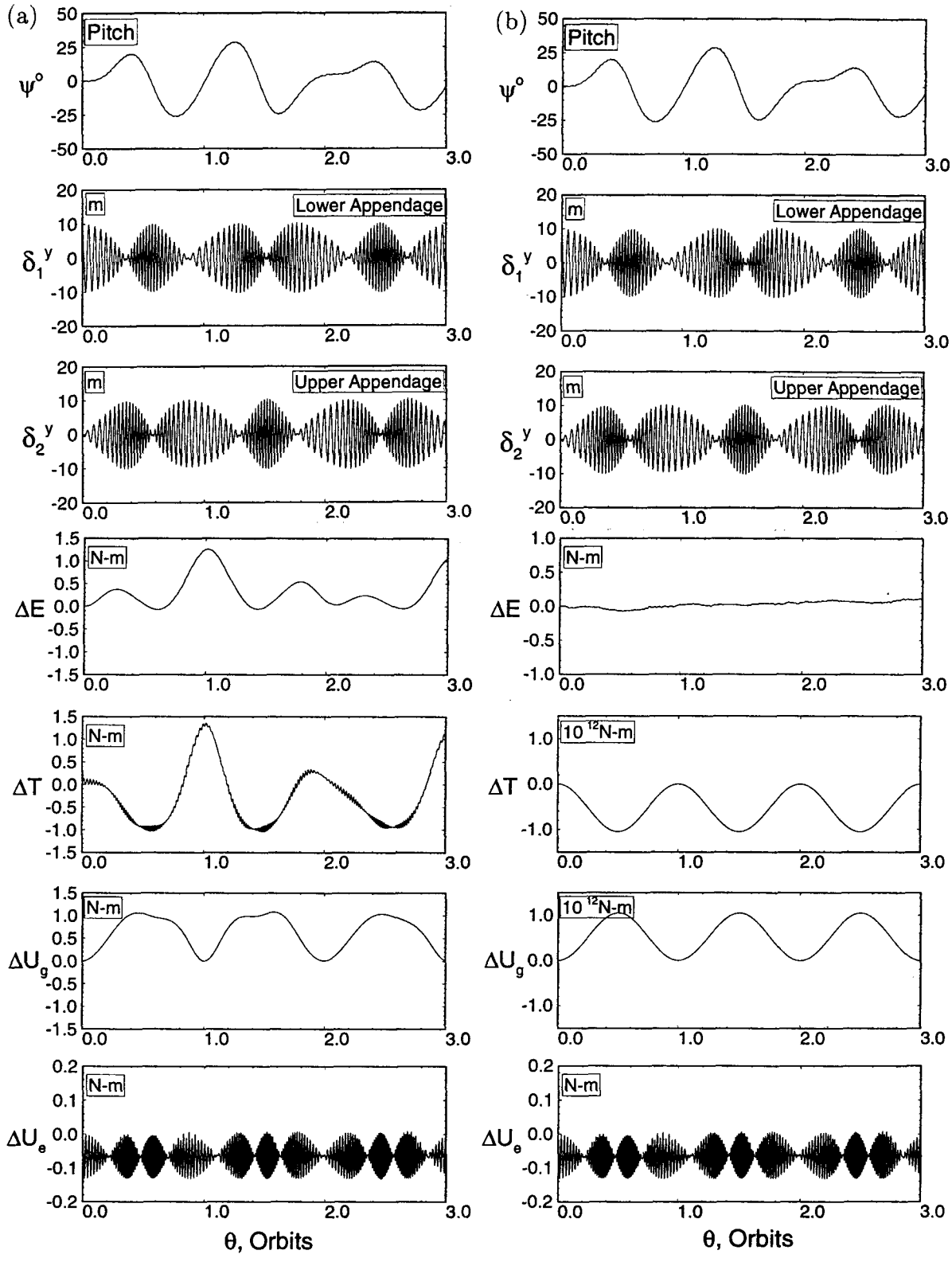

Figure 3-15 Dynamical response and energy variation of the satellite with a rigid central body and flexible appendages: $\delta_1^y(0) = 10$ m ; (a) Keplerian orbit; (b) orbital perturbations modeled.

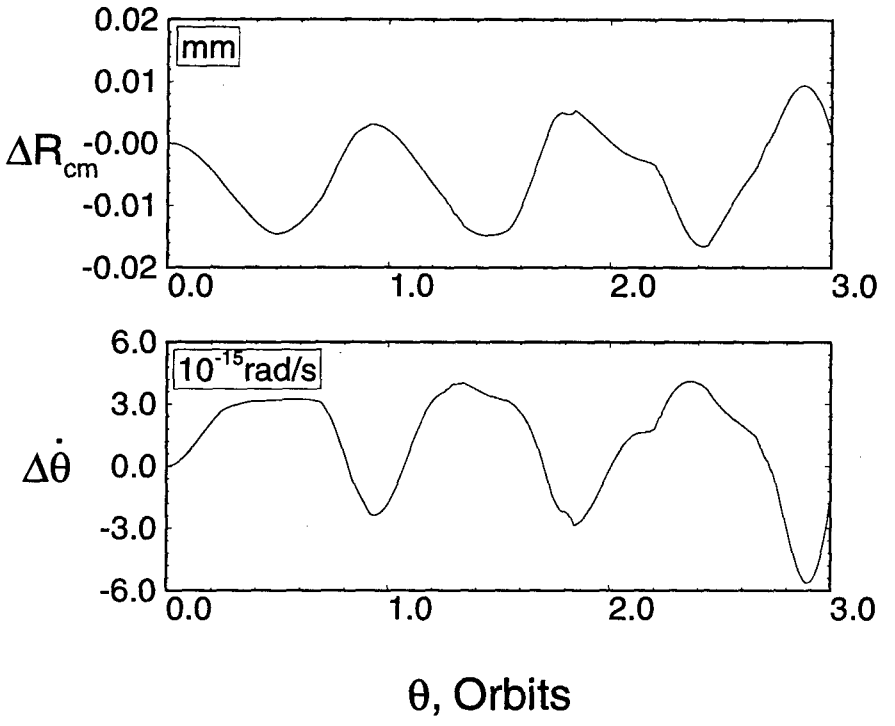

Figure 3-16 Perturbations in the orbital coordinates for the case $\delta_1^y(0) = 10$ m.

together with carefully chosen step–sizes in the finite difference algorithm should ensure the accuracy of the resulting linear model for its use in both the dynamic simulation and the control system design. This is verified by comparing the results given by the nonlinear and linear dynamic models. Another objective of this study is to gain some appreciation of the contribution of nonlinear terms in this class of problems.

The model chosen for study is the FEL configuration used previously. A series of simulations were conducted using both the linear and nonlinear models, although only two sets of results are presented here. In the first case, an initial tip deflection of 1 cm

was given to the power boom in the y direction (i.e. $\delta_c^y(0)$ =1 cm). The simulation results are shown in Figure 3-17 . Although the pitch and roll responses are in close agreement, there is a small discrepancy in the yaw. In the vibrational responses, the difference in the results, for the most part, are indiscernible. Deviations when present are indeed small and hence of little consequence. In the second case, an initial tip deflection of 1 cm was given to the power boom in the z direction (i.e. $\delta_c^z(0)$ =1 cm). These results are presented in Figure 3-18 . In this case, correlation in all the degrees of freedom is even better.

These results indicate that a linearized model can often provide sufficiently accurate results even in the presence of flexibility. Of course, the precise merit of a linear model will depend on the system characteristics and the magnitude of the disturbances. In the present case the results do provide a measure of confidence in the use of the linear model for control system synthesis. It should be noted that in most cases, it is only the actual control system design procedure that relies on the numerically linearized plant model. The multibody simulation code developed here allows for the resulting linear controller to be implemented together with the nonlinear plant model. This provides for an efficient as well as effective assessment of the control system design.

3.4 Summary

In this chapter details of the numerical implementation of the flexible multibody dynamics model were discussed. An overview of the structure of the computer code, along with description of the important subprograms were also presented. Some of the important issues related to the numerical solution of ODE's were touched upon. Also, the numerical linearization of the equations of motion, which is useful for control system synthesis, was explained. Next, the mathematical model and the related

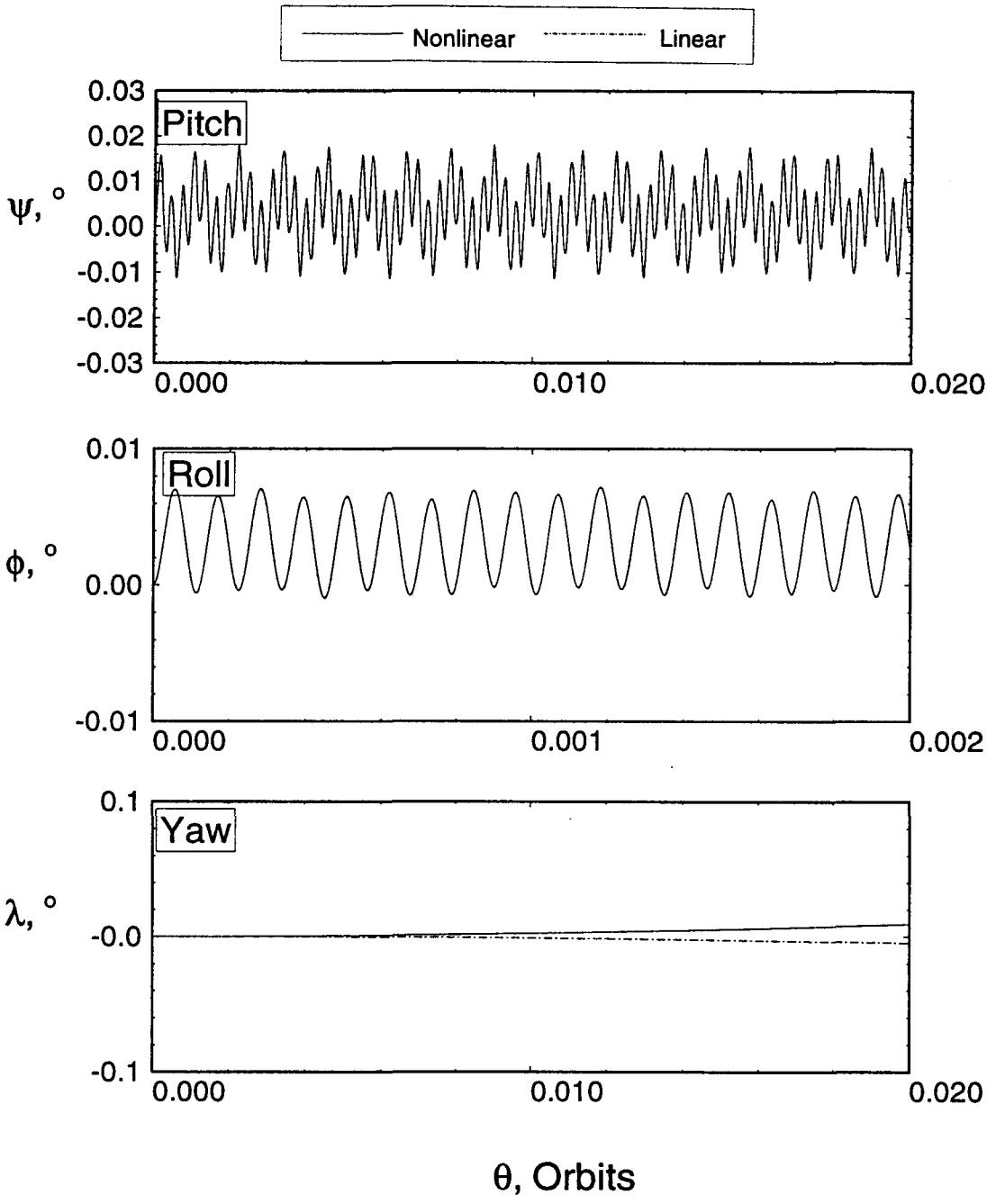

Figure 3-17 Comparison between linear and nonlinear responses of the FEL configuration to a power boom tip disturbance of $\delta_c^y(0) = 1$ cm : (a) librational time histories.

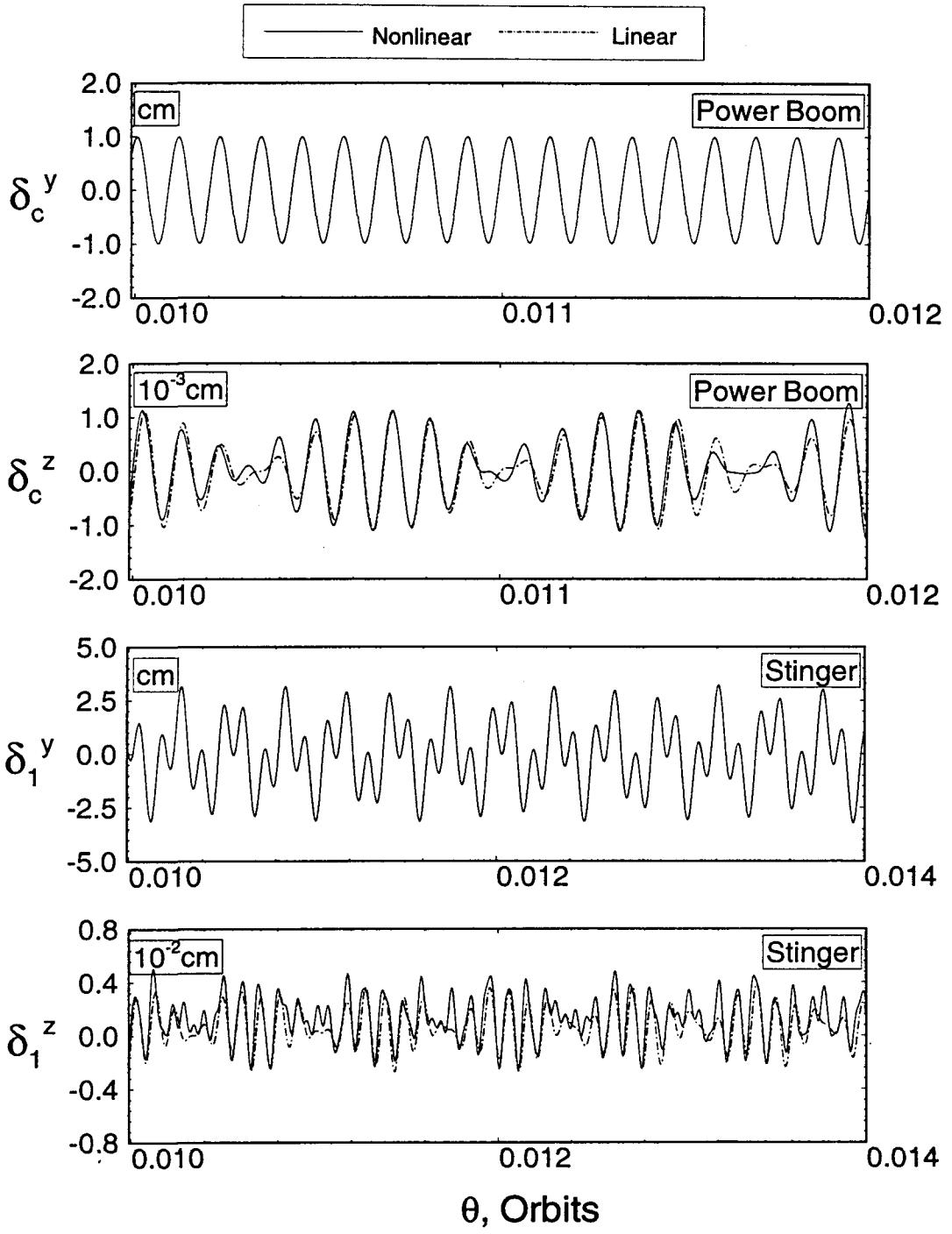

Figure 3-17 Comparison between linear and nonlinear responses of the FEL configuration to a power boom tip disturbance of $\delta_c^y(0) = 1$ cm : (b) power boom and stinger vibrational time histories.

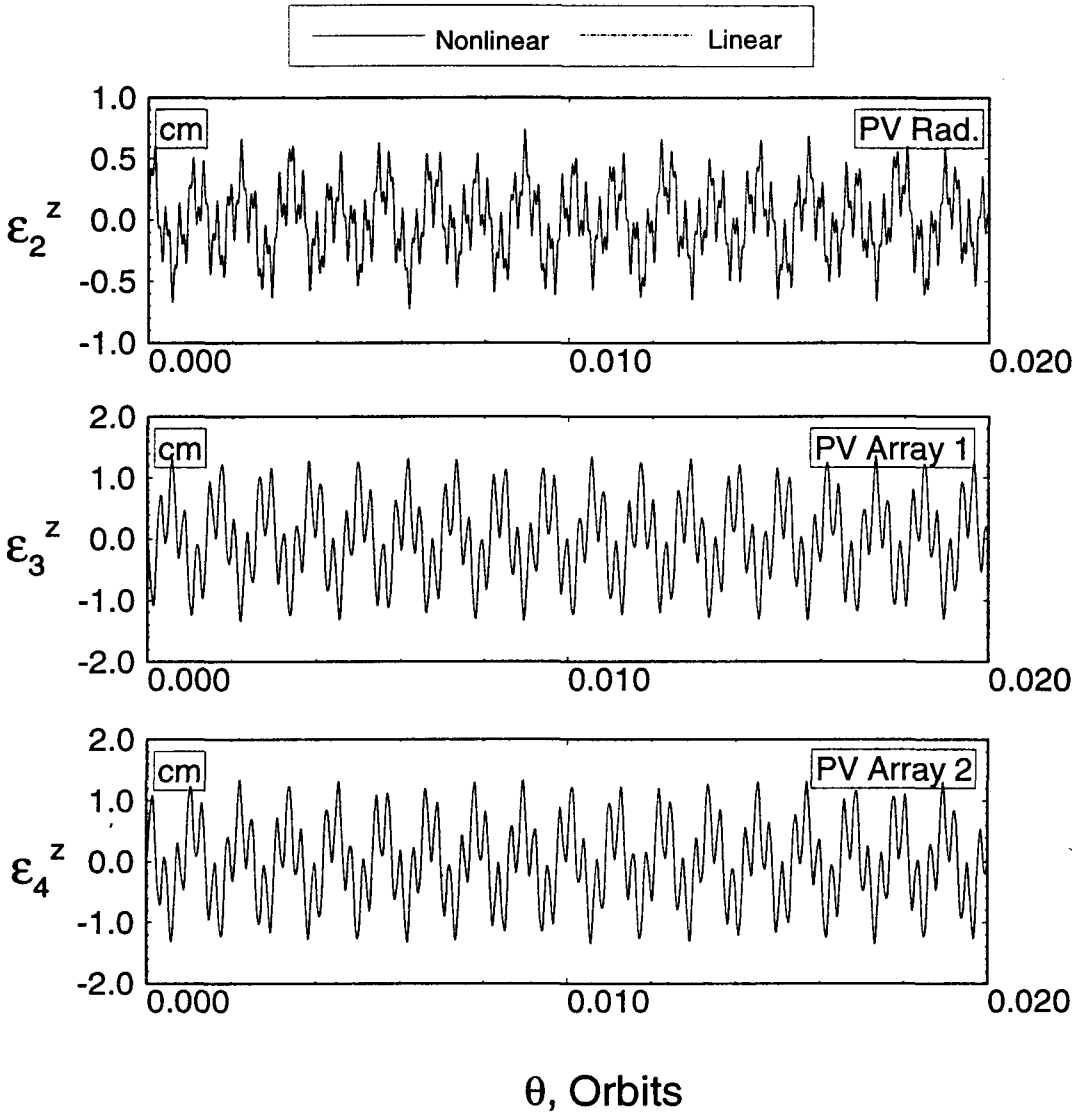

Figure 3-17 Comparison between linear and nonlinear responses of the FEL configuration to a power boom tip disturbance of $\delta_c^y(0) = 1$ cm : (c) solar arrays and radiator vibrational time histories.

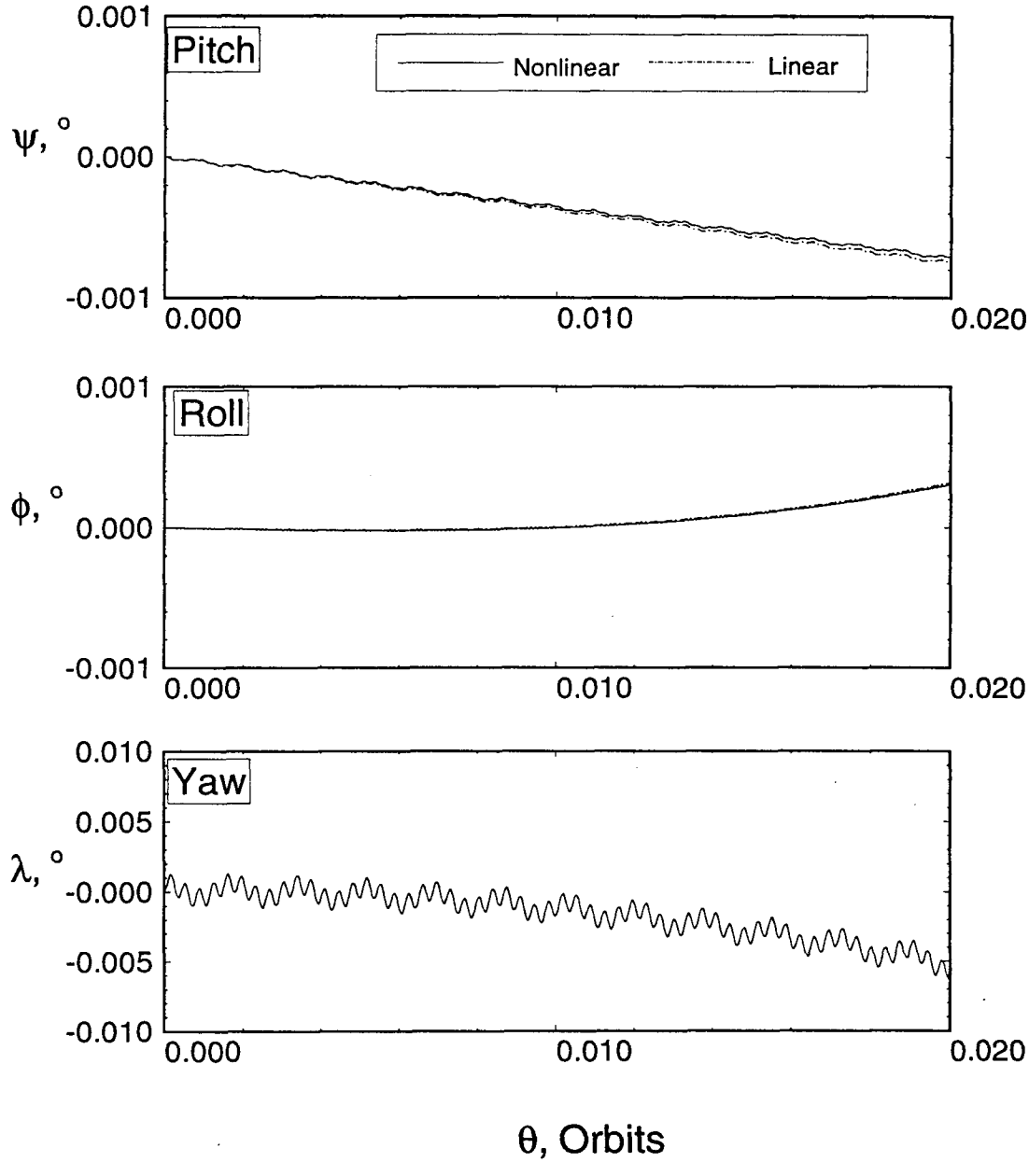

Figure 3-18 Comparison of linear and nonlinear responses of the FEL configuration to a power boom tip deflection $\delta_c^z(0) = 1$ cm : (a) librational time histories.

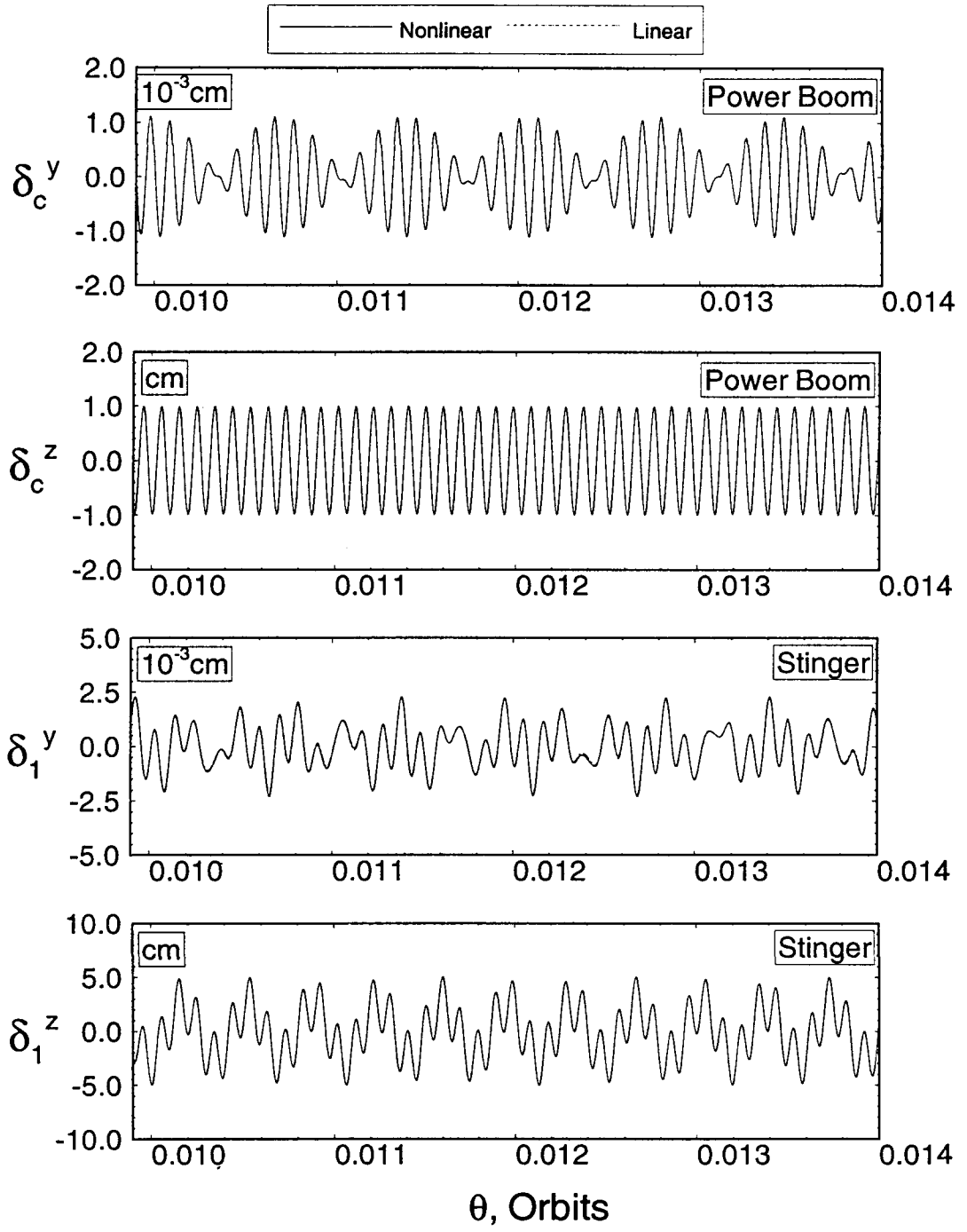

Figure 3-18 Comparison of linear and nonlinear responses of the FEL configuration to a power boom tip deflection $\delta_c^z(0) = 1$ cm : (b) power boom and stinger vibrational time histories.

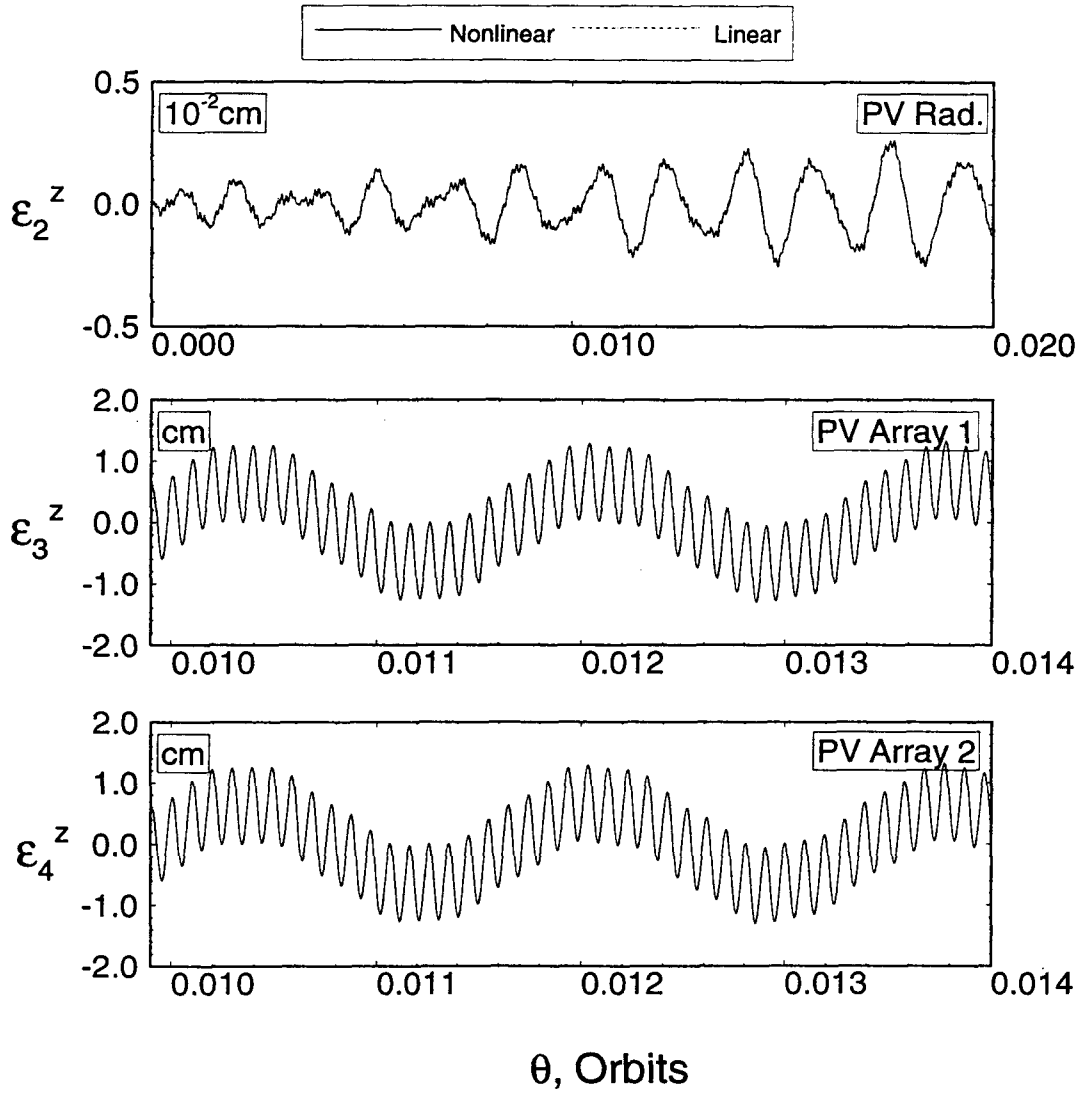

Figure 3-18 Comparison of linear and nonlinear responses of the FEL configuration to a power boom tip deflection $\delta_c^z(0) = 1$ cm : (c) solar arrays and radiator vibrational time histories.

computer program were validated by comparison with results reported by other researchers, as well as by verifying the conservation of energy for nondissipative cases. The results obtained established the fidelity of both the mathematical formulation and the computer implementation of the model. Finally, accuracy of the linearized governing equations was assessed for a specific flexible system through comparison with the complete nonlinear solution.

4. ANALYTICAL SOLUTION

4.1 Preliminary Remarks

In most cases, a numerical solution to the nonlinear governing equations of motion is sought. In general, due to the nonlinearity and time varying nature of these equations, exact analytical solutions do not exist. However, there are situations when an approximate analytical solution to the nonlinear equations of motion is desirable. The main limitation of a purely numerical approach is occasionally an insufficient understanding of the basis for certain observed phenomena, not to mention the computational cost. Often, a parametric study is needed to optimize the system design requiring substantial effort, time and expense. Thus, it is desirable to arrive at an approximate analytical solution which is able to predict the system behaviour with reasonable accuracy to establish trends and give a better appreciation of the associated physics. This chapter deals with the development and application of one such approximate analytical method to solve a system of nonlinear equations governing the dynamics of a flexible space structure. The procedure developed is an extension of the Butenin Method, which itself is a modified version of the approach proposed by Kryloff and Bogoliuboff [110].

4.2 Model Description

The model considered is similar to the FEL configuration considered in the previous chapter. However, the system is taken to be in the Lagrange configuration, where the axis of the largest inertia is parallel to the orbit normal, and the axis of minimum inertia is aligned with the local vertical. Furthermore, librational motion and structural deformations are confined to the orbital plane. Thus, pitch (motion

about the orbit normal) is the only librational degree of freedom considered while the power boom and the solar panels deformations occur in the plane of the orbit, which is taken to be circular. A schematic diagram of the model is given in Figure 4-1 .

The system dynamics is discretized through the method of assumed modes. The admissible functions for the solar panel and power boom vibration are taken as the clamped-free and free-free Euler-Bernoulli beam modes, respectively. For a multibody system where the stiffness, mass and inertia of adjacent bodies are significantly different, the method of assumed modes gives results which compare well with the system modes approach, which satisfies the boundary conditions completely [12]. This is well suited in the present study where the fundamental bending frequency of the power boom is approximately 20 times that of the solar panels. Only the first mode of vibration for each system component is considered as previous work by Modi and Suleman [111] has shown that, in most cases, sufficient accuracy in flexibility modeling can be achieved by considering only the fundamental mode and a few harmonics.

With only the first mode for the power boom and solar panels considered, the system has four degrees of freedom: the pitch angle ψ ; the generalized coordinate associated with the deformation of the power boom $q_c(t)$; and the generalized coordinates associated with the deformation of the solar panels, $q_1(t)$ and $q_2(t)$. Both the pitch motion and the vibration of the power boom tend to excite the solar panels anti-symmetrically. This axiom was validated through a series of of numerical simulations where the solar panels were free to vibrate independently. With the solar panels taken to vibrate anti-symmetrically, $\vec{\delta}_1 = -\vec{\delta}_2$. Thus, the degrees of freedom reduce from four to three. Also, as a further simplification, the shift in the system center of mass due to flexure is neglected. For a free–free beam, the shift in the system center of mass is always zero. In the present case, addition of the solar panels

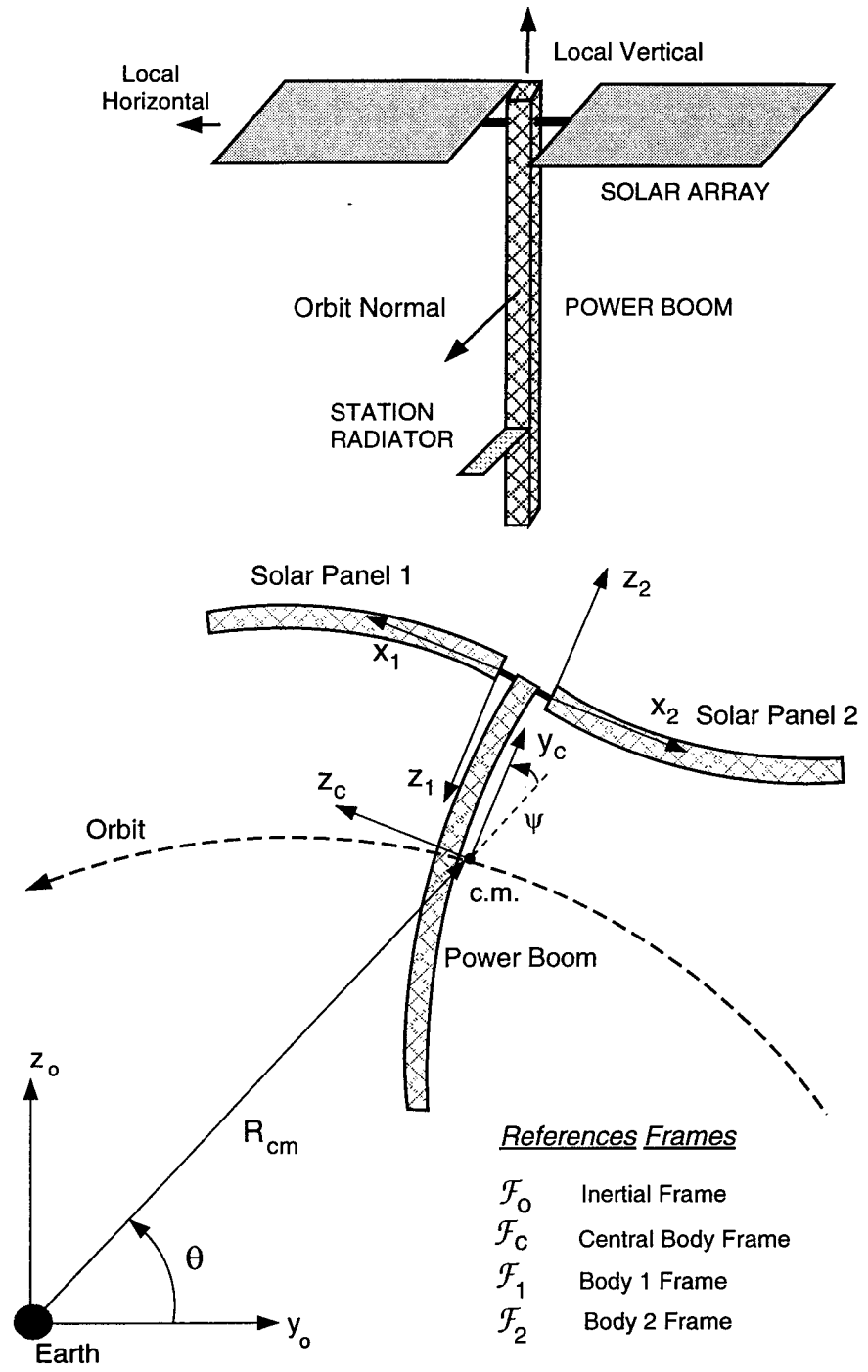

Figure 4-1 Schematic diagram of the planar FEL model.

at one end of the beam results in a nonzero shift in the c.m. However, with the large difference between the mass of the power boom and that of the solar panels (a ratio of approximately 40:1), the shift in the system c.m. is virtually negligible.

Based on the above assumptions, and the governing equations of motion in Appendix II, reduce to:

$\underline{\psi \text{ equation}}$

$$\ddot{\psi}(A_1 + A_2 q_c^2 + 2m_1 q_1^2) + \ddot{q}_c(A_4 + 2A_8 q_1^2) + \ddot{q}_1\left(\frac{2m_1 A_3}{L_1}\right) =$$
$$-(\dot{\psi}+\dot{\theta})(2A_2 q_c \dot{q}_c + 4m_1 q_1 \dot{q}_1) - 4A_8 q_1 \dot{q}_1 \dot{q}_c$$
$$+\dot{\theta}^2\Bigg\{\tfrac{3}{2}A_2 q_c^2 \sin 2\psi - 3m_1 L_c \phi_c^{'*} q_c \cos 2\psi$$
$$+\frac{6m_1 A_3 q_1}{L_1}\cos(2(\phi_c^{'*} q_c + \psi)) - 3m_1 q_1^2 \sin(2(\phi_c^{'*} q_c + \psi))$$
$$+ m_1 L_1^2 \sin(2(\phi_c^{'*} q_c + \psi)) - \tfrac{1}{4}A_7 L_c^2 \sin 2\psi\Bigg\}; \qquad (4.1)$$

$\underline{q_c \text{ equation}}$

$$\ddot{\psi}(A_4 + 2A_8 q_1^2) + \ddot{q}_c\left(A_2 + \tfrac{2}{3}A_8 L_1^2 \phi_c^{'*} + 2A_8 \phi_c^{'*} q_1^2\right) + \ddot{q}_1\left(\frac{2A_3 A_8}{L_1}\right) =$$
$$-4A_8 \phi_c^{'*} q_1 \dot{q}_c \dot{q}_1 + 2A_2 \dot{\psi}^2 q_c + 2\dot{\theta}A_2 \dot{\psi} q_c - 4\dot{\theta}A_8 q_1 \dot{q}_1$$
$$-4A_8 q_1 \dot{\psi}\dot{q}_1 - \left(A_5 - \tfrac{3}{2}\dot{\theta}^2 A_2\right) q_c + \frac{3\dot{\theta}^2}{2}\Bigg\{-A_2 q_c \cos 2\psi$$
$$-m_1 L_c \phi_c^{'*} \sin 2\psi + \frac{4A_3 A_8 q_1}{L_1}\cos(2(\phi_c^{'*} q_c + \psi))$$
$$-2A_8 q_1^2 \sin(2(\phi_c^{'*} q_c + \psi)) + \tfrac{2}{3}A_8 L_1^2 \sin(2(\phi_c^{'*} q_c + \psi))\Bigg\}; \qquad (4.2)$$

$\underline{q_1 \text{ equation}}$

$$\ddot{\psi}\left(\frac{2m_1 A_3}{L_1}\right) + \ddot{q}_c\left(\frac{2A_3 A_8}{L_1}\right) + \ddot{q}_1(2m_1) =$$

$$2A_8\phi_c^{'*}q_1\dot{q}_c^2 + 2m_1\dot{\psi}^2q_1 + 4m_1\dot{\theta}\dot{\psi}q_1 + 4A_8\dot{\theta}q_1\dot{q}_c + 4A_8q_1\dot{\psi}\dot{q}_c$$
$$+ 3\dot{\theta}^2\left\{\frac{m_1A_3}{L_1}\sin(2(\phi_c^{'*}q_c + \psi)) + m_1q_1\cos(2(\phi_c^{'*}q_c + \psi))\right\}$$
$$- (2A_6 - 3\dot{\theta}^2m_1)q_1. \qquad (4.3)$$

The quantities $A_1, \ldots, A_8$, are constants governed by physical properties and system parameters, such as the mass, length and stiffness of the bodies. For the sake of brevity these constants are not given here. $\phi_c^{'*}$ is the slope of the mode shape of the central body at the attachment point of bodies 1 and 2. It should be pointed out that in this analytical study, neither the damping nor the nonconservative generalized forces are present. Higher order terms due to the coupling between librational (pitching) and elastic motions, as well as between the elastic motion of the power boom and that of the solar arrays, are retained as they can dominate the dynamical behaviour of such a system [112].

Even with these approximations, the governing equations are not amenable to any known closed form solution procedure. A simplified set of nonlinear equations, which would still capture the dominant dynamics of the full governing equations is therefore desired. The simplified equations were obtained by retaining only the linear terms in the mass matrix of the equations (i.e. there are no nonlinearities associated with the second derivative terms), and nonlinear terms up to order three of the trigonometric terms expanded in Taylor Series. The simplified set of nonlinear equations thus obtained is:

$$A_1\ddot{\psi} + A_4\ddot{q}_c + C_1\ddot{q}_1 = -C_2\psi - C_3q_c + C_4q_1$$
$$- B_1q_1\dot{q}_1 - B_2q_c\dot{q}_c - B_3q_c^3 + \tfrac{2}{3}C_2\psi^3 + B_5\psi q_c^2$$
$$+ 3B_6\psi^2q_c - 3B_7\psi^2q_1 - B_8\psi q_1^2 - B_9q_cq_1^2 - B_{10}q_c^2q_1$$
$$- 2B_{11}\psi q_cq_1 - 2A_2q_c\dot{\psi}\dot{q}_c - 2B_{13}q_1\dot{\psi}\dot{q}_1 - 2A_8q_1\dot{q}_c\dot{q}_1; \quad (4.4)$$

$$A_4\ddot{\psi} + C_5\ddot{q}_c + C_6\ddot{q}_1 = -C_3\psi - C_7 q_c + C_8 q_1$$
$$+ B_2\dot{\psi}q_c - B_{15}q_1\dot{q}_1 + B_6\psi^3 + B_5\psi^2 q_c - B_{11}\psi^2 q_1$$
$$- 3B_3\psi q_c^2 - B_{17}\psi q_1^2 - 2B_{10}\psi q_c q_1 - B_{18}q_c^3 - 3B_{19}q_c^2 q_1$$
$$- B_{20}q_c q_1^2 + A_2\dot{\psi}^2 q_c - 4A_8 q_1\dot{\psi}\dot{q}_1 - 2B_{21}q_1\dot{q}_c\dot{q}_1; \qquad (4.5)$$

$$C_1\ddot{\psi} + C_6\ddot{q}_c + B_{13}\ddot{q}_1 = C_4\psi + C_8 q_c - C_9 q_1$$
$$+ B_1\dot{\psi}q_1 + B_{15}q_1\dot{q}_c - B_7\psi^3 - B_{11}\psi^2 q_c - B_8\psi^2 q_1$$
$$- B_{10}\psi q_c^2 - 2B_9\psi q_c q_1 - B_{19}q_c^3 - B_{20}q_c^2 q_1 + B_{13}q_1\dot{\psi}^2$$
$$+ B_{21}q_1\dot{q}_c^2 + 2A_8 q_1\dot{\psi}\dot{q}_c, \qquad (4.6)$$

where $B_1, \ldots, B_{21}$ and $C_1, \ldots, C_9$ are constants based on physical properties of the system.

A separate program was written specifically to solve the full and simplified equations numerically. Validity of both the sets of equations was established by comparing their numerical solutions to that given by the general multibody dynamics code. The results were found to be in excellent agreement except when the power boom was given a large excitation (tip deflections of more than 1 m). For large amplitude vibrations of the power boom, the assumptions of anti-symmetric bending of the solar panels and zero shift in the system c.m. are no longer valid.

4.3 Extension of the Butenin Method

The approximate analytical method employed here in solving the governing nonlinear equations is an extension of the Kryloff and Bogoliuboff method to systems with higher degrees of freedom. The method, attributed to Butenin, generally works

well with a weakly nonlinear system which has a small parameter associated with the nonlinearities. It essentially involves perturbing the generating solution of the linear system by assuming slowly varying amplitudes and phase angles, and employing the method of averaging [110]. The procedure employed here is an extension of the Butenin method to n-degree of freedom systems. In order to transform the system to a form amenable to the averaging procedure, the analytical solution to a set of $2n$ linear algebraic equations is required. For the case considered by Butenin, namely a two degree of freedom system, the solution of a set of 4 linear equations is accomplished by using Cramer's Rule. However, for the present case, this would entail an enormous amount of effort. Therefore, an alternate procedure applicable to a general n–degree of freedom second order system is developed.

Consider a weakly nonlinear system:

$$\begin{aligned} \mathbf{M}\ddot{\vec{x}} + \mathbf{K}\vec{x} = \mu\vec{f}(\vec{x},\dot{\vec{x}}), \qquad & \vec{x} \in R^n; \\ & \mathbf{M} \in R^{n\times n}; \\ & \mathbf{K} \in R^{n\times n}; \\ & \vec{f}: R^n \times R^n \rightarrow R^n; \end{aligned} \tag{4.7}$$

where both the mass matrix $\mathbf{M}$ and the stiffness matrix $\mathbf{K}$ are symmetric, positive definite, and time-invariant. $\vec{f}$ is a nonlinear vector function; and μ, a small parameter, is a measure of the strength of the nonlinearities. For the linear case ($\mu = 0$), the solution is given by

$$\vec{x}(t) = \sum_{i=1}^{n} a_i \vec{v}_i \sin(\omega_i t + \beta_i), \tag{4.8}$$

where ω_i^2 and v_i are the eigenvalues and eigenvectors of the system, respectively.

They are found by solving the eigenvalue problem

$$\left[\mathbf{K} - \omega_i^2 \mathbf{M}\right] \vec{v}_i = 0. \tag{4.9}$$

a_i and β_i are constants found by evaluating the initial conditions of the system. It can be shown [102] that all the eigenvalues are real and positive if the matrices $\mathbf{M}$ and $\mathbf{K}$ are symmetric and positive definite.

The solution of the nonlinear system ($\mu \neq 0$) is taken to have a form similar to that of the linear system, with the exception that the modal amplitudes a_i and phase angles β_i are allowed to be functions of time, rather than constants. The basic procedure for solving the nonlinear system is to replace the original set of n second order differential equations in $\vec{x}$ by a set of $2n$ first order differential equations in a_i and β_i. Because n old variables are now defined in terms of $2n$ new ones, n arbitrary conditions on the new variables may be imposed. The conditions introduced arise automatically from the particular form that the first derivative of $\vec{x}$ is taken to have. More specifically, the first derivative of $\vec{x}$ is taken to be identical in form to the linear case,

$$\dot{\vec{x}} = \sum_{i=1}^{n} a_i \omega_i \vec{v}_i \cos(\omega_i t + \beta_i), \tag{4.10}$$

which is equivalent to the equation

$$\sum_{i=1}^{n} \left\{ \dot{a}_i \vec{v}_i \sin \Theta_i + a_i \dot{\beta}_i \vec{v}_i \cos \Theta_i \right\} = 0, \tag{4.11}$$

where $\Theta_i = \omega_i t + \beta_i$. The second derivative of $\vec{x}$ is obtained through a term–by–term differentiation of Eqn. (4.10). After some manipulation, the governing equations of

motion can be expressed in terms of the new state variables as,

$$\left[\mathbf{P}\right]\left\{\begin{array}{c}\dot{a}_1\\ \vdots\\ \dot{a}_n\\ \cdots\\ a_1\dot{\beta}_1\\ \vdots\\ a_n\dot{\beta}_n\end{array}\right\}=\left\{\begin{array}{c}0\\ \vdots\\ 0\\ \cdots\\ f_1\\ \vdots\\ f_n\end{array}\right\}, \tag{4.12}$$

where $f_1, \cdots, f_n$ are the components of the nonlinear force vector, $\vec{f}$, and the matrix $\mathbf{P}$ is defined as

$$\mathbf{P}=\left[\begin{array}{ccc}\vec{\eta}_1 \sin\Theta_1 \ \ldots \ \vec{\eta}_n \sin\Theta_n & \vdots & \vec{\eta}_1 \cos\Theta_1 \ \ldots \ \vec{\eta}_n \cos\Theta_n\\ \ldots\ldots\ldots\ldots\ldots\ldots\ldots & \vdots & \ldots\ldots\ldots\ldots\ldots\ldots\ldots\\ \vec{\eta}_1\omega_1 \cos\Theta_1 \ \ldots \ \vec{\eta}_n\omega_n \cos\Theta_n & \vdots & -\vec{\eta}_1\omega_1 \sin\Theta_1 \ldots - \vec{\eta}_n\omega_n \sin\Theta_n\end{array}\right] \tag{4.13}$$

with

$$\vec{\eta}_i \equiv \mathbf{M}\vec{v}_i.$$

In order to manipulate Eqn. (4.12) to a form suitable for averaging, it has to be solved as follows,

$$\left\{\begin{array}{c}\dot{a}_1\\ \vdots\\ \dot{a}_n\\ \cdots\\ a_1\dot{\beta}_1\\ \vdots\\ a_n\dot{\beta}_n\end{array}\right\}=\left[\mathbf{P}^{-1}\right]\left\{\begin{array}{c}0\\ \vdots\\ 0\\ \cdots\\ f_1\\ \vdots\\ f_n\end{array}\right\}. \tag{4.14}$$

This would be a rather arduous task, were it not for the fact that $\mathbf{P}$ can be decomposed into a product of three matrices which, in turn, are partitioned into submatrices. The inverses of these partitioned matrices can be found with much greater ease than the inverse of $\mathbf{P}$ as it appears in Eqn. (4.13).

Defining $\mathbf{V}$ to be the matrix formed by the eigenvectors $\vec{v}_i$, i.e.

$$\mathbf{V} \equiv [\vec{v}_1 \quad \vec{v}_2 \quad \cdots \quad \vec{v}_n], \tag{4.15}$$

and $\mathbf{U}$ to be the product of $\mathbf{M}$ and $\mathbf{V}$,

$$\mathbf{U} \equiv \mathbf{MV}, \tag{4.16}$$

the matrix $\mathbf{P}$ can be partitioned as

$$\mathbf{P} = \mathbf{AB_1B_2}, \tag{4.17}$$

where:

$$\mathbf{A} = \begin{bmatrix} \mathbf{U} & \vdots & \mathbf{O} \\ \cdots & \cdots & \cdots \\ \mathbf{O} & \vdots & \mathbf{U} \end{bmatrix}; \tag{4.18}$$

$$\mathbf{B_1} = \begin{bmatrix} \mathbf{I} & \vdots & \mathbf{O} \\ \cdots & \cdots & \cdots \\ \mathbf{O} & \vdots & \mathbf{\Omega} \end{bmatrix}; \tag{4.19}$$

$$\mathbf{B_2} = \begin{bmatrix} \mathbf{S}_\theta & \vdots & \mathbf{C}_\theta \\ \cdots & \cdots & \cdots \\ \mathbf{C}_\theta & \vdots & -\mathbf{S}_\theta \end{bmatrix}. \tag{4.20}$$

The inverses of $\mathbf{A}$, $\mathbf{B_1}$ and $\mathbf{B_2}$ can be obtained readily. In particular, $\mathbf{B_2}$ is an involutory matrix (i.e. $\mathbf{B_2B_2} = \mathbf{I}$). Each submatrix is of the dimension $n \times n$. $\mathbf{I}$ and $\mathbf{O}$ are the identity and zero matrix, respectively. $\mathbf{S}_\theta$, $\mathbf{C}_\theta$ and $\mathbf{\Omega}$ are diagonal matrices defined as:

$$\mathbf{S}_\theta = \begin{bmatrix} \sin\Theta_1 & 0 & \cdots & \cdots & 0 \\ 0 & \sin\Theta_2 & 0 & \cdots & 0 \\ \vdots & & \ddots & & \vdots \\ 0 & \cdots & 0 & \sin\Theta_{n-1} & 0 \\ 0 & \cdots & \cdots & 0 & \sin\Theta_n \end{bmatrix}; \tag{4.21}$$

$$\mathbf{C}_\theta = \begin{bmatrix} \cos\Theta_1 & 0 & \dots & \dots & 0 \\ 0 & \cos\Theta_2 & 0 & \dots & 0 \\ \vdots & & \ddots & & \vdots \\ 0 & \dots & 0 & \cos\Theta_{n-1} & 0 \\ 0 & \dots & \dots & 0 & \cos\Theta_n \end{bmatrix}; \tag{4.22}$$

$$\mathbf{\Omega} = \begin{bmatrix} \omega_1 & 0 & \dots & \dots & 0 \\ 0 & \omega_2 & 0 & \dots & 0 \\ \vdots & & \ddots & & \vdots \\ 0 & \dots & 0 & \omega_{n-1} & 0 \\ 0 & \dots & \dots & 0 & \omega_n \end{bmatrix}. \tag{4.23}$$

The inverse of $\mathbf{P}$ can easily be shown to be

$$\mathbf{P}^{-1} = \begin{bmatrix} \mathbf{S}_\theta & \vdots & \mathbf{C}_\theta \\ \dots & \dots & \dots \\ \mathbf{C}_\theta & \vdots & -\mathbf{S}_\theta \end{bmatrix} \begin{bmatrix} \mathbf{I} & \vdots & \mathbf{O} \\ \dots & \dots & \dots \\ \mathbf{O} & \vdots & \mathbf{\Omega}^{-1} \end{bmatrix} \begin{bmatrix} \mathbf{U}^{-1} & \vdots & \mathbf{O} \\ \dots & \dots & \dots \\ \mathbf{O} & \vdots & \mathbf{U}^{-1} \end{bmatrix}, \tag{4.24}$$

where

$$\mathbf{\Omega}^{-1} = \begin{bmatrix} \frac{1}{\omega_1} & 0 & \dots & \dots & 0 \\ 0 & \frac{1}{\omega_2} & 0 & \dots & 0 \\ \vdots & & \ddots & & \vdots \\ 0 & \dots & 0 & \frac{1}{\omega_{n-1}} & 0 \\ 0 & \dots & \dots & 0 & \frac{1}{\omega_n} \end{bmatrix}. \tag{4.25}$$

Since $\mathbf{M}$ and $\mathbf{K}$ are both positive definite, $\omega_1, \dots, \omega_n$ are all nonzero and positive. Therefore the inverse of $\mathbf{\Omega}$ exists. $\mathbf{U}^{-1}$ can be computed numerically and is expressed as

$$\mathbf{T} = \mathbf{U}^{-1} = \begin{bmatrix} t_{11} & t_{12} & \dots & t_{1n} \\ t_{21} & t_{22} & \dots & t_{2n} \\ \vdots & \vdots & & \vdots \\ t_{n1} & t_{n2} & \dots & t_{nn} \end{bmatrix}. \tag{4.26}$$

Now, the set of first order equations expressed in a form amenable to the averaging

procedure can be written as

$$\left\{\begin{array}{c}\dot{a}_1\\ \vdots\\ \dot{a}_n\\ \cdots\\ a_1\dot{\beta}_1\\ \vdots\\ a_n\dot{\beta}_n\end{array}\right\} = \left[\mathbf{P}^{-1}\right] \left\{\begin{array}{c}0\\ \vdots\\ 0\\ \cdots\\ f_1\\ \vdots\\ f_n\end{array}\right\} = \left\{\begin{array}{c}\mathbf{C}_\theta\boldsymbol{\Omega}^{-1}\mathbf{T}\vec{f}\\ \cdots\cdots\\ -\mathbf{S}_\theta\boldsymbol{\Omega}^{-1}\mathbf{T}\vec{f}\end{array}\right\}. \tag{4.27}$$

The motivation for employing an averaging procedure is the fact that, for weakly nonlinear systems, the amplitudes and phase angles vary little over one cycle of oscillation. Therefore, the average values of the amplitudes and phase angles are considered rather than the instantaneous values. Solutions for the averaged differential equations are then sought. The averaged form of eq. (4.27) is:

$$\left\{\begin{array}{c}\dot{\bar{a}}_1\\ \vdots\\ \dot{\bar{a}}_n\\ \cdots\\ \bar{a}_1\dot{\bar{\beta}}_1\\ \vdots\\ \bar{a}_n\dot{\bar{\beta}}_n\end{array}\right\} = \left\{\begin{array}{c}\left(\sum_{i=1}^{n} F_{i1}^{c}\cdot t_{1i}\right)\frac{1}{\omega_1}\\ \vdots\\ \left(\sum_{i=1}^{n} F_{in}^{c}\cdot t_{ni}\right)\frac{1}{\omega_n}\\ \cdots\cdots\cdots\\ -\left(\sum_{i=1}^{n} F_{i1}^{s}\cdot t_{1i}\right)\frac{1}{\omega_1}\\ \vdots\\ -\left(\sum_{i=1}^{n} F_{in}^{s}\cdot t_{ni}\right)\frac{1}{\omega_n}\end{array}\right\}, \tag{4.28}$$

where the bar ($\bar{\cdot}$) denotes an averaged variable, and $F_{i1}^{c},\ldots,F_{in}^{c}$ and $F_{i1}^{s},\ldots,F_{in}^{s}$ are the expressions averaged over a complete cycle:

$$F_{ij}^{c} = \frac{1}{(2\pi)^n}\int_0^{2\pi}\cdots\int_0^{2\pi} f_i\cos\Theta_j\, d\Theta_1\cdots d\Theta_n; \tag{4.29}$$

$$F_{ij}^{s} = \frac{1}{(2\pi)^n}\int_0^{2\pi}\cdots\int_0^{2\pi} f_i\sin\Theta_j\, d\Theta_1\cdots d\Theta_n. \tag{4.30}$$

The averaged equations (4.28) may be solved to yield a first order correction to the generating solution. Any appropriate method may be employed to solve the averaged nonlinear differential equations.

4.4 Analytical and Numerical Results

The physical properties of the model used are given in Table 4-1 . The fundamental flexural frequencies for the system are taken to be a tenth of the actual FEL model described in the previous chapter. The spacecraft is placed in a circular Low Earth Orbit (LOE) at a height of 400 km.

Table 4-1 Physical characteristics of the planar FEL model

Body	Length (m)	Mass (kg)	ω_1* (rad/s)	I_{xx} (kg-m^2)	I_{yy} (kg-m^2)	I_{zz} (kg-m^2)
Power Boom	60	15,840	1.2164	1.5×10^5	4.37×10^6	4.28×10^6
PV Array	33	444	0.0628	1,332	161,172	162,504

* ω_1 is the fundamental natural frequency in bending

The Mass and Stiffness matrices of the system are taken to be as:

$$\mathbf{M} = \begin{bmatrix} 5.83112 \times 10^6 & 1.03214 \times 10^5 & 1.66689 \times 10^4 \\ & 2.71272 \times 10^4 & 2.58216 \times 10^3 \\ \text{symm.} & & 8.88000 \times 10^2 \end{bmatrix}; \tag{4.31}$$

$$\mathbf{K} = \begin{bmatrix} 1.99157 \times 10^1 & 1.28484 \times 10^{-2} & -6.40079 \times 10^{-2} \\ & 2.34367 \times 10^4 & -9.91541 \times 10^{-3} \\ \text{symm.} & & 3.44281 \end{bmatrix}. \tag{4.32}$$

The resulting natural frequencies and their corresponding eigenvectors were found to be as follows:

$$\omega_1 = 1.84789 \times 10^{-3} rad/s, \qquad \vec{v}_1 = \begin{Bmatrix} 0.99382617 \\ 0.00001451 \\ 0.03513380 \end{Bmatrix};$$

$$\omega_2 = 6.39768 \times 10^{-2} rad/s, \qquad \vec{v}_2 = \begin{Bmatrix} -0.00287077 \\ 0.00040153 \\ 0.99999580 \end{Bmatrix};$$

$$\omega_3 = 1.109036\, rad/s, \qquad \vec{v}_3 = \begin{Bmatrix} 0.00340241 \\ -0.34386914 \\ 0.939011412 \end{Bmatrix}.$$

The results indicate that the first mode of the system is dominated by the pitch motion with some coupling with the solar panel vibration, while the second is essentially comprised of the solar panel vibration and minor coupling with the pitch motion. In the third mode, the solar panel vibration is again prominent and coupled with the power boom vibration. From these results, the linear solution to the system can easily be obtained.

The averaged form of the nonlinear equations were also evaluated. Because of the relatively large number of nonlinear terms retained even in the "simplified" form, the amount of algebra involved was considerable. The averaged nonlinear differential equations are given by:

$$\dot{\overline{a}}_i = 0, \qquad i = 1, 2, 3; \tag{4.33}$$

$$\overline{a}_i \dot{\overline{\beta}}_i = \sum_{j=1}^{3} D_{ij} \overline{a}_i \overline{a}_j^2, \qquad i = 1, 2, 3. \tag{4.34}$$

Here D_{ij} are constants which depend on the physical parameters, including mass and stiffness properties, as well as the natural frequencies and eigenvectors of the system (linear). Once again, for the sake of brevity, the lengthy expressions for these constants are omitted. The solution to the averaged equations is given by:

$$\overline{a}_i(t) = \overline{a}_{i_o}, \qquad i = 1, 2, 3; \tag{4.35}$$

$$\overline{\beta}_i(t) = \sum_{j=1}^{3} D_{ij} \overline{a}_j^2 t + \overline{\beta}_{i_o}, \qquad i = 1, 2, 3. \tag{4.36}$$

This shows that the solution given by the analytical nonlinear approach results in an amplitude which is identical to that given by the linear solution. However, the nonlinear solution does 'correct' the phase through modification of the natural frequencies (obtained from the linear solution) by a constant value which depends on a weighted sum of the squares of the initial amplitudes of the system.

The numerical solutions for both the full nonlinear model and the simplified nonlinear model, as well as the analytical solutions of the simplified nonlinear model and the linear model were obtained. This was necessary to validate the analytical solution procedure. First, the response to an initial condition in the pitch angle of 20° was obtained (Figure 4-2). The results indicate that for the pitch time history taken over one orbit (5560 s) there is an excellent agreement among the numerical solutions of both the full and simplified nonlinear models, as well as with the analytical solution of the simplified nonlinear model. However, the solution given by the linear model has considerable phase error. The responses of the power boom and solar panel vibrations, given by both the linear and the analytical nonlinear solutions overpredict the amplitude of vibration by approximately 10%. However, the correlation in phase for all the solutions, is excellent here. As expected the pitching motion excites the solar panel to a much greater extent than the power boom. Note, that the pitch history is shown over one orbit, while the power boom and solar panel response is presented over one–tenth of an orbit to facilitate comparison.

Next, the response to an initial disturbance applied to the power boom, in the form of a 0.1 m excitation of the generalized coordinate (tip deflection of 0.2 m), is obtained. These results are given in Figure 4-3 . All the solutions for the power boom response are in excellent agreement. However, the linear solutions for both the pitch and the solar panel vibration are in error with the nonlinear predictions (numerical as well as analytical), all of which are in excellent agreement. The discrepancy in the linear solution takes the form of an offset error in the amplitude. Note, the error is cyclic in nature at the fundamental bending frequency of the solar panel.

Next, to complete the comparison between the various solutions, a disturbance was imparted to the solar panel. An initial condition of 0.5 m to the vibrational

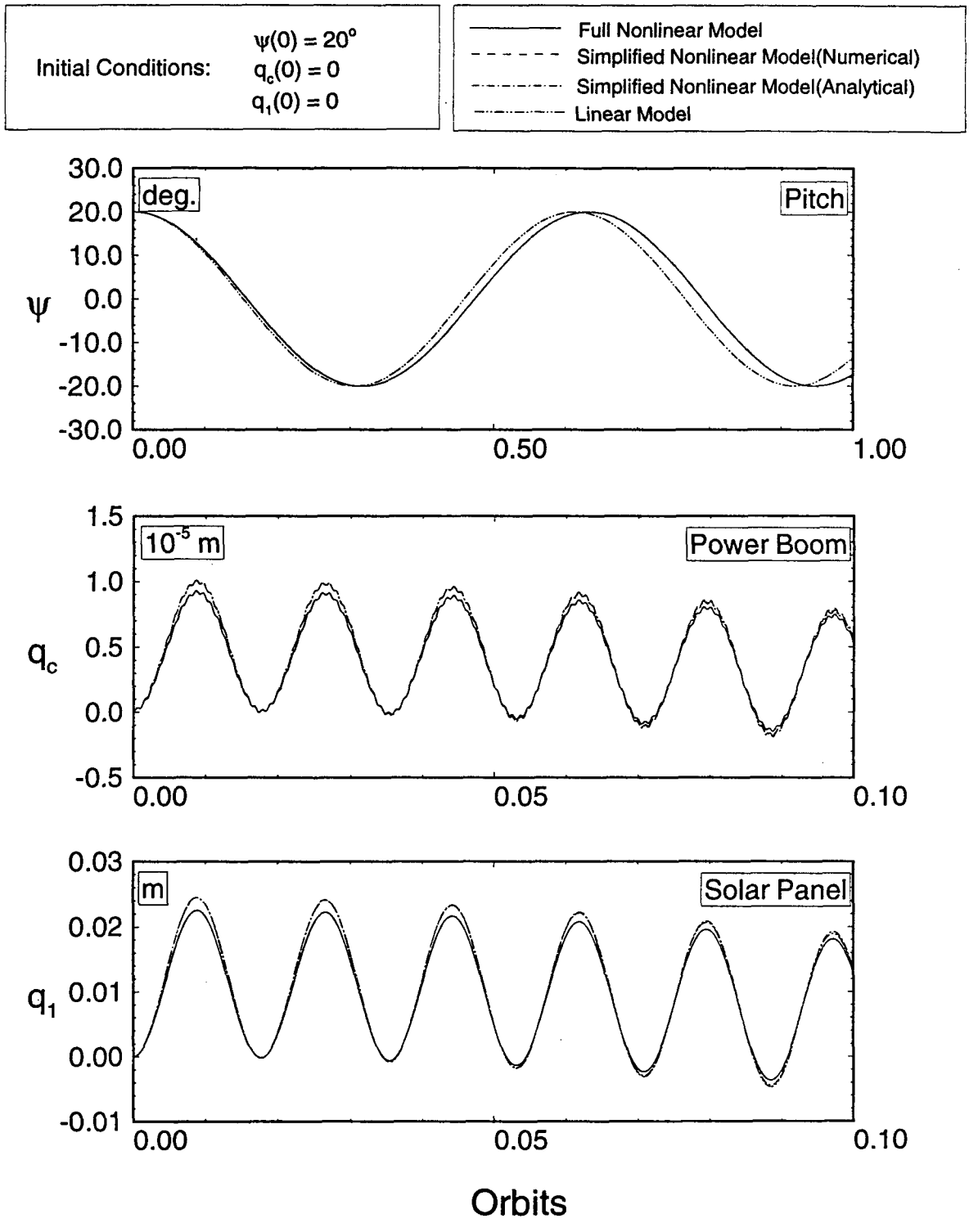

Figure 4-2 System response to an excitation in pitch: a comparison of solutions given by different models.

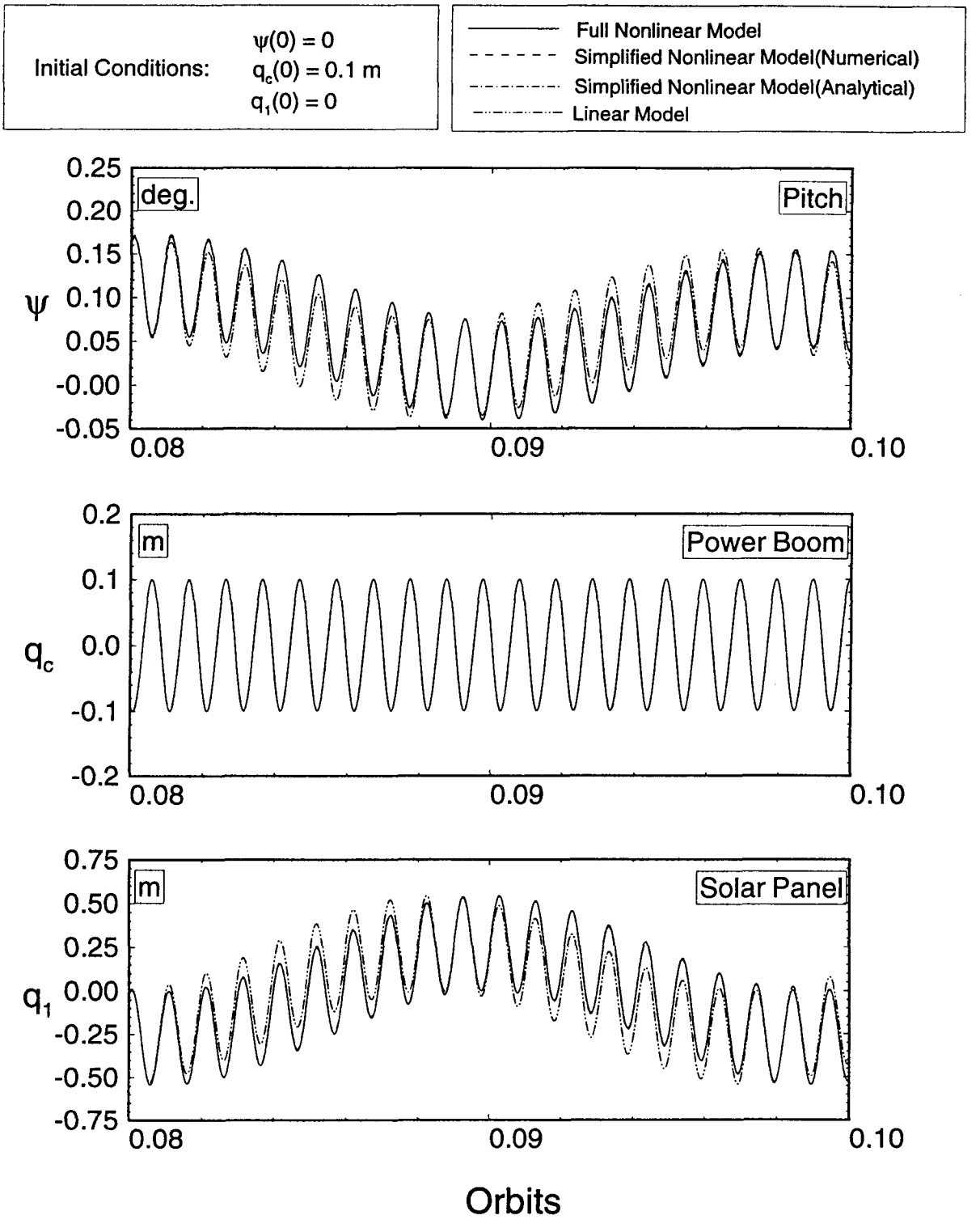

Figure 4-3 System response to the excitation of the power boom vibration: a comparison of solutions given by different models.

generalized coordinate, corresponding to a solar panel tip deflection of 1 m, was used. The results show that, apart from a negligible phase error between both the linear and analytical nonlinear solutions, and the numerical nonlinear solutions of the power boom response, the results are in excellent agreement (Figure 4-4).

The possible disturbances on a large, flexible spacecraft include environmental effects such as gravity gradient torques, solar radiation pressure, and thermal deformation, to name a few. In addition, on–board activity of the crew and maneuvers of a robotic manipulator, may excite the system. A review of the literature on environmental effects has been presented by Ng in his doctoral dissertation [13]. On the other hand, Suleman [12] has studied at length the space station response to on–board disturbances.

Some appreciation as to the effect of such disturbances can be obtained through the excitation of each generalized coordinate. For example, a small disturbance in pitch may be used to simulate the gravity gradient torque on the system, while the effects of thermal disturbances may be investigated by exciting the elastic degrees of freedom.

With this in mind, a study was undertaken using the analytical nonlinear solution, its validity having been established. To begin with, the response of all three generalized coordinates to a 20° pitch disturbance was re-examined (see Figure 4-5). Note, the time history of the flexible degrees of freedom is now extended to one orbit. The power boom response, at the pitch frequency, is modulated by high frequency oscillations corresponding to the natural frequency of the solar panel. To put it differently, the power boom responds to both the rigid body pitch as well as vibratory disturbance of the solar panel. In fact there is a small contribution at its own natural frequency (insert, center frame, Figure 4-5). The solar panel response shows similar

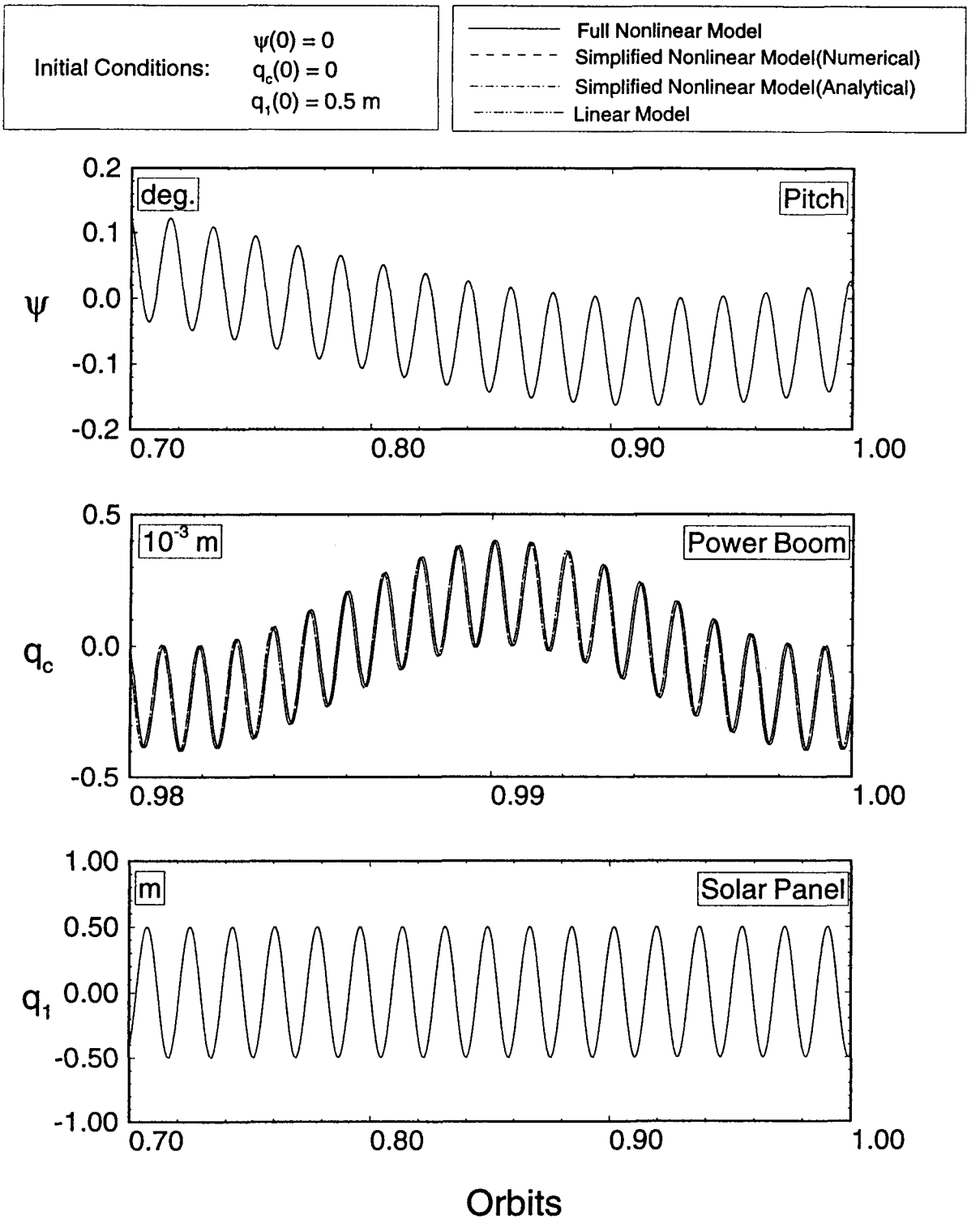

Figure 4-4 System response to the excitation of the solar panel vibration: a comparison of solutions given by different models.

trends, however, now the tip deflection is larger (5 cm compared with 0.002 cm). The results clearly illustrate the coupling between pitch motion and the flexible degrees of freedom.

Next, the response to the power boom excitation (tip deflection of 0.2 m) is investigated over one orbit (Figure 4-6). As can be expected, the power boom vibrates at its own characteristic frequency, with constant amplitude in the absence of damping. Note a strong coupling between the power boom and solar panel vibrations. In fact, the panel's vibration amplitude is approximately 5 times the power boom excitation. Two frequencies are present in the solar panel response: the higher corresponds to the power boom fundamental frequency in bending, while the lower represents the solar panel's natural frequency. The pitch response exhibits three frequencies: the two associated with the flexible degrees of freedom, while the third corresponds to the rigid body motion in pitch. Although the maximum pitch oscillation of 0.2° appears to be modest, it would be unacceptable in cases requiring high pointing accuracy of the platform (power boom) during communications.

Finally, a disturbance in the form of a tip deflection of 1 m is applied to the solar panel (Figure 4-7). The power boom's response is minimal. Although two frequencies corresponding to the vibration generalized coordinates are present, the maximum deflection is only 1 mm. The pitch motion is excited at both the solar panel as well as the pitch natural frequency with an amplitude of approximately 0.2°.

The study clearly emphasizes the presence of coupling between the librational and vibrational degrees of freedom. In particular, the solar panel vibrations are strongly coupled with the pitch and power boom responses.

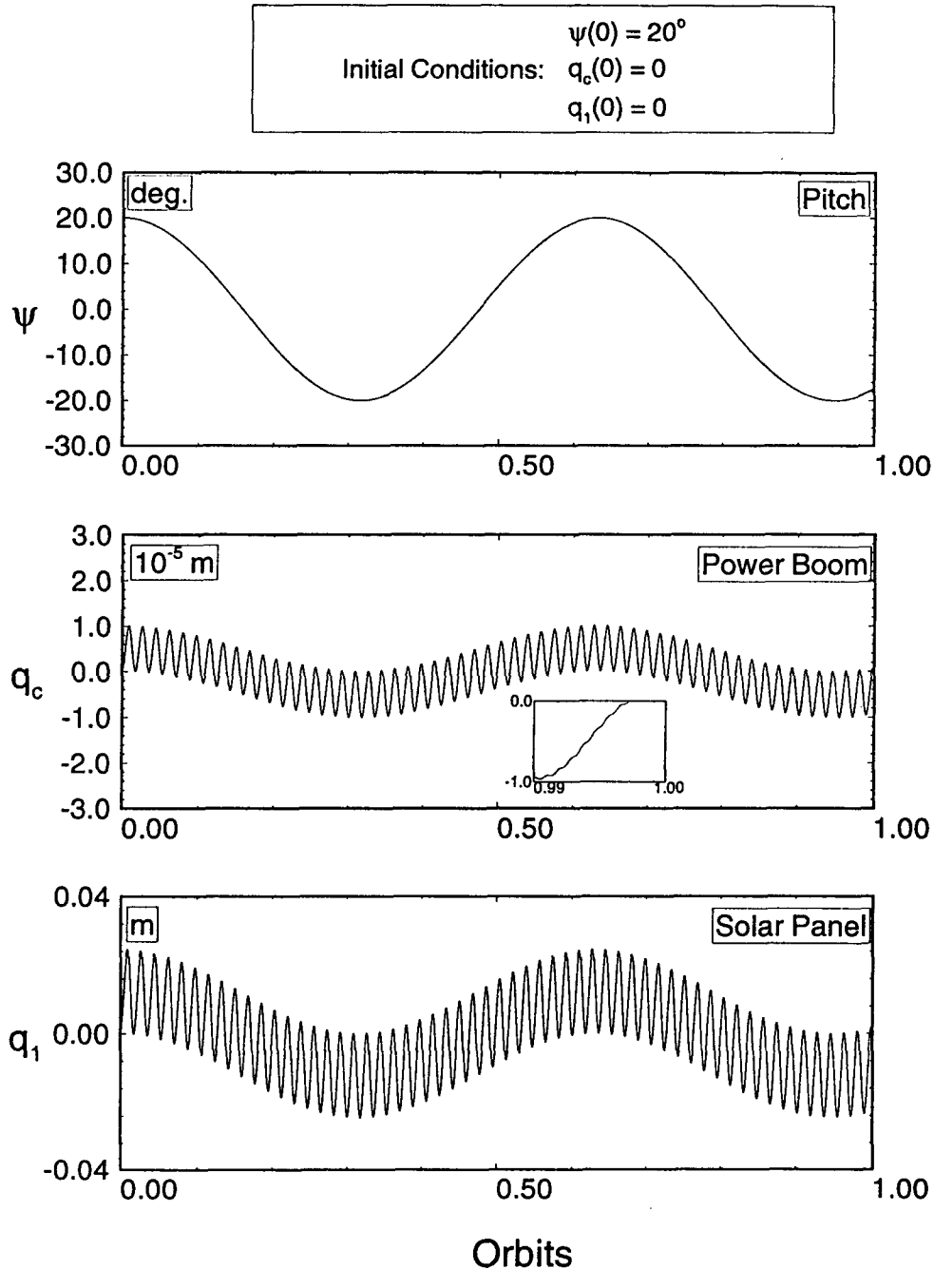

Figure 4-5 Analytical obtained system response to an excitation in pitch.

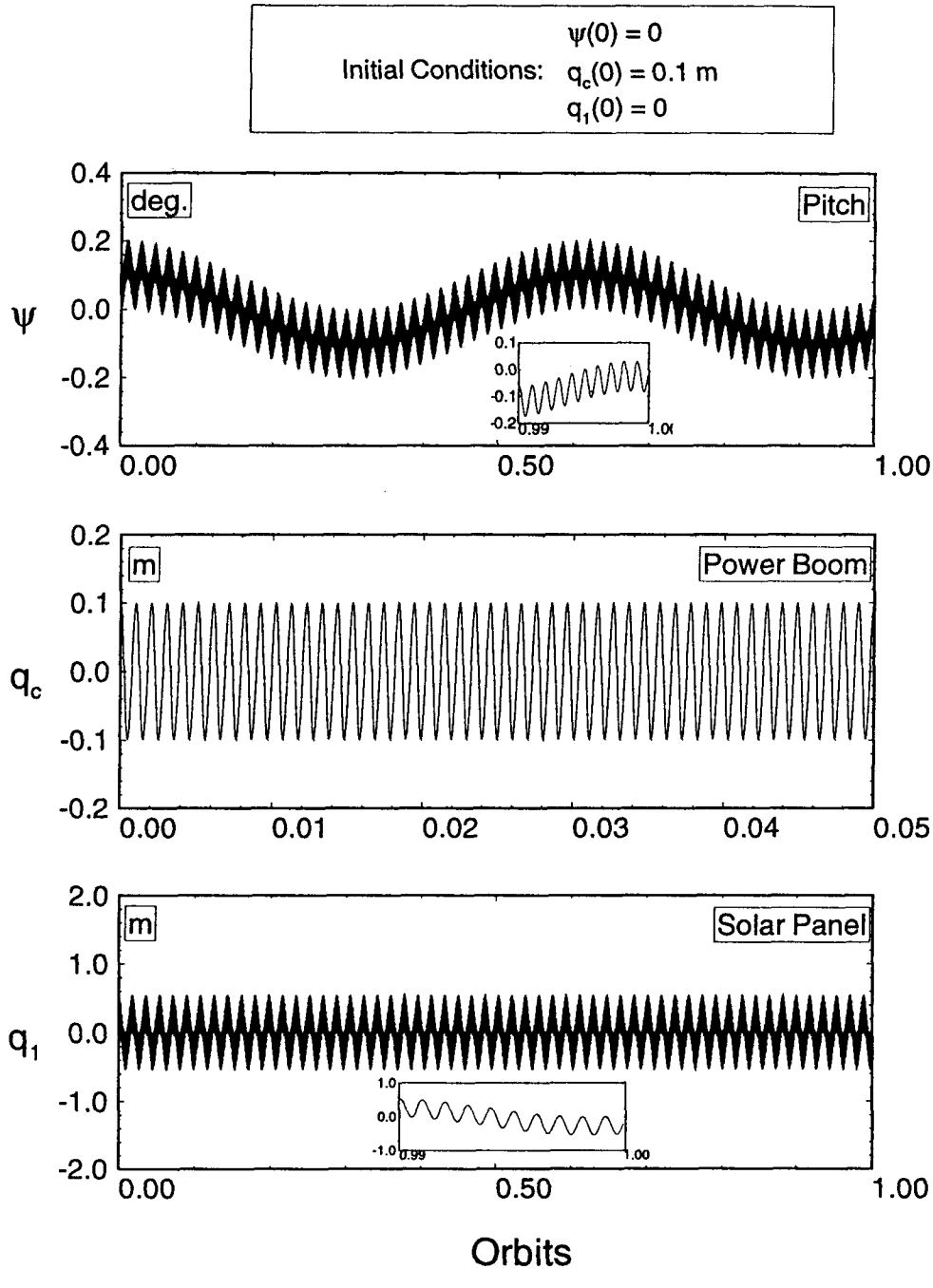

Figure 4-6 System response to an excitation of the power boom vibration: the analytical solution.

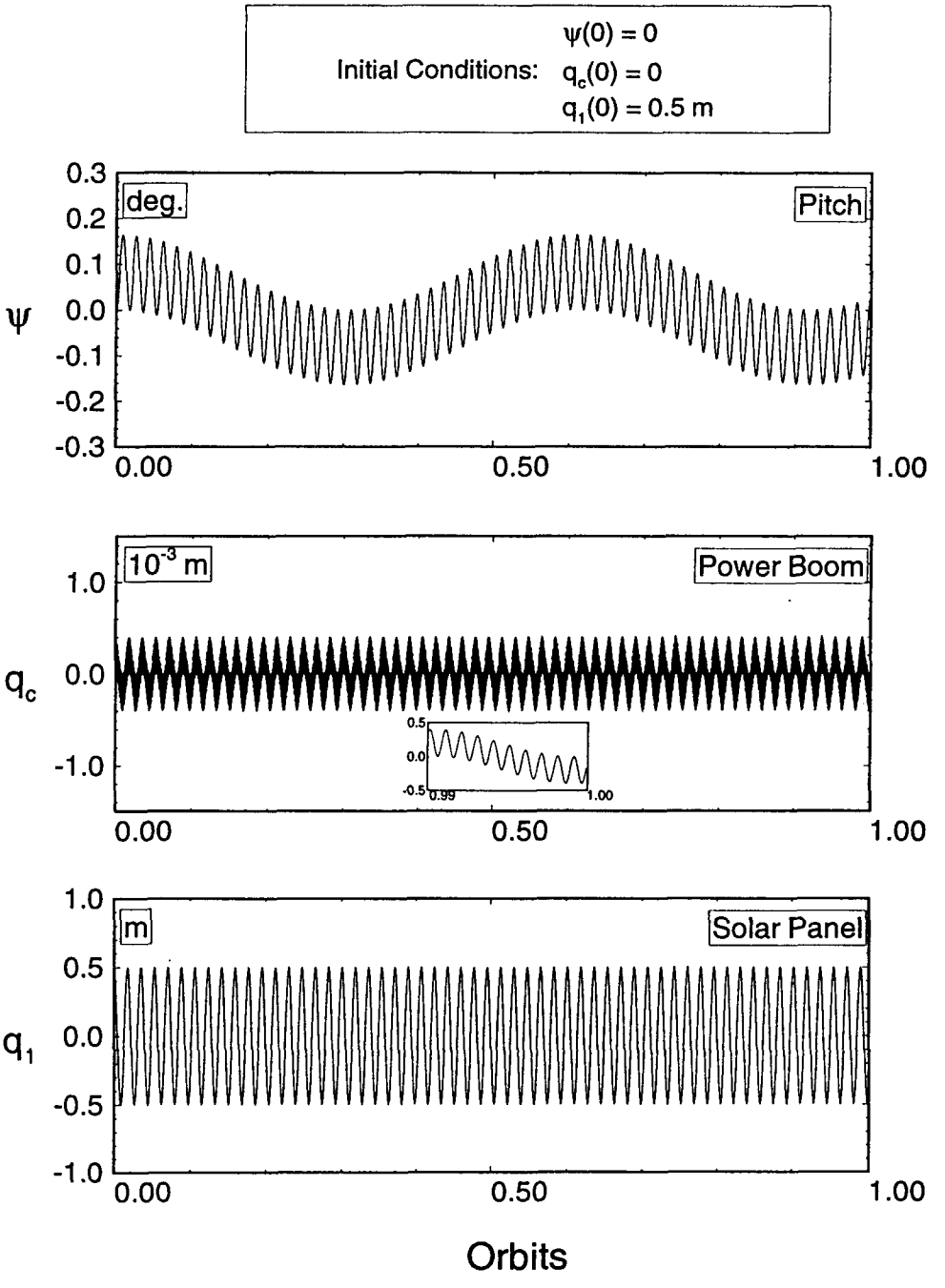

Figure 4-7 Analytically obtained system response to an excitation of the solar panel vibration.

4.5 Concluding Remarks

A procedure for the analytical solution of a weakly nonlinear system with arbitrary degrees of freedom is developed as an extension to the Butenin method. Its validity is assessed through application to a nonlinear model of a flexible space station. In general, the closed–form analytical solution predicts the response with a remarkable degree of accuracy, even when subjected to large disturbances. It clearly emphasizes the coupled character of the system. The approach can be used to advantage in gaining physical appreciation of the problem, particularly during the preliminary design stage, with significant saving in time and effort.

5. UNCONTROLLED MOTION

5.1 Preliminary Remarks

The validity of the flexible multibody formulation and the associated simulation code was established in the Chapter 3. The principal benefit in developing such a model is to predict the dynamical behaviour of a large class of flexible, multibody systems through numerical simulation. In this chapter the potential of this versatile tool is illustrated through its application in the study of the uncontrolled dynamics of a wide range of spacecraft systems.

First, the behaviour of a generic space platform with a slewing manipulator is simulated to demonstrate the foreshortening effect. Next, yet another generic space platform model with a slewing manipulator is studied to illustrate the improvement in matching of the natural boundary conditions by employing quasi–comparison functions. The proposed Space Station has numerous facets leading to its complex dynamical behaviour. It involves the evolutionary growth of a large, flexible space structure, subjected to a wide variety of disturbances including the slewing maneuvers of various structural elements, docking of the Space Shuttle, crew motion, etc. not to mention the environmental disturbances due to solar and aerodynamic effects. The influence of some of these disturbances are studied here. Specifically, the response of the First Element Launch (FEL) configuration to the docking of the Space Shuttle and maneuvers of the Remote Manipulator System (RMS) are investigated. Furthermore, the dynamics of the Permanently Manned Configuration (PMC) of the Space Station during tracking motion of its solar arrays and maneuvers of the RMS are studied.

The "turnaround" time for conducting such dynamical studies using the multibody dynamics code is relatively short; the data required for a new run can be entered

in the input file quite readily. This would enable a design engineer to conduct a systematic parametric study quite readily. Here only a few typical cases are studied to help establish trends. The purpose of the study is not to generate a vast body of design data, but to establish innovative methodologies and develop versatile tools which can be used with confidence by a community of practising as well as research engineers.

5.2 Generic Space Platforms Models with a Slewing Manipulator

5.2.1 Foreshortening Effect

As alluded to earlier, the foreshortening effect relates to the distinction between the arclength of a structural element and its projection along the axis of the reference frame [90]. To aid in the explanation of this effect consider the cantilevered beam in Figure 5-1 . In the conventional beam theory, the deflection of an element is taken to be perpendicular to the undeformed beam. Consider a beam element dm, located at M, as shown in Figure 5-1. Conventional theory implicitly states that the undeformed position of that element is at X, whereas it actually is at S. The difference between these two is insignificant if beam stiffness is high, but becomes significant as stiffness decreases. Essentially, failure to account for the foreshortening effect results in the implicit assumption of stretching or compressing of the beam[90]. Moreover, when a flexible member undergoes a fast slewing maneuver, the conventional theory fails to predict the stiffening effect due to the rotation of the beam.

In order to incorporate the foreshortening effect one must first establish a relationship between the beam arclength and position along the beam axis, x. From elementary differential geometry, the arclength, s, is related to the coordinates, x, y

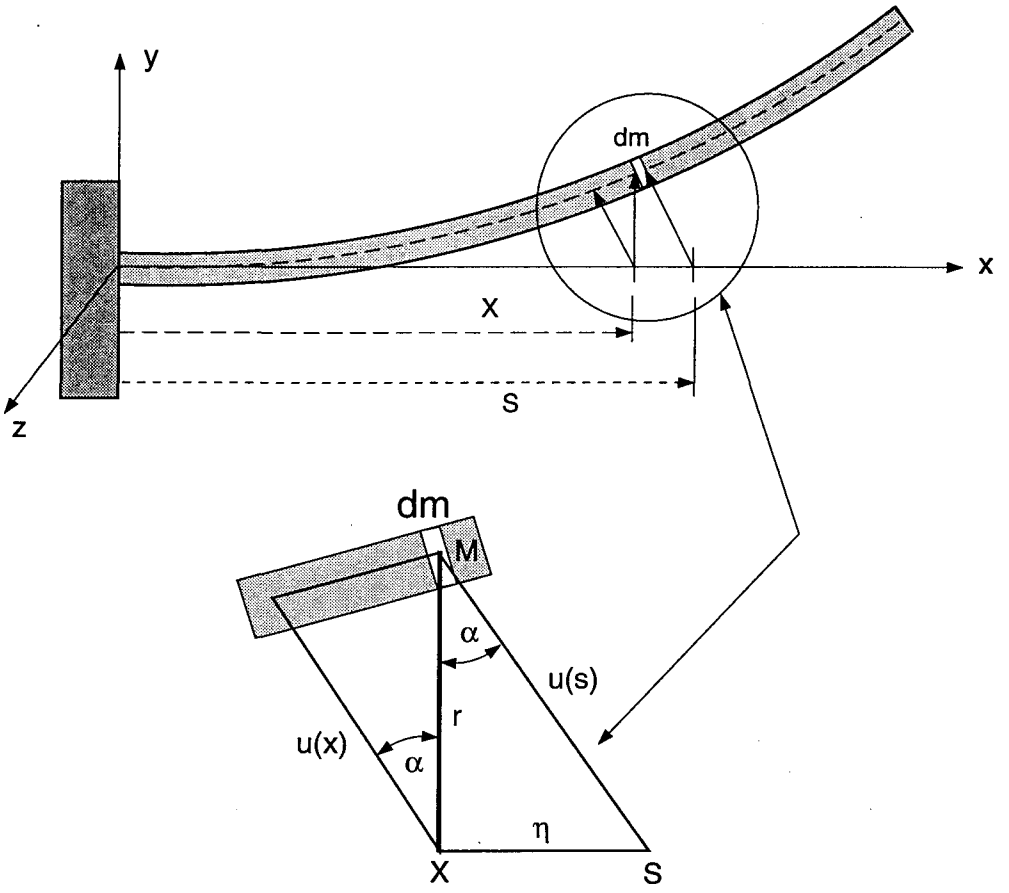

Figure 5-1 A cantilevered beam illustrating the foreshortening effect.

and z by:

$$ds = \sqrt{(dx)^2 + (dy)^2 + (dz)^2};$$
$$= \sqrt{1 + \left(\frac{\partial y}{\partial x}\right)^2 + \left(\frac{\partial z}{\partial x}\right)^2}\, dx. \tag{5.1}$$

For the case of a beam in flexure, y and z represent the beam deflections in those respective directions, i.e.

$$y \equiv v$$
$$z \equiv w. \tag{5.2}$$

Recognizing that v and w are small and using the Binomial expansion,

$$\sqrt{1+f} \approx 1 + \frac{1}{2}f.$$

Now, applying eq. (5.2), eq. (5.1) can be written as

$$ds \approx \left\{ 1 + \frac{1}{2}\left[\left(\frac{\partial v}{\partial x}\right)^2 + \left(\frac{\partial w}{\partial x}\right)^2 \right] \right\} dx. \tag{5.3}$$

Integrating eq. (5.3) and ignoring higher order terms yields [90]

$$s = x + \eta(x), \tag{5.4}$$

where

$$\eta(x) = \frac{1}{2}\int_0^x \left[\left(\frac{\partial v}{\partial \xi}\right)^2 + \left(\frac{\partial w}{\partial \xi}\right)^2 \right] d\xi. \tag{5.5}$$

η represents the difference between the arclength and its projection along the x axis and ξ is simply a dummy variable.

If the foreshortening effect is to be neglected, then terms of the form

$$\int_m x\, dm \qquad \text{and} \qquad \int_m x^2\, dm, \tag{5.6}$$

which appear in the energy expressions for a beam element are given by:

$$\begin{aligned} \int_m x\, dm &= \int_\ell \mu_m\, x\, dx; \\ \int_m x^2\, dm &= \int_\ell \mu_m\, x^2\, dx; \end{aligned} \tag{5.7}$$

where μ_m is the mass per unit length of the beam element. If, however, the foreshortening effect is to be modeled, then terms of the form shown in eq. (5.6) are given by the following expressions:

$$\int_m x\, dm = \int_\ell \mu_m\, x\, ds;$$

$$\int_m x^2\, dm = \int_\ell \mu_m\, x^2\, ds. \tag{5.8}$$

Substituting eq. (5.4) into eq. (5.8) and neglecting $\mathcal{O}(\eta^2)$ terms gives:

$$\int_\ell \mu_m\, x\, ds = \int_\ell \mu_m\, (s-\eta)\, ds; \tag{5.9}$$

$$\begin{aligned}\int_\ell \mu_m\, x^2\, ds &= \int_\ell \mu_m\, (s-\eta)^2\, ds \\ &= \int_\ell \mu_m\, (s^2 - 2s\eta)\, ds + \mathcal{O}(v^4, w^4).\end{aligned} \tag{5.10}$$

Note that $\eta = \mathcal{O}(v^2, w^2)$. One can see that the first terms in eqs. (5.9) and (5.10) represent the expressions when the foreshortening effect is neglected, while the second terms in the respective equations represent the corrective terms. It can be shown through integration by parts [90] that the corrective terms for

$$\int_\ell s\, ds \qquad \text{and} \qquad \int_\ell s^2\, ds$$

are:

$$-\int_0^\ell \eta\, ds = \frac{1}{2}\int_0^\ell (s-\ell)\left[\left(\frac{\partial v}{\partial s}\right)^2 + \left(\frac{\partial w}{\partial s}\right)^2\right] ds; \tag{5.11}$$

$$-2\int_0^\ell s\eta\, ds = \frac{1}{2}\int_0^\ell (s^2-\ell^2)\left[\left(\frac{\partial v}{\partial s}\right)^2 + \left(\frac{\partial w}{\partial s}\right)^2\right] ds; \tag{5.12}$$

respectively. Corrections are required for the: T_{cm}, T_s and $T_{h,s}$ terms of the kinetic energy expression; $\mathbf{I_{cm}}$, $\mathbf{I_r}$ and $\mathbf{I_{h,r}}$ terms of the system inertia matrix; and the $\vec{H}_{cm}$, $\vec{H}_{hr}$, $\vec{H}_{rs}$ and $\vec{H}_{hs}$ terms of the angular momentum vector. Their contribution to the governing equations of motion is incorporated in the model. As an example, consider the relevant portion of the T_s expression for a system with only B_i bodies,

$$T_s = \frac{1}{2}\sum_{i=1}^{N}\left[\int_{m_i} (\dot{\mathbf{C}}_\mathbf{i}^\mathbf{c}\vec{\rho}_i)\cdot(\dot{\mathbf{C}}_\mathbf{i}^\mathbf{c}\vec{\rho}_i)\, dm_i\right]. \tag{5.13}$$

Consider the case when the central body is rigid, and each of the B_i bodies are flexible beam–type appendages undergoing prescribed slewing maneuvers. The corrective terms (for the equations of motion) due to foreshortening, for the m-th flexibility coordinate of the l-th B_i body are:

$$\frac{\partial T_s^{cor}}{\partial P_l^m} = \frac{1}{2}\mu_l \,\text{trace}\left[\dot{\mathbf{C}}_\mathbf{l}^\mathbf{c}\mathbf{1}\dot{\mathbf{C}}_\mathbf{l}^{\mathbf{c}^T}\right]\sum_j P_l^j A_{jm}^l; \tag{5.14}$$

$$\frac{\partial T_s^{cor}}{\partial Q_l^m} = \frac{1}{2}\mu_l \,\text{trace}\left[\dot{\mathbf{C}}_\mathbf{l}^\mathbf{c}\mathbf{1}\dot{\mathbf{C}}_\mathbf{l}^{\mathbf{c}^T}\right]\sum_j Q_l^j A_{jm}^l; \tag{5.15}$$

where:

$$A_{jm}^l = \int_0^{\ell_l}\left(x_l^2 - \ell_l^2\right)\left(\frac{d\psi_l^j}{dx_l}\right)\left(\frac{d\psi_l^m}{dx_l}\right)dx_l; \tag{5.16}$$

$$\mathbf{1} = \begin{bmatrix}1 & 0 & 0\\ 0 & 0 & 0\\ 0 & 0 & 0\end{bmatrix}. \tag{5.17}$$

When $j = m$, it is clear that A_{jm}^l is negative. Therefore, the contributions of the corrective terms to the governing equations are such that the stiffness of the system increases. This explains the observed phenomenon of stiffening encountered when flexible systems are spun.

The foreshortening effect is demonstrated through computer simulations of a rigid space platform with a flexible manipulator undergoing a fast slewing maneuver. The physical characteristics of the system are given in Table 5-1 . The system, in a circular Low Earth Orbit at an altitude of 400 km, is oriented in the gravity gradient configuration with the long axis of the platform along the local vertical. The manipulator, located at the nadir end of the platform, slews at a constant angular velocity of 0.1454 rad/s. At time $t = 0$, the manipulator tip is oriented towards zenith, and is given a tip deflection of 1 cm in each of the transverse directions. A schematic

diagram of the system is shown in Figure 5-2 . The manipulator is discretized using a single clamped–free beam shape function in each transverse direction.

Table 5-1 Physical characteristics of the rigid space platform with a flexible manipulator

Body	Length (m)	Mass (kg)	ω_1* (rad/s)	I_{xx} (kg-m^2)	I_{yy} (kg-m^2)	I_{zz} (kg-m^2)
Platform	60	120,000	rigid	1.0×10^6	3.6×10^7	3.6×10^7
Manipulator	15	750	0.494	400	5.625×10^4	5.625×10^4

* ω_1 is the fundamental bending natural frequency

The results comparing the system response with and without the foreshortening effect are shown in Figure 5-3 . There is no discernible difference in the pitch response, which, as expected, shows the platform motion in the clockwise sense (-ive ψ) to conserve the system angular momentum (Figure 5-3a). In the roll and yaw responses, both of which are much smaller than the pitch excitation, a slight increase in stiffness due to foreshortening is clearly discernible through higher frequency. Note, unlike the roll and yaw, the pitch response is essentially unaffected by the manipulator vibration. Part (b) of the figure studies the vibrational response of the manipulator. Note, δ_1^y is the transverse deflection of the arm in the plane of the rotation, while δ_1^z is the deflection in the out–of–plane direction. These results also confirm the stiffening effect. It should be noted that the fundamental flexural frequency of the manipulator is approximately 3.5 times the rotation rate of the manipulator. This accounts for the significant effect of beam foreshortening.

Next, the stiffness of the manipulator is increased tenfold, resulting in a fundamental bending frequency (ω_1) of 1.56 rad/s. The slewing rate is maintained at 0.1454 rad/s. The results are presented in Figure 5-4 . Note, the pitch response is

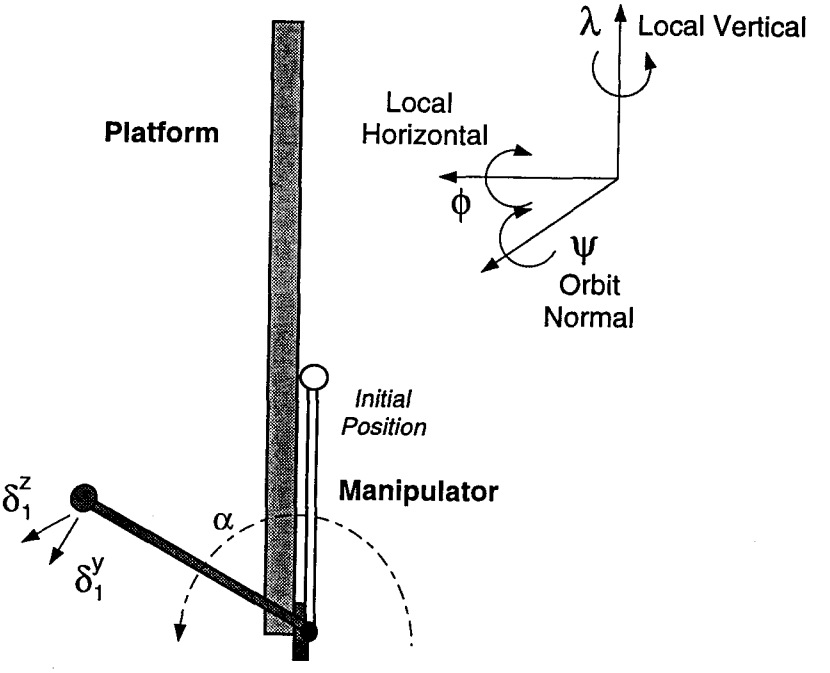

Figure 5-2 Schematic of the rigid space platform with a flexible manipulator.

virtually unchanged from the previous case, when the manipulator was less stiff. The roll response exhibits, logically, a higher frequency of oscillation although the amplitude remains essentially unchanged. The basic trend in yaw is also the same. The responses predicted by the model which incorporates foreshortening are virtually the same as the model which neglects it. The same trend is also reflected in the vibratory response of the manipulator. It is of interest to recognize that the tip deflection perpendicular to the plane of slew (i.e. δ_1^z) is virtually unaffected by foreshortening. However, the manipulator tip deflection in the plane of rotation (i.e. δ_1^y) is quite sensitive to the foreshortening effect in terms of amplitude attenuation. The general

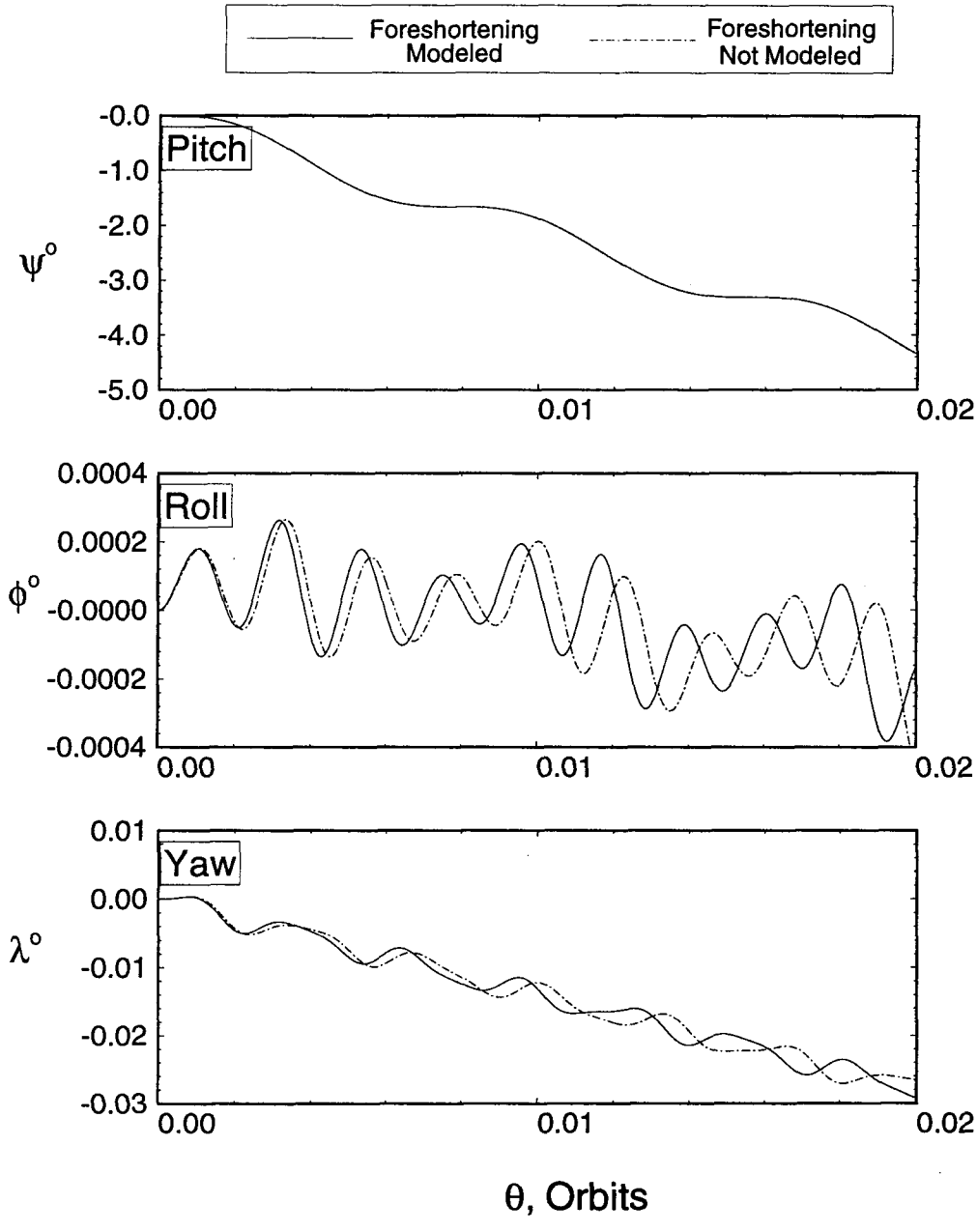

Figure 5-3 Response of a rigid platform with slewing flexible manipulator, $\omega_1 = 0.494$ rad/s: (a) librational time histories.

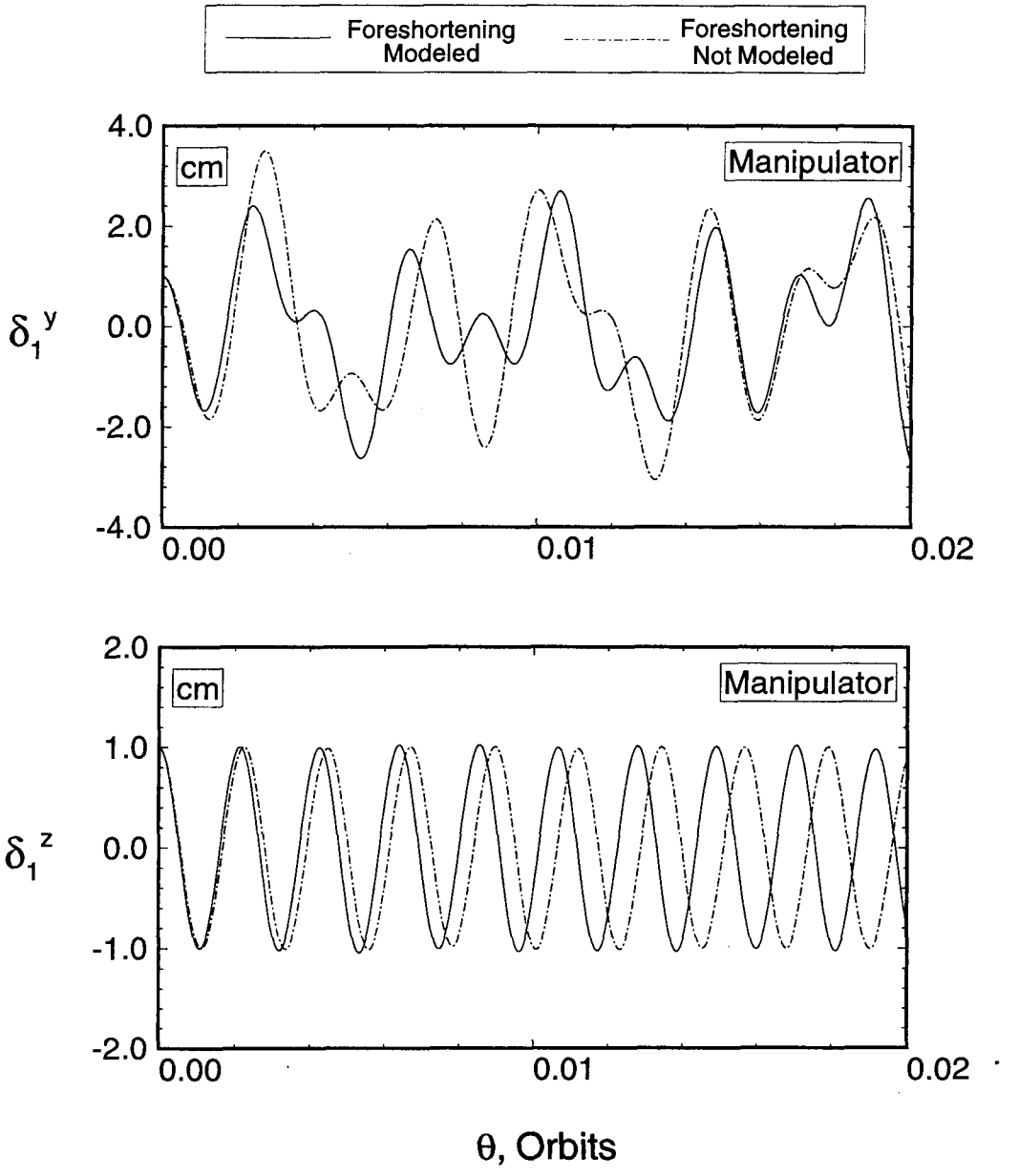

Figure 5-3 Response of a rigid platform with slewing flexible manipulator, $\omega_1 = 0.494$ rad/s: (b) vibrational generalized coordinates.

trend indicates that as the flexural stiffness of the system increases, the foreshortening effect becomes less important. For ω_1 greater than 10 times the frequency of rotation, the increase in stiffness due to foreshortening was essentially absent.

5.2.2 Improved Performance using Quasi–Comparison Functions

The various options for discretizing continuous variable flexible systems to their approximate discrete variable analogues were discussed in Chapter 2. To summarize, the use of Rayleigh–Ritz type approaches, e.g. the method of assumed modes, theoretically guarantees convergence of the solution as more admissible functions are used. Admissible functions, which only satisfy the geometric boundary conditions of the system, are attractive because of their abundance. On the other hand, comparison functions, which satisfy both the geometric and the natural boundary conditions are relatively limited in number.

The poor convergence often observed with the use of admissible functions may be attributed to the fact that, in some cases, no finite set of these functions is capable of satisfying the natural boundary conditions. Meirovitch and Kwak [93–95] have shown that the use of quasi–comparison functions can improve the convergence. These functions, individually, do not satisfy both types of boundary conditions but do so as a whole. Typically, a set of quasi–comparison functions is formed by augmenting admissible functions with a set of functions which satisfy the natural boundary conditions. It is common to select eigenfunctions of a closely related problem as the admissible functions. Similarly, the second set of functions constituting the quasi–comparison functions are also often chosen as eigenfunctions of related systems.

The improvement in modeling multibody systems has been demonstrated by Meirovitch and Kwak [94] on a ground–based planar frame–type structure resembling an inverted "U". Various combinations of beam eigenfunctions were used to

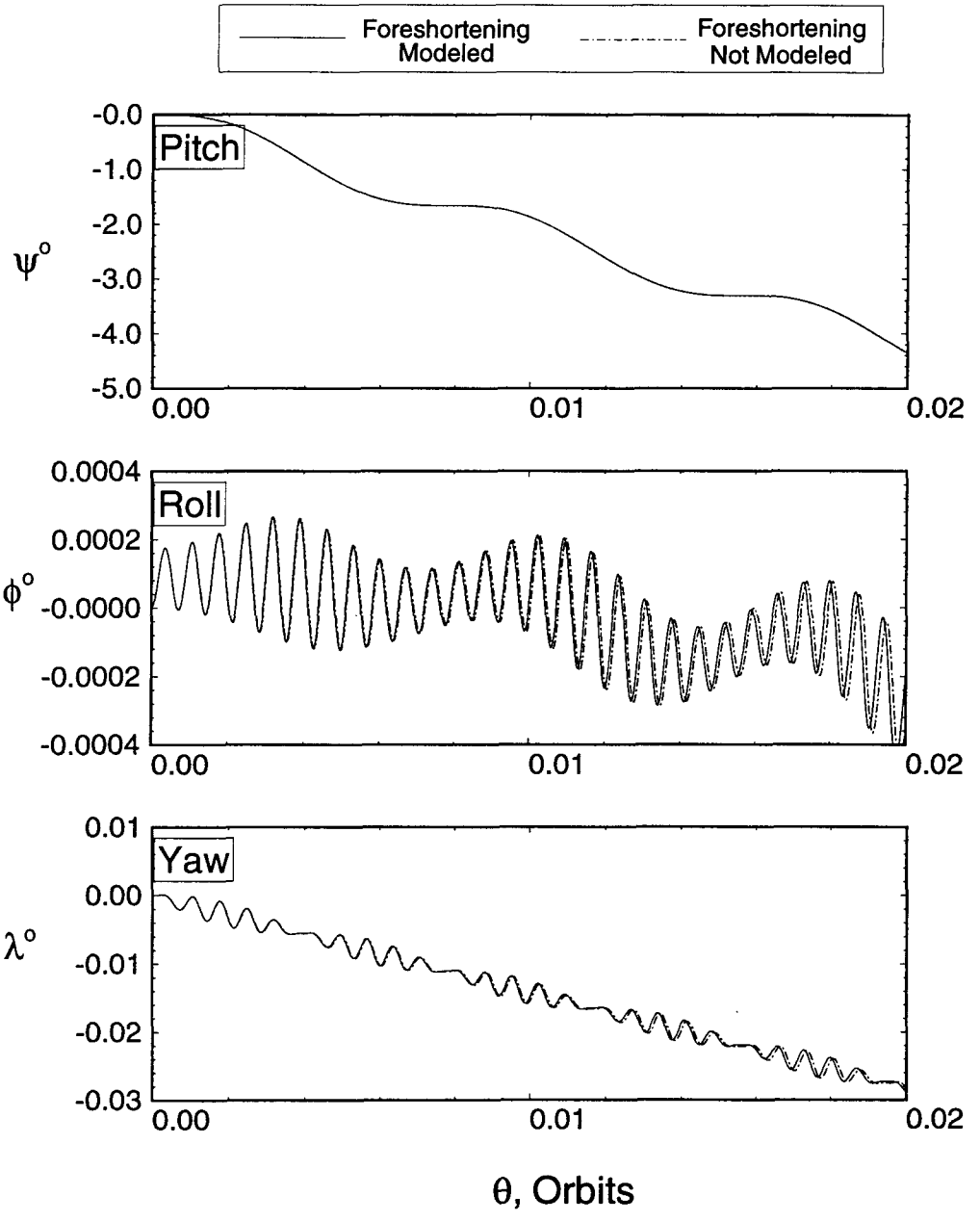

Figure 5-4 Response of a rigid platform with slewing flexible manipulator, $\omega_1 = 1.56$ rad/s: (a) librational degrees of freedom.

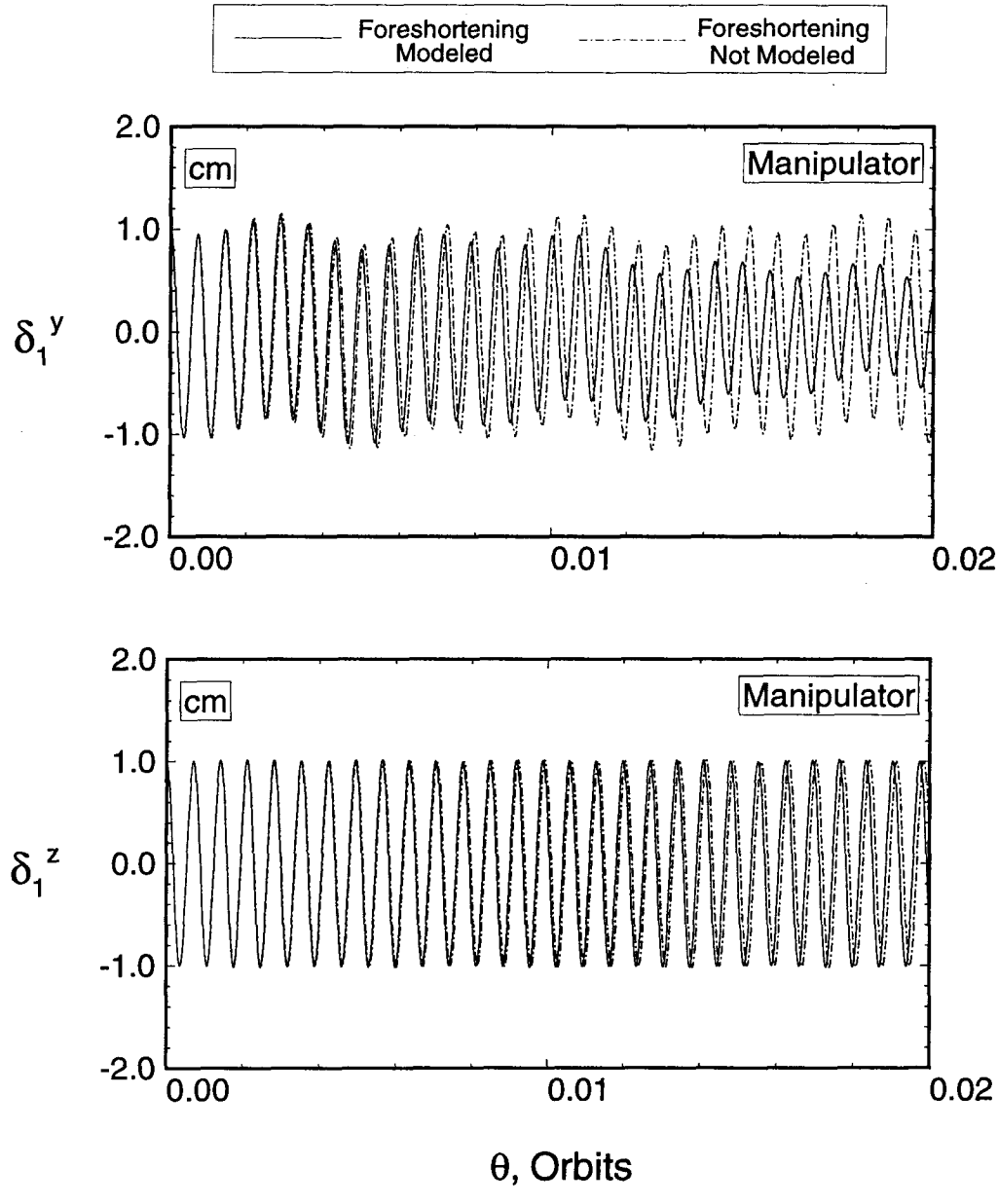

Figure 5-4 Response of a rigid platform with slewing flexible manipulator, $\omega_1 = 1.56$ rad/s: (b) vibrational generalized coordinates.

form the set of quasi–comparison functions for each of the 3 components of the structure. The results generally indicate good matching of natural boundary conditions at the interfaces of the constituent beams.

In the present study, a flexible space platform with a slewing flexible manipulator is used to investigate the convergence of quasi–comparison function based discretization for orbiting space structures with time–varying geometry. The system is similar to the one employed in the previous subsection (5.2.1). The beam–like platform is placed in a gravity gradient configuration in a circular orbit at an altitude of 400 km. The manipulator is placed at the nadir end of the platform and performs slewing maneuver of 180° in 2 minutes. The manipulator, which has a mass of 150 kg and a tip (payload) mass of 50 kg, commences the sinusoidal–ramp maneuver while oriented toward zenith and terminates it oriented towards nadir. Simulations are carried out using 2 and 3 shape functions each for the platform and manipulator, both of the admissible function (AF) and quasi–comparison function (QCF) variety. The admissible functions for the platform are free–free Euler–Bernoulli beam eigenfunctions, while those for the manipulator represent clamped–free beam modes. These admissible functions are augmented by the clamped–free and clamped–clamped beam modes to form the set of quasi–comparison functions for the the platform and manipulator, respectively. For example, when 2 shape functions were used for the platform, the QCF solution employed the first free–free and the first clamped–free eigenfunctions. For the 3 shape functions case, the first two free–free and the first clamped–free eigenfunctions were used to form the QCF set. The physical characteristics of the system are given in Table 5-2 , and a schematic of the system is shown in Figure 5-5 .

The simulation results for the case when 2 AF's are used for the power boom and the manipulator are shown in Figure 5-6 . The librational response indicates, as

Table 5-2 Physical characteristics of the flexible space platform with a flexible manipulator

Body	Length (m)	Mass (kg)	EI (N-m^2)	I_{xx} (kg-m^2)	I_{yy} (kg-m^2)	I_{zz} (kg-m^2)
Platform	60	3000	1.0×10^7	2.5×10^4	9.0×10^5	9.0×10^5
Manipulator	15	150†	5.0×10^4	400	1.125×10^4	1.125×10^4

† excluding the payload mass

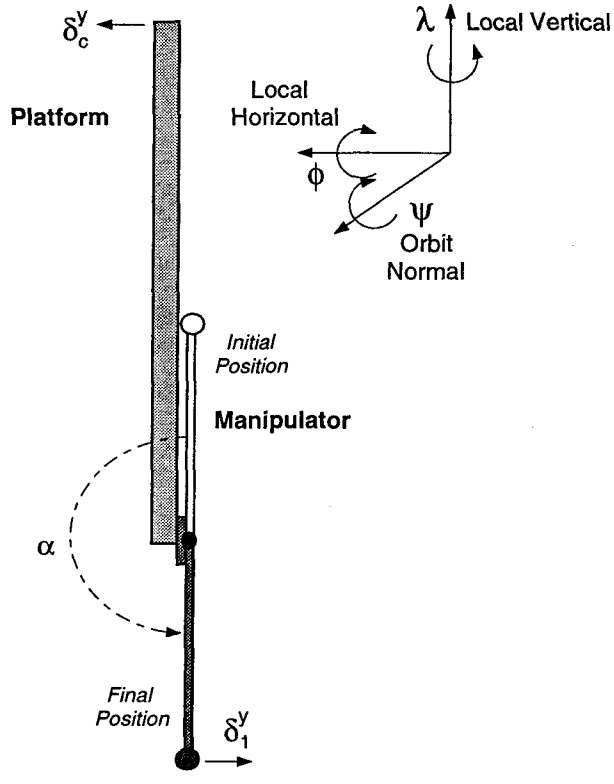

Figure 5-5 Schematic of the flexible space platform with a flexible manipulator.

expected, that only the pitch motion is excited by the maneuver. The pitch degree of freedom experiences a peak deviation of approximately 1.5°. The vibrational response

suggests that the maximum tip deflection of the power boom is only 1 mm, however that of the manipulator is about 4 cm! Note, the deflections during the maneuver are considerably greater than those during the post–maneuver phase. It may be pointed out that no structural damping is assumed.

In order to assess how well the natural boundary conditions are satisfied, the bending moments at the base of the manipulator and the tip of the platform were computed. These results are shown in part (b) of the figure. As expected, the bending moment at the power boom end is zero because of the free–free shape functions used. The manipulator's bending moment time history which has a peak value of about 40 N-m, is quite similar to its tip deflection response, except for the 180° phase difference. This is consistent with the physics of the problem, because as the manipulator is accelerated from rest, the tip tends to lag the base. The situation is reversed as the manipulator decelerates back to rest.

Next, the simulation was run using two QCF's for the platform and manipulator (Figure 5-7). There is no discernible difference between the pitch response for this case and the one presented before. The same is true for the manipulator response. However, there is a considerable difference in the power boom tip response. While the shape of the response is similar, it appears to be magnified by a factor of 4. Furthermore, now the bending moment shows very good agreement, both in the maneuver and post–maneuver phases.

The results for the simulation with three AF's are presented in Figure 5-8 . These are essentially indistinguishable from the two admissible functions case. There is, however, some departure in the power boom's peak tip deflection (at around 0.0015 orbits), with the three shape functions case predicting a larger value.

The final case considered involved 3 QCF's. The simulation results are given

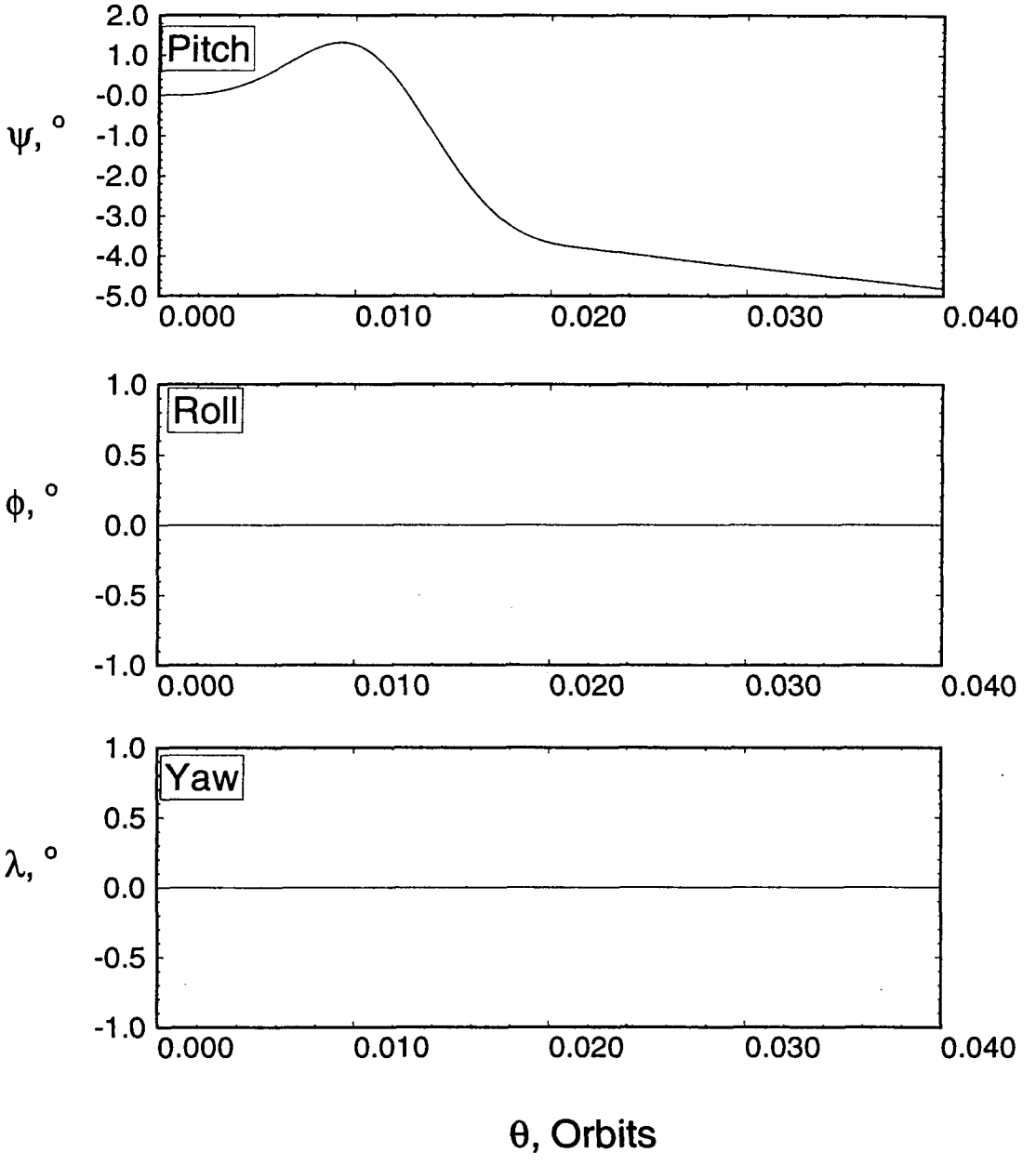

Figure 5-6 Response of the flexible platform to a slewing flexible manipulator using two admissible functions for discretization: (a) librational response.

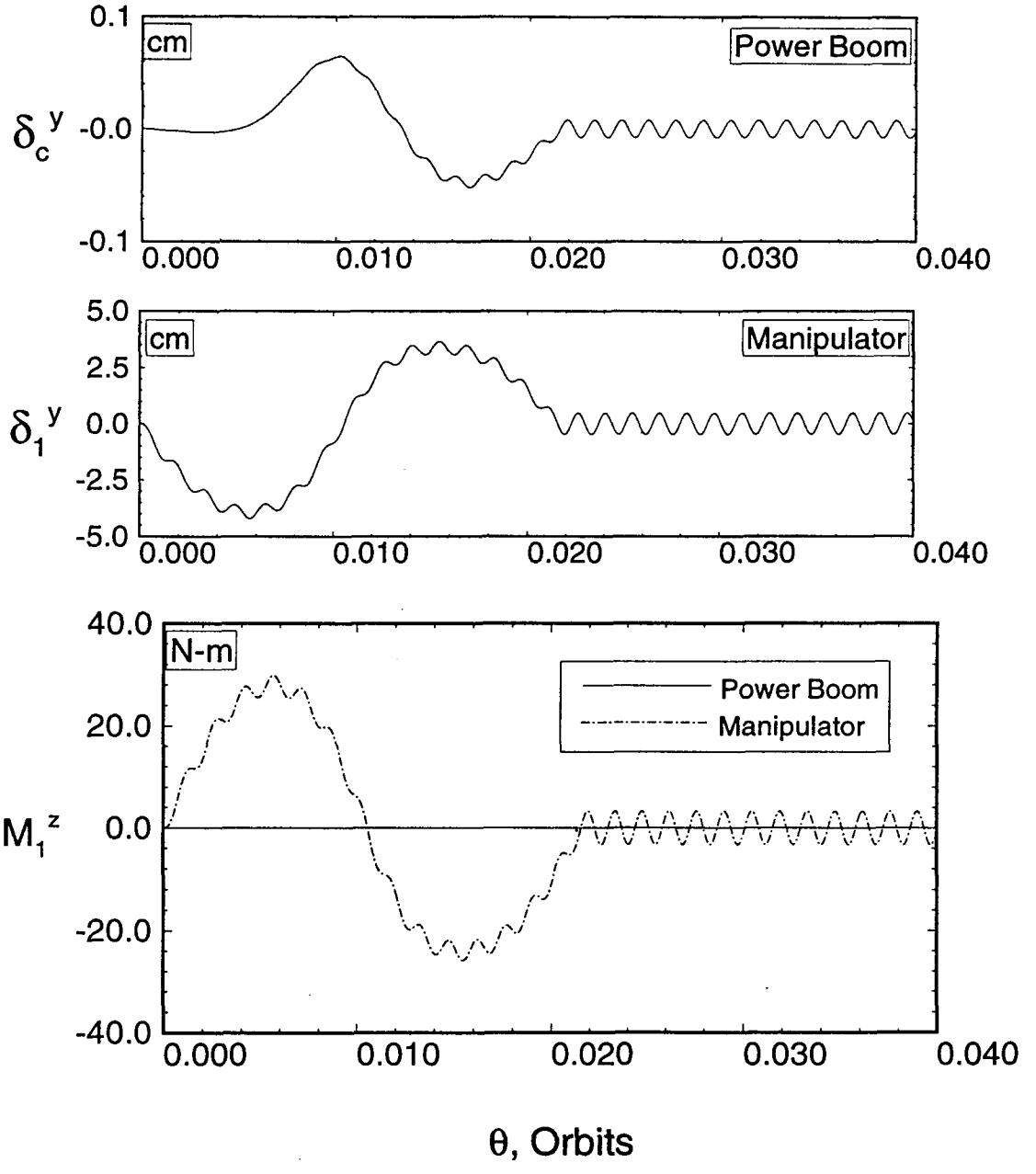

Figure 5-6 Response of the flexible platform to a slewing flexible manipulator using two admissible functions for discretization: (b) vibrational and bending moment response.

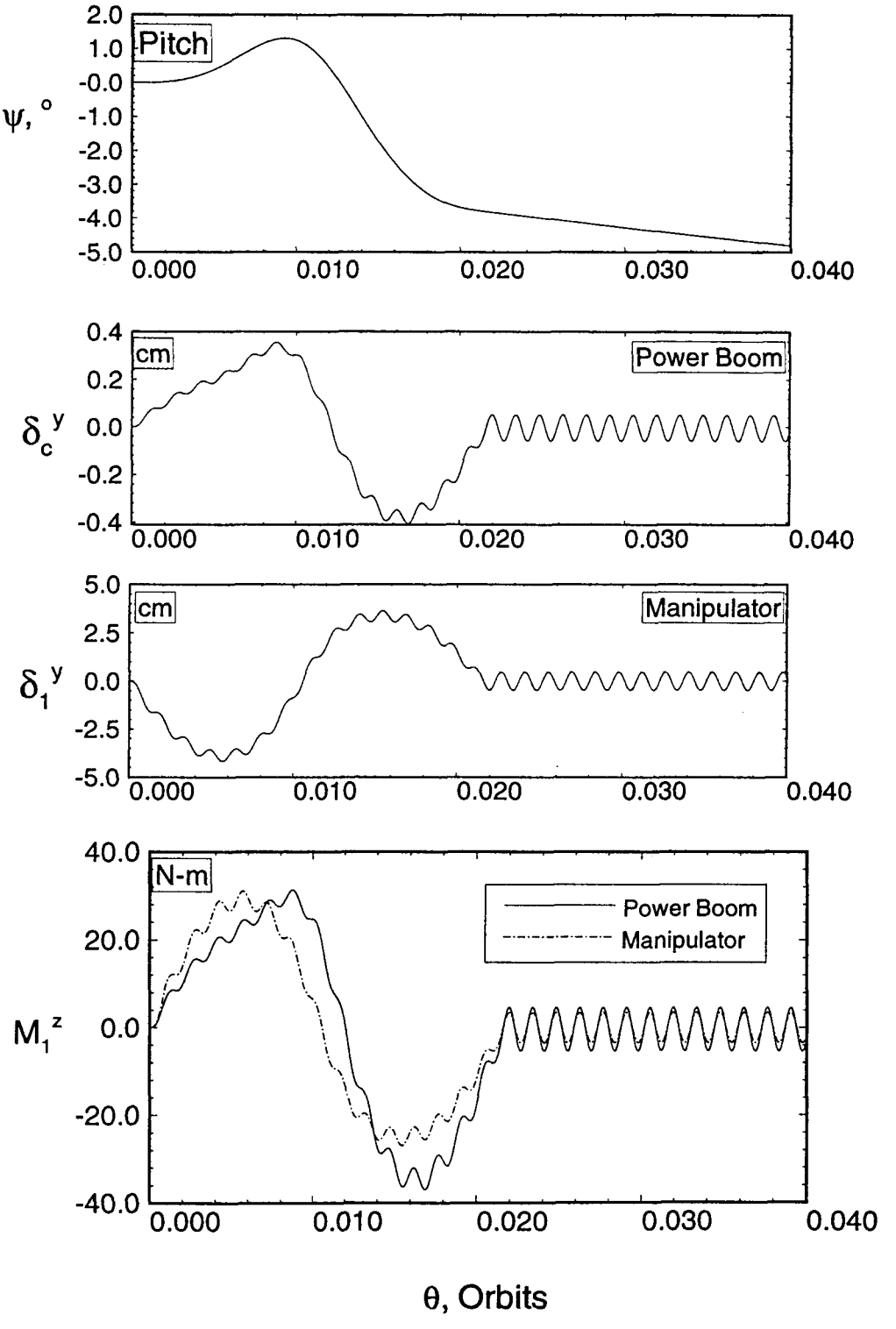

Figure 5-7 Response for the flexible platform with slewing flexible manipulator using two quasi–comparison functions.

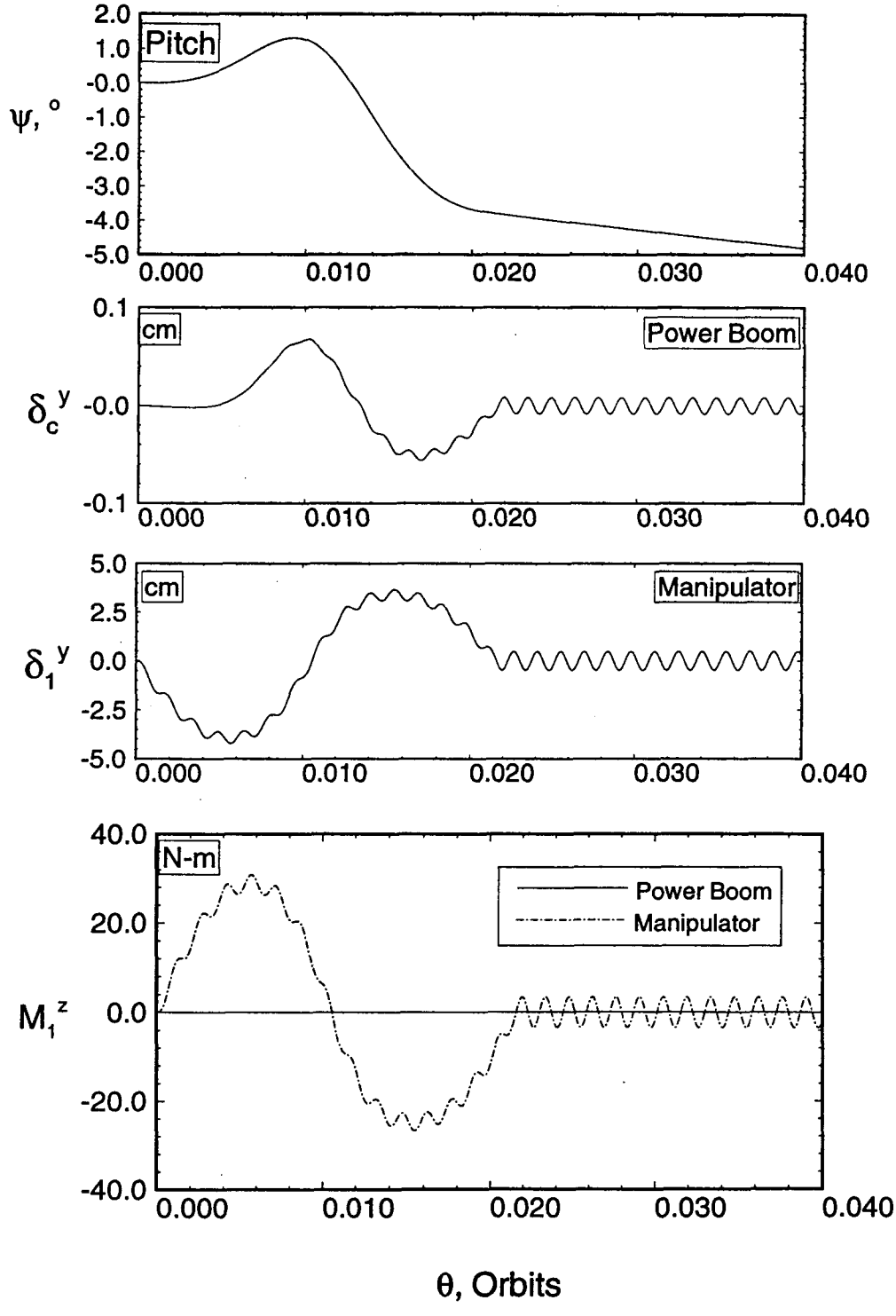

Figure 5-8 Response for the flexible platform with slewing flexible manipulator using three admissible functions.

in Figure 5-9 . The response is close to the 2 QCF case, although there are some noteworthy differences. For the platform tip deflection, the 3 QCF case predicts lower peak values during the maneuvering phase, however the correlation is rather good subsequently. There also appears to be some high frequency modulations of the platform response at around 0.01 orbits, however, it attenuates rather quickly. For the bending moment, there is a slightly better agreement compared to the two QCF case. The pitch and the manipulator tip deflection responses compare rather well.

The results indicate that in some cases, the performance of conventional discretization methods, such as the method of assumed modes, when applied to interconnected, flexible bodies, can be improved by augmenting the standard admissible functions with ones which satisfy the natural boundary conditions. These auxiliary functions themselves need not even satisfy the geometric boundary conditions. The totality of these augmented functions, called quasi–comparison functions, however, are capable of satisfying all the boundary conditions. This approach was applied here successfully to an orbiting flexible space platform with a flexible slewing manipulator. Moreover, the results suggest an accurate prediction of the response by employing relatively few shape functions.

5.3 First Element Launch (FEL)

The response of the FEL configuration of the proposed Space Station to various librational and vibrational initial conditions were studied by Ng [13]. As seen earlier his results were used in validating the flexible multibody spacecraft model and code developed in this study.

As pointed out earlier, the Space Station will be subject to numerous disturbances, both of the natural and operational variety. Operational disturbances include crew activity, the docking of the space shuttle, and the maneuvers of the remote manipulator

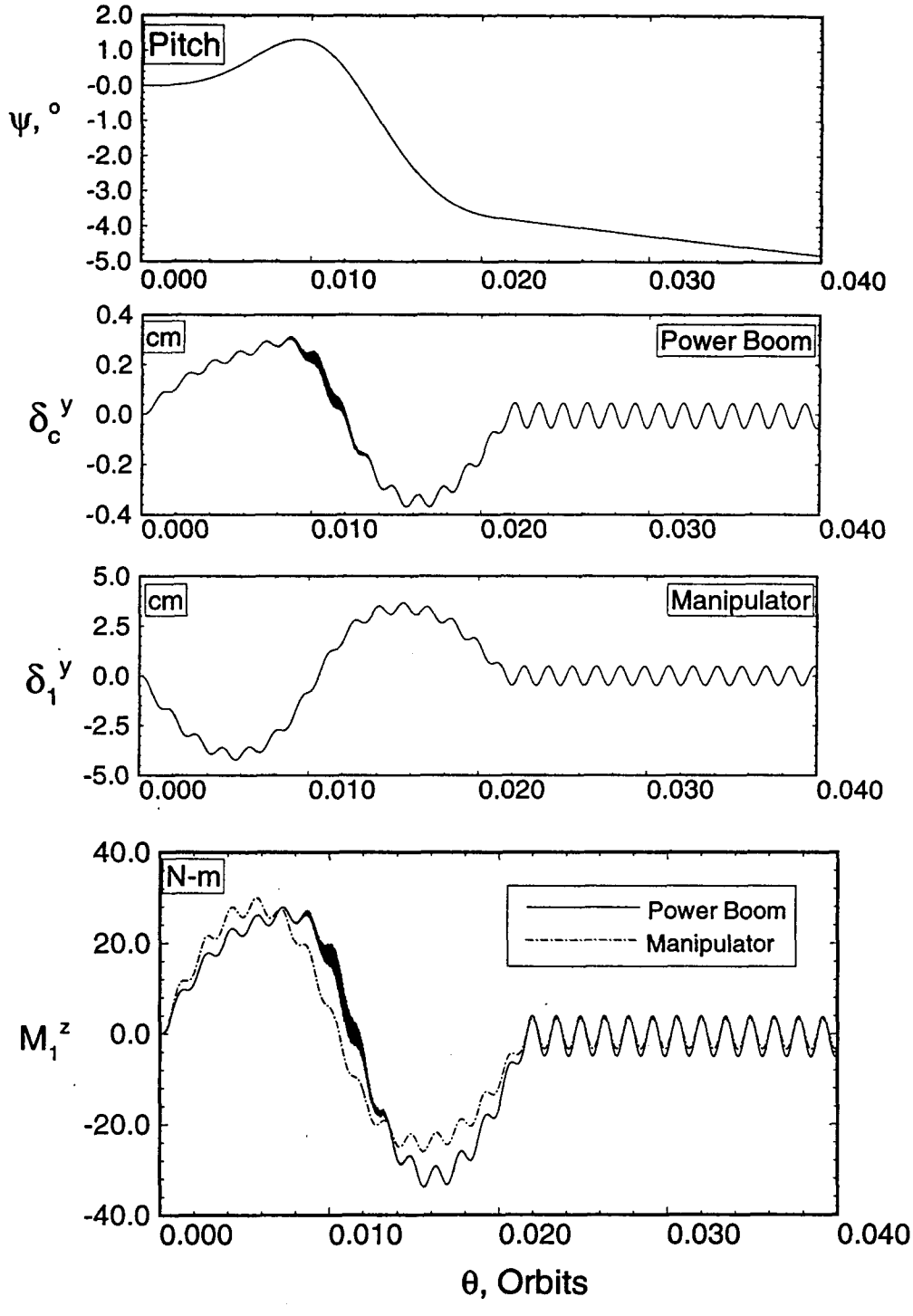

Figure 5-9 Response of the flexible platform with a slewing flexible manipulator using three quasi-comparison functions.

system. Response of the latter two types of operational disturbances is investigated in this section.

5.3.1 Responses to docking of the Space Shuttle

The physical characteristics of the FEL were given in Table 3-1 and a schematic diagram of the system was shown in Figure 3-9. It is important to note that the system is placed in a nonequilibrium orientation which is unstable in the librational degrees of freedom. The equilibrium orientation of the system was found to be: $\psi_e = 0$, $\phi_e = 0$, $\lambda_e = 0.74°$. Therefore, a control system would have to be designed to stabilize the system. The synthesis of control systems for the Space Station is investigated in the following chapter. Here, the open loop response of the FEL to the docking of the Shuttle is considered.

The orbiter berthing is a complicated process. Docking units are designed to soften the impact [113]. One docking mechanism, consisting of active and passive units, is based on the one used in the Apollo–Soyuz project. The active element, located on the orbiter, incorporates an attenuator supported standoff ring which engages and latches the passive unit mounted on the Space Station.

A detailed model of the dynamics of the docking procedure is still not established. For the purposes of this investigation, it is modeled as follows. An average docking force, along with a docking time interval, and the direction of approach are considered as specified. For the duration of the docking process, non–conservative generalized forces are computed and incorporated in the dynamics model. At the end of that interval, the system mass and inertias are recomputed to include the effect of the docked orbiter, which is modeled as a rigid body.

The properties of the shuttle are obtained from NASA report SSE-E-88-R8 [114].

The mass of the orbiter is taken to be 9×10^4 kg with the inertia matrix as:

$$\mathbf{I}_{ss} = \begin{bmatrix} 1.09 \times 10^6 & 0 & 3.2 \times 10^5 \\ 0 & 8.65 \times 10^6 & 0 \\ 3.2 \times 10^5 & 0 & 8.38 \times 10^6 \end{bmatrix} \text{kg-m}^2.$$

A diagram of the orbiter is shown in Figure 5-10 . For the simulation, the power boom is modeled as a free–free beam, while the stinger is taken to be a cantilever beam. The PV radiator and the PV arrays are modeled as cantilever plates. A single generalized coordinate is employed for the discretization of the plates, while two modes are used for the beam–type members in each transverse direction. The orbital perturbations are also modeled. Thus, a total of 32 degrees of freedom are considered. The orbiter is assumed to approach the Space Station in the direction opposite to the local horizontal (i.e. the $-Z$ direction). Two cases are considered: the average force transmitted during docking to be 200 N or 2000 N. In both the cases, docking commences at $\theta = 0.01$ orbit and its duration is 1 s. The docking ring is taken to be situated at the stinger end of the power boom, i.e. 27.5 m from its center.

The results for the first case are shown in in Figure 5-11 . Although all the librational d.o.f. are excited, the yaw is affected most, reaching a value of almost 30° within 0.09 orbit. Given the relatively large moment–arm to the docking force with respect to the c.m., this is as expected. Moreover, the fact that the docking procedure results in an impulsive loading is verified by the yaw response which demonstrates a constant angular rate. The coupling between the librational d.o.f. is responsible for the pitch and roll motion.

The vibrational responses of the power boom and the stinger are given in part (b). The power boom is excited mainly in the z_c transverse direction. Again, this is the anticipated results as the docking impact takes place in this direction. The tip

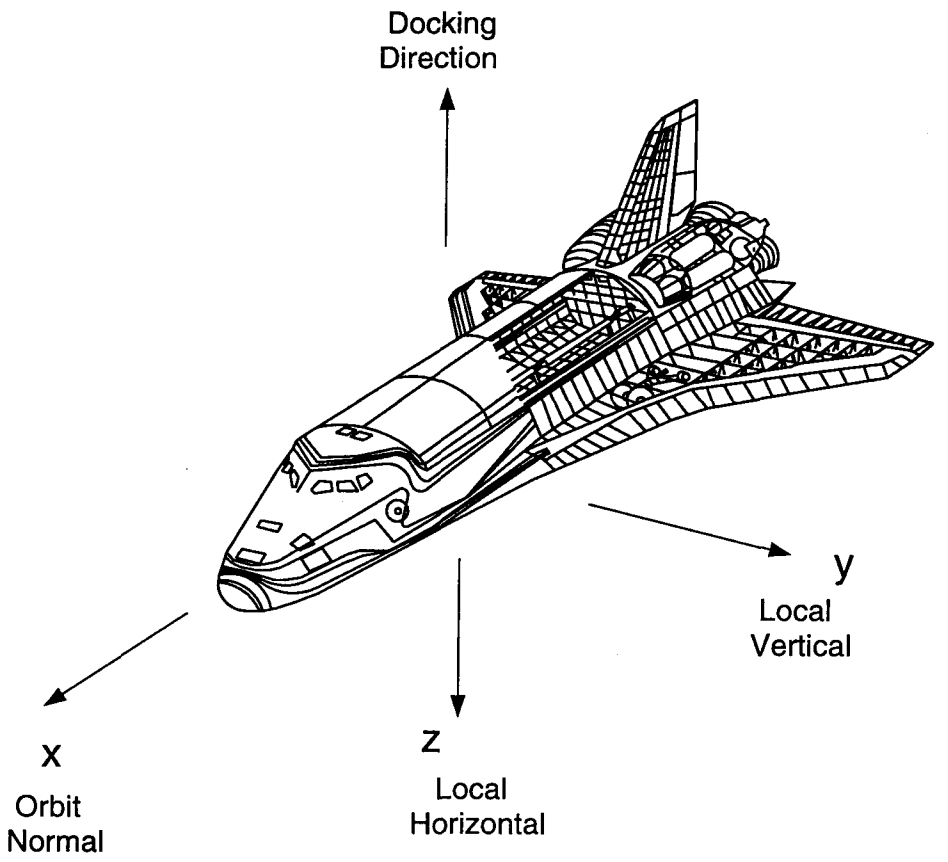

Figure 5-10 A diagram of the Space Shuttle showing the docking direction.

excitation in the z_c direction is approximately 0.4 mm compared to around 5×10^{-3} mm in the y_c direction. The power boom vibrates at a frequency significantly lower than the computed fundamental free–free beam frequency (1.93 Hz) because of the presence of the docked orbiter. The observed frequency of vibration for the power boom is 0.65 Hz. The analytically computed fundamental frequency for a beam with a rigid body corresponding to the orbiter mass at one end is 0.53 Hz. The small

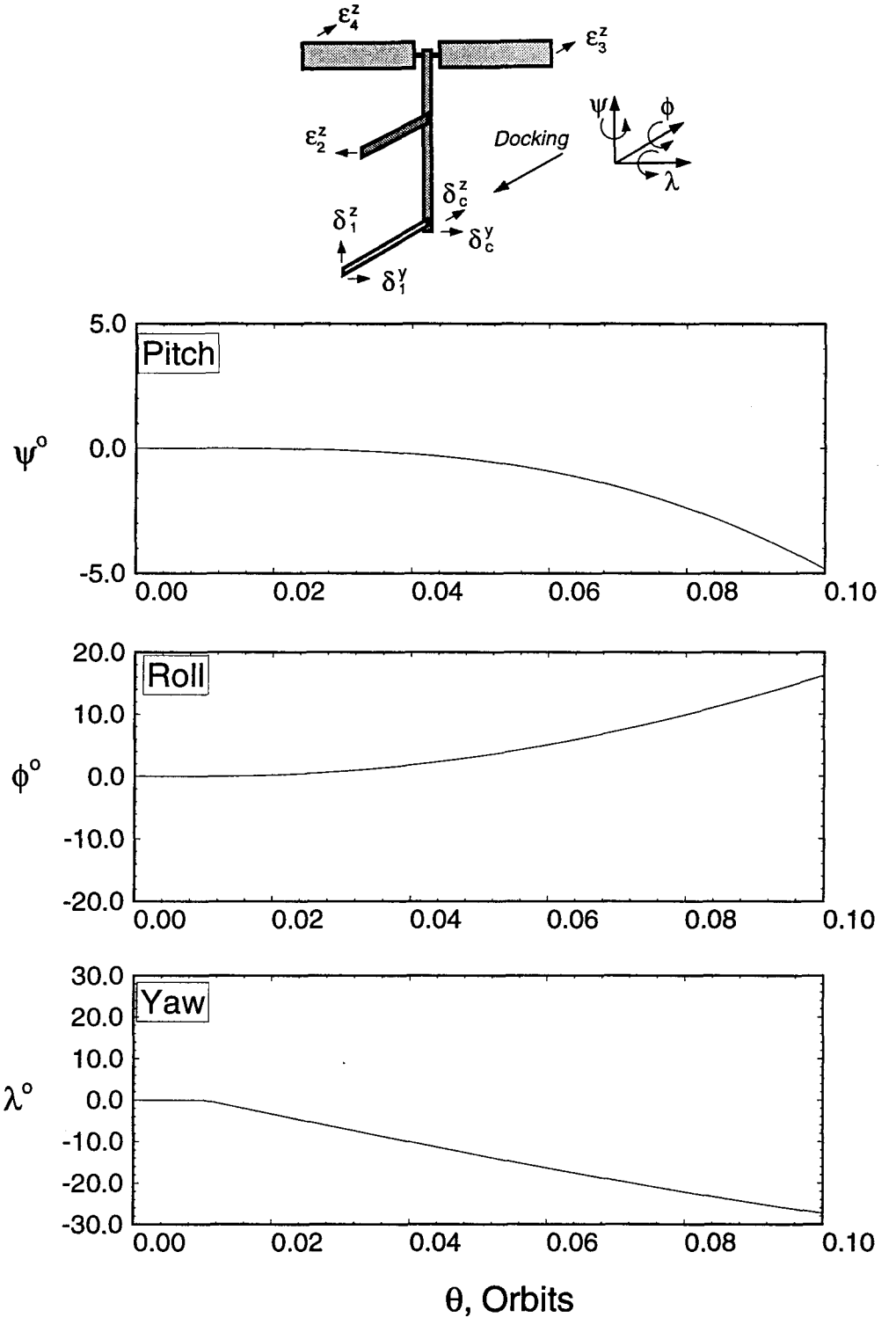

Figure 5-11 Response to the orbiter docking, $F_{av} = 200$ N: (a) librational time histories.

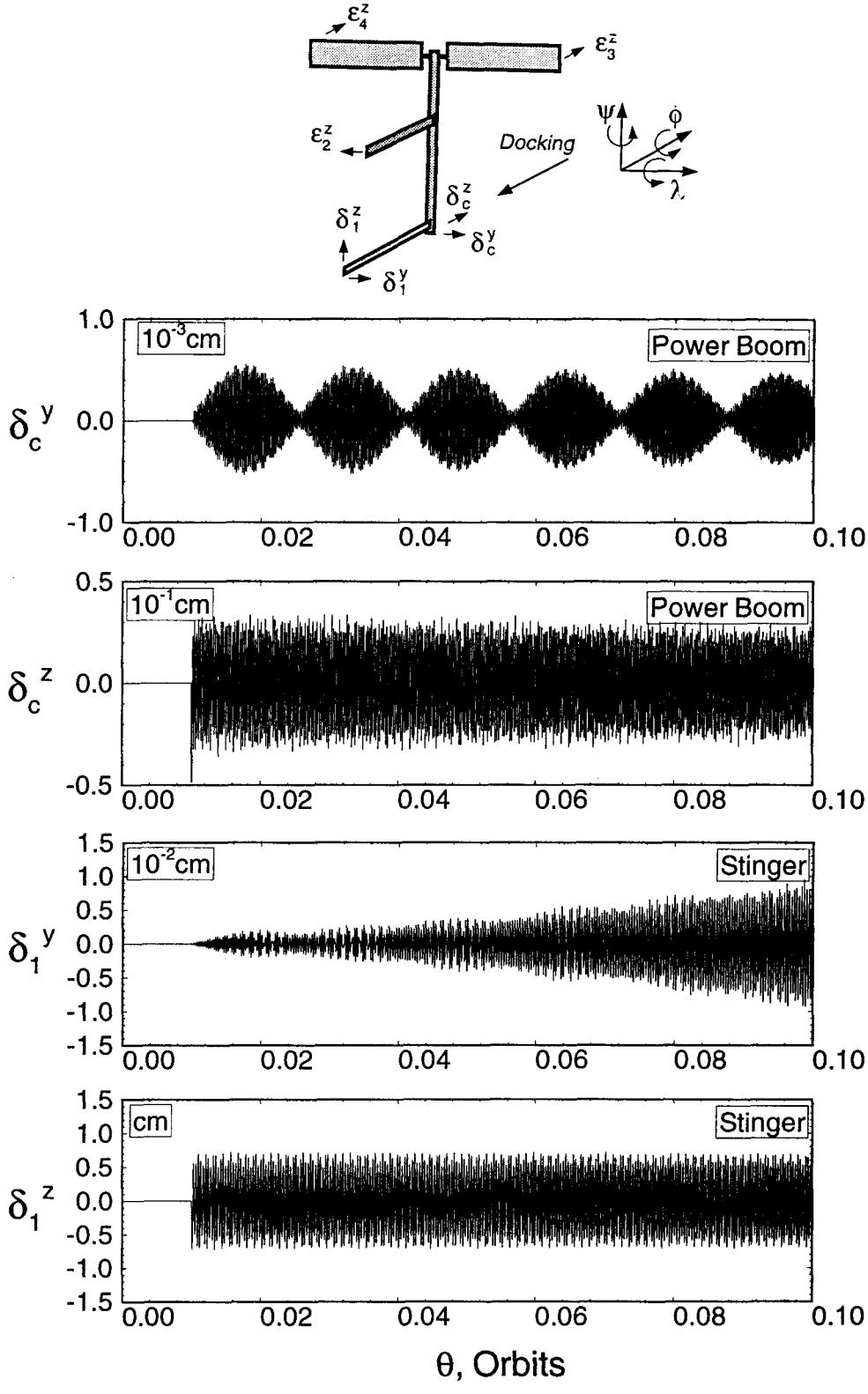

Figure 5-11 Response to the orbiter docking, $F_{av} = 200$ N: (b) power boom and stinger tip deflections.

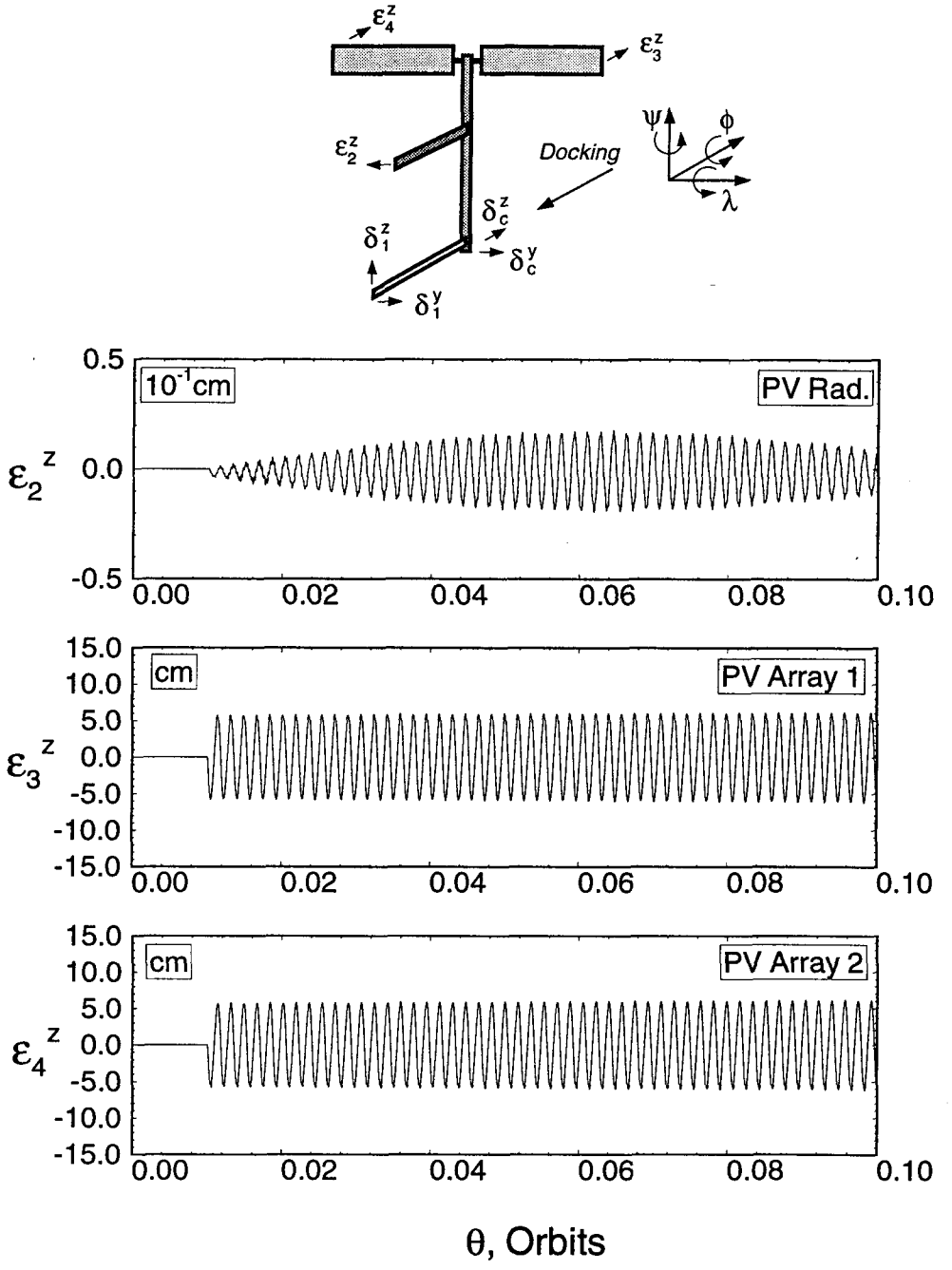

Figure 5-11 Response to the orbiter docking, $F_{av} = 200$ N: (c) PV radiator and array tip vibrational histories.

difference is attributed to the free–free shape functions used in the discretization. The stinger's vibration in the z_1 direction is excited principally by the rotational motion due to flexure of the power boom at the stinger's attachment point. The stinger's response in the other transverse direction grows with time suggesting that it is excited through coupling with the pitch motion which has an increasing angular rate.

The responses of the PV radiator and arrays are presented in part (c) of the figure. The tip deflections of the arrays are significantly greater than that of the radiator. Again, these are caused by the rotation of the power boom due to flexure. It is apparent that this rotational motion tends to excite the arrays in their transverse direction, but has no effect on the PV radiator in its transverse direction. Hence, the maximum array tip deflection is around 6 cm while that of the radiator is less than 0.3 mm.

Next, the average docking force is increased to 2000 N, while the time interval is maintained at 1 s (Figure 5-12). The trends are essentially the same as before except for the oscillatory character of the pitch and roll responses. The pitch and yaw librations are approximately 10 times larger than the previous case, which is consistent with the fact that the impulse in this case is 10 times greater. The power boom response also exhibits the same trend with approximately a tenfold increase in amplitude. The beat–type character of the power boom vibration, suggesting interaction between closely spaced frequencies, degenerates to a more conventional response by 0.1 orbit. The stinger response is also significantly higher, as expected. The behaviour of the PV radiator and arrays are similar in nature to the previous case, with amplitudes 10 times greater in the case of the array responses, and almost 100 times higher for the radiator response. Among the structural members, tip deflections

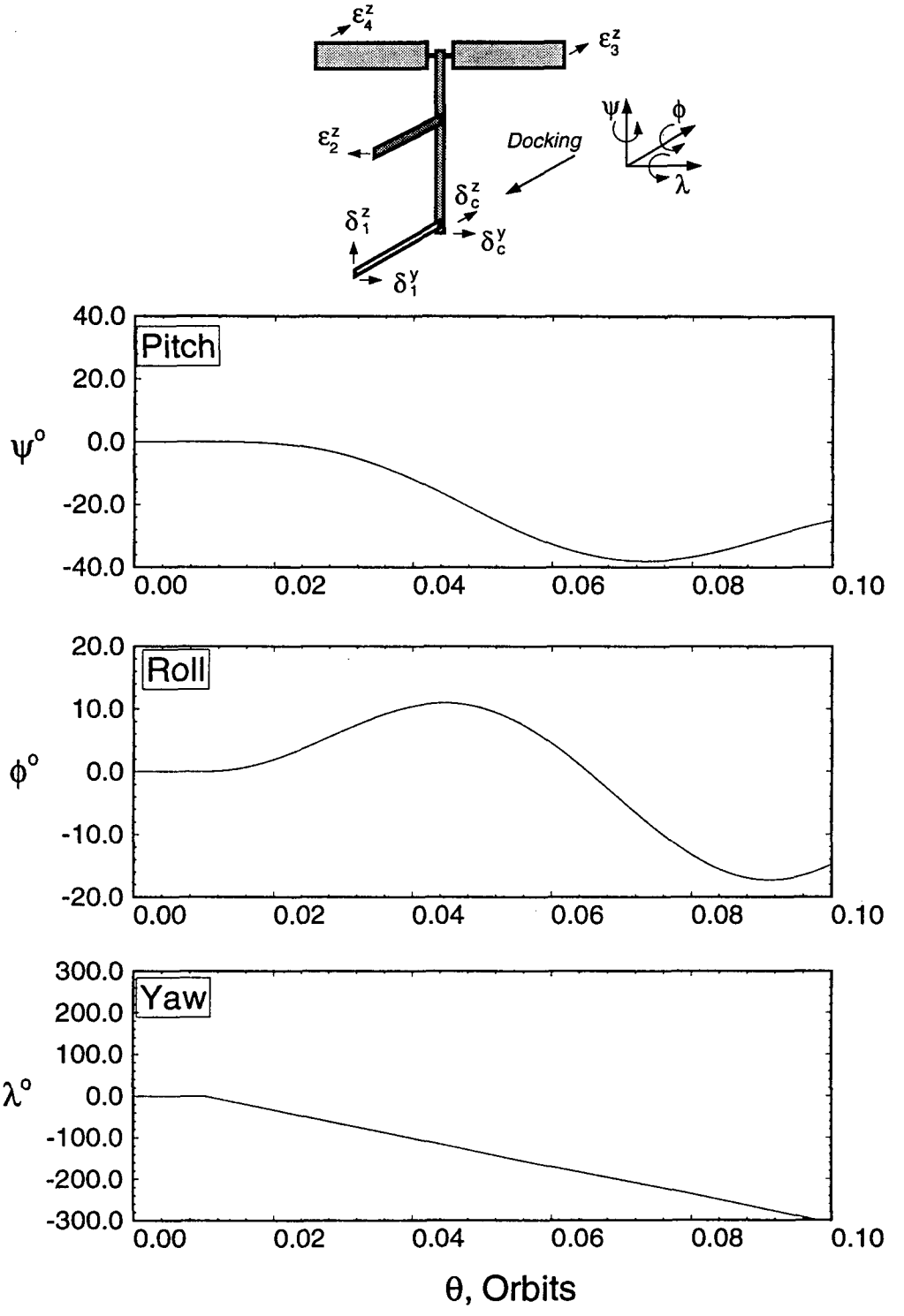

Figure 5-12 System response to the orbiter docking, $F_{av} = 2000$ N: (a) librational time histories.

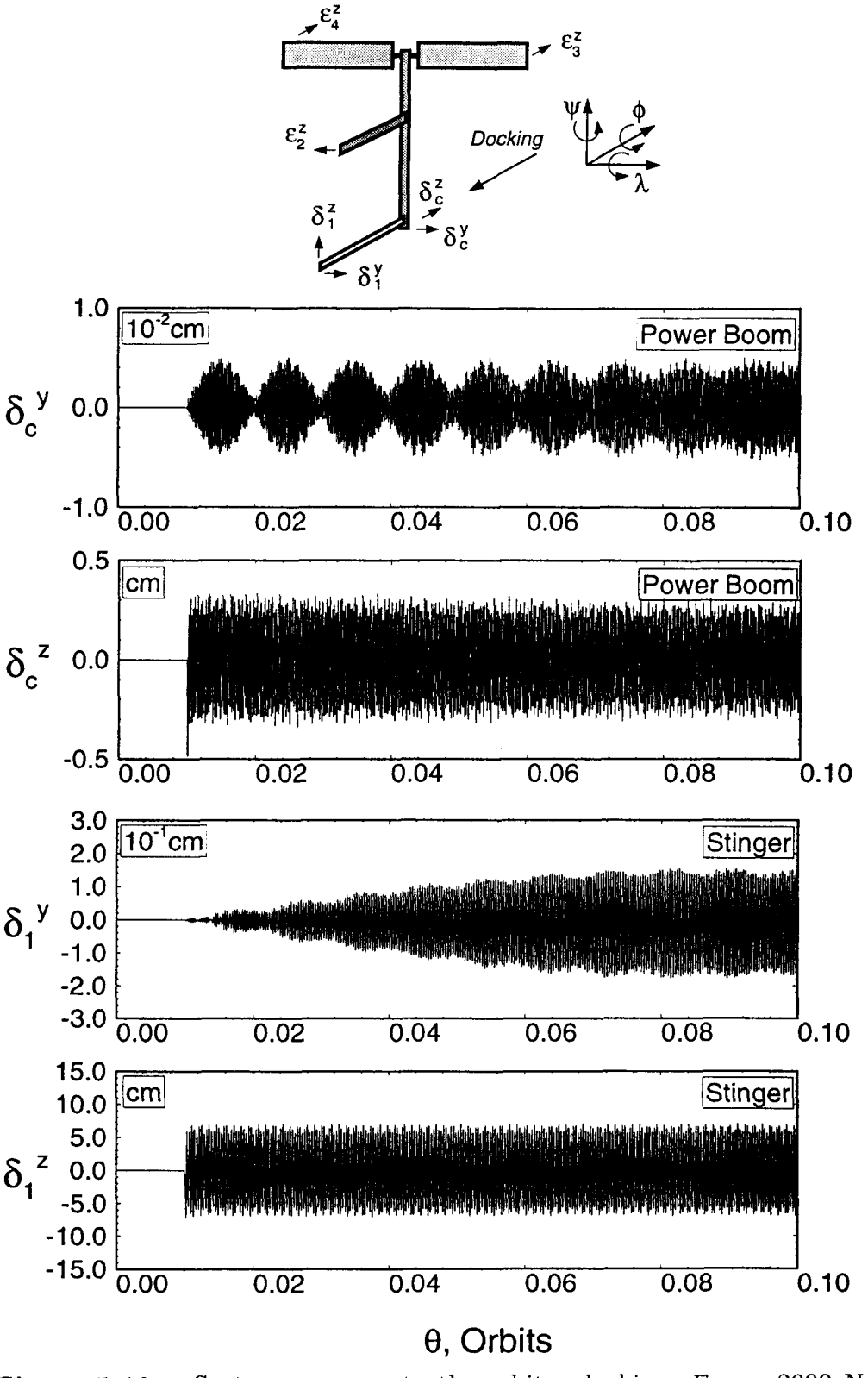

Figure 5-12 System response to the orbiter docking, F_{av} = 2000 N: (b) power boom and stinger tip deflections.

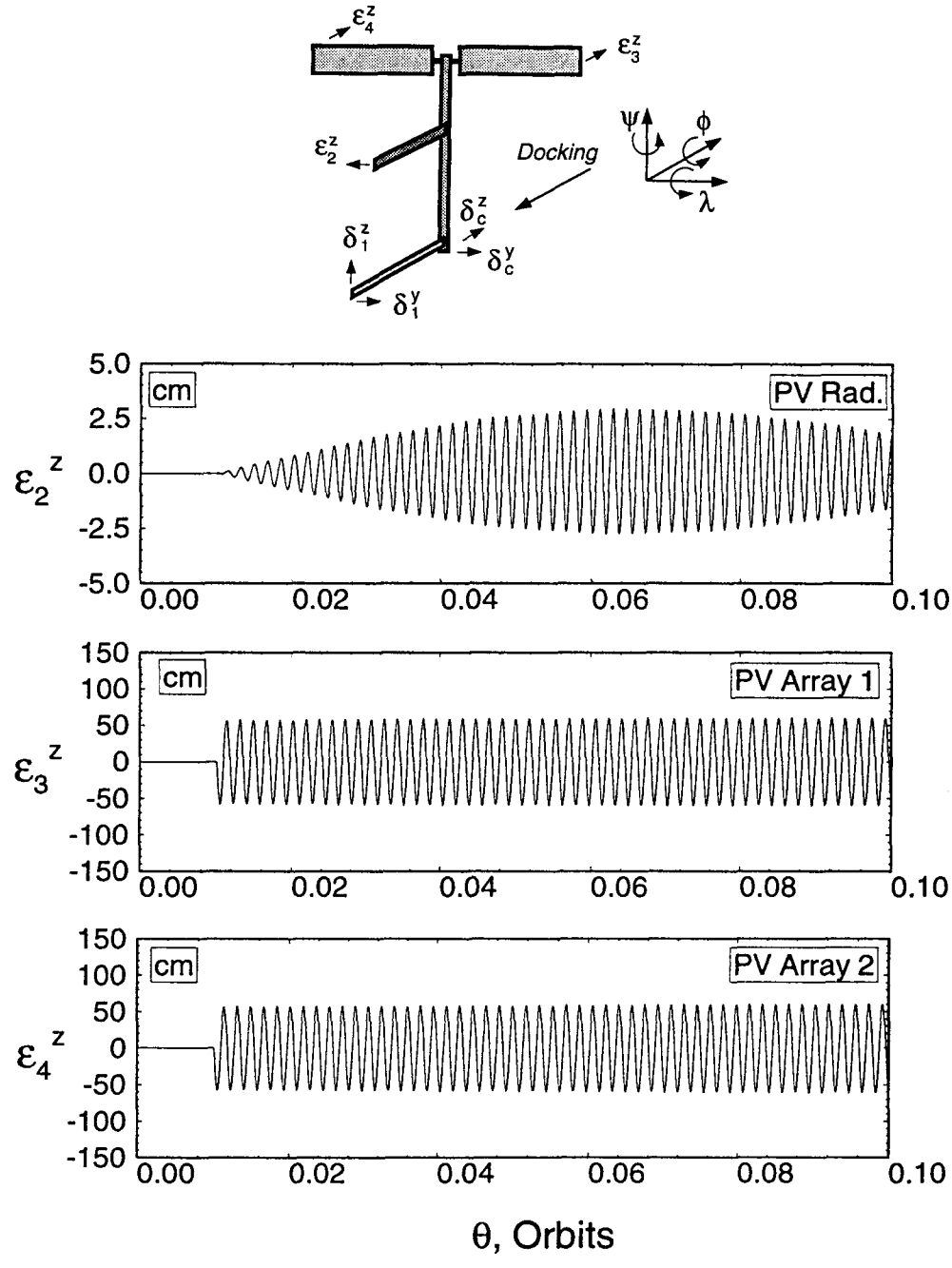

Figure 5-12 System response to the orbiter docking, $F_{av} = 2000$ N: (c) PV radiator and array tip deflections.

of the solar arrays were the highest, i.e. over 50 cm.

As expected, the results show that the docking of the space shuttle represents a major disturbance to the space station. A relatively modest impact force of 200 N for a duration of 1 s is sufficient to cause significant librational and vibrational motions. The need for active control of the librational d.o.f.'s has already been established. The above results suggest that the active control of the vibrational d.o.f.'s may also be required.

5.3.2 Response to manipulator maneuvers

In addition to operational maneuvers, the Space Station based manipulator will also be employed during the construction of the Station. It is envisaged that a manipulator system will be exploited even at the FEL stage of the evolving Space Station. Thus the operation of such a robotic system will constitute a significant disturbance. The physical characteristics of the manipulator considered in the simulation are given in Table 5-3 . The payload is represented by a point mass of 800 kg at its tip.

Table 5-3 Physical characteristics of the FEL manipulator

Body	Length (m)	Mass (kg)	EI (N-m^2)	I_{xx} (kg-m^2)	I_{yy} (kg-m^2)	I_{zz} (kg-m^2)
Manipulator	7.5	800*	5×10^5	45	6.0×10^4	6.0×10^4

* excluding payload mass of 800 kg

The effect of a typical maneuver of the manipulator on the dynamics of the Station is investigated by simulating a combined translation and rotation maneuver shown in Figure 5-13 . The base of the manipulator is initially situated 15 m from the center of the power boom (towards the solar panels), with the the long axis of the manipulator located along the orbit normal. The manipulator slews in the plane defined by the

orbit normal and local horizontal through 180°, while its base translates by 30 m along the power boom towards the stinger end. Both the translation and rotation profiles are taken to be of the sine–on ramp type, and the maneuver is completed in 60 s. Note that the fundamental flexural frequency of the manipulator is approximately 4.3 rad/s, while its average rotational speed is only about 0.05 rad/s. Therefore, the foreshortening effect can be neglected.

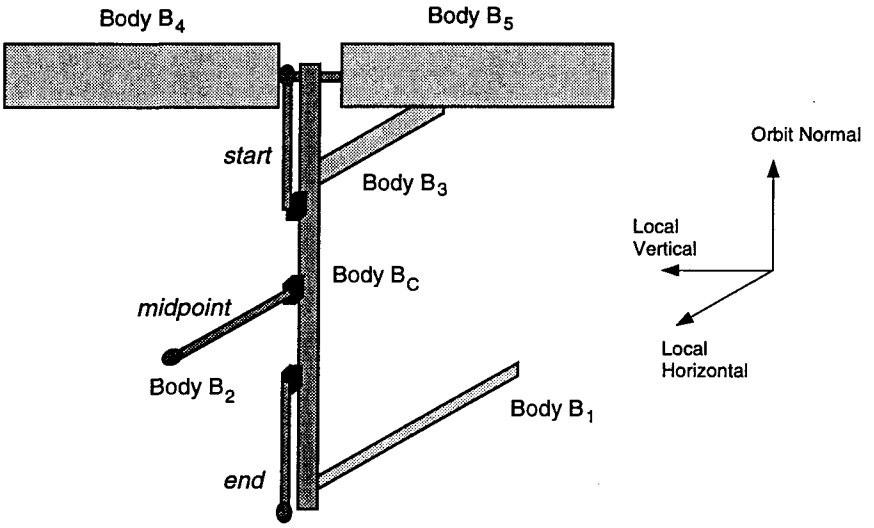

Body	Description
B_C	Power Boom
B_1	Stinger
B_2	Manipulator
B_3	PV Radiator
B_4, B_5	PV Arrays

Figure 5-13 Schematic of the FEL configuration showing a combined slew–translation maneuver of the manipulator.

Three cases are investigated corresponding to one, two, or three shape functions employed for discretizing the flexible nature of the power boom, manipulator and

stinger in each transverse direction. As before, the PV arrays and radiator are modeled as cantilever plates represented by a single shape function in the longitudinal and transverse directions. The mass of the power boom (15,840 kg) is much greater than those of the other structural elements, the most massive of which is the manipulator with payload (total mass of 1600 kg). Therefore, the power boom dynamics is adequately represented by eigenfunctions of a free–free beam. Eigenfunctions of a cantilevered beam are taken as admissible functions for the manipulator and stinger.

In the first simulation, one shape function is used to model the flexibility of the beam elements. The librational responses to the maneuver are shown in Figure 5-14 (a) over 0.02 orbit which corresponds to approximately 110 seconds. The major librational d.o.f. excited by the maneuver is the yaw angle, which is perturbed by almost 7°. Interestingly, the yaw angle at the end of the maneuver appears to stabilize about this value. The pitch degree of freedom is the least affected, with a maximum deviation of less than 0.2° over the period shown. The roll response starts to grow considerably in the negative direction, especially at about 20 seconds after the start of the maneuver. The growth is essentially linear, reaching a value of 0.7° by 0.02 orbit.

The vibrational response of the power boom and stinger is shown in Figure 5-14 (b). The results indicate that the effect of the maneuver on the power boom tip deflections is quite minor. The tip deflection in the z_c transverse direction is significantly greater than the deflection in the y_c direction (2.5×10^{-2} mm and 1×10^{-3} mm, respectively). This is as expected because the z_c direction lies in the plane of the slew maneuver. This, in turn, leads to the stinger vibration occurring principally in the z_1 direction. The maximum stinger tip deflection in this direction is about 0.7 mm, compared to 0.05 mm in the y_1 direction.

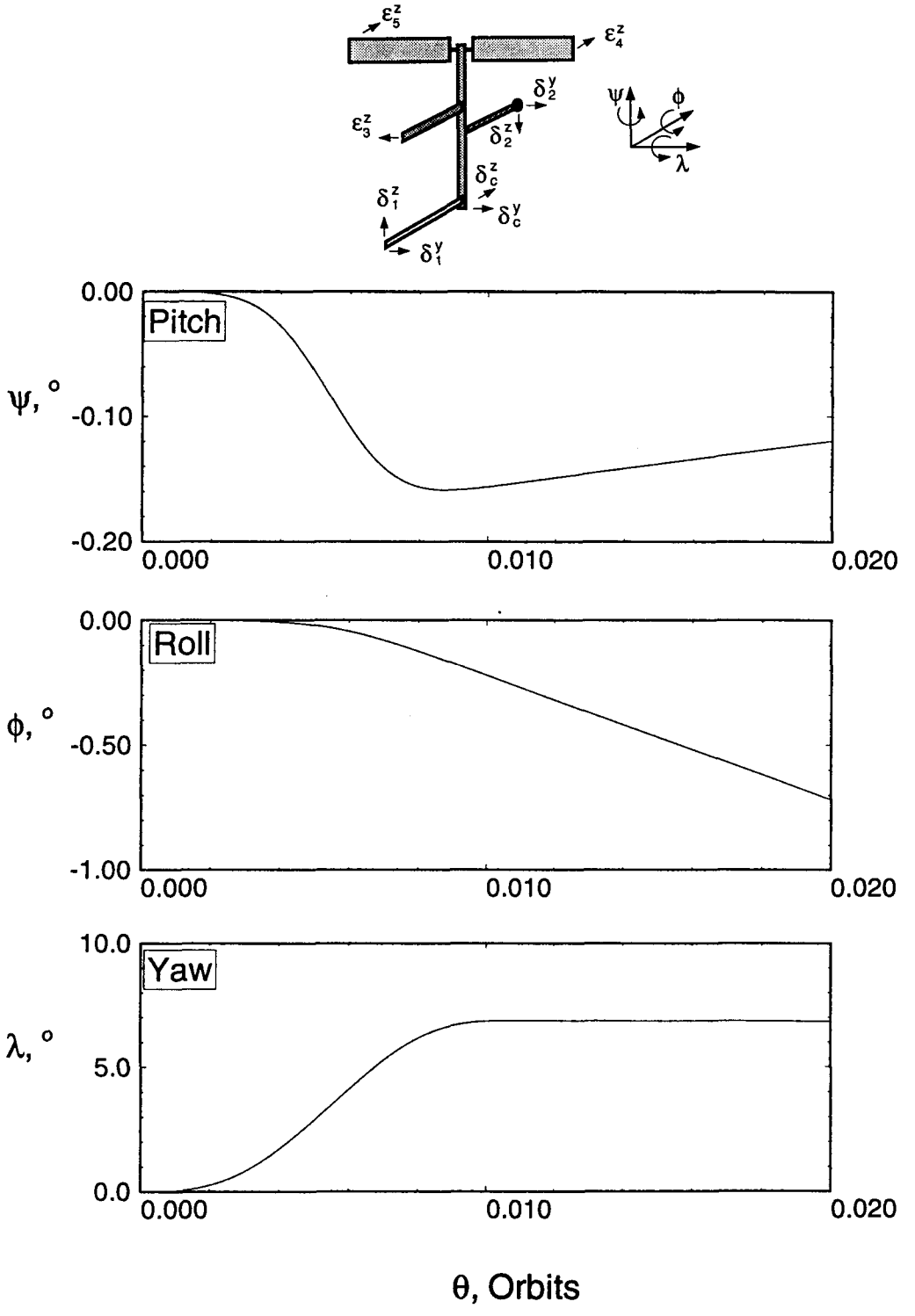

Figure 5-14 FEL dynamics during a manipulator maneuver using one admissible function for discretization: (a) librational response.

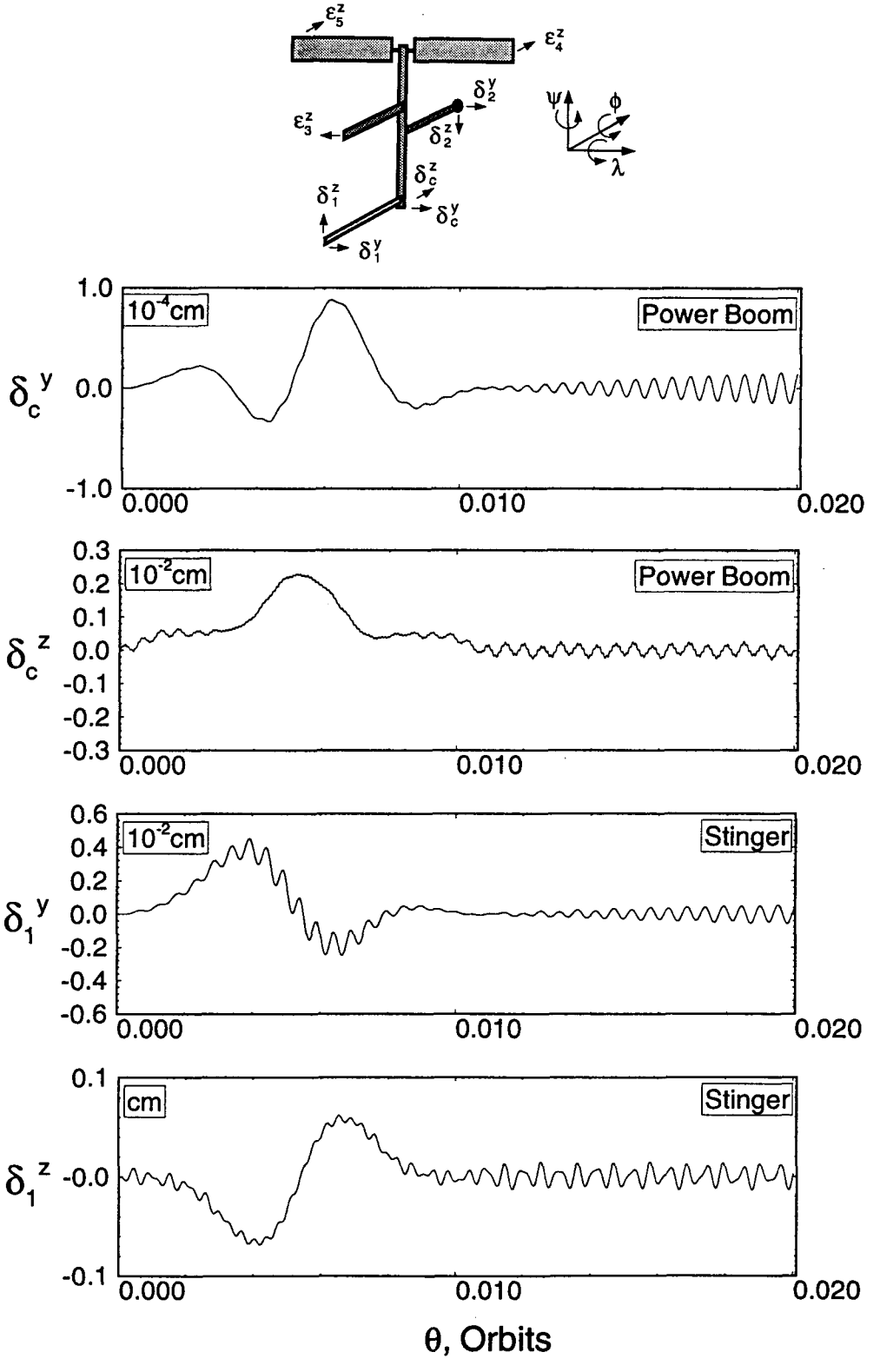

Figure 5-14 FEL dynamics during a manipulator maneuver using one admissible function for discretization: (b) vibrational response of the power boom and stinger.

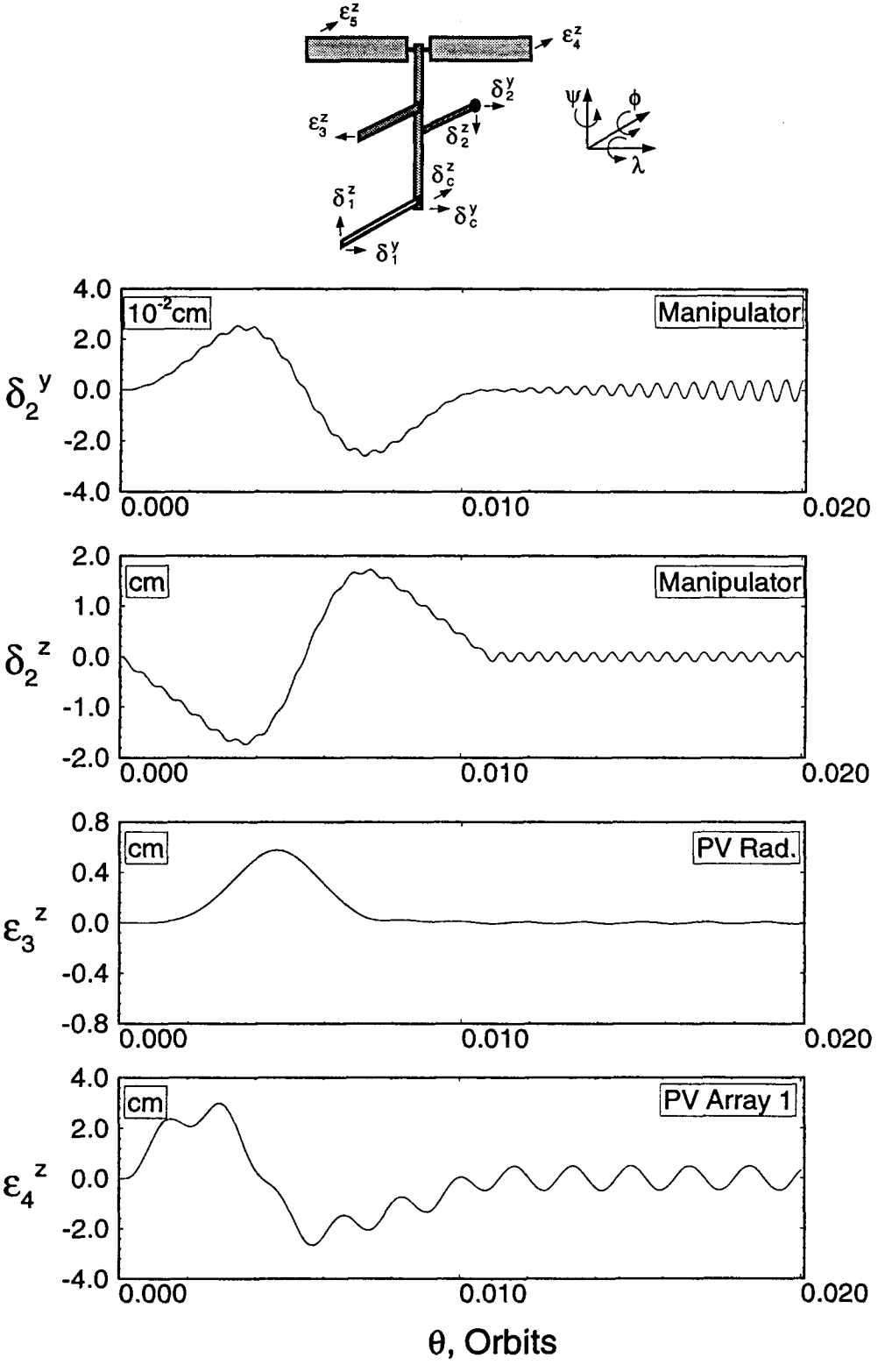

Figure 5-14 FEL dynamics during a manipulator maneuver using one admissible function for discretization: (c) vibrational response of the manipulator, PV radiator and arrays.

The manipulator dynamics is shown in Figure 5-14 (c), along with the vibrational responses of the PV radiator and arrays. Again, the tip deflection of the manipulator is significantly higher (approximately 50 times) in the z_2 direction than in the y_2 direction. This is again due to the fact that the z_2 direction lies in the plane of the maneuver. Moreover, at the start of the maneuver the deflection is in the $-z_2$ direction because the torque applied at the base of the arm results in the tip lagging behind. The shape of the tip deflection curve resembles the sinusoidal profile of the angular acceleration of the manipulator. The maximum tip deflection of manipulator is approximately two cm. The post maneuver response for all the members is relatively small. As pointed out before, the structural damping is purposely not modeled for any of the bodies as accurate, reliable models are still not available. However, the formulation can readily account for damping once its precise value is known. The deflection of the PV radiator remains generally quite small, with a maximum value of 0.6 cm at, approximately, the midpoint of the maneuver. The large deflections in the system occur at the tips of the solar panels (maximum 3 cm). Recognizing that the direction of the array vibration lies in the plane of the maneuver, and that the power boom flexure induces the "flapping" motion of the arrays, this result is not surprising.

Next, the simulation was repeated using two admissible functions in the discretization of the beam elements (Figure 5-15). The results showed close correlation with the one admissible function case except for minor differences. Finally, with 3 admissible functions for discretization of the power boom, stinger and manipulator, the response results (Figure 5-16) were virtually indistinguishable from the previous case. This clearly shows that a considerable degree of convergence in the results has been accomplished with the use of 3 admissible shape functions

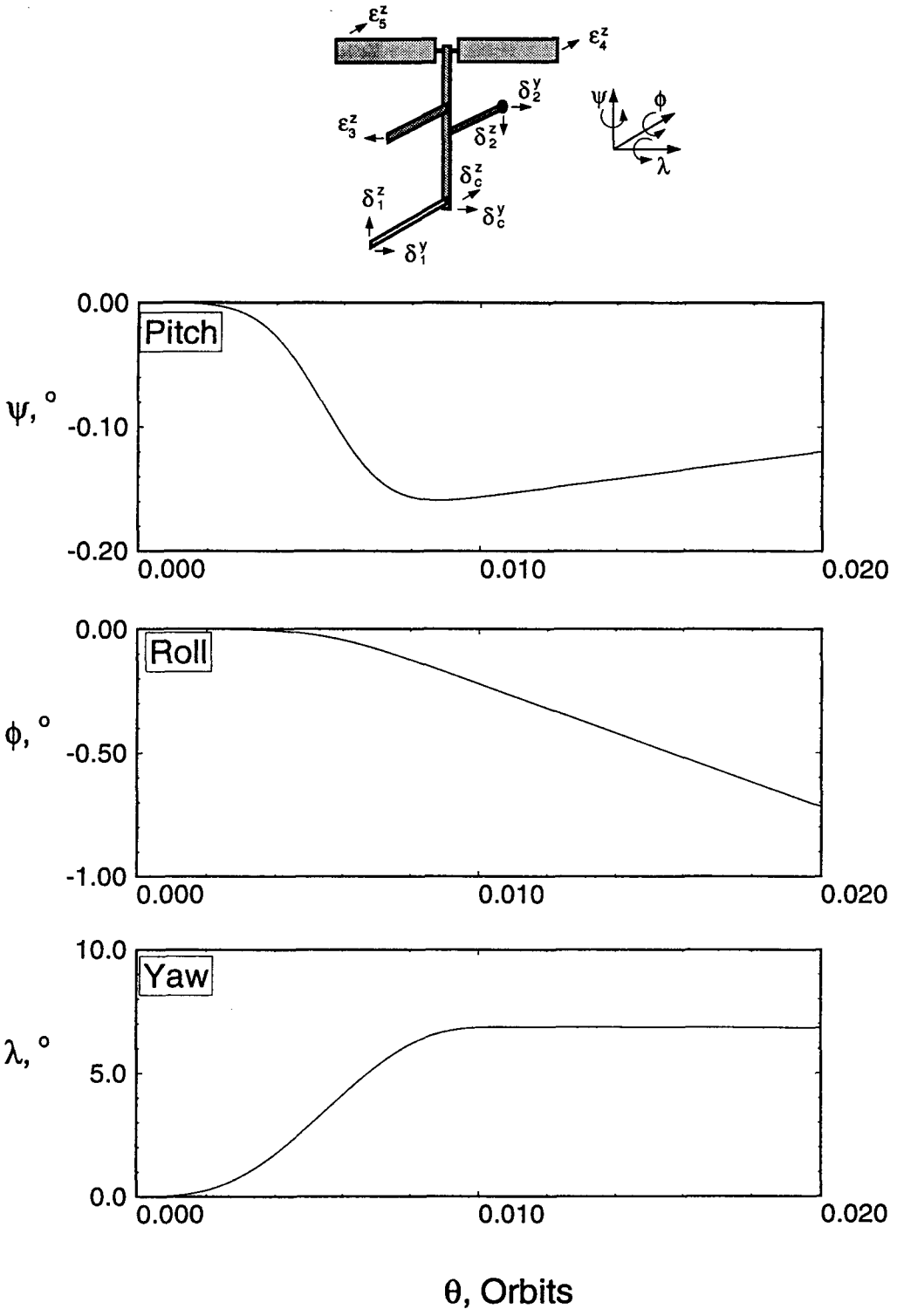

Figure 5-15 FEL response to a manipulator maneuver obtained using two admissible functions: (a) librational time histories.

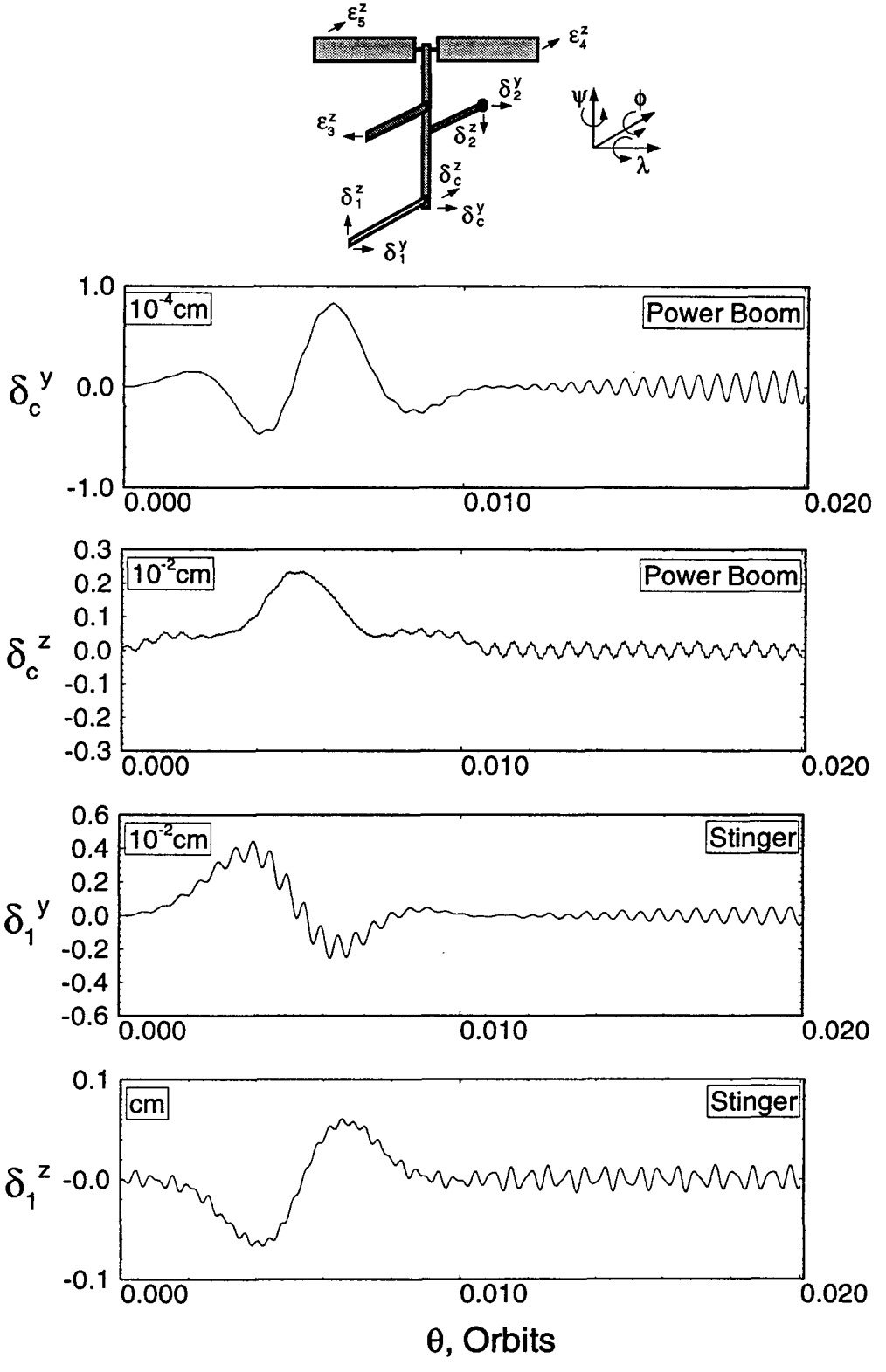

Figure 5-15 FEL response to a manipulator maneuver obtained using two admissible functions: (b) tip vibrational motions of the power boom and stinger.

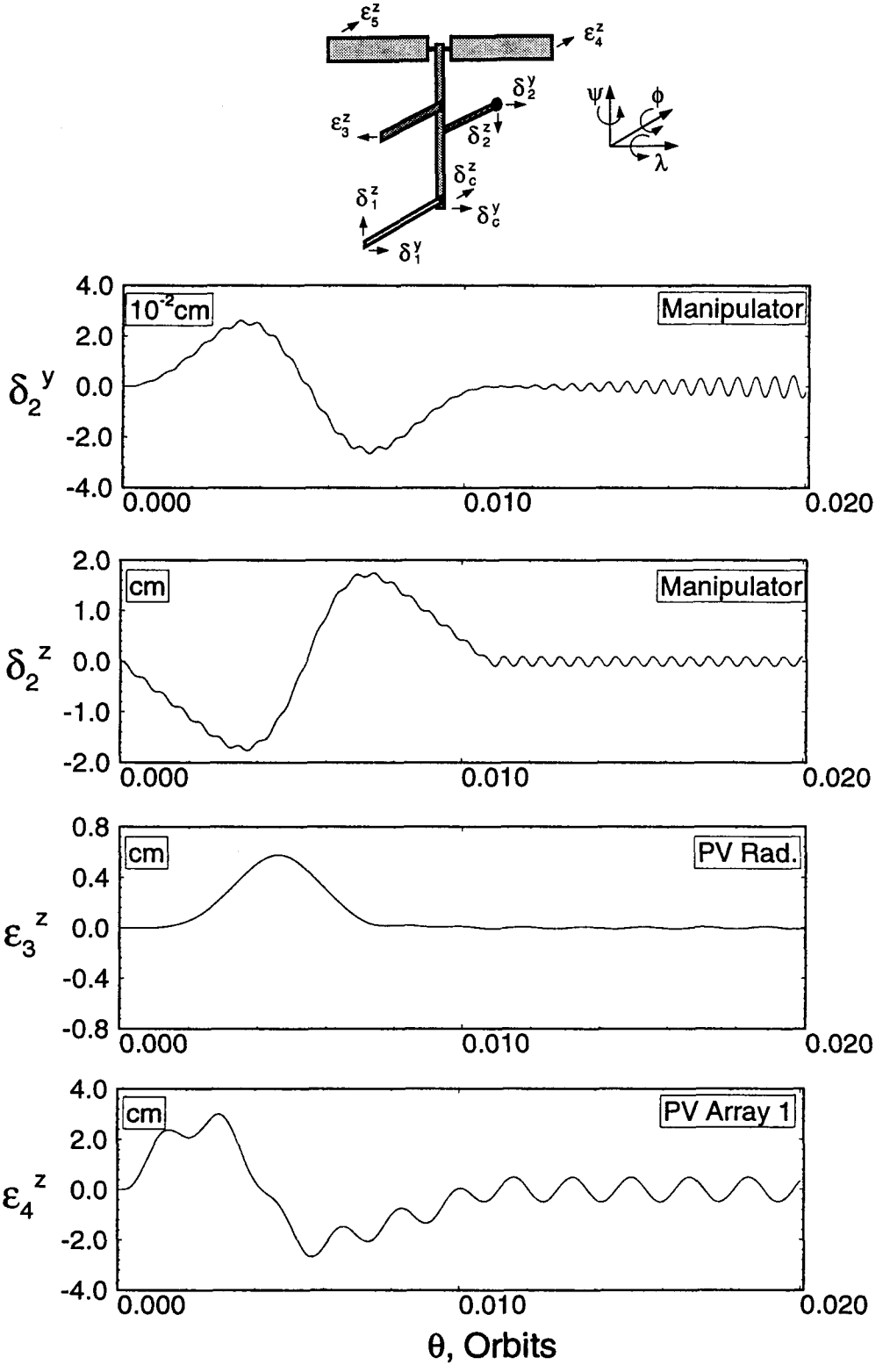

Figure 5-15 FEL response to a manipulator maneuver obtained using two admissible functions: (c) tip vibrational motions of the manipulator, PV radiator and arrays.

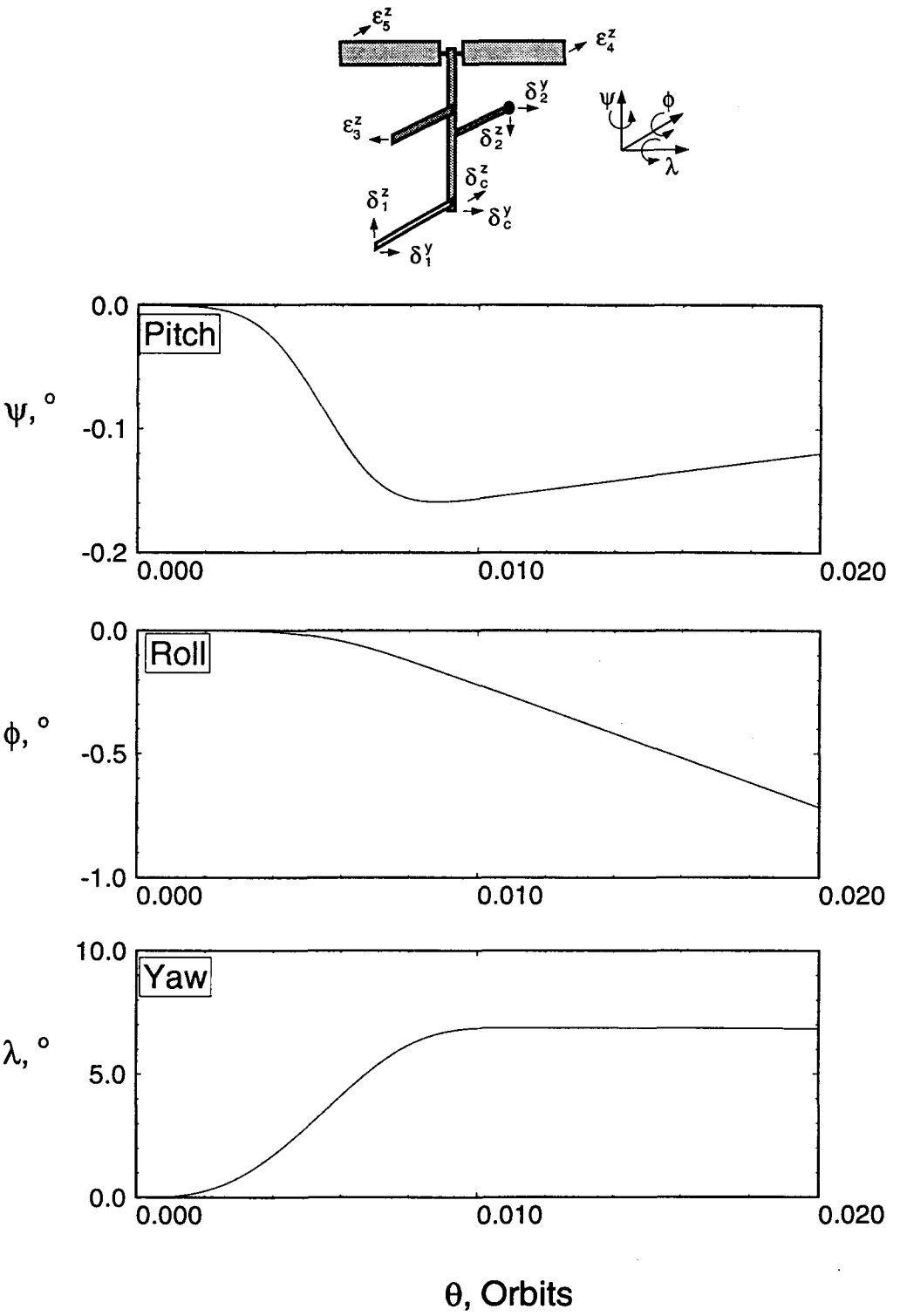

Figure 5-16 Response of the FEL configuration of the proposed Space Station to a manipulator maneuver. The discretization process uses three admissible functions: (a) librational motion.

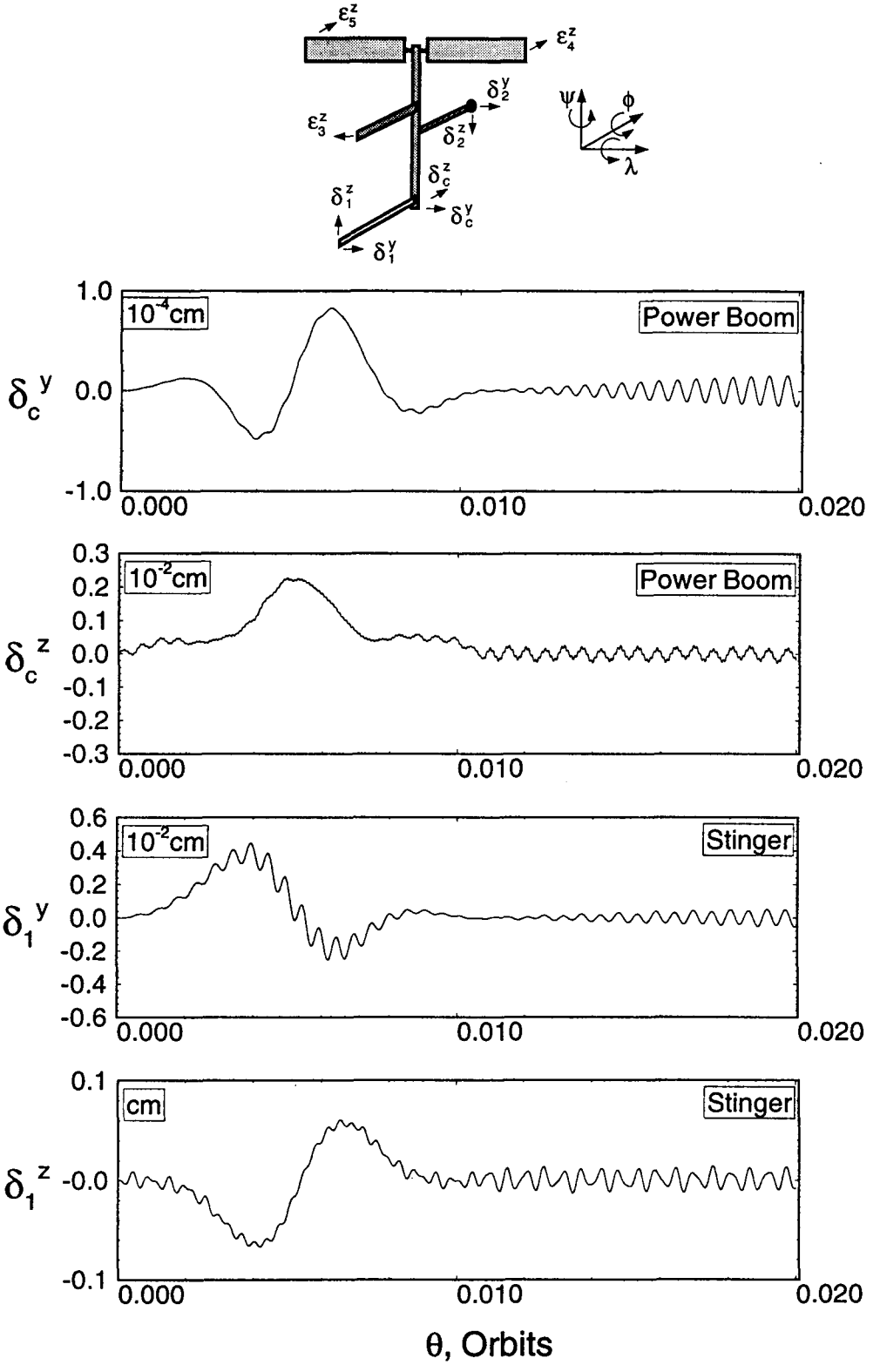

Figure 5-16 Response of the FEL configuration of the proposed Space Station to a manipulator maneuver. The discretization process uses three admissible functions: (b) tip vibrations of the power boom and stinger.

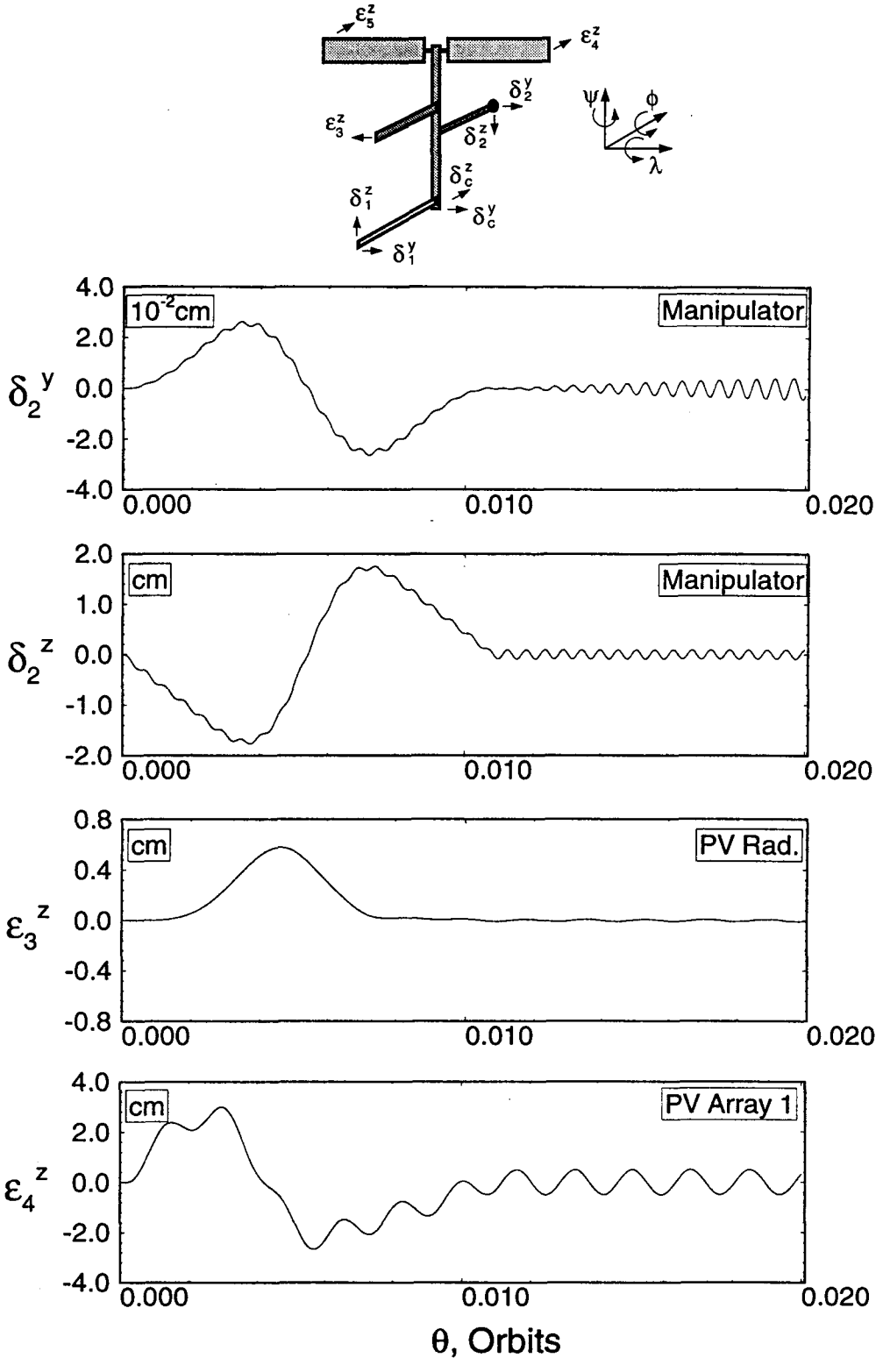

Figure 5-16 Response of the FEL configuration of the proposed Space Station to a manipulator maneuver. The discretization process uses three admissible functions: (c) tip vibrations of the manipulator, PV radiator and arrays.

5.4 Permanently Manned Configuration (PMC)

The Permanently Manned Configuration (PMC) of the proposed space station is close to the final operational design. The orientation of the PMC is identical to that of the FEL, with the power boom aligned along the orbit normal. The overall length of the structure is 115 m, and the total mass is about 160,000 kg. The primary difference between the FEL and the PMC is the latter's greater length, and the presence of an additional pair of solar arrays, a second PV radiator and a pair of of station radiators. As in the case of the FEL, admissible functions for the power boom are taken from the set of free–free beam eigenfunctions, while the stinger and manipulator are discretized using cantilevered beam shape functions. The PV radiators, arrays and station radiators are treated as cantilever plates. A schematic of the PMC is shown in Figure 5-17 with physical characteristics of the principal components of the PMC given in Table 5-4 . In addition to the parameters listed, the power boom is assumed to have a non–zero product of inertia term, I_{xz}, equal to 1.845×10^4 kg-m^2 because of the asymmetric arrangement of the module cluster. Also, each elastic element is taken to have structural damping corresponding to 1% of the critical value. This represents the upper limit for typical materials used in the construction of space structures. The widths of the station radiators, PV radiators and PV arrays are 5.75 m, 1.15 m, and 6 m, respectively.

The equilibrium configuration of the system can be evaluated using the linearized equations. To determine the equilibrium state, $\mathbf{z}^{\mathbf{e}}$, the governing equations of motion (eq.3.1) are solved for the specific state vector whose time derivative is identically zero,

$$\dot{\mathbf{z}}^{\mathbf{e}} = \mathbf{0} = \mathbf{g}(\mathbf{z}^{\mathbf{e}}, \mathbf{0}, t). \tag{5.18}$$

Table 5-4 Physical characteristics of the major components of the PMC.

Body	Length (m)	Mass (kg)	EI (N-m^2)	I_{xx} (kg-m^2)	I_{yy} (kg-m^2)	I_{zz} (kg-m^2)
Power Boom	115	154,583	6.9×10^8	1.48×10^6	4.45×10^7	4.33×10^7
Stinger	26.7	270	4.103×10^6	10	64,160	64,160
Manipulator	15	1000*	1.725×10^6	100	75,000	75,000
Station Radiator	11.5	1,395	6.165×10^4	3,840	61,496	65,340
PV Radiator	11.5	450	1.988×10^4	50	19,837	19,887
PV Array	33	444	4.647×10^5	1,332	161,172	162,504

* excluding payload mass of 300 kg

Equation (5.18) is then linearized about a state $\mathbf{z^o}(0)$ which is sufficiently close to the equilibrium state such that a Taylor series expansion of (5.18) about $\mathbf{z^o}$ is valid,

$$\mathbf{g}(\mathbf{z^e}, \mathbf{0}, t) = \mathbf{g}(\mathbf{z^o}, \mathbf{0}, 0) + \left[\frac{\partial \mathbf{g}}{\partial \mathbf{z}}\right]_{\mathbf{z^o}} (\mathbf{z^e} - \mathbf{z^o}) + \tilde{\mathbf{h}}(t), \tag{5.19}$$

where $\tilde{\mathbf{h}}(t)$ represents the higher order terms. Ignoring $\tilde{\mathbf{h}}(t)$, and solving for the equilibrium state gives

$$\mathbf{z^e} = \mathbf{z^o} - \left[\frac{\partial \mathbf{g}}{\partial \mathbf{z}}\right]^{-1}_{\mathbf{z^o}} \mathbf{g}(\mathbf{z^o}, \mathbf{0}, 0). \tag{5.20}$$

The Jacobian $\left[\frac{\partial \mathbf{g}}{\partial \mathbf{z}}\right]_{\mathbf{z^o}}$ is computed numerically as described in Chapter 3. The resulting $\mathbf{z^e}$ can be substituted for $\mathbf{z^o}$ to obtain a better estimate for the equilibrium state.

Using the above procedure, the equilibrium position of the PMC was found for three different cases: the PMC without the manipulator system; with the manipulator before the slewing maneuver; and the manipulator configuration at the end of the maneuver (Figure 5-17). In all the cases, only the yaw angle at equilibrium is nonzero

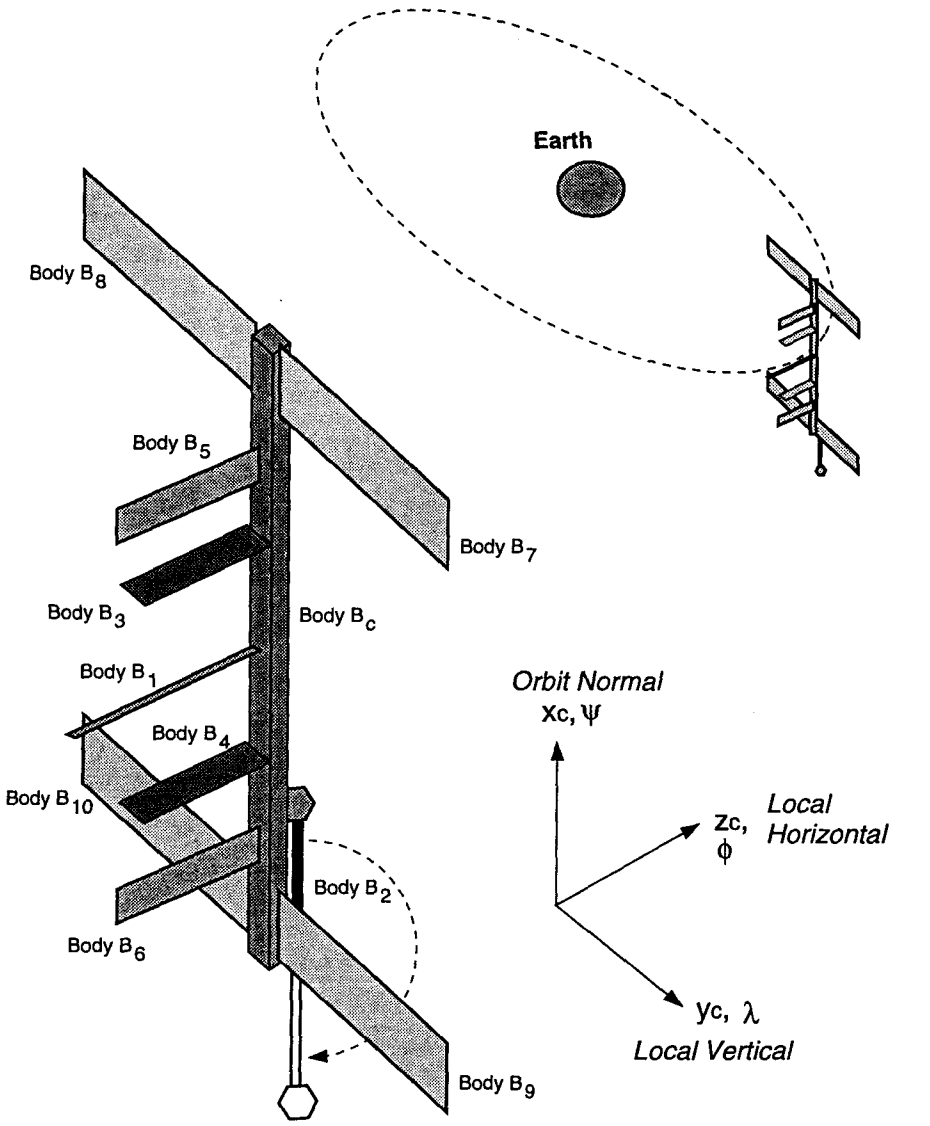

Body	Description
B_c	Power Boom
B_1	Stinger
B_2	Manipulator with payload
B_3 , B_4	Station Radiator
B_5 , B_6	PV Radiator
B_7 , B_8 , B_9 , B_{10}	PV Array

Figure 5-17 Schematic diagram of the PMC showing its major components.

by a significant amount; the remaining states are very close to zero. The equilibrium yaw angle, λ_e, for the 3 cases are:

$$\begin{aligned} &\text{without manipulator,} && \lambda_e = -0.021^\circ; \\ &\text{manipulator inboard,} && \lambda_e = 0.0158^\circ; \\ &\text{manipulator outboard,} && \lambda_e = -0.0578^\circ. \end{aligned}$$

In all the three cases, linearization was performed about the zero state. The closeness of the equilibrium state to the zero state indicates that the values for the equilibrium yaw angles are quite accurate. Furthermore, accuracy of the computed equilibrium values were verified by simulating the system with initial conditions corresponding to the equilibrium state. In all the cases the simulation results confirmed the veracity of the computed equilibrium values.

5.4.1 Response to PV Array Tracking

In order to maximize the power generation the plane of the PV array is maintained normal to the incident sun rays. The proposed orbital plane of the Space Station being close to the ecliptic, this can be achieved, approximately, by slewing about the orbit normal at a rate of -1 revolution per orbit. The motion of the arrays act as a disturbance to the station that must be corrected or minimized through an appropriate control system. This is investigated the following chapter. Here, the uncontrolled response of the system to a prescribed solar array slew rate of 1 rev./orbit is studied. The pitch and vibrations in the orbital plane are likely to be affected most. The formulation and code developed is capable of assessing this effect rather well.

In the present study, three admissible functions were used in each transverse direction for the power boom, and two admissible functions for the manipulator and

stinger. Furthermore, a pair of longitudinal cantilever modes and a single free–free transverse mode were used for each of the PV arrays and radiators. The resulting system has a total of 66 d.o.f.. The arrays were slewed at a constant angular rate for one orbit and then stopped.

The response of the attitude degrees of freedom is depicted in Figure 5-18 (a). As expected, the pitch angle is the most affected by slewing however, due to coupling, roll and yaw are also excited by a significant amount. At the end of 1 orbit (5554 s), the pitch angle has grown to around 360° while the yaw and roll reach the values of 90° and 45°, respectively. The closeness of the slewing rate to the librational natural frequencies accentuates the response. At the end of the orbit when the arrays stop slewing, the pitch tends to zero, however the roll (ϕ) and yaw (λ) show large amplitude modulations.

In contrast to the vibratory response of the FEL to the manipulator maneuver discussed earlier, the corresponding excitation of the PMC due to the array slewing is significantly lower (Figures 5-18 b-d). This is principally due to the low rate of the array rotation ($\approx$ 0.001 rad./s) compared to the manipulator slew rate ($\approx$ 0.052 rad./s). Note, the high frequency transient component of the power boom response, near the beginning and termination of the maneuver, attenuates quickly due to the structural damping. Damped transients are also exhibited by the other members, at the beginning or end of the slew maneuver. Like the roll and yaw responses, amplitudes of the power boom vibrations increase on termination of the maneuver suggesting coupling with the rigid degrees of freedom. Indeed the dominant frequencies of the attitude and elastic responses are very close. Note, the stinger response in the y_1 direction is similar to that of the arrays (Figure 5-18 d), indicating significant coupling between the two. Similar interactions are also evident between

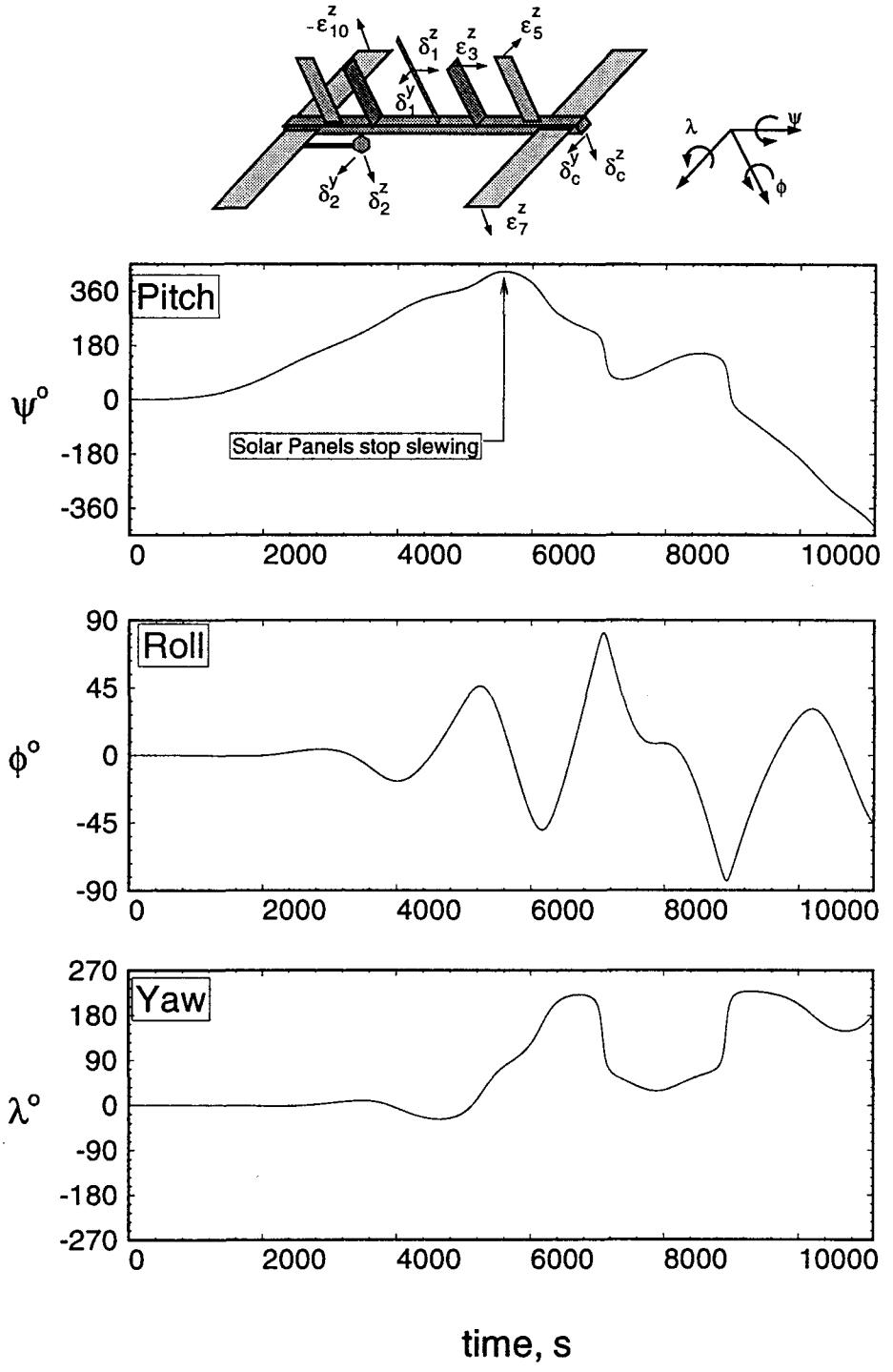

Figure 5-18 Response of the PMC to a PV array slewing: (a) librational motion.

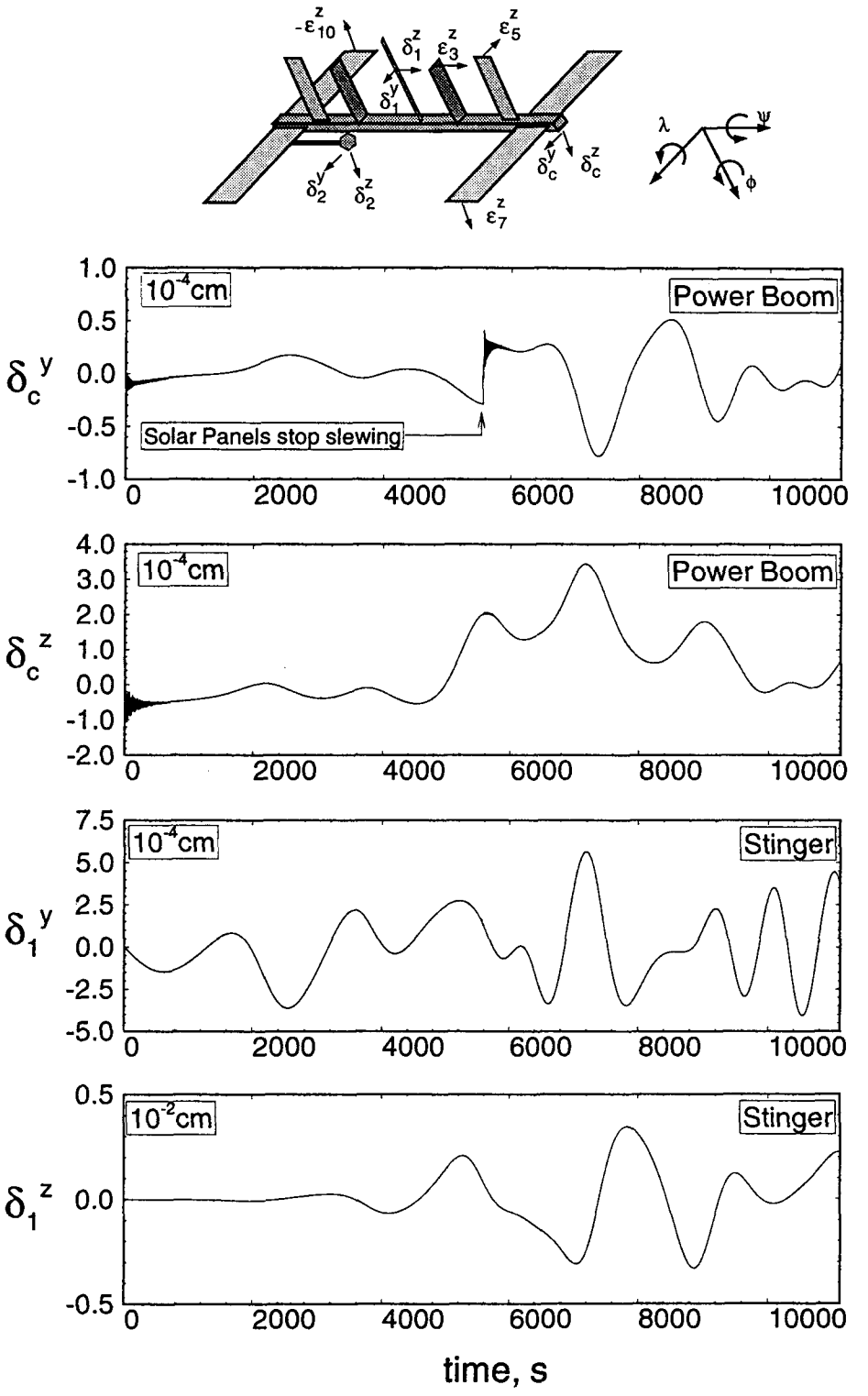

Figure 5-18 Response of the PMC to a PV array slewing: (b) vibrational time histories of the power boom and stinger.

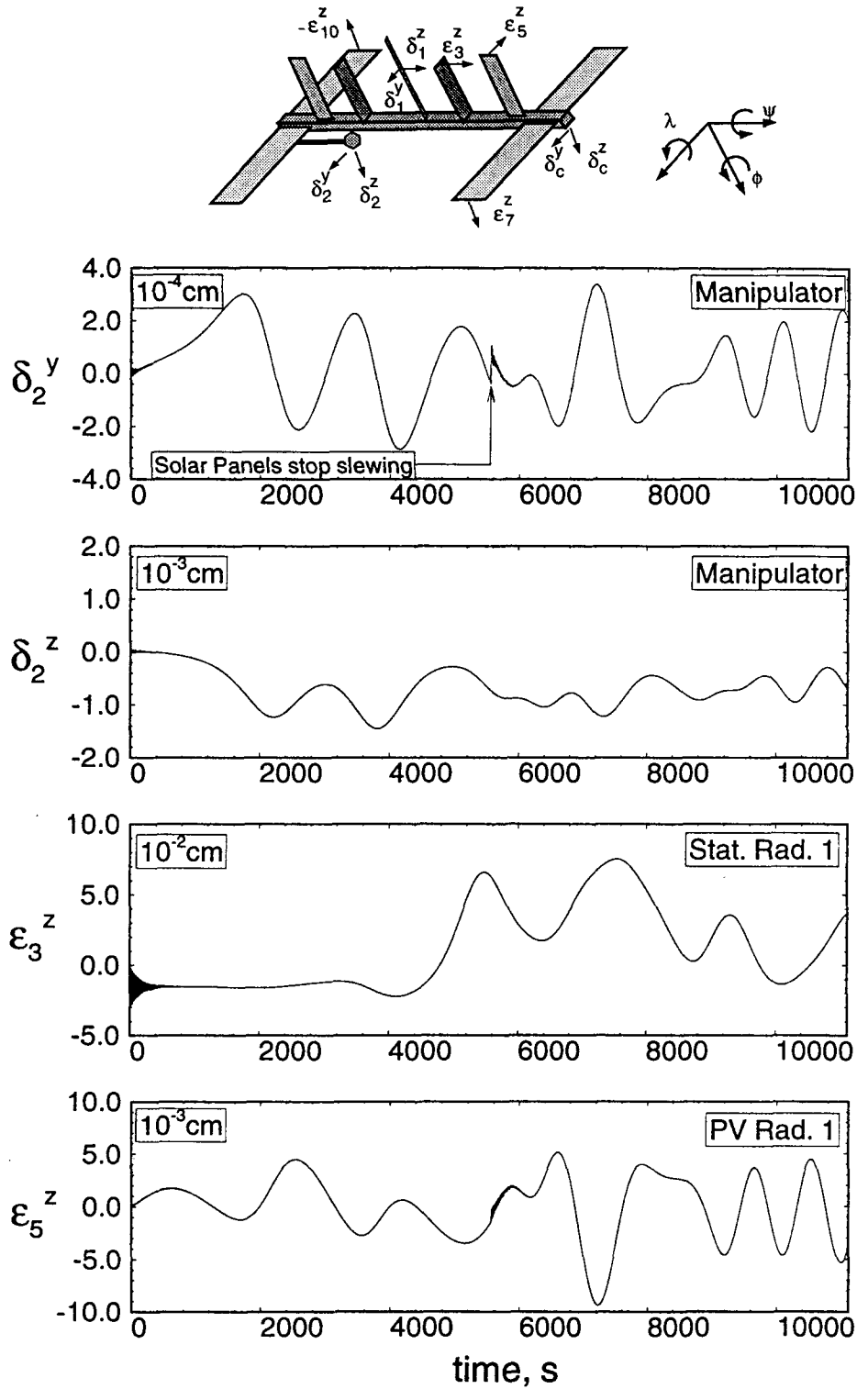

Figure 5-18 Response of the PMC to a PV array slewing: (c) vibrational time histories of the manipulator, station radiator and PV radiator.

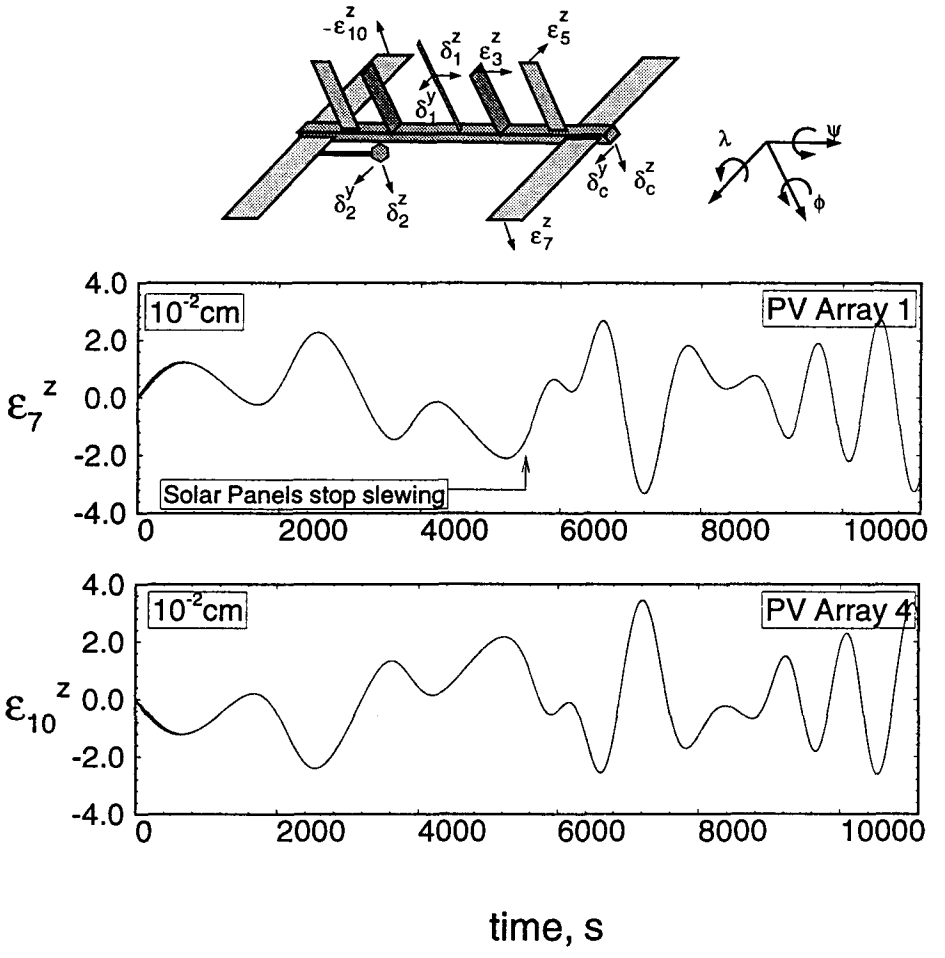

Figure 5-18 Response of the PMC to a PV array slewing: (d) vibrational time histories of the PV arrays.

the stinger response in the z_1 direction and the roll and yaw librations. Curiously, the largest tip vibration is not associated with the solar arrays, but rather occurs at the station radiators and is quite small (< 1 mm). The location and orientation of the station radiator suggest significant coupling among the roll, yaw, power boom vibration in the z_c direction, stinger vibration in the z_1 direction, and station radiator vibration. Note, arrays 1 and 4 respond in a similar fashion, albeit out of phase, as expected being located on opposite sides of the power boom.

5.4.2 Response to Manipulator Maneuvers

The effects of some typical maneuvers of the RMS on the dynamics of the PMC are investigated next. For this series of simulations, two admissible functions are employed for the power boom in each transverse direction, while a single admissible function is employed for the remaining flexible components, resulting in 19 generalized coordinates. Three cases are investigated, with the manipulator at the end of the power boom performing a purely rotational maneuver of 180° from the inboard to the outboard position. In the first case, the maneuver is performed in the Orbit Normal–Local Horizontal (ONLH) plane (i.e. in the $-y_c$ direction), while in the second, it takes place in the Orbit Normal–Local Vertical (ONLV) plane (i.e. in the $+z_c$ direction, Fig. 5-17). In both the cases, the maneuver takes place in 60 s. In the third case the maneuver in the ONLH plane is performed in 600 s. As before, sine–on ramp maneuver profiles are employed. As in the case of the FEL, the fundamental frequency of flexure for the manipulator (2.5 rad/s) is considerably greater than the average angular velocity of the manipulator (0.05 rad/s), allowing for the foreshortening effect to be neglected.

Maneuver in the ONLH plane ($-y_c$ direction) performed in 60 s

The librational response for this case is given in Figure 5-19 . The yaw degree of freedom is the most sensitive during the maneuver, exhibiting an oscillatory response from $-0.5°$ to $+0.5°$. The pitch response is less than $0.1°$, while the roll is hardly excited. However, after the maneuver, all librational d.o.f. exhibit unstable behaviour.

On the other hand, the vibrational response (Figures 5-19b-d) all exhibit good settling behaviour in the post–maneuver phase due to the structural damping present in the system. Also, in all the cases, the response during the maneuver is significantly higher. As can be anticipated, tip deflections of the beam–type elements (bodies B_c,

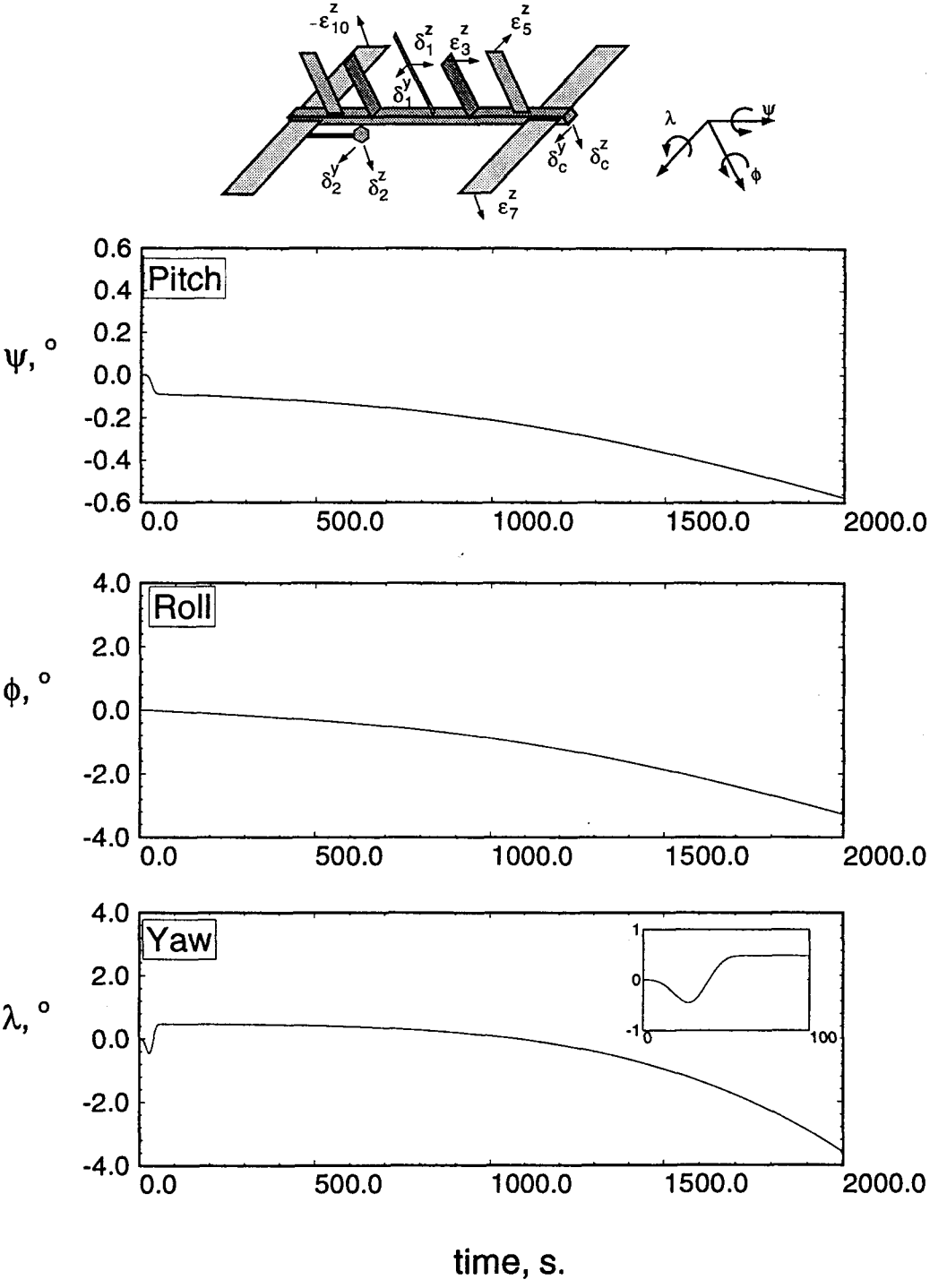

Figure 5-19 Dynamics of the PMC due to a manipulator slew maneuver, in the ONLH plane, performed in 60 s: (a) librational response.

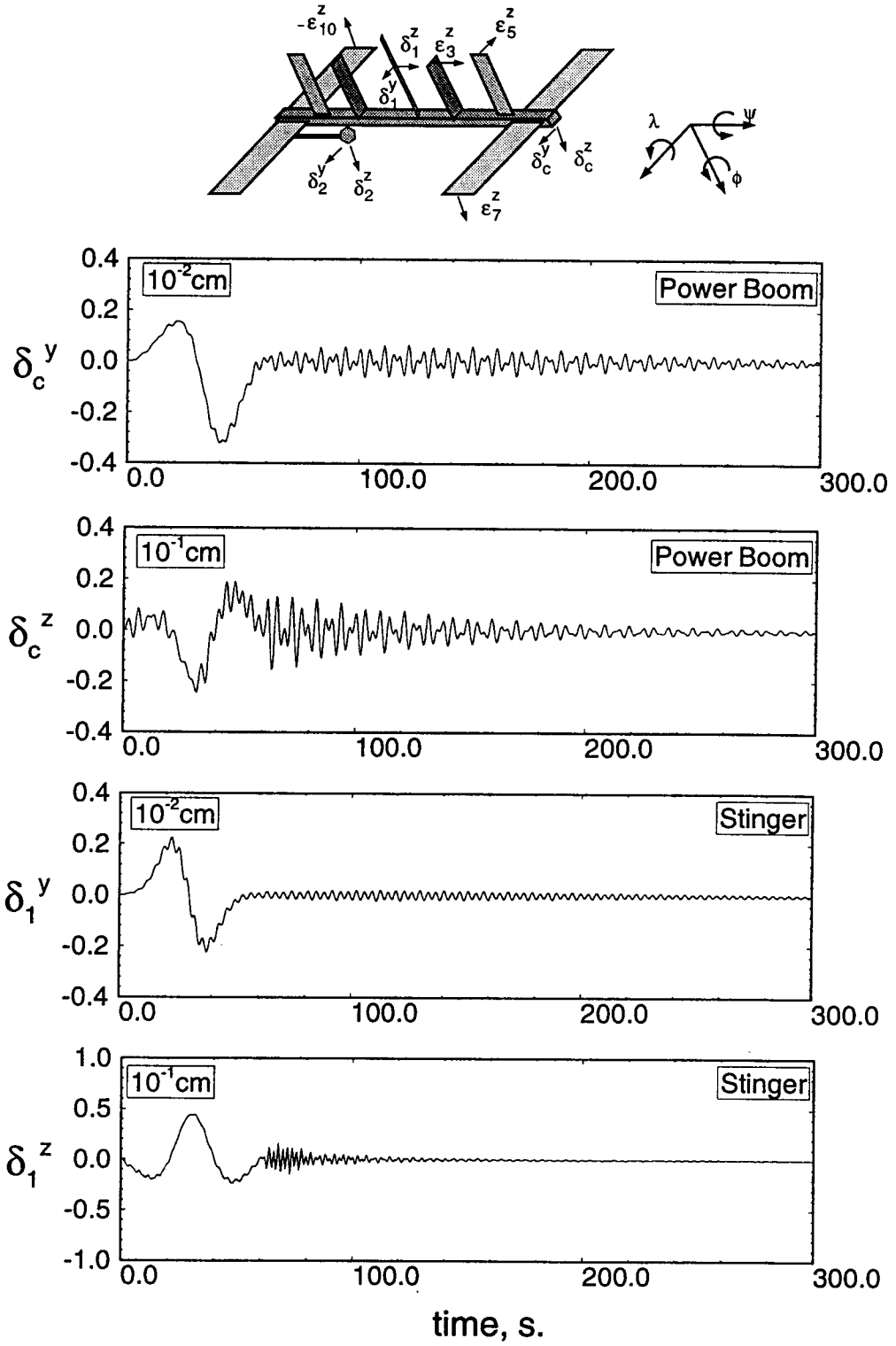

Figure 5-19 Dynamics of the PMC due to a manipulator slew maneuver, in the ONLH plane, performed in 60 s: (b) tip vibrations of the power boom and stinger.

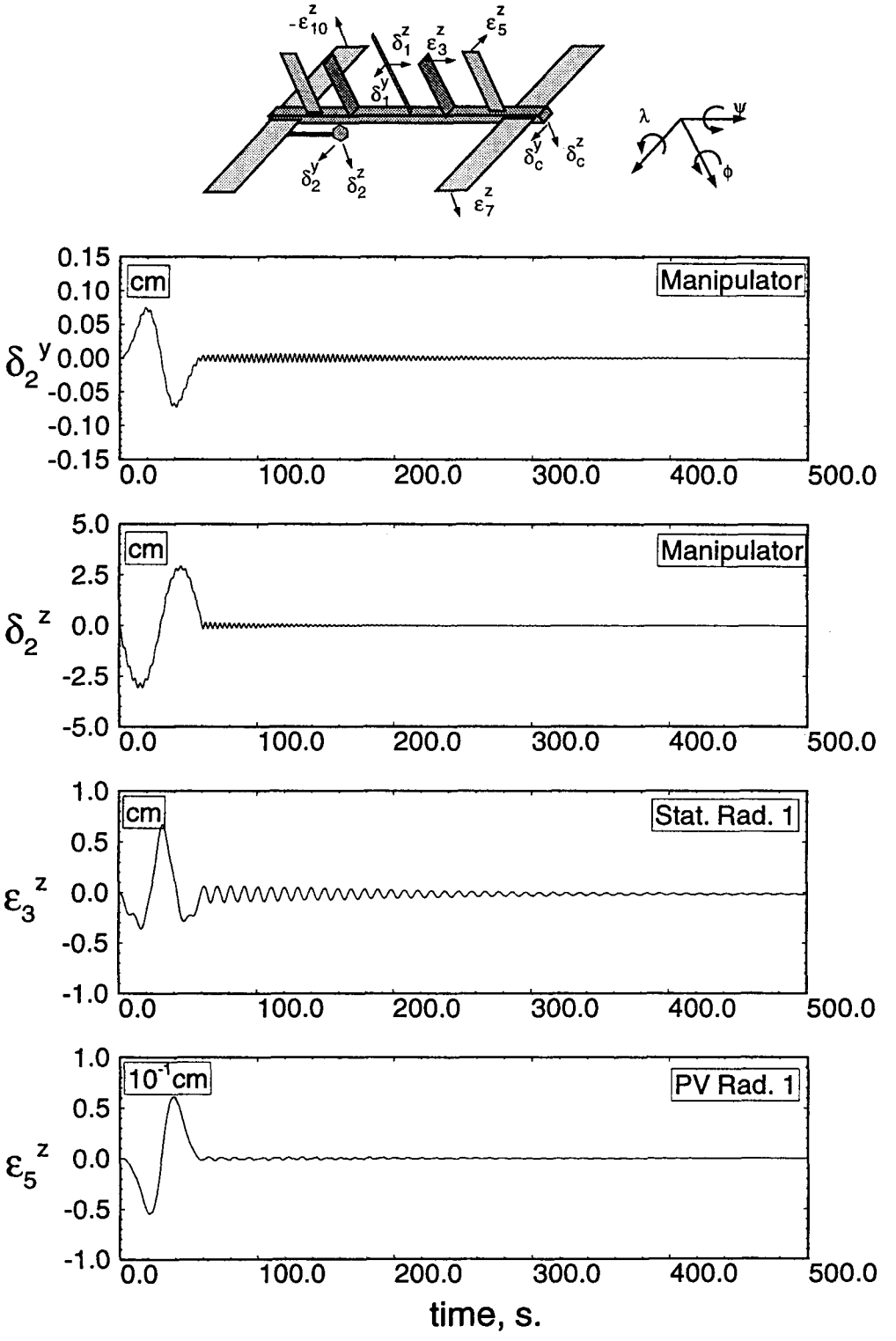

Figure 5-19 Dynamics of the PMC due to a manipulator slew maneuver, in the ONLH plane, performed in 60 s: (c) vibrational response of the manipulator, station radiator and PV radiator.

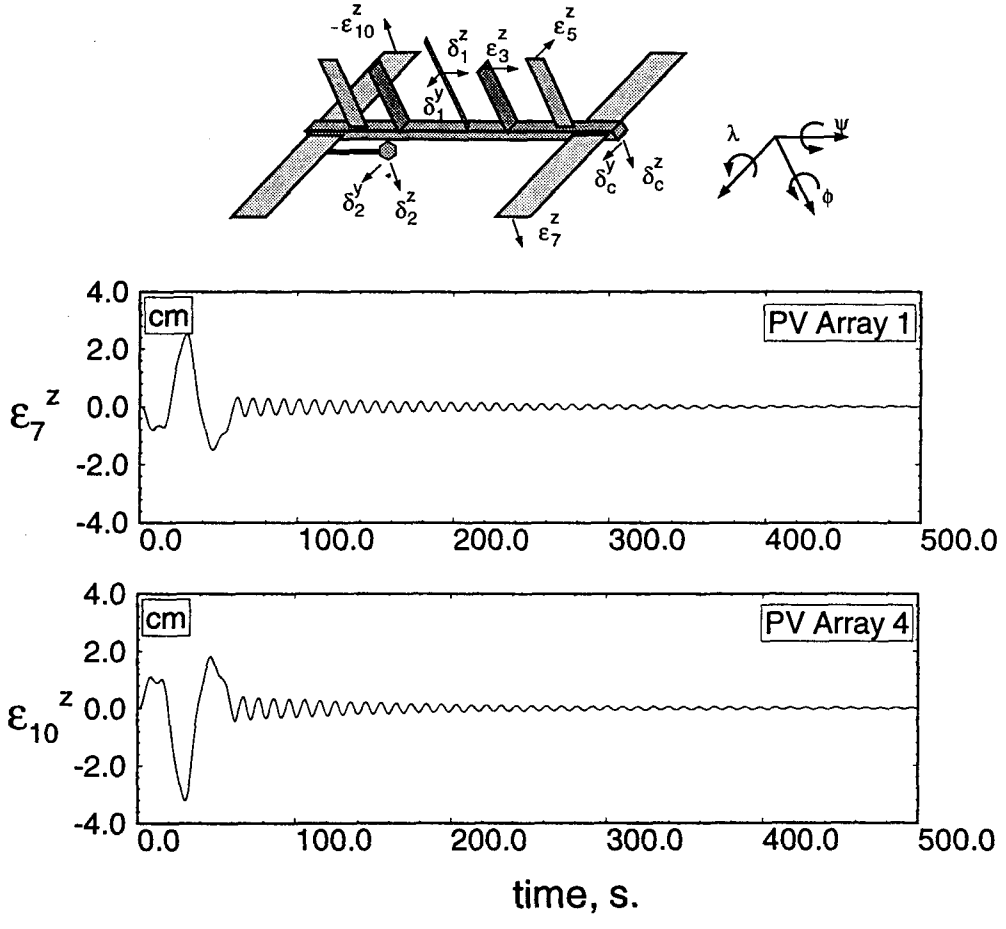

Figure 5-19 Dynamics of the PMC due to a manipulator slew maneuver, in the ONLH plane, performed in 60 s: (d) vibrational response of the PV arrays.

B_1, and B_2) in the plane of the maneuver are more pronounced. Also, the plate–type elements in the plane of the maneuver (bodies B_5 and B_6) are relatively less affected than those located in the orthogonal planes (bodies B_3, B_5, B_7, B_8, B_9 and B_{10}). This may be attributed to the transfer of angular momentum from the slewing manipulator, first to the central body and subsequently to other members.

The largest tip deflections were associated with the manipulator and the PV arrays. In both the cases, the maximum value is approximately 3 cm.

Maneuver in the ONLV plane ($+z_c$ direction) performed in 60 s

Figure 5-20 presents response time histories for this case. The librational results indicate that, during the maneuver, the system is primarily excited in pitch and roll. In fact, the pitch perturbation during the maneuver ($\approx 0.65°$), is greater than the roll response. The reason for a strong coupling between the pitch and the roll is the relatively large product of inertia term (I_{xz}) present in the PMC. Hence, in terms of the librational response, the maneuver in the $-y_c$ direction has less disturbing influence on the system although the final orientation of the manipulator is the same.

The tip vibration time histories of the flexible members show the trends similar to the ones observed earlier in Figure 5-19. The maximum tip deflection of the power boom is essentially the same in both the cases. The same is true for the manipulator tip deflection. However, in the present case, the deflection of station radiator 1 (body B_3) is significantly smaller (0.25 cm versus 0.7 cm) as well as of the PV arrays 1 and 4 (bodies B_7 and B_{10}) where the peak deformations are approximately half as large as the previous case (1.5 cm versus 3 cm). In contrast to this, the deflection of the PV radiator 1 (body B_5) is significantly higher (3 cm versus 0.06 cm). Thus there are no well established trends for the vibratory response of the flexible members. Hence depending on the mission, the operator may prefer one maneuver over the other. What is important is to recognize the fact that this versatile tool (formulation and the code) permits systematic parametric analysis in the presence of diverse disturbances resulting in information useful for design as well as operation of the space station.

Maneuver in the ONLH plane ($-y_c$ direction) performed in 600 s

As can be expected, the longer maneuvering time leads to local variations in the

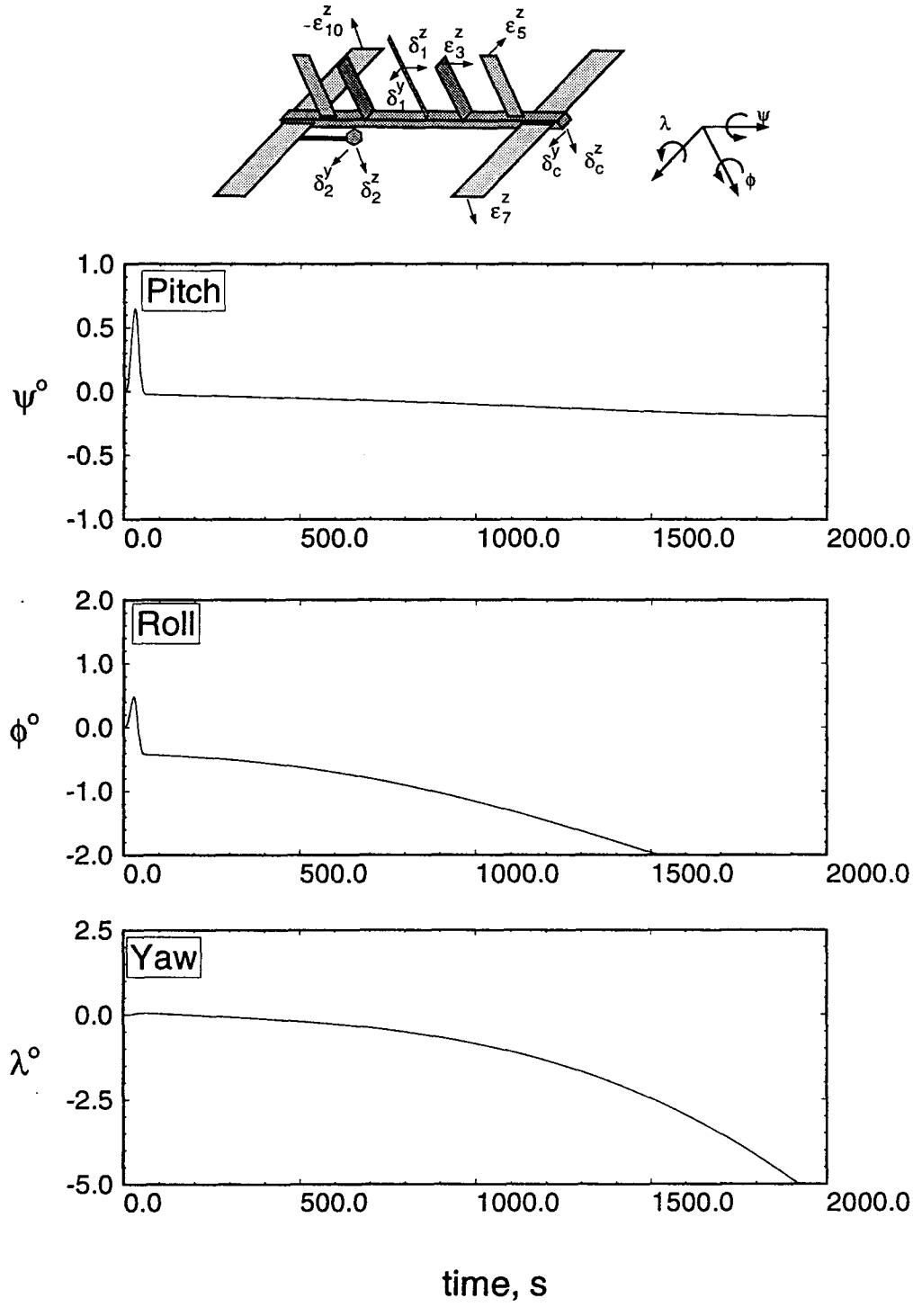

Figure 5-20 Response of the PMC to a 180° slew maneuver of the manipulator, in the ONLV plane, performed in 60 s: (a) librational dynamics.

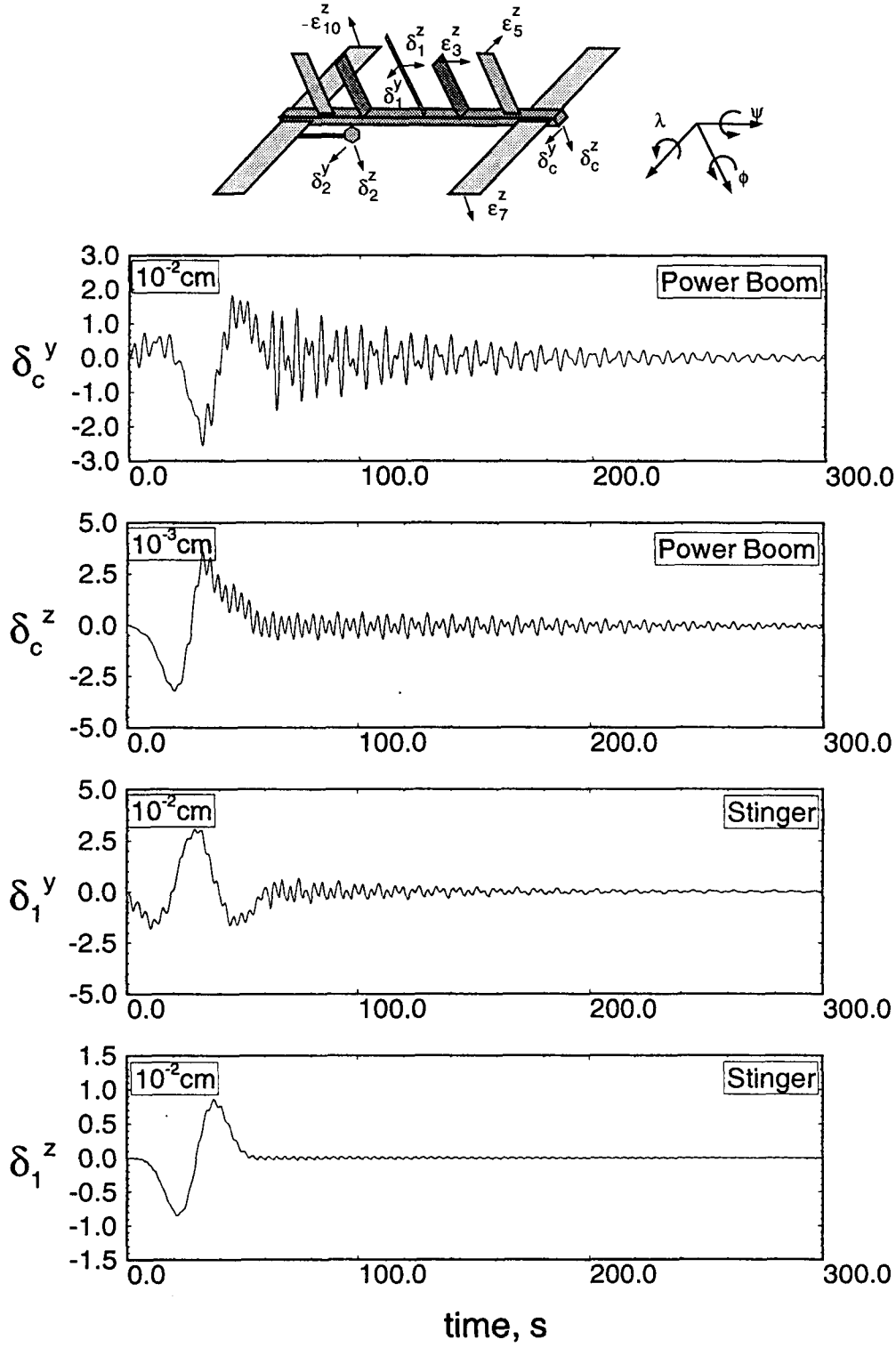

Figure 5-20 Response of the PMC to a 180° slew maneuver of the manipulator, in the ONLV plane, performed in 60 s: (b) tip vibrational response of the power boom and stinger.

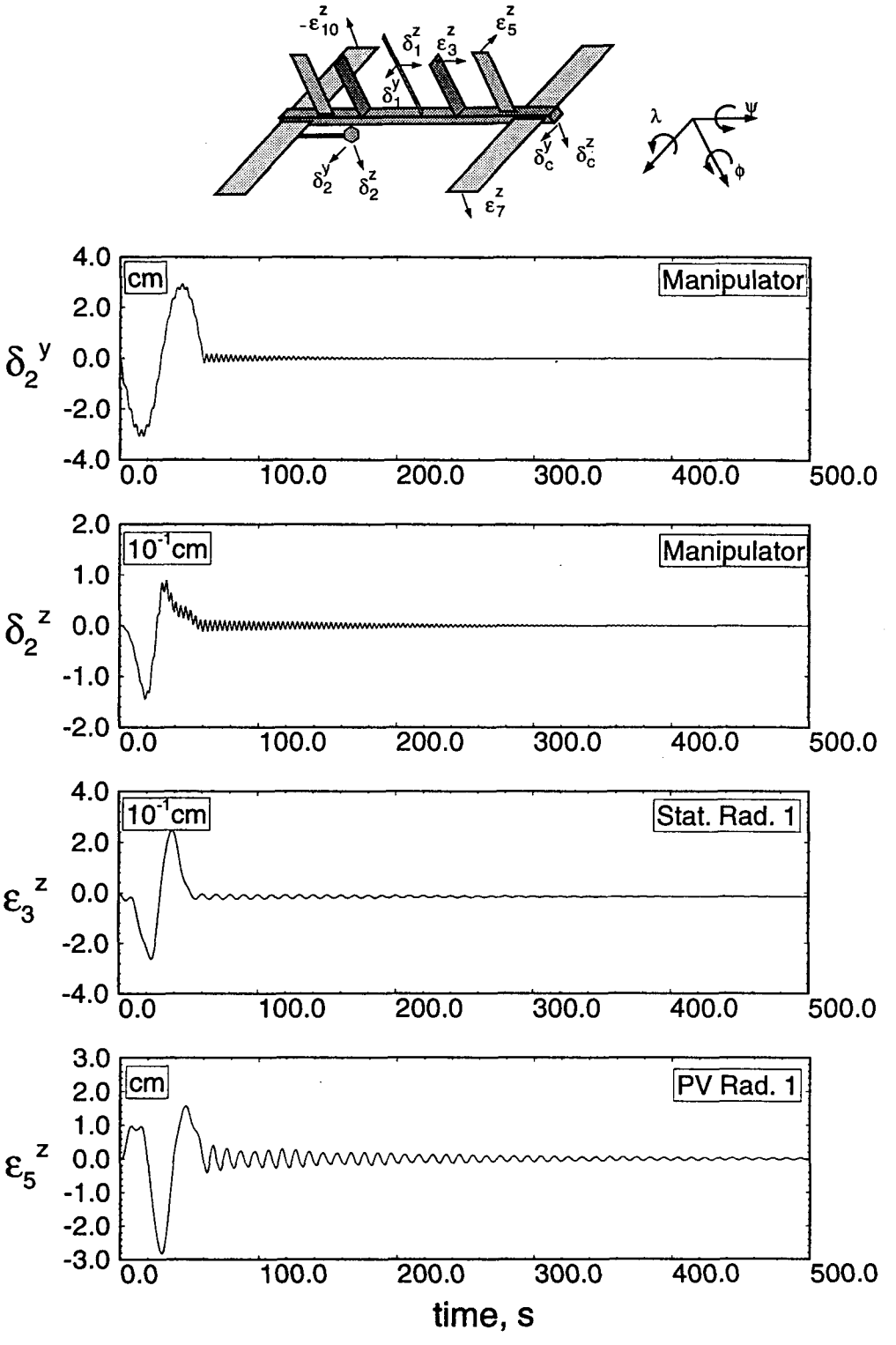

Figure 5-20 Response of the PMC to a 180° slew maneuver of the manipulator, in the ONLV plane, performed in 60 s: (c) tip vibrational response of the manipulator, station radiator and PV radiator.

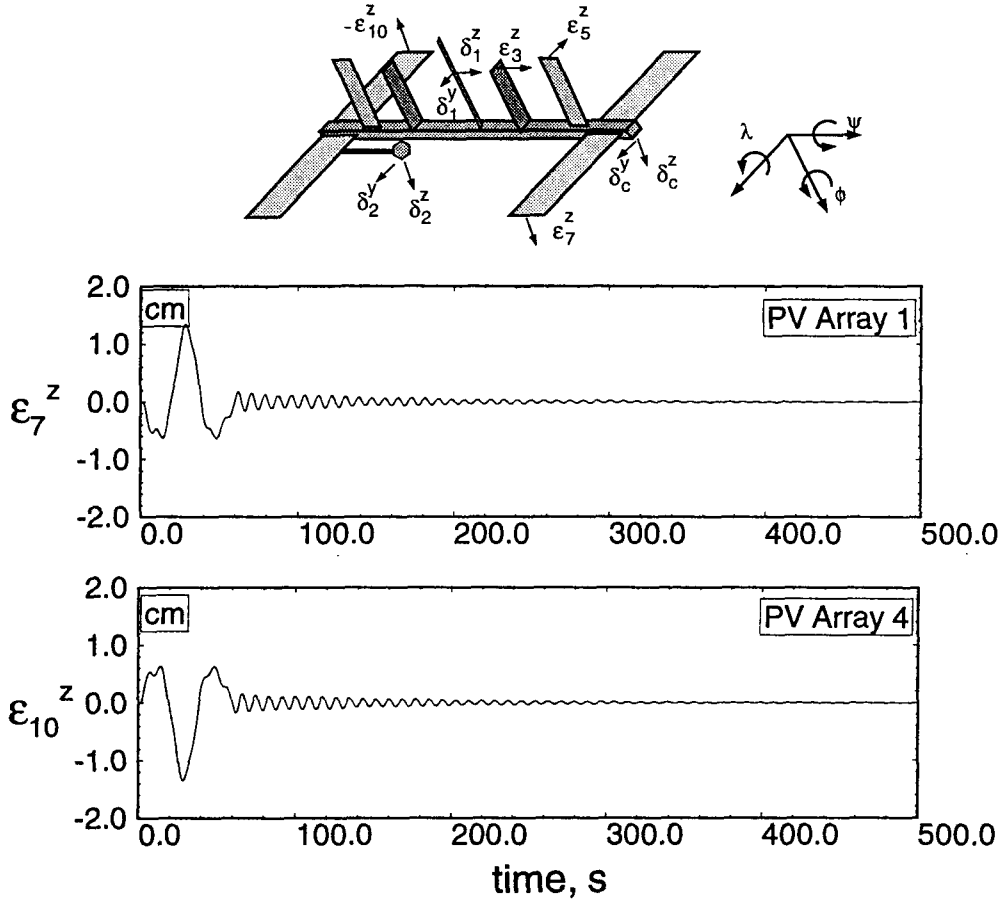

Figure 5-20 Response of the PMC to a 180° slew maneuver of the manipulator, in the ONLV plane, performed in 60 s: (d) tip vibrational response of the PV arrays.

response but the general trends are essentially the same (Figure 5-21). The librational degrees of freedom show instability as before, however, the deviations grow at different rates. Tip vibratory responses of the flexible members remain small and show faster attenuation.

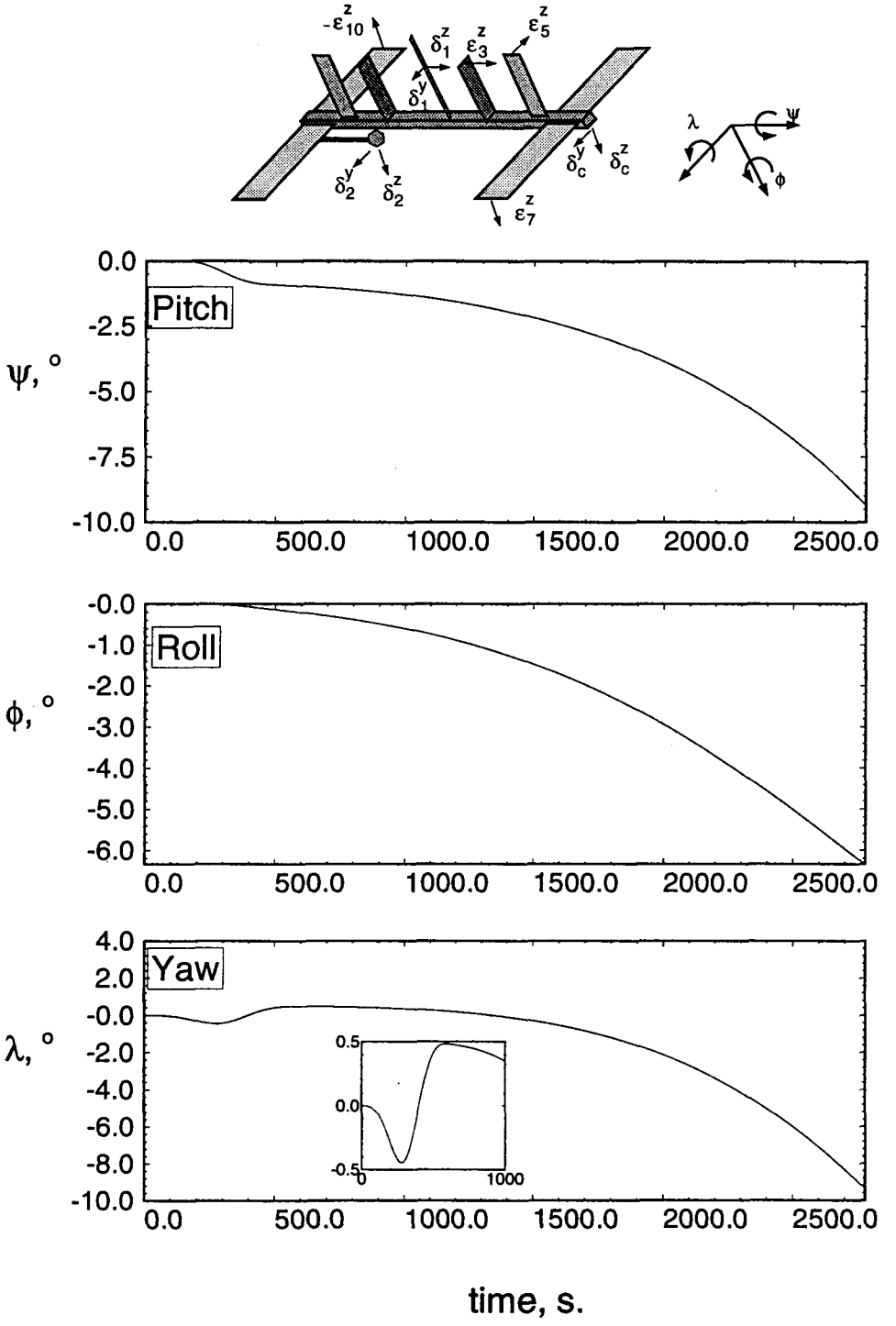

Figure 5-21 Response of the PMC to a slower manipulator maneuver, in the ONLH plane, performed in 600 s: (a) librational time histories.

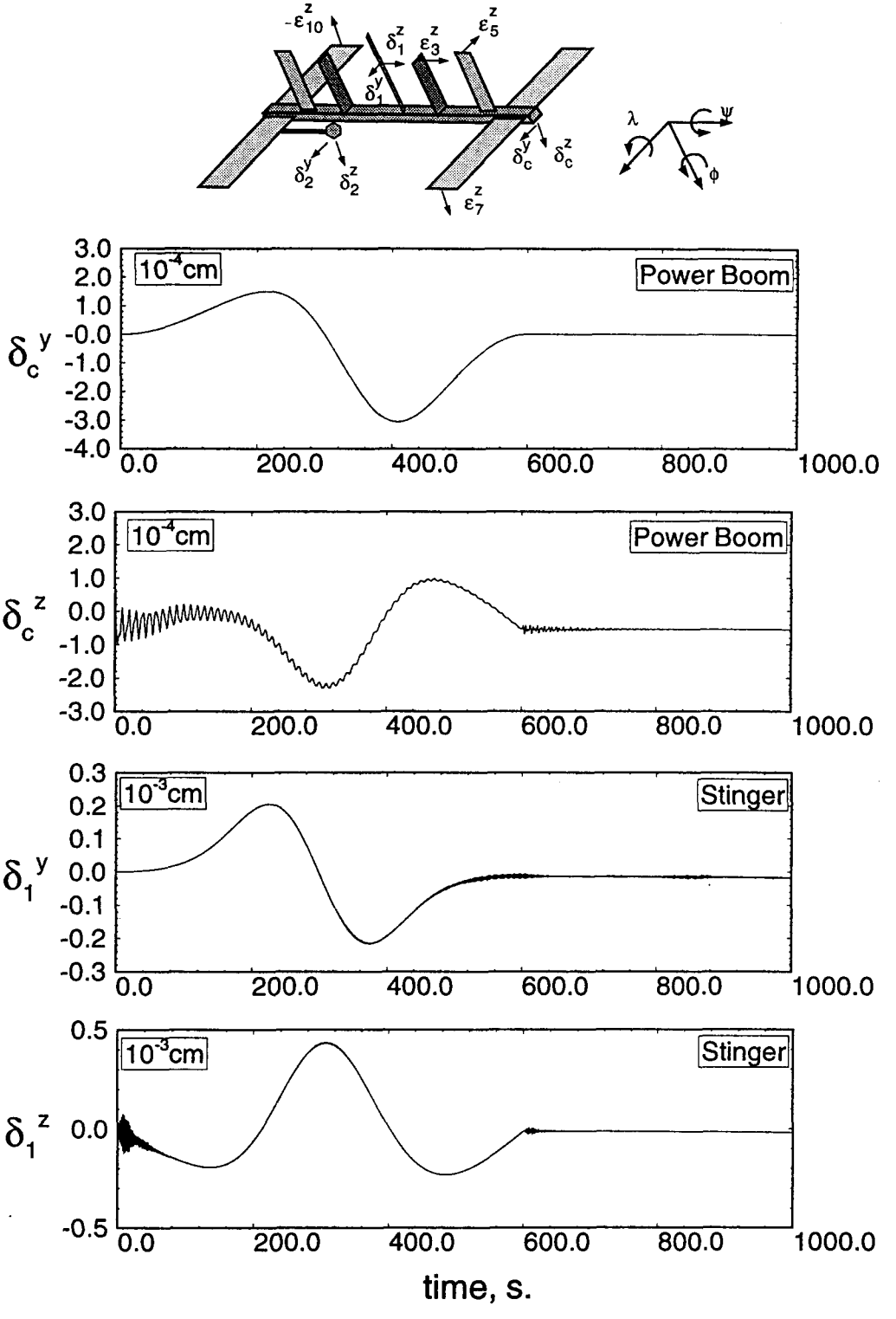

Figure 5-21 Response of the PMC to a slower manipulator maneuver, in the ONLH plane, performed in 600 s: (b) vibrational response of the power boom and stinger.

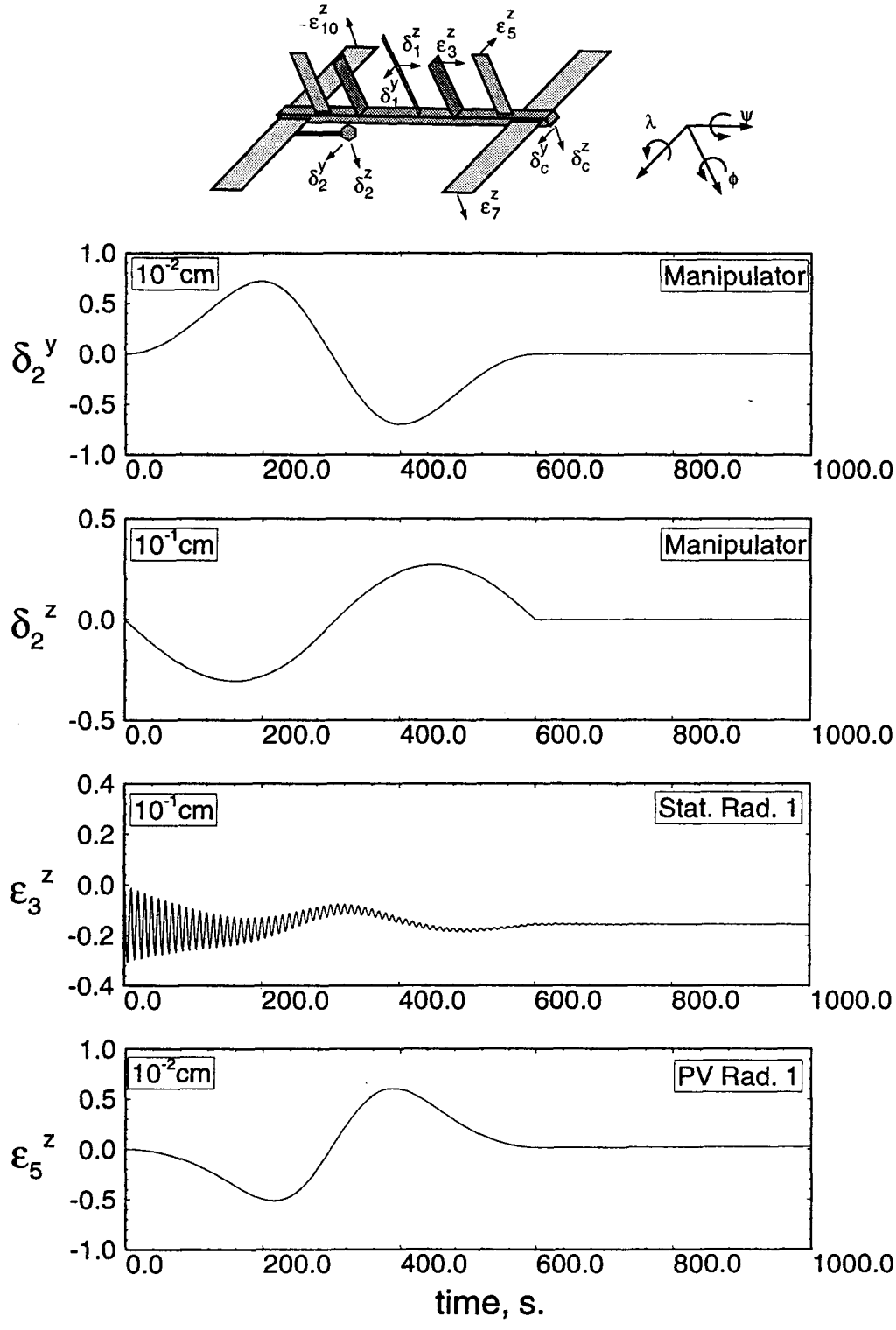

Figure 5-21 Response of the PMC to a slower manipulator maneuver, in the ONLH plane, performed in 600 s: (c) vibrational response of the manipulator, station radiator and PV radiator.

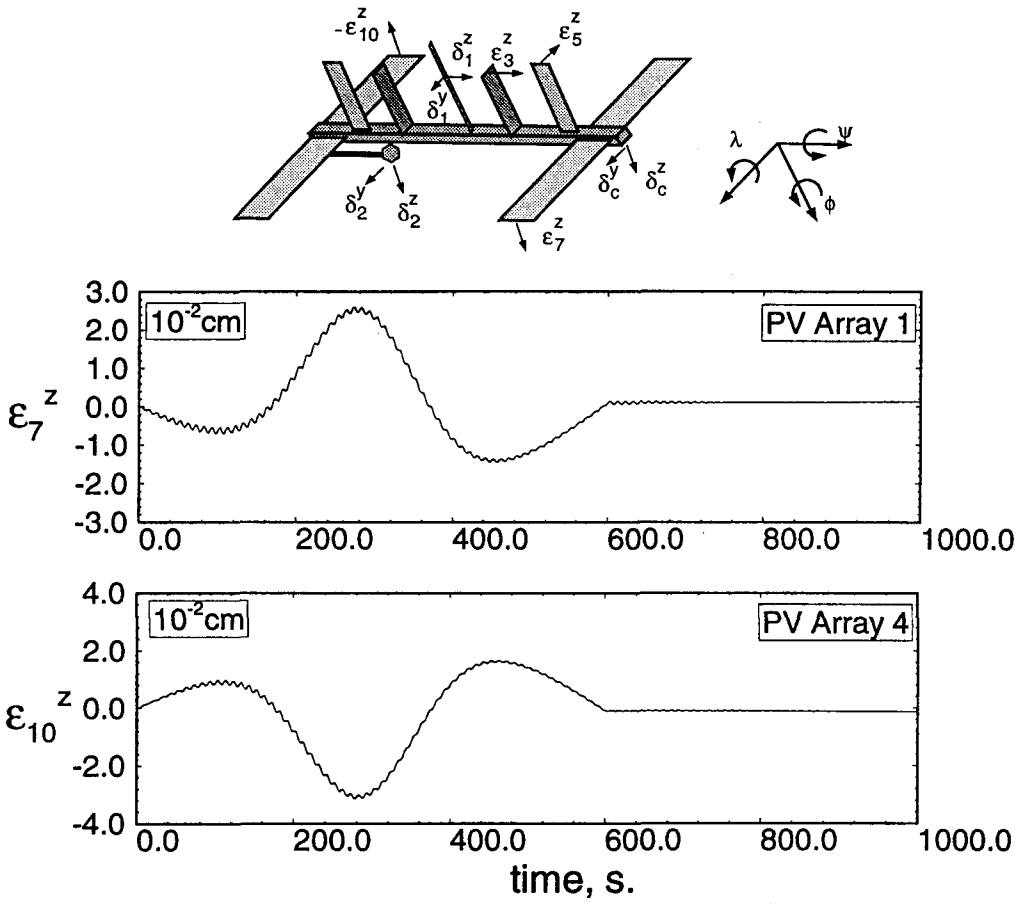

Figure 5-21 Response of the PMC to a slower manipulator maneuver, in the ONLH plane, performed in 600 s: (d) vibrational response of the PV arrays.

5.5 Summary

The versatility of the dynamical formulation and simulation code was demonstrated in this chapter through its use in a variety of applications. First, the ability of the model to accurately incorporate the foreshortening effect was demonstrated.

Next, the improved flexibility modeling through the use of quasi–comparison functions was established. Both these features were illustrated through the use of generic space platform models with a slewing appendage. Next, the effects of shuttle docking and manipulator maneuvers on the dynamics of the First Element Launch (FEL) configuration of the Space Station were investigated. Finally, the influence of solar array slewing and manipulator maneuvers on the Permanently Manned Configuration (PMC) of the Station were studied. Besides providing useful results on the performance of the various space station configurations when exposed to different disturbances, it clearly establishes the potential of this powerful tool in the design and operational management of complex multibody flexible systems.

6. CONTROLLED MOTION

6.1 Preliminary Remarks

For various operational reasons, at times spacecraft have to be placed in unstable orientations. For example, in order to maximize the earth viewing area for the proposed space station, its power boom will be aligned with the orbit normal resulting in unstable librational motion. In many cases, even a stable orientation results in unacceptable librational response due to the various environmentally induced and operational disturbances. Systems for attitude control are an integral part of almost all present–day spacecraft. For flexible satellites, the disturbances may result in large vibrations, partly due to low damping. Passive means of control is often not feasible or adequate, and hence one is forced to resort to some active control procedure for successful completion of the mission.

In the previous chapter, the unstable and nonequilibrium character of the attitude dynamics of the space station was shown, and the need for active attitude control established. One of the principal objectives of the space station program is the exploitation of the space environment for scientific and commercial benefits, including the production of high purity drugs and crystals. In order to achieve this goal, low microgravity levels in the vicinity of the experimental modules are necessary. Therefore, active vibration control of the power boom, to which the modules are attached, may be required to improve upon its structural damping characteristics.

In this chapter, a number of linear control design techniques are applied to two configurations of the proposed space station. For the FEL configuration, the Linear Quadratic Regulator (LQR), Linear Quadratic Gaussian/Loop Transfer Recovery (LQG/LTR) and the H_∞ techniques are applied for attitude control. Vibrations

are not controlled, however, the effect of flexibility is incorporated as modeling error. Thus, the controller design can be made robust against the unmodeled flexible dynamics, ensuring that instability in the closed loop system will not arise.

Next, simultaneous attitude and vibration control of the PMC of the space station is considered. A high order linearized model is first obtained. It is partitioned into the rigid and flexible subsystems. Working first with the flexible subsystem after applying robust model reduction, a controller is designed using the LQG/LTR approach. The error between the reduced order (design) and the original model is evaluated, and the controller design is forced to satisfy a robustness test based on that error. The resulting "flexible" controller is then applied to the full (unpartitioned) system, to obtain an augmented model. The LQG/LTR technique is again applied to the augmented model, after model reduction, to design a "rigid" controller. As in the previous step, the robustness of the design against the unmodeled dynamics is ensured. Finally the "rigid" and "flexible" controllers are combined to give the "complete" controller. For both the FEL and PMC, the effectiveness of the resulting controller is assessed through its application to the original nonlinear, time–varying system. Controlled performance during the slewing of manipulators and solar arrays is also studied for the original nonlinear system. For a simulation based investigation, this represents a logical procedure for assessing the performance of the control system synthesis.

6.2 First Element Launch (FEL)

The FEL configuration of the proposed space station (Figure 3-9) was described in Chapter 3, with its physical characteristics given in Table 3-1. In this case, a structural damping coefficient equal to 1% of its critical value is assumed to be present. To summarize, the simulation results in Chapters 3 and 5 conclude that the FEL is

unstable in libration and is prone to excitation from operational disturbances such as orbiter docking and RMS maneuvers. In terms of dynamic performance, attitude stability and the response characteristics are of primary importance. Therefore, for the FEL an attitude control system is designed employing three different control techniques: the LQR, LQG/LTR and H_∞ methods.

6.2.1 Linear Quadratic Regulator (LQR) Control

The LQR theory is described in detail in Ref. 105 and its application to Linear Time–Invariant (LTI) systems is briefly summarized in Appendix VIII.

The proposed space station will be provided with Control Moment Gyros (CMG's) for attitude stabilization and control. For the purposes of this investigation, the CMG's are taken to be simple torque generating devices located at the center of the power boom. A set of three CMG's are assumed, one for each direction. Colocated at the CMG position are a set of three sensors (say position gyroscopes) which measure the system output, i.e. the pitch, roll and yaw angles. Two linearized models of the FEL are obtained from the flexible multibody program: (i) the design model, which considers the system rigid; and (ii) the truth model, which accounts for the flexibility with discretization using a single shape function for each flexible member. For this control study the manipulator is taken to be absent. The design model consists of a set of three second–order ODE's (i.e. 6 states), while the truth model is described by a set of ten second–order ODE's (20 states). Both the models are linearized about the zero state. As seen before (p. 166), the only nonzero equilibrium state of the system is the yaw angle, which has an equilibrium value of $\lambda_e = 0.74°$. Both the models have the following mathematical form:

$$\dot{\mathbf{x}} = \mathbf{A}\mathbf{x} + \mathbf{B}\mathbf{u};$$

$$\mathbf{y} = \mathbf{C}\mathbf{x}. \tag{6.1}$$

$\mathbf{x}$, $\mathbf{y}$, and $\mathbf{u}$ are the state, output and control input vectors of the system, respectively, while $\mathbf{A}$, $\mathbf{B}$, and $\mathbf{C}$ are time–invariant matrices. Their details (for the design and truth models) are given in Appendix IX.

The system controllability, $\mathcal{C}$, and observability, $\mathcal{O}$, matrices are evaluated as follows:

$$\begin{aligned} \mathcal{C} &= [\,\mathbf{B} \quad \mathbf{AB} \quad \mathbf{A^2B} \quad \cdots \quad \mathbf{A^{n-1}B}\,]; \\ \mathcal{O} &= \begin{bmatrix} \mathbf{C} \\ \mathbf{CA} \\ \mathbf{CA^2} \\ \vdots \\ \mathbf{CA^{n-1}} \end{bmatrix}. \end{aligned} \tag{6.2}$$

The truth model is unobservable and uncontrollable, while the design model is controllable and observable.

The objectives of the controller design are as follows: (i) stabilization of the attitude motion; (ii) sufficiently high bandwidth for the system, resulting in a relatively fast response; (iii) adequate damping of the attitude motion to avoid excessive overshoot; and (iv) acceptable control requirement for expected disturbances to avoid saturation of the CMG's. As is the case with most engineering designs, some of the goals are not entirely compatible, and hence one has to introduce some rational compromises. The maximum levels for the CMG torque and its total momentum capacity are taken as 270 N-m, and 27 kN-m-s, respectively [39]. The station is required to maintain an attitude within $\pm 1^\circ$ of the nominal orientation.

A common design procedure for multivariable control systems involves the representation of the performance specification as a low frequency barrier, and identifying a model uncertainty as a high frequency bound. Then, the robustness of the controller

design to model uncertainty as well as the specified performance can be ensured by employing various tests. In the present case, the stability robustness test for model uncertainty in employed, although the performance test is not used. Rather, the system response to disturbances is simulated, and the resulting control input requirements are determined to ensure that CMG saturation is avoided.

In this investigation, a pre–multiplicative model uncertainty or error is employed. The error, denoted by $\mathbf{E_m}(s)$, is defined as follows:

$$\mathbf{G_f}(s) = [\mathbf{I} + \mathbf{E_m}(s)]\,\mathbf{G_r}(s); \tag{6.3}$$

where $\mathbf{G_f}(s)$ and $\mathbf{G_r}(s)$ are the transfer function matrices of the truth and design models, respectively. The relationship between the models and the error is shown in a block diagram form in Figure 6-1 .

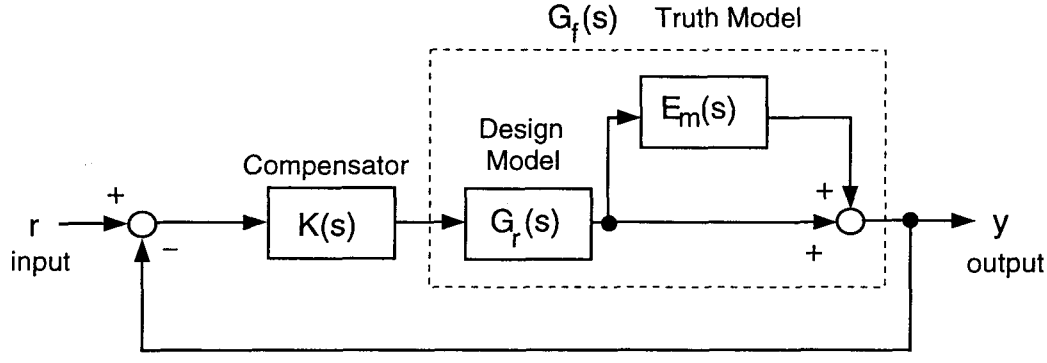

Figure 6-1 Multiplicative model error.

The criterion for a Multi–Input, Multi–Output (MIMO) system to be robust, from the stability point of view, to model uncertainty is obtained from a generalization of the Nyquist criterion for Single–Input, Single–Output (SISO) systems [115]. The

condition for multiplicative model error or uncertainty is

$$\underline{\sigma}\left[\mathbf{I}+(\mathbf{G_r}(j\omega)\mathbf{K_c}(j\omega))^{-1}\right] > \overline{\sigma}[\mathbf{E_m}(j\omega)], \tag{6.4}$$

where $\overline{\sigma}[\cdot]$ and $\underline{\sigma}[\cdot]$ are the maximum and minimum singular values, respectively.

The LQR design procedure was repeated with various values of the state weighting matrix, $\mathbf{Q}$, and the control weighting matrix, $\mathbf{R}$, until an acceptable performance (bandwidth) was achieved, along with the stability robustness criterion satisfied. The MATLAB software package with the *Control System Toolbox* [116] were employed for the LQR design. The final weighting matrices for the final design were found to be:

$$\mathbf{Q} = \begin{bmatrix} 1 & 0 & 0 & 0 & 0 & 0 \\ 0 & 1 & 0 & 0 & 0 & 0 \\ 0 & 0 & 1 & 0 & 0 & 0 \\ 0 & 0 & 0 & 0 & 0 & 0 \\ 0 & 0 & 0 & 0 & 0 & 0 \\ 0 & 0 & 0 & 0 & 0 & 0 \end{bmatrix}; \tag{6.5}$$

$$\mathbf{R} = \begin{bmatrix} 50 & 0 & 0 \\ 0 & 50 & 0 \\ 0 & 0 & 50 \end{bmatrix}; \tag{6.6}$$

with the resulting state feedback gain matrix $\mathbf{K_{lqr}}$ as

$$\mathbf{K_{lqr}} = \begin{bmatrix} 1.4066e-01 & -2.079e-03 & -5.499e-04 & \cdots \\ -1.232e-07 & -4.293e-02 & 1.4118e-01 & \cdots \\ 1.8251e-03 & 1.6027e-01 & 4.2388e-02 & \cdots \\ \cdots & 1.3689e+01 & -5.410e-01 & 4.6726e-03 \\ \cdots & -1.115e-06 & -3.737e-01 & 3.8629e+01 \\ \cdots & 1.7770e-01 & 4.1700e+01 & -3.602e-01 \end{bmatrix}. \tag{6.7}$$

The implementation scheme as shown in Figure 6-2 .

In order to ensure that the closed loop system exhibits good tracking properties, the standard LQR state feedback configuration was altered to provide two feedback loops: an output feedback loop which is compared with the reference input, $\mathbf{r}$, and then passed through a constant gain prefilter matrix, $\mathbf{K_{pf}}$; and a pure state feedback

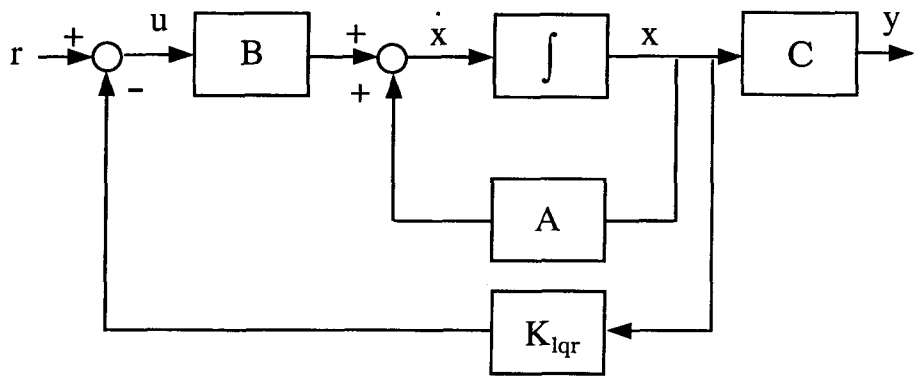

Figure 6-2 The plant with full state feedback.

which is multiplied by a state feedback matrix, $\mathbf{K_{sf}}$. This configuration is shown in Figure 6-3 . The two gain matrices are chosen to ensure that the closed loop poles are identical to those of the standard state feedback system, which yields the equation

$$\mathbf{K_{sf}} + \mathbf{K_{pf}C} = \mathbf{K_{lqr}}, \tag{6.8}$$

and the d.c. (i.e. $\omega = 0$) closed loop gain as unity. This requires that the prefilter gain, $\mathbf{K_{pf}}$, satisfy the relationship

$$\mathbf{K_{pf}} = -\left[\mathbf{C}[\mathbf{A} - \mathbf{B}\mathbf{K_{lqr}}]^{-1}\mathbf{B}\right]^{-1}. \tag{6.9}$$

The resulting prefilter and state feedback gain matrices are:

$$\mathbf{K_{sf}} = \begin{bmatrix} -7.5323e-04 & -3.048e-04 & 0 & \cdots \\ 0 & 0 & 6.1262e-03 & \cdots \\ -9.7164e-06 & 2.3499e-02 & 0 & \cdots \end{bmatrix}$$
$$\begin{bmatrix} \cdots & 1.3689e+01 & -5.4098e-01 & 4.6726e-03 \\ \cdots & -1.115e-06 & -3.7366e-01 & 3.8629e+01 \\ \cdots & 1.7770e-01 & 4.17000e+01 & -3.602e-01 \end{bmatrix}; \tag{6.10}$$

$$\mathbf{K_{pf}} = \begin{bmatrix} 1.4142e-03 & -5.499e-06 & 6.0200e-07 \\ 5.5688e-06 & 1.3506e-03 & -4.293e-04 \\ 6.0215e-07 & 4.2388e-04 & 1.3678e-03 \end{bmatrix}. \tag{6.11}$$

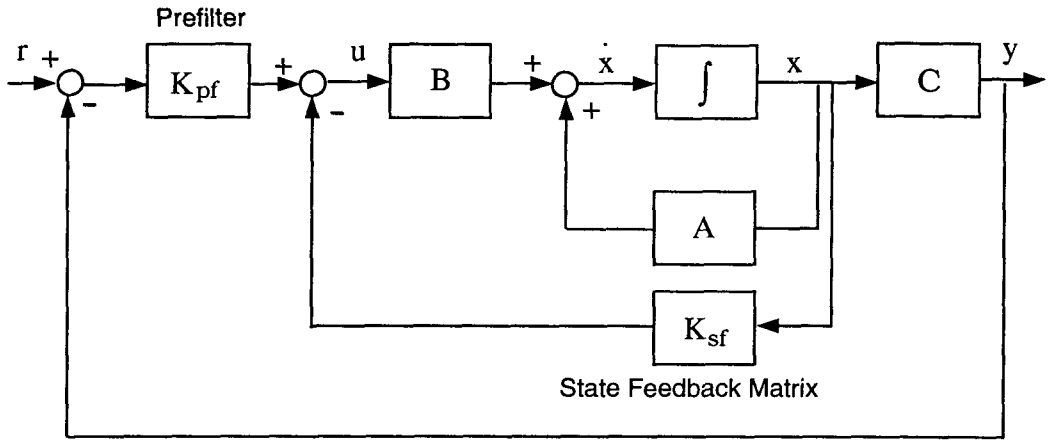

Figure 6-3 State feedback implemented with a prefilter.

With the LQR controller described above, the open loop poles of the system which are located at:

$$\begin{array}{ll} & \pm j1.0634e-03; \\ -1.1677e-03 & \pm j9.3692e-04; \\ 1.1677e-03 & \pm j9.3692e-04; \end{array} \tag{6.12}$$

are shifted via state feedback to:

$$\begin{array}{ll} -1.0275e-02 & \pm j1.0330e-02; \\ -3.7390e-03 & \pm j4.5932e-03; \\ -3.7600e-03 & \pm j2.4595e-03. \end{array} \tag{6.13}$$

The unstable open loop poles are stabilized with a reasonable level of damping. Moreover, the bandwidth of system is also increased. The robustness of the system to the unmodelled flexible dynamics is shown in Figure 6-4 . Note, the system is quite robust to disturbances in the entire frequency range except around 1 rad/s, and to a lesser extent at approximately 4 rad/s, which correspond to system modes dominated by anti–symmetric solar panel and stinger vibration, respectively. The singular values of $\mathbf{K_{lqr}}(s\mathbf{I}-\mathbf{A})^{-1}\mathbf{B}$, which provide a measure of the bandwidth of the system, are shown in Figure 6-5 .

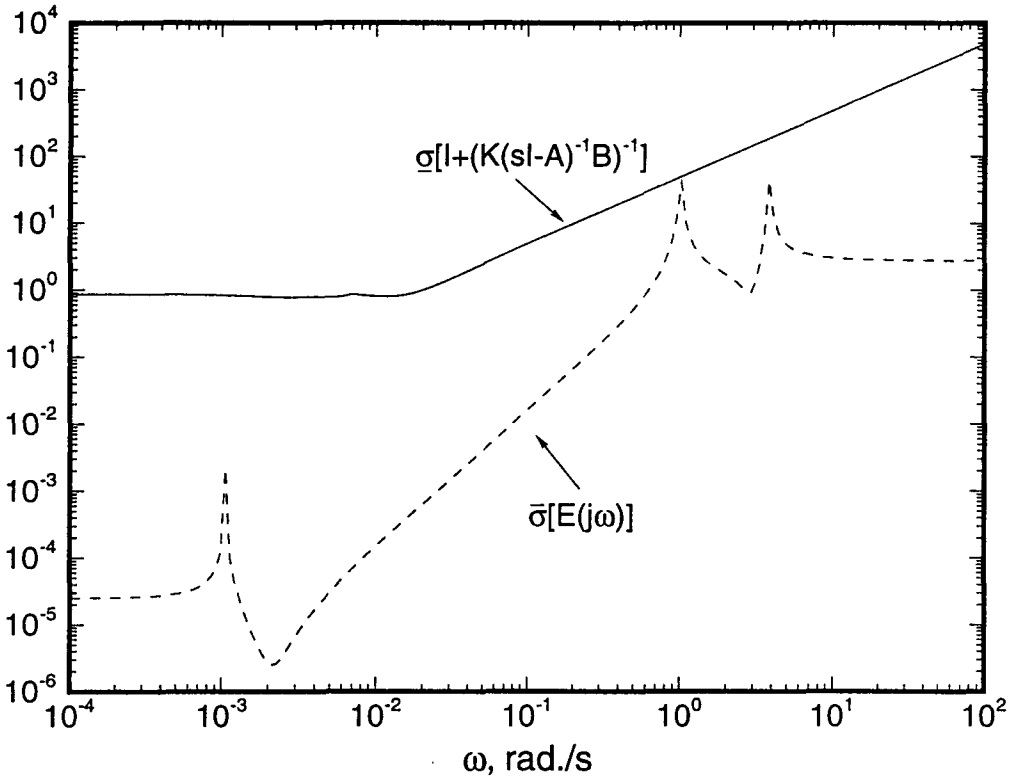

Figure 6-4 Stability robustness test for the LQR design.

A comprehensive set of controlled and uncontrolled nonlinear simulation results were obtained. For brevity, only two cases are presented here: one corresponding to an initial disturbance in roll; while the other involves an initial tip deflection imparted to the power boom. The truth model described earlier, which includes a single flexible d.o.f. for each plate member, and two flexible d.o.f. for each beam element (one for each transverse direction), was used. Note, any excitation of the flexible d.o.f.'s by the controller will be apparent. First, the controller's ability to regulate a roll disturbance of 5° is investigated. The controlled librational response is given in Figure 6-6 a. The FEL experiences minor pitch perturbations in the first

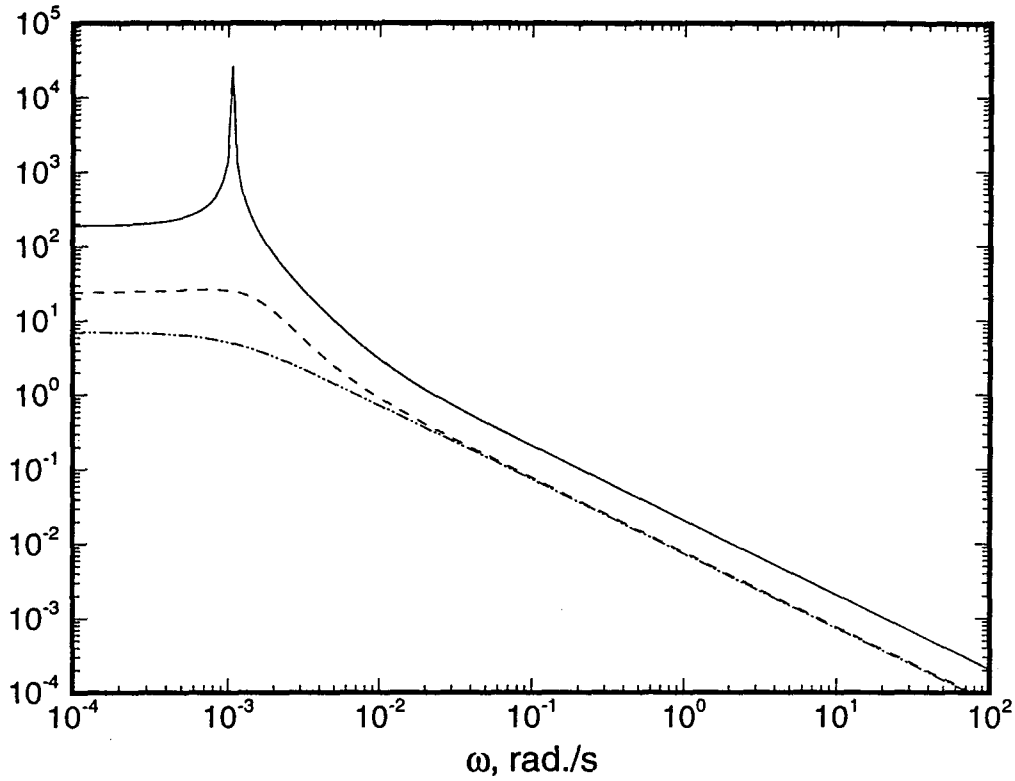

Figure 6-5 Singular values of $\mathbf{K_{lqr}}(s\mathbf{I} - \mathbf{A})^{-1}\mathbf{B}$.

300 s. The high frequency of this response indicates that its source is the dynamic coupling with the vibration of a flexible member, most likely the PV radiator. The roll response settles down relatively quickly without any significant overshoot, and there is some minor excitation ($< 0.4°$) in the yaw which reduces appreciably within 10 minutes. To help appreciate the effectiveness of the controller through comparison, the uncontrolled librational responses are given in Figure 6-6b. In general, the flexible members are hardly excited (Figures 6-6c,d). Even for the most significant response associated with the PV radiator the tip deflection is only 0.3 mm. The CMG torque demand in each direction is shown in Figure 6-6e. As expected, the highest torque

requirement is in the roll direction, where a maximum torque of 15 N-m is needed initially. Due to the coupling between the librational degrees of freedom, there is some torque required in the other directions, notably in the yaw direction. However, it is apparent that the demand on the controller, even for this relatively large librational disturbance of 5°in roll, is quite small. This may lead one to believe that the system bandwidth can be increased, resulting in a faster response. However, the limiting factor in this case is the robustness of the system to the unmodelled dynamics. A larger bandwidth would violate the stability robustness criterion.

To further assess the effect of flexibility on the overall closed loop performance of the system, simulations involving initial conditions to the flexibility d.o.f. were also conducted. One such case is discussed here where the power boom is given a tip deflection of 1 cm in the y_c direction. The librational coordinates exhibited only small perturbations and hence are not presented. The controlled responses of the power boom and stinger exhibit good settling behaviour (Figure 6-7 a). The same can be said of the vibrational responses of the PV arrays and radiator (Figure 6-7b). The CMG torque histories in Figure 6-7c show a relatively large demand, especially for the pitch and roll directions (i.e. about the orbit normal and local horizontal, respectively). The uncontrolled response of the power boom and stinger is shown in Figure 6-7d. In both cases, the vibration amplitudes are slightly larger than when the system is controlled. The same is true for the PV radiator and the arrays (Figure 6-7e). This indicates that the coupling between the flexible degrees of freedom and the controlled librational coordinates results in some attenuation of the vibrational responses.

These series of simulations verify the performance of the control design as indicated by the librational response, as well as the robustness of the control system to

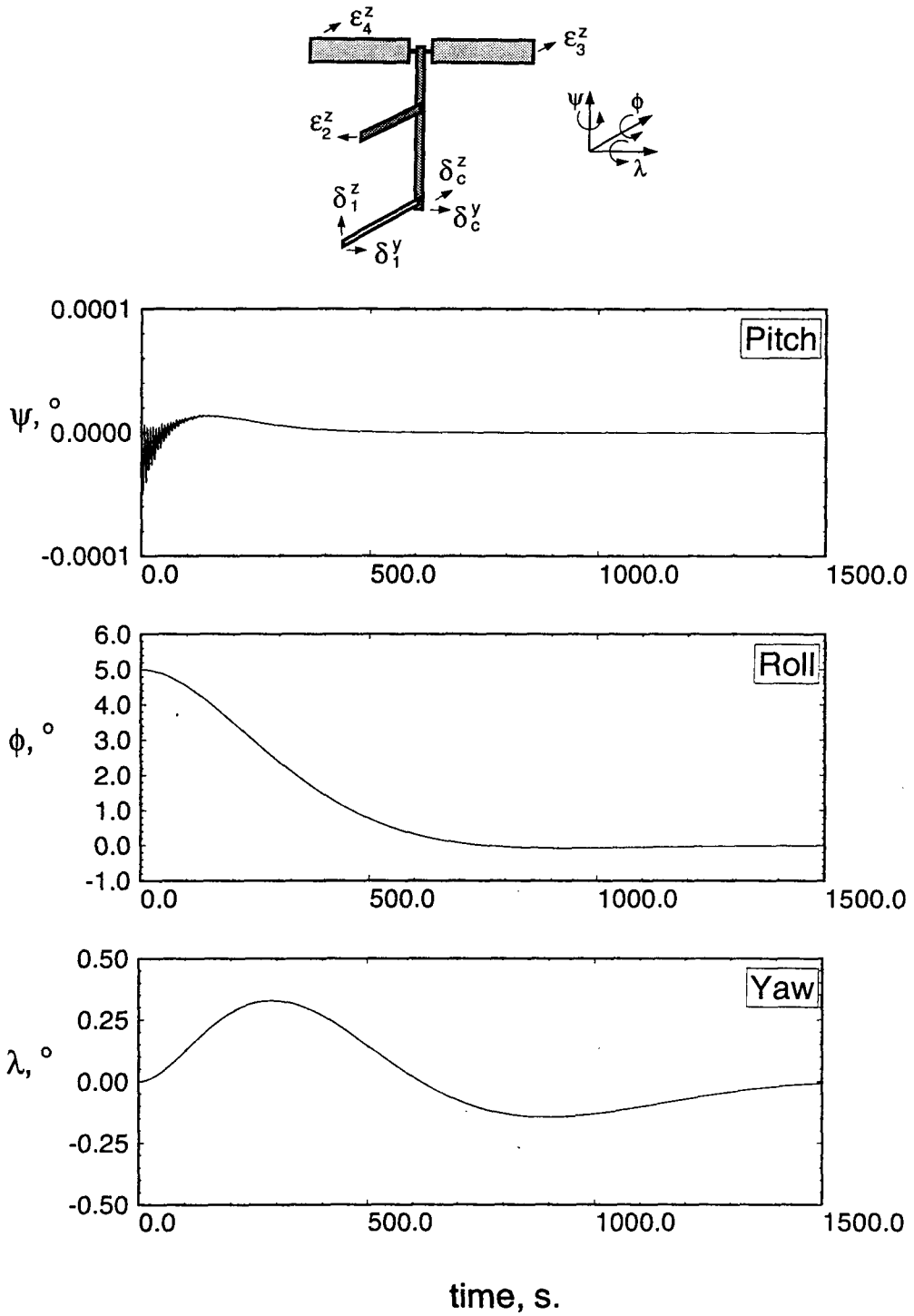

Figure 6-6 (a) Controlled Response: LQR; librational coordinates; $\phi(0) = 5°$.

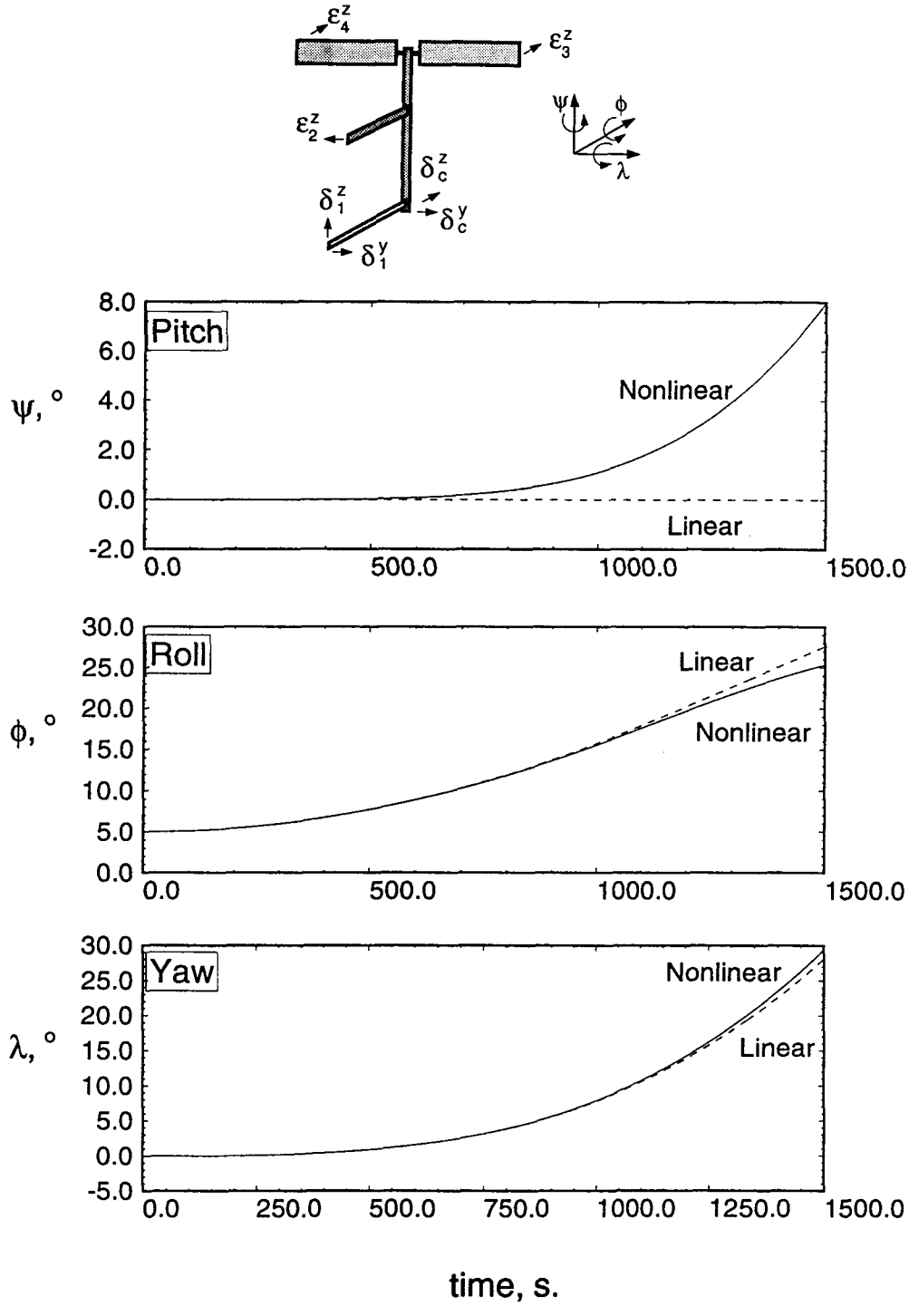

Figure 6-6 (b) Uncontrolled Response: librational coordinates; $\phi(0) = 5°$.

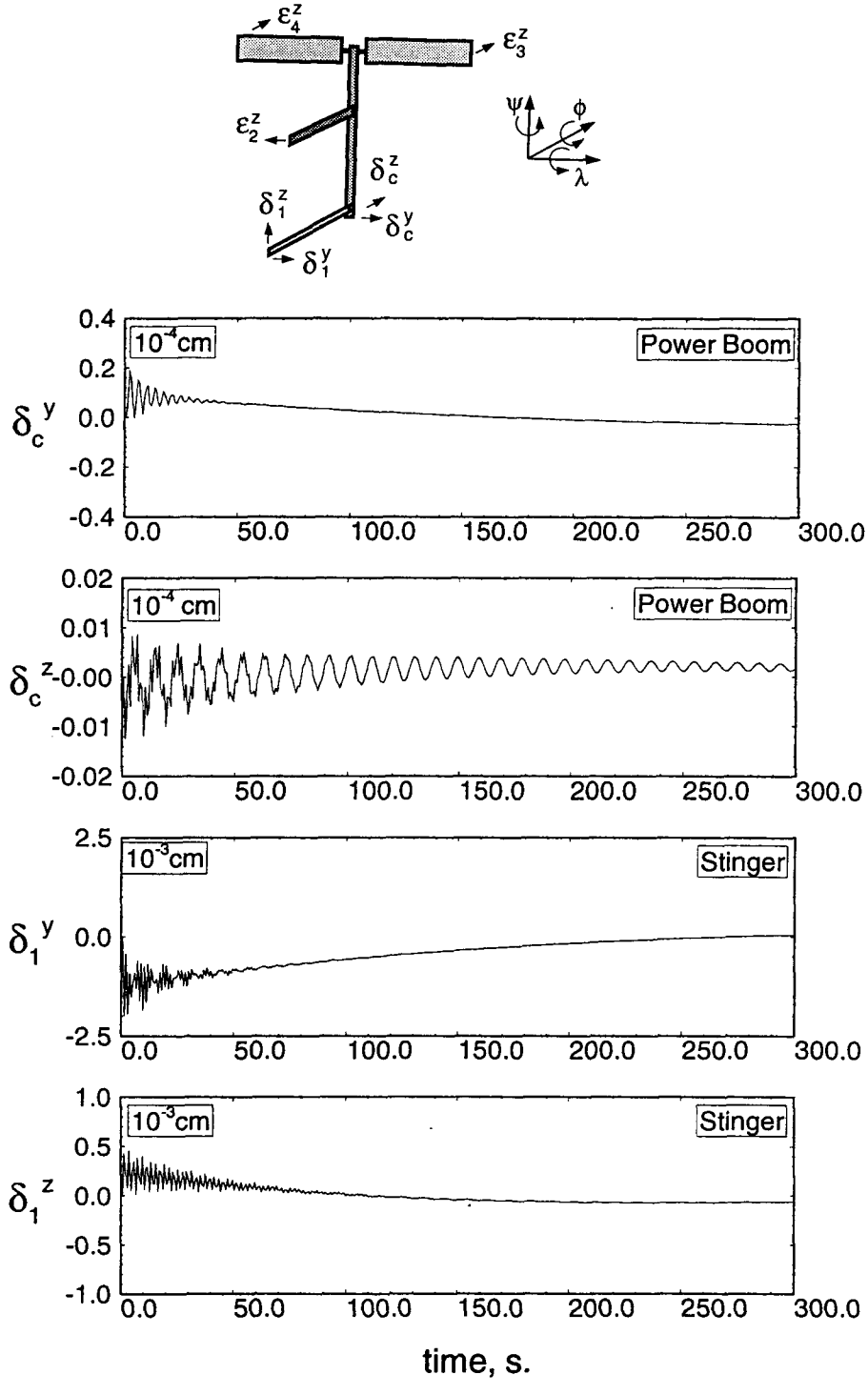

Figure 6-6 (c) Controlled Response: LQR; power boom and stinger tip deflection time histories; $\phi(0) = 5°$.

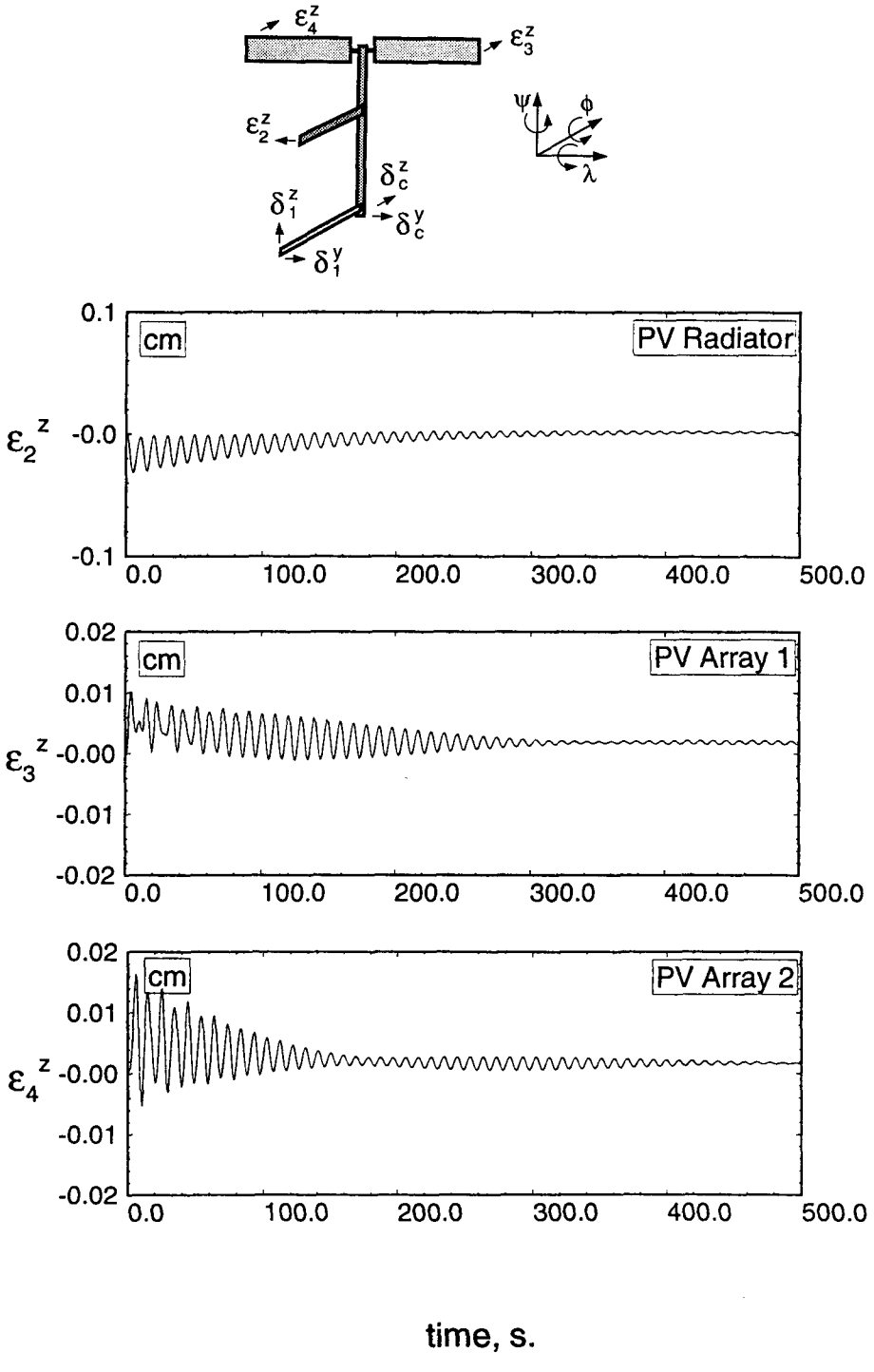

Figure 6-6 (d) Controlled Response: LQR; PV radiator and array tip vibration, $\phi(0) = 5°$.

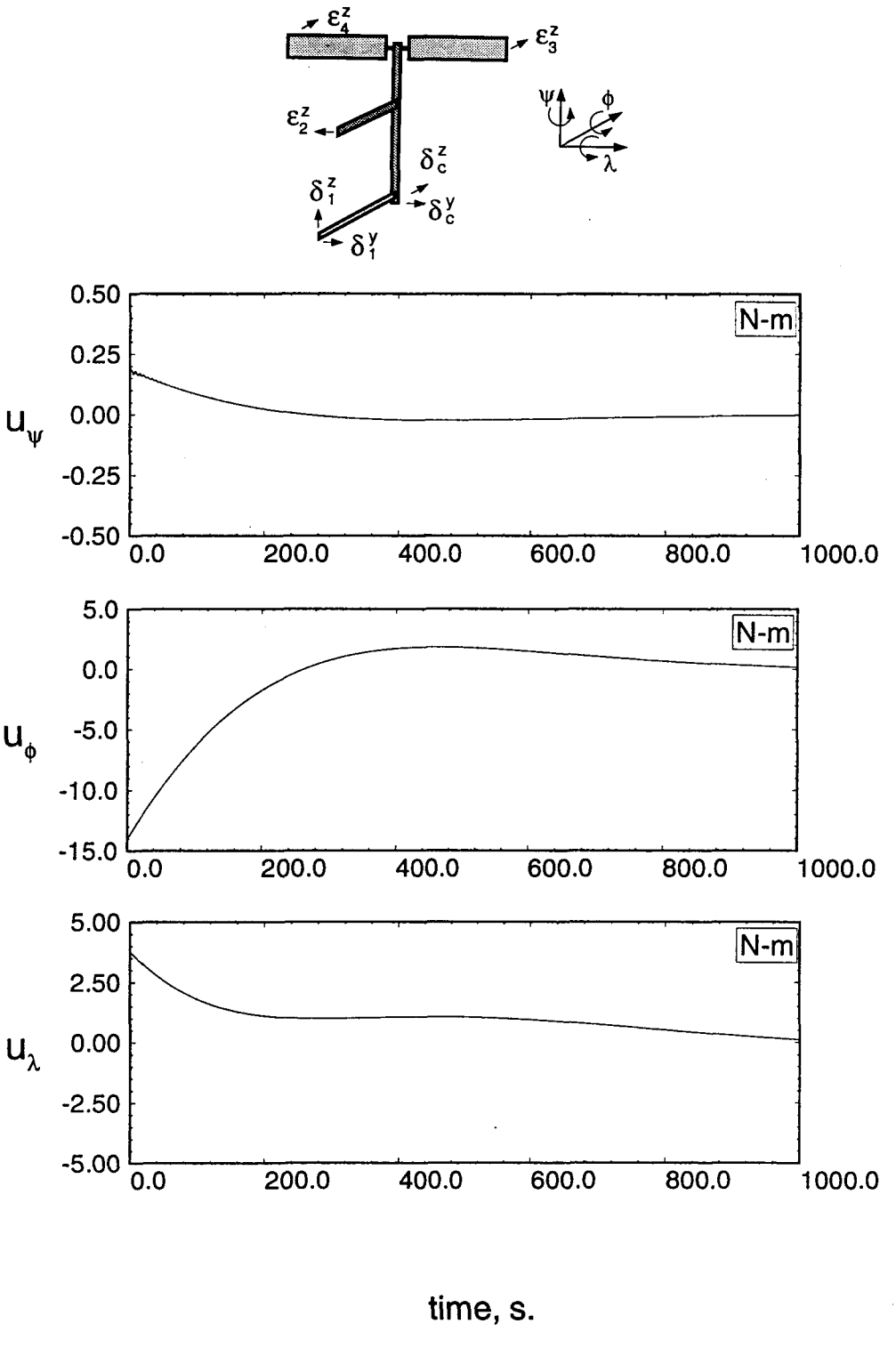

Figure 6-6 (e) Control Torque Requirement: LQR; $\phi(0) = 5°$.

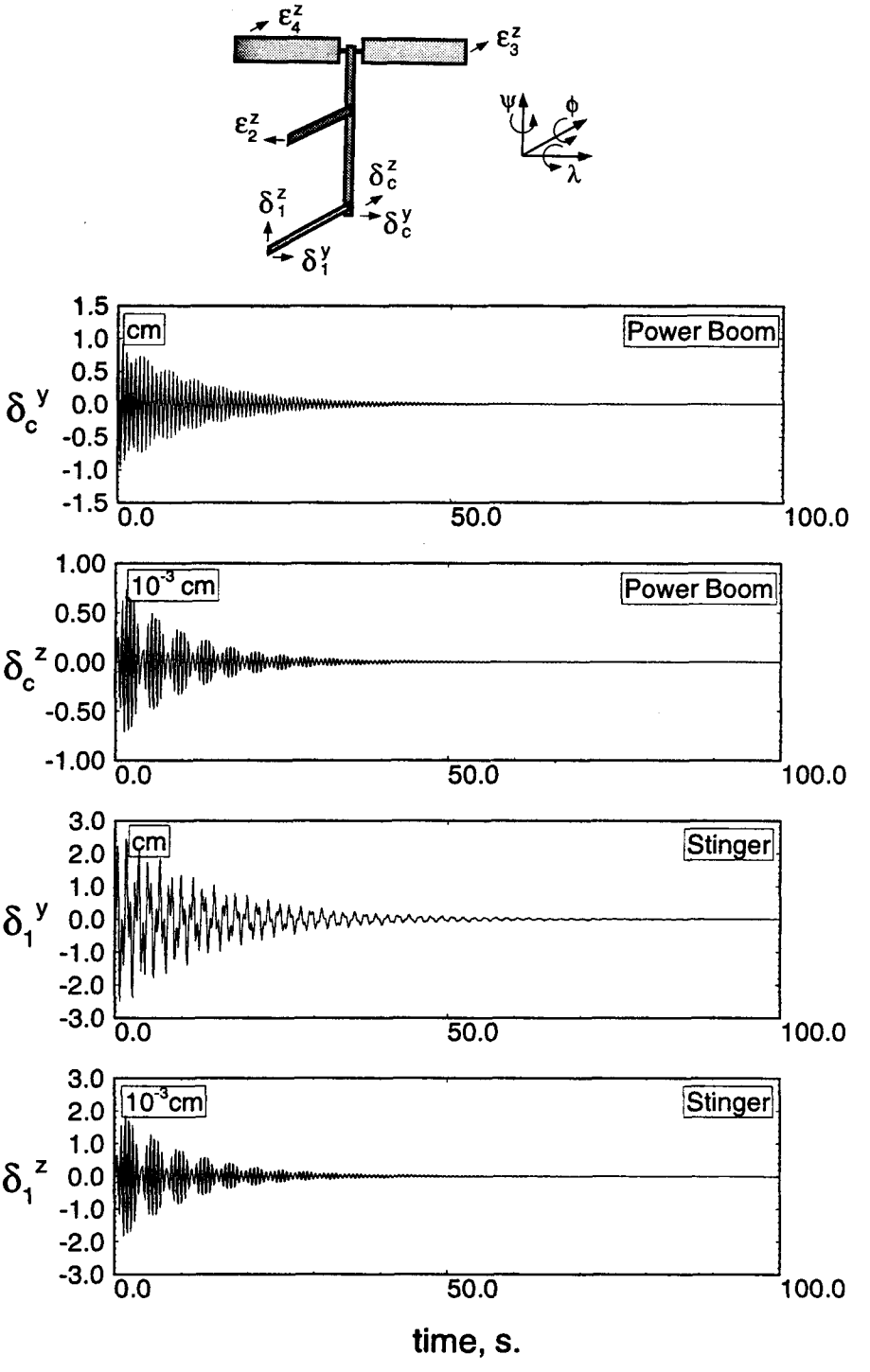

Figure 6-7 (a) Controlled Response: LQR; power boom and stinger tip vibration; $\delta_c^y(0) = 1$ cm.

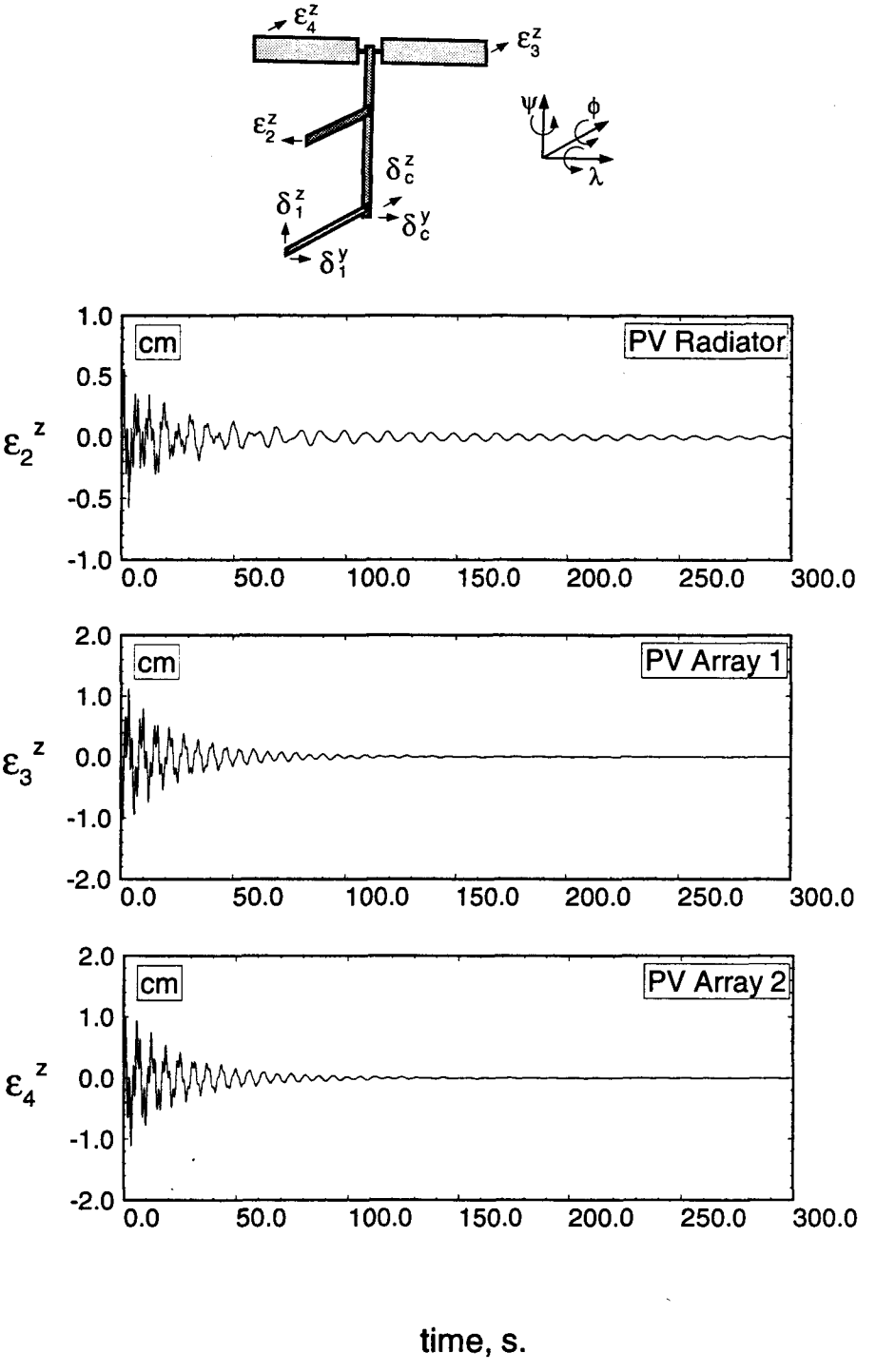

Figure 6-7 (b) Controlled Response: LQR; PV radiator and array tip vibration; $\delta_c^y(0) = 1$ cm.

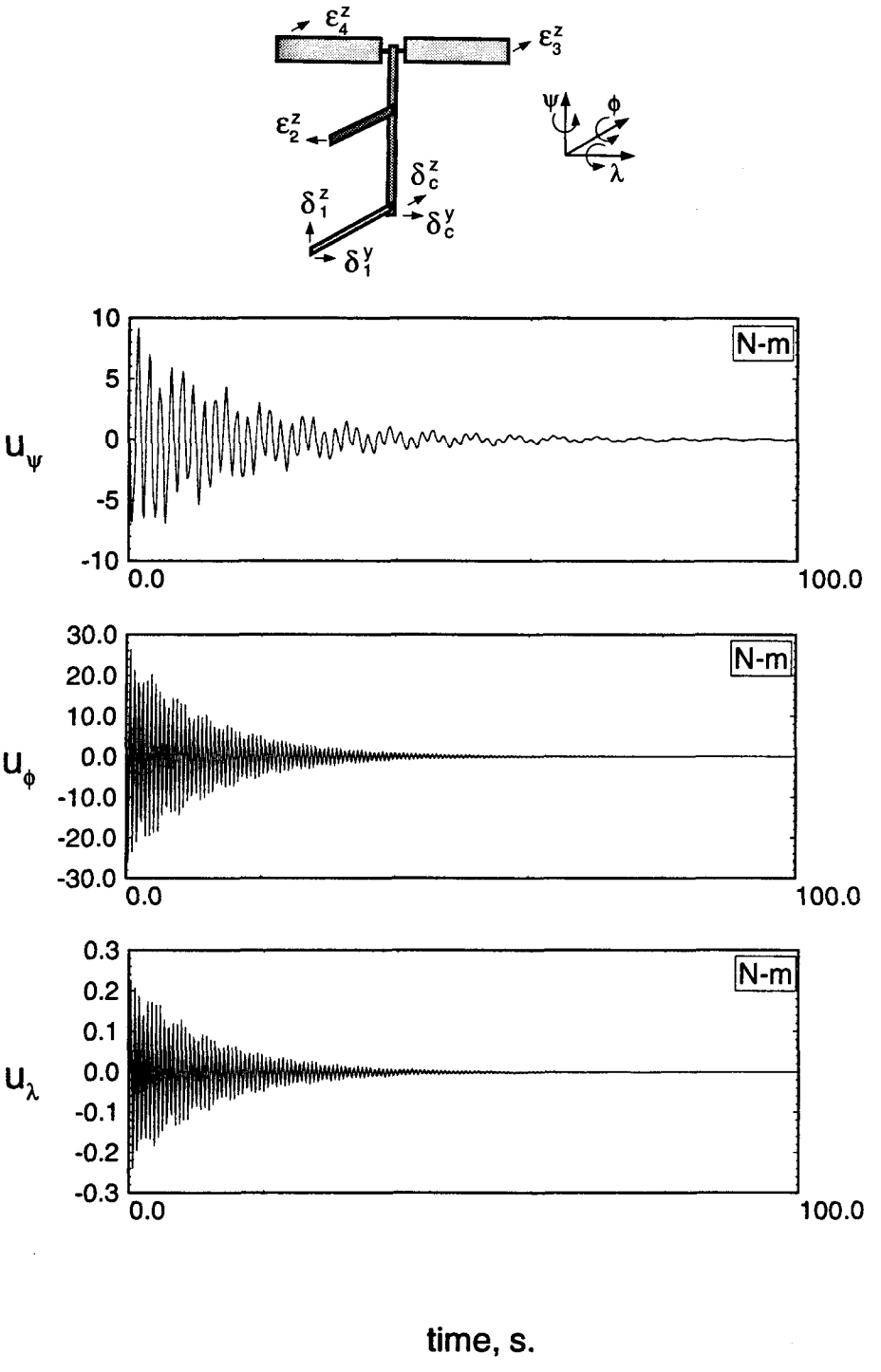

Figure 6-7 (c) Control Torque Requirement: LQR; $\delta_c^y(0) = 1$ cm.

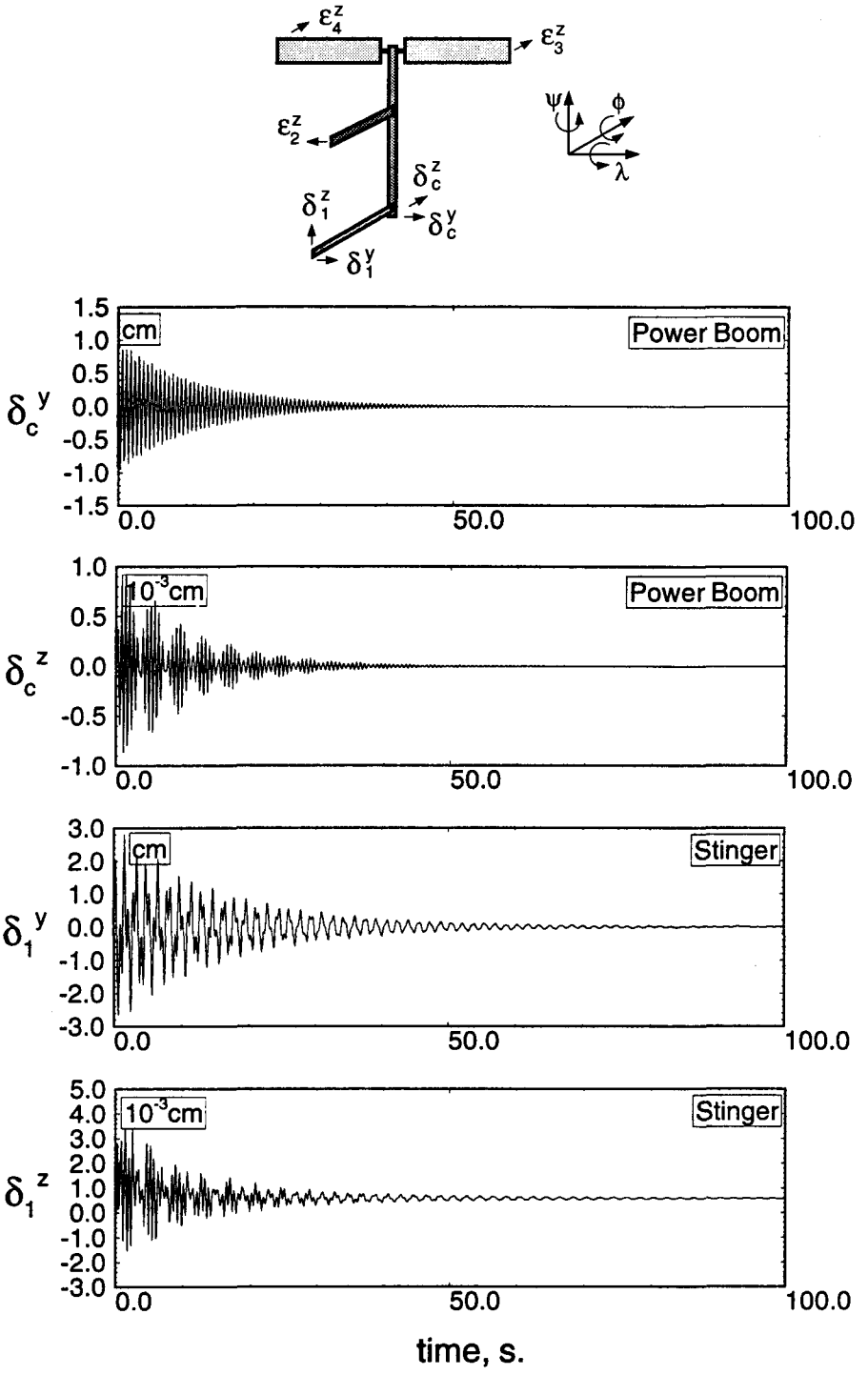

Figure 6-7 (d) Uncontrolled Response: LQR; power boom and stinger tip vibration; $\delta_c^y(0) = 1$ cm.

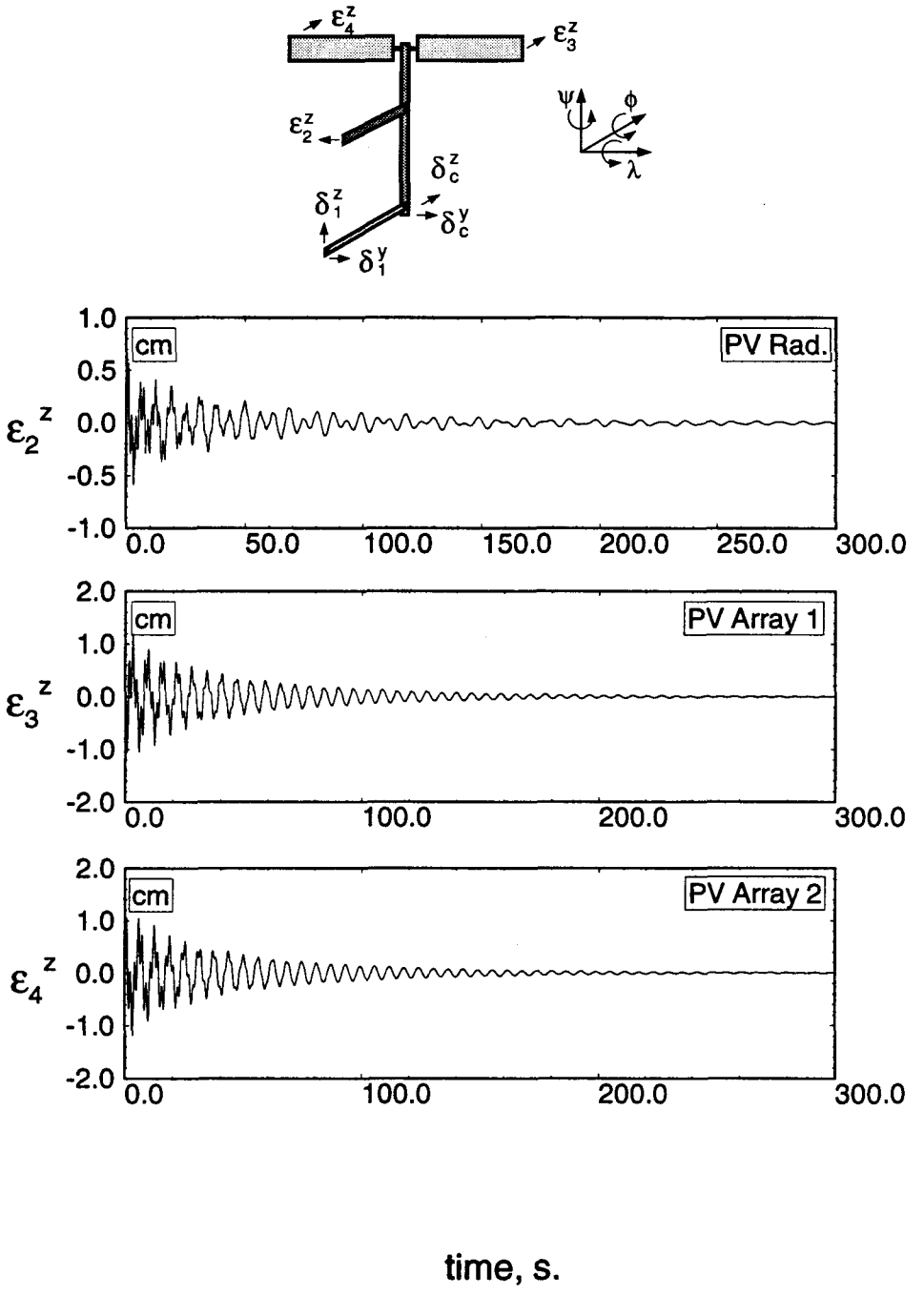

Figure 6-7 (e) Uncontrolled Response: LQR; PV radiator and array tip vibration; $\delta_c^y(0) = 1$ cm.

the unmodelled flexible dynamics. The latter feature is confirmed by the closed loop simulation results to vibrational disturbances.

6.2.2 LQG/LTR Control

The Linear Quadratic Gaussian/ Loop Transfer Recovery (LQG/LTR) design procedure is quite well established [117,118]. Issues pertaining to model uncertainty for multivariable systems have also been explored [115] together with the convergence of the performance of LQG/LTR controllers to those obtained by the LQR procedure [119,120]. A brief outline of the procedure is given in Appendix VIII. Salient features of the LQG/LTR design centers around its suitability for so–called real systems, which are corrupted by noise and have some states which cannot be measured readily. The LQG/LTR procedure involves "recovering" the properties of the LQR, in absence of the full state feedback, through reconstruction of the state using an optimal state estimator or Kalman filter with specific characteristics. Two procedures are available: (a) initially establish an optimal estimator and then recover the design through a Linear Regulator; (b) establish the Linear Quadratic Regulator first, and subsequently recover the design using a Kalman filter. For the FEL, the latter path is followed since the LQR design is already available. Thus, the approach involves recovery of the previous LQR design.

The LTR step is rather straightforward for a minimum–phase system such as the one at hand. It involves design of a Kalman filter (i.e. an optimal observer) with the input noise influence matrix, $\mathbf{\Gamma}$, equal to the the control influence matrix, $\mathbf{B}$ (Appendix VIII). The covariances of the input and measurement noise intensities are taken to be $q\mathbf{I}$ and $\mathbf{I}$, respectively, where q is a scalar quantity. The variable q is used as a tuning parameter which is increased until sufficient recovery is achieved. In the limit as $q \rightarrow \infty$, the LQR loop transfer function approaches the loop transfer

function for the combined compensator–plant system (broken at the plant input),

$$\lim_{q\to\infty} \mathbf{K_c}(s\mathbf{I}-\mathbf{A}+\mathbf{B}\mathbf{K_c}+\mathbf{K_f}\mathbf{C})^{-1}\mathbf{K_f}\mathbf{C}(s\mathbf{I}-\mathbf{A})^{-1}\mathbf{B}$$
$$= \mathbf{K_c}(s\mathbf{I}-\mathbf{A})^{-1}\mathbf{B}. \tag{6.14}$$

However, to avoid a loss in robustness, the parameter q should not be increased beyond the value neccessary to recover the bandwidth of the LQR design. An acceptable degree of recovery for the FEL was found with $q = 10^7$. The dynamic model of the resulting compensator can be represented in state space form as:

$$\dot{\mathbf{x}}_\mathbf{c} = \mathbf{A_c}\mathbf{x_c} + \mathbf{B_c}(\mathbf{r}-\mathbf{y});$$
$$\mathbf{u} = \mathbf{C_c}\mathbf{x_c}; \tag{6.15}$$

where $\mathbf{u}$ and $\mathbf{y}$ are the input and output vectors of the plant, respectively. The matrices $\mathbf{A_c}$, $\mathbf{B_c}$ and $\mathbf{C_c}$ are given in Appendix IX. The transmission zeros of the compensator are:

$$\begin{array}{l} -3.7482e-03 \pm j1.0578e-03; \\ -1.0272e-02; \end{array} \tag{6.16}$$

and the resulting closed–loop poles of the compensator–plant arrangement are:

$$\begin{array}{l} -2.7397e+1 \pm j2.7397e+1; \\ -9.5762e+0 \pm j9.5762e+0; \\ -9.7533e+0 \pm j9.7533e+0; \\ -1.0275e-2 \pm j1.0330e-2; \\ -5.7182e-3 \pm j5.1001e-3; \\ -1.7808e-3 \pm j2.9816e-3. \end{array} \tag{6.17}$$

The first three pairs are the compensator poles. Note, the first two zeros are close to two of the open loop poles of the plant (eq. 6.12). This suggests some cancellation between the compensator and plant dynamics. The singular values of the LQG/LTR compensator $\mathbf{K_c}(s)$ are shown in Figure 6-8 .

The constant gain precompensator, $\mathbf{P}$, used to improve the tracking behaviour of

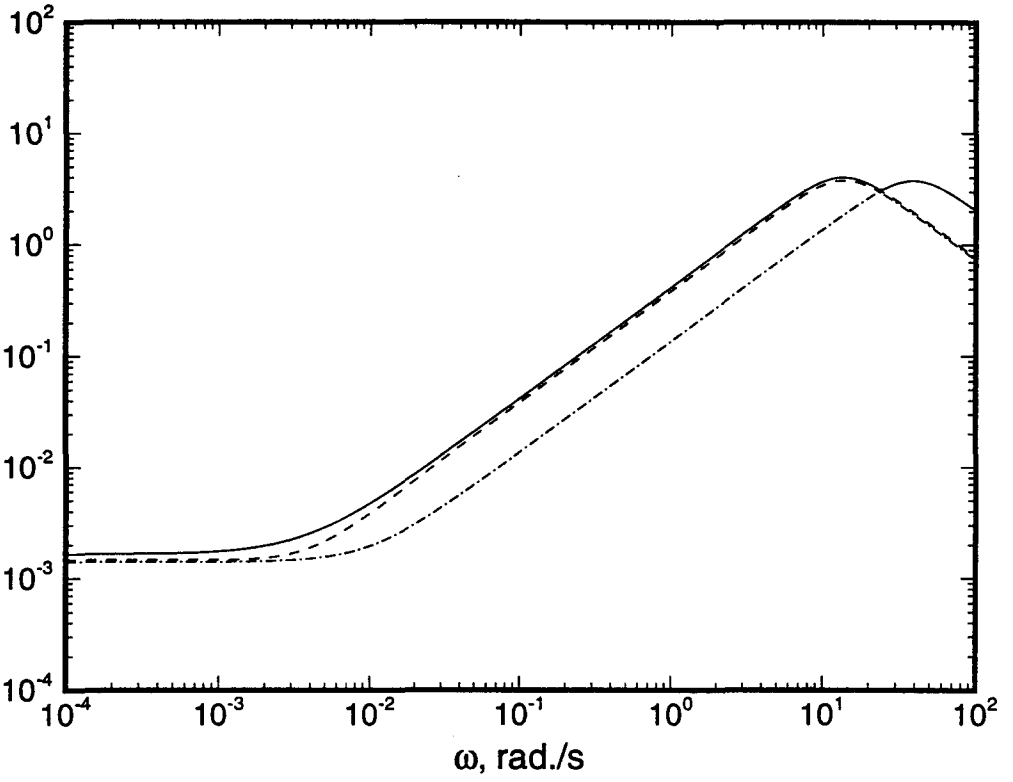

Figure 6-8 Singular values of the LQG/LTR compensator.

the closed–loop system, is found by forcing the closed–loop d.c. gain to unity. The implementation of the precompensator is shown in Figure 6-9 and its value is found to be

$$\mathbf{P} = \begin{bmatrix} 1.0053e+00 & 1.3963e-04 & 1.8308e-03 \\ -5.289e-04 & 9.5981e-01 & 4.0769e-02 \\ 1.8309e-03 & -1.076e-02 & 8.6422e-01 \end{bmatrix}. \tag{6.18}$$

The LQG/LTR design is robust against the modelling error. The test is presented in Figure 6-10 , along with the results for the LQR state feedback design. The closeness of the two results demonstrates the high degree of recovery achieved. Except

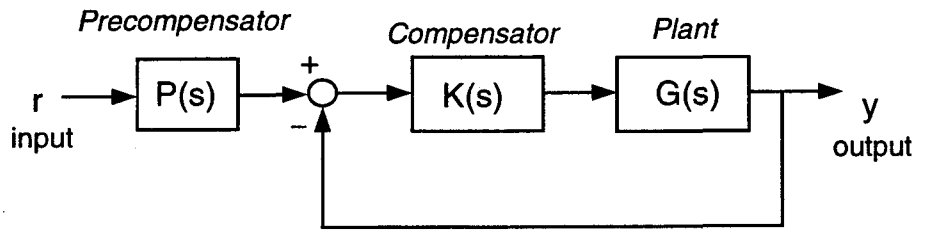

Figure 6-9 Implementation of the tracking precompensator.

for some departure in the 0.001 to 0.01 rad/s region, the singular values of the two loop transfer functions are extremely close up to, approximately, 30 rad/s. The bandwidth of the system is revealed by examining the singular values of the loop transfer function, i.e. $\mathbf{K_c}(s)\mathbf{G}(s)$. These results, along with those for the LQR design, are shown in Figure 6-11 . Again, the high extent of recovery is apparent. As in the case with the stability robustness test there is some departure between the two designs in the 0.001 to 0.01 rad/s frequency range. Also, the roll–off after 10 rad/s is greater for the LQG/LTR design. This is a desirable feature, indicating the improved high frequency disturbance rejection.

The LQG/LTR compensator is implemented in the nonlinear simulation code by incorporating the controller dynamics in the overall system model. A saturation limit of 270 N-m was set for the CMG's. The cases simulated are the same as those considered in the LQR control study.

As before, the system was subjected to an initial disturbance in roll of 5° (Figure 6-12). The roll response converges to equilibrium with a small overshoot and

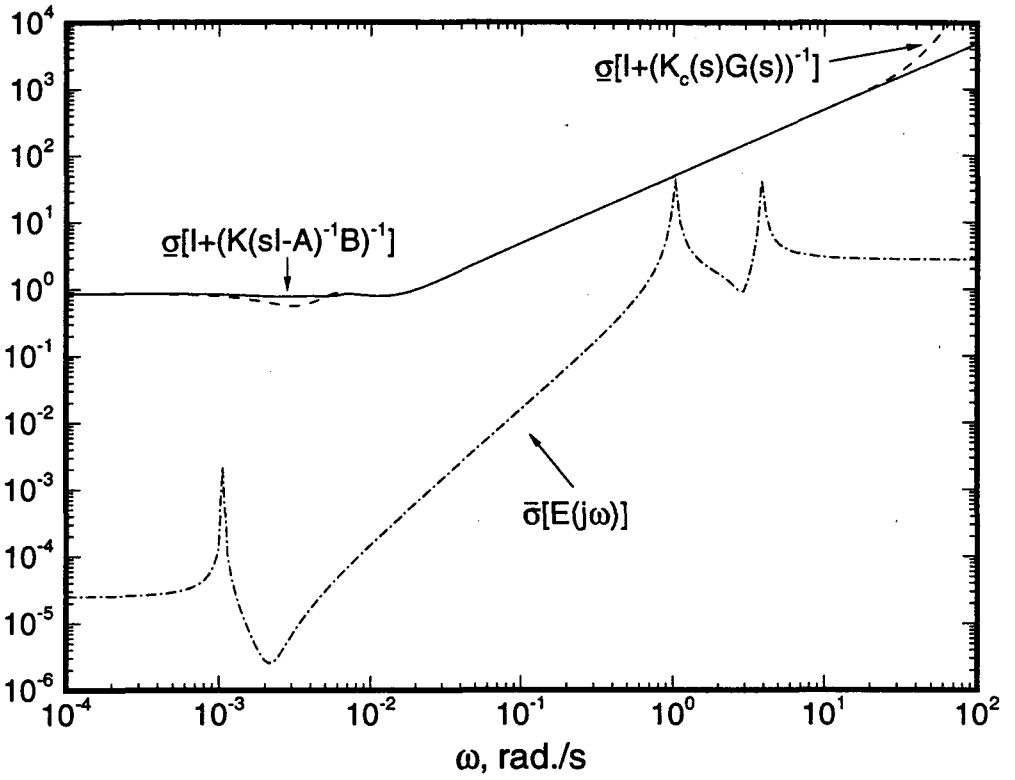

Figure 6-10 Stability robustness test for the LQG/LTR compensator.

at a slower rate than that in the LQR case. The slower response may be attributed to the imposed saturation level which limits both the pitch and roll control efforts during the first second (Figure 6-12d). Compared to the LQR case, the pitch and yaw transients are also more pronounced. In around 0.36 orbit (2000 s), however, all the librational d.o.f. settle down to their steady state values. The transient vibrational displacements are also significantly higher than those in the LQR case (Figures 6-12b,c). This is especially true of the stinger vibration in the y_1 direction which has a maximum tip deflection value of 0.2 cm. This is almost two orders of magnitude greater than that with the LQR procedure. The same trend persists with the PV

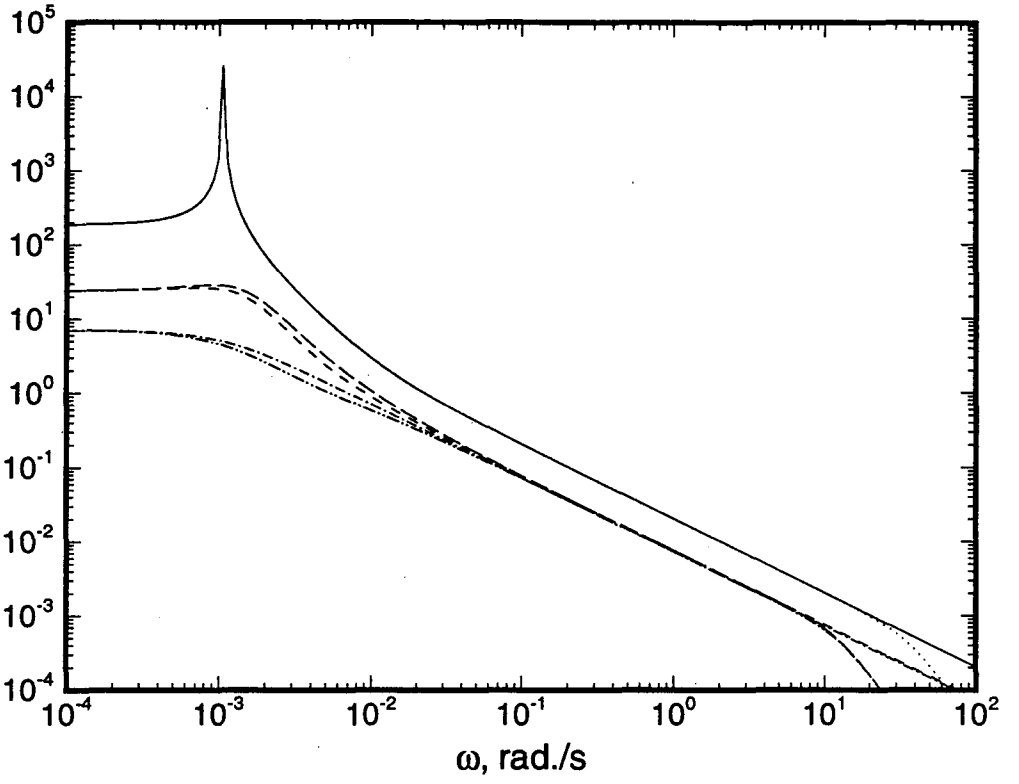

Figure 6-11 Singular values of $\mathbf{K_c}(s)\mathbf{G}(s)$ for the LQG/LTR compensator .

arrays and radiator tip deflection time histories. However, here the transients attenuate faster. The required CMG control torque histories for the first two seconds are given in Figure 6-12d, while Figure 6-12e presents the results for longer time periods. The peak CMG demand occurs in the first second, after which the requirements are quite modest.

Next, the controlled response of the system to an initial power boom tip deflection of 1 cm in the y_c direction was examined (Figure 6-13). As mentioned previously, this provides some indication of the extent to which the flexible dynamics, unmodelled in the control design, is excited by the controller. Although the stability robustness test

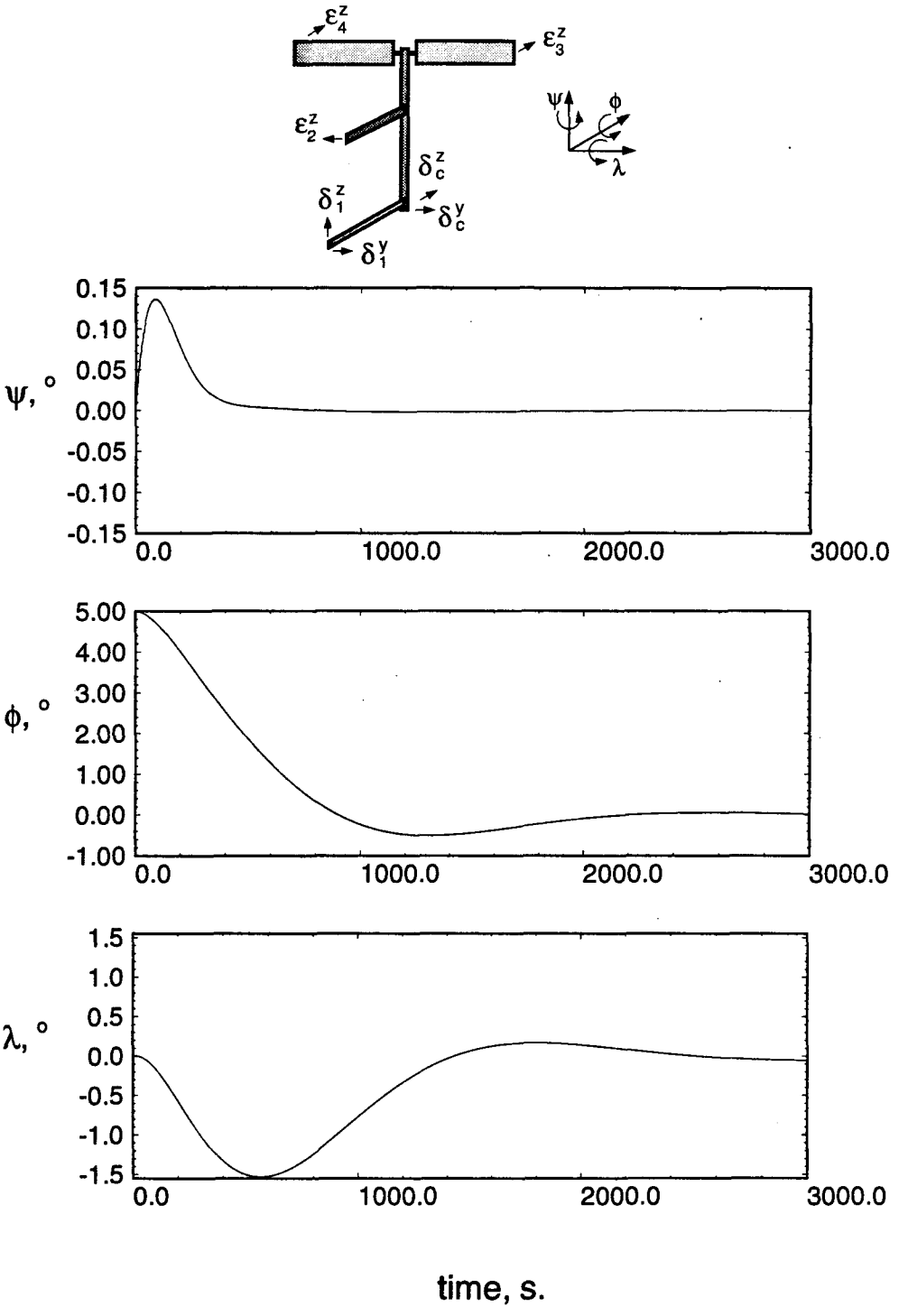

Figure 6-12 Controlled response of the FEL configuration using the LQG/LTR procedure with the initial disturbance in roll of $\phi(0) = 5°$: (a) librational coordinates.

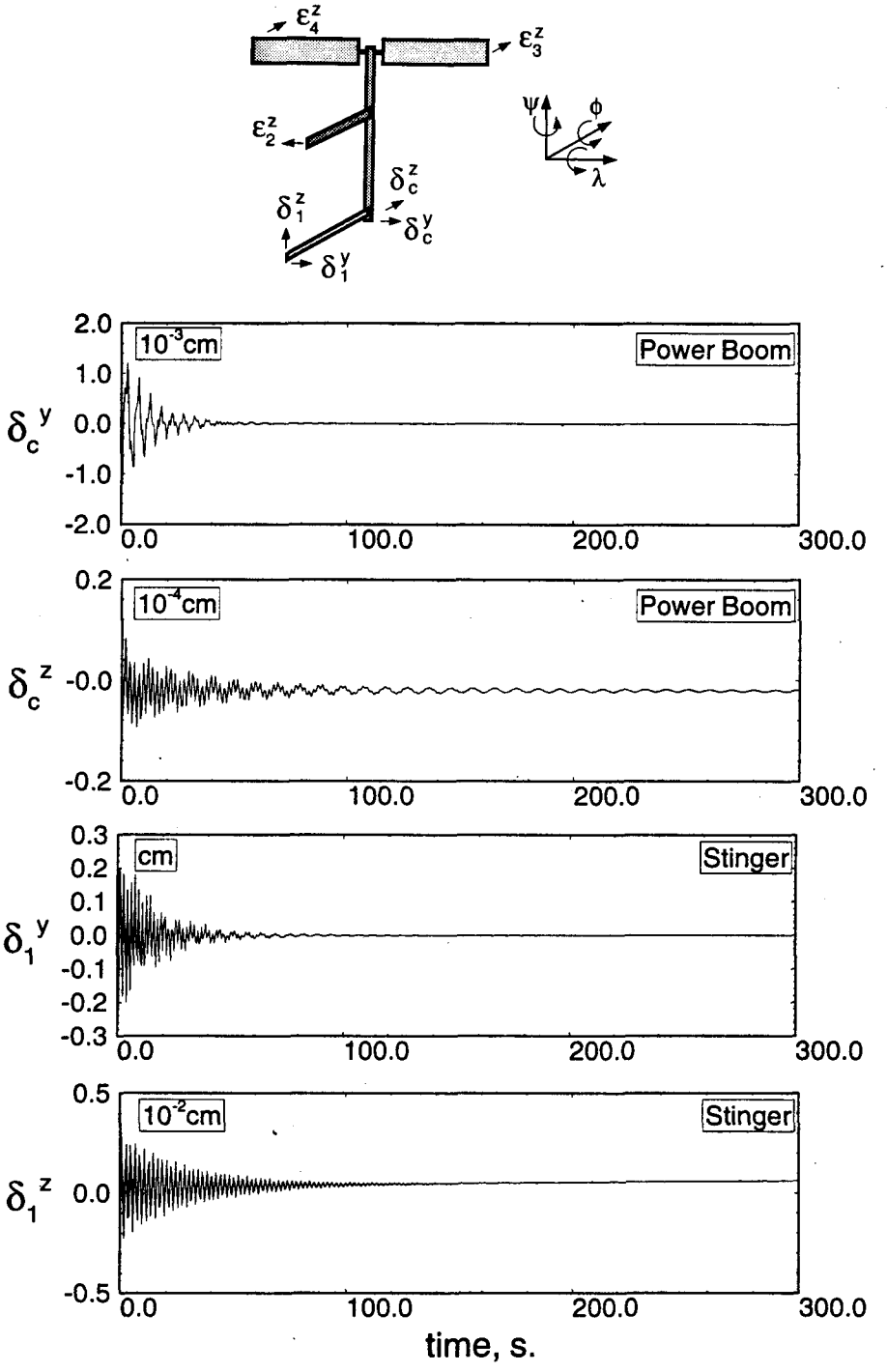

Figure 6-12 Controlled response of the FEL configuration using the LQG/LTR procedure with the initial disturbance in roll of $\phi(0) = 5°$: (b) power boom and stinger tip vibrations.

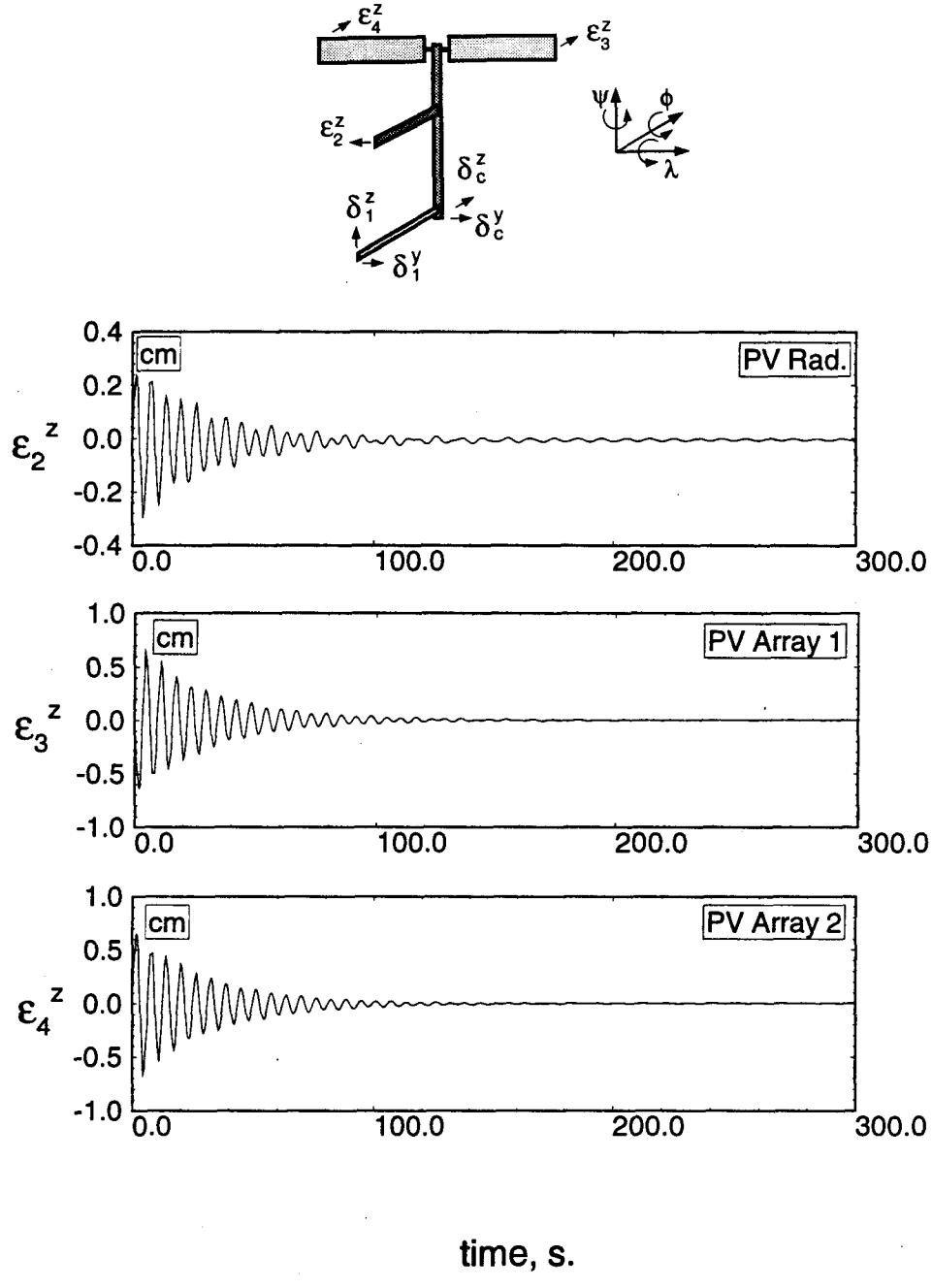

Figure 6-12 Controlled response of the FEL configuration using the LQG/LTR procedure with the initial disturbance in roll of $\phi(0) = 5°$: (c) PV radiator and array tip vibrations.

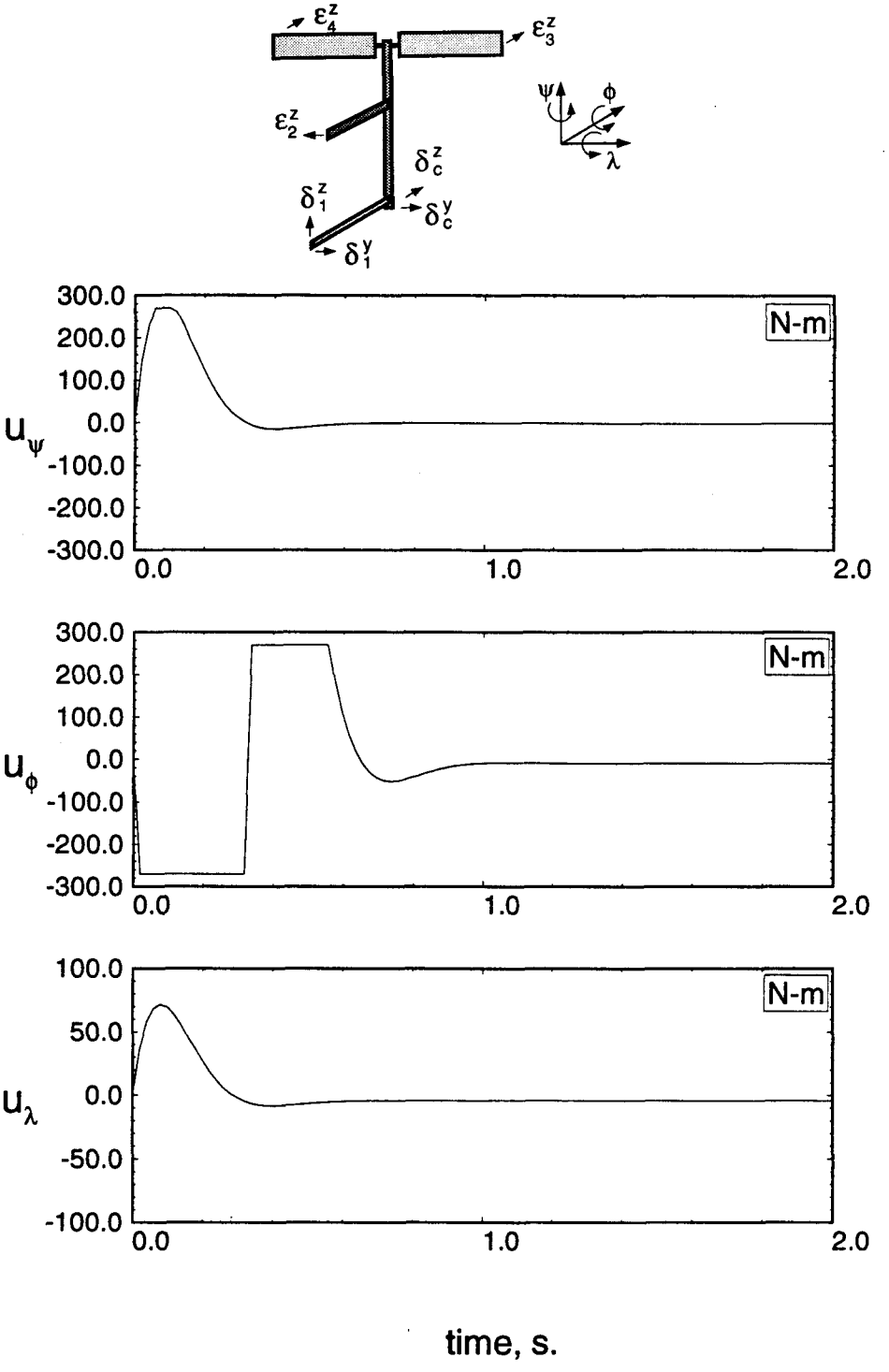

Figure 6-12 Controlled response of the FEL configuration using the LQG/LTR procedure with the initial disturbance in roll of $\phi(0) = 5°$: (d) control torque requirement close to the application of the disturbance.

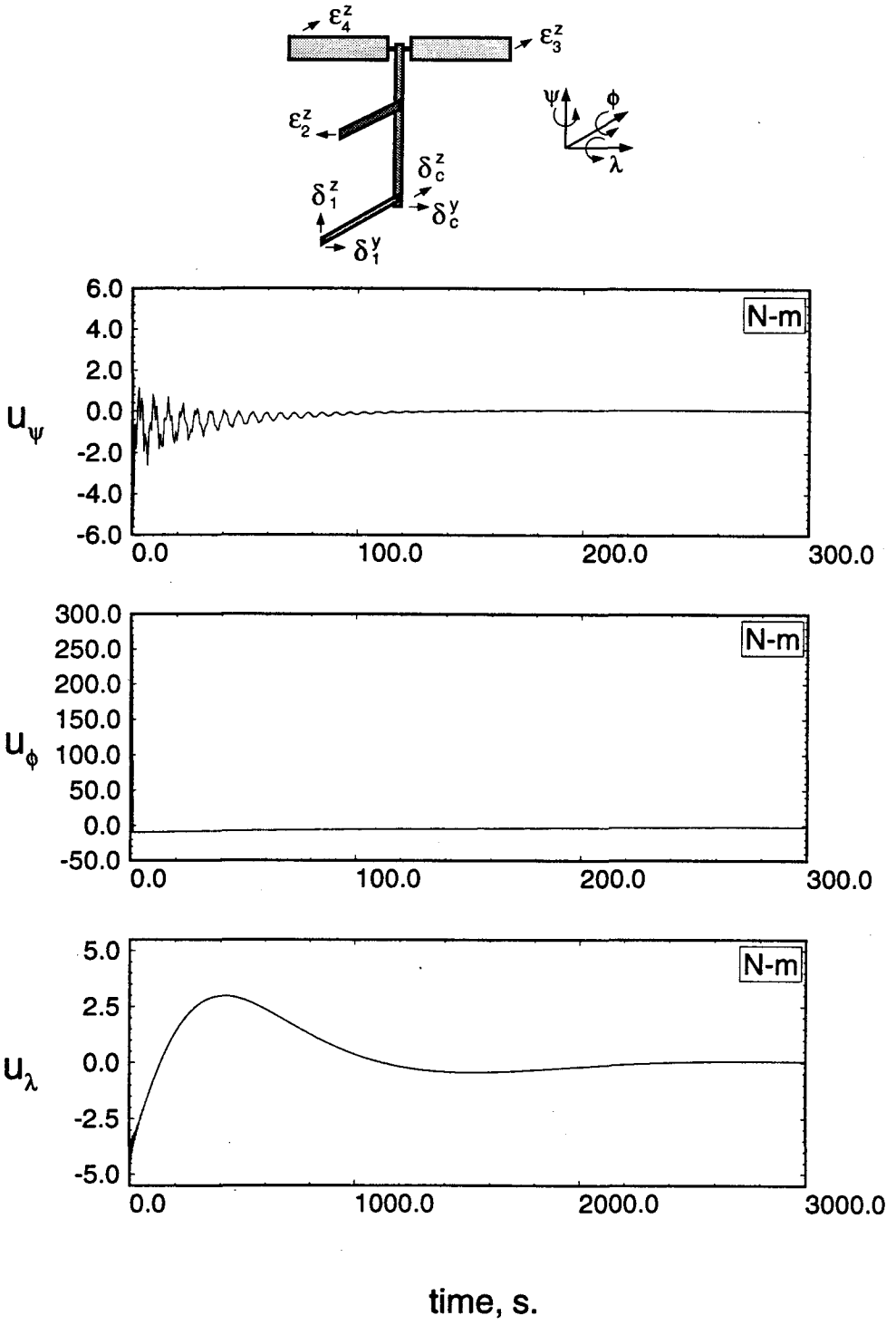

Figure 6-12 Controlled response of the FEL configuration using the LQG/LTR procedure with the initial disturbance in roll of $\phi(0) = 5°$: (e) control torque requirement; long duration time history.

was satisfied, greater confidence in the robustness of the controller can be gained by studying the simulation results. The vibrational responses of the power boom and stinger are similar to those obtained with the LQR controller except for the stinger vibration in the z direction. However, in this case, not only is the rate of decay of the transient significantly slower, but the peak value of the vibration is also greater (Figure 6-13a). Note, the dominant response of the stinger vibration is not along z, but rather in the y direction. The tip deflections of the plate elements (i.e. the PV radiator and arrays) are almost identical to those given by the LQR controller (Figure 6-13b). The CMG torque requirements (Figure 6-13c) also exhibit similarities to those given by the LQR case. However, in the present case, the peak input torque demand is significantly higher.

6.2.3 H_∞ Control

In the LQG/LTR control, the synthesis was accomplished by employing an optimal observer designed in a particular way to recover the properties of the LQR state feedback design. Moreover, the LQR design procedure involves the minimization of a quadratic performance index (eq. VIII-2). This, indirectly, leads to the minimization of the H_2 norm of the system transfer function matrix $\mathbf{M}(s)$ [59, 117]

$$\|\mathbf{M}\|_2 = \sqrt{\frac{1}{2\pi}\int_{-\infty}^{\infty} \mathrm{tr}\left[\mathbf{M}(j\omega)\mathbf{M}^T(-j\omega)\right]\, d\omega}. \tag{6.19}$$

The indirect nature of the optimization results in only a moderate control over the loop–shaping, a desirable feature, through the use of the quadratic weights in the performance index. H_∞ synthesis refers to an approach to linear control system design which entails the minimization of the H_∞ norm of the system transfer function(s).

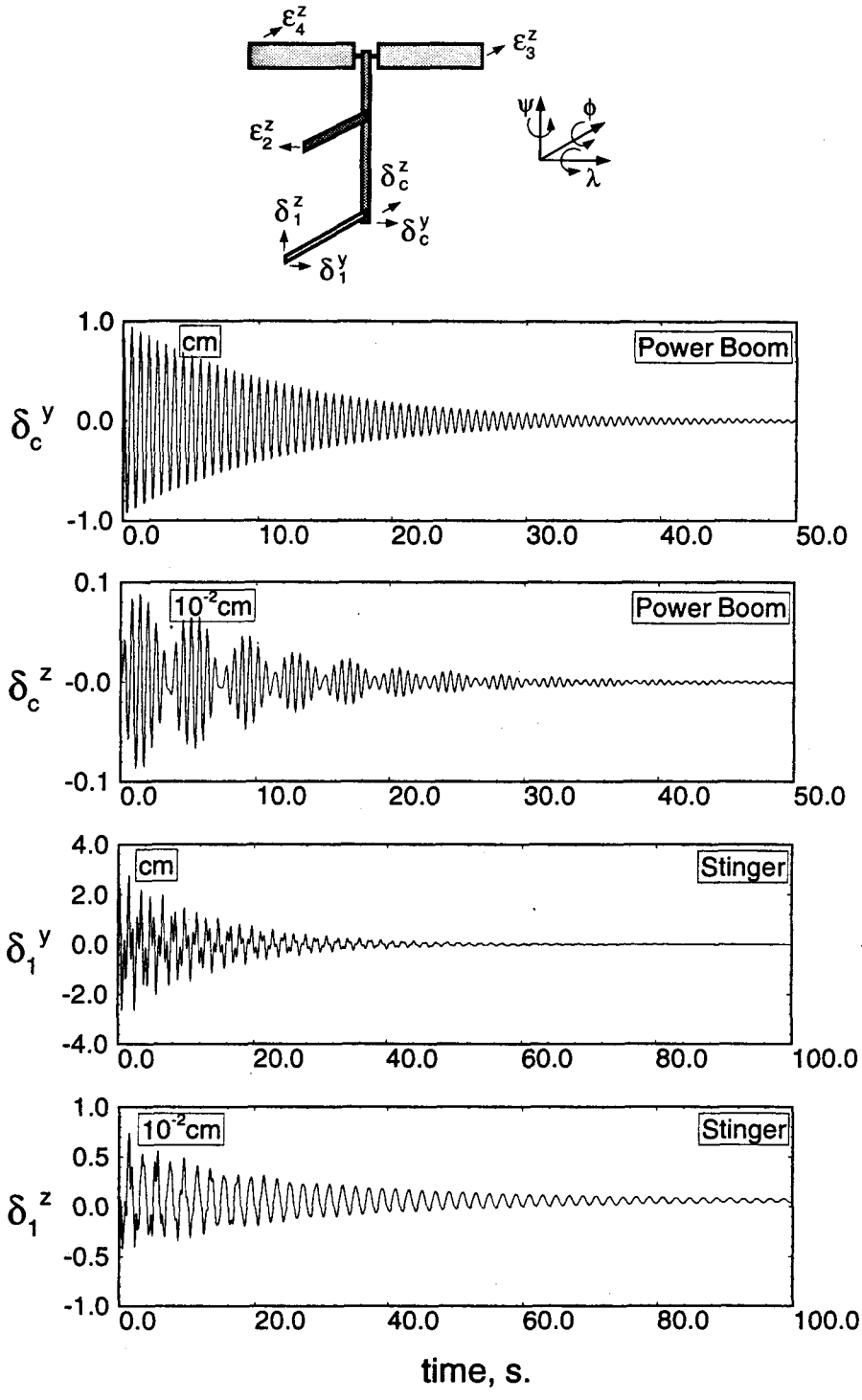

Figure 6-13 FEL response to the power boom tip disturbance of $\delta_c^y(0) = 1$ cm in the presence of LQG/LTR control: (a) power boom and stinger tip deflection time histories.

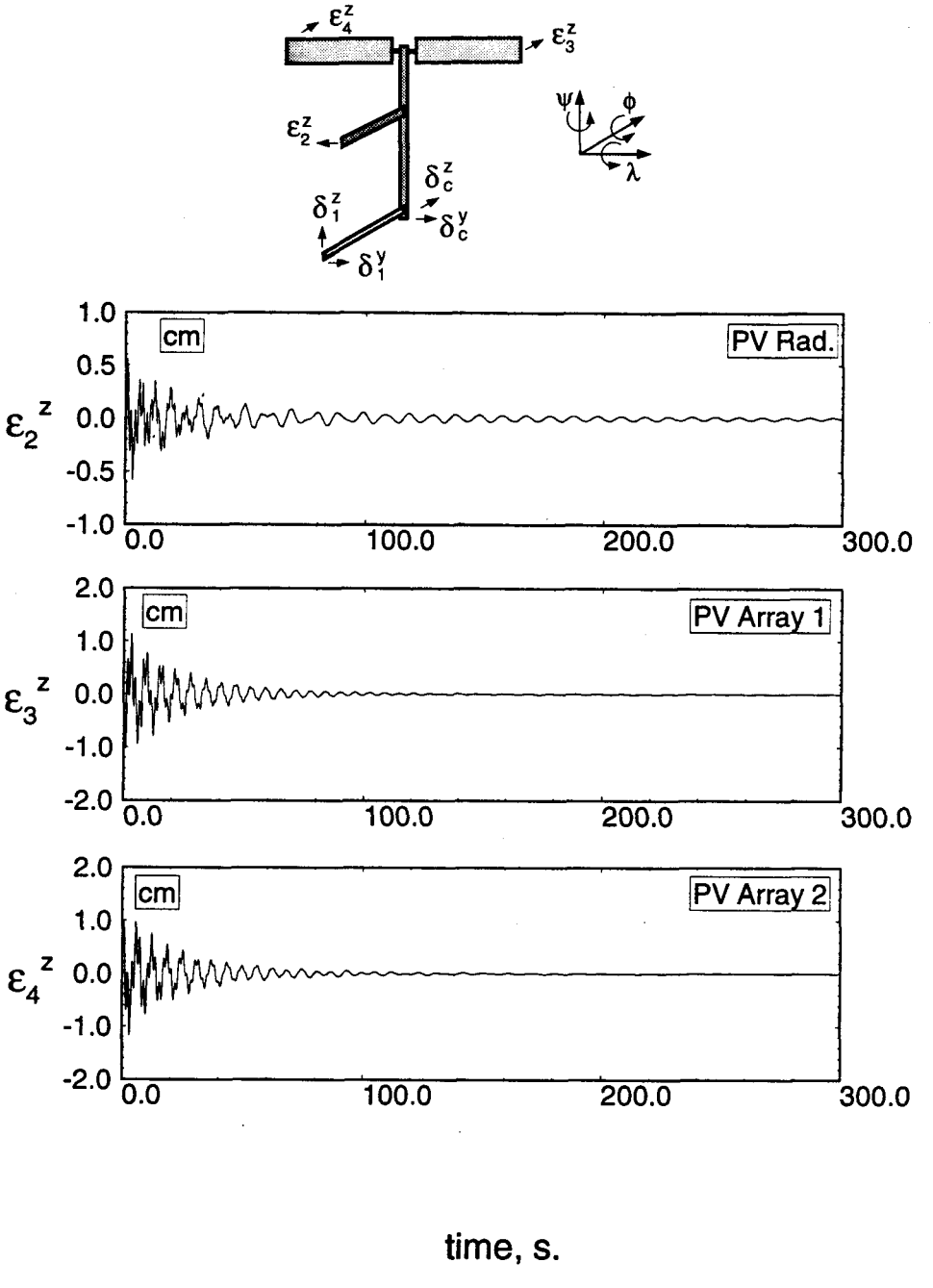

Figure 6-13 FEL response to the power boom tip disturbance of $\delta_c^y(0) = 1$ cm in the presence of LQG/LTR control: (b) PV radiator and array tip vibrations.

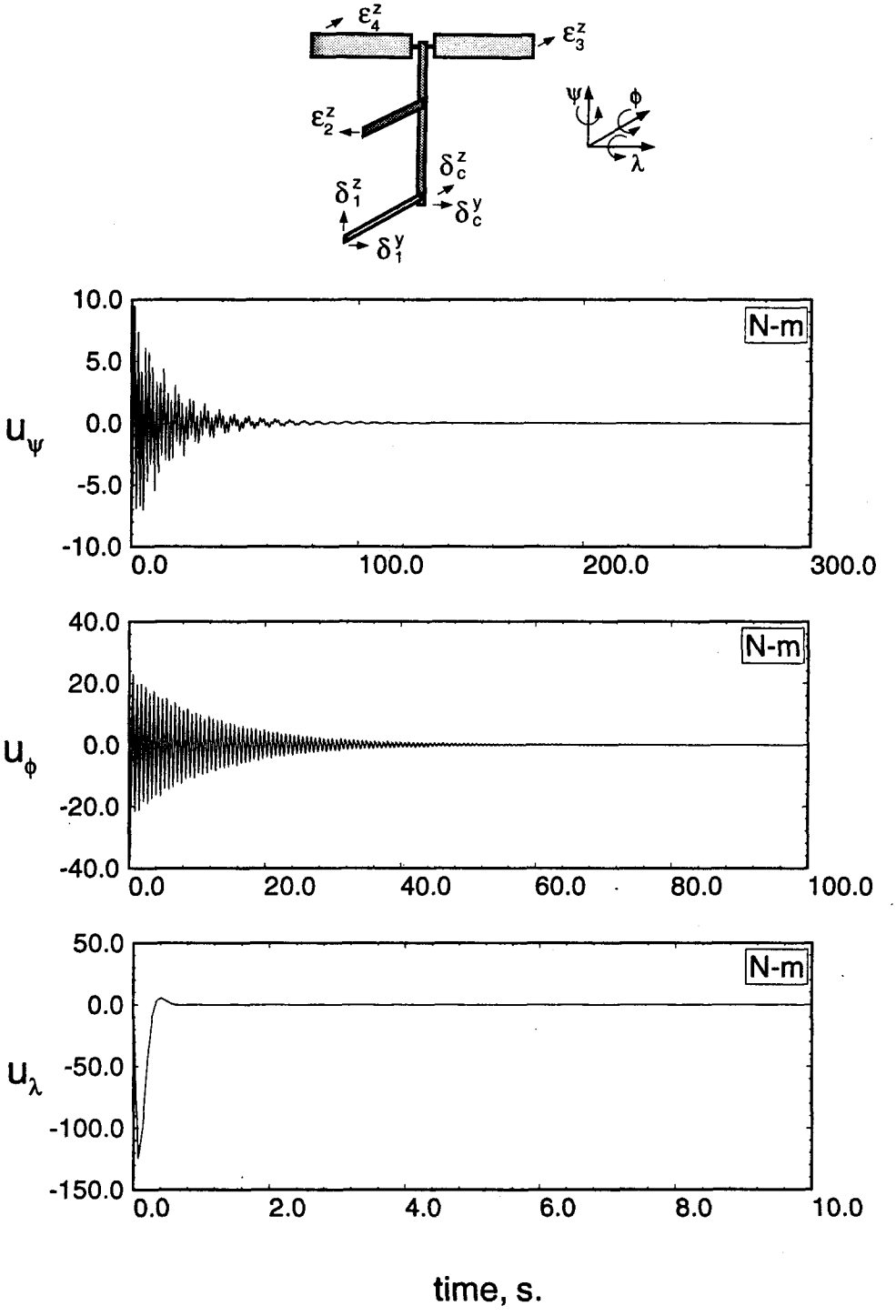

Figure 6-13 FEL response to the power boom tip disturbance of $\delta_c^y(0) = 1$ cm in the presence of LQG/LTR control: (c) demand on the control torque.

The H_∞ norm of a proper transfer function matrix, $\mathbf{M}(s)$, is defined as

$$\|\mathbf{M}\|_\infty = \sup_\omega \bar{\sigma}\left[\mathbf{M}(j\omega)\right]. \tag{6.20}$$

The use of the H_∞ norm allows for precise shaping of the system transfer function matrices in order to simultaneously satisfy performance, stability, disturbance rejection, etc. criteria through the use of dynamic weights. This represents a far more direct procedure to the design of a controller than the LQG/LTR approach, which iteratively satisfies the design criteria. As in the case with the LQG/LTR procedure, the controller obtained using the H_∞ technique is observer based. There is a large body of literature in the area of H_∞ control ranging from tutorial papers [121] and monographs [122] to mathematically oriented papers which concern themselves with the implementation of algorithms [123,124]. The method has been been applied to to many aerospace systems, including space structures [71,125] as well as aircraft [126,127]. A brief summary of the procedure is given in Appendix VIII.

The H_∞ control design procedure is applied to the same plant model as the one employed for the LQR and LQG/LTR controller designs, namely a rigid model of the FEL configuration of the proposed space station. As in the previous control designs, the multiplicative error was computed assuming the true system to consist of a 20 state flexible model described earlier. The mixed–sensitivity problem formulation was adopted, whereby the rigid design model was augmented with two weighting function, $W_1(j\omega)$ and $W_3(j\omega)$, which penalize the sensitivity, $\mathbf{S}(j\omega)$, and complementary sensitivity, $\mathbf{I} - \mathbf{S}(j\omega)$, transfer functions of the un–augmented plant–controller system (Appendix VIII). The procedure used for the H_∞ design is referred to as the Glover–Doyle or two–Riccati algorithm. It was implemented with the *Robust Control Toolbox* [128] used in conjunction with MATLAB.

The sensitivity transfer function is given by

$$\mathbf{S}(j\omega) = [\mathbf{I} + \mathbf{G}(j\omega)\mathbf{K_c}(j\omega)]^{-1}. \tag{6.21}$$

The weighting function $W_1(j\omega)$ essentially penalizes the error between the plant output and the desired output, while $W_3(j\omega)$ penalizes the plant output. Furthermore, $W_1(j\omega)$ establishes the performance (bandwidth) specification for the design, while $W_3(j\omega)$ defines the bound required to maintain stability robustness.

For the present design, $W_3(j\omega)$ is taken to be an upper limit of the multiplicative model error to ensure the stability robustness of the design against unmodelled dynamics, while $W_1(j\omega)$ is used as a design parameter which is manipulated until an acceptable performance is achieved. The criteria used to establish whether the final design is acceptable or not include the speed of the response and the control effort (CMG torque) required. The initial torque demand during librational disturbances are particularly high. For the present case $W_3(j\omega)$ is chosen to be

$$\frac{s^2}{0.02}. \tag{6.22}$$

A plot of $\frac{1}{|W_3|}$ and $\frac{1}{\bar{\sigma}[\mathbf{E_m}]}$ is shown in in Figure 6-14 . Note that the region above the 10^0 (0 dB) line is of no consequence because the value of the complementary sensitivity transfer function will be very close to 0 dB in the bandwidth (i.e. low frequency) region.

The following form is taken for the performance weighting function W_1,

$$W_1 = \frac{s^2 + 2\zeta_{c_1}\,\omega_{c_1}\,s + \omega_{c_1}^2}{100\gamma(s^2 + 2\zeta_{c_2}\,\omega_{c_2}\,s + \omega_{c_2}^2)}. \tag{6.23}$$

The resulting augmented plant model has 12 states. The H_∞ design procedure, which is described in Appendix VIII, was repeated for different values of the parameters

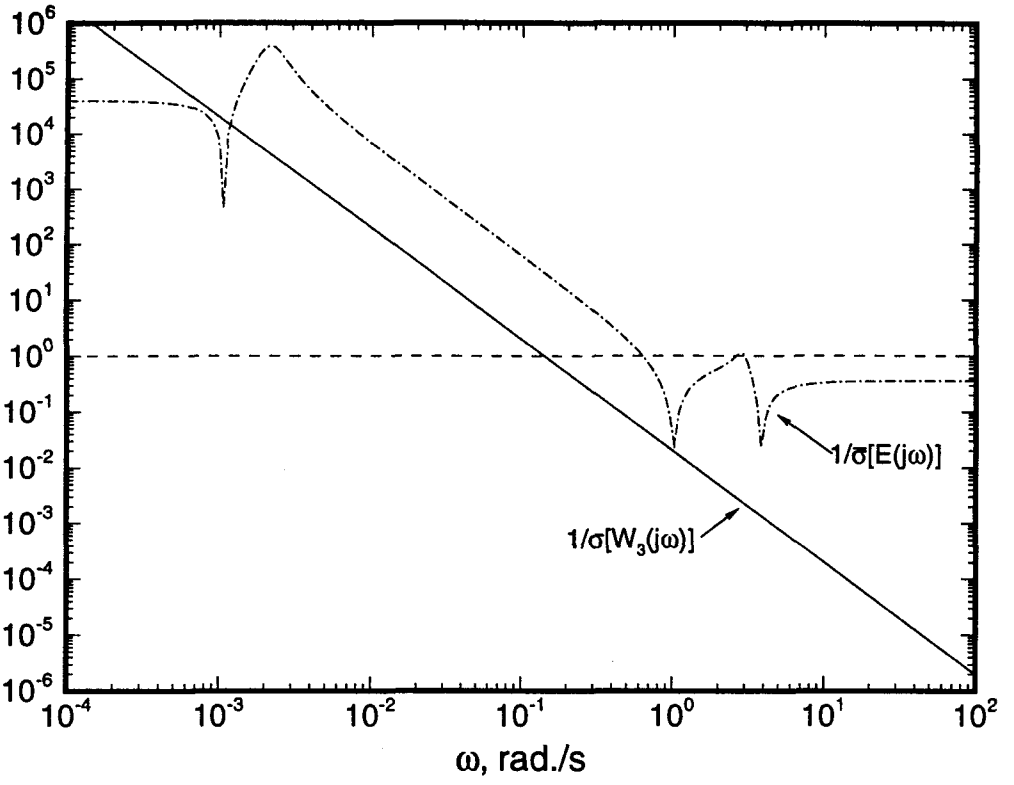

Figure 6-14 Singular values of the multiplicative model error and the W_3 weighting function.

governing W_1. The values corresponding to the final design are:

$$\begin{aligned} \omega_{c_1} &= 1; \qquad \zeta_{c_1} = 5; \\ \omega_{c_2} &= 0.005; \quad \zeta_{c_1} = 20; \\ \gamma &= 10. \end{aligned} \tag{6.24}$$

The compensator returned by the H_∞ algorithm is given in the state space form in Appendix IX. Note that this model also has 12 states. The transmission zeros of the

compensator are:

$$
\begin{aligned}
Z_{1,2,3} &= -1.9893e-1; \\
Z_{4,5} &= -2.8130e-03 \pm j8.1579e-4; \\
Z_{6,7} &= -1.1677e-03 \pm j9.3692e-4; \\
Z_{8,9} &= -1.8516e-03 \pm j1.0369e-3;
\end{aligned} \tag{6.25}
$$

and its poles are located at:

$$
\begin{aligned}
P_{1,2} &= -5.1172e-2 \pm j4.9962e-2; \\
P_{3,4} &= -5.0506e-2 \pm j4.9316e-2; \\
P_{5,6} &= -5.0196e-2 \pm j4.9017e-2; \\
P_{7,8,9} &= -2.0087e-1; \\
P_{10,11,12} &= -1.1251e-3.
\end{aligned} \tag{6.26}
$$

It may be pointed out that the sixth and seventh zeros of the compensator cancel the stable open loop poles of the plant given in eq. (6.12). Singular values of the compensator are shown in Figure 6-15 , while those for the sensitivity, $\mathbf{S}$, complementary sensitivity, $\mathbf{I}-\mathbf{S}$, transfer functions, and the weighting functions W_1, W_3 are given in Figure 6-16 . It is apparent that the controller significantly exceeds the design specifications, both in terms of performance and stability robustness. The stability robustness test of the design is presented in Figure 6-17 . The system is clearly far more robust to the unmodelled plant dynamics then in the case of the LQG/LTR compensator, mainly due to the greater slope of $\underline{\sigma}\left[\mathbf{I}+[\mathbf{G}(s)\mathbf{K}(s)]^{-1}\right]$ (40dB per decade) for $\omega > 0.1$ rad/s. The higher slope is due to the second order dependence of W_3 on s. The increased bandwidth of the H_∞ compensator (≈ 0.03 rad/s), compared to the LQG/LTR compensator (≈ 0.006 rad/s), is apparent from the singular value plot of

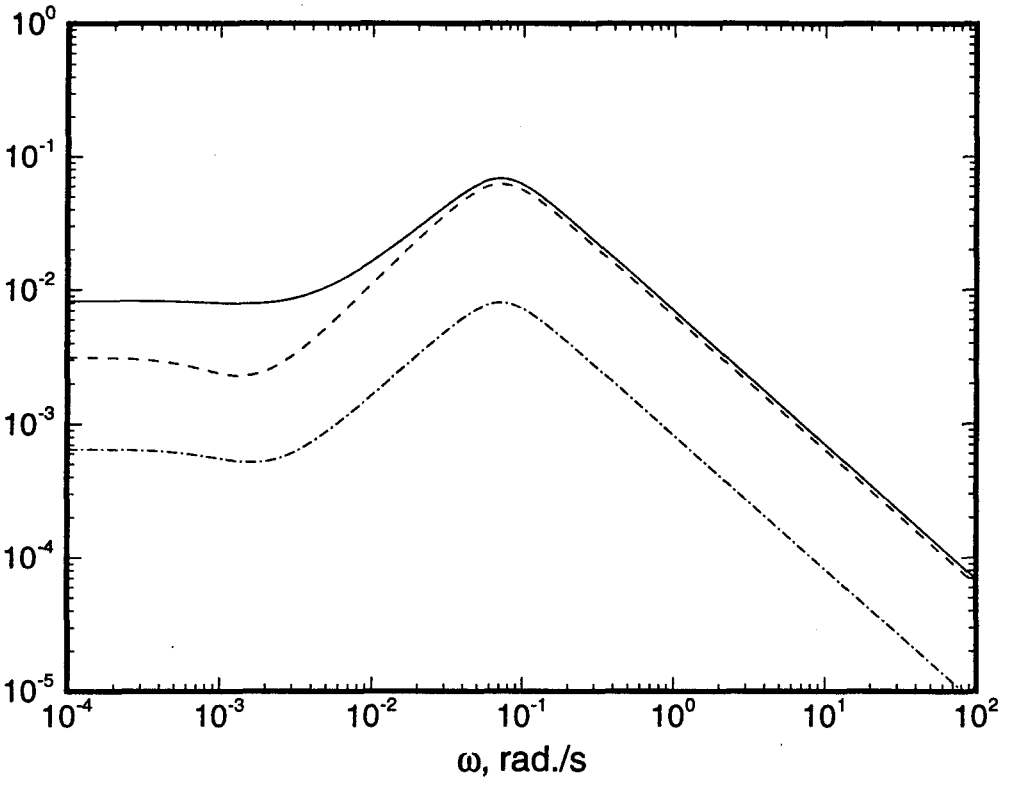

Figure 6-15 Singular values of the H_∞ compensator.

the loop transfer function (Figure 6-18).

As with the LQG/LTR design, the H_∞ controller was implemented on the non-linear plant model. The objective was to assess its effectiveness over a wide range of librational and vibrational disturbances. Only a few typical results, corresponding to the initial conditions used during the LQR and LQG/LTR studies, are discussed here. In particular, the performance of the closed loop system is compared to the LQG/LTR case.

Figure 6-19 a shows the controlled response of the system to a 5° disturbance in roll. The improved performance with the H_∞ controller is apparent. The pitch

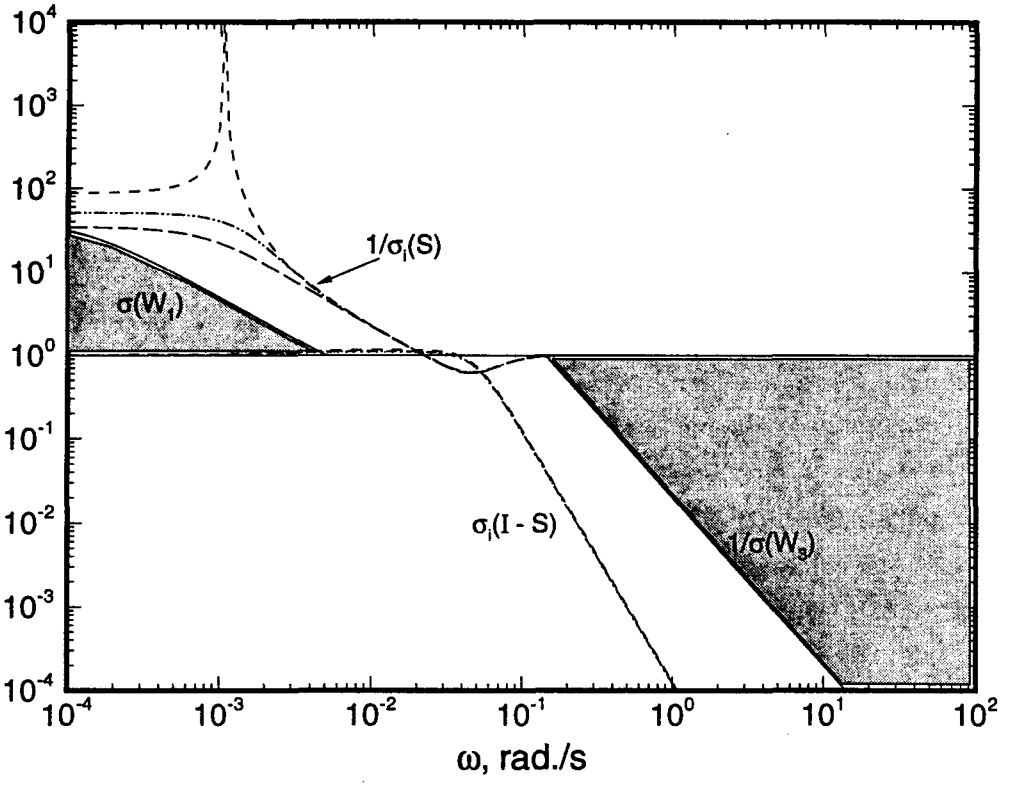

Figure 6-16 Singular values of the sensitivity and complementary sensitivity transfer functions and the associated weights.

transient response is considerably smaller in this case (maximum value of $\approx 0.07°$ for H_∞, compared to $\approx 0.14°$ with LQG/LTR). The same is true with the yaw response (maximum value of $\approx 0.2°$ for H_∞, compared to $\approx 1.5°$ for LQG/LTR). Furthermore, the roll disturbance attenuates much faster, in less than 400 s, compared to more than 2000 s for the LQG/LTR controller. Note, the vibrational time histories of the flexible members are similar to the control torque profiles, particularly for the power boom and stinger tip responses. These results show a lower level of control effort, especially for the pitch and yaw CMG's. For example, in the LQG/LTR case, peak torques of

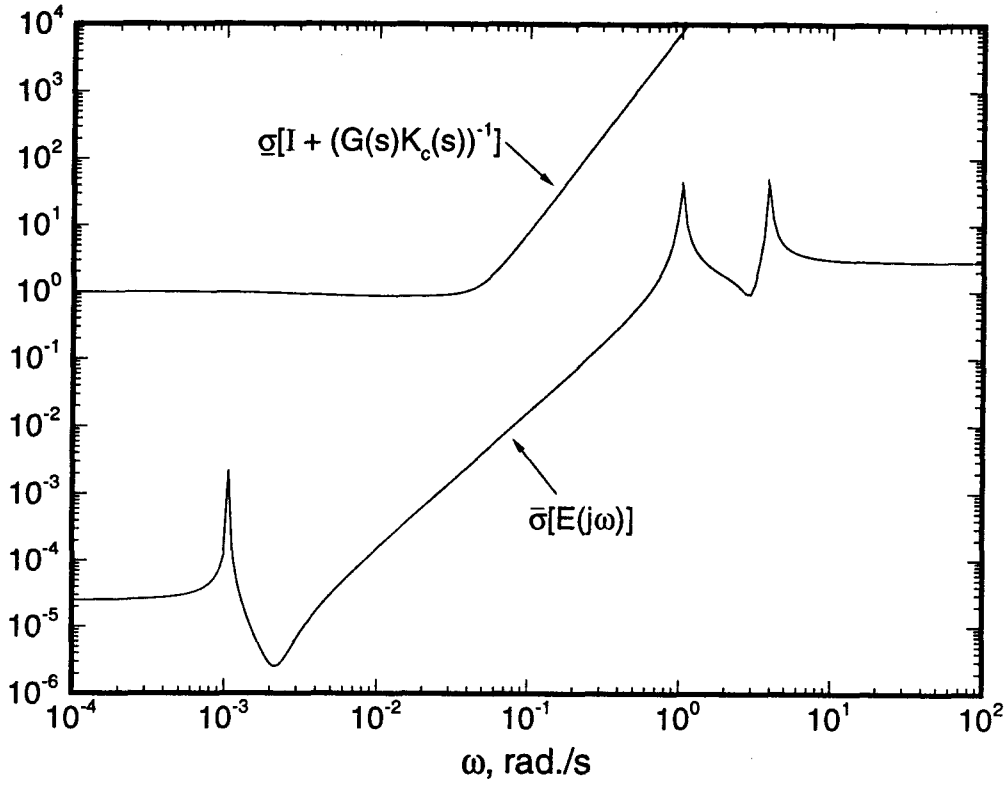

Figure 6-17 Stability robustness test for the H_∞ compensator design.

270 N-m and 70 N-m were required for the the pitch and yaw CMG's, respectively. For the H_∞ controller these values are 5 N-m and 25 N-m, respectively (Figure 6-19 d). Furthermore, the control torque demand for the roll CMG is relatively smooth. It does not exhibit any fast 'switching' as in the case of the LQG/LTR control (–270 N-m to +270 N-m, Figure 6-12d).

Response results for the FEL to a power boom tip deflection of 1 cm in the y_c direction are presented in Figure 6-20 . They are virtually identical to those obtained with the LQG/LTR controller. However, the CMG torque histories exhibit lower values (Figure 6-20c). This can be traced to the fact that the poles of the flexible

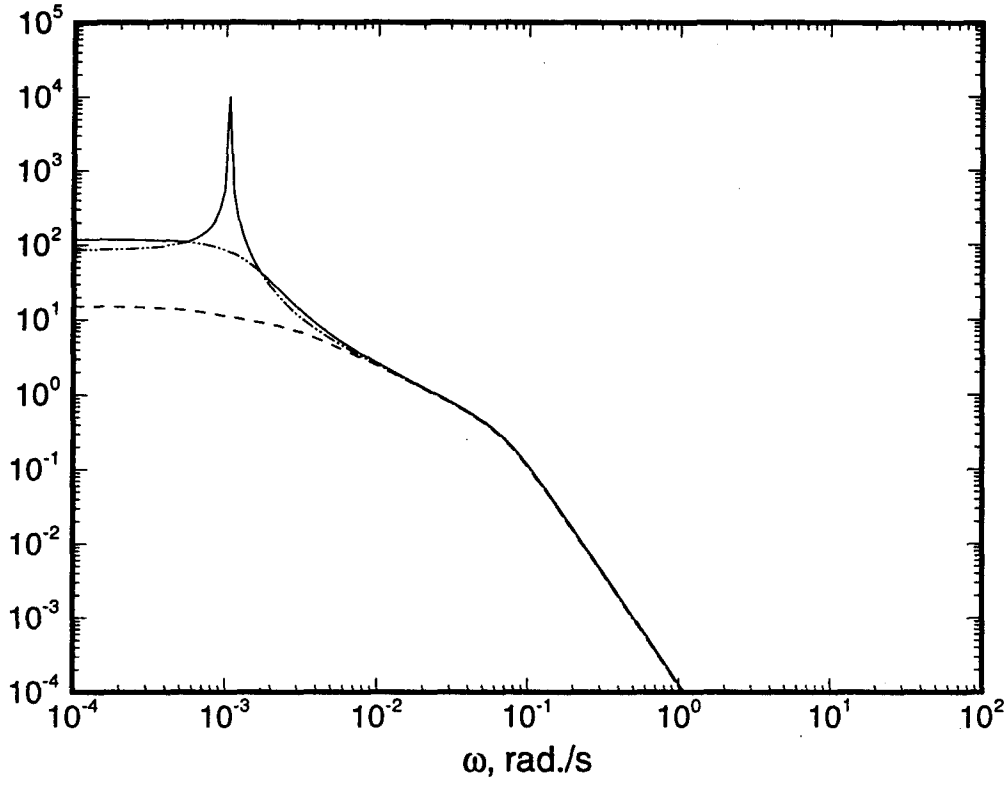

Figure 6-18 Singular values of $\mathbf{K}(s)\mathbf{G}(s)$.

modes, which are at:

$$\begin{aligned}
&-0.08398 \pm j10.063;\\
&-0.11512 \pm j11.704;\\
&-0.05125 \pm j3.8542;\\
&-0.03183 \pm j3.1702;\\
&-0.01597 \pm j1.0117;\\
&-0.00648 \pm j0.6370;\\
&-0.00685 \pm j0.6551;
\end{aligned} \tag{6.27}$$

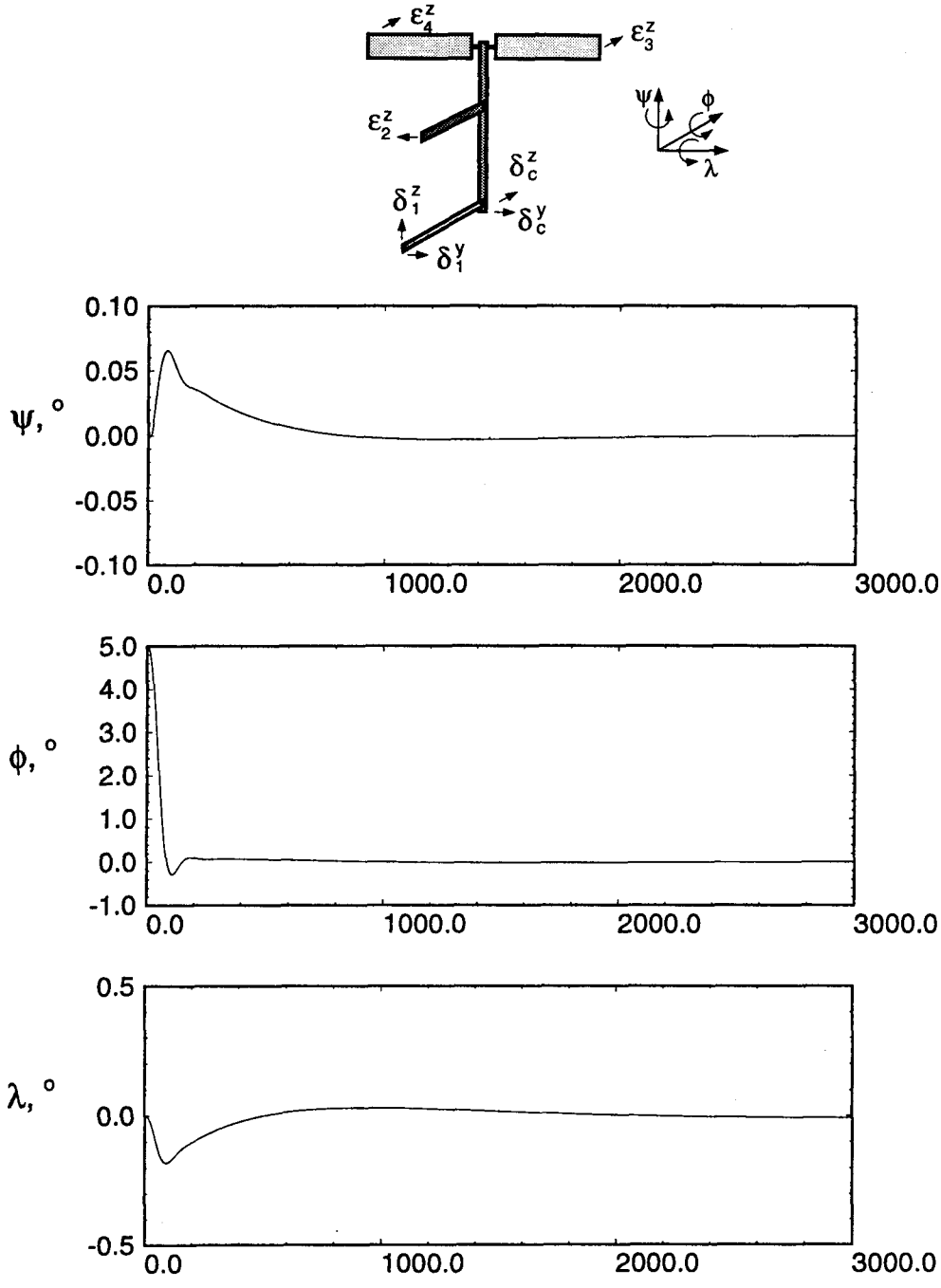

Figure 6-19 FEL response to a roll disturbance of $\phi(0) = 5°$ with the H_∞ control: (a) librational motion.

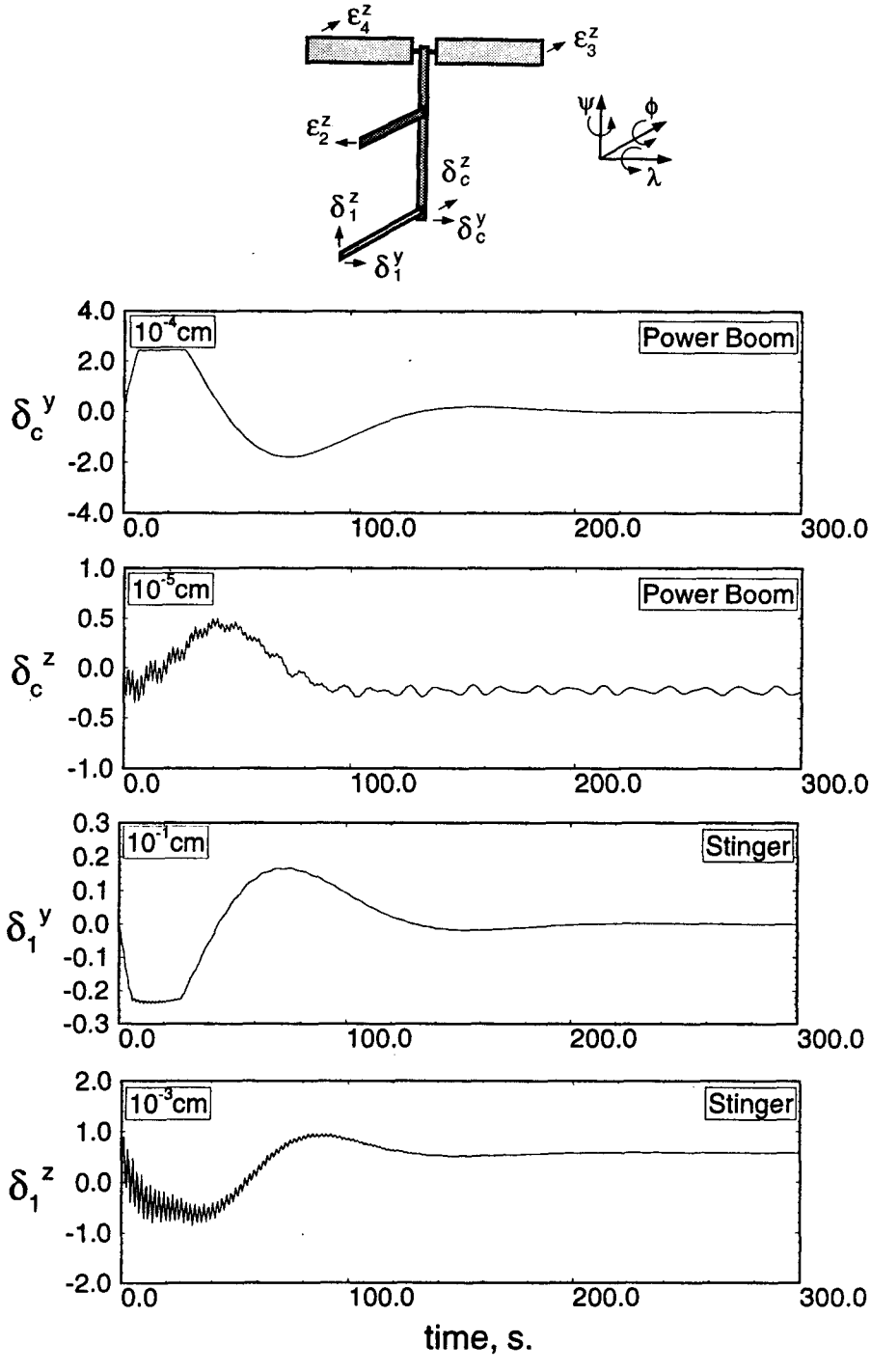

Figure 6-19 FEL response to a roll disturbance of $\phi(0) = 5°$ with the H_∞ control: (b) power boom and stinger tip vibrations.

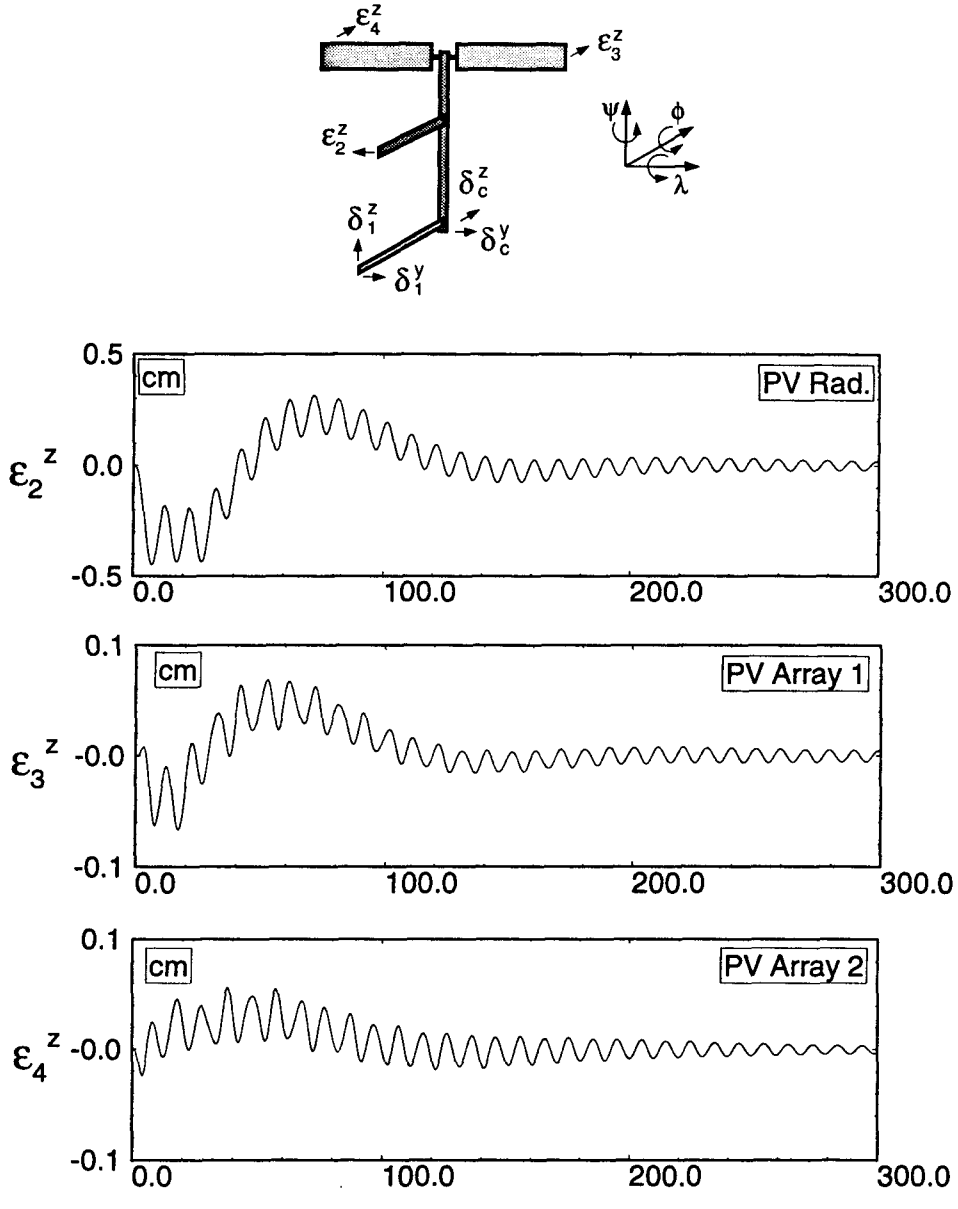

Figure 6-19 FEL response to a roll disturbance of $\phi(0) = 5°$ with the H_∞ control: (c) PV radiator and array tip deflection time histories.

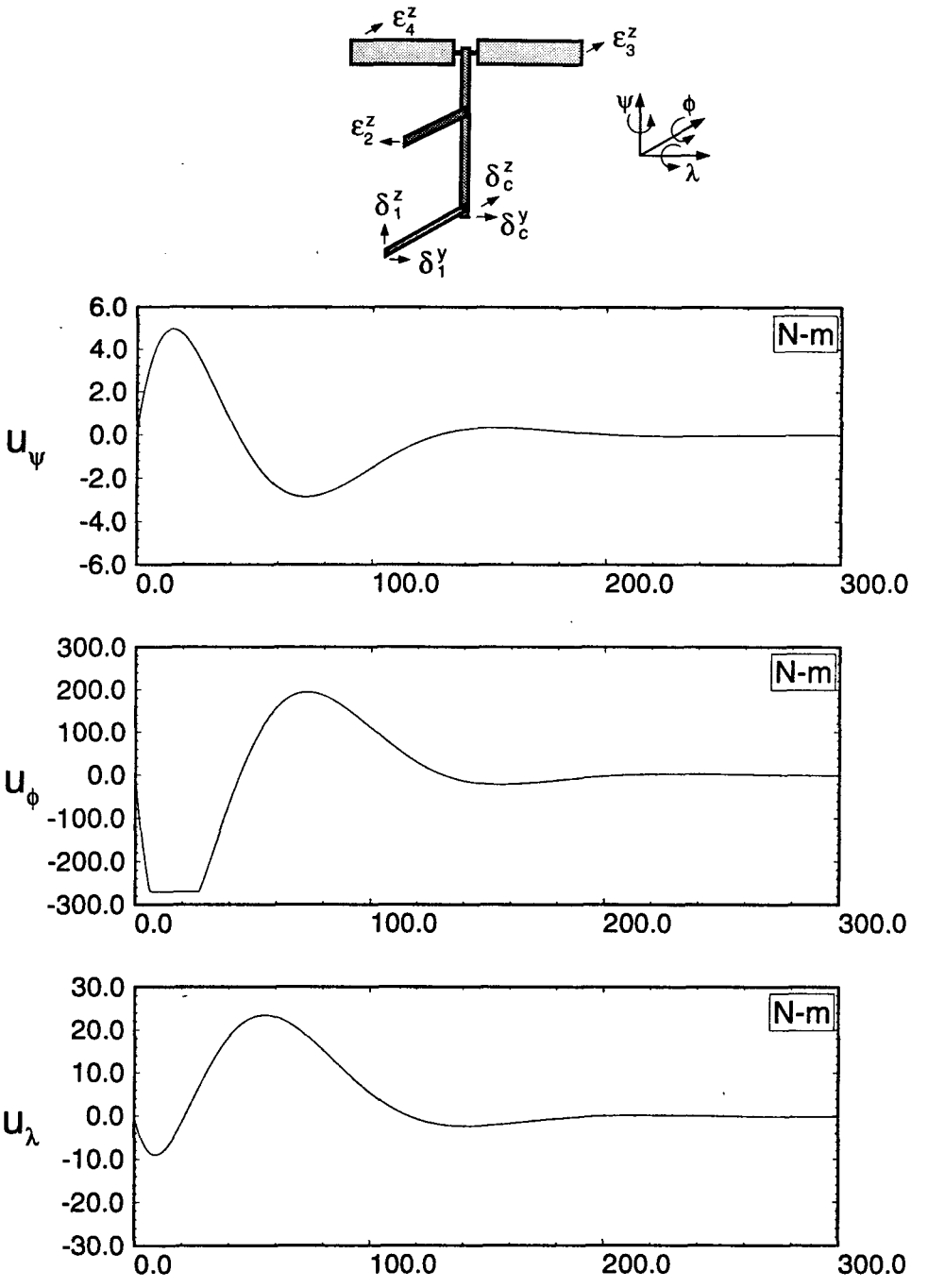

Figure 6-19 FEL response to a roll disturbance of $\phi(0) = 5°$ with the H_∞ control: (d) control effort.

are farther from the poles of the H_∞ compensator (eq. 6.26) than the poles of the LQG/LTR compensator (eq. 6.17). Hence, the vibratory motion does not excite the modes of the H_∞ controller as much as it does the modes of the LQG/LTR controller. This is preferable because the control action is, in a sense, not useful. That is, the CMG torques for the LQG/LTR control, although considerable, are unable to attenuate the vibratory motion appreciably.

To summarize, the H_∞ controller appears to be superior to the LQG/LTR design in many respects. It is more robust to the unmodelled (flexible) dynamics. This is borne out not only in the robustness test, but also in the simulation results. In terms of performance, the H_∞ design leads to quicker settling times for librational disturbances. The control torques required in the directions normal to the disturbance are significantly lower. Also, because of the ability to tailor the closed loop characteristics of the design, the H_∞ procedure requires significantly less iteration effort compared to the LQG/LTR case, to achieve the desired loop shape. In fact, this was achieved in a single step using the the weighting functions in the H_∞ design. Of course, a certain degree of iteration was required in the H_∞ procedure to obtain designs which did not saturate the CMG's, however, the effort involved in achieving this was substantially less than that in the LQG/LTR controller synthesis.

It must be emphasized that the H_∞ controller is relatively more complex. In the present study it gave a 12^{th} order controller, while the LQG/LTR procedure resulted in a 6^{th} order one. Therefore, in terms of implementation, the H_∞ controller would demand more computing effort. However, the possibility of reducing the order of the resulting compensator, which was not pursued here, may result in a more attractive design.

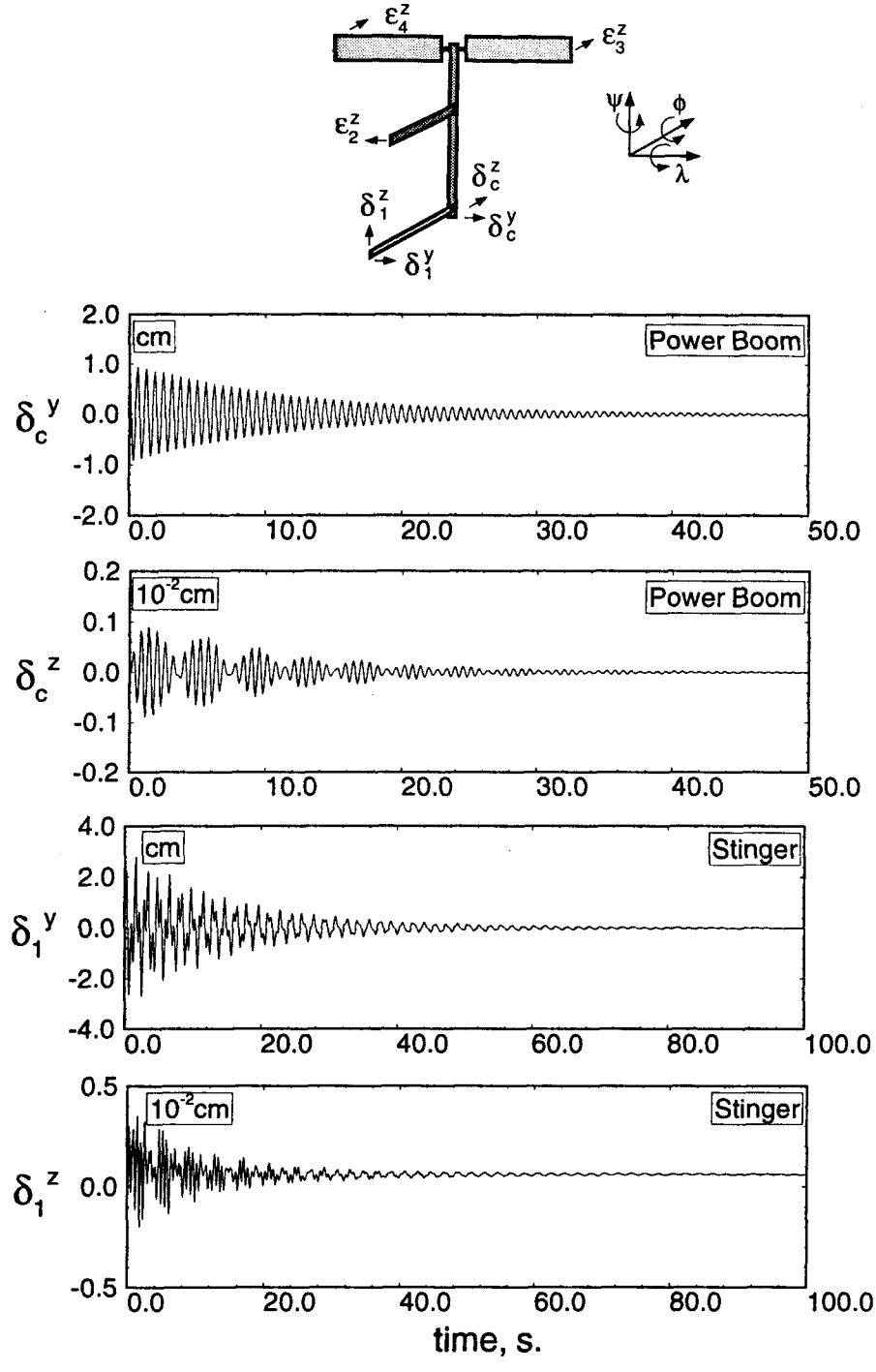

Figure 6-20 H_∞ control of the FEL to a power boom disturbance $\delta_c^y(0) = 1$ cm : (a) power boom and stinger tip deflections.

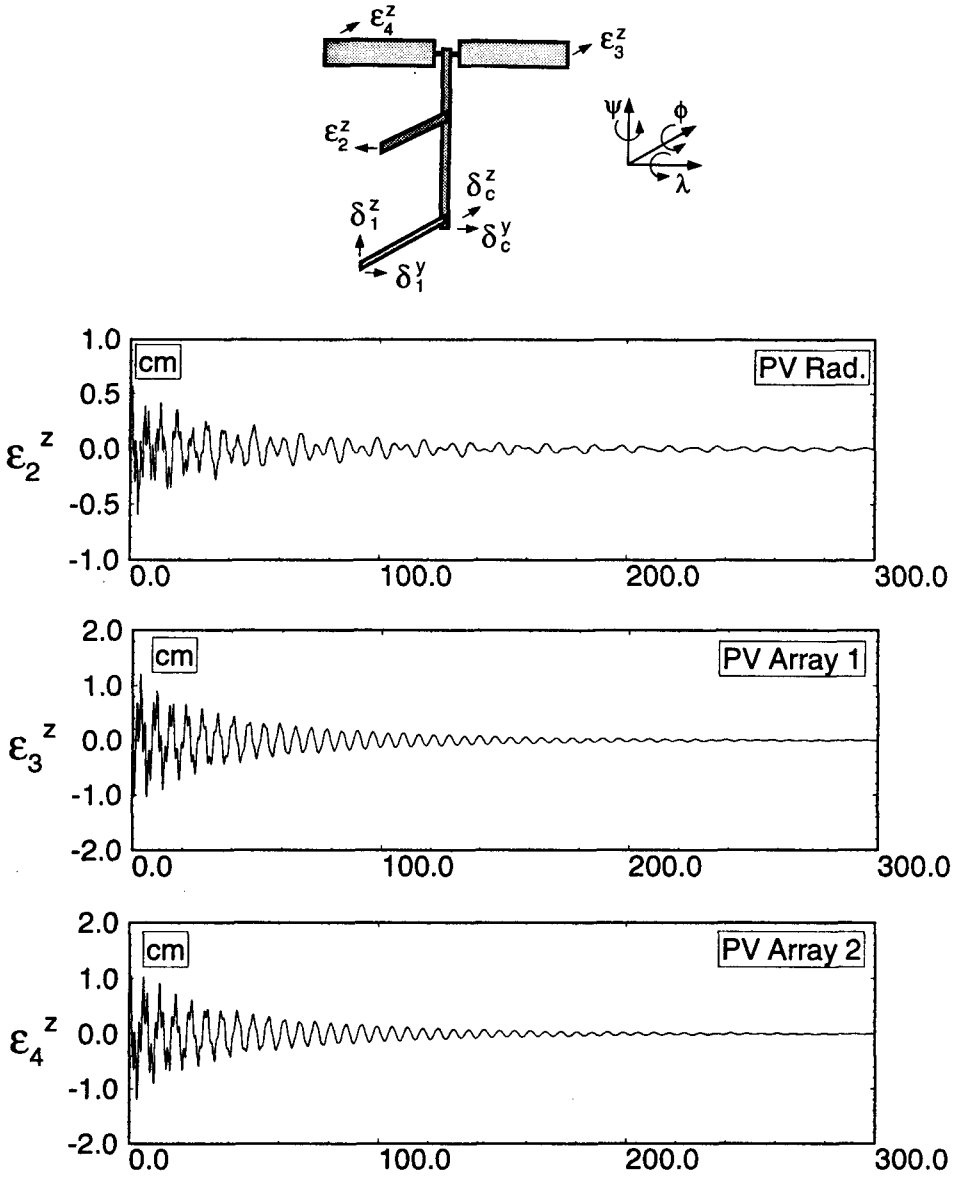

Figure 6-20 H_∞ control of the FEL to a power boom disturbance $\delta_c^y(0) = 1$ cm : (b) PV radiator and array tip deflections.

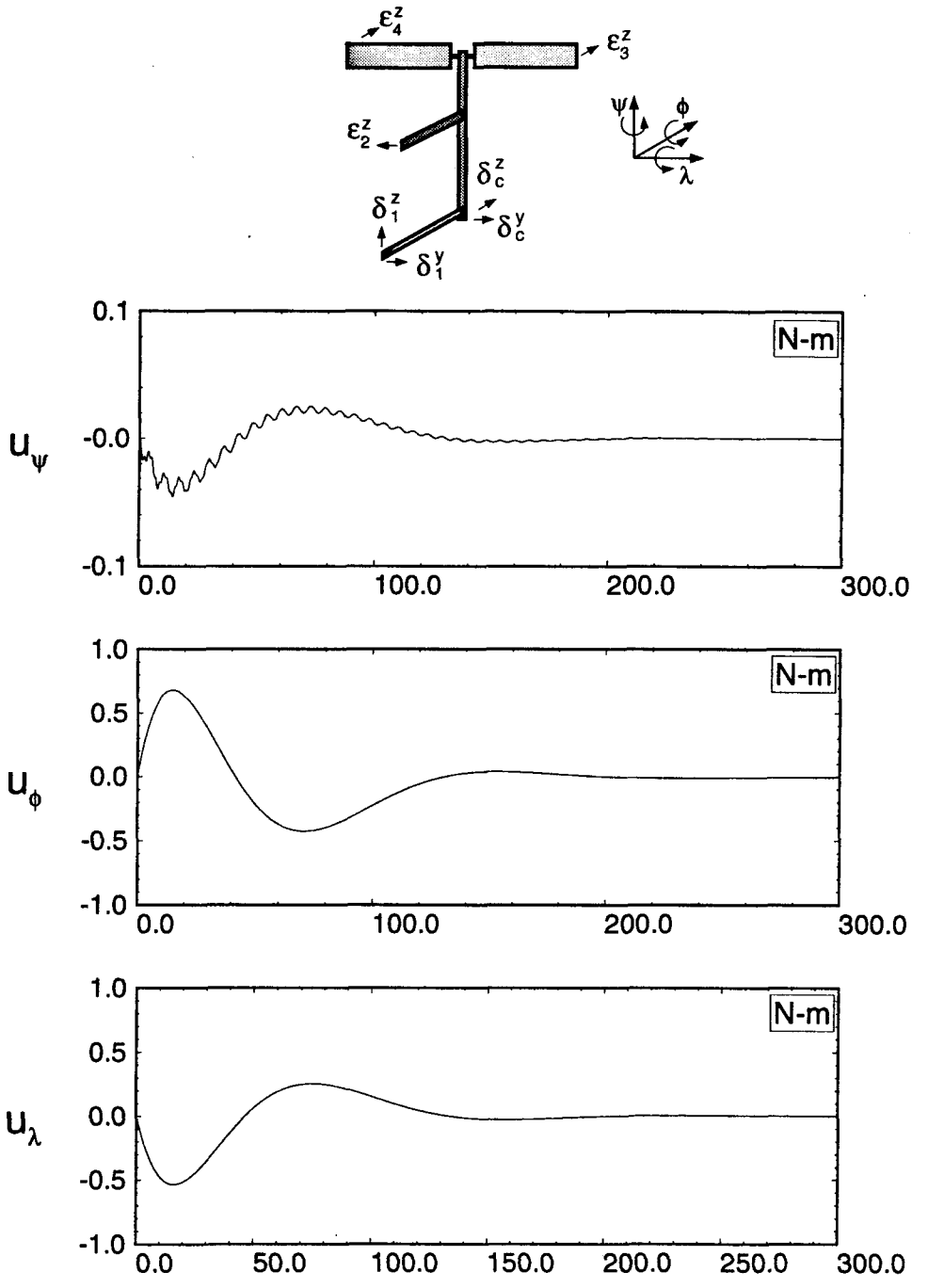

Figure 6-20 H_∞ control of the FEL to a power boom disturbance $\delta_c^y(0) = 1$ cm : (c) control torque requirement.

6.3 Permanently Manned Configuration (PMC)

Many of the proposed experiments for the Space Station will rely on its low microgravity level. This will be adversely affected by the presence of vibration in the power boom to which the various experimental modules will be attached. To overcome this problem, the suppression of the power boom vibration through active control is proposed.

The simultaneous control of vibration and attitude motion is difficult to accomplish in a single controller design, principally due to the widely different natural frequencies associated with the rigid body motion and flexure. Manipulating the weighting matrices in the LQG/LTR procedure to obtain the desired loop shapes to meet the performance criteria for both the rigid and flexible subsystems is a challenging task. For the PMC, the eigenvalues of the rigid modes are:

$$\begin{array}{cll} & 1.2427 \times 10^{-3} \pm j9.5562 \times 10^{-4} & \text{rad/s;} \\ - & 1.2427 \times 10^{-3} \pm j9.5623 \times 10^{-4} & \text{rad/s;} \\ \pm & 1.2385 \times 10^{-3} & \text{rad/s.} \end{array}$$

In the 66–state PMC model described in Chapter 5, the 60 eigenvalues for flexure lie in the range of $-6.2502 \times 10^{-3} \pm j0.62756$ to $-1.2384 \pm j19.684$ rad/s. The rigid and flexible natural frequencies differ almost by three orders of magnitude.

In order to overcome this problem a number of investigators have employed a 2–level controller whereby a so-called Low Authority Controller (LAC) is initially used to enhance the damping of the critical flexure modes [71, 129–132]. Typically this is accomplished by using colocated rate feedback. Subsequently, a High Authority Controller (HAC) is introduced to provide the necessary performance characteristics. Apart from stabilizing the higher flexural modes, the LAC does not provide any performance enhancement. In the present study, an alternative procedure is proposed to achieve simultaneous attitude and vibration suppression control. Using the linearized

equations obtained through the multibody code, control of the proposed Space Station is achieved by designing the compensator in two stages. Initially the vibration suppression controller is synthesized. Next, the attitude control system is designed. The LQG/LTR procedure is employed at both the stages, after appropriate model reduction. The resulting controller is implemented on a higher order nonlinear plant, simulating the entire closed loop system in the presence of realistic disturbances.

Attitude control of the PMC is achieved by employing a 3-axis CMG located at the center of the power boom (Figure 5-17). Also, a 2-axis CMG is placed on the power boom, 31 m from the center (i.e. at $x_c = -31$), to provide torques in the two transverse directions, y_c and z_c, for vibration suppression of the power boom. This position was chosen to coincide with the point of maximum slope for the first admissible function of the power boom, thus providing the highest possible control and sensing of the first mode. Colocated along with the CMG's are sets of attitude sensors which measure the local slope due to both attitude motion and flexure. Thus, a total of 5 control inputs and 5 measured outputs are available. Among all the elastic members, vibration control of the power boom is the most critical. Studies have shown that power boom vibration can cause microgravity levels at locations of the experimental modules to exceed the maximum allowable value [12]. The saturation level of the attitude CMG is taken as 270 N-m in each axis, while for the vibration suppression CMG it was left unspecified. It is anticipated that due to the high flexural rigidity of the power boom, relatively large torque demands will be placed on the vibration suppression actuator.

6.3.1 Control System Synthesis

The truth model for the PMC with 66 states was described earlier. The complete

linear state equations are:

$$\dot{\mathbf{x}} = \mathbf{A}\mathbf{x} + \mathbf{B}\mathbf{u};$$
$$\mathbf{y} = \mathbf{C}\mathbf{x}; \tag{6.28}$$

where $\mathbf{x} \in \Re^{66}$, $\mathbf{y} \in \Re^{5}$, $\mathbf{u} \in \Re^{5}$ are the state, output and control vectors, respectively. $\mathbf{A} \in \Re^{66\times 66}$, $\mathbf{B} \in \Re^{66\times 5}$ and $\mathbf{C} \in \Re^{5\times 66}$ are time invariant matrices. Prior to commencing the design of the controller, the system output is manipulated in the following way: the roll and yaw channels of the 3-axis attitude sensor are subtracted from the output of the 2-axis sensor so that the local slope due to flexure is isolated from the rigid motion. Also the system is scaled so that outputs 1 to 3 (rigid) are expressed in centiradians, while outputs 4 and 5 (flexible) are in milliradians. The inputs are measured in kN-m. The singular value plots of the open loop system is shown in Figure 6-21 .

Next eq. (6.28) is partitioned into the flexible and rigid subsystems as follows:

$$\begin{Bmatrix} \dot{\mathbf{x}}_\mathbf{r} \\ \dot{\mathbf{x}}_\mathbf{f} \end{Bmatrix} = \begin{bmatrix} \mathbf{A}_\mathbf{r} & \mathbf{A}_\mathbf{rf} \\ \mathbf{A}_\mathbf{fr} & \mathbf{A}_\mathbf{f} \end{bmatrix} \begin{Bmatrix} \mathbf{x}_\mathbf{r} \\ \mathbf{x}_\mathbf{f} \end{Bmatrix} + \begin{bmatrix} \mathbf{B}_\mathbf{r} & \mathbf{B}_\mathbf{rf} \\ \mathbf{B}_\mathbf{fr} & \mathbf{B}_\mathbf{f} \end{bmatrix} \begin{Bmatrix} \mathbf{u}_\mathbf{r} \\ \mathbf{u}_\mathbf{f} \end{Bmatrix};$$
$$\begin{Bmatrix} \mathbf{y}_\mathbf{r} \\ \mathbf{y}_\mathbf{f} \end{Bmatrix} = \begin{bmatrix} \mathbf{C}_\mathbf{r} & \mathbf{C}_\mathbf{rf} \\ \mathbf{C}_\mathbf{fr} & \mathbf{C}_\mathbf{f} \end{bmatrix} \begin{Bmatrix} \mathbf{x}_\mathbf{r} \\ \mathbf{x}_\mathbf{f} \end{Bmatrix}. \tag{6.29}$$

Here $\mathbf{x_r} \in \Re^{6}$, $\mathbf{u_r} \in \Re^{3}$ and $\mathbf{y_r} \in \Re^{3}$ are the state, input and output vectors of the rigid subsystem, respectively. Similarly, $\mathbf{x_f} \in \Re^{60}$, $\mathbf{u_f} \in \Re^{2}$ and $\mathbf{y_f} \in \Re^{2}$ represent the state, input and output vectors for the flexible subsystem. The first step is to design the controller for vibration suppression. For this, the flexural dynamics is considered alone, i.e. neglecting the effect of the rigid body motion. This can be justified due to the widely separated time scales of the two subsystems. Thus, in the time scale of the elastic motions, the attitude dynamics remains essentially unchanged. The resulting vibration controller is connected to the unpartitioned system. Next, the attitude

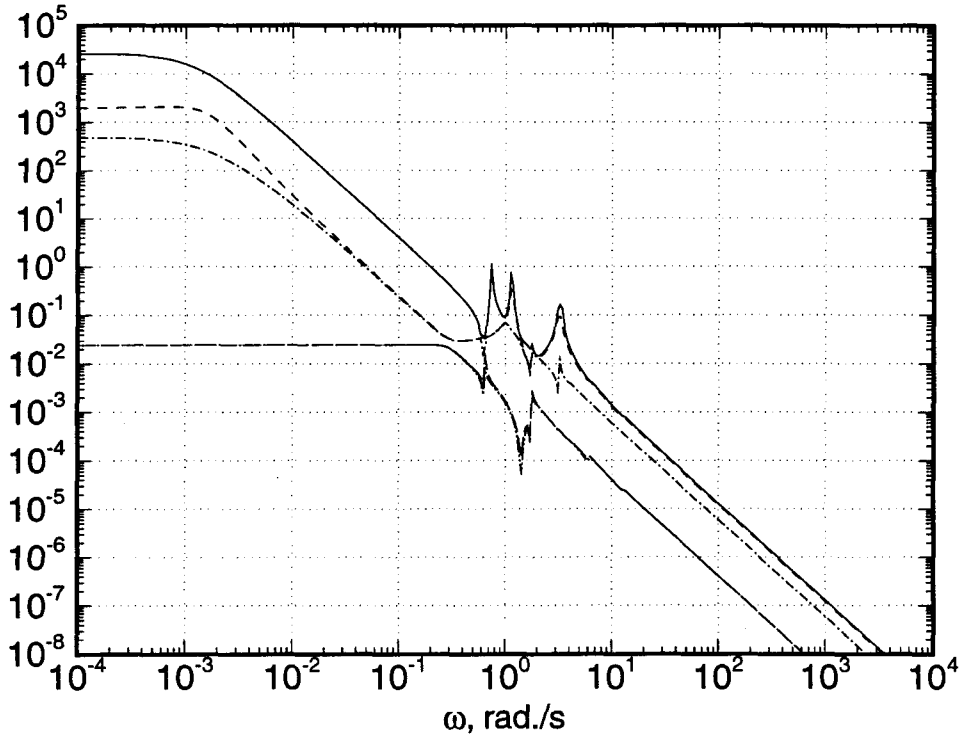

Figure 6-21 Singular values of the open–loop plant.

controller for this augmented system is designed. Note, in this second design stage, the flexible dynamics is not neglected. This is important, because it is principally the inaccurate representation of the high frequency dynamics which leads to unacceptable performance. The overall design procedure is represented schematically in Figure 6-22

.

The vibration of the PMC is governed by:

$$\dot{\mathbf{x}}_\mathbf{f} = \mathbf{A}_\mathbf{f}\mathbf{x}_\mathbf{f} + \mathbf{B}_\mathbf{f}\mathbf{u}_\mathbf{f};$$

$$\mathbf{y}_\mathbf{f} = \mathbf{C}_\mathbf{f}\mathbf{x}_\mathbf{f}. \tag{6.30}$$

The above 60-state model is unacceptably large for the controller design. Moreover, the model is both uncontrollable and unobservable, which precludes the possibility

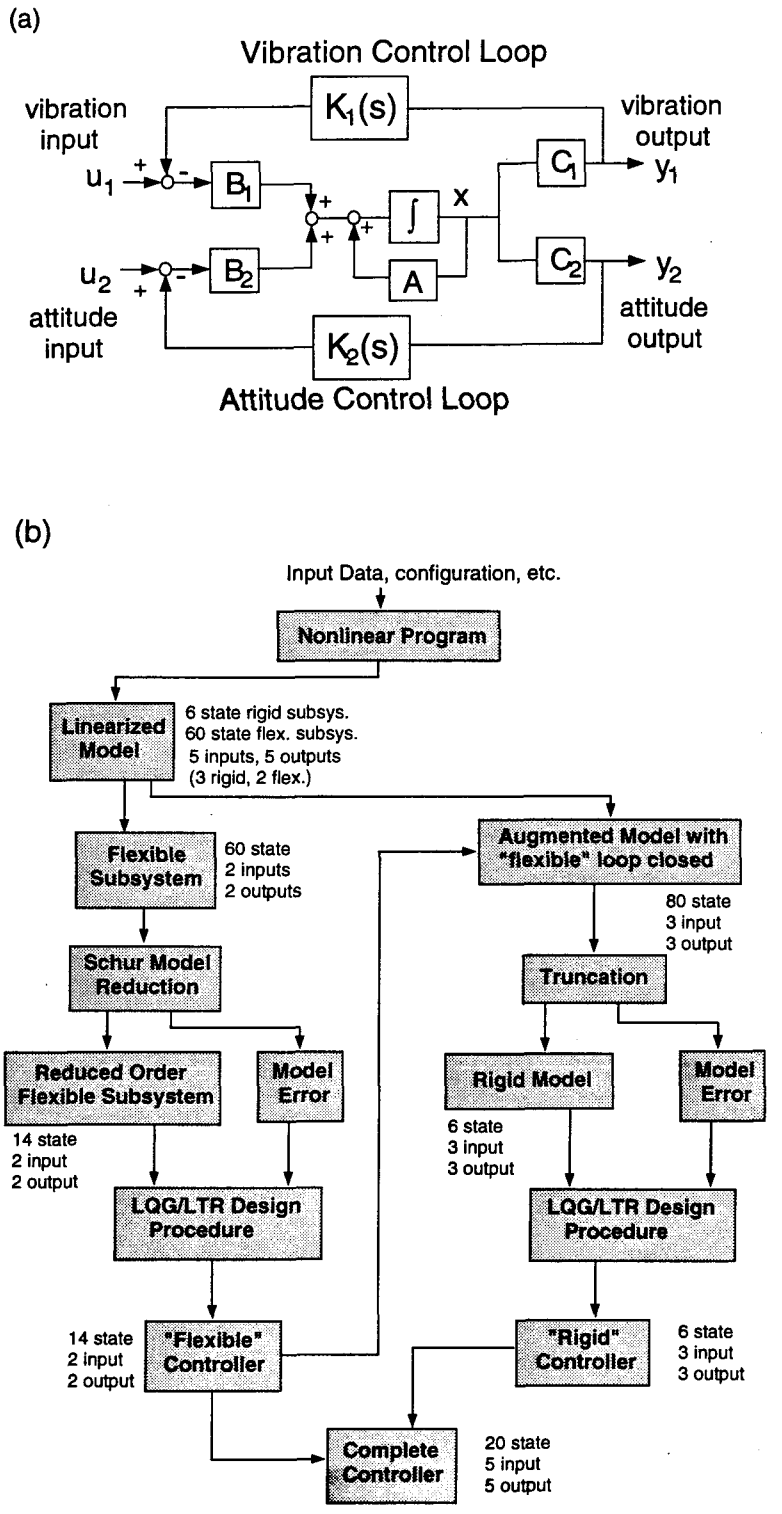

Figure 6-22 Overview of the control design procedure for the PMC: (a) structure of the two-level controller; (b) flowchart.

of its use in design. Therefore, prior to applying the LQG/LTR procedure, model reduction is imperative. The Schur procedure [133] was implemented using the MATLAB *Robust-Control Toolbox* [128] to obtain an observable and controllable 14-state reduced order model. The details are given in Appendix X. In order to ensure robustness against unmodelled dynamics, the multiplicative model error, $\mathbf{E_f}(s)$, between full flexible, $\mathbf{G_{60}}(s)$ and the reduced flexible, $\mathbf{G_{14}}(s)$ models was developed. For the present application of the LQG/LTR procedure, the optimal state estimator $\mathbf{L_f}$ is first established, followed by the design of the state feedback matrix $\mathbf{K_{sf}}$ to recover the properties of the state estimator. The design procedure is an iterative one, accomplished by manipulating the input and output error covariance matrices of the state estimator, until a design which satisfies the stability robustness criterion and does not require overly large control torques is obtained. The resulting compensator $\mathbf{K_v}(s)$ has the same order as the design model (i.e. 14 in this case). Details of the LQG/LTR design and the compensator model are presented in Appendix X. The singular values of both the optimal estimator and the loop transfer function $\mathbf{G_{14}}(s)\mathbf{K_v}(s)$ are shown in Figure 6-23. A greater extent of recovery could have been achieved, but at the cost of higher peak actuator torques. The stability robustness test, which requires $\underline{\sigma}\left[\mathbf{I} + [\mathbf{G_{14}}(s)\mathbf{K_v}(s)]^{-1}\right] > \overline{\sigma}[\mathbf{E_f}(s)]$ [115], is shown in Figure 6-24 . It is clear that the design of the vibration suppression controller is robust to the unmodelled higher frequency elastic states.

The state equation for the vibration controller can be written in terms of the plant input and output as:

$$\begin{aligned} \dot{\mathbf{x}}_{\mathbf{cf}} &= \mathbf{A_{cf}}\mathbf{x_{cf}} + \mathbf{B_{cf}}(\mathbf{r_f} - \mathbf{y_f}); \\ \mathbf{u_f} &= \mathbf{C_{cf}}\mathbf{x_{cf}}; \end{aligned} \tag{6.31}$$

where $\mathbf{x_{cf}} \in \Re^{14}$ is the vector of controller states and $\mathbf{r_f} \in \Re^2$ is the reference input

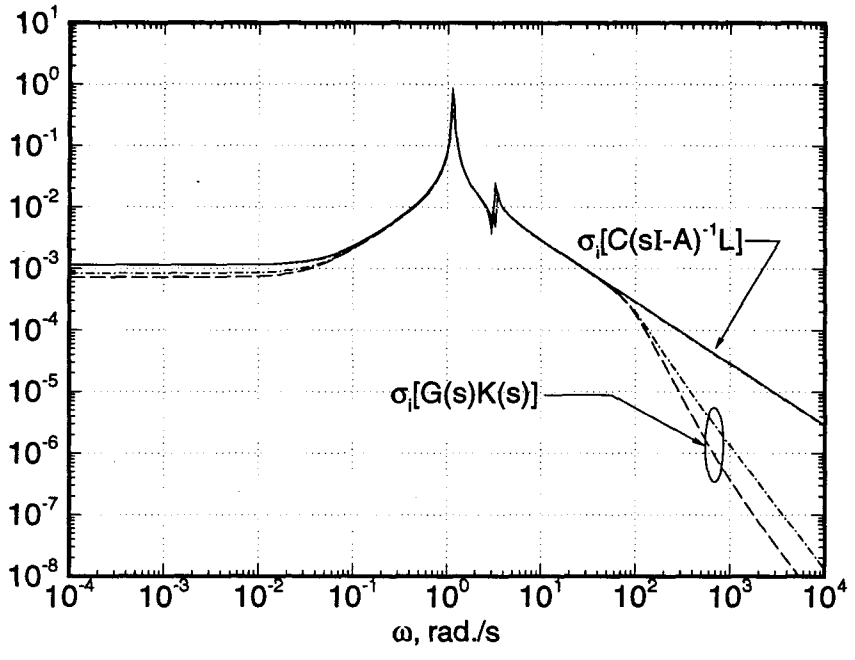

Figure 6-23 Singular values of the loop transfer function: flexible subsystem.

for the flexible subsystem. The details of the time invariant matrices $\mathbf{A_{cf}}$, $\mathbf{B_{cf}}$ and $\mathbf{C_{cf}}$ are given in Appendix X.

The vibration controller is then connected, in feedback, to the original 66-state system. The result is an 80-state, 5-input, 5-output augmented system, although the inputs and outputs of the flexible part are not of interest in the design of the attitude controller. The truth model for the attitude control design is taken to be the 80-state, 3-input, 3-output system obtained by neglecting the 2 inputs and 2 outputs associated with the flexible subsystem:

$$\begin{Bmatrix} \dot{\mathbf{x}}_\mathbf{r} \\ \dot{\mathbf{x}}_\mathbf{f} \\ \dot{\mathbf{x}}_\mathbf{cf} \end{Bmatrix} = \begin{bmatrix} \mathbf{A_r} & \mathbf{A_{rf}} & \mathbf{B_{rf}C_{cf}} \\ \mathbf{A_{fr}} & \mathbf{A_f} & \mathbf{B_fC_{cf}} \\ -\mathbf{B_{cf}C_{fr}} & -\mathbf{B_{cf}C_f} & \mathbf{A_{cf}} \end{bmatrix} \begin{Bmatrix} \mathbf{x_r} \\ \mathbf{x_f} \\ \mathbf{x_{cf}} \end{Bmatrix} + \begin{bmatrix} \mathbf{B_r} \\ \mathbf{B_{fr}} \\ \mathbf{0} \end{bmatrix} \mathbf{u_r};$$

$$\mathbf{y_r} = \begin{bmatrix} \mathbf{C_r} & \mathbf{C_{rf}} & \mathbf{0} \end{bmatrix} \begin{Bmatrix} \mathbf{x_r} \\ \mathbf{x_f} \\ \mathbf{x_{cf}} \end{Bmatrix}. \tag{6.32}$$

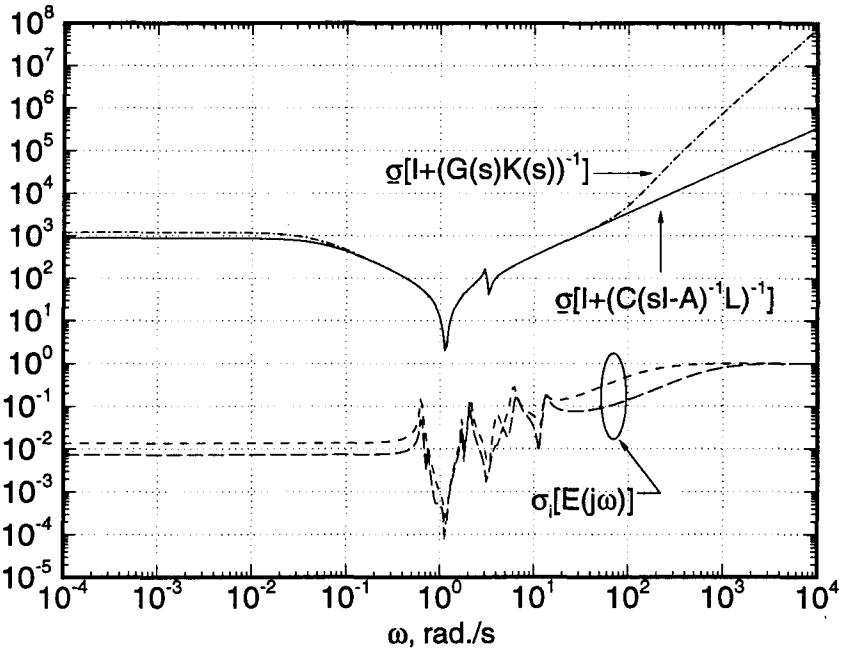

Figure 6-24 Stability robustness test: flexible subsystem.

Again, the large order necessitates model reduction. For this case, the model is reduced by truncating all the non–rigid states. The multiplicative model error between the truth model and the truncated model is evaluated and, as in the design of the vibration suppression controller, the robustness of the synthesized controller to the unmodelled dynamics is ensured. The LQG/LTR procedure is applied, again by designing the state estimator first, and recovering the design with the state feedback (Appendix X).

The singular values of the loop transfer function of the plant with both the LQG/LTR compensator and the state estimator matrix $\mathbf{L_r}$ are presented in Figure 6-25 . This plot shows the extent to which the estimator properties are recovered. In order to lower the required CMG torques, recovery only in the low frequency performance area is obtained. The stability robustness test of the design is presented in Figure 6-26 . The design is quite robust except in the low frequency region ($< 10^{-3}$

rad/s). This is of little consequence since most disturbances occur at considerably higher frequencies, where the robustness of the system is quite good.

The state equation for the attitude controller can be expressed as:

$$\begin{aligned} \dot{\mathbf{x}}_{\mathbf{cr}} &= \mathbf{A}_{\mathbf{cr}}\mathbf{x}_{\mathbf{cr}} + \mathbf{B}_{\mathbf{cr}}(\mathbf{r}_{\mathbf{r}} - \mathbf{y}_{\mathbf{r}}); \\ \mathbf{u}_{\mathbf{r}} &= \mathbf{C}_{\mathbf{cr}}\mathbf{x}_{\mathbf{cr}}; \end{aligned} \tag{6.33}$$

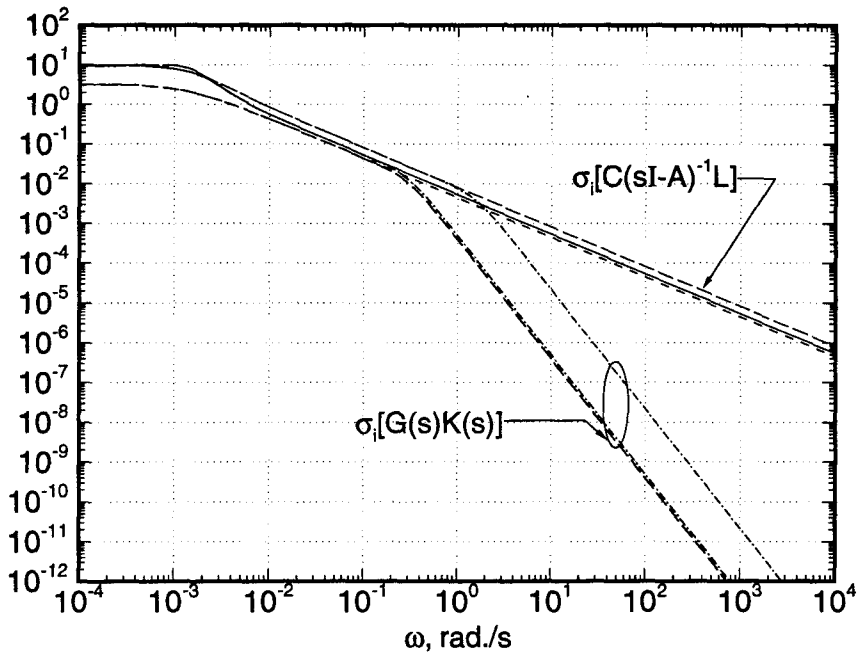

Figure 6-25 Singular values of the loop transfer function: rigid subsystem.

where $\mathbf{x}_{\mathbf{cr}} \in \Re^6$ is the vector of the attitude controller states and $\mathbf{r}_{\mathbf{r}} \in \Re^3$ is the reference input for the rigid subsystem. The vibration and attitude controllers are now combined to form a single 20-state controller $\mathbf{K}_{\mathbf{20}}(s)$ with the following structure:

$$\begin{aligned} \dot{\mathbf{x}}_{\mathbf{c}} &= \begin{bmatrix} \mathbf{A}_{\mathbf{cr}} & \mathbf{0} \\ \mathbf{0} & \mathbf{A}_{\mathbf{cf}} \end{bmatrix} \mathbf{x}_{\mathbf{c}} + \begin{bmatrix} \mathbf{B}_{\mathbf{cr}} & \mathbf{0} \\ \mathbf{0} & \mathbf{B}_{\mathbf{cf}} \end{bmatrix} (\mathbf{r} - \mathbf{y}); \\ \mathbf{u} &= \begin{bmatrix} \mathbf{C}_{\mathbf{cr}} & \mathbf{0} \\ \mathbf{0} & \mathbf{C}_{\mathbf{cf}} \end{bmatrix} \mathbf{x}_{\mathbf{c}}; \end{aligned} \tag{6.34}$$

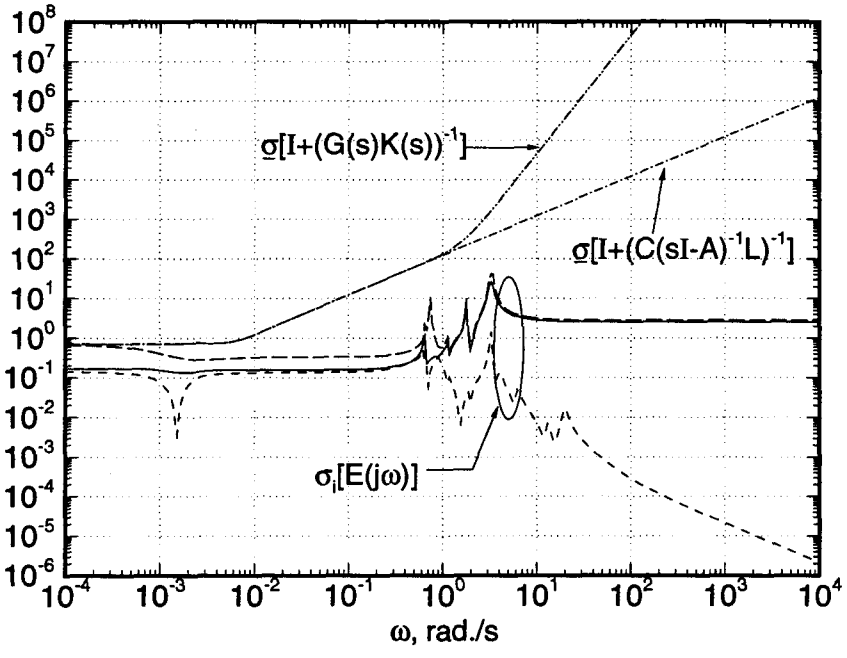

Figure 6-26 Stability robustness test: rigid subsystem.

where

$$\mathbf{x_c} = \begin{Bmatrix} \mathbf{x_{cr}} \\ \mathbf{x_{cf}} \end{Bmatrix}.$$

Note that **u** and **y** refer to the plant input and output vectors, respectively. The singular values of the complete (20-state) compensator are given in Figure 6-27 and the loop transfer function for the 20-state compensator and 66-state plant model pair (i.e. $\mathbf{G_{66}}(s)\mathbf{K_{20}}(s)$) are presented in Figure 6-28 .

6.3.2 Numerical Simulation of the Controlled System

In order to assess the effectiveness of the controller a comprehensive set of simulations were conducted. The controlled response of the PMC was obtained over a range of external disturbances. Only a few of the results useful in establishing trends are discussed here.

For the controlled dynamical studies, the 66-state nonlinear plant model described

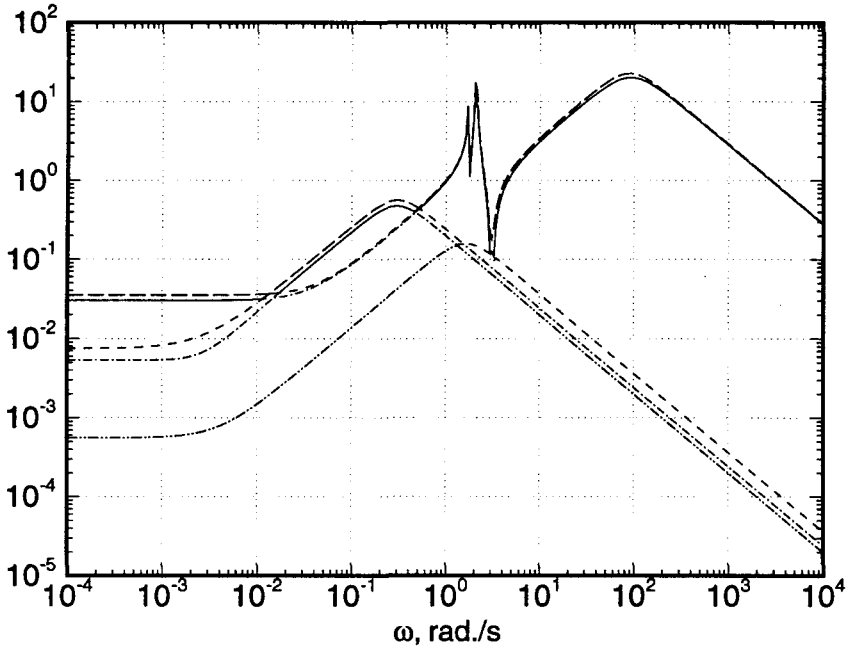

Figure 6-27 Singular values of the complete controller.

earlier was employed. This allows for the closed-loop simulation of the manipulator maneuvers, as well as the slewing of the PV arrays to track the sun. Both the maneuvers require that a nonlinear, time-varying model be used in representing the system dynamics. LQG/LTR control, on the other hand, is linear. However, it has robustness properties which may allow it to cope with the time varying nature of the system during the aforementioned maneuvers. Cases which demonstrate the vibration suppression as well as the attitude control are also presented. The use of a higher order plant model is necessary to indicate the presence of spillover, if it is a problem. This requires that the equations governing the attitude and flexural dynamics of the system be augmented with those for the compensator dynamics.

Responses to Attitude Disturbances

The first case considered is the system response to an initial pitch disturbance of 0.5°. Both the controlled and uncontrolled responses of the librational degrees

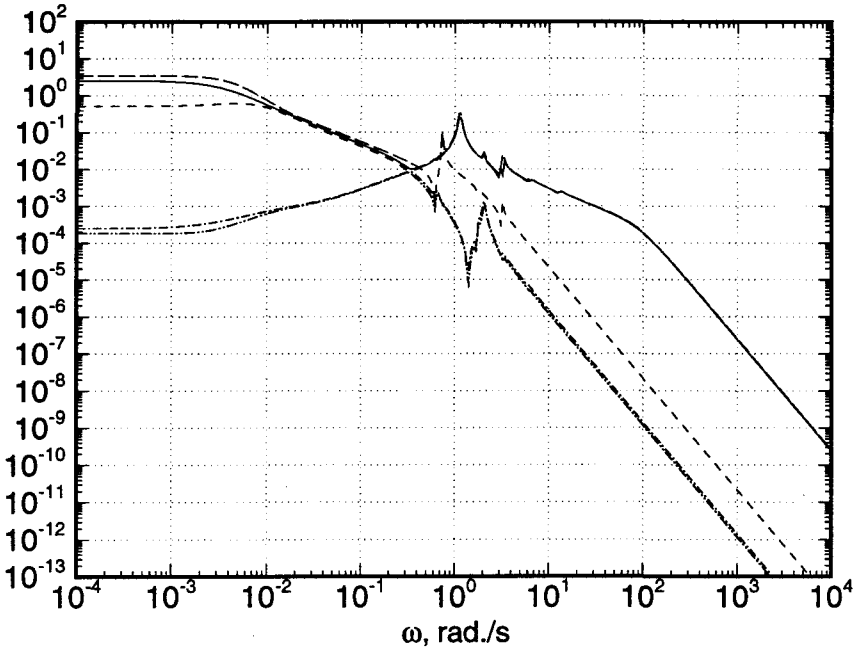

Figure 6-28 Singular values of $\mathbf{G_{66}}(s)\mathbf{K_{20}}(s)$.

of freedom are shown in Figure 6-29 . The controller is able to settle the pitch disturbance in approximately 15 minutes with very little overshoot. The coupled transient roll and yaw excitations are indeed quite small.

Figure 6-30 presents the closed–loop response of flexible members in terms of tip deflections in transverse directions. Note, the beam elements are hardly excited. The peak tip deflections, which are experienced by the PV arrays and radiators, are less than 0.5 cm. As can be expected, these small amplitude vibrations are confined to the pitch plane.

The control torque histories show the effort required to be relatively moderate (Figure 6-31). The peak CMG torque in pitch is less than 100 N-m. The control effort needed for the vibration suppression is very small ($<$ 1 N-m) and hence are not shown. The response to disturbances in other librational degrees of freedom exhibited

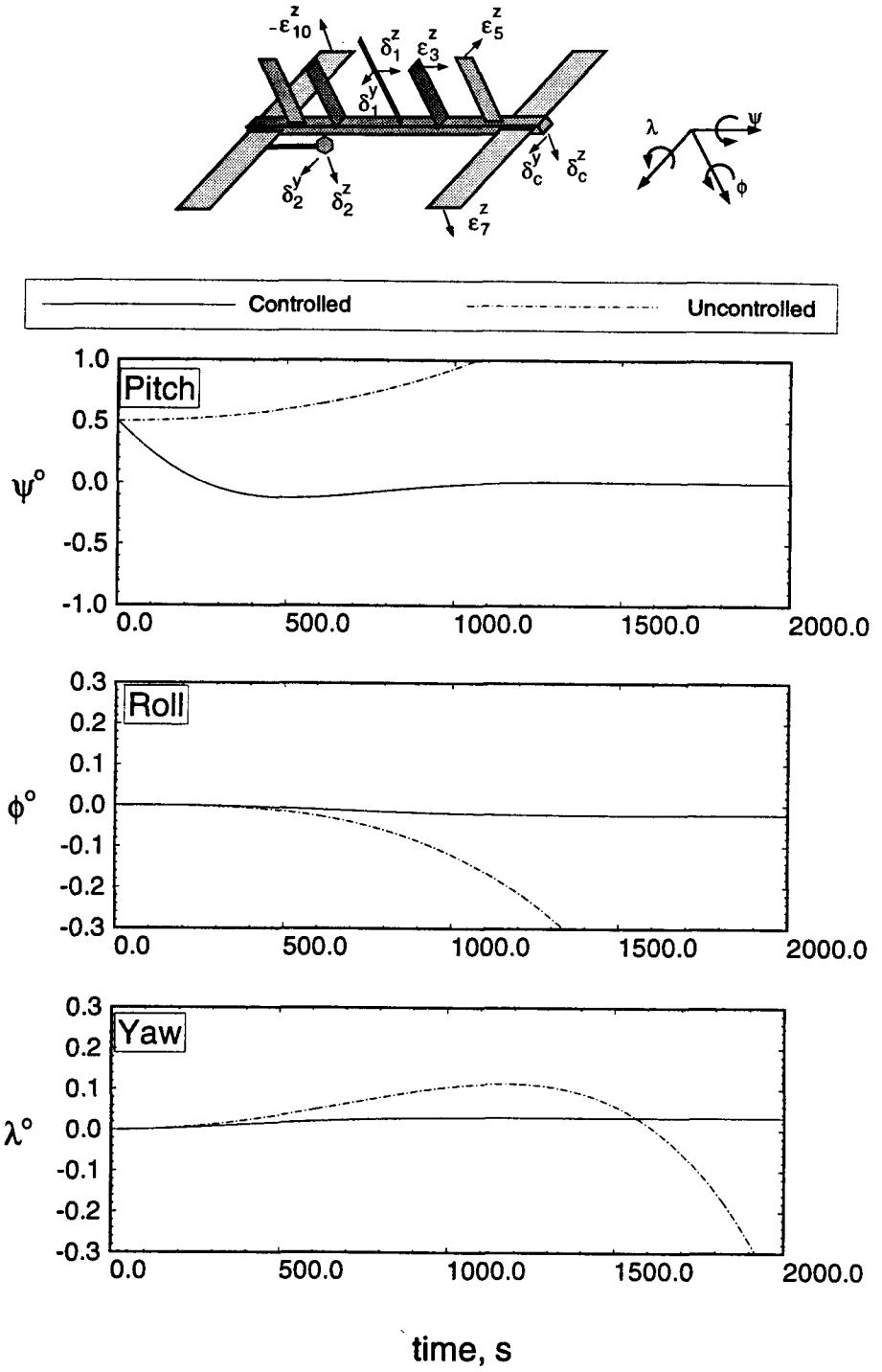

Figure 6-29 Librational response of the PMC to a pitch disturbance of $\psi(0) = 0.5°$.

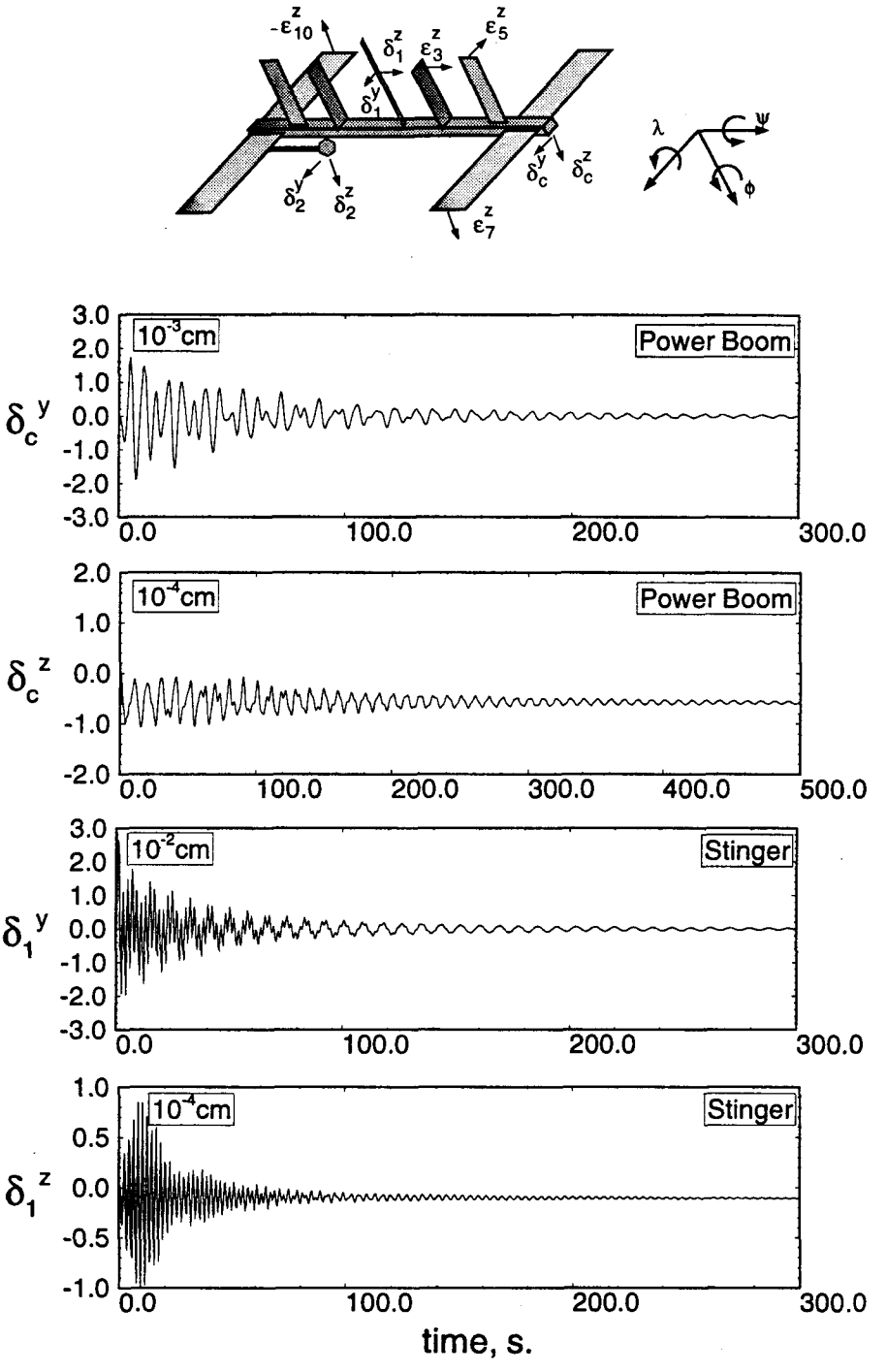

Figure 6-30 Controlled flexural response showing tip deflection time histories for a librational disturbance of $\psi(0) = 0.5°$: (a) power boom and stinger.

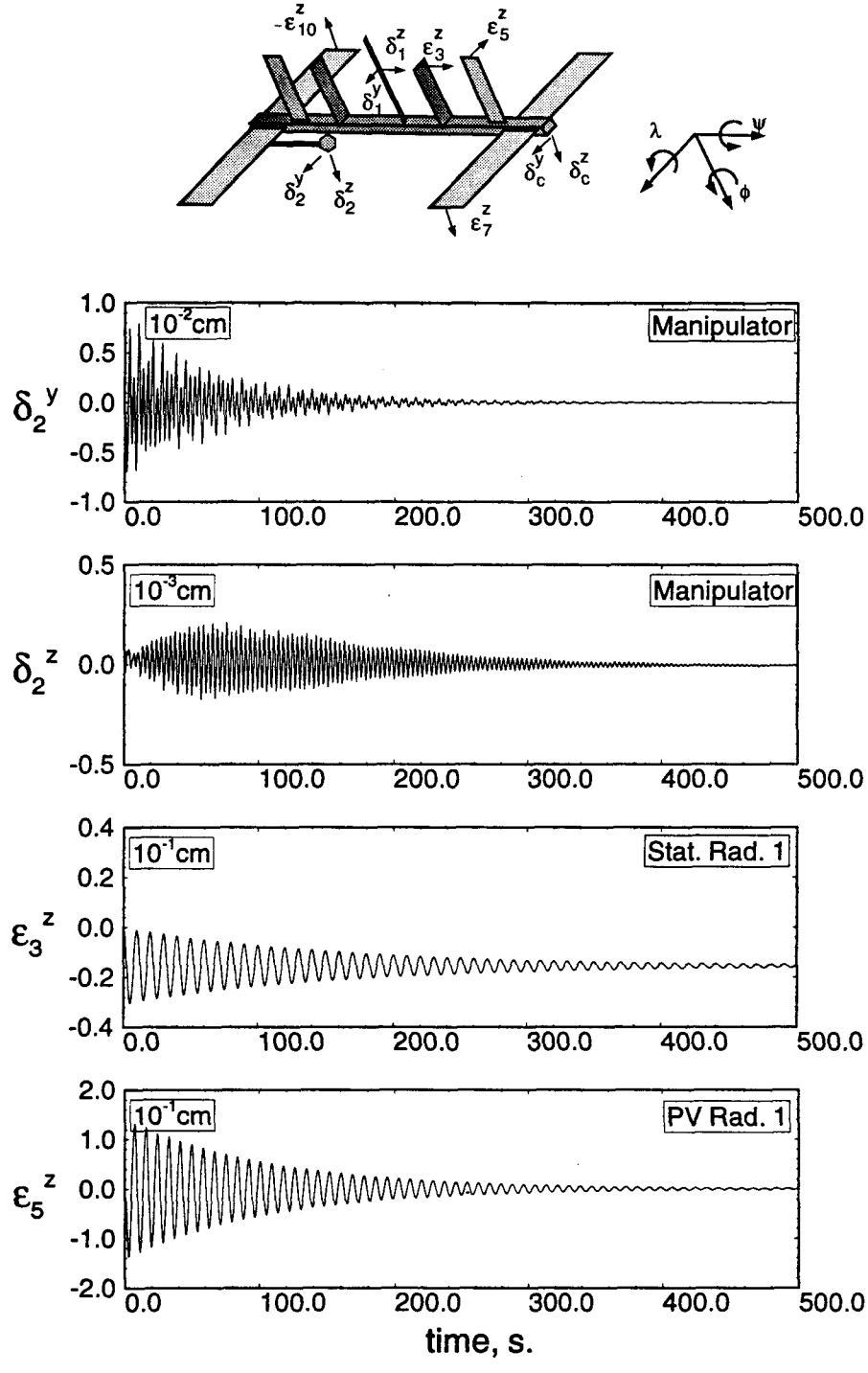

Figure 6-30 Controlled flexural response showing tip deflection time histories for a librational disturbance of $\psi(0) = 0.5°$: (b) manipulator and radiators.

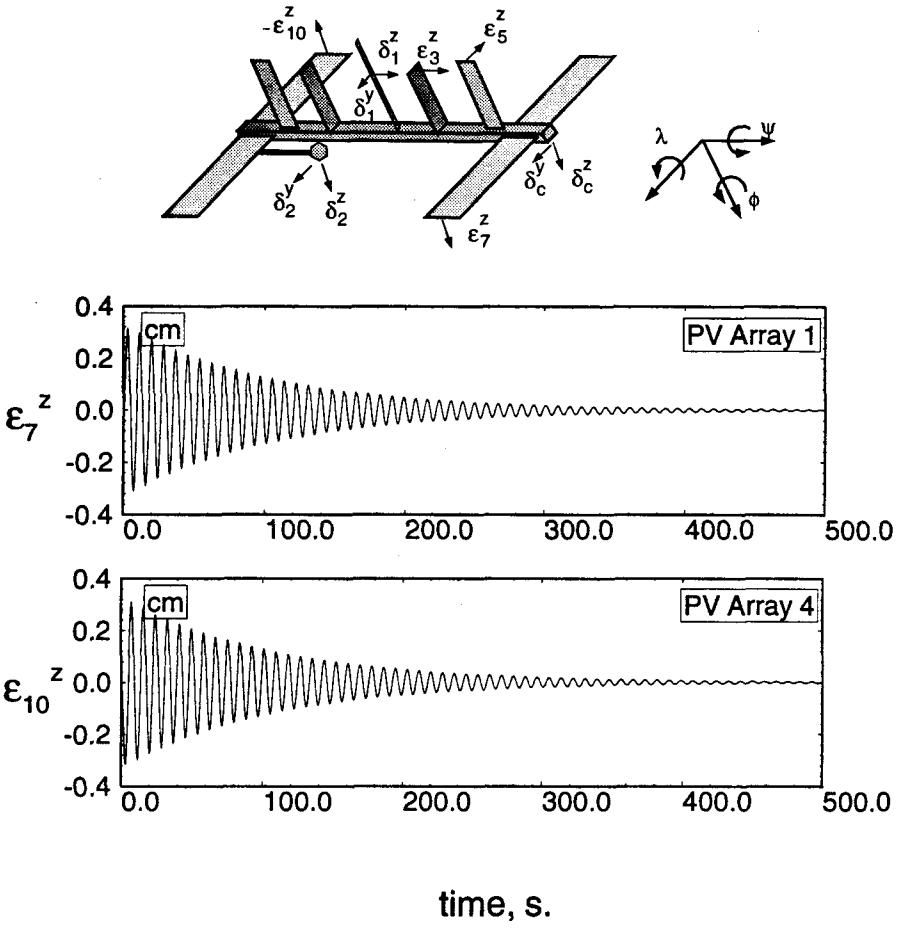

Figure 6-30 Controlled flexural response showing tip deflection time histories for a librational disturbance of $\psi(0) = 0.5°$: (c) PV arrays.

similar trends.

Responses to Flexural Disturbances

In order to evaluate the vibration suppression performance of the compensator, the system response to an initial power boom tip deflection of 1.5 cm ($\delta_c^y(0) = 1.5$ cm) was simulated. The first two shape functions of the power boom were deflected by 1 cm and 0.5 cm, respectively, to provide the prescribed initial tip motion. The controlled and uncontrolled vibrations of the power boom and stinger tips are shown in Figures 6-32 and 6-33 , respectively. The controller is able to suppress the dominant

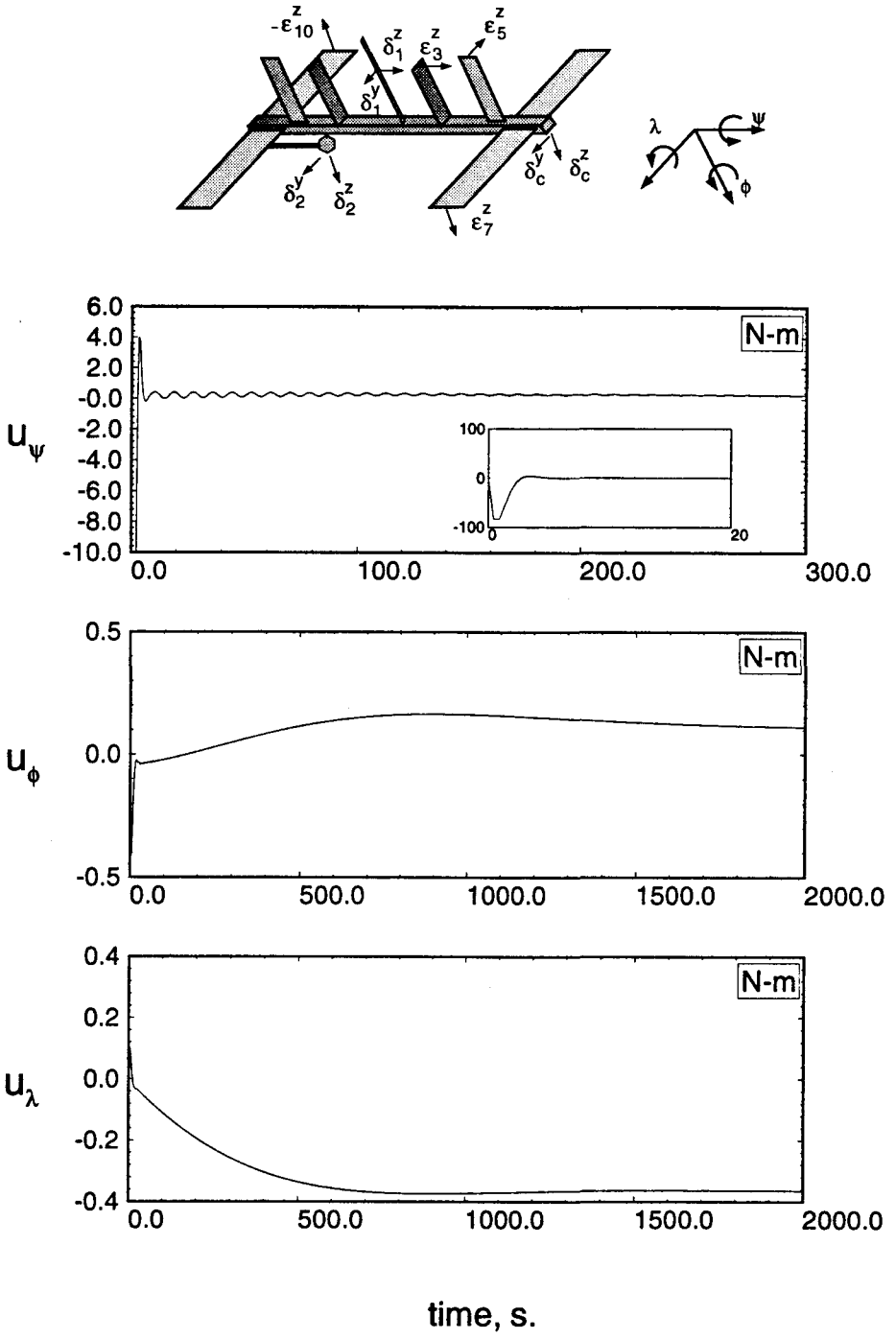

Figure 6-31 Time histories of the control effort to damp the response caused by a pitch disturbance of $\psi(0) = 0.5°$.

power boom vibration (δ_c^y) within 150 seconds. With structural damping alone (i.e. without control), the same degree of attenuation required approximately 400 seconds. Similarly, the power boom vibration in the other transverse direction (δ_c^z) is also attenuated significantly. Through coupling, the stinger vibration in the y_1 direction is also abated compared to the uncontrolled case. The attenuating effect of the controller on the other elastic members, although present, is not as significant as that on the stinger.

The required attitude CMG torques were found be minimal (< 2 N-m) and hence are not shown. The torque time histories for the vibration suppression are given in Figure 6-34 . A peak torque of approximately 900 N-m is required in the z_c direction. This high value is not surprising, given the high flexural rigidity of the power boom as well as the degree of vibration suppression achieved.

Responses to Operational Maneuver

The first maneuver considered is that of the PV arrays. To simulate the tracking of the sun, the 4 PV arrays are slewed about the orbit normal at a rate of 1 revolution per orbit. The maneuver is performed for 1 orbit, after which the arrays remain fixed with respect to the PMC. The uncontrolled response to this maneuver was discussed in Chapter 5.

The time histories of the attitude angles are shown in Figure 6-35 for both the controlled and uncontrolled cases. The controller is able to maintain the pitch angle within $\pm 2^\circ$, while the uncontrolled response is quite unstable. Due to the slow slew rate, the vibrational response of all the flexible members was found to be very small. The highest tip deflection, as expected, occurred in the PV arrays, although even that was found to be less than 0.3 mm in amplitude. The vibration time histories are, therefore, purposely omitted here. The required CMG torque levels (Figure 6-36)

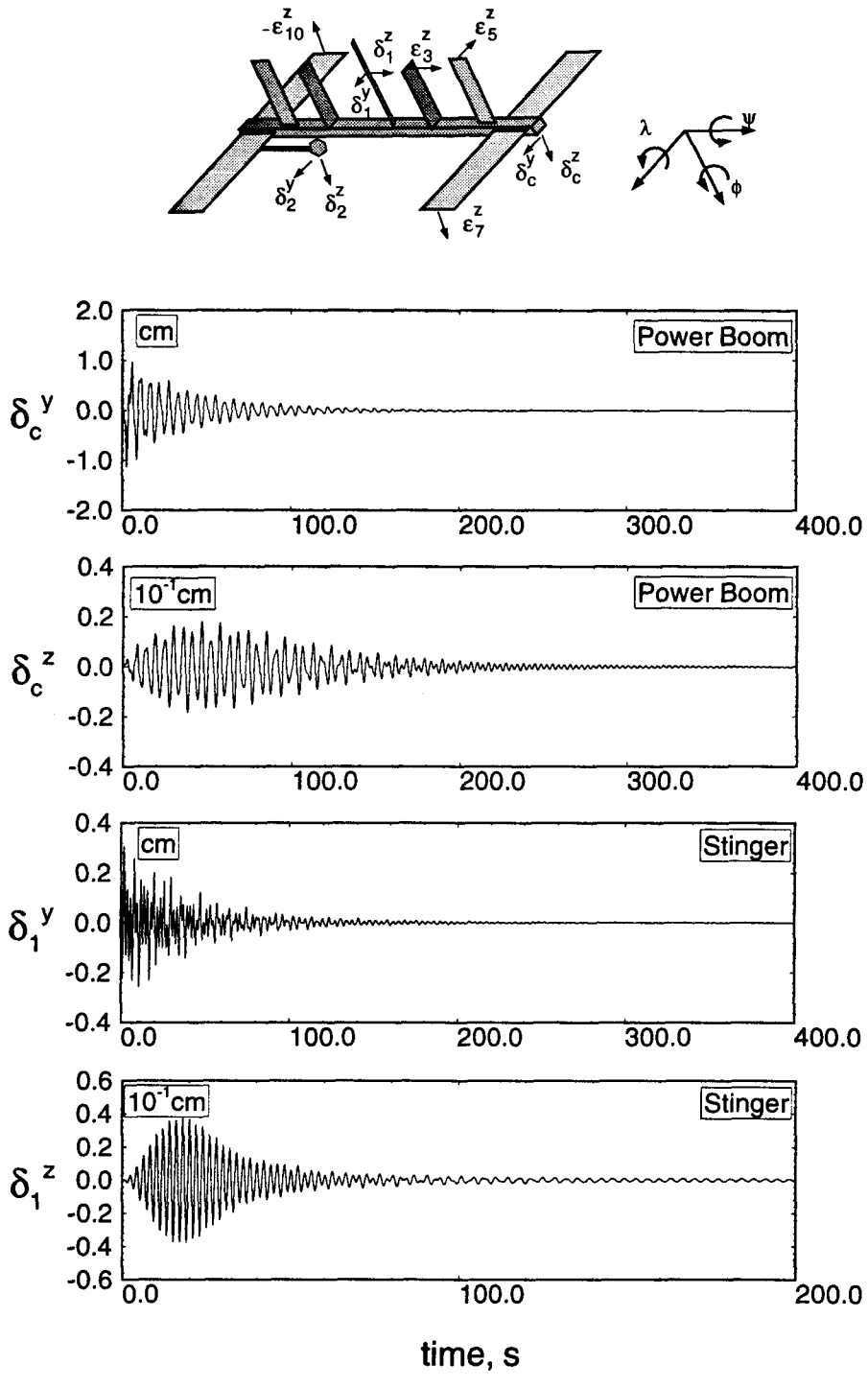

Figure 6-32 Controlled flexural response of the power boom and stinger to a disturbance $\delta_c^y(0) = 1.5$ cm.

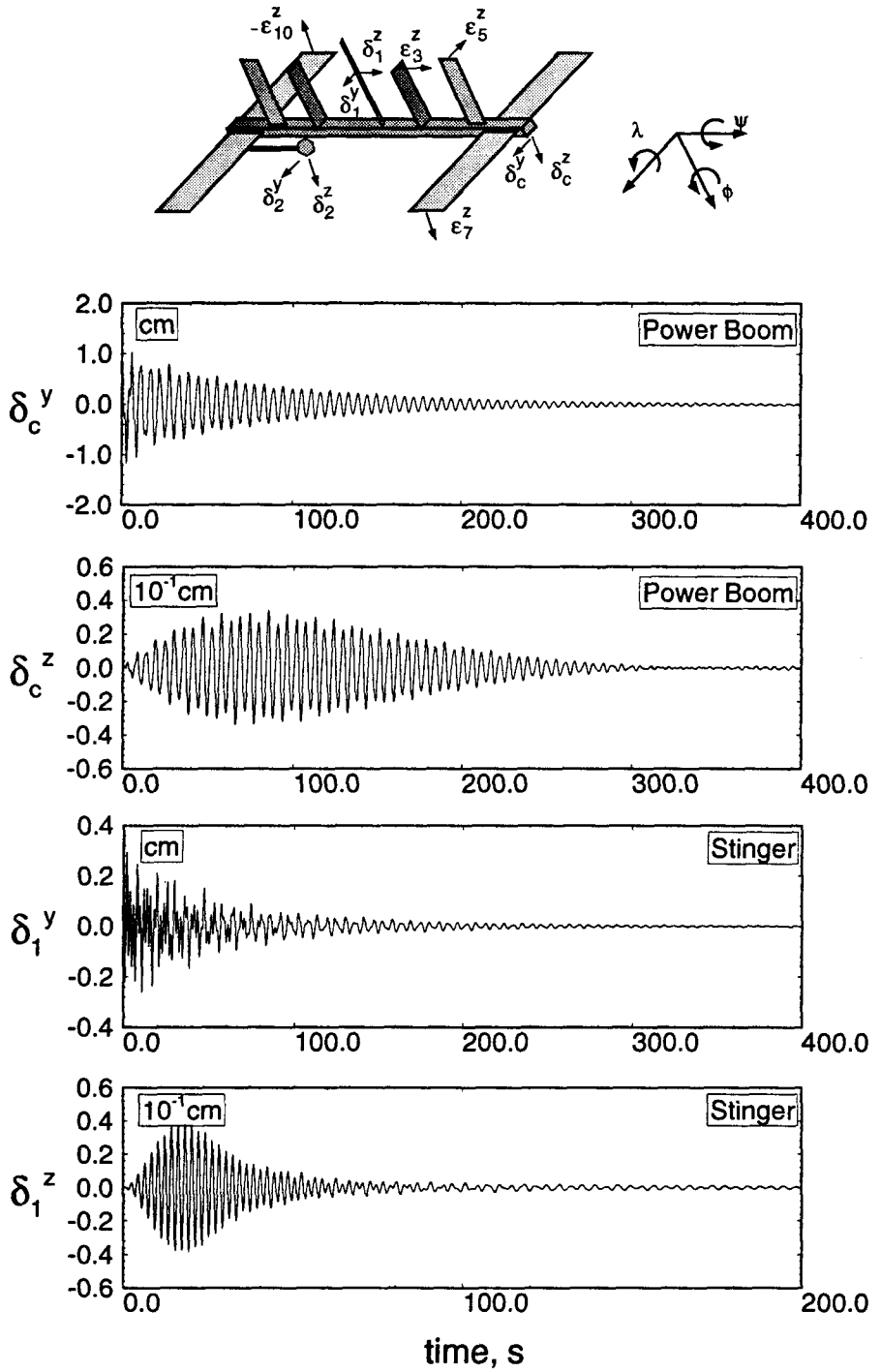

Figure 6-33 Uncontrolled flexural response of the power boom and stinger to a disturbance $\delta_c^y(0) = 1.5$ cm.

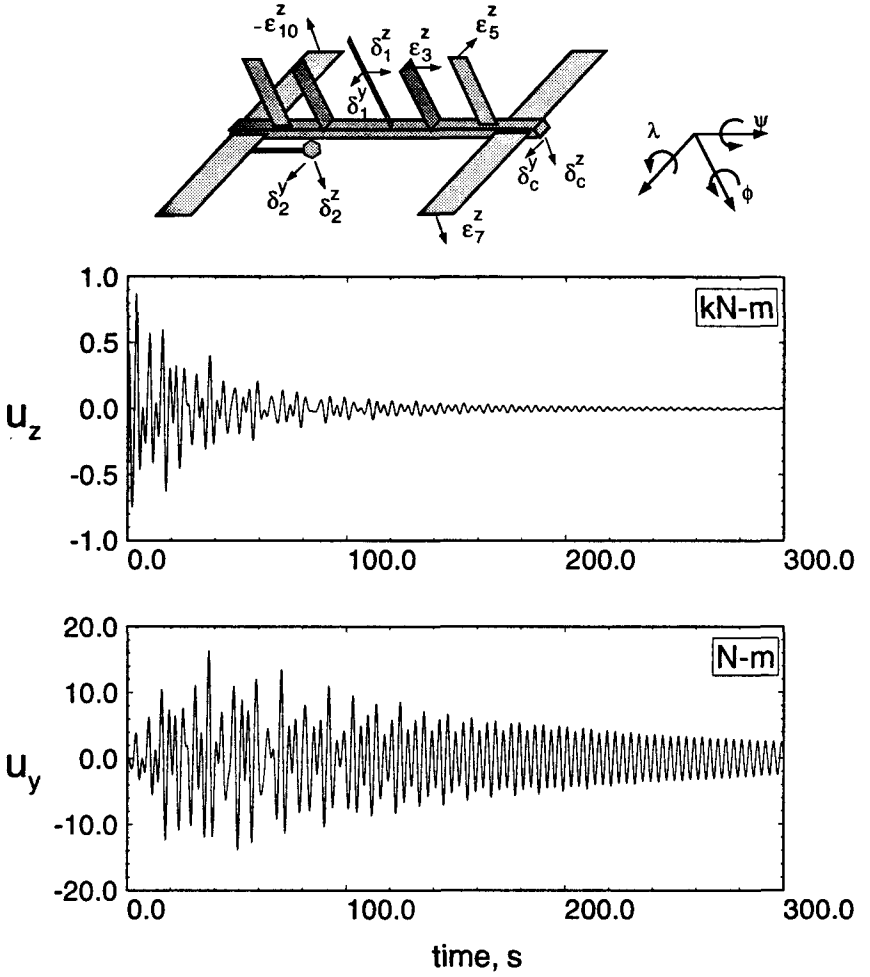

Figure 6-34 Vibration suppression CMG torque histories: $\delta_c^y(0) = 1.5$ cm.

are quite modest, with the peak value about the pitch axis of only 2 N-m. The ability of the time invariant controller to maintain the attitude angles within acceptable limits is perhaps a little surprising, given the nonautonomous character of the system. With the addition of a simple nonlinear control effort based on the computed torque method, even the relatively small cyclic variation of $\pm 2^\circ$ can be eliminated. Because of the known nature of the disturbance, i.e. the slewing maneuver, the design of such a controller is not a major challenge.

The final case considered is a 180° rotational maneuver of the manipulator in the ONLV plane with a payload located at its tip. The uncontrolled response to

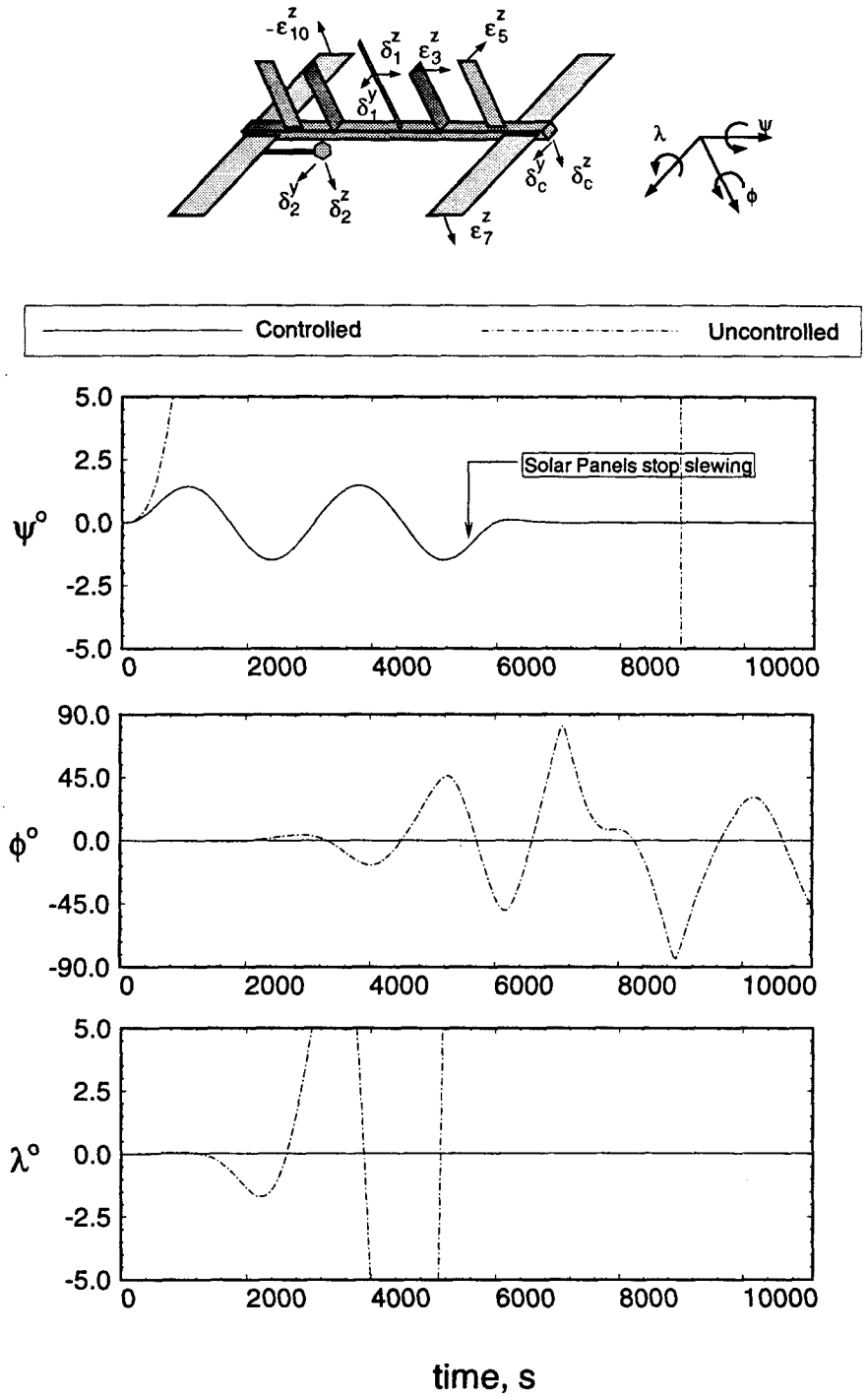

Figure 6-35 Librational response to the PV array slewing maneuver.

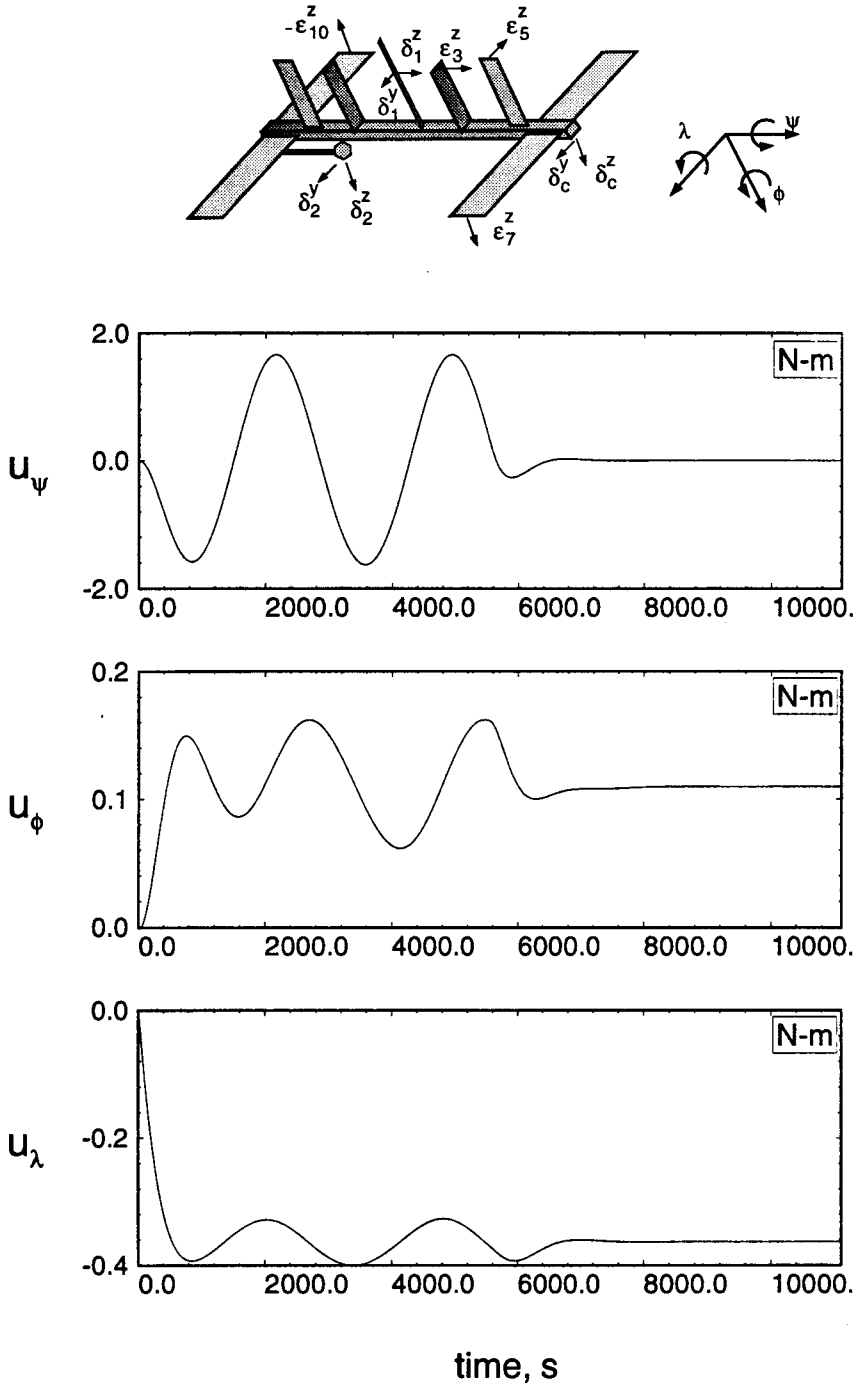

Figure 6-36 Attitude CMG's torque time histories to attenuate the response induced by the PV array slew maneuvers.

this maneuver was studied in the previous chapter. A schematic diagram illustrating the model and the maneuver was given in Figure 5-17. The maneuver is executed in 1 minute and has a sine-on ramp profile, commencing and terminating the action with both zero angular acceleration and velocity. Figure 6-37 shows the librational response. As can be expected, the yaw degree of freedom is affected most, although the pitch and roll are also disturbed due to the dynamic coupling. Because of the speed of the maneuver, the controller is unable to reduce the librational excursions during the maneuver. However, in the post maneuver phase, the controller is quite effective in regulating the attitude motion. A nonlinear controller may improve the behaviour during the maneuver.

The power boom and stinger remained relatively unaffected by the maneuver, however, the same cannot be said of the other elastic members. The manipulator experienced a peak tip deformation of approximately 3 cm (Figure 6-38). The station radiators also show relatively large tip deflections. Note, the PV arrays exhibit a peak deflection of almost 4 cm (Figure 6-39). Of course, all the large displacements occur in directions which lie in the plane of the maneuver. Thus the PV radiators, which are free to deflect in the direction normal to the plane of the maneuver, remain unaffected.

The attitude control effort required is shown in Figure 6-40 . The demand imposed on the vibration suppression CMG during the maneuver was found to be very small and hence is not presented here. Note that the CMG torques during the maneuver are relatively large, especially in the yaw channel. Nevertheless, the corrective action is not observed until after the maneuver is complete. To reiterate, this may be attributed to the bandwidth of the controller which is not large enough to cope with the relatively fast maneuver. If the actuators were capable of providing the necessary torque, the control system can be designed with a greater bandwidth, provided that

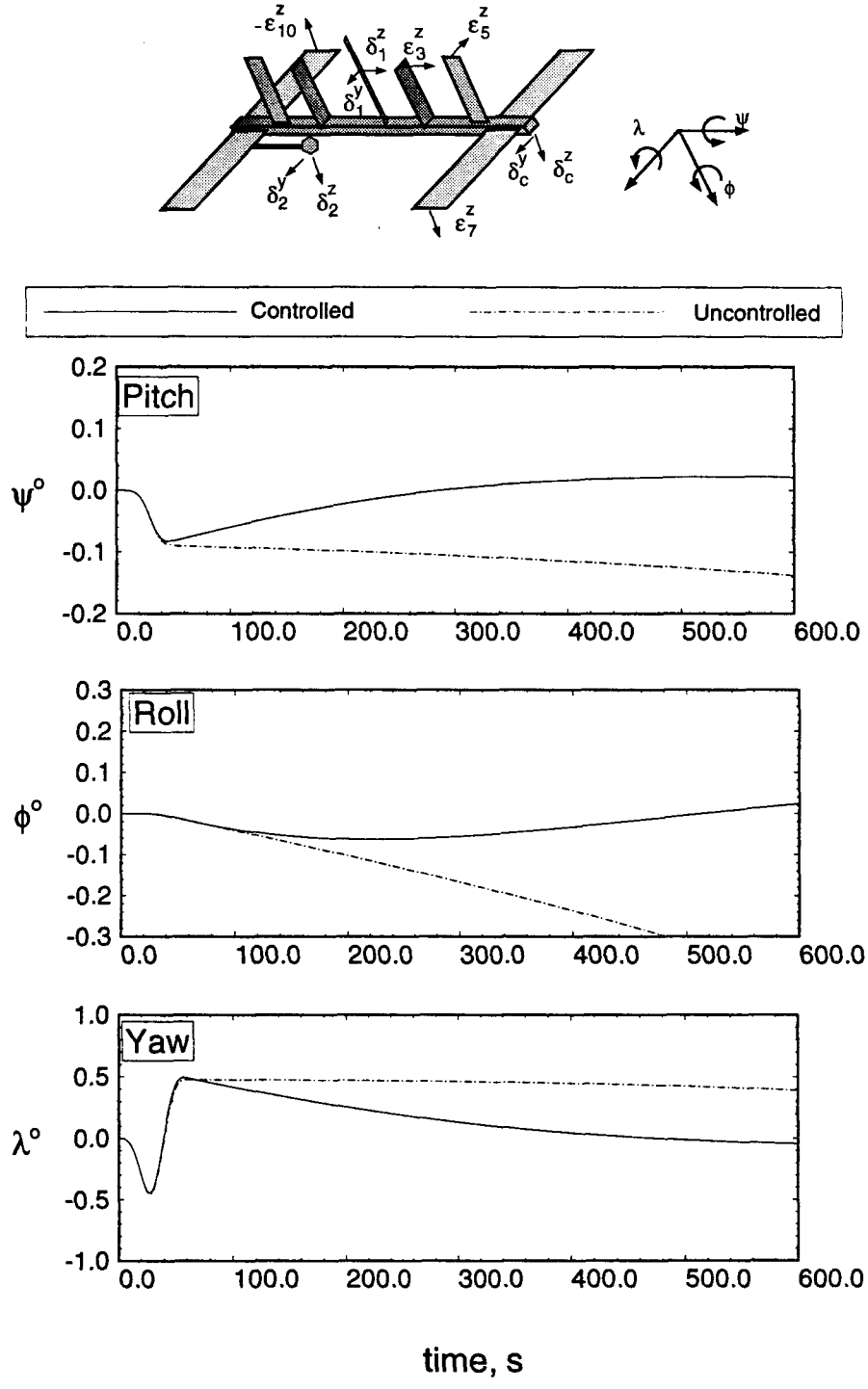

Figure 6-37 Librational response to the manipulator maneuver.

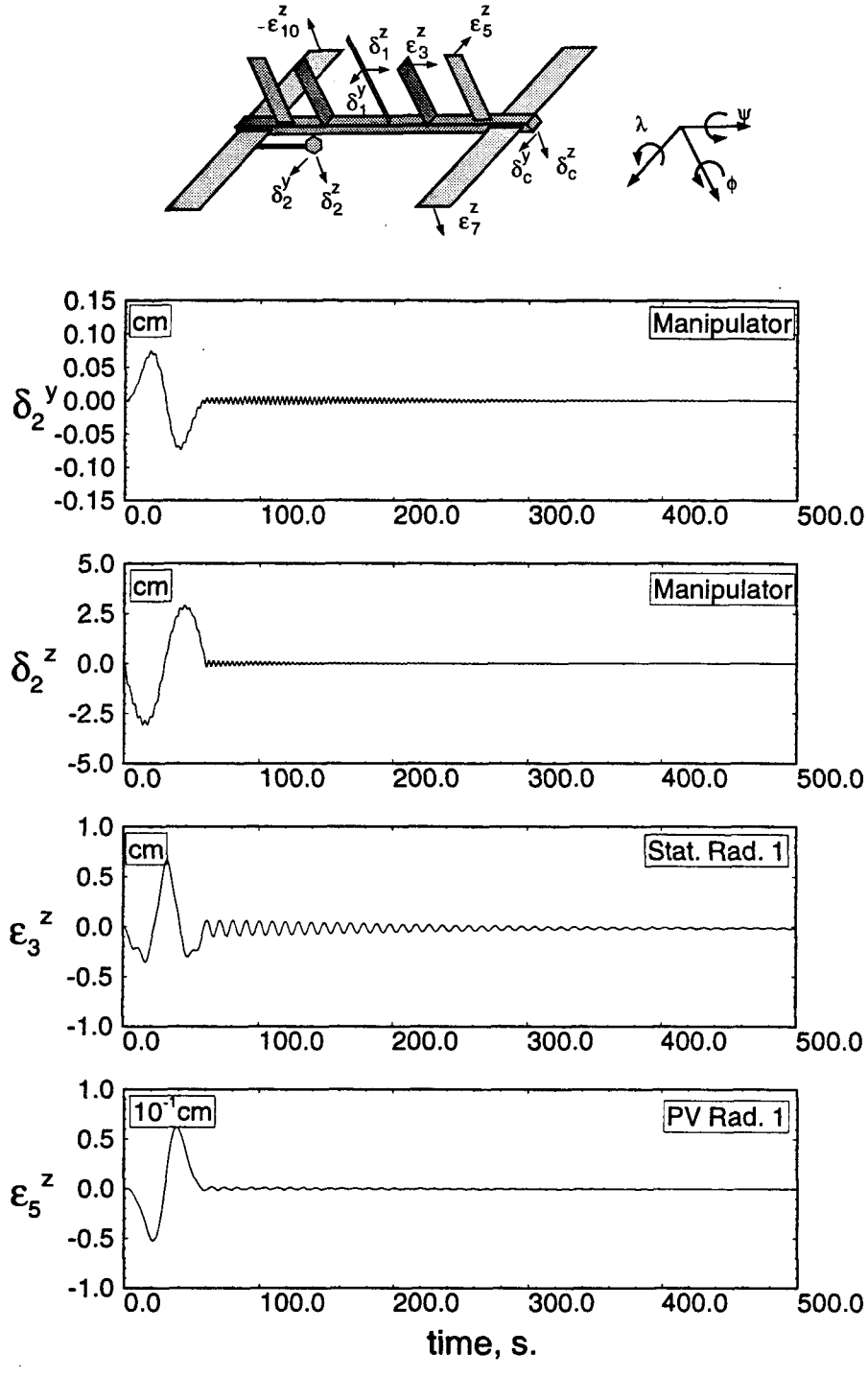

Figure 6-38 Controlled vibrational dynamics of the radiators and manipulator to the 180° slew maneuver.

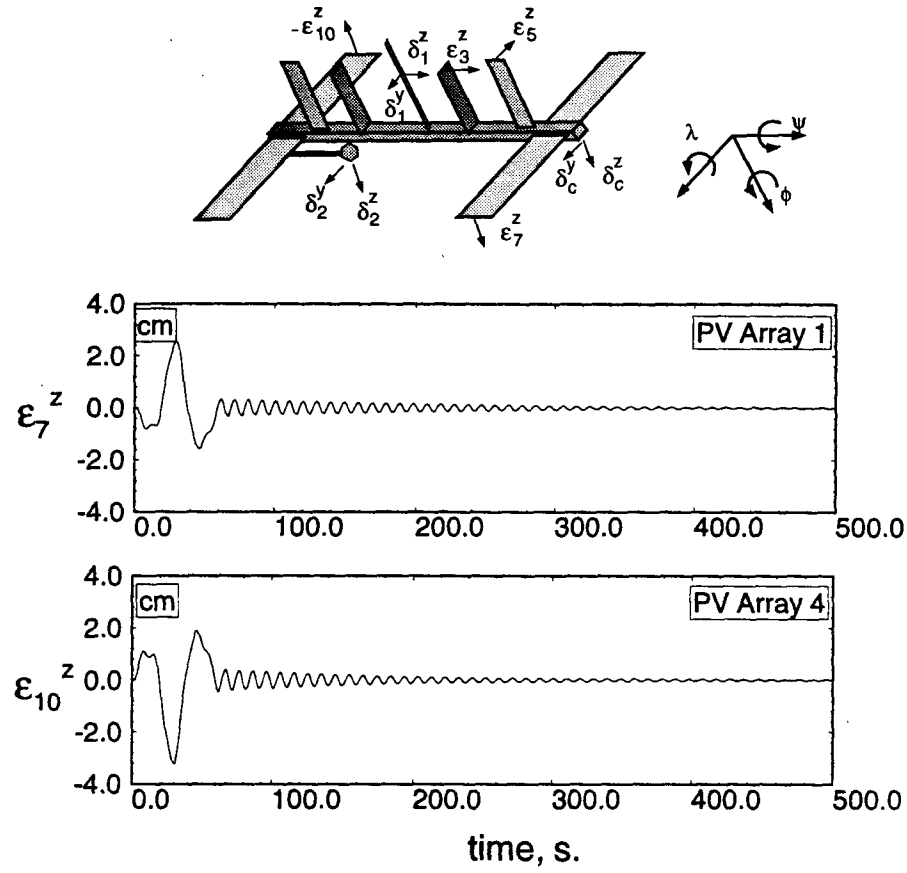

Figure 6-39 Controlled vibrational response of the PV arrays to the 180° slew maneuver of the manipulator.

the robustness criterion is not violated.

6.4 Summary

Three linear control strategies, namely the LQR, LQG/LTR and H_∞, were applied to synthesize an attitude controller for the FEL configuration of the proposed Space Station. The procedures employed ensured the robustness of the design to the unmodelled dynamics. The resulting controllers were implemented on the nonlinear plant model which included both the attitude and the flexible system dynamics. The

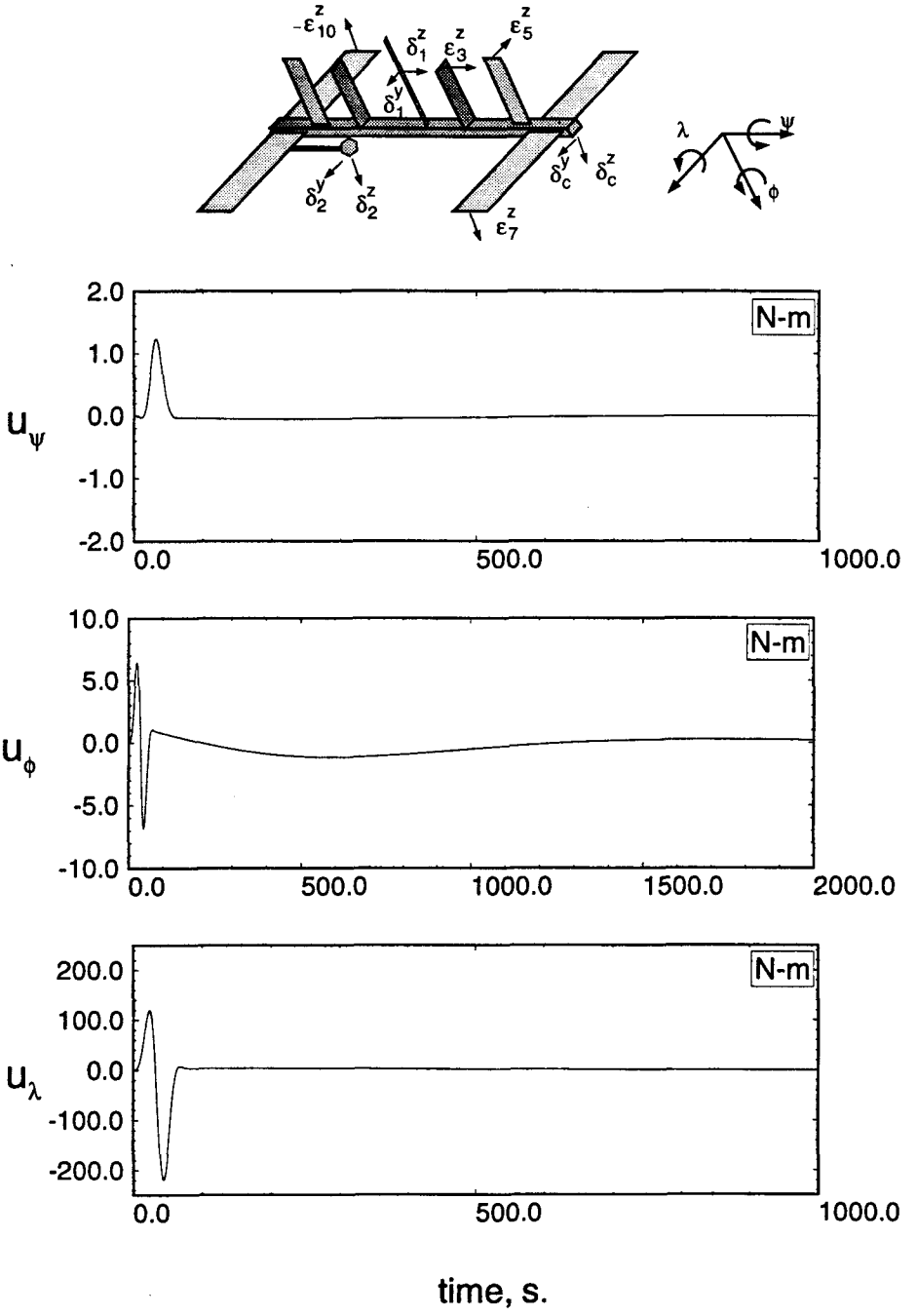

Figure 6-40 Attitude CMG's torque requirements for the manipulator maneuver.

results of the closed loop simulations indicate that the performance of the H_∞ controller is superior. However, it involves a larger size of the compensator model, which may require careful consideration during its implementation.

For the PMC, a two-level LQG/LTR controller for both the attitude and vibration control was synthesized. The controller was subsequently incorporated into the nonlinear code, and dynamics of the closed loop system to attitude, vibration and slew disturbances were simulated. The results show excellent attitude control and vibration suppression behaviour. This is indeed gratifying considering the fact that the linear controller was designed based on a time–invariant plant model. Moreover, no spillover effect was observed.

7. CLOSING COMMENTS

7.1 Concluding Remarks

The thesis represents a comprehensive study aimed at the dynamics and control of flexible multibody systems. In the process it deals with several important aspects of this challenging problem:

(i) A relatively general dynamical formulation applicable to a large class of systems, characterized by interconnected flexible structures in a tree topology, has a number of attractive features all of them not found in any single formulation reported in the open literature. Beam as well as plate type members in an arbitrary elliptical trajectory free to undergo slewing and translational motion; coupling between the orbital, librational and vibrational motions; accounting of the shifting c.m., foreshortening effect and structural damping; compact character of the governing equations through cancellation of terms; incorporation of quasi–comparison functions for discretization; arbitrary number of force and moment actuators on each member; etc. lead to a powerful and versatile tool for studying this class of problems. As the nature of the deflection is kept general in the formulation, it can be readily extended to other structural members (shells, membranes, tethers) undergoing a wide range of deformations (axial, bending, torsion).

(ii) An efficient numerical code has been developed for the integration of the nonlinear, nonautonomous and coupled equations of motion. Its modular character is ideally suited to assess the relative importance of various system parameters, thus assisting in the evaluation of system performance and design. The versatile formulation together with the numerical code, both with attractive features,

represent a significant contribution to the field.

(iii) The conservation of energy to a high level of accuracy as well as comparison with results for particular cases reported in the literature substantiate the validity of the formulation and code.

(iv) The versatility of the approach has been illustrated through its application to study uncontrolled dynamics of several different configurations, of contemporary and future importance, under a variety of disturbances. This clearly suggests its potential role during the design as well as operational phases of complex multibody systems. In terms of the dynamical response, disturbances represented by the Shuttle docking, PV array slew and the manipulator maneuvers resulted in significant excitation of the attitude angles and/or of the flexural members. As can be expected, the degree of freedom most affected depended on the character of the disturbance as well as the system. For example, the docking of the Space Shuttle on the FEL resulted in significant excitation of both librational and vibrational degrees of freedom (particularly the PV arrays). Solar tracking by the PV arrays on the PMC affects the attitude angles but the elastic members remain virtually unaffected. On the other hand, the effect of the manipulator maneuvers is primarily on the elastic degrees of freedom.

(v) An approximate analytical solution to the dynamics of a flexible multibody system through an extension of the Butenin method represents an important development. The approach is attractive because of its applicability to a set of n second order differential equations. It gives results of sufficient accuracy, at least during the preliminary design stage, and promises considerable savings in time as well as effort.

(vi) A fresh approach to the linearization of the complex model through the compu-

tation of the system Jacobian matrices by finite differences has been developed. Linearized equations are often indispensable for the controller design.

(vii) The effectiveness of three control strategies is studied with reference to two evolving configurations of the proposed Space Station. The provision for a dynamic compensator permits simulation of the closed loop system consisting of both the nonlinear plant and the linear controller. The controller design ensures robustness to unmodelled dynamics. When applied to the FEL, results show superior performance of the H_∞ controller, however, it involves a larger size of the compensator. The two–level LQG/LTR controller showed excellent attitude and vibration suppression behaviour, when applied to the PMC, without any spillover effect, although it was based on a time–invariant plant.

(viii) The comprehensive study involving formulation, numerical code, validation, dynamics and control provides a versatile and powerful tool for studying a wide range of dynamics and control problems associated with space based multibody flexible systems.

7.2 Recommendations for Future Work

The field of dynamics and control of flexible multibody systems, like any other area of inquiry, is full of endless challenges. The present study, though comprehensive, has tried to address only some of the issues. Attention to several other aspects indicated below may prove to be fruitful, satisfying and improving our understanding of the subject:

(a) The mathematical formulation presented in the thesis considers a topological tree with two levels of branching. An extension to higher levels with open and/or closed geometry as well as an extension of the numerical code would be

the next logical step. Incorporation of the joint degrees of freedom as generalized coordinates in the code would further enhance its versatility.

(b) In order to improve verification of the energy conservation, a generalized coordinate for the out–of–plane orbital motion may be incorporated in the model.

(c) The use of quasi–comparison functions was found to improve the discretization process. For more complex interconnected systems, the selection of these functions requires closer attention. For example, when secondary or tertiary bodies are not connected at the extremities of the preceding ones, the use of eigenfunctions with moments and forces applied at the appropriate locations may be investigated. This would provide the shape functions with the necessary discontinuities in their second and third derivatives.

(d) Structural elements such as shells and membranes, not considered in the thesis, may be incorporated in the code. This would add to the versatility.

(e) The application of the H_∞ method to the simultaneous attitude and vibration suppression control of the PMC would be an important contribution.

(f) The use of piezoelectric elements for vibration control can be readily incorporated in the formulation and code. This method of sensing and actuation has numerous benefits for space structures.

(g) Attention should be directed towards control of complex multibody systems accounting for their nonlinear dynamics. Application of the Feedback Linearization Technique (FLT) would represent an important step forward in that direction.

BIBLIOGRAPHY

[1] Glasstone, S., *Sourcebook on the Space Sciences*, D. Van Nostrand Co., Princeton, New Jersey, 1965, pp. 158–171.

[2] Hughes, P.C., *Spacecraft Attitude Dynamics*, John Wiley & Sons, New York, N.Y., 1986, pp. 18–30, 409–410.

[3] Likins, P., "Spacecraft Attitude Dynamics and Control – A Personal Perspective on Early Developments," *Journal of Guidance, Control, and Dynamics*, Vol. 9, No. 2, March – April 1986, pp. 129–134.

[4] Ho, J.Y.L., and Herber, D.R., "Development of Dynamics and Control Simulation of Large Flexible Space Systems," *Journal of Guidance, Control, and Dynamics*, Vol. 8, No. 3, May – June 1985, pp. 374–383.

[5] Ho, J.Y.L., "Direct Path Method for Flexible Multibody Spacecraft Dynamics," *Journal of Spacecraft and Rockets*, Vol. 14, No. 2, February 1977, pp. 102–110.

[6] Singh, R.P., VanderVoot, R.J., and Likins, P.W., "Dynamics of Flexible Bodies in Tree Topology – A Computer–Oriented Approach," *Journal of Guidance, Control, and Dynamics*, Vol. 8, No. 5, September – October 1985, pp. 584–590.

[7] Chun, H.M., Turner, J.D., and Frisch, H.P., "Experimental Validation of Order (N) DISCOS," *AAS/AIAA Astrodynamics Specialist Conference*, Stowe, Vermont, August 1989, Paper No. AAS–89–457.

[8] Shrivastava, S.K., Tschann, C., and Modi, V.J., "Librational Dynamics of Earth Oriented Satellites – A Brief Review," *Proceedings of the 14th Congress on Theoretical and Applied Mechanics*, Kurukshetra, India, 1969, pp. 284–306.

[9] Modi, V.J., "Attitude Dynamics of Satellites with Flexible Appendages – A Brief Review," *Journal of Spacecraft and Rockets*, Vol. 11, No. 11, November 1974, pp. 743–751.

[10] Roberson, R.E., "Two Decades of Spacecraft Attitude Control," *Journal of Guidance and Control*, Vol. 2, No. 1, January–February 1979, pp. 3–8.

[11] Modi, V.J., and Shrivastava, S.K., "Satellite Attitude Dynamics and Control in the Presence of Environmental Torques – A Brief Survey," *Journal of Guidance, Control, and Dynamics*, Vol. 6, No. 6, November–December 1983, pp. 461–471.

[12] Suleman, A., *Dynamics and Control of Evolving Space Platforms: An Approach with Application*, Ph.D. Thesis, The University of British Columbia, August 1992.

[13] Ng, C. K. A., *Dynamics and Control of Orbiting Flexible Systems: A Formulation with Applications*, Ph.D. Thesis, The University of British Columbia, April 1992.

[14] Ibrahim, A. M., *Mathematical Modelling of Flexible Multibody Dynamics with Applications to Orbiting Systems*, Ph.D. Thesis, The University of British Columbia, April 1988.

[15] Hooker, W.W., and Margulies, G., "The Dynamical Attitude Equations for an n-Body Satellite," *The Journal of the Astronautical Sciences*, Vol. 12, No. 4, 1965, pp. 123–128.

[16] Roberson, R.E., and Wittenburg, J., "A Dynamical Formalism for an Arbitrary Number of Interconnected Rigid Bodies, with Reference to the Problem of Satellite Attitude Control," *Proceedings of the 3rd International Federation on Automatic Control*, London, England, 1966, Paper No. 46D.

[17] Roberson, R.E., "A Form of the Translational Dynamical Equations for Relative Motion in Systems of Many Non-Rigid Bodies," *Acta Mechanica*, Vol. 14, 1972, pp. 297–308.

[18] Hooker, W.W., "A Set of r Dynamical Attitude Equations for an Arbitrary n-Body Satellite Having r Rotational Degrees of Freedom," *AIAA Journal*, Vol. 8, No. 7, July 1970, pp. 1205-1207.

[19] Hooker, W.W., "Equations of Motion for Interconnected Rigid and Elastic Bodies: A Derivation Independent of Angular Momentum," *Celestial Mechanics*, Vol. 11, No. 1, 1975, pp. 337–359.

[20] Jerkovsky, W., "The Structure of Multibody Dynamics Equations," *Journal of Guidance and Control*, Vol. 1, No. 3, May – June 1978, pp. 173–182.

[21] Hughes, P.C., "Dynamics of a Chain of Flexible Bodies," *The Journal of the Astronautical Sciences*, Vol. 27, No. 4, October – December 1979, pp. 359–380.

[22] Kane, T.R., and Levinson, D.A., "Formulation of Equations of Motion for Complex Spacecraft," *Journal of Guidance and Control*, Vol. 3, No. 2, March – April 1980, pp. 99–112.

[23] Modi, V.J., and Ibrahim, A.M., "A General Formulation for Librational Dynamics of Spacecraft with Deploying Appendages," *Journal of Guidance, Control, and*

Dynamics, Vol. 7, No. 5, September – October, 1984, pp. 563–569.

[24] Meirovitch, L., and Quinn, R.D., "Equations of Motion for Maneuvring Flexible Spacecraft," *Journal of Guidance, Control, and Dynamics*, Vol. 10, No. 5, September – October 1987, pp. 453–465.

[25] Vu-Quoc, L., and Simo, J.C., "Dynamics of Earth–Orbiting Flexible Satellites with Multibody Components," *Journal of Guidance, Control, and Dynamics*, Vol. 10, No. 6, November – December 1987, pp. 549–558.

[26] Keat, J.E., "Multibody System Order n Dynamics Formulation Based on Velocity Transform Method," *Journal of Guidance, Control, and Dynamics*, Vol. 13, No. 2, March – April 1990, pp. 207–212.

[27] Jain, A., "United Formulation of Dynamics for Serial Rigid Multibody Systems," *Journal of Guidance, Control, and Dynamics*, Vol. 14, No. 3, May – June 1991, pp. 531–542.

[28] Jain, A., and Rodriguez, G., "Recursive Flexible Multibody System Dynamics Using Spatial Operators," *Journal of Guidance, Control, and Dynamics*, Vol. 15, No. 6, November – December 1992, pp. 1453–1466.

[29] Banerjee, A.K., "Block–Diagonal Equations for Multibody Elastodynamics with Geometric Stiffness and Constraints," *Journal of Guidance, Control, and Dynamics*, Vol. 16, No. 6, November – December 1993, pp. 1092–1100.

[30] Kurdila, A.J., Menon, R.G., and Sunkel, J.W., "Nonrecursive Order N Formulation of Multibody Dynamics," *Journal of Guidance, Control, and Dynamics*, Vol, 16, No. 5, September – October 1993, pp. 839–844.

[31] Balas, M.J., "Trends in Large Space Structure Control Theory: Fondest Hopes, Wildest Dreams," *IEEE Transactions on Automatic Control*, Vol. AC-27, No. 3, June 1982, pp. 522–535.

[32] Meirovitch, L., Baruh, H., and Öz, H., "A Comparison of Control Techniques for Large Flexible Systems," *Journal of Guidance, Control, and Dynamics*, Vol. 6, No. 4, July – August 1983, pp. 302–310.

[33] Meirovitch, L., and Öz, H., "An Assessment of Methods for the Control of Large Space Structures," *Proceedings of the 1979 Joint Automatic Control*, Denver, Colorado, June 1979, pp. 34–41.

[34] Van Woerkom, P.Th.L.M., "Synthesis and Survey of Control Laws for Large Flexi-

ble Spacecraft," *Control–Theory and Advanced Technology*, Vol. 9, No. 3, September 1993, pp. 639–669.

[35] Balas, M.J., "Modal Control of Certain Flexible Dynamic Systems," *SIAM Journal of Control and Optimization*, Vol. 16, May 1978, pp. 450–462.

[36] Meirovitch, L., and Öz, H., "Modal–Space Control of Distributed Gyroscopic Systems," *Journal of Guidance and Control*, Vol. 3, No. 2, March – April 1980, pp. 140–149.

[37] Öz, H., and Meirovitch, L., "Optimal Modal–Space Control of Flexible Gyroscopic Systems," *Journal of Guidance and Control*, Vol. 3, No. 3, May – June 1980, pp. 218–226.

[38] Woo, H.H., Morgan, H.D., and Falangas, E.T., "Momentum Management and Attitude Control Design for a Space Station," *Journal of Guidance, Control, and Dynamics*, Vol. 11, No. 1, January – February 1988, pp. 19–25.

[39] Chu, P.Y., Wie, B., Gretz, B., and Plescia, C., "Space Station Attitude Control: Modeling and Design," *AIAA Guidance, Navigation and Control Conference*, August 1988, Minneapolis, Minnesota, Paper No. AIAA–88–4133.

[40] Sunkel, J.W., and Shieh, L.S., "Optimal Momentum Management Controller for the Space Station," *Journal of Guidance, Control, and Dynamics*, Vol. 13, No. 4, July – August 1990, pp. 659–668.

[41] Sunkel, J.W., Shieh, L.S., and Zhang, J.L., "Digital Redesign of an Optimal Momentum Management Controller for the Space Station," *Journal of Guidance, Control, and Dynamics*, Vol. 14, No. 4, July – August 1991, pp. 712–723.

[42] Sunkel, J.W., and Shieh, L.S., "Multistage Design of an Optimal Momentum Management Controller for the Space Station," *Journal of Guidance, Control, and Dynamics*, Vol. 14, No. 3, May – June 1991, pp. 492–502.

[43] Vadali, S.R., and Oh, H-S., "Attitude Control and Momentum Management of the Space Station," *AAS/AIAA Spaceflight Mechanics Meeting*, February 1991, Houston, Texas, Paper No. AAS 91–145.

[44] Harduvel, J.T., "Continuous Momentum Management of Earth–Oriented Spacecraft," *Journal of Guidance, Control, and Dynamics*, Vol. 15, No. 6, November – December 1992, pp. 1417–1426.

[45] Byun, K–W, Wie, B., Geller, D., and Sunkel, J., "Robust H_∞ Control Design for

the Space Station with Structured Parameter Uncertainty," *Journal of Guidance, Control, and Dynamics*, Vol. 14, No. 6, November – December 1991, pp. 1115–1122.

[46] Bainum, P.M., and Li, F., "Optimal Large Angle Maneuvers of a Flexible Spacecraft," *Acta Astronautica*, Vol. 25, No. 3, 1991, pp. 141–148.

[47] Sharony, Y., and Meirovitch, L., "Accomodation of Kinematic Disturbances During Minimum–Time Maneuvers of Flexible Spacecraft," *Journal of Guidance, Control, and Dynamics*, Vol. 14, No. 2, March – April 1991, pp. 268–277.

[48] Meirovitch, L., and Kwak, M.K., "Control of Spacecraft with Multi–Targeted Flexible Antennas," *The Journal of the Astronautical Sciences*, Vol. 38, No. 2, April – June 1990, pp. 187-199.

[49] Singh, T., and Vadali, S.R., "Input–Shaped Control of Three–Dimensional Maneuvers of Flexible Spacecraft," *Journal of Guidance, Control, and Dynamics*, Vol. 16, No. 6, November – December 1993, pp. 1061–1086.

[50] Junkins, J.L., Rahman, Z., and Bang, H., "Near–Minimum–Time Maneuvers of Flexible Vehicles: A Liapunov Control Law Design Method," *Mechanics and Control of Large Flexible Structures, edited by: J.L. Junkins*, Vol. 129 Progress in Astronautics and Aeronautics, AIAA, Inc., Washington, D.C., 1990, pp. 565–593.

[51] Li, Z., and Bainum, P.M., "Momentum Exchange: Feedback Control of Flexible Spacecraft Maneuvers and Vibration," *Journal of Guidance, Control, and Dynamics*, Vol. 15, No. 6, November – December 1992, pp. 1354–1360.

[52] Junkins, J.L., and Bang, H., "Maneuver and Vibration Control of Hybrid Coordinate Systems Using Lyapunov Stability Theory," *Journal of Guidance, Control, and Dynamics*, Vol. 16, No. 4, July – August 1993, pp. 668–676.

[53] Hecht, N.K., and Junkins, J.L., "Near–Minimum–Time Control of a Flexible Manipulator," *Journal of Guidance, Control, and Dynamics*, Vol. 15, No. 2, March – April 1992, pp. 477–481.

[54] Bell, M.J., and Junkins, J.L., 'Near–Minimum–Time Three–Dimensional Maneuvers of Rigid and Flexible Spacecraft," *AAS/AIAA Astrodynamics Specialist Conference*, August 1993, Victoria, Canada, Paper No. AAS 93–586.

[55] Parlos, A.G., and Sunkel, J.W., "Adaptive Attitude Control and Momentum Management for Large–Angle Spacecraft Maneuvers," *Journal of Guidance, Control, and Dynamics*, Vol. 15, No. 4, July – August 1992, pp. 1018–1028.

[56] Zhao, X.M., Shieh, L.S., Sunkel, J.W., and Yuan, Z.Z., 'Self–Tuning Control of Attitude and Momentum Management for the Space Station," *Journal of Guidance, Control, and Dynamics*, Vol. 15, No. 1, January – February 1992, pp. 17–27.

[57] Garcia, E., and Inman, D.J., "Modeling of the Slewing Control of a Flexible Structure," *Journal of Guidance, Control, and Dynamics*, Vol. 14, No. 4, July – August 1991, pp. 736–742.

[58] Kumar, R.R., Cooper, P.A., and Lim, T.W., "Sensitivity of Space Station Alpha Joint Robust Controller to Structural Modal Parameter Variations," *Journal of Guidance, Control, and Dynamics*, Vol. 15, No. 6, November – December 1992, pp. 1427–1433.

[59] Hyland, D.C., Junkins, J.L., and Longman, R.W., "Active Control Technology for Large Space Structures," *Journal of Guidance, Control, and Dynamics*, Vol. 16, No. 5, September – October 1993, pp. 801–821.

[60] Balas, M.J., "Active Control of Flexible Systems," *Journal of Optimization Theory and Applications*, Vol. 25, No. 3, July 1978, pp. 415–436.

[61] Balas, M.J., "Feedback Control of Flexible Systems," *IEEE Transactions on Automatic Control*, Vol. AC–23, No. 4, August 1978, pp. 673–679.

[62] Balas, M.J., "Direct Velocity Feedback Control of Large Space Structures," *Journal of Guidance and Control*, Vol. 2, No. 3, May – June 1979, pp. 252–253.

[63] Yedavalli, R.K., "Critical Parameter Selection in the Vibration Suppression of Large Space Structures," *Journal of Guidance, Control, and Dynamics*, Vol. 7, No. 3, May – June 1984, pp. 274–278.

[64] Goh, C.J., and Caughney, T.K., "A Quasi–Linear Vibration Suppression Technique for Large Space Structures via Stiffness Modification," *International Journal of Control*, Vol. 41, No. 3, 1985, pp. 803–811.

[65] Sundararajan, N., Joshi, S.M., and Armstrong, E.S., "Robust Controller Synthesis for a Large Flexible Space Antenna," *Journal of Guidance, Control, and Dynamics*, Vol. 10, No. 2, March – April 1987, pp. 201–208.

[66] Wie, B., "Active Vibration Control Synthesis for the Control of Flexible Structures Mast Flight System," *Journal of Guidance, Control, and Dynamics*, Vol. 11, No. 3, May – June 1988, pp. 271–277.

[67] Heise, S., Banda, S., and Yeh, H., "Robust Control of a Flexible Space Structure in the Presence of Parameter Variations and Unmodeled Dynamics," *AIAA 28th Aerospace Sciences Meeting*, January 1990, Reno, Nevada, Paper No. AIAA–90–0752.

[68] Williams, T., and Juang, J–N., "Pole/Zero Cancellations in Flexible Space Structures," *Journal of Guidance, Control, and Dynamics*, Vol. 13, No. 4, July – August 1990, pp. 684–690.

[69] Hanagud, S., Obal, M.W., and Calise, A.J., "Optimal Vibration Control by the Use of Piezoceramic Sensors and Actuators," *Journal of Guidance, Control, and Dynamics*, Vol. 15, No. 5, September – October 1992, pp. 1199–1206.

[70] Reddy, A.S.S.R., Bainum, P.M., Krishna, R., and Hamer, H.A., "Control of a Large Flexible Platform in Orbit," *Journal of Guidance and Control*, Vol. 4, No. 6, November – December 1981, pp. 642–649.

[71] Safonov, M.G., Chiang, R.Y., and Flasher, H., "H_∞ Robust Control Synthesis for a Large Space Structure," *Journal of Guidance, Control, and Dynamics*, Vol. 14, No. 3, May – June 1991, pp. 513–520.

[72] Sparks, D.W., and Juang, J–N., "Survey of Experiments and Experimental Facilities for Control of Flexible Structures," *Journal of Guidance, Control, and Dynamics*, Vol. 15, No. 4, July – August 1992, pp. 801–816.

[73] Wie, B., "Experimental Demonstration of a Classical Approach to Flexible Structure Control," *Journal of Guidance, Control, and Dynamics*, Vol. 15, No. 6, November – December 1992, pp. 1327–1333.

[74] Dunn, H.J., "Experimental Results of Active Control on a Large Structure to Suppress Vibration," *Journal of Guidance, Control, and Dynamics*, Vol. 15, No. 6, November – December 1992, pp. 1334–1341.

[75] Buddie, S.A., Georgiou, T.T., Özgüner, U., and Smith, M.C., "Flexible Structure Experiments at JPL and WPAFB: H_∞ Controller Designs," *International Journal of Control*, Vol. 58, No. 1, 1993, pp. 1–19.

[76] Ih, C–H. C., Bayard, D.S., Ahmed, A., and Wang, S.J., "Experiments in Multivariable Adaptive Control of a Large Flexible Structure," *Journal of Guidance, Control, and Dynamics*, Vol. 16, No. 1, January – February 1993, pp. 9–13.

[77] Ih, C–H. C., Bayard, D.S., Ahmed, A., and Wang, S.J., "Experimental Study of Robustness in Adaptive Control for Large Flexible Structures," *Journal of*

Guidance, Control, and Dynamics, Vol. 16, No. 1, January – February 1993, pp. 14–20.

[78] Townsend, M.A., "Kane's Equations, Lagrange's Equations, and Virtual Work," *Journal of Guidance, Control, and Dynamics*, Vol. 15, No. 1, January – February 1992, pp. 277–280.

[79] Hughes, P.C., "Space Structure Vibration Modes: How Many Exist? Which Ones Are Important?," *IEEE Control Systems Magazine*, Vol. 7, No. 1, February 1987, pp. 22–28.

[80] Smith, M.J., *An Evaluation of Component Mode Synthesis for Modal Analysis of Finite Element Models*, Ph.D. Thesis, The University of British Columbia, April 1993.

[81] Hughes, T.J.R., *The Finite Element Method: Linear Static and Dynamic Finite Element Analysis*, Prentice–Hall, Inc., Englewood Cliffs, New Jersey, 1987, pp. 1–13.

[82] Meirovitch, L., *Dynamics and Control of Structures*, John Wiley and Sons, New York, N.Y., 1989, pp. 283–309.

[83] Hurty, W.C., *Dynamic Analysis of Structural Systems by Component Mode Synthesis*, Report 32–530, Jet Propulsion Lab., Pasadena, California, 1964.

[84] Hurty, W.C., "Dynamic Analysis of Structural Systems Using Component Modes," *AIAA Journal*, Vol. 3, No. 4, April 1965, pp. 678–685.

[85] Craig, R.R., Jr., and Bampton, M.C.C., "Coupling of Substructures for Dynamic Analyses," *AIAA Journal*, Vol. 6, No. 7, July 1968, pp. 1313–1319.

[86] Benfield, W.A., and Hruda, R.F., "Vibration Analysis of Structures by Component Mode Substitution," *AIAA Journal*, Vol. 9, No. 7, July 1971, pp. 1255–1261.

[87] MacNeal, R.H., "A Hybrid Method of Component Mode Synthesis," *Computers and Structures*, Vol. 1, December 1971, pp. 581–601.

[88] Rubin, S., "Improved Component–Mode Representation for Structural Dynamic Analysis," *AIAA Journal*, Vol. 13, No. 8, August 1975, pp. 995–1006.

[89] Spanos, J.T., and Tsuha, W.S., "Selection of Component Modes for the Simulation of Flexible Multibody Spacecraft," *AAS/AIAA Astrodynamics Specialist Conference*, August 1989, Stowe, Vermont, Paper AAS-89-438.

[90] Junkins, J.L., and Turner, J.D., *Optimal Spacecraft Rotational Maneuvers*, Elsevier Science Publishers B.V., Amsterdam, The Netherlands, 1986, pp. 144–156.

[91] Hale, A.L., and Meirovitch, L., "A General Substructure Synthesis Method for the Dynamic Simulation of Complex Structures," *Journal of Sound and Vibration*, Vol. 69, No. 2, 1980, pp. 309–326.

[92] Meirovitch, L., and Hale, A.L., "On the Substructure Synthesis Method," *AIAA Journal*, Vol. 19, No. 7, July 1981, pp. 940–947.

[93] Meirovitch, L., and Kwak, M.K., "Convergence of the Classical Rayleigh–Ritz Method and the Finite Element Method," *AIAA Journal*, Vol. 28, No. 8, August 1990, pp. 1509–1516.

[94] Meirovitch, L., and Kwak, M.K., "Rayleigh–Ritz Based Substructure Synthesis for Flexible Multibody Systems," *AIAA Journal*, Vol. 29, No. 10, October 1991, pp. 1709–1719.

[95] Meirovitch, L., and Kwak, M.K., "Inclusion Principle for the Rayleigh–Ritz Based Substructure Synthesis," *AIAA Journal*, Vol. 30, No. 5, May 1992, pp. 1344–1351.

[96] Clough, R.W., and Penzien, J., *Dynamics of Structures*, McGraw–Hill Book Co., New York, N.Y., 1975, pp. 281–326.

[97] Blevins, R.D., *Formulas for Natural Frequencies and Mode Shapes*, Van Nostrand Reinhold, New York, N.Y., 1979, pp. 101–170.

[98] Warburton, G.B., "The Vibration of Rectangular Plates," *Proceedings of the Institution of Mechanical Engineers*, Vol. 168, No. 12, 1954, pp. 371–384.

[99] Timoshenko, S., and Woinowsky–Krieger, S., "Theory of Plates and Shells," McGraw–Hill Book Company, New York, N.Y., 1959, pp 79–104.

[100] Leissa, A.W., "The Free Vibration of Rectangular Plates," *Journal of Sound and Vibration*, Vol. 31, No. 3, 1973, pp. 257–293.

[101] W.C. Hurty, and M.F. Rubinstein, *Dynamics of Structures*, Prentice Hall Inc., Englewood Cliffs, New Jersey, pp. 141–187.

[102] Greenwood, D.T., *Principles of Dynamics*, Prentice Hall Inc., Englewood Cliffs, New Jersey, pp. 455–472, 489–490.

[103] Thomson, W.T., *Space Dynamics*, John Wiley and Sons, New York, N.Y., 1961, pp. 56–59.

[104] Moran, J.P., "Effects of Plane Librations on the Orbital Motion of a Dumbbell Satellite," *ARS Journal*, Vol. 31, No. 8, August 1961, pp. 1089–1096.

[105] Kwakernaak, H., and Sivan, R., *Linear Optimal Control Systems*, Wiley–Interscience, New York, N.Y., 1972, pp. 1–3, 201–243, 377-409.

[106] Press, W.H., Teukolsky, S.A., Vetterling, W.T., and Flannery, B.P., *Numerical Recipes in Fortran*, Cambridge University Press, Cambridge, England, 1992, pp. 180–182.

[107] *IMSL Library Reference Manual*, Vol. 1, IMSL Inc., Houston, Texas, June 1980, pp. DGEAR-1 – DGEAR-9.

[108] Chan, J.K.W., *Dynamics and Control of an Orbiting Space Platform Based Mobile Flexible Manipulator*, M.A.Sc. Thesis, The University of British Columbia, April 1990.

[109] Ng, A.C., and Modi, V.J., "Dynamics of Gravity Oriented Satellites with Thermally Flexed Appendages," *AAS/AIAA Astrodynamics Specialist Conference*, Kalispell, Montana, August 1987, Paper No. AAS–87–432.

[110] Butenin, N.V., *Elements of Nonlinear Oscillations*, Blaisdell, New York, 1965, pp. 102–137.

[111] Modi, V.J. and Suleman, A., "System Modes and Dynamics of the Proposed Space Station Type Configuration," *Proceedings of the first International Conference on the Dynamics of Flexible Structures in Space*,Cranfield, UK, C.L. Kirk and J.L. Junkins, eds., 1990, pp. 645–659.

[112] Modi, V.J., Ng, A.C., and Suleman, A., "Transient Dynamics of the Proposed Space Station During Integration: A General Formulation and Response Analysis," *The Journal of the Astronautical Sciences*, Vol. 39, 1991, pp. 393–410.

[113] *Space Station Preliminary Design Report*, JSC–18555, Structures Division, Engineering and Development Directorate, NASA Johnson Space Center, Houston, Texas, September 1982.

[114] *Modal Analysis of Selected Space Station Configurations*, NASA SSE-E-88-R8, NASA Space Station Program Office, Washington, D.C., June 1988.

[115] Doyle, J.C., and Stein, G., "Multivariable Feedback Design: Concepts for Classical/Modern Synthesis," *IEEE Transactions on Automatic Control*, Vol. AC–26, No.1, February 1981, pp. 4–16.

[116] Grace, A., et al., *Control System Toolbox*, The MathWorks, Inc., Natick, Mass., 1992.

[117] Maciejowski, J.M., *Multivariable Feedback Design*, Addison-Wesley, Wokingham, England, 1989, pp. 222–317.

[118] Stein, G., and Athans, M., "The LQR/LTR Procedure for Multivariable Feedback Control Design," *IEEE Transactions on Automatic Control*, Vol. AC–32, No.2, February 1987, pp. 105–114.

[119] Doyle, J.C., "Guaranteed Margins for LQG Regulators," *IEEE Transactions on Automatic Control*, Vol. AC–23, No.4, August 1978, pp. 756–757.

[120] Doyle, J.C., and Stein, G., "Robustness with Observers," *IEEE Transactions on Automatic Control*, Vol. AC–24, No.4, August 1979, pp. 607–611.

[121] Kwakernaak, H., "Robust Control and H_∞ Optimization – Tutorial Paper," *Automatica*, Vol. 29, No. 2, 1993, pp. 255–273.

[122] McFarlane, D.C., and Glover, K., *Robust Controller Design Using Normalized Coprime Factor Plant Descriptions*, Lecture Notes in Control and Information Sciences, Vol. 138, Springer–Verlag, Berlin, 1990.

[123] Francis, B.A., Helton, J.W., and Zames, G., "H_∞ – Optimal Feedback Controllers for Linear Multivariable Systems," *IEEE Transactions on Automatic Control*, Vol. AC–29, No. 10, October 1984., pp. 888–900.

[124] Glover, K., and Doyle, J.C., "State–Space Formulae For All Stabilizing Controllers That Satisfy An H_∞–Norm Bound and Relations to Risk Sensitivity," *Systems and Control Letters*, Vol. 11, 1988, pp. 167–172.

[125] McFarlane, D., Glover, K., and Noton, M., "Robust Stabilization of a Flexible Space Platform: An H_∞ Coprime Factor Approach," Proceedings of the IEE 'Control 88' Conference, Oxford, U.K., 1988, pp. 677–682.

[126] Chiang, R.Y., et. al., "A Fixed H_∞ Controller for a Supermaneuverable Fighter Performing the Herbst Maneuver," *Automatica*, Vol. 29, No. 1, 1993, pp. 111–127.

[127] Garg, S., "Robust Integrated Flight/Propulsion Control Design for a STOVL Aircraft Using H_∞ Control Design Techniques," *Automatica*, Vol. 29, No. 1, 1993, pp. 129–145.

[128] Chiang, R.Y., and Safonov, M.G., *Robust–Control Toolbox*, The MathWorks, Inc., Natick, Mass., 1992.

[129] Joshi, S.M., "Control Systems Synthesis for a Large Flexible Space Antenna," *Acta Astronautica*, Vol. 10, No. 5–6, 1983, pp. 365–380.

[130] Joshi, S.M., "A Class of Stable, Robust Feedback Controllers for Large Space Structures," *Acta Astronautica*, Vol. 9, No. 5, 1982, pp. 291–295.

[131] Gregory, C.Z., "Reduction of Large Flexible Spacecraft Models Using Internal Balancing Theory," *Journal of Guidance, Control, and Dynamics*, Vol. 7, No. 6, November–December 1984, pp. 725–732.

[132] Aubrun, J.-N., Ratner, M.J., and Lyons, M.G., "Structural Control for a Circular Plate," *Journal of Guidance, Control, and Dynamics*, Vol. 7, No. 5, September–October 1984, pp. 535–545.

[133] Safonov, M.G., and Chiang, R.Y., "A Schur Method for Balanced–Truncation Model Reduction," *IEEE Transactions on Automatic Control*, Vol. 34, No. 7, July 1989, pp. 729–733.

Appendix I: Details of System Kinetic Energy, Inertia Matrix and Angular Momentum

The details of the terms which constitute the system kinetic energy (equation 2.20) are given below:

$$T_{orb} = \frac{1}{2}(\dot{\vec{R}}_{cm} \cdot \dot{\vec{R}}_{cm})M;$$

$$T_{cm} = -\frac{1}{2}(\dot{\vec{C}}_{cm} \cdot \dot{\vec{C}}_{cm})M;$$

$$T_h = \frac{1}{2}\sum_{i=1}^{N}\left[(\dot{\vec{d}}_i \cdot \dot{\vec{d}}_i)m_i + \sum_{j=1}^{N_i}\left[\dot{\vec{d}}_i \cdot \dot{\vec{d}}_i + 2(\mathbf{C_i^c}\dot{\vec{d}}_{i,j}) \cdot \dot{\vec{d}}_i + \dot{\vec{d}}_{i,j} \cdot \dot{\vec{d}}_{i,j}\right] m_{i,j}\right];$$

$$T_v = \frac{1}{2}\left\{\int_{m_c}(\dot{\vec{\delta}}_c \cdot \dot{\vec{\delta}}_c)\, dm_c + \sum_{i=1}^{N}\left[\int_{m_i}(\dot{\vec{\delta}}_i \cdot \dot{\vec{\delta}}_i)\, dm_i + \sum_{j=1}^{N_i}\int_{m_{i,j}}(\dot{\vec{\delta}}_{i,j} \cdot \dot{\vec{\delta}}_{i,j})\, dm_{i,j}\right]\right\};$$

$$\begin{aligned} T_s = \frac{1}{2}\sum_{i=1}^{N}\Bigg[\int_{m_i} \dot{\mathbf{C}}_\mathbf{i}^\mathbf{c}(\vec{\rho}_i + \vec{\delta}_i) \cdot \dot{\mathbf{C}}_\mathbf{i}^\mathbf{c}(\vec{\rho}_i + \vec{\delta}_i)\, dm_i + \sum_{j=1}^{N_i}\Bigg[(\dot{\mathbf{C}}_\mathbf{i}^\mathbf{c}\vec{d}_{i,j}) \cdot (\dot{\mathbf{C}}_\mathbf{i}^\mathbf{c}\vec{d}_{i,j})m_{i,j} \\ + \int_{m_{i,j}}\Big[2(\dot{\mathbf{C}}_\mathbf{i}^\mathbf{c}\vec{d}_{i,j}) \cdot \mathbf{C}_\mathbf{i}^\mathbf{c}\dot{\mathbf{C}}_{\mathbf{i,j}}^\mathbf{i}(\vec{\rho}_{i,j} + \vec{\delta}_{i,j}) + 2(\dot{\mathbf{C}}_\mathbf{i}^\mathbf{c}\vec{d}_{i,j}) \cdot \dot{\mathbf{C}}_\mathbf{i}^\mathbf{c}\mathbf{C}_{\mathbf{i,j}}^\mathbf{i}(\vec{\rho}_{i,j} + \vec{\delta}_{i,j}) \\ + \dot{\mathbf{C}}_{\mathbf{i,j}}^\mathbf{i}(\vec{\rho}_{i,j} + \vec{\delta}_{i,j}) \cdot \dot{\mathbf{C}}_{\mathbf{i,j}}^\mathbf{i}(\vec{\rho}_{i,j} + \vec{\delta}_{i,j}) + \dot{\mathbf{C}}_\mathbf{i}^\mathbf{c}\mathbf{C}_{\mathbf{i,j}}^\mathbf{i}(\vec{\rho}_{i,j} + \vec{\delta}_{i,j}) \cdot \dot{\mathbf{C}}_\mathbf{i}^\mathbf{c}\mathbf{C}_{\mathbf{i,j}}^\mathbf{i}(\vec{\rho}_{i,j} + \vec{\delta}_{i,j}) \\ + 2\dot{\mathbf{C}}_\mathbf{i}^\mathbf{c}\mathbf{C}_{\mathbf{i,j}}^\mathbf{i}(\vec{\rho}_{i,j} + \vec{\delta}_{i,j}) \cdot \mathbf{C}_\mathbf{i}^\mathbf{c}\dot{\mathbf{C}}_{\mathbf{i,j}}^\mathbf{i}(\vec{\rho}_{i,j} + \vec{\delta}_{i,j})\Big]\, dm_{i,j}\Bigg]\Bigg]; \end{aligned}$$

$$\begin{aligned} T_{h,s} = \sum_{i=1}^{N}\Bigg[\int_{m_i} \dot{\vec{d}}_i \cdot \dot{\mathbf{C}}_\mathbf{i}^\mathbf{c}(\vec{\rho}_i + \vec{\delta}_i)\, dm_i + \sum_{j=1}^{N_i}\Bigg[\int_{m_{i,j}}\Big[(\dot{\vec{d}}_i + \mathbf{C}_\mathbf{i}^\mathbf{c}\dot{\vec{d}}_{i,j}) \cdot \dot{\mathbf{C}}_\mathbf{i}^\mathbf{c}\mathbf{C}_{\mathbf{i,j}}^\mathbf{i}(\vec{\rho}_{i,j} + \vec{\delta}_{i,j}) \\ + \dot{\vec{d}}_i \cdot \mathbf{C}_\mathbf{i}^\mathbf{c}\dot{\mathbf{C}}_{\mathbf{i,j}}^\mathbf{i}(\vec{\rho}_{i,j} + \vec{\delta}_{i,j}) + \dot{\vec{d}}_{i,j} \cdot \dot{\mathbf{C}}_{\mathbf{i,j}}^\mathbf{i}(\vec{\rho}_{i,j} + \vec{\delta}_{i,j})\Big]\, dm_{i,j} \\ + (\dot{\vec{d}}_i + \mathbf{C}_\mathbf{i}^\mathbf{c}\dot{\vec{d}}_{i,j}) \cdot (\dot{\mathbf{C}}_\mathbf{i}^\mathbf{c}\vec{d}_{i,j})m_{i,j}\Bigg]\Bigg]; \end{aligned}$$

$$T_{h,v} = \sum_{i=1}^{N} \left[\int_{m_i} \dot{\vec{d}}_i \cdot (\mathbf{C_i^c} \dot{\vec{\delta}}_i)\, dm_i + \sum_{j=1}^{N_i} \left[\int_{m_{i,j}} \left[\dot{\vec{d}}_i \cdot (\mathbf{C_i^c C_{i,j}^i} \dot{\vec{\delta}}_{i,j}) + \dot{\vec{d}}_{i,j} \cdot (\mathbf{C_{i,j}^i} \dot{\vec{\delta}}_{i,j}) \right] dm_{i,j} \right] \right];$$

$$T_{s,v} = \sum_{i=1}^{N} \left[\int_{m_i} \dot{\mathbf{C}}_{\mathbf{i}}^{\mathbf{c}} (\vec{\rho}_i + \vec{\delta}_i) \cdot (\mathbf{C_i^c} \dot{\vec{\delta}}_i)\, dm_i + \sum_{j=1}^{N_i} \left[\int_{m_{i,j}} \left[\dot{\mathbf{C}}_{\mathbf{i,j}}^{\mathbf{i}} (\vec{\rho}_{i,j} + \vec{\delta}_{i,j}) \cdot (\mathbf{C_{i,j}^i} \dot{\vec{\delta}}_{i,j}) + (\dot{\mathbf{C}}_{\mathbf{i}}^{\mathbf{c}} \dot{\vec{d}}_{i,j} + \dot{\mathbf{C}}_{\mathbf{i}}^{\mathbf{c}} \mathbf{C}_{\mathbf{i,j}}^{\mathbf{i}} (\vec{\rho}_{i,j} + \vec{\delta}_{i,j})) \cdot (\mathbf{C_i^c C_{i,j}^i} \dot{\vec{\delta}}_{i,j}) \right] dm_{i,j} \right] \right]. \quad \text{(I-1)}$$

The system inertia matrix $\mathbf{I_{sys}}$, which is given by equation (2.39), is comprised of the following terms:

$$\mathbf{I_{cm}} = -M \left[(\vec{C}_{cm} \cdot \vec{C}_{cm}) \mathbf{E} - (\vec{C}_{cm})(\vec{C}_{cm})^T \right];$$

$$\mathbf{I_r} = \int_{m_c} \left[(\vec{\rho}_c \cdot \vec{\rho}_c) \mathbf{E} - (\vec{\rho}_c \vec{\rho}_c^{\,T}) \right] dm_c + \sum_{i=1}^{N} \left[\int_{m_i} \left[(\vec{\rho}_i \cdot \vec{\rho}_i) \mathbf{E} - (\mathbf{C_i^c} \vec{\rho}_i)(\mathbf{C_i^c} \vec{\rho}_i)^T \right] dm_i + \sum_{j=1}^{N_i} \left[\int_{m_{i,j}} \left[(\vec{\rho}_{i,j} \cdot \vec{\rho}_{i,j}) \mathbf{E} - (\mathbf{C_i^c C_{i,j}^i} \vec{\rho}_{i,j})(\mathbf{C_i^c C_{i,j}^i} \vec{\rho}_{i,j})^T \right] dm_{i,j} \right] \right];$$

$$\mathbf{I_h} = \sum_{i=1}^{N} \left[\left[(\vec{d}_i \cdot \vec{d}_i) \mathbf{E} - (\vec{d}_i \vec{d}_i^{\,T}) \right] m_i + \sum_{j=1}^{N_i} \left[\left[(\vec{d}_i + \mathbf{C_i^c} \vec{d}_{i,j}) \cdot (\vec{d}_i + \mathbf{C_i^c} \vec{d}_{i,j}) \mathbf{E} - (\vec{d}_i + \mathbf{C_i^c} \vec{d}_{i,j})(\vec{d}_i + \mathbf{C_i^c} \vec{d}_{i,j})^T \right] m_{i,j} \right] \right];$$

$$\mathbf{I_v} = \int_{m_c} \left[(\vec{\delta}_c \cdot \vec{\delta}_c) \mathbf{E} - (\vec{\delta}_c \vec{\delta}_c^{\,T}) \right] dm_c + \sum_{i=1}^{N} \left[\int_{m_i} \left[(\vec{\delta}_i \cdot \vec{\delta}_i) \mathbf{E} - (\mathbf{C_i^c} \vec{\delta}_i)(\mathbf{C_i^c} \vec{\delta}_i)^T \right] dm_i + \sum_{j=1}^{N_i} \left[\int_{m_{i,j}} \left[(\vec{\delta}_{i,j} \cdot \vec{\delta}_{i,j}) \mathbf{E} - (\mathbf{C_i^c C_{i,j}^i} \vec{\delta}_{i,j})(\mathbf{C_i^c C_{i,j}^i} \vec{\delta}_{i,j})^T \right] dm_{i,j} \right] \right];$$

$$\mathbf{I_{h,r}} = \sum_{i=1}^{N} \left[\int_{m_i} \left[(2\vec{d}_i \cdot (\mathbf{C_i^c} \vec{\rho}_i)) \mathbf{E} - \vec{d}_i (\mathbf{C_i^c} \vec{\rho}_i)^T - (\mathbf{C_i^c} \vec{\rho}_i) \vec{d}_i^{\,T} \right] dm_i \right.$$

$$+\sum_{j=1}^{N_i}\left[\int_{m_{i,j}}\left[2(\vec{d}_i+\mathbf{C}_{\mathbf{i}}^{\mathbf{c}}\vec{d}_{i,j})\cdot(\mathbf{C}_{\mathbf{i}}^{\mathbf{c}}\mathbf{C}_{\mathbf{i,j}}^{\mathbf{i}}\vec{\rho}_{i,j})\mathbf{E}\right.\right.$$

$$\left.\left.-(\vec{d}_i+\mathbf{C}_{\mathbf{i}}^{\mathbf{c}}\vec{d}_{i,j})(\mathbf{C}_{\mathbf{i}}^{\mathbf{c}}\mathbf{C}_{\mathbf{i,j}}^{\mathbf{i}}\vec{\rho}_{i,j})^{T}-(\mathbf{C}_{\mathbf{i}}^{\mathbf{c}}\mathbf{C}_{\mathbf{i,j}}^{\mathbf{i}}\vec{\rho}_{i,j})(\vec{d}_i+\mathbf{C}_{\mathbf{i}}^{\mathbf{c}}\vec{d}_{i,j})^{T}\right]dm_{i,j}\right]\Bigg];$$

$$\mathbf{I_{h,v}}=\sum_{i=1}^{N}\left[\int_{m_i}\left[(2\vec{d}_i\cdot(\mathbf{C}_{\mathbf{i}}^{\mathbf{c}}\vec{\delta}_i))\mathbf{E}-\vec{d}_i(\mathbf{C}_{\mathbf{i}}^{\mathbf{c}}\vec{\delta}_i)^{T}-(\mathbf{C}_{\mathbf{i}}^{\mathbf{c}}\vec{\delta}_i)\vec{d}_i^{\,T}\right]dm_i\right.$$

$$+\sum_{j=1}^{N_i}\left[\int_{m_{i,j}}\left[2(\vec{d}_i+\mathbf{C}_{\mathbf{i}}^{\mathbf{c}}\vec{d}_{i,j})\cdot(\mathbf{C}_{\mathbf{i}}^{\mathbf{c}}\mathbf{C}_{\mathbf{i,j}}^{\mathbf{i}}\vec{\delta}_{i,j})\mathbf{E}\right.\right.$$

$$\left.\left.\left.-(\vec{d}_i+\mathbf{C}_{\mathbf{i}}^{\mathbf{c}}\vec{d}_{i,j})(\mathbf{C}_{\mathbf{i}}^{\mathbf{c}}\mathbf{C}_{\mathbf{i,j}}^{\mathbf{i}}\vec{\delta}_{i,j})^{T}-(\mathbf{C}_{\mathbf{i}}^{\mathbf{c}}\mathbf{C}_{\mathbf{i,j}}^{\mathbf{i}}\vec{\delta}_{i,j})(\vec{d}_i+\mathbf{C}_{\mathbf{i}}^{\mathbf{c}}\vec{d}_{i,j})^{T}\right]dm_{i,j}\right]\right];$$

$$\mathbf{I_{r,v}}=\int_{m_c}\left[(2\vec{\rho}_c\cdot\vec{\delta}_c)\mathbf{E}-\vec{\rho}_c\vec{\delta}_c^{\,T}-\vec{\delta}_c\vec{\rho}_c^{\,T}\right]dm_c+\sum_{i=1}^{N}\left[\int_{m_i}\left[(2\vec{\rho}_i\cdot\vec{\delta}_i)\mathbf{E}\right.\right.$$

$$-(\mathbf{C}_{\mathbf{i}}^{\mathbf{c}}\vec{\rho}_i)(\mathbf{C}_{\mathbf{i}}^{\mathbf{c}}\vec{\delta}_i)^{T}-(\mathbf{C}_{\mathbf{i}}^{\mathbf{c}}\vec{\delta}_i)(\mathbf{C}_{\mathbf{i}}^{\mathbf{c}}\vec{\rho}_i)^{T}\left.\right]dm_i+\sum_{j=1}^{N_i}\left[\int_{m_{i,j}}\left[(2\vec{\rho}_{i,j}\cdot\vec{\delta}_{i,j})\mathbf{E}\right.\right.$$

$$\left.\left.\left.-(\mathbf{C}_{\mathbf{i}}^{\mathbf{c}}\mathbf{C}_{\mathbf{i,j}}^{\mathbf{i}}\vec{\rho}_{i,j})(\mathbf{C}_{\mathbf{i}}^{\mathbf{c}}\mathbf{C}_{\mathbf{i,j}}^{\mathbf{i}}\vec{\delta}_{i,j})^{T}-(\mathbf{C}_{\mathbf{i}}^{\mathbf{c}}\mathbf{C}_{\mathbf{i,j}}^{\mathbf{i}}\vec{\delta}_{i,j})(\mathbf{C}_{\mathbf{i}}^{\mathbf{c}}\mathbf{C}_{\mathbf{i,j}}^{\mathbf{i}}\vec{\rho}_{i,j})^{T}\right]dm_{i,j}\right]\right]; \quad \text{(I-2)}$$

where $\mathbf{E}$ is the 3×3 identity matrix.

Contributions to the system angular momentum vector, which is given in equation (2.40), are as follows:

$$\vec{H}_{cm}=-M\left[\vec{C}_{cm}\times\dot{\vec{C}}_{cm}\right];$$

$$\vec{H}_h=\sum_{i=1}^{N}\left[(\vec{d}_i\times\dot{\vec{d}}_i)m_i+\sum_{j=1}^{N_i}\left[\left[(\vec{d}_i+\mathbf{C}_{\mathbf{i}}^{\mathbf{c}}\vec{d}_{i,j})\times(\dot{\vec{d}}_i+\mathbf{C}_{\mathbf{i}}^{\mathbf{c}}\dot{\vec{d}}_{i,j})\right]m_{i,j}\right]\right];$$

$$\vec{H}_v=\int_{m_c}(\vec{\delta}_c\times\dot{\vec{\delta}}_c)\,dm_c+\sum_{i=1}^{N}\left[\int_{m_i}\left[(\mathbf{C}_{\mathbf{i}}^{\mathbf{c}}\vec{\delta}_i)\times(\mathbf{C}_{\mathbf{i}}^{\mathbf{c}}\dot{\vec{\delta}}_i)\right]dm_i\right.$$

$$+\sum_{j=1}^{N_i}\left[\int_{m_{i,j}}\left[(\mathbf{C}_{\mathbf{i}}^{\mathbf{c}}\mathbf{C}_{\mathbf{i,j}}^{\mathbf{i}}\vec{\delta}_{i,j})\times(\mathbf{C}_{\mathbf{i}}^{\mathbf{c}}\mathbf{C}_{\mathbf{i,j}}^{\mathbf{i}}\dot{\vec{\delta}}_{i,j})\right]dm_{i,j}\right]\Bigg];$$

$$\vec{H}_{h,r}=\sum_{i=1}^{N}\left[\int_{m_i}((\mathbf{C}_{\mathbf{i}}^{\mathbf{c}}\vec{\rho}_i)\times\dot{\vec{d}}_i)\,dm_i+\sum_{j=1}^{N_i}\left[\left[(\mathbf{C}_{\mathbf{i}}^{\mathbf{c}}\mathbf{C}_{\mathbf{i,j}}^{\mathbf{i}}\vec{\rho}_{i,j})\times(\dot{\vec{d}}_i+\mathbf{C}_{\mathbf{i}}^{\mathbf{c}}\dot{\vec{d}}_{i,j})\right]dm_{i,j}\right]\right];$$

$$\vec{H}_{h,v}=\sum_{i=1}^{N}\left[\int_{m_i}\left[(\mathbf{C}_{\mathbf{i}}^{\mathbf{c}}\vec{\delta}_i)\times\dot{\vec{d}}_i+\vec{d}_i\times(\mathbf{C}_{\mathbf{i}}^{\mathbf{c}}\dot{\vec{\delta}}_i)\right]dm_i+\sum_{j=1}^{N_i}\left[\int_{m_{i,j}}\left[(\mathbf{C}_{\mathbf{i}}^{\mathbf{c}}\mathbf{C}_{\mathbf{i,j}}^{\mathbf{i}}\vec{\delta}_{i,j})\right.\right.\right.$$
$$\left.\left.\left.\times(\dot{\vec{d}}_i+\mathbf{C}_{\mathbf{i}}^{\mathbf{c}}\dot{\vec{d}}_{i,j})+(\vec{d}_i+\mathbf{C}_{\mathbf{i}}^{\mathbf{c}}\vec{d}_{i,j})\times(\mathbf{C}_{\mathbf{i}}^{\mathbf{c}}\mathbf{C}_{\mathbf{i,j}}^{\mathbf{i}}\dot{\vec{\delta}}_{i,j})\right]dm_{i,j}\right]\right];$$

$$\vec{H}_{r,v}=\int_{m_c}(\vec{\rho}_c\times\dot{\vec{\delta}}_c)\,dm_c+\sum_{i=1}^{N}\left[\int_{m_i}\left[(\mathbf{C}_{\mathbf{i}}^{\mathbf{c}}\vec{\rho}_i)\times(\mathbf{C}_{\mathbf{i}}^{\mathbf{c}}\dot{\vec{\delta}}_i)\right]dm_i\right.$$
$$\left.+\sum_{j=1}^{N_i}\left[\int_{m_{i,j}}\left[(\mathbf{C}_{\mathbf{i}}^{\mathbf{c}}\mathbf{C}_{\mathbf{i,j}}^{\mathbf{i}}\vec{\rho}_{i,j})\times(\mathbf{C}_{\mathbf{i}}^{\mathbf{c}}\mathbf{C}_{\mathbf{i,j}}^{\mathbf{i}}\dot{\vec{\delta}}_{i,j})\right]dm_{i,j}\right]\right];$$

$$\vec{H}_{r,s}=\sum_{i=1}^{N}\left[\int_{m_i}\left[(\mathbf{C}_{\mathbf{i}}^{\mathbf{c}}\vec{\rho}_i)\times\dot{\mathbf{C}}_{\mathbf{i}}^{\mathbf{c}}(\vec{\rho}_i+\vec{\delta}_i)\right]dm_i+\sum_{j=1}^{N_i}\left[\int_{m_{i,j}}\left[(\mathbf{C}_{\mathbf{i}}^{\mathbf{c}}\mathbf{C}_{\mathbf{i,j}}^{\mathbf{i}}\vec{\rho}_{i,j})\right.\right.\right.$$
$$\left.\left.\left.\times\left[\dot{\mathbf{C}}_{\mathbf{i}}^{\mathbf{c}}\mathbf{C}_{\mathbf{i,j}}^{\mathbf{i}}(\vec{\rho}_{i,j}+\vec{\delta}_{i,j})+\mathbf{C}_{\mathbf{i}}^{\mathbf{c}}\dot{\mathbf{C}}_{\mathbf{i,j}}^{\mathbf{i}}(\vec{\rho}_{i,j}+\vec{\delta}_{i,j})+\dot{\mathbf{C}}_{\mathbf{i}}^{\mathbf{c}}\vec{d}_{i,j}\right]\right]dm_{i,j}\right]\right];$$

$$\vec{H}_{v,s}=\sum_{i=1}^{N}\left[\int_{m_i}\left[(\mathbf{C}_{\mathbf{i}}^{\mathbf{c}}\vec{\delta}_i)\times\dot{\mathbf{C}}_{\mathbf{i}}^{\mathbf{c}}(\vec{\rho}_i+\vec{\delta}_i)\right]dm_i+\sum_{j=1}^{N_i}\left[\int_{m_{i,j}}\left[(\mathbf{C}_{\mathbf{i}}^{\mathbf{c}}\mathbf{C}_{\mathbf{i,j}}^{\mathbf{i}}\vec{\delta}_{i,j})\right.\right.\right.$$
$$\left.\left.\left.\times\left[\dot{\mathbf{C}}_{\mathbf{i}}^{\mathbf{c}}\mathbf{C}_{\mathbf{i,j}}^{\mathbf{i}}(\vec{\rho}_{i,j}+\vec{\delta}_{i,j})+\mathbf{C}_{\mathbf{i}}^{\mathbf{c}}\dot{\mathbf{C}}_{\mathbf{i,j}}^{\mathbf{i}}(\vec{\rho}_{i,j}+\vec{\delta}_{i,j})+\dot{\mathbf{C}}_{\mathbf{i}}^{\mathbf{c}}\vec{d}_{i,j}\right]\right]dm_{i,j}\right]\right];$$

$$\vec{H}_{h,s}=\sum_{i=1}^{N}\left[\int_{m_i}\left[\vec{d}_i\times\dot{\mathbf{C}}_{\mathbf{i}}^{\mathbf{c}}(\vec{\rho}_i+\vec{\delta}_i)\right]dm_i+\sum_{j=1}^{N_i}\left[\int_{m_{i,j}}\left[(\vec{d}_i+\mathbf{C}_{\mathbf{c}}^{\mathbf{i}}\vec{d}_{i,j})\right.\right.\right.$$
$$\left.\left.\left.\times\left[\dot{\mathbf{C}}_{\mathbf{i}}^{\mathbf{c}}\mathbf{C}_{\mathbf{i,j}}^{\mathbf{i}}(\vec{\rho}_{i,j}+\vec{\delta}_{i,j})+\mathbf{C}_{\mathbf{i}}^{\mathbf{c}}\dot{\mathbf{C}}_{\mathbf{i,j}}^{\mathbf{i}}(\vec{\rho}_{i,j}+\vec{\delta}_{i,j})+\dot{\mathbf{C}}_{\mathbf{i}}^{\mathbf{c}}\vec{d}_{i,j}\right]\right]dm_{i,j}\right]\right]. \qquad \text{(I–3)}$$

Appendix II: Governing Equations of Motion

The complete equations of motion governing the orbital generalized coordinates R_{cm} and θ are:

$$\ddot{R}_{cm} = R_{cm}\dot{\theta}^2 - \mu_e/R_{cm}^2 - \frac{3\mu_e}{2MR_{cm}^4}\text{trace}[\mathbf{I_{sys}}] + \frac{9\mu_e}{2MR_{cm}^4}\vec{\ell}^T\mathbf{I_{sys}}\vec{\ell};$$

$$R_{cm}\ddot{\theta} = -2\dot{R}_{cm}\dot{\theta} - \frac{1}{MR_{cm}}\left[\frac{d}{dt}\left(\frac{\partial\vec{\omega}}{\partial\dot{\theta}}\right)^T\mathbf{I_{sys}}\vec{\omega} + \frac{\partial\vec{\omega}}{\partial\dot{\theta}}^T\dot{\mathbf{I}}_{\mathbf{sys}}\vec{\omega} + \frac{\partial\vec{\omega}}{\partial\dot{\theta}}^T\mathbf{I_{sys}}\dot{\vec{\omega}}\right.$$
$$\left. + \frac{d}{dt}\left(\frac{\partial\vec{\omega}}{\partial\dot{\theta}}\right)^T\vec{H} + \frac{\partial\vec{\omega}}{\partial\dot{\theta}}^T\dot{\vec{H}}\right]. \qquad \text{(II-1)}$$

The time derivatives of $\mathbf{I_{sys}}$ and $\vec{H}$ as well as the derivatives of $\vec{\omega}$ are given in Appendix IV.

The kinetic energy contribution to the equations governing librational motion is:

$$\frac{d}{dt}\left(\frac{\partial T}{\partial\dot{\psi}}\right) - \frac{\partial T}{\partial\psi} = \frac{d}{dt}\left(\frac{\partial\vec{\omega}}{\partial\dot{\psi}}\right)^T[\mathbf{I_{sys}}]\vec{\omega} + \frac{\partial\vec{\omega}}{\partial\dot{\psi}}^T[\dot{\mathbf{I}}_{\mathbf{sys}}]\vec{\omega} + \frac{\partial\vec{\omega}}{\partial\dot{\psi}}^T[\mathbf{I_{sys}}]\dot{\vec{\omega}}$$
$$+ \frac{d}{dt}\left(\frac{\partial\vec{\omega}}{\partial\dot{\psi}}\right)^T\vec{H} + \frac{\partial\vec{\omega}}{\partial\dot{\psi}}^T\dot{\vec{H}};$$

$$\frac{d}{dt}\left(\frac{\partial T}{\partial\dot{\phi}}\right) - \frac{\partial T}{\partial\phi} = \frac{d}{dt}\left(\frac{\partial\vec{\omega}}{\partial\dot{\phi}}\right)^T[\mathbf{I_{sys}}]\vec{\omega} + \frac{\partial\vec{\omega}}{\partial\dot{\phi}}^T[\dot{\mathbf{I}}_{\mathbf{sys}}]\vec{\omega} + \frac{\partial\vec{\omega}}{\partial\dot{\phi}}^T[\mathbf{I_{sys}}]\dot{\vec{\omega}} - \frac{\partial\vec{\omega}}{\partial\phi}^T[\mathbf{I_{sys}}]\vec{\omega}$$
$$+ \left[\frac{d}{dt}\left(\frac{\partial\vec{\omega}}{\partial\dot{\phi}}\right)^T - \frac{\partial\vec{\omega}}{\partial\phi}^T\right]\vec{H} + \frac{\partial\vec{\omega}}{\partial\dot{\phi}}^T\dot{\vec{H}};$$

$$\frac{d}{dt}\left(\frac{\partial T}{\partial\dot{\lambda}}\right) - \frac{\partial T}{\partial\lambda} = \frac{\partial\vec{\omega}}{\partial\dot{\lambda}}^T[\dot{\mathbf{I}}_{\mathbf{sys}}]\vec{\omega} + \frac{\partial\vec{\omega}}{\partial\dot{\lambda}}^T[\mathbf{I_{sys}}]\dot{\vec{\omega}} - \frac{\partial\vec{\omega}}{\partial\lambda}^T[\mathbf{I_{sys}}]\vec{\omega} - \frac{\partial\vec{\omega}}{\partial\lambda}^T\vec{H}$$
$$+ \frac{\partial\vec{\omega}}{\partial\dot{\lambda}}^T\dot{\vec{H}}. \qquad \text{(II-2)}$$

The kinetic energy contribution to the equation governing the central body flexibility

generalized coordinates, q_{cm}, is:

$$\frac{d}{dt}\left(\frac{\partial T}{\partial \dot{q}_{cm}}\right) - \frac{\partial T}{\partial q_{cm}} =$$

$$-M\ddot{\vec{C}}_{cm} \cdot \left(\frac{\partial \vec{C}_{cm}}{\partial q_{cm}}\right) + \int_{m_c} (\vec{\phi}_{cm} \cdot \ddot{\vec{\delta}}_c)\, dm_c$$

$$+\sum_{i=1}^{N}\Bigg\{ \int_{m_i} \Bigg[\Big(\frac{\partial \mathbf{C_i^c}}{\partial q_{cm}}(\vec{\rho}_i + \vec{\delta}_i)\Big) \cdot \Big(\ddot{\mathbf{C}}_\mathbf{i}^\mathbf{c}(\vec{\rho}_i + \vec{\delta}_i)\Big) + 2\Big(\frac{\partial \mathbf{C_i^c}}{\partial q_{cm}}(\vec{\rho}_i + \vec{\delta}_i)\Big) \cdot (\dot{\mathbf{C}}_\mathbf{i}^\mathbf{c}\dot{\vec{\delta}}_i)$$

$$+\Big(\frac{\partial \mathbf{C_i^c}}{\partial q_{cm}}(\vec{\rho}_i + \vec{\delta}_i)\Big) \cdot (\mathbf{C}_\mathbf{i}^\mathbf{c}\ddot{\vec{\delta}}_i) + \vec{\phi}_{cm}(o_i) \cdot \Big(\ddot{\mathbf{C}}_\mathbf{i}^\mathbf{c}(\vec{\rho}_i + \vec{\delta}_i)\Big) + 2\vec{\phi}_{cm}(o_i) \cdot (\dot{\mathbf{C}}_\mathbf{i}^\mathbf{c}\dot{\vec{\delta}}_i)$$

$$+\vec{\phi}_{cm}(o_i) \cdot (\mathbf{C}_\mathbf{i}^\mathbf{c}\ddot{\vec{\delta}}_i) + \ddot{\vec{d}}_i \cdot \Big(\frac{\partial \mathbf{C_i^c}}{\partial q_{cm}}(\vec{\rho}_i + \vec{\delta}_i)\Big)\Bigg]\, dm_i + \big[\vec{\phi}_{cm}(o_i) \cdot \ddot{\vec{d}}_i\big] m_i$$

$$+\sum_{j=1}^{N_i}\Bigg[\int_{m_{i,j}} \Bigg[\Big(\frac{\partial \mathbf{C_i^c}}{\partial q_{cm}}\mathbf{C_{i,j}^i}(\vec{\rho}_{i,j} + \vec{\delta}_{i,j})\Big) \cdot \Big(\ddot{\mathbf{C}}_\mathbf{i}^\mathbf{c}\mathbf{C_{i,j}^i}(\vec{\rho}_{i,j} + \vec{\delta}_{i,j})\Big)$$

$$+2\Big(\frac{\partial \mathbf{C_i^c}}{\partial q_{cm}}\mathbf{C_{i,j}^i}(\vec{\rho}_{i,j} + \vec{\delta}_{i,j})\Big) \cdot (\dot{\mathbf{C}}_\mathbf{i}^\mathbf{c}\mathbf{C_{i,j}^i}\dot{\vec{\delta}}_{i,j})$$

$$+2\Big(\frac{\partial \mathbf{C_i^c}}{\partial q_{cm}}\mathbf{C_{i,j}^i}(\vec{\rho}_{i,j} + \vec{\delta}_{i,j})\Big) \cdot \Big(\dot{\mathbf{C}}_\mathbf{i}^\mathbf{c}\dot{\mathbf{C}}_\mathbf{i,j}^\mathbf{i}(\vec{\rho}_{i,j} + \vec{\delta}_{i,j})\Big)$$

$$+2\Big(\frac{\partial \mathbf{C_i^c}}{\partial q_{cm}}\mathbf{C_{i,j}^i}(\vec{\rho}_{i,j} + \vec{\delta}_{i,j})\Big) \cdot (\mathbf{C}_\mathbf{i}^\mathbf{c}\dot{\mathbf{C}}_\mathbf{i,j}^\mathbf{i}\dot{\vec{\delta}}_{i,j})$$

$$+\Big(\frac{\partial \mathbf{C_i^c}}{\partial q_{cm}}\mathbf{C_{i,j}^i}(\vec{\rho}_{i,j} + \vec{\delta}_{i,j})\Big) \cdot \Big(\mathbf{C}_\mathbf{i}^\mathbf{c}\ddot{\mathbf{C}}_\mathbf{i,j}^\mathbf{i}(\vec{\rho}_{i,j} + \vec{\delta}_{i,j})\Big)$$

$$+\Big(\frac{\partial \mathbf{C_i^c}}{\partial q_{cm}}\mathbf{C_{i,j}^i}(\vec{\rho}_{i,j} + \vec{\delta}_{i,j})\Big) \cdot (\mathbf{C}_\mathbf{i}^\mathbf{c}\mathbf{C_{i,j}^i}\ddot{\vec{\delta}}_{i,j}) + \Big(\frac{\partial \mathbf{C_i^c}}{\partial q_{cm}}\vec{d}_{i,j}\Big) \cdot \Big(\ddot{\mathbf{C}}_\mathbf{i}^\mathbf{c}\mathbf{C_{i,j}^i}(\vec{\rho}_{i,j} + \vec{\delta}_{i,j})\Big)$$

$$+2\Big(\frac{\partial \mathbf{C_i^c}}{\partial q_{cm}}\vec{d}_{i,j}\Big) \cdot \Big(\dot{\mathbf{C}}_\mathbf{i}^\mathbf{c}\dot{\mathbf{C}}_\mathbf{i,j}^\mathbf{i}(\vec{\rho}_{i,j} + \vec{\delta}_{i,j})\Big) + 2\Big(\frac{\partial \mathbf{C_i^c}}{\partial q_{cm}}\vec{d}_{i,j}\Big) \cdot (\dot{\mathbf{C}}_\mathbf{i}^\mathbf{c}\mathbf{C_{i,j}^i}\dot{\vec{\delta}}_{i,j})$$

$$+2\Big(\frac{\partial \mathbf{C_i^c}}{\partial q_{cm}}\vec{d}_{i,j}\Big) \cdot (\mathbf{C}_\mathbf{i}^\mathbf{c}\dot{\mathbf{C}}_\mathbf{i,j}^\mathbf{i}\dot{\vec{\delta}}_{i,j}) + \Big(\frac{\partial \mathbf{C_i^c}}{\partial q_{cm}}\vec{d}_{i,j}\Big) \cdot \Big(\mathbf{C}_\mathbf{i}^\mathbf{c}\ddot{\mathbf{C}}_\mathbf{i,j}^\mathbf{i}(\vec{\rho}_{i,j} + \vec{\delta}_{i,j})\Big)$$

$$+\Big(\frac{\partial \mathbf{C_i^c}}{\partial q_{cm}}\vec{d}_{i,j}\Big) \cdot (\mathbf{C}_\mathbf{i}^\mathbf{c}\mathbf{C_{i,j}^i}\ddot{\vec{\delta}}_{i,j}) + (\ddot{\mathbf{C}}_\mathbf{i}^\mathbf{c}\vec{d}_{i,j}) \cdot \Big(\frac{\partial \mathbf{C_i^c}}{\partial q_{cm}}\mathbf{C_{i,j}^i}(\vec{\rho}_{i,j} + \vec{\delta}_{i,j})\Big)$$

$$+2(\dot{\mathbf{C}}_\mathbf{i}^\mathbf{c}\dot{\vec{d}}_{i,j}) \cdot \Big(\frac{\partial \mathbf{C_i^c}}{\partial q_{cm}}\mathbf{C_{i,j}^i}(\vec{\rho}_{i,j} + \vec{\delta}_{i,j})\Big) + (\mathbf{C}_\mathbf{i}^\mathbf{c}\ddot{\vec{d}}_{i,j}) \cdot \Big(\frac{\partial \mathbf{C_i^c}}{\partial q_{cm}}\mathbf{C_{i,j}^i}(\vec{\rho}_{i,j} + \vec{\delta}_{i,j})\Big)$$

$$+\vec{\phi}_{cm}(o_i) \cdot \Big(\ddot{\mathbf{C}}_\mathbf{i}^\mathbf{c}\mathbf{C_{i,j}^i}(\vec{\rho}_{i,j} + \vec{\delta}_{i,j})\Big) + 2\vec{\phi}_{cm}(o_i) \cdot (\dot{\mathbf{C}}_\mathbf{i}^\mathbf{c}\mathbf{C_{i,j}^i}\dot{\vec{\delta}}_{i,j})$$

$$
\begin{aligned}
&+2\vec{\phi}_{c_m}(o_i)\cdot\left(\dot{\mathbf{C}}^{\mathbf{c}}_{\mathbf{i}}\dot{\mathbf{C}}^{\mathbf{i}}_{\mathbf{i,j}}(\vec{\rho}_{i,j}+\vec{\delta}_{i,j})\right)+2\vec{\phi}_{c_m}(o_i)\cdot(\mathbf{C}^{\mathbf{c}}_{\mathbf{i}}\dot{\mathbf{C}}^{\mathbf{i}}_{\mathbf{i,j}}\dot{\vec{\delta}}_{i,j})\\
&+\vec{\phi}_{c_m}(o_i)\cdot\left(\mathbf{C}^{\mathbf{c}}_{\mathbf{i}}\ddot{\mathbf{C}}^{\mathbf{i}}_{\mathbf{i,j}}(\vec{\rho}_{i,j}+\vec{\delta}_{i,j})\right)+\vec{\phi}_{c_m}(o_i)\cdot(\mathbf{C}^{\mathbf{c}}_{\mathbf{i}}\mathbf{C}^{\mathbf{i}}_{\mathbf{i,j}}\ddot{\vec{\delta}}_{i,j})\\
&+\ddot{\vec{d}}_i\cdot\left(\frac{\partial\mathbf{C}^{\mathbf{c}}_{\mathbf{i}}}{\partial q_{c_m}}\mathbf{C}^{\mathbf{i}}_{\mathbf{i,j}}(\vec{\rho}_{i,j}+\vec{\delta}_{i,j})\right)\Big]\,dm_{i,j}\\
&+\Big[\vec{\phi}_{c_m}(o_i)\cdot\ddot{\vec{d}}_i+2\vec{\phi}_{c_m}(o_i)\cdot(\dot{\mathbf{C}}^{\mathbf{c}}_{\mathbf{i}}\dot{\vec{d}}_{i,j})+\vec{\phi}_{c_m}(o_i)\cdot(\mathbf{C}^{\mathbf{c}}_{\mathbf{i}}\ddot{\vec{d}}_{i,j})\\
&+\vec{\phi}_{c_m}(o_i)\cdot(\ddot{\mathbf{C}}^{\mathbf{c}}_{\mathbf{i}}\vec{d}_{i,j})+\ddot{\vec{d}}_i\cdot\left(\frac{\partial\mathbf{C}^{\mathbf{c}}_{\mathbf{i}}}{\partial q_{c_m}}\vec{d}_{i,j}\right)+(\mathbf{C}^{\mathbf{c}}_{\mathbf{i}}\ddot{\vec{d}}_{i,j})\cdot\left(\frac{\partial\mathbf{C}^{\mathbf{c}}_{\mathbf{i}}}{\partial q_{c_m}}\vec{d}_{i,j}\right)\\
&+(\ddot{\mathbf{C}}^{\mathbf{c}}_{\mathbf{i}}\vec{d}_{i,j})\cdot\left(\frac{\partial\mathbf{C}^{\mathbf{c}}_{\mathbf{i}}}{\partial q_{c_m}}\vec{d}_{i,j}\right)+2(\dot{\mathbf{C}}^{\mathbf{c}}_{\mathbf{i}}\dot{\vec{d}}_{i,j})\cdot\left(\frac{\partial\mathbf{C}^{\mathbf{c}}_{\mathbf{i}}}{\partial q_{c_m}}\vec{d}_{i,j}\right)\Big]m_{i,j}-\frac{1}{2}\vec{\omega}^{\,T}\left[\frac{\partial\mathbf{I_{sys}}}{\partial q_{c_m}}\right]\vec{\omega}\\
&+\dot{\vec{\omega}}^{\,T}\left(\frac{\partial\vec{H}}{\partial\dot{q}_{c_m}}\right)+\vec{\omega}^{\,T}\left[\frac{d}{dt}\left(\frac{\partial\vec{H}}{\partial\dot{q}_{c_m}}\right)-\frac{\partial\vec{H}}{\partial q_{c_m}}\right],
\end{aligned}
\tag{II-3}
$$

where

$$m=1,\ldots,Nm_c,$$

and Nm_c denotes the number of assumed modes (and hence generalized coordinates) used in discretizing the flexible nature of the central body. $\vec{\phi}_{c_m}(o_i)$ is the value of the m-th mode shape vector for body B_c evaluated at the point of attachment of the body B_i. Details of $\left[\frac{\partial\mathbf{I_{sys}}}{\partial q_{c_m}}\right]$, $\left(\frac{\partial\vec{H}}{\partial\dot{q}_{c_m}}\right)$ and $\left[\frac{d}{dt}\left(\frac{\partial\vec{H}}{\partial\dot{q}_{c_m}}\right)-\frac{\partial\vec{H}}{\partial q_{c_m}}\right]$ are given in Appendix V.

The kinetic energy contribution to the equation governing the flexibility generalized coordinates q_{i_n} of body B_i is

$$
\begin{aligned}
&\frac{d}{dt}\left(\frac{\partial T}{\partial\dot{q}_{i_n}}\right)-\frac{\partial T}{\partial q_{i_n}}=-M\ddot{\vec{C}}_{cm}\cdot\left(\frac{\partial\vec{C}_{cm}}{\partial q_{i_n}}\right)\\
&+\int_{m_i}\left[(\vec{\phi}_{i_n}\cdot\ddot{\vec{\delta}}_i)+(\mathbf{C}^{\mathbf{c}}_{\mathbf{i}}\vec{\phi}_{i_n})\cdot\ddot{\vec{d}}_i+(\mathbf{C}^{\mathbf{c}}_{\mathbf{i}}\vec{\phi}_{i_n})\cdot\ddot{\mathbf{C}}^{\mathbf{c}}_{\mathbf{i}}(\vec{\rho}_i+\vec{\delta}_i)+2(\mathbf{C}^{\mathbf{c}}_{\mathbf{i}}\vec{\phi}_{i_n})\cdot(\dot{\mathbf{C}}^{\mathbf{c}}_{\mathbf{i}}\dot{\vec{\delta}}_i)\right]dm_i\\
&+\sum_{j=1}^{N_i}\Bigg[\int_{m_{i,j}}\Big[\Big(\frac{\partial\mathbf{C}^{\mathbf{i}}_{\mathbf{i,j}}}{\partial q_{i_n}}(\vec{\rho}_{i,j}+\vec{\delta}_{i,j})\Big)\cdot\Big(\ddot{\mathbf{C}}^{\mathbf{i}}_{\mathbf{i,j}}(\vec{\rho}_{i,j}+\vec{\delta}_{i,j})\Big)\\
&+2\Big(\frac{\partial\mathbf{C}^{\mathbf{i}}_{\mathbf{i,j}}}{\partial q_{i_n}}(\vec{\rho}_{i,j}+\vec{\delta}_{i,j})\Big)\cdot(\dot{\mathbf{C}}^{\mathbf{i}}_{\mathbf{i,j}}\dot{\vec{\delta}}_{i,j})+\Big(\frac{\partial\mathbf{C}^{\mathbf{i}}_{\mathbf{i,j}}}{\partial q_{i_n}}(\vec{\rho}_{i,j}+\vec{\delta}_{i,j})\Big)\cdot(\mathbf{C}^{\mathbf{i}}_{\mathbf{i,j}}\ddot{\vec{\delta}}_{i,j})
\end{aligned}
$$

$$
\begin{aligned}
&+\left(\mathbf{C_i^c}\frac{\partial \mathbf{C_{i,j}^i}}{\partial q_{in}}(\vec{\rho}_{i,j}+\vec{\delta}_{i,j})\right)\cdot\left(\ddot{\mathbf{C}}_\mathbf{i}^\mathbf{c}\mathbf{C_{i,j}^i}(\vec{\rho}_{i,j}+\vec{\delta}_{i,j})\right)\\
&+2\left(\mathbf{C_i^c}\frac{\partial \mathbf{C_{i,j}^i}}{\partial q_{in}}(\vec{\rho}_{i,j}+\vec{\delta}_{i,j})\right)\cdot\left(\dot{\mathbf{C}}_\mathbf{i}^\mathbf{c}\dot{\mathbf{C}}_\mathbf{i,j}^\mathbf{i}(\vec{\rho}_{i,j}+\vec{\delta}_{i,j})\right)\\
&+2\left(\mathbf{C_i^c}\frac{\partial \mathbf{C_{i,j}^i}}{\partial q_{in}}(\vec{\rho}_{i,j}+\vec{\delta}_{i,j})\right)\cdot(\dot{\mathbf{C}}_\mathbf{i}^\mathbf{c}\mathbf{C_{i,j}^i}\dot{\vec{\delta}}_{i,j})+\left(\mathbf{C_i^c}\frac{\partial \mathbf{C_{i,j}^i}}{\partial q_{in}}(\vec{\rho}_{i,j}+\vec{\delta}_{i,j})\right)\cdot\ddot{\vec{d}}_i\\
&+\left(\frac{\partial \mathbf{C_{i,j}^i}}{\partial q_{in}}(\vec{\rho}_{i,j}+\vec{\delta}_{i,j})\right)\cdot\ddot{\vec{d}}_{i,j}+\left(\mathbf{C_i^c}\frac{\partial \mathbf{C_{i,j}^i}}{\partial q_{in}}(\vec{\rho}_{i,j}+\vec{\delta}_{i,j})\right)\cdot(\ddot{\mathbf{C}}_\mathbf{i}^\mathbf{c}\vec{d}_{i,j})\\
&+2\left(\mathbf{C_i^c}\frac{\partial \mathbf{C_{i,j}^i}}{\partial q_{in}}(\vec{\rho}_{i,j}+\vec{\delta}_{i,j})\right)\cdot(\dot{\mathbf{C}}_\mathbf{i}^\mathbf{c}\dot{\vec{d}}_{i,j})+\left(\ddot{\mathbf{C}}_\mathbf{i,j}^\mathbf{i}(\vec{\rho}_{i,j}+\vec{\delta}_{i,j})\right)\cdot\vec{\phi}_{in}(o_{i,j})\\
&+2(\dot{\mathbf{C}}_\mathbf{i,j}^\mathbf{i}\dot{\vec{\delta}}_{i,j})\cdot\vec{\phi}_{in}(o_{i,j})\\
&+(\mathbf{C_{i,j}^i}\ddot{\vec{\delta}}_{i,j})\cdot\vec{\phi}_{in}(o_{i,j})+\left(\ddot{\mathbf{C}}_\mathbf{i}^\mathbf{c}\mathbf{C_{i,j}^i}(\vec{\rho}_{i,j}+\vec{\delta}_{i,j})\right)\cdot(\mathbf{C_i^c}\vec{\phi}_{in}(o_{i,j}))\\
&+2\left(\dot{\mathbf{C}}_\mathbf{i}^\mathbf{c}\dot{\mathbf{C}}_\mathbf{i,j}^\mathbf{i}(\vec{\rho}_{i,j}+\vec{\delta}_{i,j})\right)\cdot(\mathbf{C_i^c}\vec{\phi}_{in}(o_{i,j}))+2(\dot{\mathbf{C}}_\mathbf{i}^\mathbf{c}\mathbf{C_{i,j}^i}\dot{\vec{\delta}}_{i,j})\cdot(\mathbf{C_i^c}\vec{\phi}_{in}(o_{i,j}))\Big]\,dm_{i,j}\\
&+\Big[\ddot{\vec{d}}_i\cdot(\mathbf{C_i^c}\vec{\phi}_{in}(o_{i,j}))+\ddot{\vec{d}}_{i,j}\cdot\vec{\phi}_{in}(o_{i,j})+(\ddot{\mathbf{C}}_\mathbf{i}^\mathbf{c}\vec{d}_{i,j})\cdot(\mathbf{C_i^c}\vec{\phi}_{in}(o_{i,j}))\\
&+2(\dot{\mathbf{C}}_\mathbf{i}^\mathbf{c}\dot{\vec{d}}_{i,j})\cdot(\mathbf{C_i^c}\vec{\phi}_{in}(o_{i,j}))\Big]m_{i,j}\Big]-\frac{1}{2}\vec{\omega}^{\,T}\left[\frac{\partial \mathbf{I_{sys}}}{\partial q_{in}}\right]\vec{\omega}+\dot{\vec{\omega}}^{\,T}\left(\frac{\partial \vec{H}}{\partial \dot{q}_{in}}\right)\\
&+\vec{\omega}^{\,T}\left[\frac{d}{dt}\left(\frac{\partial \vec{H}}{\partial \dot{q}_{in}}\right)-\frac{\partial \vec{H}}{\partial q_{in}}\right],
\end{aligned}
\tag{II-4}
$$

where:

$$
i=1,\ldots,N;\quad n=1,\ldots,Nm_i;
$$

and Nm_i denotes the number of assumed modes (and hence generalized coordinates) used in discretizing the flexible nature of body B_i. $\vec{\phi}_{in}(o_{i,j})$ is the value of the n-th mode shape vector of body B_i evaluated at the point of attachment for the body $B_{i,j}$. Details of $\left[\frac{\partial \mathbf{I_{sys}}}{\partial q_{in}}\right]$, $\left(\frac{\partial \vec{H}}{\partial \dot{q}_{in}}\right)$ and $\left[\frac{d}{dt}\left(\frac{\partial \vec{H}}{\partial \dot{q}_{in}}\right)-\frac{\partial \vec{H}}{\partial q_{in}}\right]$ are given in Appendix V.

The kinetic energy contribution to the equation governing the flexibility general-

ized coordinates q_{i,j_p} of body $B_{i,j}$ is given by

$$\frac{d}{dt}\left(\frac{\partial T}{\partial \dot{q}_{i,j_p}}\right) - \frac{\partial T}{\partial q_{i,j_p}} = -M\ddot{\vec{C}}_{cm} \cdot \left(\frac{\partial \vec{C}_{cm}}{\partial q_{i,j_p}}\right)$$
$$+ \int_{m_{i,j}} \Big[(\vec{\phi}_{i,j_p} \cdot \ddot{\vec{\delta}}_{i,j}) + \ddot{\vec{d}}_i \cdot (\mathbf{C_i^c C_{i,j}^i}\vec{\phi}_{i,j_p}) + \ddot{\vec{d}}_{i,j} \cdot (\mathbf{C_{i,j}^i}\vec{\phi}_{i,j_p})$$
$$+(\ddot{\mathbf{C}}_\mathbf{i}^\mathbf{c}\vec{d}_{i,j}) \cdot (\mathbf{C_i^c C_{i,j}^i}\vec{\phi}_{i,j_p}) + 2(\dot{\mathbf{C}}_\mathbf{i}^\mathbf{c}\dot{\vec{d}}_{i,j}) \cdot (\mathbf{C_i^c C_{i,j}^i}\vec{\phi}_{i,j_p})$$
$$+(\ddot{\mathbf{C}}_{\mathbf{i,j}}^\mathbf{i}(\vec{\rho}_{i,j} + \vec{\delta}_{i,j})) \cdot (\mathbf{C_{i,j}^i}\vec{\phi}_{i,j_p}) + 2(\dot{\mathbf{C}}_{\mathbf{i,j}}^\mathbf{i}\dot{\vec{\delta}}_{i,j}) \cdot (\mathbf{C_{i,j}^i}\vec{\phi}_{i,j_p})$$
$$+(\ddot{\mathbf{C}}_\mathbf{i}^\mathbf{c}\mathbf{C}_{\mathbf{i,j}}^\mathbf{i}(\vec{\rho}_{i,j} + \vec{\delta}_{i,j})) \cdot (\mathbf{C_i^c C_{i,j}^i}\vec{\phi}_{i,j_p}) + 2(\dot{\mathbf{C}}_\mathbf{i}^\mathbf{c}\dot{\mathbf{C}}_{\mathbf{i,j}}^\mathbf{i}(\vec{\rho}_{i,j} + \vec{\delta}_{i,j})) \cdot (\mathbf{C_i^c C_{i,j}^i}\vec{\phi}_{i,j_p})$$
$$+2(\dot{\mathbf{C}}_\mathbf{i}^\mathbf{c}\mathbf{C}_{\mathbf{i,j}}^\mathbf{i}\dot{\vec{\delta}}_{i,j}) \cdot (\mathbf{C_i^c C_{i,j}^i}\vec{\phi}_{i,j_p})\Big]\, dm_{i,j} - \frac{1}{2}\vec{\omega}^{\,T}\left[\frac{\partial \mathbf{I_{sys}}}{\partial q_{i,j_p}}\right]\vec{\omega} + \dot{\vec{\omega}}^{\,T}\left(\frac{\partial \vec{H}}{\partial \dot{q}_{i,j_p}}\right)$$
$$+\vec{\omega}^{\,T}\left[\frac{d}{dt}\left(\frac{\partial \vec{H}}{\partial \dot{q}_{i,j_p}}\right) - \frac{\partial \vec{H}}{\partial q_{i,j_p}}\right], \qquad \text{(II–5)}$$

where:

$$i = 1, \ldots, N; \quad j = 1, \ldots, N_i; \quad p = 1, \ldots, Nm_{i,j};$$

and $Nm_{i,j}$ denotes the number of assumed modes (and hence the generalized coordinates) used in discretizing the flexible nature of the body $B_{i,j}$. Again, details of $\left[\frac{\partial \mathbf{I_{sys}}}{\partial q_{i,j_p}}\right]$, $\left(\frac{\partial \vec{H}}{\partial \dot{q}_{i,j_p}}\right)$ and $\left[\frac{d}{dt}\left(\frac{\partial \vec{H}}{\partial \dot{q}_{i_n}}\right) - \frac{\partial \vec{H}}{\partial q_{i,j_p}}\right]$ are given in Appendix V.

The equations governing the degrees of freedom for the joint between the bodies B_i and $B_{i,j}$ ($\alpha_{a_i}^s$, $a = 1, 2, 3$) are:

$$\frac{d}{dt}\left(\frac{\partial T}{\partial \dot{\alpha}_{a_i}^s}\right) - \frac{\partial T}{\partial \alpha_{a_i}^s} = -M\ddot{\vec{C}}_{cm} \cdot \left(\frac{\partial \vec{C}_{cm}}{\partial \alpha_{a_i}^s}\right)$$
$$+ \int_{m_i} \left[\left(\frac{\partial \mathbf{C_i^c}}{\partial \alpha_{a_i}^s}(\vec{\rho}_i + \vec{\delta}_i)\right) \cdot \left(\ddot{\mathbf{C}}_\mathbf{i}^\mathbf{c}(\vec{\rho}_i + \vec{\delta}_i)\right) + 2\left(\frac{\partial \mathbf{C_i^c}}{\partial \alpha_{a_i}^s}(\vec{\rho}_i + \vec{\delta}_i)\right) \cdot (\dot{\mathbf{C}}_\mathbf{i}^\mathbf{c}\dot{\vec{\delta}}_i)\right.$$
$$\left.+\left(\frac{\partial \mathbf{C_i^c}}{\partial \alpha_{a_i}^s}(\vec{\rho}_i + \vec{\delta}_i)\right) \cdot (\mathbf{C}_\mathbf{i}^\mathbf{c}\ddot{\vec{\delta}}_i) + \ddot{\vec{d}}_i \cdot \left(\frac{\partial \mathbf{C_i^c}}{\partial \alpha_{a_i}}(\vec{\rho}_i + \vec{\delta}_i)\right)\right] dm_i$$
$$+ \sum_{j=1}^{N_i}\left[\int_{m_{i,j}} \left[\left(\frac{\partial \mathbf{C_i^c}}{\partial \alpha_{a_i}^s}\mathbf{C}_{\mathbf{i,j}}^\mathbf{i}(\vec{\rho}_{i,j} + \vec{\delta}_{i,j})\right) \cdot \left(\ddot{\mathbf{C}}_\mathbf{i}^\mathbf{c}\mathbf{C}_{\mathbf{i,j}}^\mathbf{i}(\vec{\rho}_{i,j} + \vec{\delta}_{i,j})\right)\right.\right.$$

$$
\begin{aligned}
&+2\Big(\frac{\partial \mathbf{C}_{\mathbf{i}}^{\mathbf{c}}}{\partial \alpha_{a_i}^s}\mathbf{C}_{\mathbf{i,j}}^{\mathbf{i}}(\vec{\rho}_{i,j}+\vec{\delta}_{i,j})\Big)\cdot(\dot{\mathbf{C}}_{\mathbf{i}}^{\mathbf{c}}\mathbf{C}_{\mathbf{i,j}}^{\mathbf{i}}\dot{\vec{\delta}}_{i,j})\\
&+2\Big(\frac{\partial \mathbf{C}_{\mathbf{i}}^{\mathbf{c}}}{\partial \alpha_{a_i}^s}\mathbf{C}_{\mathbf{i,j}}^{\mathbf{i}}(\vec{\rho}_{i,j}+\vec{\delta}_{i,j})\Big)\cdot\Big(\dot{\mathbf{C}}_{\mathbf{i}}^{\mathbf{c}}\dot{\mathbf{C}}_{\mathbf{i,j}}^{\mathbf{i}}(\vec{\rho}_{i,j}+\vec{\delta}_{i,j})\Big)\\
&+2\Big(\frac{\partial \mathbf{C}_{\mathbf{i}}^{\mathbf{c}}}{\partial \alpha_{a_i}^s}\mathbf{C}_{\mathbf{i,j}}^{\mathbf{i}}(\vec{\rho}_{i,j}+\vec{\delta}_{i,j})\Big)\cdot(\mathbf{C}_{\mathbf{i}}^{\mathbf{c}}\dot{\mathbf{C}}_{\mathbf{i,j}}^{\mathbf{i}}\dot{\vec{\delta}}_{i,j})\\
&+\Big(\frac{\partial \mathbf{C}_{\mathbf{i}}^{\mathbf{c}}}{\partial \alpha_{a_i}^s}\mathbf{C}_{\mathbf{i,j}}^{\mathbf{i}}(\vec{\rho}_{i,j}+\vec{\delta}_{i,j})\Big)\cdot\Big(\mathbf{C}_{\mathbf{i}}^{\mathbf{c}}\ddot{\mathbf{C}}_{\mathbf{i,j}}^{\mathbf{i}}(\vec{\rho}_{i,j}+\vec{\delta}_{i,j})\Big)\\
&+\Big(\frac{\partial \mathbf{C}_{\mathbf{i}}^{\mathbf{c}}}{\partial \alpha_{a_i}^s}\mathbf{C}_{\mathbf{i,j}}^{\mathbf{i}}(\vec{\rho}_{i,j}+\vec{\delta}_{i,j})\Big)\cdot(\mathbf{C}_{\mathbf{i}}^{\mathbf{c}}\mathbf{C}_{\mathbf{i,j}}^{\mathbf{i}}\ddot{\vec{\delta}}_{i,j})+\Big(\frac{\partial \mathbf{C}_{\mathbf{i}}^{\mathbf{c}}}{\partial \alpha_{a_i}^s}\vec{d}_{i,j}\Big)\cdot\Big(\ddot{\mathbf{C}}_{\mathbf{i}}^{\mathbf{c}}\mathbf{C}_{\mathbf{i,j}}^{\mathbf{i}}(\vec{\rho}_{i,j}+\vec{\delta}_{i,j})\Big)\\
&+2\Big(\frac{\partial \mathbf{C}_{\mathbf{i}}^{\mathbf{c}}}{\partial \alpha_{a_i}^s}\vec{d}_{i,j}\Big)\cdot\Big(\dot{\mathbf{C}}_{\mathbf{i}}^{\mathbf{c}}\dot{\mathbf{C}}_{\mathbf{i,j}}^{\mathbf{i}}(\vec{\rho}_{i,j}+\vec{\delta}_{i,j})\Big)+2\Big(\frac{\partial \mathbf{C}_{\mathbf{i}}^{\mathbf{c}}}{\partial \alpha_{a_i}^s}\vec{d}_{i,j}\Big)\cdot(\dot{\mathbf{C}}_{\mathbf{i}}^{\mathbf{c}}\mathbf{C}_{\mathbf{i,j}}^{\mathbf{i}}\dot{\vec{\delta}}_{i,j})\\
&+2\Big(\frac{\partial \mathbf{C}_{\mathbf{i}}^{\mathbf{c}}}{\partial \alpha_{a_i}^s}\vec{d}_{i,j}\Big)\cdot(\mathbf{C}_{\mathbf{i}}^{\mathbf{c}}\dot{\mathbf{C}}_{\mathbf{i,j}}^{\mathbf{i}}\dot{\vec{\delta}}_{i,j})+\Big(\frac{\partial \mathbf{C}_{\mathbf{i}}^{\mathbf{c}}}{\partial \alpha_{a_i}^s}\vec{d}_{i,j}\Big)\cdot\Big(\mathbf{C}_{\mathbf{i}}^{\mathbf{c}}\ddot{\mathbf{C}}_{\mathbf{i,j}}^{\mathbf{i}}(\vec{\rho}_{i,j}+\vec{\delta}_{i,j})\Big)\\
&\quad+\Big(\frac{\partial \mathbf{C}_{\mathbf{i}}^{\mathbf{c}}}{\partial \alpha_{a_i}^s}\vec{d}_{i,j}\Big)\cdot(\mathbf{C}_{\mathbf{i}}^{\mathbf{c}}\mathbf{C}_{\mathbf{i,j}}^{\mathbf{i}}\ddot{\vec{\delta}}_{i,j})+(\ddot{\mathbf{C}}_{\mathbf{i}}^{\mathbf{c}}\vec{d}_{i,j})\cdot\Big(\frac{\partial \mathbf{C}_{\mathbf{i}}^{\mathbf{c}}}{\partial \alpha_{a_i}^s}\mathbf{C}_{\mathbf{i,j}}^{\mathbf{i}}(\vec{\rho}_{i,j}+\vec{\delta}_{i,j})\Big)\\
&+2(\dot{\mathbf{C}}_{\mathbf{i}}^{\mathbf{c}}\dot{\vec{d}}_{i,j})\cdot\Big(\frac{\partial \mathbf{C}_{\mathbf{i}}^{\mathbf{c}}}{\partial \alpha_{a_i}^s}\mathbf{C}_{\mathbf{i,j}}^{\mathbf{i}}(\vec{\rho}_{i,j}+\vec{\delta}_{i,j})\Big)+(\mathbf{C}_{\mathbf{i}}^{\mathbf{c}}\ddot{\vec{d}}_{i,j})\cdot\Big(\frac{\partial \mathbf{C}_{\mathbf{i}}^{\mathbf{c}}}{\partial \alpha_{a_i}^s}\mathbf{C}_{\mathbf{i,j}}^{\mathbf{i}}(\vec{\rho}_{i,j}+\vec{\delta}_{i,j})\Big)\\
&+\ddot{\vec{d}}_i\cdot\Big(\frac{\partial \mathbf{C}_{\mathbf{i}}^{\mathbf{c}}}{\partial \alpha_{a_i}^s}\mathbf{C}_{\mathbf{i,j}}^{\mathbf{i}}(\vec{\rho}_{i,j}+\vec{\delta}_{i,j})\Big)\Big]\,dm_i\\
&+\Big[\ddot{\vec{d}}_i\cdot\Big(\frac{\partial \mathbf{C}_{\mathbf{i}}^{\mathbf{c}}}{\partial \alpha_{a_i}^s}\vec{d}_{i,j}\Big)+(\mathbf{C}_{\mathbf{i}}^{\mathbf{c}}\ddot{\vec{d}}_{i,j})\cdot\Big(\frac{\partial \mathbf{C}_{\mathbf{i}}^{\mathbf{c}}}{\partial \alpha_{a_i}^s}\vec{d}_{i,j}\Big)+(\ddot{\mathbf{C}}_{\mathbf{i}}^{\mathbf{c}}\vec{d}_{i,j})\cdot\Big(\frac{\partial \mathbf{C}_{\mathbf{i}}^{\mathbf{c}}}{\partial \alpha_{a_i}^s}\vec{d}_{i,j}\Big)\\
&+2(\dot{\mathbf{C}}_{\mathbf{i}}^{\mathbf{c}}\dot{\vec{d}}_{i,j})\cdot\Big(\frac{\partial \mathbf{C}_{\mathbf{i}}^{\mathbf{c}}}{\partial \alpha_{a_i}^s}\vec{d}_{i,j}\Big)\Big]m_{i,j}-\frac{1}{2}\vec{\omega}^{\,T}\left[\frac{\partial \mathbf{I_{sys}}}{\partial \alpha_{a_i}^s}\right]\vec{\omega}+\dot{\vec{\omega}}^{\,T}\left(\frac{\partial \vec{H}}{\partial \dot{\alpha}_{a_i}^s}\right)\\
&+\vec{\omega}^{\,T}\left[\frac{d}{dt}\left(\frac{\partial \vec{H}}{\partial \dot{\alpha}_{a_i}^s}\right)-\frac{\partial \vec{H}}{\partial \alpha_{a_i}^s}\right],
\end{aligned}
\tag{II-6}
$$

where:

$$a=1,2,3;\qquad i=1,\ldots,N.$$

Details of $\left[\frac{\partial \mathbf{I_{sys}}}{\partial \alpha_{a_i}^s}\right]$, $\left(\frac{\partial \vec{H}}{\partial \dot{\alpha}_{a_i}^s}\right)$ and $\left[\frac{d}{dt}\left(\frac{\partial \vec{H}}{\partial \dot{\alpha}_{a_i}^s}\right)-\frac{\partial \vec{H}}{\partial \alpha_{a_i}^s}\right]$ are given in Appendix VI.

Similarly, the contribution from the Kinetic Energy to the equations of motion governing the dynamics of the joints between the bodies B_i and $B_{i,j}$ ($\alpha_{a_{i,j}}^s$, $a=1,2,3$)

is given below:

$$\frac{d}{dt}\left(\frac{\partial T}{\partial \dot{\alpha}^s_{a_{i,j}}}\right) - \frac{\partial T}{\partial \alpha^s_{a_{i,j}}} = -M\ddot{\vec{C}}_{cm}\cdot\left(\frac{\partial \vec{C}_{cm}}{\partial \alpha^s_{a_{i,j}}}\right)$$

$$+\int_{m_{i,j}}\Big[\Big(\frac{\partial \mathbf{C^i_{i,j}}}{\partial \alpha^s_{a_{i,j}}}(\vec{\rho}_{i,j}+\vec{\delta}_{i,j})\Big)\cdot\Big(\ddot{\mathbf{C}}^{\mathbf{i}}_{\mathbf{i,j}}(\vec{\rho}_{i,j}+\vec{\delta}_{i,j})\Big)+2\Big(\frac{\partial \mathbf{C^i_{i,j}}}{\partial \alpha^s_{a_{i,j}}}(\vec{\rho}_{i,j}+\vec{\delta}_{i,j})\Big)\cdot(\dot{\mathbf{C}}^{\mathbf{i}}_{\mathbf{i,j}}\dot{\vec{\delta}}_{i,j})$$

$$+\Big(\frac{\partial \mathbf{C^i_{i,j}}}{\partial \alpha^s_{a_{i,j}}}(\vec{\rho}_{i,j}+\vec{\delta}_{i,j})\Big)\cdot(\mathbf{C}^{\mathbf{i}}_{\mathbf{i,j}}\ddot{\vec{\delta}}_{i,j})+\Big(\mathbf{C^c_i}\frac{\partial \mathbf{C^i_{i,j}}}{\partial \alpha^s_{a_{i,j}}}(\vec{\rho}_{i,j}+\vec{\delta}_{i,j})\Big)\cdot\Big(\ddot{\mathbf{C}}^{\mathbf{c}}_{\mathbf{i}}\mathbf{C}^{\mathbf{i}}_{\mathbf{i,j}}(\vec{\rho}_{i,j}+\vec{\delta}_{i,j})\Big)$$

$$+2\Big(\mathbf{C^c_i}\frac{\partial \mathbf{C^i_{i,j}}}{\partial \alpha^s_{a_{i,j}}}(\vec{\rho}_{i,j}+\vec{\delta}_{i,j})\Big)\cdot\Big(\dot{\mathbf{C}}^{\mathbf{c}}_{\mathbf{i}}\dot{\mathbf{C}}^{\mathbf{i}}_{\mathbf{i,j}}(\vec{\rho}_{i,j}+\vec{\delta}_{i,j})\Big)$$

$$+2\Big(\mathbf{C^c_i}\frac{\partial \mathbf{C^i_{i,j}}}{\partial \alpha^s_{a_{i,j}}}(\vec{\rho}_{i,j}+\vec{\delta}_{i,j})\Big)\cdot(\dot{\mathbf{C}}^{\mathbf{c}}_{\mathbf{i}}\mathbf{C}^{\mathbf{i}}_{\mathbf{i,j}}\dot{\vec{\delta}}_{i,j})+\Big(\mathbf{C^c_i}\frac{\partial \mathbf{C^i_{i,j}}}{\partial \alpha^s_{a_{i,j}}}(\vec{\rho}_{i,j}+\vec{\delta}_{i,j})\Big)\cdot\ddot{\vec{d}}_i$$

$$+\Big(\frac{\partial \mathbf{C^i_{i,j}}}{\partial \alpha^s_{a_{i,j}}}(\vec{\rho}_{i,j}+\vec{\delta}_{i,j})\Big)\cdot\ddot{\vec{d}}_{i,j}+\Big(\mathbf{C^c_i}\frac{\partial \mathbf{C^i_{i,j}}}{\partial \alpha^s_{a_{i,j}}}(\vec{\rho}_{i,j}+\vec{\delta}_{i,j})\Big)\cdot(\ddot{\mathbf{C}}^{\mathbf{c}}_{\mathbf{i}}\vec{d}_{i,j})$$

$$+2\Big(\mathbf{C^c_i}\frac{\partial \mathbf{C^i_{i,j}}}{\partial \alpha^s_{a_{i,j}}}(\vec{\rho}_{i,j}+\vec{\delta}_{i,j})\Big)\cdot(\dot{\mathbf{C}}^{\mathbf{c}}_{\mathbf{i}}\dot{\vec{d}}_{i,j})\Big]\,dm_{i,j}-\frac{1}{2}\vec{\omega}^{\,T}\left[\frac{\partial \mathbf{I_{sys}}}{\partial \alpha^s_{a_{i,j}}}\right]\vec{\omega}+\dot{\vec{\omega}}^{\,T}\left(\frac{\partial \vec{H}}{\partial \dot{\alpha}^s_{a_{i,j}}}\right)$$

$$+\vec{\omega}^{\,T}\left[\frac{d}{dt}\left(\frac{\partial \vec{H}}{\partial \dot{\alpha}^s_{a_{i,j}}}\right)-\frac{\partial \vec{H}}{\partial \alpha^s_{a_{i,j}}}\right]; \qquad \text{(II–7)}$$

where:

$$a=1,2,3;\quad i=1,\ldots,N;\quad j=1,\ldots,N_i.$$

Details of $\left[\frac{\partial \mathbf{I_{sys}}}{\partial \alpha^s_{a_{i,j}}}\right]$, $\left(\frac{\partial \vec{H}}{\partial \dot{\alpha}^s_{a_{i,j}}}\right)$ and $\left[\frac{d}{dt}\left(\frac{\partial \vec{H}}{\partial \dot{\alpha}^s_{a_{i,j}}}\right)-\frac{\partial \vec{H}}{\partial \alpha^s_{a_{i,j}}}\right]$ are given in Appendix VI.

The gravitational potential energy contribution to the equations governing librational motion are:

$$\frac{\partial U_g}{\partial \psi}=\frac{3\mu_e}{R^3_{cm}}\frac{\partial \vec{\ell}^{\,T}}{\partial \psi}\left[\mathbf{I_{sys}}\right]\vec{\ell};$$

$$\frac{\partial U_g}{\partial \phi}=\frac{3\mu_e}{R^3_{cm}}\frac{\partial \vec{\ell}^{\,T}}{\partial \phi}\left[\mathbf{I_{sys}}\right]\vec{\ell};$$

$$\frac{\partial U_g}{\partial \lambda} = \frac{3\mu_e}{R_{cm}^3} \frac{\partial \vec{\ell}^T}{\partial \lambda} \left[\mathbf{I_{sys}}\right] \vec{\ell}. \tag{II-8}$$

The details of $\frac{\partial \vec{\ell}}{\partial \psi}$, $\frac{\partial \vec{\ell}}{\partial \phi}$ and $\frac{\partial \vec{\ell}}{\partial \lambda}$ are presented in Appendix III.

The gravitational potential energy contribution to the equations governing the vibration of the B_c, B_i and $B_{i,j}$ bodies are:

$$\begin{aligned}
\frac{\partial U_g}{\partial q_{c_m}} &= -\frac{\mu_e}{2R_{cm}^3} \text{trace} \left[\frac{\partial \mathbf{I_{sys}}}{\partial q_{c_m}}\right] + \frac{3\mu_e}{2R_{cm}^3} \vec{\ell}^T \left[\frac{\partial \mathbf{I_{sys}}}{\partial q_{c_m}}\right] \vec{\ell}; \\
\frac{\partial U_g}{\partial q_{i_n}} &= -\frac{\mu_e}{2R_{cm}^3} \text{trace} \left[\frac{\partial \mathbf{I_{sys}}}{\partial q_{i_n}}\right] + \frac{3\mu_e}{2R_{cm}^3} \vec{\ell}^T \left[\frac{\partial \mathbf{I_{sys}}}{\partial q_{i_n}}\right] \vec{\ell}; \\
\frac{\partial U_g}{\partial q_{i,j_p}} &= -\frac{\mu_e}{2R_{cm}^3} \text{trace} \left[\frac{\partial \mathbf{I_{sys}}}{\partial q_{i,j_p}}\right] + \frac{3\mu_e}{2R_{cm}^3} \vec{\ell}^T \left[\frac{\partial \mathbf{I_{sys}}}{\partial q_{i,j_p}}\right] \vec{\ell};
\end{aligned} \tag{II-9}$$

where:

$$\begin{aligned}
i &= 1, \ldots, N; \qquad j = 1, \ldots, N_i; \\
m &= 1, \ldots, Nm_c; \quad n = 1, \ldots, Nm_i; \\
p &= 1, \ldots, Nm_{i,j}.
\end{aligned}$$

The contribution of the strain energy to the equations of motion can easily be determined by differentiating the strain energy expression, given in equation (2.46), with respect to the appropriate flexibility generalized coordinates. There is, of course, no strain energy contribution to the equations governing the librational or joint degrees of freedom. For the equations governing the flexibility generalized coordinates of the central body, the contribution is given by:

$$\frac{\partial U_e}{\partial q_{c_m}} = \left\{ \begin{array}{ll} \frac{\partial U_e}{\partial P_c^a} & \text{for odd } m \left(a = \frac{m+1}{2}\right) \\ \frac{\partial U_e}{\partial Q_c^a} & \text{for even } m \left(a = \frac{m}{2}\right) \end{array} \right\}; \tag{II-10}$$

where:

$$\frac{\partial U_e}{\partial P_c^a} = \int_{l_c} \left[E_c I_{czz} \left(\sum_{\ell=1}^{Mm_c} P_c^\ell(t) \frac{d^2\psi_{cy}^\ell}{dx_c^2} \right) \left(\frac{d^2\psi_{cy}^a}{dx_c^2} \right) \right] dx_c;$$

$$\frac{\partial U_e}{\partial Q_c^a} = \int_{l_c} \left[E_c I_{cyy} \left(\sum_{\ell=1}^{Mm_c} Q_c^\ell(t) \frac{d^2\psi_{cz}^\ell}{dx_c^2} \right) \left(\frac{d^2\psi_{cz}^a}{dx_c^2} \right) \right] dx_c; \qquad \text{(II-11)}$$

and:

$$m = 1, \ldots, Nm_c; \quad a = 1, \ldots, Mm_c.$$

Implicit in the above equations is the "matching" of the generic flexibility generalized coordinates q_{c_m} with the beam flexibility generalized coordinates P_c^ℓ (for the y direction), and Q_c^ℓ (for the z direction). To make this more clear, the relationship between the two is given below,

$$\left\{ \begin{array}{c} q_{c_1} \\ q_{c_2} \\ q_{c_3} \\ q_{c_4} \\ \cdot \\ \cdot \\ \cdot \\ q_{c_{Nm_c-1}} \\ q_{c_{Nmc}} \end{array} \right\} = \left\{ \begin{array}{c} P_c^1 \\ Q_c^1 \\ P_c^2 \\ Q_c^2 \\ \cdot \\ \cdot \\ \cdot \\ P_c^{Mm_c} \\ Q_c^{Mm_c} \end{array} \right\}. \qquad \text{(II-12)}$$

The contribution of the strain energy to the equations governing the elastic degrees of freedom of the beam–type B_i bodies is:

$$\frac{\partial U_e}{\partial q_{i_n}} = \left\{ \begin{array}{ll} \frac{\partial U_e}{\partial P_i^b} & \text{for odd } n \left(b = \frac{n+1}{2} \right) \\ \frac{\partial U_e}{\partial Q_i^b} & \text{for even } n \left(b = \frac{n}{2} \right) \end{array} \right\}; \qquad \text{(II-13)}$$

where:

$$\frac{\partial U_e}{\partial P_i^b} = \int_{l_i} \left[E_i I_{i_{zz}} \left(\sum_{\ell=1}^{Mm_i} P_i^\ell(t) \frac{d^2\psi_{i_y}^\ell}{dx_i^2} \right) \left(\frac{d^2\psi_{i_y}^b}{dx_i^2} \right) \right] dx_i;$$

$$\frac{\partial U_e}{\partial Q_i^b} = \int_{l_i} \left[E_i I_{i_{yy}} \left(\sum_{\ell=1}^{Mm_i} Q_i^\ell(t) \frac{d^2\psi_{i_z}^\ell}{dx_i^2} \right) \left(\frac{d^2\psi_{i_z}^b}{dx_i^2} \right) \right] dx_i; \qquad \text{(II-14)}$$

and:

$$i = 1, \ldots, N_b; \quad n = 1, \ldots, Nm_i; \quad b = 1, \ldots, Mm_i.$$

The contribution to the equations governing the elastic degrees of freedom of the plate–type B_i bodies is,

$$\begin{aligned}
\frac{\partial U_e}{\partial q_{i_n}} =& \frac{\partial U_e}{\partial H_i^{u,v}} \\
=& D_i \int_{w_i} \int_{l_i} \left[\left(\sum_{s=1}^{m_i} \sum_{t=1}^{n_i} H_i^{s,t}(t) \frac{d^2\phi_i^s}{dx_i^2} \psi_i^t(y_i) \right) \left(\frac{d^2\phi_i^u}{dx_i^2} \psi_i^v(y_i) \right) \right. \\
&+ \nu_i \left(\sum_{s=1}^{m_i} \sum_{t=1}^{n_i} H_i^{s,t}(t) \frac{d^2\phi_i^s}{dx_i^2} \psi_i^t(y_i) \right) \left(\phi_i^u(x_i) \frac{d^2\psi_i^v}{dy_i^2} \right) \\
&+ \nu_i \left(\sum_{s=1}^{m_i} \sum_{t=1}^{n_i} H_i^{s,t}(t) \phi_i^s(x_i) \frac{d^2\psi_i^t}{dy_i^2} \right) \left(\frac{d^2\phi_i^u}{dx_i^2} \psi_i^v(y_i) \right) \\
&+ 2(1-\nu_i) \left(\sum_{s=1}^{m_i} \sum_{t=1}^{n_i} H_i^{s,t}(t) \frac{d\phi_i^s}{dx_i} \frac{d\psi_i^t}{dy_i} \right) \left(\frac{d\phi_i^u}{dx_i} \frac{d\psi_i^v}{dy_i} \right) \\
&\left. + \left(\sum_{s=1}^{m_i} \sum_{t=1}^{n_i} H_i^{s,t}(t) \phi_i^s(x_i) \frac{d^2\psi_i^t}{dy_i^2} \right) \left(\phi_i^u(x_i) \frac{d^2\psi_i^v}{dy_i^2} \right) \right] dx_i \, dy_i, \qquad \text{(II-15)}
\end{aligned}$$

where:

$$i = N_b + 1, \ldots, N; \quad u = 1, \ldots, m_i; \quad v = 1, \ldots, n_i; \quad n = 1, \ldots, Nm_i.$$

The ordering of the generalized coordinates for the plate-type B_i bodies (i.e. $i = N_B + 1, \ldots, N$) is slightly more complicated. The m_i shape functions are used along

the x-direction and n_i functions along the y-direction. So, a total of $m_i n_i$ generalized coordinates are required for representation of the body B_i. The following convention is adopted

$$\left\{\begin{array}{c} q_{i_1} \\ q_{i_2} \\ \cdot \\ \cdot \\ \cdot \\ q_{i_{(m_i)}} \\ q_{i_{(m_i+1)}} \\ \cdot \\ \cdot \\ \cdot \\ q_{i_{(2m_i)}} \\ \cdot \\ \cdot \\ \cdot \\ q_{i_{((n_i-1)m_i+1)}} \\ \cdot \\ \cdot \\ \cdot \\ q_{i_{(m_i n_i)}} \end{array}\right\} = \left\{\begin{array}{c} H_i^{1,1} \\ H_i^{2,1} \\ \cdot \\ \cdot \\ \cdot \\ H_i^{m_i,1} \\ H_i^{1,2} \\ \cdot \\ \cdot \\ \cdot \\ H_i^{m_i,2} \\ \cdot \\ \cdot \\ \cdot \\ H_i^{1,n_i} \\ \cdot \\ \cdot \\ \cdot \\ H_i^{m_i,n_i} \end{array}\right\}.$$

Contribution of the strain energy to the equations governing the elastic degrees of freedom of the beam–type $B_{i,j}$ bodies is given by:

$$\frac{\partial U_e}{\partial q_{i,j_p}} = \left\{\begin{array}{ll} \frac{\partial U_e}{\partial P_{i,j}^c} & \text{for odd } p \left(c = \frac{p+1}{2}\right) \\ \frac{\partial U_e}{\partial Q_{i,j}^c} & \text{for even } p \left(c = \frac{p}{2}\right) \end{array}\right\}; \qquad \text{(II–16)}$$

where:

$$\frac{\partial U_e}{\partial P_{i,j}^c} = \int_{l_{i,j}} \left[E_{i,j} I_{i,j_{zz}} \left(\sum_{\ell=1}^{M m_{i,j}} P_{i,j}^{\ell}(t) \frac{d^2 \psi_{i,j_y}^{\ell}}{dx_{i,j}^2} \right) \left(\frac{d^2 \psi_{i,j_y}^{c}}{dx_{i,j}^2} \right) \right] dx_{i,j};$$

$$\frac{\partial U_e}{\partial Q^c_{i,j}} = \int_{l_{i,j}} \left[E_{i,j} I_{i,jyy} \left(\sum_{\ell=1}^{M m_{i,j}} Q^{\ell}_{i,j}(t) \frac{d^2 \psi^{\ell}_{i,jz}}{dx^2_{i,j}} \right) \left(\frac{d^2 \psi^{c}_{i,jz}}{dx^2_{i,j}} \right) \right] dx_{i,j};$$

(II−17)

and:

$$i = 1, \ldots, N_b; \quad j = 1, \ldots, N_{b_i}; \quad p = 1, \ldots, N m_{i,j}; \quad c = 1, \ldots, M m_{i,j}.$$

Similarly, corresponding contribution to the equations governing the plate–type $B_{i,j}$ bodies is

$$\begin{aligned}
\frac{\partial U_e}{\partial q_{i,jp}} =& \frac{\partial U_e}{\partial H^{u,v}_{i,j}} \\
=& D_{i,j} \int_{w_{i,j}} \int_{l_{i,j}} \left[\left(\sum_{s=1}^{m_{i,j}} \sum_{t=1}^{n_{i,j}} H^{s,t}_{i,j}(t) \frac{d^2 \phi^{s}_{i,j}}{dx^2_{i,j}} \psi^{t}_{i,j}(y_{i,j}) \right) \left(\frac{d^2 \phi^{u}_{i,j}}{dx^2_{i,j}} \psi^{v}_{i,j}(y_{i,j}) \right) \right. \\
&+ \nu_{i,j} \left(\sum_{s=1}^{m_{i,j}} \sum_{t=1}^{n_{i,j}} H^{s,t}_{i,j}(t) \frac{d^2 \phi^{s}_{i,j}}{dx^2_{i,j}} \psi^{t}_{i,j}(y_{i,j}) \right) \left(\phi^{u}_{i,j}(x_{i,j}) \frac{d^2 \psi^{v}_{i,j}}{dy^2_{i,j}} \right) \\
&+ \nu_{i,j} \left(\sum_{s=1}^{m_{i,j}} \sum_{t=1}^{n_{i,j}} H^{s,t}_{i,j}(t) \phi^{s}_{i,j}(x_{i,j}) \frac{d^2 \psi^{t}_{i,j}}{dy^2_{i,j}} \right) \left(\frac{d^2 \phi^{u}_{i,j}}{dx^2_{i,j}} \psi^{v}_{i,j}(y_{i,j}) \right) \\
&+ 2(1 - \nu_{i,j}) \left(\sum_{s=1}^{m_{i,j}} \sum_{t=1}^{n_{i,j}} H^{s,t}_{i,j}(t) \frac{d\phi^{s}_{i,j}}{dx_{i,j}} \frac{d\psi^{t}_{i,j}}{dy_{i,j}} \right) \left(\frac{d\phi^{u}_{i,j}}{dx_{i,j}} \frac{d\psi^{v}_{i,j}}{dy_{i,j}} \right) \\
&+ \left. \left(\sum_{s=1}^{m_{i,j}} \sum_{t=1}^{n_{i,j}} H^{s,t}_{i,j}(t) \phi^{s}_{i,j}(x_{i,j}) \frac{d^2 \psi^{t}_{i,j}}{dy^2_{i,j}} \right) \left(\phi^{u}_{i,j}(x_{i,j}) \frac{d^2 \psi^{v}_{i,j}}{dy^2_{i,j}} \right) \right] dx_{i,j}\, dy_{i,j},
\end{aligned}$$

(II−18)

where:

$$i = 1, \ldots, N_b; \quad j = N_{b_i} + 1, \ldots, N_i; \quad u = 1, \ldots, m_{i,j};$$

$$v = 1, \ldots, n_{i,j}; \quad p = 1, \ldots, N m_{i,j}.$$

Appendix III: Derivatives of $\vec{\omega}$ and $\vec{\ell}$

The terms related to the librational angular velocity $\vec{\omega}$ are given by:

$$\begin{aligned}\dot{\vec{\omega}} =&\big[(\ddot{\psi}+\ddot{\theta})\cos\phi\cos\lambda-(\dot{\psi}+\dot{\theta})\dot{\phi}\sin\phi\cos\lambda\\&-(\dot{\psi}+\dot{\theta})\dot{\lambda}\cos\phi\sin\lambda-\ddot{\phi}\sin\lambda-\dot{\phi}\dot{\lambda}\cos\lambda\big]\hat{i}_p\\&+\big[-(\ddot{\psi}+\ddot{\theta})\sin\phi-(\dot{\psi}+\dot{\theta})\dot{\phi}\cos\phi+\ddot{\lambda}\big]\hat{j}_p\\&+\big[(\ddot{\psi}+\ddot{\theta})\cos\phi\sin\lambda-(\dot{\psi}+\dot{\theta})\dot{\phi}\sin\phi\sin\lambda\\&+(\dot{\psi}+\dot{\theta})\dot{\lambda}\cos\phi\cos\lambda+\ddot{\phi}\cos\lambda-\dot{\phi}\dot{\lambda}\sin\lambda\big]\hat{k}_p;\end{aligned}\qquad\text{(III–1)}$$

$$\frac{\partial\vec{\omega}}{\partial\dot{\psi}}=\big[\cos\phi\cos\lambda\big]\hat{i}_p-\big[\sin\phi\big]\hat{j}_p+\big[\cos\phi\sin\lambda\big]\hat{k}_p;\qquad\text{(III–2)}$$

$$\begin{aligned}\frac{d}{dt}\left(\frac{\partial\vec{\omega}}{\partial\dot{\psi}}\right)=&\big[-\dot{\phi}\sin\phi\cos\lambda-\dot{\lambda}\cos\phi\sin\lambda\big]\hat{i}_p-\big[\dot{\phi}\cos\phi\big]\hat{j}_p\\&+[-\dot{\phi}\sin\phi\sin\lambda+\dot{\lambda}\cos\phi\cos\lambda\big]\hat{k}_p;\end{aligned}\qquad\text{(III–3)}$$

$$\frac{\partial\vec{\omega}}{\partial\psi}=0;\qquad\text{(III–4)}$$

$$\frac{\partial\vec{\omega}}{\partial\dot{\phi}}=-\big[\sin\lambda\big]\hat{i}_p+\big[\cos\lambda\big]\hat{k}_p;\qquad\text{(III–5)}$$

$$\frac{d}{dt}\left(\frac{\partial\vec{\omega}}{\partial\dot{\phi}}\right)=-\big[\dot{\lambda}\cos\lambda\big]\hat{i}_p-\big[\dot{\lambda}\sin\lambda\big]\hat{k}_p;\qquad\text{(III–6)}$$

$$\begin{aligned}\frac{\partial\vec{\omega}}{\partial\phi}=&-\big[(\dot{\psi}+\dot{\theta})\sin\phi\cos\lambda\big]\hat{i}_p-\big[(\dot{\psi}+\dot{\theta})\cos\phi\big]\hat{j}_p\\&-\big[(\dot{\psi}+\dot{\theta})\sin\phi\sin\lambda\big]\hat{k}_p;\end{aligned}\qquad\text{(III–7)}$$

$$\frac{\partial \vec{\omega}}{\partial \dot{\lambda}} = \hat{j}_p; \tag{III-8}$$

$$\frac{d}{dt}\left(\frac{\partial \vec{\omega}}{\partial \dot{\lambda}}\right) = 0; \tag{III-9}$$

$$\begin{aligned}\frac{\partial \vec{\omega}}{\partial \lambda} = &- \left[(\dot{\psi} + \dot{\theta})\cos\phi \sin\lambda + \dot{\phi}\cos\lambda\right]\hat{i}_p \\ &+ \left[(\dot{\psi} + \dot{\theta})\cos\phi\cos\lambda - \dot{\phi}\sin\lambda\right]\hat{k}_p.\end{aligned} \tag{III-10}$$

The direction cosine vector and its derivatives with respect to the Euler angles are:

$$\begin{aligned}\vec{\ell} = &(\cos\psi\sin\phi\cos\lambda + \sin\psi\sin\lambda)\hat{i}_p + \cos\psi\cos\phi\hat{j}_p \\ &+ (\cos\psi\sin\phi\sin\lambda - \sin\psi\cos\lambda)\hat{k}_p;\end{aligned} \tag{III-11}$$

$$\begin{aligned}\frac{\partial \vec{\ell}}{\partial \psi} = &(-\sin\psi\sin\phi\cos\lambda + \cos\psi\sin\lambda)\hat{i}_p - \sin\psi\cos\phi\hat{j}_p \\ &- (\sin\psi\sin\phi\sin\lambda + \cos\psi\cos\lambda)\hat{k}_p;\end{aligned} \tag{III-12}$$

$$\frac{\partial \vec{\ell}}{\partial \phi} = \cos\psi\cos\phi\cos\lambda\hat{i}_p - \cos\psi\sin\phi\hat{j}_p + \cos\psi\cos\phi\sin\lambda\hat{k}_p; \tag{III-13}$$

$$\begin{aligned}\frac{\partial \vec{\ell}}{\partial \lambda} = &(-\cos\psi\sin\phi\sin\lambda + \sin\psi\cos\lambda)\hat{i}_p \\ &+ (\cos\psi\sin\phi\cos\lambda + \sin\psi\sin\lambda)\hat{k}_p.\end{aligned} \tag{III-14}$$

Appendix IV: Time Derivatives of $\mathbf{I_{sys}}$ and $\vec{H}$

The time rate of change of the moment of inertia matrix $\dot{\mathbf{I}}_{\mathbf{sys}}$ can also be written as the sum of the different contributions,

$$\dot{\mathbf{I}}_{\mathbf{sys}} = \dot{\mathbf{I}}_{\mathbf{cm}} + \dot{\mathbf{I}}_{\mathbf{r}} + \dot{\mathbf{I}}_{\mathbf{h}} + \dot{\mathbf{I}}_{\mathbf{v}} + \dot{\mathbf{I}}_{\mathbf{h,r}} + \dot{\mathbf{I}}_{\mathbf{h,v}} + \dot{\mathbf{I}}_{\mathbf{r,v}},$$

where:

$$\dot{\mathbf{I}}_{\mathbf{cm}} = -M\left[2\dot{\vec{C}}_{cm}{}^{T}\vec{C}_{cm}\mathbf{E} - \dot{\vec{C}}_{cm}\vec{C}_{cm}{}^{T} - \vec{C}_{cm}\dot{\vec{C}}_{cm}{}^{T}\right];$$

$$\dot{\mathbf{I}}_{\mathbf{r}} = \sum_{i=1}^{N}\left[-\dot{\mathbf{C}}_{\mathbf{i}}^{\mathbf{c}}\mathbf{P}_{\mathbf{i}}^{\mathbf{2}}\mathbf{C}_{\mathbf{i}}^{\mathbf{c}T} - \mathbf{C}_{\mathbf{i}}^{\mathbf{c}}\mathbf{P}_{\mathbf{i}}^{\mathbf{2}}\dot{\mathbf{C}}_{\mathbf{i}}^{\mathbf{c}T} + \sum_{j=1}^{N_i}\left[-\dot{\mathbf{C}}_{\mathbf{i}}^{\mathbf{c}}\mathbf{C}_{\mathbf{i,j}}^{\mathbf{i}}\mathbf{P}_{\mathbf{i,j}}^{\mathbf{2}}\mathbf{C}_{\mathbf{i,j}}^{\mathbf{i}}{}^{T}\mathbf{C}_{\mathbf{i}}^{\mathbf{c}T}\right.\right.$$
$$\left.\left.-\mathbf{C}_{\mathbf{i}}^{\mathbf{c}}\dot{\mathbf{C}}_{\mathbf{i,j}}^{\mathbf{i}}\mathbf{P}_{\mathbf{i,j}}^{\mathbf{2}}\mathbf{C}_{\mathbf{i,j}}^{\mathbf{i}}{}^{T}\mathbf{C}_{\mathbf{i}}^{\mathbf{c}T} - \mathbf{C}_{\mathbf{i}}^{\mathbf{c}}\mathbf{C}_{\mathbf{i,j}}^{\mathbf{i}}\mathbf{P}_{\mathbf{i,j}}^{\mathbf{2}}\dot{\mathbf{C}}_{\mathbf{i,j}}^{\mathbf{i}}{}^{T}\mathbf{C}_{\mathbf{i}}^{\mathbf{c}T} - \mathbf{C}_{\mathbf{i}}^{\mathbf{c}}\mathbf{C}_{\mathbf{i,j}}^{\mathbf{i}}\mathbf{P}_{\mathbf{i,j}}^{\mathbf{2}}\mathbf{C}_{\mathbf{i,j}}^{\mathbf{i}}{}^{T}\dot{\mathbf{C}}_{\mathbf{i}}^{\mathbf{c}T}\right]\right],$$

$$\text{with}\quad \mathbf{P}_{\mathbf{i}}^{\mathbf{2}} = \int_{m_i}\vec{\rho}_i\vec{\rho}_i{}^{T}\,dm_i \quad\text{and}\quad \mathbf{P}_{\mathbf{i,j}}^{\mathbf{2}} = \int_{m_{i,j}}\vec{\rho}_{i,j}\vec{\rho}_{i,j}{}^{T}\,dm_{i,j};$$

$$\dot{\mathbf{I}}_{\mathbf{h}} = \sum_{i=1}^{N}\left[\left[2\vec{d}_i{}^{T}\dot{\vec{d}}_i\mathbf{E} - \dot{\vec{d}}_i\vec{d}_i{}^{T} - \vec{d}_i\dot{\vec{d}}_i{}^{T}\right]m_i + \sum_{j=1}^{N_i}\left[\left[2\left[\vec{d}_i{}^{T}\dot{\vec{d}}_i + \dot{\vec{d}}_{i,j}{}^{T}\mathbf{C}_{\mathbf{i}}^{\mathbf{c}T}\vec{d}_i\right.\right.\right.\right.$$
$$\left.+\vec{d}_{i,j}{}^{T}\dot{\mathbf{C}}_{\mathbf{i}}^{\mathbf{c}T}\vec{d}_i + \vec{d}_{i,j}{}^{T}\mathbf{C}_{\mathbf{i}}^{\mathbf{c}T}\dot{\vec{d}}_i + \vec{d}_{i,j}{}^{T}\dot{\vec{d}}_{i,j}\right]\mathbf{E} - \left[\dot{\vec{d}}_i\vec{d}_i{}^{T} + \vec{d}_i\dot{\vec{d}}_i{}^{T}\right.$$
$$\left.+\dot{\vec{d}}_i\vec{d}_{i,j}{}^{T}\mathbf{C}_{\mathbf{i}}^{\mathbf{c}T} + \vec{d}_i\dot{\vec{d}}_{i,j}{}^{T}\mathbf{C}_{\mathbf{i}}^{\mathbf{c}T} + \vec{d}_i\vec{d}_{i,j}{}^{T}\dot{\mathbf{C}}_{\mathbf{i}}^{\mathbf{c}T} + \dot{\mathbf{C}}_{\mathbf{i}}^{\mathbf{c}}\vec{d}_{i,j}\vec{d}_i{}^{T}\right.$$
$$\left.+\mathbf{C}_{\mathbf{i}}^{\mathbf{c}}\dot{\vec{d}}_{i,j}\vec{d}_i{}^{T} + \mathbf{C}_{\mathbf{i}}^{\mathbf{c}}\vec{d}_{i,j}\dot{\vec{d}}_i{}^{T} + \dot{\mathbf{C}}_{\mathbf{i}}^{\mathbf{c}}\vec{d}_{i,j}\vec{d}_{i,j}{}^{T}\mathbf{C}_{\mathbf{i}}^{\mathbf{c}T} + \mathbf{C}_{\mathbf{i}}^{\mathbf{c}}\dot{\vec{d}}_{i,j}\vec{d}_{i,j}{}^{T}\mathbf{C}_{\mathbf{i}}^{\mathbf{c}T}\right.$$
$$\left.\left.+\mathbf{C}_{\mathbf{i}}^{\mathbf{c}}\vec{d}_{i,j}\dot{\vec{d}}_{i,j}{}^{T}\mathbf{C}_{\mathbf{i}}^{\mathbf{c}T} + \mathbf{C}_{\mathbf{i}}^{\mathbf{c}}\vec{d}_{i,j}\vec{d}_{i,j}{}^{T}\dot{\mathbf{C}}_{\mathbf{i}}^{\mathbf{c}T}\right]\right]m_{i,j}\right]\right];$$

$$\dot{\mathbf{I}}_{\mathbf{v}} = \int_{m_c}\left[2\vec{\delta}_c{}^{T}\dot{\vec{\delta}}_c\mathbf{E} - \dot{\vec{\delta}}_c\vec{\delta}_c{}^{T} - \vec{\delta}_c\dot{\vec{\delta}}_c{}^{T}\right]dm_c + \sum_{i=1}^{N}\left[\int_{m_i}2\vec{\delta}_i{}^{T}\dot{\vec{\delta}}_i\,dm_i\mathbf{E}\right.$$

$$
\begin{aligned}
&-\dot{\mathbf{C}}_{\mathbf{i}}^{\mathbf{c}}\mathbf{D}_{\mathbf{i}}^{\mathbf{2}}\mathbf{C}_{\mathbf{i}}^{\mathbf{c}^T}-\mathbf{C}_{\mathbf{i}}^{\mathbf{c}}\left\{\int_{m_i}\dot{\vec{\delta}}_i\vec{\delta}_i{}^T\,dm_i\right\}\mathbf{C}_{\mathbf{i}}^{\mathbf{c}^T}-\mathbf{C}_{\mathbf{i}}^{\mathbf{c}}\left\{\int_{m_i}\vec{\delta}_i\dot{\vec{\delta}}_i{}^T\,dm_i\right\}\mathbf{C}_{\mathbf{i}}^{\mathbf{c}^T}\\
&-\mathbf{C}_{\mathbf{i}}^{\mathbf{c}}\mathbf{D}_{\mathbf{i}}^{\mathbf{2}}\dot{\mathbf{C}}_{\mathbf{i}}^{\mathbf{c}^T}+\sum_{j=1}^{N_i}\left[\int_{m_{i,j}}2\vec{\delta}_{i,j}{}^T\dot{\vec{\delta}}_{i,j}\,dm_{i,j}\mathbf{E}-\dot{\mathbf{C}}_{\mathbf{i}}^{\mathbf{c}}\mathbf{C}_{\mathbf{i,j}}^{\mathbf{i}}\mathbf{D}_{\mathbf{i,j}}^{\mathbf{2}}\mathbf{C}_{\mathbf{i,j}}^{\mathbf{i}}{}^T\mathbf{C}_{\mathbf{i}}^{\mathbf{c}^T}\right.\\
&-\mathbf{C}_{\mathbf{i}}^{\mathbf{c}}\dot{\mathbf{C}}_{\mathbf{i,j}}^{\mathbf{i}}\mathbf{D}_{\mathbf{i,j}}^{\mathbf{2}}\mathbf{C}_{\mathbf{i,j}}^{\mathbf{i}}{}^T\mathbf{C}_{\mathbf{i}}^{\mathbf{c}^T}-\mathbf{C}_{\mathbf{i}}^{\mathbf{c}}\mathbf{C}_{\mathbf{i,j}}^{\mathbf{i}}\left\{\int_{m_{i,j}}\dot{\vec{\delta}}_{i,j}\vec{\delta}_{i,j}{}^T\,dm_{i,j}\right\}\mathbf{C}_{\mathbf{i,j}}^{\mathbf{i}}{}^T\mathbf{C}_{\mathbf{i}}^{\mathbf{c}^T}\\
&-\mathbf{C}_{\mathbf{i}}^{\mathbf{c}}\mathbf{C}_{\mathbf{i,j}}^{\mathbf{i}}\left\{\int_{m_{i,j}}\vec{\delta}_{i,j}\dot{\vec{\delta}}_{i,j}{}^T\,dm_{i,j}\right\}\mathbf{C}_{\mathbf{i,j}}^{\mathbf{i}}{}^T\mathbf{C}_{\mathbf{i}}^{\mathbf{c}^T}-\mathbf{C}_{\mathbf{i}}^{\mathbf{c}}\mathbf{C}_{\mathbf{i,j}}^{\mathbf{i}}\mathbf{D}_{\mathbf{i,j}}^{\mathbf{2}}\dot{\mathbf{C}}_{\mathbf{i,j}}^{\mathbf{i}}{}^T\mathbf{C}_{\mathbf{i}}^{\mathbf{c}^T}\\
&\left.-\mathbf{C}_{\mathbf{i}}^{\mathbf{c}}\mathbf{C}_{\mathbf{i,j}}^{\mathbf{i}}\mathbf{D}_{\mathbf{i,j}}^{\mathbf{2}}\mathbf{C}_{\mathbf{i,j}}^{\mathbf{i}}{}^T\dot{\mathbf{C}}_{\mathbf{i}}^{\mathbf{c}^T}\right]\Bigg],
\end{aligned}
$$

$$
\text{with}\quad \mathbf{D}_{\mathbf{i}}^{\mathbf{2}}=\int_{m_i}\vec{\delta}_i\vec{\delta}_i{}^T\,dm_i\quad\text{and}\quad \mathbf{D}_{\mathbf{i,j}}^{\mathbf{2}}=\int_{m_{i,j}}\vec{\delta}_{i,j}\vec{\delta}_{i,j}{}^T\,dm_{i,j};
$$

$$
\begin{aligned}
\dot{\mathbf{I}}_{\mathbf{h,r}}=\sum_{i=1}^{N}\Bigg[&2\left[\dot{\vec{d}}_i{}^T\mathbf{C}_{\mathbf{i}}^{\mathbf{c}}\vec{P}_i+\vec{d}_i{}^T\dot{\mathbf{C}}_{\mathbf{i}}^{\mathbf{c}}\vec{P}_i\right]\mathbf{E}-\dot{\vec{d}}_i\vec{P}_i{}^T\mathbf{C}_{\mathbf{i}}^{\mathbf{c}^T}-\vec{d}_i\vec{P}_i{}^T\dot{\mathbf{C}}_{\mathbf{i}}^{\mathbf{c}^T}\\
&-\dot{\mathbf{C}}_{\mathbf{i}}^{\mathbf{c}}\vec{P}_i\vec{d}_i{}^T-\mathbf{C}_{\mathbf{i}}^{\mathbf{c}}\vec{P}_i\dot{\vec{d}}_i{}^T+\sum_{j=1}^{N_i}\Bigg[2\Big[\dot{\vec{d}}_i{}^T\mathbf{C}_{\mathbf{i}}^{\mathbf{c}}\mathbf{C}_{\mathbf{i,j}}^{\mathbf{i}}\vec{P}_{i,j}+\vec{d}_i{}^T\dot{\mathbf{C}}_{\mathbf{i}}^{\mathbf{c}}\mathbf{C}_{\mathbf{i,j}}^{\mathbf{i}}\vec{P}_{i,j}\\
&+\vec{d}_i{}^T\mathbf{C}_{\mathbf{i}}^{\mathbf{c}}\dot{\mathbf{C}}_{\mathbf{i,j}}^{\mathbf{i}}\vec{P}_{i,j}+\dot{\vec{d}}_{i,j}{}^T\mathbf{C}_{\mathbf{i,j}}^{\mathbf{i}}\vec{P}_{i,j}+\vec{d}_{i,j}{}^T\dot{\mathbf{C}}_{\mathbf{i,j}}^{\mathbf{i}}\vec{P}_{i,j}\Big]\mathbf{E}\\
&-\Big[\dot{\vec{d}}_i\vec{P}_{i,j}{}^T\mathbf{C}_{\mathbf{i,j}}^{\mathbf{i}}{}^T\mathbf{C}_{\mathbf{i}}^{\mathbf{c}^T}+\vec{d}_i\vec{P}_{i,j}{}^T\dot{\mathbf{C}}_{\mathbf{i,j}}^{\mathbf{i}}{}^T\mathbf{C}_{\mathbf{i}}^{\mathbf{c}^T}+\vec{d}_i\vec{P}_{i,j}{}^T\mathbf{C}_{\mathbf{i,j}}^{\mathbf{i}}{}^T\dot{\mathbf{C}}_{\mathbf{i}}^{\mathbf{c}^T}\\
&+\dot{\mathbf{C}}_{\mathbf{i}}^{\mathbf{c}}\vec{d}_{i,j}\vec{P}_{i,j}{}^T\mathbf{C}_{\mathbf{i,j}}^{\mathbf{i}}{}^T\mathbf{C}_{\mathbf{i}}^{\mathbf{c}^T}+\mathbf{C}_{\mathbf{i}}^{\mathbf{c}}\dot{\vec{d}}_{i,j}\vec{P}_{i,j}{}^T\mathbf{C}_{\mathbf{i,j}}^{\mathbf{i}}{}^T\mathbf{C}_{\mathbf{i}}^{\mathbf{c}^T}+\mathbf{C}_{\mathbf{i}}^{\mathbf{c}}\vec{d}_{i,j}\vec{P}_{i,j}{}^T\dot{\mathbf{C}}_{\mathbf{i,j}}^{\mathbf{i}}{}^T\mathbf{C}_{\mathbf{i}}^{\mathbf{c}^T}\\
&+\mathbf{C}_{\mathbf{i}}^{\mathbf{c}}\vec{d}_{i,j}\vec{P}_{i,j}{}^T\mathbf{C}_{\mathbf{i,j}}^{\mathbf{i}}{}^T\dot{\mathbf{C}}_{\mathbf{i}}^{\mathbf{c}^T}+\dot{\mathbf{C}}_{\mathbf{i}}^{\mathbf{c}}\mathbf{C}_{\mathbf{i,j}}^{\mathbf{i}}\vec{P}_{i,j}\vec{d}_i{}^T+\mathbf{C}_{\mathbf{i}}^{\mathbf{c}}\dot{\mathbf{C}}_{\mathbf{i,j}}^{\mathbf{i}}\vec{P}_{i,j}\vec{d}_i{}^T\\
&+\mathbf{C}_{\mathbf{i}}^{\mathbf{c}}\mathbf{C}_{\mathbf{i,j}}^{\mathbf{i}}\vec{P}_{i,j}\dot{\vec{d}}_i{}^T+\dot{\mathbf{C}}_{\mathbf{i}}^{\mathbf{c}}\mathbf{C}_{\mathbf{i,j}}^{\mathbf{i}}\vec{P}_{i,j}\vec{d}_{i,j}{}^T\mathbf{C}_{\mathbf{i}}^{\mathbf{c}^T}+\mathbf{C}_{\mathbf{i}}^{\mathbf{c}}\dot{\mathbf{C}}_{\mathbf{i,j}}^{\mathbf{i}}\vec{P}_{i,j}\vec{d}_{i,j}{}^T\mathbf{C}_{\mathbf{i}}^{\mathbf{c}^T}\\
&+\mathbf{C}_{\mathbf{i}}^{\mathbf{c}}\mathbf{C}_{\mathbf{i,j}}^{\mathbf{i}}\vec{P}_{i,j}\dot{\vec{d}}_{i,j}{}^T\mathbf{C}_{\mathbf{i}}^{\mathbf{c}^T}+\mathbf{C}_{\mathbf{i}}^{\mathbf{c}}\mathbf{C}_{\mathbf{i,j}}^{\mathbf{i}}\vec{P}_{i,j}\vec{d}_{i,j}{}^T\dot{\mathbf{C}}_{\mathbf{i}}^{\mathbf{c}^T}\Big]\Bigg]\Bigg],
\end{aligned}
$$

$$
\text{with}\quad \vec{P}_i=\int_{m_i}\vec{\rho}_i\,dm_i\quad\text{and}\quad \vec{P}_{i,j}=\int_{m_{i,j}}\vec{\rho}_{i,j}\,dm_{i,j};
$$

$$
\begin{aligned}
\dot{\mathbf{I}}_{\mathbf{h,v}} = \sum_{i=1}^{N} \Bigg[& 2\Big[\dot{\vec{d}}_i{}^T \mathbf{C}_{\mathbf{i}}^{\mathbf{c}} \vec{D}_i + \vec{d}_i{}^T \dot{\mathbf{C}}_{\mathbf{i}}^{\mathbf{c}} \vec{D}_i + \vec{d}_i{}^T \mathbf{C}_{\mathbf{i}}^{\mathbf{c}} \dot{\vec{D}}_i\Big]\mathbf{E} - \dot{\vec{d}}_i \vec{D}_i{}^T \mathbf{C}_{\mathbf{i}}^{\mathbf{c}T} \\
& - \vec{d}_i \dot{\vec{D}}_i{}^T \mathbf{C}_{\mathbf{i}}^{\mathbf{c}T} - \vec{d}_i \vec{D}_i{}^T \dot{\mathbf{C}}_{\mathbf{i}}^{\mathbf{c}T} - \dot{\mathbf{C}}_{\mathbf{i}}^{\mathbf{c}} \vec{D}_i \vec{d}_i{}^T - \mathbf{C}_{\mathbf{i}}^{\mathbf{c}} \dot{\vec{D}}_i \vec{d}_i{}^T - \mathbf{C}_{\mathbf{i}}^{\mathbf{c}} \vec{D}_i \dot{\vec{d}}_i{}^T \\
& + \sum_{j=1}^{N_i} \Bigg[2\Big[\dot{\vec{d}}_i{}^T \mathbf{C}_{\mathbf{i}}^{\mathbf{c}} \mathbf{C}_{\mathbf{i,j}}^{\mathbf{i}} \vec{D}_{i,j} + \vec{d}_i{}^T \dot{\mathbf{C}}_{\mathbf{i}}^{\mathbf{c}} \mathbf{C}_{\mathbf{i,j}}^{\mathbf{i}} \vec{D}_{i,j} + \vec{d}_i{}^T \mathbf{C}_{\mathbf{i}}^{\mathbf{c}} \dot{\mathbf{C}}_{\mathbf{i,j}}^{\mathbf{i}} \vec{D}_{i,j} \\
& + \vec{d}_i{}^T \mathbf{C}_{\mathbf{i}}^{\mathbf{c}} \mathbf{C}_{\mathbf{i,j}}^{\mathbf{i}} \dot{\vec{D}}_{i,j} + \dot{\vec{d}}_{i,j}{}^T \mathbf{C}_{\mathbf{i,j}}^{\mathbf{i}} \vec{D}_{i,j} + \vec{d}_{i,j}{}^T \dot{\mathbf{C}}_{\mathbf{i,j}}^{\mathbf{i}} \vec{D}_{i,j} + \vec{d}_{i,j}{}^T \mathbf{C}_{\mathbf{i,j}}^{\mathbf{i}} \dot{\vec{D}}_{i,j}\Big]\mathbf{E} \\
& - \Big[\dot{\vec{d}}_i \vec{D}_{i,j}{}^T \mathbf{C}_{\mathbf{i,j}}^{\mathbf{i}}{}^T \mathbf{C}_{\mathbf{i}}^{\mathbf{c}T} + \vec{d}_i \dot{\vec{D}}_{i,j}{}^T \mathbf{C}_{\mathbf{i,j}}^{\mathbf{i}}{}^T \mathbf{C}_{\mathbf{i}}^{\mathbf{c}T} + \vec{d}_i \vec{D}_{i,j}{}^T \dot{\mathbf{C}}_{\mathbf{i,j}}^{\mathbf{i}}{}^T \mathbf{C}_{\mathbf{i}}^{\mathbf{c}T} \\
& + \vec{d}_i \vec{D}_{i,j}{}^T \mathbf{C}_{\mathbf{i,j}}^{\mathbf{i}}{}^T \dot{\mathbf{C}}_{\mathbf{i}}^{\mathbf{c}T} + \dot{\mathbf{C}}_{\mathbf{i}}^{\mathbf{c}} \vec{d}_{i,j} \vec{D}_{i,j}{}^T \mathbf{C}_{\mathbf{i,j}}^{\mathbf{i}}{}^T \mathbf{C}_{\mathbf{i}}^{\mathbf{c}T} + \mathbf{C}_{\mathbf{i}}^{\mathbf{c}} \dot{\vec{d}}_{i,j} \vec{D}_{i,j}{}^T \mathbf{C}_{\mathbf{i,j}}^{\mathbf{i}}{}^T \mathbf{C}_{\mathbf{i}}^{\mathbf{c}T} \\
& + \mathbf{C}_{\mathbf{i}}^{\mathbf{c}} \vec{d}_{i,j} \dot{\vec{D}}_{i,j}{}^T \mathbf{C}_{\mathbf{i,j}}^{\mathbf{i}}{}^T \mathbf{C}_{\mathbf{i}}^{\mathbf{c}T} + \mathbf{C}_{\mathbf{i}}^{\mathbf{c}} \vec{d}_{i,j} \vec{D}_{i,j}{}^T \dot{\mathbf{C}}_{\mathbf{i,j}}^{\mathbf{i}}{}^T \mathbf{C}_{\mathbf{i}}^{\mathbf{c}T} + \mathbf{C}_{\mathbf{i}}^{\mathbf{c}} \vec{d}_{i,j} \vec{D}_{i,j}{}^T \mathbf{C}_{\mathbf{i,j}}^{\mathbf{i}}{}^T \dot{\mathbf{C}}_{\mathbf{i}}^{\mathbf{c}T} \\
& + \dot{\mathbf{C}}_{\mathbf{i}}^{\mathbf{c}} \mathbf{C}_{\mathbf{i,j}}^{\mathbf{i}} \vec{D}_{i,j} \vec{d}_i{}^T + \mathbf{C}_{\mathbf{i}}^{\mathbf{c}} \dot{\mathbf{C}}_{\mathbf{i,j}}^{\mathbf{i}} \vec{D}_{i,j} \vec{d}_i{}^T + \mathbf{C}_{\mathbf{i}}^{\mathbf{c}} \mathbf{C}_{\mathbf{i,j}}^{\mathbf{i}} \dot{\vec{D}}_{i,j} \vec{d}_i{}^T \\
& + \mathbf{C}_{\mathbf{i}}^{\mathbf{c}} \mathbf{C}_{\mathbf{i,j}}^{\mathbf{i}} \vec{D}_{i,j} \dot{\vec{d}}_i{}^T + \dot{\mathbf{C}}_{\mathbf{i}}^{\mathbf{c}} \mathbf{C}_{\mathbf{i,j}}^{\mathbf{i}} \vec{D}_{i,j} \vec{d}_{i,j}{}^T \mathbf{C}_{\mathbf{i}}^{\mathbf{c}T} + \mathbf{C}_{\mathbf{i}}^{\mathbf{c}} \dot{\mathbf{C}}_{\mathbf{i,j}}^{\mathbf{i}} \vec{D}_{i,j} \vec{d}_{i,j}{}^T \mathbf{C}_{\mathbf{i}}^{\mathbf{c}T} \\
& + \mathbf{C}_{\mathbf{i}}^{\mathbf{c}} \mathbf{C}_{\mathbf{i,j}}^{\mathbf{i}} \dot{\vec{D}}_{i,j} \vec{d}_{i,j}{}^T \mathbf{C}_{\mathbf{i}}^{\mathbf{c}T} + \mathbf{C}_{\mathbf{i}}^{\mathbf{c}} \mathbf{C}_{\mathbf{i,j}}^{\mathbf{i}} \vec{D}_{i,j} \dot{\vec{d}}_{i,j}{}^T \mathbf{C}_{\mathbf{i}}^{\mathbf{c}T} + \mathbf{C}_{\mathbf{i}}^{\mathbf{c}} \mathbf{C}_{\mathbf{i,j}}^{\mathbf{i}} \vec{D}_{i,j} \vec{d}_{i,j}{}^T \dot{\mathbf{C}}_{\mathbf{i}}^{\mathbf{c}T}\Big]\Bigg]\Bigg],
\end{aligned}
$$

$$
\text{with} \quad \vec{D}_i = \int_{m_i} \vec{\delta}_i \, dm_i \quad \text{and} \quad \vec{D}_{i,j} = \int_{m_{i,j}} \vec{\delta}_{i,j} \, dm_{i,j};
$$

$$
\begin{aligned}
\dot{\mathbf{I}}_{\mathbf{r,v}} = & \int_{m_c} \Big[2\vec{\rho}_c{}^T \dot{\vec{\delta}}_c \mathbf{E} - \vec{\rho}_c \dot{\vec{\delta}}_c{}^T - \dot{\vec{\delta}}_c \vec{\rho}_c{}^T\Big] \, dm_c + \sum_{i=1}^{N} \Bigg[\int_{m_i} 2\vec{\rho}_i{}^T \dot{\vec{\delta}}_i \, dm_i \mathbf{E} \\
& - \dot{\mathbf{C}}_{\mathbf{i}}^{\mathbf{c}} \mathbf{D}_{\mathbf{i}}^{\mathbf{r}}{}^T \mathbf{C}_{\mathbf{i}}^{\mathbf{c}T} - \mathbf{C}_{\mathbf{i}}^{\mathbf{c}} \Bigg\{ \int_{m_i} \vec{\rho}_i \dot{\vec{\delta}}_i{}^T \, dm_i \Bigg\} \mathbf{C}_{\mathbf{i}}^{\mathbf{c}T} - \mathbf{C}_{\mathbf{i}}^{\mathbf{c}} \mathbf{D}_{\mathbf{i}}^{\mathbf{r}}{}^T \dot{\mathbf{C}}_{\mathbf{i}}^{\mathbf{c}T} \\
& - \dot{\mathbf{C}}_{\mathbf{i}}^{\mathbf{c}} \mathbf{D}_{\mathbf{i}}^{\mathbf{r}} \mathbf{C}_{\mathbf{i}}^{\mathbf{c}T} - \mathbf{C}_{\mathbf{i}}^{\mathbf{c}} \Bigg\{ \int_{m_i} \dot{\vec{\delta}}_i \vec{\rho}_i{}^T \, dm_i \Bigg\} \mathbf{C}_{\mathbf{i}}^{\mathbf{c}T} - \mathbf{C}_{\mathbf{i}}^{\mathbf{c}} \mathbf{D}_{\mathbf{i}}^{\mathbf{r}} \dot{\mathbf{C}}_{\mathbf{i}}^{\mathbf{c}T} \\
& + \sum_{j=1}^{N_i} \Bigg[\int_{m_{i,j}} 2\vec{\rho}_{i,j}{}^T \dot{\vec{\delta}}_{i,j} \, dm_{i,j} \mathbf{E} - \dot{\mathbf{C}}_{\mathbf{i}}^{\mathbf{c}} \mathbf{C}_{\mathbf{i,j}}^{\mathbf{i}} \mathbf{D}_{\mathbf{i,j}}^{\mathbf{r}}{}^T \mathbf{C}_{\mathbf{i,j}}^{\mathbf{i}}{}^T \mathbf{C}_{\mathbf{i}}^{\mathbf{c}T} \\
& - \mathbf{C}_{\mathbf{i}}^{\mathbf{c}} \dot{\mathbf{C}}_{\mathbf{i,j}}^{\mathbf{i}} \mathbf{D}_{\mathbf{i,j}}^{\mathbf{r}}{}^T \mathbf{C}_{\mathbf{i,j}}^{\mathbf{i}}{}^T \mathbf{C}_{\mathbf{i}}^{\mathbf{c}T} - \mathbf{C}_{\mathbf{i}}^{\mathbf{c}} \mathbf{C}_{\mathbf{i,j}}^{\mathbf{i}} \Bigg\{ \int_{m_{i,j}} \vec{\rho}_{i,j} \dot{\vec{\delta}}_{i,j}{}^T \, dm_{i,j} \Bigg\} \mathbf{C}_{\mathbf{i,j}}^{\mathbf{i}}{}^T \mathbf{C}_{\mathbf{i}}^{\mathbf{c}T} \\
& - \mathbf{C}_{\mathbf{i}}^{\mathbf{c}} \mathbf{C}_{\mathbf{i,j}}^{\mathbf{i}} \mathbf{D}_{\mathbf{i,j}}^{\mathbf{r}}{}^T \dot{\mathbf{C}}_{\mathbf{i,j}}^{\mathbf{i}}{}^T \mathbf{C}_{\mathbf{i}}^{\mathbf{c}T} - \mathbf{C}_{\mathbf{i}}^{\mathbf{c}} \mathbf{C}_{\mathbf{i,j}}^{\mathbf{i}} \mathbf{D}_{\mathbf{i,j}}^{\mathbf{r}}{}^T \mathbf{C}_{\mathbf{i,j}}^{\mathbf{i}}{}^T \dot{\mathbf{C}}_{\mathbf{i}}^{\mathbf{c}T}
\end{aligned}
$$

$$
\begin{aligned}
&-\dot{\mathbf{C}}_{\mathbf{i}}^{\mathbf{c}}\mathbf{C}_{\mathbf{i,j}}^{\mathbf{i}}\mathbf{D}_{\mathbf{i,j}}^{\mathbf{r}}\mathbf{C}_{\mathbf{i,j}}^{\mathbf{i}\,T}\mathbf{C}_{\mathbf{i}}^{\mathbf{c}T}-\mathbf{C}_{\mathbf{i}}^{\mathbf{c}}\dot{\mathbf{C}}_{\mathbf{i,j}}^{\mathbf{i}}\mathbf{D}_{\mathbf{i,j}}^{\mathbf{r}}\mathbf{C}_{\mathbf{i,j}}^{\mathbf{i}\,T}\mathbf{C}_{\mathbf{i}}^{\mathbf{c}T}\\
&-\mathbf{C}_{\mathbf{i}}^{\mathbf{c}}\mathbf{C}_{\mathbf{i,j}}^{\mathbf{i}}\left\{\int_{m_{i,j}}\dot{\vec{\delta}}_{i,j}\vec{\rho}_{i,j}{}^{T}dm_{i,j}\right\}\mathbf{C}_{\mathbf{i,j}}^{\mathbf{i}\,T}\mathbf{C}_{\mathbf{i}}^{\mathbf{c}T}-\mathbf{C}_{\mathbf{i}}^{\mathbf{c}}\mathbf{C}_{\mathbf{i,j}}^{\mathbf{i}}\mathbf{D}_{\mathbf{i,j}}^{\mathbf{r}}\dot{\mathbf{C}}_{\mathbf{i,j}}^{\mathbf{i}\,T}\mathbf{C}_{\mathbf{i}}^{\mathbf{c}T}\\
&-\mathbf{C}_{\mathbf{i}}^{\mathbf{c}}\mathbf{C}_{\mathbf{i,j}}^{\mathbf{i}}\mathbf{D}_{\mathbf{i,j}}^{\mathbf{r}}\mathbf{C}_{\mathbf{i,j}}^{\mathbf{i}\,T}\dot{\mathbf{C}}_{\mathbf{i}}^{\mathbf{c}T}\Big]\Big], \qquad \text{(IV-1)}
\end{aligned}
$$

$$
\text{with}\quad \mathbf{D}_{\mathbf{i}}^{\mathbf{r}}=\int_{m_i}\vec{\delta}_i\vec{\rho}_i{}^{T}dm_i \quad\text{and}\quad \mathbf{D}_{\mathbf{i,j}}^{\mathbf{r}}=\int_{m_{i,j}}\vec{\delta}_{i,j}\vec{\rho}_{i,j}{}^{T}dm_{i,j}.
$$

In much the same way, the time rate of change of the angular momentum vector $\dot{\vec{H}}$ can also be written as the sum of the different contributions,

$$
\dot{\vec{H}}=\dot{\vec{H}}_{cm}+\dot{\vec{H}}_h+\dot{\vec{H}}_v+\dot{\vec{H}}_{h,r}+\dot{\vec{H}}_{h,v}+\dot{\vec{H}}_{r,v}+\dot{\vec{H}}_{r,s}+\dot{\vec{H}}_{v,s}+\dot{\vec{H}}_{h,s},
$$

where:

$$
\dot{\vec{H}}_{cm}=-M\left[\vec{C}_{cm}\times\ddot{\vec{C}}_{cm}\right];
$$

$$
\begin{aligned}
\dot{\vec{H}}_h=&\sum_{i=1}^{N}\left[(\vec{d}_i\times\ddot{\vec{d}}_i)m_i+\sum_{j=1}^{N_i}\left[\left[\vec{d}_i\times(\ddot{\vec{d}}_i+\dot{\mathbf{C}}_{\mathbf{i}}^{\mathbf{c}}\dot{\vec{d}}_{i,j}+\mathbf{C}_{\mathbf{i}}^{\mathbf{c}}\ddot{\vec{d}}_{i,j})-\dot{\vec{d}}_i\times\dot{\mathbf{C}}_{\mathbf{i}}^{\mathbf{c}}\vec{d}_{i,j}\right.\right.\right.\\
&\left.\left.\left.-\ddot{\vec{d}}_i\times\mathbf{C}_{\mathbf{i}}^{\mathbf{c}}\vec{d}_{i,j}+\dot{\mathbf{C}}_{\mathbf{i}}^{\mathbf{c}}(\vec{d}_{i,j}\times\dot{\vec{d}}_{i,j})+\mathbf{C}_{\mathbf{i}}^{\mathbf{c}}(\vec{d}_{i,j}\times\ddot{\vec{d}}_{i,j})\right]m_{i,j}\right]\right];
\end{aligned}
$$

$$
\begin{aligned}
\dot{\vec{H}}_v=&\int_{m_c}(\vec{\delta}_c\times\ddot{\vec{\delta}}_c)\,dm_c+\sum_{i=1}^{N}\left[\int_{m_i}\left[\dot{\mathbf{C}}_{\mathbf{i}}^{\mathbf{c}}(\vec{\delta}_i\times\dot{\vec{\delta}}_i)+\mathbf{C}_{\mathbf{i}}^{\mathbf{c}}(\vec{\delta}_i\times\ddot{\vec{\delta}}_i)\right]dm_i\right.\\
&+\sum_{j=1}^{N_i}\left[\int_{m_{i,j}}\left[\dot{\mathbf{C}}_{\mathbf{i}}^{\mathbf{c}}\mathbf{C}_{\mathbf{i,j}}^{\mathbf{i}}(\vec{\delta}_{i,j}\times\dot{\vec{\delta}}_{i,j})+\mathbf{C}_{\mathbf{i}}^{\mathbf{c}}\dot{\mathbf{C}}_{\mathbf{i,j}}^{\mathbf{i}}(\vec{\delta}_{i,j}\times\dot{\vec{\delta}}_{i,j})\right.\right.\\
&\left.\left.\left.+\mathbf{C}_{\mathbf{i}}^{\mathbf{c}}\mathbf{C}_{\mathbf{i,j}}^{\mathbf{i}}(\vec{\delta}_{i,j}\times\ddot{\vec{\delta}}_{i,j})\right]dm_{i,j}\right]\right];
\end{aligned}
$$

$$\dot{\vec{H}}_{h,r} = \sum_{i=1}^{N} \left[\int_{m_i} \left[\dot{\mathbf{C}}_{\mathbf{i}}^{\mathbf{c}} \vec{\rho}_i \times \dot{\vec{d}}_i + \mathbf{C}_{\mathbf{i}}^{\mathbf{c}} \vec{\rho}_i \times \ddot{\vec{d}}_i \right] dm_i \right.$$
$$+ \sum_{j=1}^{N_i} \left[\int_{m_{i,j}} \left[\dot{\mathbf{C}}_{\mathbf{i}}^{\mathbf{c}} \mathbf{C}_{\mathbf{i,j}}^{\mathbf{i}} \vec{\rho}_{i,j} \times \dot{\vec{d}}_i + \mathbf{C}_{\mathbf{i}}^{\mathbf{c}} \dot{\mathbf{C}}_{\mathbf{i,j}}^{\mathbf{i}} \vec{\rho}_{i,j} \times \dot{\vec{d}}_i + \mathbf{C}_{\mathbf{i}}^{\mathbf{c}} \mathbf{C}_{\mathbf{i,j}}^{\mathbf{i}} \vec{\rho}_{i,j} \times \ddot{\vec{d}}_i \right.\right.$$
$$\left.\left. + \dot{\mathbf{C}}_{\mathbf{i}}^{\mathbf{c}} (\mathbf{C}_{\mathbf{i,j}}^{\mathbf{i}} \vec{\rho}_{i,j} \times \dot{\vec{d}}_{i,j}) + \mathbf{C}_{\mathbf{i}}^{\mathbf{c}} (\dot{\mathbf{C}}_{\mathbf{i,j}}^{\mathbf{i}} \vec{\rho}_{i,j} \times \dot{\vec{d}}_{i,j}) + \mathbf{C}_{\mathbf{i}}^{\mathbf{c}} (\mathbf{C}_{\mathbf{i,j}}^{\mathbf{i}} \vec{\rho}_{i,j} \times \ddot{\vec{d}}_{i,j}) \right] dm_{i,j} \right] \Bigg];$$

$$\dot{\vec{H}}_{h,v} = \sum_{i=1}^{N} \left[\int_{m_i} \left[\dot{\mathbf{C}}_{\mathbf{i}}^{\mathbf{c}} \vec{\delta}_i \times \dot{\vec{d}}_i + \mathbf{C}_{\mathbf{i}}^{\mathbf{c}} \vec{\delta}_i \times \ddot{\vec{d}}_i + \vec{d}_i \times (\dot{\mathbf{C}}_{\mathbf{i}}^{\mathbf{c}} \dot{\vec{\delta}}_i + \mathbf{C}_{\mathbf{i}}^{\mathbf{c}} \ddot{\vec{\delta}}_i) \right] dm_i \right.$$
$$+ \sum_{j=1}^{N_i} \left[\int_{m_{i,j}} \left[(\dot{\mathbf{C}}_{\mathbf{i}}^{\mathbf{c}} \mathbf{C}_{\mathbf{i,j}}^{\mathbf{i}} \vec{\delta}_{i,j} + \mathbf{C}_{\mathbf{i}}^{\mathbf{c}} \dot{\mathbf{C}}_{\mathbf{i,j}}^{\mathbf{i}} \vec{\delta}_{i,j}) \times \dot{\vec{d}}_i + \dot{\mathbf{C}}_{\mathbf{i}}^{\mathbf{c}} (\mathbf{C}_{\mathbf{i,j}}^{\mathbf{i}} \vec{\delta}_{i,j} \times \dot{\vec{d}}_{i,j}) \right.\right.$$
$$+ \mathbf{C}_{\mathbf{i}}^{\mathbf{c}} (\dot{\mathbf{C}}_{\mathbf{i,j}}^{\mathbf{i}} \vec{\delta}_{i,j} \times \dot{\vec{d}}_{i,j}) + \mathbf{C}_{\mathbf{i}}^{\mathbf{c}} (\mathbf{C}_{\mathbf{i,j}}^{\mathbf{i}} \vec{\delta}_{i,j} \times \ddot{\vec{d}}_{i,j}) + \vec{d}_i \times \dot{\mathbf{C}}_{\mathbf{i}}^{\mathbf{c}} \mathbf{C}_{\mathbf{i,j}}^{\mathbf{i}} \dot{\vec{\delta}}_{i,j}$$
$$+ \vec{d}_i \times \mathbf{C}_{\mathbf{i}}^{\mathbf{c}} \dot{\mathbf{C}}_{\mathbf{i,j}}^{\mathbf{i}} \dot{\vec{\delta}}_{i,j} + \vec{d}_i \times \mathbf{C}_{\mathbf{i}}^{\mathbf{c}} \mathbf{C}_{\mathbf{i,j}}^{\mathbf{i}} \ddot{\vec{\delta}}_{i,j} + \dot{\mathbf{C}}_{\mathbf{i}}^{\mathbf{c}} (\vec{d}_{i,j} \times \mathbf{C}_{\mathbf{i,j}}^{\mathbf{i}} \dot{\vec{\delta}}_{i,j})$$
$$\left.\left. + \mathbf{C}_{\mathbf{i}}^{\mathbf{c}} (\vec{d}_{i,j} \times \dot{\mathbf{C}}_{\mathbf{i,j}}^{\mathbf{i}} \dot{\vec{\delta}}_{i,j}) + \mathbf{C}_{\mathbf{i}}^{\mathbf{c}} (\vec{d}_{i,j} \times \mathbf{C}_{\mathbf{i,j}}^{\mathbf{i}} \ddot{\vec{\delta}}_{i,j}) \right] dm_{i,j} \right] \Bigg];$$

$$\dot{\vec{H}}_{r,v} = \int_{m_c} (\vec{\rho}_c \times \ddot{\vec{\delta}}_c)\, dm_c + \sum_{i=1}^{N} \left[\int_{m_i} \left[\dot{\mathbf{C}}_{\mathbf{i}}^{\mathbf{c}} (\vec{\rho}_i \times \dot{\vec{\delta}}_i) + \mathbf{C}_{\mathbf{i}}^{\mathbf{c}} (\vec{\rho}_i \times \ddot{\vec{\delta}}_i) \right] dm_i \right.$$
$$+ \sum_{j=1}^{N_i} \left[\int_{m_{i,j}} \left[\dot{\mathbf{C}}_{\mathbf{i}}^{\mathbf{c}} \mathbf{C}_{\mathbf{i,j}}^{\mathbf{i}} (\vec{\rho}_{i,j} \times \dot{\vec{\delta}}_{i,j}) + \mathbf{C}_{\mathbf{i}}^{\mathbf{c}} \dot{\mathbf{C}}_{\mathbf{i,j}}^{\mathbf{i}} (\vec{\rho}_{i,j} \times \dot{\vec{\delta}}_{i,j}) \right.\right.$$
$$\left.\left. + \mathbf{C}_{\mathbf{i}}^{\mathbf{c}} \mathbf{C}_{\mathbf{i,j}}^{\mathbf{i}} (\vec{\rho}_{i,j} \times \ddot{\vec{\delta}}_{i,j}) \right] dm_{i,j} \right] \Bigg];$$

$$\dot{\vec{H}}_{r,s} = \sum_{i=1}^{N} \left[\int_{m_i} \left[\dot{\mathbf{C}}_{\mathbf{i}}^{\mathbf{c}} \vec{\rho}_i \times \dot{\mathbf{C}}_{\mathbf{i}}^{\mathbf{c}} \vec{\delta}_i + \mathbf{C}_{\mathbf{i}}^{\mathbf{c}} \vec{\rho}_i \times (\ddot{\mathbf{C}}_{\mathbf{i}}^{\mathbf{c}} (\vec{\rho}_i + \vec{\delta}_i) + \dot{\mathbf{C}}_{\mathbf{i}}^{\mathbf{c}} \dot{\vec{\delta}}_i) \right] dm_i \right.$$
$$+ \sum_{j=1}^{N_i} \left[\int_{m_{i,j}} \left[\dot{\mathbf{C}}_{\mathbf{i}}^{\mathbf{c}} \mathbf{C}_{\mathbf{i,j}}^{\mathbf{i}} \vec{\rho}_{i,j} \times \dot{\mathbf{C}}_{\mathbf{i}}^{\mathbf{c}} \mathbf{C}_{\mathbf{i,j}}^{\mathbf{i}} \vec{\delta}_{i,j} + \mathbf{C}_{\mathbf{i}}^{\mathbf{c}} \dot{\mathbf{C}}_{\mathbf{i,j}}^{\mathbf{i}} \vec{\rho}_{i,j} \times \dot{\mathbf{C}}_{\mathbf{i}}^{\mathbf{c}} \mathbf{C}_{\mathbf{i,j}}^{\mathbf{i}} (\vec{\rho}_{i,j} + \vec{\delta}_{i,j}) \right.\right.$$
$$\left.\left. + \mathbf{C}_{\mathbf{i}}^{\mathbf{c}} \mathbf{C}_{\mathbf{i,j}}^{\mathbf{i}} \vec{\rho}_{i,j} \times \left(\ddot{\mathbf{C}}_{\mathbf{i}}^{\mathbf{c}} \mathbf{C}_{\mathbf{i,j}}^{\mathbf{i}} (\vec{\rho}_{i,j} + \vec{\delta}_{i,j}) + \dot{\mathbf{C}}_{\mathbf{i}}^{\mathbf{c}} \dot{\mathbf{C}}_{\mathbf{i,j}}^{\mathbf{i}} (\vec{\rho}_{i,j} + \vec{\delta}_{i,j}) + \dot{\mathbf{C}}_{\mathbf{i}}^{\mathbf{c}} \mathbf{C}_{\mathbf{i,j}}^{\mathbf{i}} \dot{\vec{\delta}}_{i,j} \right) \right.\right.$$

$$
\begin{aligned}
&+\dot{\mathbf{C}}_{\mathbf{i}}^{\mathbf{c}}\left[\mathbf{C}_{\mathbf{i},\mathbf{j}}^{\mathbf{i}}\vec{\rho}_{i,j}\times\dot{\mathbf{C}}_{\mathbf{i},\mathbf{j}}^{\mathbf{i}}(\vec{\rho}_{i,j}+\vec{\delta}_{i,j})\right]+\mathbf{C}_{\mathbf{i}}^{\mathbf{c}}\left[\dot{\mathbf{C}}_{\mathbf{i},\mathbf{j}}^{\mathbf{i}}\vec{\rho}_{i,j}\times\dot{\mathbf{C}}_{\mathbf{i},\mathbf{j}}^{\mathbf{i}}\vec{\delta}_{i,j}\right]\\
&+\mathbf{C}_{\mathbf{i}}^{\mathbf{c}}\left[\mathbf{C}_{\mathbf{i},\mathbf{j}}^{\mathbf{i}}\vec{\rho}_{i,j}\times\left(\ddot{\mathbf{C}}_{\mathbf{i},\mathbf{j}}^{\mathbf{i}}(\vec{\rho}_{i,j}+\vec{\delta}_{i,j})+\dot{\mathbf{C}}_{\mathbf{i},\mathbf{j}}^{\mathbf{i}}\dot{\vec{\delta}}_{i,j}\right)\right]\\
&+(\dot{\mathbf{C}}_{\mathbf{i}}^{\mathbf{c}}\mathbf{C}_{\mathbf{i},\mathbf{j}}^{\mathbf{i}}\vec{\rho}_{i,j}+\mathbf{C}_{\mathbf{i}}^{\mathbf{c}}\dot{\mathbf{C}}_{\mathbf{i},\mathbf{j}}^{\mathbf{i}}\vec{\rho}_{i,j})\times\dot{\mathbf{C}}_{\mathbf{i}}^{\mathbf{c}}\vec{d}_{i,j}\\
&+\mathbf{C}_{\mathbf{i}}^{\mathbf{c}}\mathbf{C}_{\mathbf{i},\mathbf{j}}^{\mathbf{i}}\vec{\rho}_{i,j}\times(\ddot{\mathbf{C}}_{\mathbf{i}}^{\mathbf{c}}\vec{d}_{i,j}+\dot{\mathbf{C}}_{\mathbf{i}}^{\mathbf{c}}\dot{\vec{d}}_{i,j})\Big]\,dm_{i,j}\Bigg]\Bigg];
\end{aligned}
$$

$$
\begin{aligned}
\dot{\vec{H}}_{v,s}=&\sum_{i=1}^{N}\Bigg[\int_{m_i}\Big[\dot{\mathbf{C}}_{\mathbf{i}}^{\mathbf{c}}\vec{\delta}_i\times\dot{\mathbf{C}}_{\mathbf{i}}^{\mathbf{c}}\vec{\rho}_i+\mathbf{C}_{\mathbf{i}}^{\mathbf{c}}\dot{\vec{\delta}}_i\times\dot{\mathbf{C}}_{\mathbf{i}}^{\mathbf{c}}(\vec{\rho}_i+\vec{\delta}_i)\\
&+\mathbf{C}_{\mathbf{i}}^{\mathbf{c}}\vec{\delta}_i\times\left(\ddot{\mathbf{C}}_{\mathbf{i}}^{\mathbf{c}}(\vec{\rho}_i+\vec{\delta}_i)+\dot{\mathbf{C}}_{\mathbf{i}}^{\mathbf{c}}\dot{\vec{\delta}}_i\right)\Big]\,dm_i\\
&+\sum_{j=1}^{N_i}\Bigg[\int_{m_{i,j}}\Big[\dot{\mathbf{C}}_{\mathbf{i}}^{\mathbf{c}}\mathbf{C}_{\mathbf{i},\mathbf{j}}^{\mathbf{i}}\vec{\delta}_{i,j}\times(\dot{\mathbf{C}}_{\mathbf{i}}^{\mathbf{c}}\mathbf{C}_{\mathbf{i},\mathbf{j}}^{\mathbf{i}}\vec{\rho}_{i,j}+\dot{\mathbf{C}}_{\mathbf{i}}^{\mathbf{c}}\vec{d}_{i,j})\\
&+\mathbf{C}_{\mathbf{i}}^{\mathbf{c}}(\dot{\mathbf{C}}_{\mathbf{i},\mathbf{j}}^{\mathbf{i}}\vec{\delta}_{i,j}+\mathbf{C}_{\mathbf{i},\mathbf{j}}^{\mathbf{i}}\dot{\vec{\delta}}_{i,j})\times\left(\dot{\mathbf{C}}_{\mathbf{i}}^{\mathbf{c}}\mathbf{C}_{\mathbf{i},\mathbf{j}}^{\mathbf{i}}(\vec{\rho}_{i,j}+\vec{\delta}_{i,j})+\dot{\mathbf{C}}_{\mathbf{i}}^{\mathbf{c}}\vec{d}_{i,j}\right)\\
&+\mathbf{C}_{\mathbf{i}}^{\mathbf{c}}\mathbf{C}_{\mathbf{i},\mathbf{j}}^{\mathbf{i}}\vec{\delta}_{i,j}\times\Big(\ddot{\mathbf{C}}_{\mathbf{i}}^{\mathbf{c}}\mathbf{C}_{\mathbf{i},\mathbf{j}}^{\mathbf{i}}(\vec{\rho}_{i,j}+\vec{\delta}_{i,j})+\dot{\mathbf{C}}_{\mathbf{i}}^{\mathbf{c}}\dot{\mathbf{C}}_{\mathbf{i},\mathbf{j}}^{\mathbf{i}}(\vec{\rho}_{i,j}+\vec{\delta}_{i,j})\\
&+\dot{\mathbf{C}}_{\mathbf{i}}^{\mathbf{c}}\mathbf{C}_{\mathbf{i},\mathbf{j}}^{\mathbf{i}}\dot{\vec{\delta}}_{i,j}+\ddot{\mathbf{C}}_{\mathbf{i}}^{\mathbf{c}}\vec{d}_{i,j}+\dot{\mathbf{C}}_{\mathbf{i}}^{\mathbf{c}}\dot{\vec{d}}_{i,j}\Big)\\
&+\dot{\mathbf{C}}_{\mathbf{i}}^{\mathbf{c}}\Big(\mathbf{C}_{\mathbf{i},\mathbf{j}}^{\mathbf{i}}\vec{\delta}_{i,j}\times\dot{\mathbf{C}}_{\mathbf{i},\mathbf{j}}^{\mathbf{i}}(\vec{\rho}_{i,j}+\vec{\delta}_{i,j})\Big)+\mathbf{C}_{\mathbf{i}}^{\mathbf{c}}(\dot{\mathbf{C}}_{\mathbf{i},\mathbf{j}}^{\mathbf{i}}\vec{\delta}_{i,j}\times\dot{\mathbf{C}}_{\mathbf{i},\mathbf{j}}^{\mathbf{i}}\vec{\rho}_{i,j})\\
&+\mathbf{C}_{\mathbf{i}}^{\mathbf{c}}\Big((\dot{\mathbf{C}}_{\mathbf{i},\mathbf{j}}^{\mathbf{i}}\vec{\delta}_{i,j}+\mathbf{C}_{\mathbf{i},\mathbf{j}}^{\mathbf{i}}\dot{\vec{\delta}}_{i,j})\times\dot{\mathbf{C}}_{\mathbf{i},\mathbf{j}}^{\mathbf{i}}(\vec{\rho}_{i,j}+\vec{\delta}_{i,j})\Big)\\
&+\mathbf{C}_{\mathbf{i}}^{\mathbf{c}}\Big(\mathbf{C}_{\mathbf{i},\mathbf{j}}^{\mathbf{i}}\vec{\delta}_{i,j}\times(\ddot{\mathbf{C}}_{\mathbf{i}}^{\mathbf{c}}(\vec{\rho}_{i,j}+\vec{\delta}_{i,j})+\dot{\mathbf{C}}_{\mathbf{i},\mathbf{j}}^{\mathbf{i}}\dot{\vec{\delta}}_{i,j})\Big)\Big]\,dm_{i,j}\Bigg]\Bigg];
\end{aligned}
$$

$$
\begin{aligned}
\dot{\vec{H}}_{h,s}=&\sum_{i=1}^{N}\Bigg[\int_{m_i}\Big[\dot{\vec{d}}_i\times\dot{\mathbf{C}}_{\mathbf{i}}^{\mathbf{c}}(\vec{\rho}_{i,j}+\vec{\delta}_{i,j})+\vec{d}_i\times\left(\ddot{\mathbf{C}}_{\mathbf{i}}^{\mathbf{c}}(\vec{\rho}_{i,j}+\vec{\delta}_{i,j})+\dot{\mathbf{C}}_{\mathbf{i}}^{\mathbf{c}}\dot{\vec{\delta}}_{i,j}\right)\Big]\,dm_i\\
&+\sum_{j=1}^{N_i}\Bigg[\int_{m_{i,j}}\Big[(\dot{\vec{d}}_i+\mathbf{C}_{\mathbf{i}}^{\mathbf{c}}\dot{\vec{d}}_{i,j})\times\left(\dot{\mathbf{C}}_{\mathbf{i}}^{\mathbf{c}}\vec{d}_{i,j}+\dot{\mathbf{C}}_{\mathbf{i}}^{\mathbf{c}}\mathbf{C}_{\mathbf{i},\mathbf{j}}^{\mathbf{i}}(\vec{\rho}_{i,j}+\vec{\delta}_{i,j})\right)\\
&+\dot{\mathbf{C}}_{\mathbf{i}}^{\mathbf{c}}\vec{d}_{i,j}\times\dot{\mathbf{C}}_{\mathbf{i}}^{\mathbf{c}}\mathbf{C}_{\mathbf{i},\mathbf{j}}^{\mathbf{i}}(\vec{\rho}_{i,j}+\vec{\delta}_{i,j})+(\vec{d}_i+\mathbf{C}_{\mathbf{i}}^{\mathbf{c}}\vec{d}_{i,j})\times\left(\ddot{\mathbf{C}}_{\mathbf{i}}^{\mathbf{c}}\vec{d}_{i,j}+\dot{\mathbf{C}}_{\mathbf{i}}^{\mathbf{c}}\dot{\vec{d}}_{i,j}\right.\\
&\left.+\ddot{\mathbf{C}}_{\mathbf{i}}^{\mathbf{c}}\mathbf{C}_{\mathbf{i},\mathbf{j}}^{\mathbf{i}}(\vec{\rho}_{i,j}+\vec{\delta}_{i,j})+\dot{\mathbf{C}}_{\mathbf{i}}^{\mathbf{c}}\dot{\mathbf{C}}_{\mathbf{i},\mathbf{j}}^{\mathbf{i}}(\vec{\rho}_{i,j}+\vec{\delta}_{i,j})+\dot{\mathbf{C}}_{\mathbf{i}}^{\mathbf{c}}\mathbf{C}_{\mathbf{i},\mathbf{j}}^{\mathbf{i}}\dot{\vec{\delta}}_{i,j}\right)\\
&+\dot{\vec{d}}_i\times\mathbf{C}_{\mathbf{i}}^{\mathbf{c}}\dot{\mathbf{C}}_{\mathbf{i},\mathbf{j}}^{\mathbf{i}}(\vec{\rho}_{i,j}+\vec{\delta}_{i,j})+\vec{d}_i\times\Big(\dot{\mathbf{C}}_{\mathbf{i}}^{\mathbf{c}}\dot{\mathbf{C}}_{\mathbf{i},\mathbf{j}}^{\mathbf{i}}(\vec{\rho}_{i,j}+\vec{\delta}_{i,j})
\end{aligned}
$$

$$+\mathbf{C_i^c}\ddot{\mathbf{C}}_{\mathbf{i,j}}^{\mathbf{i}}(\vec{\rho}_{i,j}+\vec{\delta}_{i,j})+\mathbf{C_i^c}\dot{\mathbf{C}}_{\mathbf{i,j}}^{\mathbf{i}}\dot{\vec{\delta}}_{i,j}\Big)+\dot{\mathbf{C}}_{\mathbf{i}}^{\mathbf{c}}\Big(\vec{d}_{i,j}\times\dot{\mathbf{C}}_{\mathbf{i,j}}^{\mathbf{i}}(\vec{\rho}_{i,j}+\vec{\delta}_{i,j})\Big)$$
$$+\mathbf{C_i^c}\Big(\dot{\vec{d}}_{i,j}\times\dot{\mathbf{C}}_{\mathbf{i,j}}^{\mathbf{i}}(\vec{\rho}_{i,j}+\vec{\delta}_{i,j})\Big)+\mathbf{C_i^c}\Big(\vec{d}_{i,j}\times\Big(\ddot{\mathbf{C}}_{\mathbf{i,j}}^{\mathbf{i}}(\vec{\rho}_{i,j}+\vec{\delta}_{i,j})$$
$$+\dot{\mathbf{C}}_{\mathbf{i,j}}^{\mathbf{i}}\dot{\vec{\delta}}_{i,j}\Big)\Big)\Big]\,dm_{i,j}\Big]\Big]. \qquad \text{(IV-2)}$$

A significant degree of simplification, mainly due to the cancellation of terms, does take place, and $\dot{\vec{H}}$ can be reduced to

$$\dot{\vec{H}} = -M\Big[\vec{C}_{cm}\times\ddot{\vec{C}}_{cm}\Big]+\int_{m_c}\Big[(\vec{\rho}_c\times\ddot{\vec{\delta}}_c)+(\vec{\delta}_c\times\ddot{\vec{\delta}}_c)\Big]\,dm_c$$
$$\sum_{i=1}^{N}\Bigg[(\vec{d}_i\times\ddot{\vec{d}}_i)m_i+\int_{m_i}\Big[\mathbf{C_i^c}\vec{\rho}_i\times\ddot{\vec{d}}_i+\mathbf{C_i^c}\vec{\delta}_i\times\ddot{\vec{d}}_i$$
$$+\vec{d}_i\times\Big(\mathbf{C_i^c}\ddot{\vec{\delta}}_i+2\dot{\mathbf{C}}_{\mathbf{i}}^{\mathbf{c}}\dot{\vec{\delta}}_i+\ddot{\mathbf{C}}_{\mathbf{i}}^{\mathbf{c}}(\vec{\rho}_i+\vec{\delta}_i)\Big)+\mathbf{C_i^c}(\vec{\rho}_i\times\ddot{\vec{\delta}}_i)+\mathbf{C_i^c}(\vec{\delta}_i\times\ddot{\vec{\delta}}_i)$$
$$+\mathbf{C_i^c}\vec{\rho}_i\times\Big(2\dot{\mathbf{C}}_{\mathbf{i}}^{\mathbf{c}}\dot{\vec{\delta}}_i+\ddot{\mathbf{C}}_{\mathbf{i}}^{\mathbf{c}}(\vec{\rho}_i+\vec{\delta}_i)\Big)+\mathbf{C_i^c}\vec{\delta}_i\times\Big(2\dot{\mathbf{C}}_{\mathbf{i}}^{\mathbf{c}}\dot{\vec{\delta}}_i+\ddot{\mathbf{C}}_{\mathbf{i}}^{\mathbf{c}}(\vec{\rho}_i+\vec{\delta}_i)\Big)\Big]\,dm_i$$
$$+\sum_{j=1}^{N_i}\Bigg[\Big[(\vec{d}_i+\mathbf{C_i^c}\vec{d}_{i,j})\times\big(\ddot{\vec{d}}_i+\ddot{\mathbf{C}}_{\mathbf{i}}^{\mathbf{c}}\vec{d}_{i,j}+2\dot{\mathbf{C}}_{\mathbf{i}}^{\mathbf{c}}\dot{\vec{d}}_{i,j}+\mathbf{C_i^c}\ddot{\vec{d}}_{i,j}\big)\Big]m_{i,j}$$
$$+\int_{m_{i,j}}\Big[\mathbf{C_i^c}\mathbf{C}_{\mathbf{i,j}}^{\mathbf{i}}\vec{\rho}_{i,j}\times\big(\ddot{\vec{d}}_i+\ddot{\mathbf{C}}_{\mathbf{i}}^{\mathbf{c}}\vec{d}_{i,j}+2\dot{\mathbf{C}}_{\mathbf{i}}^{\mathbf{c}}\dot{\vec{d}}_{i,j}+\mathbf{C_i^c}\ddot{\vec{d}}_{i,j}\big)$$
$$+\mathbf{C_i^c}\mathbf{C}_{\mathbf{i,j}}^{\mathbf{i}}\vec{\delta}_{i,j}\times\big(\ddot{\vec{d}}_i+\ddot{\mathbf{C}}_{\mathbf{i}}^{\mathbf{c}}\vec{d}_{i,j}+2\dot{\mathbf{C}}_{\mathbf{i}}^{\mathbf{c}}\dot{\vec{d}}_{i,j}+\mathbf{C_i^c}\ddot{\vec{d}}_{i,j}\big)$$
$$+\mathbf{C_i^c}\mathbf{C}_{\mathbf{i,j}}^{\mathbf{i}}\vec{\rho}_{i,j}\times\Big(\ddot{\mathbf{C}}_{\mathbf{i}}^{\mathbf{c}}\mathbf{C}_{\mathbf{i,j}}^{\mathbf{i}}(\vec{\rho}_{i,j}+\vec{\delta}_{i,j})+2\dot{\mathbf{C}}_{\mathbf{i}}^{\mathbf{c}}\dot{\mathbf{C}}_{\mathbf{i,j}}^{\mathbf{i}}(\vec{\rho}_{i,j}+\vec{\delta}_{i,j})+2\dot{\mathbf{C}}_{\mathbf{i}}^{\mathbf{c}}\mathbf{C}_{\mathbf{i,j}}^{\mathbf{i}}\dot{\vec{\delta}}_{i,j}$$
$$+\mathbf{C_i^c}\ddot{\mathbf{C}}_{\mathbf{i,j}}^{\mathbf{i}}(\vec{\rho}_{i,j}+\vec{\delta}_{i,j})+2\mathbf{C_i^c}\dot{\mathbf{C}}_{\mathbf{i,j}}^{\mathbf{i}}\dot{\vec{\delta}}_{i,j}+\mathbf{C_i^c}\mathbf{C}_{\mathbf{i,j}}^{\mathbf{i}}\ddot{\vec{\delta}}_{i,j}\Big)$$
$$+\mathbf{C_i^c}\mathbf{C}_{\mathbf{i,j}}^{\mathbf{i}}\vec{\delta}_{i,j}\times\Big(\ddot{\mathbf{C}}_{\mathbf{i}}^{\mathbf{c}}\mathbf{C}_{\mathbf{i,j}}^{\mathbf{i}}(\vec{\rho}_{i,j}+\vec{\delta}_{i,j})+2\dot{\mathbf{C}}_{\mathbf{i}}^{\mathbf{c}}\dot{\mathbf{C}}_{\mathbf{i,j}}^{\mathbf{i}}(\vec{\rho}_{i,j}+\vec{\delta}_{i,j})+2\dot{\mathbf{C}}_{\mathbf{i}}^{\mathbf{c}}\mathbf{C}_{\mathbf{i,j}}^{\mathbf{i}}\dot{\vec{\delta}}_{i,j}$$
$$+\mathbf{C_i^c}\ddot{\mathbf{C}}_{\mathbf{i,j}}^{\mathbf{i}}(\vec{\rho}_{i,j}+\vec{\delta}_{i,j})+2\mathbf{C_i^c}\dot{\mathbf{C}}_{\mathbf{i,j}}^{\mathbf{i}}\dot{\vec{\delta}}_{i,j}+\mathbf{C_i^c}\mathbf{C}_{\mathbf{i,j}}^{\mathbf{i}}\ddot{\vec{\delta}}_{i,j}\Big)$$
$$+(\vec{d}_i+\mathbf{C_i^c}\vec{d}_{i,j})\times\Big(\ddot{\mathbf{C}}_{\mathbf{i}}^{\mathbf{c}}\mathbf{C}_{\mathbf{i,j}}^{\mathbf{i}}(\vec{\rho}_{i,j}+\vec{\delta}_{i,j})+2\dot{\mathbf{C}}_{\mathbf{i}}^{\mathbf{c}}\dot{\mathbf{C}}_{\mathbf{i,j}}^{\mathbf{i}}(\vec{\rho}_{i,j}+\vec{\delta}_{i,j})+2\dot{\mathbf{C}}_{\mathbf{i}}^{\mathbf{c}}\mathbf{C}_{\mathbf{i,j}}^{\mathbf{i}}\dot{\vec{\delta}}_{i,j}$$
$$+\mathbf{C_i^c}\ddot{\mathbf{C}}_{\mathbf{i,j}}^{\mathbf{i}}(\vec{\rho}_{i,j}+\vec{\delta}_{i,j})+2\mathbf{C_i^c}\dot{\mathbf{C}}_{\mathbf{i,j}}^{\mathbf{i}}\dot{\vec{\delta}}_{i,j}+\mathbf{C_i^c}\mathbf{C}_{\mathbf{i,j}}^{\mathbf{i}}\ddot{\vec{\delta}}_{i,j}\Big)\Big]\,dm_{i,j}\Big]\Big]. \qquad \text{(IV-3)}$$

Appendix V: Derivatives of $\mathbf{I_{sys}}$ and $\vec{H}$ w.r.t. the Flexibility Generalized Coordinates

The derivative of the moment of inertia matrix with respect to q_{cm}, i.e. $\frac{\partial \mathbf{I_{sys}}}{\partial q_{cm}}$, can be written as the sum of the different contributions,

$$\frac{\partial \mathbf{I_{sys}}}{\partial q_{cm}} = \frac{\partial \mathbf{I_{cm}}}{\partial q_{cm}} + \frac{\partial \mathbf{I_r}}{\partial q_{cm}} + \frac{\partial \mathbf{I_h}}{\partial q_{cm}} + \frac{\partial \mathbf{I_v}}{\partial q_{cm}} + \frac{\partial \mathbf{I_{h,r}}}{\partial q_{cm}} + \frac{\partial \mathbf{I_{h,v}}}{\partial q_{cm}} + \frac{\partial \mathbf{I_{r,v}}}{\partial q_{cm}},$$

where:

$$\frac{\partial \mathbf{I_{cm}}}{\partial q_{cm}} = -M\left[2\left(\frac{\partial \vec{C}_{cm}}{\partial q_{cm}}\right)^T \vec{C}_{cm}\mathbf{E} - \left(\frac{\partial \vec{C}_{cm}}{\partial q_{cm}}\right)\vec{C}_{cm}^T - \vec{C}_{cm}\left(\frac{\partial \vec{C}_{cm}}{\partial q_{cm}}\right)^T\right];$$

$$\begin{aligned}\frac{\partial \mathbf{I_r}}{\partial q_{cm}} = &\sum_{i=1}^{N}\Bigg[-\left(\frac{\partial \mathbf{C_i^c}}{\partial q_{cm}}\right)\mathbf{P_i^2}\mathbf{C_i^{c^T}} - \mathbf{C_i^c}\mathbf{P_i^2}\left(\frac{\partial \mathbf{C_i^c}}{\partial q_{cm}}\right)^T \\ &+\sum_{j=1}^{N_i}\Bigg[-\left(\frac{\partial \mathbf{C_i^c}}{\partial q_{cm}}\right)\mathbf{C_{i,j}^i}\mathbf{P_{i,j}^2}\mathbf{C_{i,j}^i}^T\mathbf{C_i^{c^T}} - \mathbf{C_i^c}\mathbf{C_{i,j}^i}\mathbf{P_{i,j}^2}\mathbf{C_{i,j}^i}^T\left(\frac{\partial \mathbf{C_i^c}}{\partial q_{cm}}\right)^T\Bigg]\Bigg];\end{aligned}$$

$$\begin{aligned}\frac{\partial \mathbf{I_h}}{\partial q_{cm}} = &\sum_{i=1}^{N}\Bigg[\Big[2\vec{d}_i^{\,T}\vec{\phi}_{cm}(o_i)\mathbf{E} - \vec{\phi}_{cm}(o_i)\vec{d}_i^{\,T} - \vec{d}_i\vec{\phi}_{cm}(o_i)^T\Big]m_i \\ &+\sum_{j=1}^{N_i}\Bigg[\Big[2\Big[\vec{d}_i^{\,T}\vec{\phi}_{cm}(o_i) + \vec{d}_{i,j}^{\,T}\left(\frac{\partial \mathbf{C_i^c}}{\partial q_{cm}}\right)^T\vec{d}_i + \vec{d}_{i,j}^{\,T}\mathbf{C_i^{c^T}}\vec{\phi}_{cm}(o_i)\Big]\mathbf{E} \\ &-\Big[\vec{\phi}_{cm}(o_i)\vec{d}_i^{\,T} + \vec{d}_i\vec{\phi}_{cm}(o_i)^T + \left(\frac{\partial \mathbf{C_i^c}}{\partial q_{cm}}\right)\vec{d}_{i,j}\vec{d}_i^{\,T} + \mathbf{C_i^c}\vec{d}_{i,j}\vec{\phi}_{cm}(o_i)^T \\ &+\vec{\phi}_{cm}(o_i)\vec{d}_{i,j}^{\,T}\mathbf{C_i^{c^T}} + \left(\frac{\partial \mathbf{C_i^c}}{\partial q_{cm}}\right)\vec{d}_{i,j}\vec{d}_{i,j}^{\,T}\mathbf{C_i^{c^T}} \\ &+\mathbf{C_i^c}\vec{d}_{i,j}\vec{d}_{i,j}^{\,T}\left(\frac{\partial \mathbf{C_i^c}}{\partial q_{cm}}\right)^T + \vec{d}_i\vec{d}_{i,j}^{\,T}\left(\frac{\partial \mathbf{C_i^c}}{\partial q_{cm}}\right)^T\Big]\Big]m_{i,j}\Bigg]\Bigg];\end{aligned}$$

$$\frac{\partial \mathbf{I_v}}{\partial q_{cm}} = \int_{m_c}\left[2\vec{\delta}_c^{\,T}\vec{\phi}_{cm}\mathbf{E} - \vec{\phi}_{cm}\vec{\delta}_c^{\,T} - \vec{\delta}_c\vec{\phi}_{cm}^{\,T}\right]dm_c$$

$$+\sum_{i=1}^{N}\left[-\left(\frac{\partial \mathbf{C_i^c}}{\partial q_{c_m}}\right)\mathbf{D_i^2}\mathbf{C_i^{c}}^{T}-\mathbf{C_i^c}\mathbf{D_i^2}\left(\frac{\partial \mathbf{C_i^c}}{\partial q_{c_m}}\right)^{T}\right.$$
$$\left.+\sum_{j=1}^{N_i}\left[-\left(\frac{\partial \mathbf{C_i^c}}{\partial q_{c_m}}\right)\mathbf{C_{i,j}^i}\mathbf{D_{i,j}^2}\mathbf{C_{i,j}^i}^{T}\mathbf{C_i^{c}}^{T}-\mathbf{C_i^c}\mathbf{C_{i,j}^i}\mathbf{D_{i,j}^2}\mathbf{C_{i,j}^i}^{T}\left(\frac{\partial \mathbf{C_i^c}}{\partial q_{c_m}}\right)^{T}\right]\right];$$

$$\frac{\partial \mathbf{I_{h,r}}}{\partial q_{c_m}}=\sum_{i=1}^{N}\left[2\left[\vec{\phi}_{c_m}(o_i)^T\mathbf{C_i^c}\vec{P}_i+\vec{d}_i{}^T\left(\frac{\partial \mathbf{C_i^c}}{\partial q_{c_m}}\right)\vec{P}_i\right]\mathbf{E}-\vec{\phi}_{c_m}(o_i)\vec{P}_i{}^T\mathbf{C_i^{c}}^{T}\right.$$
$$-\vec{d}_i\vec{P}_i{}^T\left(\frac{\partial \mathbf{C_i^c}}{\partial q_{c_m}}\right)^{T}-\left(\frac{\partial \mathbf{C_i^c}}{\partial q_{c_m}}\right)\vec{P}_i\vec{d}_i{}^T-\mathbf{C_i^c}\vec{P}_i\vec{\phi}_{c_m}(o_i)^T$$
$$+\sum_{j=1}^{N_i}\left[2\left[\vec{\phi}_{c_m}(o_i)^T\mathbf{C_i^c}\mathbf{C_{i,j}^i}\vec{P}_{i,j}+\vec{d}_i{}^T\left(\frac{\partial \mathbf{C_i^c}}{\partial q_{c_m}}\right)\mathbf{C_{i,j}^i}\vec{P}_{i,j}\right]\mathbf{E}\right.$$
$$-\left[\vec{\phi}_{c_m}(o_i)\vec{P}_{i,j}{}^T\mathbf{C_{i,j}^i}{}^T\mathbf{C_i^{c}}^{T}+\vec{d}_i\vec{P}_{i,j}{}^T\mathbf{C_{i,j}^i}{}^T\left(\frac{\partial \mathbf{C_i^c}}{\partial q_{c_m}}\right)^{T}\right.$$
$$+\left(\frac{\partial \mathbf{C_i^c}}{\partial q_{c_m}}\right)\vec{d}_{i,j}\vec{P}_{i,j}{}^T\mathbf{C_{i,j}^i}{}^T\mathbf{C_i^{c}}^{T}+\mathbf{C_i^c}\vec{d}_{i,j}\vec{P}_{i,j}{}^T\mathbf{C_{i,j}^i}{}^T\left(\frac{\partial \mathbf{C_i^c}}{\partial q_{c_m}}\right)^{T}$$
$$+\left(\frac{\partial \mathbf{C_i^c}}{\partial q_{c_m}}\right)\mathbf{C_{i,j}^i}\vec{P}_{i,j}\vec{d}_i{}^T+\mathbf{C_i^c}\mathbf{C_{i,j}^i}\vec{P}_{i,j}\vec{\phi}_{c_m}(o_i)^T$$
$$\left.\left.+\left(\frac{\partial \mathbf{C_i^c}}{\partial q_{c_m}}\right)\mathbf{C_{i,j}^i}\vec{P}_{i,j}\vec{d}_{i,j}{}^T\mathbf{C_i^{c}}^{T}+\mathbf{C_i^c}\mathbf{C_{i,j}^i}\vec{P}_{i,j}\vec{d}_{i,j}{}^T\left(\frac{\partial \mathbf{C_i^c}}{\partial q_{c_m}}\right)^{T}\right]\right]\right];$$

$$\frac{\partial \mathbf{I_{h,v}}}{\partial q_{c_m}}=\sum_{i=1}^{N}\left[2\left[\vec{\phi}_{c_m}(o_i)^T\mathbf{C_i^c}\vec{D}_i+\vec{d}_i{}^T\left(\frac{\partial \mathbf{C_i^c}}{\partial q_{c_m}}\right)\vec{D}_i\right]\mathbf{E}-\vec{\phi}_{c_m}(o_i)\vec{D}_i{}^T\mathbf{C_i^{c}}^{T}\right.$$
$$-\vec{d}_i\vec{D}_i{}^T\left(\frac{\partial \mathbf{C_i^c}}{\partial q_{c_m}}\right)^{T}-\left(\frac{\partial \mathbf{C_i^c}}{\partial q_{c_m}}\right)\vec{D}_i\vec{d}_i{}^T-\mathbf{C_i^c}\vec{D}_i\vec{\phi}_{c_m}(o_i)^T$$
$$+\sum_{j=1}^{N_i}\left[2\left[\vec{\phi}_{c_m}(o_i)^T\mathbf{C_i^c}\mathbf{C_{i,j}^i}\vec{D}_{i,j}+\vec{d}_i{}^T\left(\frac{\partial \mathbf{C_i^c}}{\partial q_{c_m}}\right)\mathbf{C_{i,j}^i}\vec{D}_{i,j}\right]\mathbf{E}\right.$$
$$-\left[\vec{\phi}_{c_m}(o_i)\vec{D}_{i,j}{}^T\mathbf{C_{i,j}^i}{}^T\mathbf{C_i^{c}}^{T}+\vec{d}_i\vec{D}_{i,j}{}^T\mathbf{C_{i,j}^i}{}^T\left(\frac{\partial \mathbf{C_i^c}}{\partial q_{c_m}}\right)^{T}\right.$$
$$+\left(\frac{\partial \mathbf{C_i^c}}{\partial q_{c_m}}\right)\vec{d}_{i,j}\vec{D}_{i,j}{}^T\mathbf{C_{i,j}^i}{}^T\mathbf{C_i^{c}}^{T}+\mathbf{C_i^c}\vec{d}_{i,j}\vec{D}_{i,j}{}^T\mathbf{C_{i,j}^i}{}^T\left(\frac{\partial \mathbf{C_i^c}}{\partial q_{c_m}}\right)^{T}$$
$$+\left(\frac{\partial \mathbf{C_i^c}}{\partial q_{c_m}}\right)\mathbf{C_{i,j}^i}\vec{D}_{i,j}\vec{d}_i{}^T+\mathbf{C_i^c}\mathbf{C_{i,j}^i}\vec{D}_{i,j}\vec{\phi}_{c_m}(o_i)^T$$

$$+\left(\frac{\partial \mathbf{C_i^c}}{\partial q_{cm}}\right)\mathbf{C_{i,j}^i}\vec{D}_{i,j}\vec{d}_{i,j}{}^T\mathbf{C_i^{c^T}}+\mathbf{C_i^c C_{i,j}^i}\vec{D}_{i,j}\vec{d}_{i,j}{}^T\left(\frac{\partial \mathbf{C_i^c}}{\partial q_{cm}}\right)^T\Bigg]\Bigg]\Bigg];$$

$$\begin{aligned}\frac{\partial \mathbf{I_{r,v}}}{\partial q_{cm}} &= \int_{m_c}\left[2\vec{\rho}_c{}^T\vec{\phi}_{cm}\mathbf{E}-\vec{\rho}_c\vec{\phi}_{cm}{}^T-\vec{\phi}_{cm}\vec{\rho}_c{}^T\right]dm_c\\
&+\sum_{i=1}^{N}\Bigg[-\left(\frac{\partial \mathbf{C_i^c}}{\partial q_{cm}}\right)\mathbf{D_i^r}\mathbf{C_i^{c^T}}-\mathbf{C_i^c D_i^r}{}^T\left(\frac{\partial \mathbf{C_i^c}}{\partial q_{cm}}\right)^T\\
&-\left(\frac{\partial \mathbf{C_i^c}}{\partial q_{cm}}\right)\mathbf{D_i^r}\mathbf{C_i^{c^T}}-\mathbf{C_i^c D_i^r}\left(\frac{\partial \mathbf{C_i^c}}{\partial q_{cm}}\right)^T\\
&+\sum_{j=1}^{N_i}\Bigg[-\left(\frac{\partial \mathbf{C_i^c}}{\partial q_{cm}}\right)\mathbf{C_{i,j}^i D_{i,j}^r}{}^T\mathbf{C_{i,j}^i}{}^T\mathbf{C_i^{c^T}}-\mathbf{C_i^c C_{i,j}^i D_{i,j}^r}{}^T\mathbf{C_{i,j}^i}{}^T\left(\frac{\partial \mathbf{C_i^c}}{\partial q_{cm}}\right)^T\\
&-\left(\frac{\partial \mathbf{C_i^c}}{\partial q_{cm}}\right)\mathbf{C_{i,j}^i D_{i,j}^r C_{i,j}^i}{}^T\mathbf{C_i^{c^T}}-\mathbf{C_i^c C_{i,j}^i D_{i,j}^r C_{i,j}^i}{}^T\left(\frac{\partial \mathbf{C_i^c}}{\partial q_{cm}}\right)^T\Bigg]\Bigg]. \qquad \text{(V-1)}\end{aligned}$$

The derivative of the moment of inertia matrix with respect to q_{in}, $\frac{\partial \mathbf{I_{sys}}}{\partial q_{in}}$, can be written as the sum of the different contributions,

$$\frac{\partial \mathbf{I_{sys}}}{\partial q_{in}}=\frac{\partial \mathbf{I_{cm}}}{\partial q_{in}}+\frac{\partial \mathbf{I_r}}{\partial q_{in}}+\frac{\partial \mathbf{I_h}}{\partial q_{in}}+\frac{\partial \mathbf{I_v}}{\partial q_{in}}+\frac{\partial \mathbf{I_{h,r}}}{\partial q_{in}}+\frac{\partial \mathbf{I_{h,v}}}{\partial q_{in}}+\frac{\partial \mathbf{I_{r,v}}}{\partial q_{in}},$$

where:

$$\frac{\partial \mathbf{I_{cm}}}{\partial q_{in}}=-M\left[2\left(\frac{\partial \vec{C}_{cm}}{\partial q_{in}}\right)^T\vec{C}_{cm}\mathbf{E}-\left(\frac{\partial \vec{C}_{cm}}{\partial q_{in}}\right)\vec{C}_{cm}^T-\vec{C}_{cm}\left(\frac{\partial \vec{C}_{cm}}{\partial q_{in}}\right)^T\right];$$

$$\frac{\partial \mathbf{I_r}}{\partial q_{in}}=-\sum_{j=1}^{N_i}\left[\mathbf{C_i^c}\left(\frac{\partial \mathbf{C_{i,j}^i}}{\partial q_{in}}\right)\mathbf{P_{i,j}^2 C_{i,j}^i}{}^T\mathbf{C_i^{c^T}}+\mathbf{C_i^c C_{i,j}^i P_{i,j}^2}\left(\frac{\partial \mathbf{C_{i,j}^i}}{\partial q_{in}}\right)^T\mathbf{C_i^{c^T}}\right];$$

$$\begin{aligned}\frac{\partial \mathbf{I_h}}{\partial q_{in}} &= \sum_{j=1}^{N_i}\Bigg[\Big[2\Big[\vec{\phi}_i(o_{i,j})^T\mathbf{C_i^{c^T}}\vec{d}_i+\vec{\phi}_i(o_{i,j})^T\vec{d}_{i,j}\Big]\mathbf{E}-\Big[\mathbf{C_i^c}\vec{\phi}_i(o_{i,j})\vec{d}_i{}^T\\
&+\vec{d}_i\vec{\phi}_i(o_{i,j})^T\mathbf{C_i^{c^T}}+\mathbf{C_i^c}\vec{\phi}_i(o_{i,j})\vec{d}_{i,j}{}^T\mathbf{C_i^{c^T}}+\mathbf{C_i^c}\vec{d}_{i,j}\vec{\phi}_i(o_{i,j})^T\mathbf{C_i^{c^T}}\Big]\Big]m_{i,j}\Bigg];\end{aligned}$$

$$\frac{\partial \mathbf{I_v}}{\partial q_{in}} = \int_{m_i} 2\vec{\delta_i}^T \vec{\phi}_{in}\, dm_i \mathbf{E} - \mathbf{C_i^c}\left\{ \int_{m_i} \vec{\phi}_{in} \vec{\delta_i}^T dm_i \right\} \mathbf{C_i^{cT}}$$
$$-\mathbf{C_i^c}\left\{ \int_{m_i} \vec{\delta_i} \vec{\phi_{in}}^T dm_i \right\} \mathbf{C_i^{cT}} - \sum_{j=1}^{N_i} \left[\mathbf{C_i^c} \left(\frac{\partial \mathbf{C_{i,j}^i}}{\partial q_{in}} \right) \mathbf{D_{i,j}^2} \mathbf{C_{i,j}^i}^T \mathbf{C_i^{cT}} \right.$$
$$\left. + \mathbf{C_i^c C_{i,j}^i D_{i,j}^2} \left(\frac{\partial \mathbf{C_{i,j}^i}}{\partial q_{in}} \right)^T \mathbf{C_i^{cT}} \right];$$

$$\frac{\partial \mathbf{I_{h,r}}}{\partial q_{in}} = \sum_{j=1}^{N_i} \left[2 \left[\vec{\phi}_{in}(o_{i,j})^T \mathbf{C_{i,j}^i} \vec{P}_{i,j} + \vec{d_i}^T \mathbf{C_i^c} \left(\frac{\partial \mathbf{C_{i,j}^i}}{\partial q_{in}} \right) \vec{P}_{i,j} \right.\right.$$
$$\left. + \vec{d}_{i,j}^{\,T} \left(\frac{\partial \mathbf{C_{i,j}^i}}{\partial q_{in}} \right) \vec{P}_{i,j} \right] \mathbf{E}$$
$$- \left[\vec{d_i} \vec{P}_{i,j}^{\,T} \left(\frac{\partial \mathbf{C_{i,j}^i}}{\partial q_{in}} \right)^T \mathbf{C_i^{cT}} + \mathbf{C_i^c} \vec{\phi}_{in}(o_{i,j}) \vec{P}_{i,j}^{\,T} \mathbf{C_{i,j}^i}^T \mathbf{C_i^{cT}} \right.$$
$$+ \mathbf{C_i^c} \vec{d}_{i,j} \vec{P}_{i,j}^{\,T} \left(\frac{\partial \mathbf{C_{i,j}^i}}{\partial q_{in}} \right)^T \mathbf{C_i^{cT}} + \mathbf{C_i^c} \left(\frac{\partial \mathbf{C_{i,j}^i}}{\partial q_{in}} \right) \vec{P}_{i,j} \vec{d_i}^T$$
$$\left.\left. + \mathbf{C_i^c} \left(\frac{\partial \mathbf{C_{i,j}^i}}{\partial q_{in}} \right) \vec{P}_{i,j} \vec{d}_{i,j}^{\,T} \mathbf{C_i^{cT}} + \mathbf{C_i^c C_{i,j}^i} \vec{P}_{i,j} \vec{\phi}_{in}(o_{i,j})^T \mathbf{C_i^{cT}} \right] \right];$$

$$\frac{\partial \mathbf{I_{h,v}}}{\partial q_{in}} = 2\vec{d_i}^T \mathbf{C_i^c} \left\{ \int_{m_i} \vec{\phi}_{in} dm_i \right\} \mathbf{E} - \vec{d_i} \left\{ \int_{m_i} \vec{\phi}_{in}^{\,T} dm_i \right\} \mathbf{C_i^{cT}}$$
$$-\mathbf{C_i^c} \left\{ \int_{m_i} \vec{\phi}_{in} dm_i \right\} \vec{d_i}^T$$
$$+ \sum_{j=1}^{N_i} \left[2 \left[\vec{d_i}^T \mathbf{C_i^c} \left(\frac{\partial \mathbf{C_{i,j}^i}}{\partial q_{in}} \right) \vec{D}_{i,j} + \vec{\phi}_{in}(o_{i,j})^T \mathbf{C_{i,j}^i} \vec{D}_{i,j} \right.\right.$$
$$\left. + \vec{d}_{i,j}^{\,T} \left(\frac{\partial \mathbf{C_{i,j}^i}}{\partial q_{in}} \right) \vec{D}_{i,j} \right] \mathbf{E} - \left[\vec{d_i} \vec{D}_{i,j}^{\,T} \left(\frac{\partial \mathbf{C_{i,j}^i}}{\partial q_{in}} \right)^T \mathbf{C_i^{cT}} \right.$$
$$\left. + \mathbf{C_i^c} \vec{\phi}_{in}(o_{i,j}) \vec{D}_{i,j}^{\,T} \mathbf{C_{i,j}^i}^T \mathbf{C_i^{cT}} + \mathbf{C_i^c} \vec{d}_{i,j} \vec{D}_{i,j}^{\,T} \left(\frac{\partial \mathbf{C_{i,j}^i}}{\partial q_{in}} \right)^T \mathbf{C_i^{cT}} \right.$$

$$+\mathbf{C_i^c}\left(\frac{\partial \mathbf{C_{i,j}^i}}{\partial q_{in}}\right)\vec{D}_{i,j}\vec{d}_i{}^T+\mathbf{C_i^c}\left(\frac{\partial \mathbf{C_{i,j}^i}}{\partial q_{in}}\right)\vec{D}_{i,j}\vec{d}_{i,j}{}^T\mathbf{C_i^{cT}}$$

$$+\mathbf{C_i^c C_{i,j}^i}\vec{D}_{i,j}\vec{\phi}_{in}(o_{i,j})^T\mathbf{C_i^{cT}}\Big]\Big];$$

$$\frac{\partial \mathbf{I_{r,v}}}{\partial q_{in}}=\int_{m_i}2\vec{\rho}_i{}^T\vec{\phi}_{in}\mathbf{E}-\mathbf{C_i^c}\left\{\int_{m_i}\vec{\rho}_i\vec{\phi}_{in}{}^T dm_i\right\}\mathbf{C_i^{cT}}$$

$$-\mathbf{C_i^c}\left\{\int_{m_i}\vec{\phi}_{in}\vec{\rho}_i{}^T dm_i\right\}\mathbf{C_i^{cT}}-\sum_{j=1}^{N_i}\Bigg[\mathbf{C_i^c}\left(\frac{\partial \mathbf{C_{i,j}^i}}{\partial q_{in}}\right)\mathbf{D_{i,j}^r}{}^T\mathbf{C_{i,j}^i}{}^T\mathbf{C_i^{cT}}$$

$$+\mathbf{C_i^c C_{i,j}^i D_{i,j}^r}{}^T\left(\frac{\partial \mathbf{C_{i,j}^i}}{\partial q_{in}}\right)^T\mathbf{C_i^{cT}}+\mathbf{C_i^c}\left(\frac{\partial \mathbf{C_{i,j}^i}}{\partial q_{in}}\right)\mathbf{D_{i,j}^r C_{i,j}^i}{}^T\mathbf{C_i^{cT}}$$

$$+\mathbf{C_i^c C_{i,j}^i D_{i,j}^r}\left(\frac{\partial \mathbf{C_{i,j}^i}}{\partial q_{in}}\right)^T\mathbf{C_i^{cT}}. \qquad \text{(V-2)}$$

The derivative of the moment of inertia matrix with respect to q_{i,j_p}, $\frac{\partial \mathbf{I_{sys}}}{\partial q_{i,j_p}}$, can be written as the sum of the different contributions,

$$\frac{\partial \mathbf{I_{sys}}}{\partial q_{i,j_p}}=\frac{\partial \mathbf{I_{cm}}}{\partial q_{i,j_p}}+\frac{\partial \mathbf{I_r}}{\partial q_{i,j_p}}+\frac{\partial \mathbf{I_h}}{\partial q_{i,j_p}}+\frac{\partial \mathbf{I_v}}{\partial q_{i,j_p}}+\frac{\partial \mathbf{I_{h,r}}}{\partial q_{i,j_p}}+\frac{\partial \mathbf{I_{h,v}}}{\partial q_{i,j_p}}+\frac{\partial \mathbf{I_{r,v}}}{\partial q_{i,j_p}},$$

where:

$$\frac{\partial \mathbf{I_{cm}}}{\partial q_{i,j_p}}=-M\Big[2\left(\frac{\partial \vec{C}_{cm}}{\partial q_{i,j_p}}\right)^T\vec{C}_{cm}\mathbf{E}-\left(\frac{\partial \vec{C}_{cm}}{\partial q_{i,j_p}}\right)\vec{C}_{cm}{}^T-\vec{C}_{cm}\left(\frac{\partial \vec{C}_{cm}^f}{\partial q_{i,j_p}}\right)^T\Big];$$

$$\frac{\partial \mathbf{I_r}}{\partial q_{i,j_p}}=0;$$

$$\frac{\partial \mathbf{I_h}}{\partial q_{i,j_p}}=0;$$

$$\frac{\partial \mathbf{I_v}}{\partial q_{i,j_p}}=2\int_{m_{i,j}}\vec{\phi}_{i,j_p}{}^T\vec{\delta}_{i,j}\,dm_{i,j}\mathbf{E}-\mathbf{C_i^c C_{i,j}^i}\Big\{\int_{m_{i,j}}\vec{\phi}_{i,j_p}\vec{\delta}_{i,j}{}^T dm_{i,j}\Big\}\mathbf{C_{i,j}^i}{}^T\mathbf{C_i^{cT}}$$

$$-\mathbf{C_i^c C_{i,j}^i}\Big\{\int_{m_{i,j}} \vec{\delta}_{i,j}\vec{\phi}_{i,j_p}{}^T dm_{i,j}\Big\}\mathbf{C_{i,j}^i}{}^T\mathbf{C_i^{cT}};$$

$$\frac{\partial \mathbf{I_{h,r}}}{\partial q_{i,j_p}} = 0;$$

$$\begin{aligned}\frac{\partial \mathbf{I_{h,v}}}{\partial q_{i,j_p}} =& 2\vec{d}_i{}^T\mathbf{C_i^c C_{i,j}^i}\Big\{\int_{m_{i,j}} \vec{\phi}_{i,j_p} dm_{i,j}\Big\}\mathbf{E} + 2\vec{d}_{i,j}{}^T\mathbf{C_{i,j}^i}\Big\{\int_{m_{i,j}} \vec{\phi}_{i,j_p} dm_{i,j}\Big\}\mathbf{E} \\ &-\vec{d}_i\Big\{\int_{m_{i,j}} \vec{\phi}_{i,j_p}{}^T dm_{i,j}\Big\}\mathbf{C_{i,j}^i}{}^T\mathbf{C_i^{cT}} - \mathbf{C_i^c}\vec{d}_{i,j}\Big\{\int_{m_{i,j}} \vec{\phi}_{i,j_p}{}^T dm_{i,j}\Big\}\mathbf{C_{i,j}^i}{}^T\mathbf{C_i^{cT}} \\ &-\mathbf{C_i^c C_{i,j}^i}\int_{m_{i,j}} \Big\{\vec{\phi}_{i,j_p} dm_{i,j}\Big\}\vec{d}_i{}^T - \mathbf{C_i^c C_{i,j}^i}\Big\{\int_{m_{i,j}} \vec{\phi}_{i,j_p} dm_{i,j}\Big\}\vec{d}_{i,j}{}^T\mathbf{C_i^{cT}};\end{aligned}$$

$$\begin{aligned}\frac{\partial \mathbf{I_{r,v}}}{\partial q_{i,j_p}} =& 2\Big\{\int_{m_{i,j}} \vec{\rho}_{i,j}{}^T\vec{\phi}_{i,j_p} dm_{i,j}\Big\}\mathbf{E} - \mathbf{C_i^c C_{i,j}^i}\Big\{\int_{m_{i,j}} \vec{\rho}_{i,j}\vec{\phi}_{i,j_p}{}^T dm_{i,j}\Big\}\mathbf{C_{i,j}^i}{}^T\mathbf{C_i^{cT}} \\ &-\mathbf{C_i^c C_{i,j}^i}\Big\{\int_{m_{i,j}} \vec{\phi}_{i,j_p}\vec{\rho}_{i,j}{}^T dm_{i,j}\Big\}\mathbf{C_{i,j}^i}{}^T\mathbf{C_i^{cT}}.\end{aligned} \qquad (V-3)$$

As mentioned before, considerable simplification of various expressions takes place due to cancellation of terms. Reduced expressions are presented below:

$$\begin{aligned}\frac{\partial \vec{H}}{\partial \dot{q}_{c_m}} =& \int_{m_c}\Big[(\vec{\rho}_c \times \vec{\phi}_{c_m}) + (\vec{\delta}_c \times \vec{\phi}_{c_m})\Big]dm_c + \sum_{i=1}^{N}\Bigg[\Big[\vec{d}_i \times \vec{\phi}_{c_m}(o_i)\Big]m_i \\ &+\int_{m_i}\Big[\mathbf{C_i^c}\vec{\rho}_i \times \vec{\phi}_{c_m}(o_i) + \mathbf{C_i^c}\vec{\delta}_i \times \vec{\phi}_{c_m}(o_i) + \mathbf{C_i^c}\vec{\rho}_i \times \left(\frac{\partial \mathbf{C_i^c}}{\partial q_{c_m}}(\vec{\rho}_i + \vec{\delta}_i)\right) \\ &+\mathbf{C_i^c}\vec{\delta}_i \times \left(\frac{\partial \mathbf{C_i^c}}{\partial q_{c_m}}(\vec{\rho}_i + \vec{\delta}_i)\right) + \vec{d}_i \times \left(\frac{\partial \mathbf{C_i^c}}{\partial q_{c_m}}(\vec{\rho}_i + \vec{\delta}_i)\right)\Big]dm_i \\ &+\sum_{j=1}^{N_i}\Bigg[\Big[(\vec{d}_i + \mathbf{C_i^c}\vec{d}_{i,j}) \times \vec{\phi}_{c_m}(o_i) + (\vec{d}_i + \mathbf{C_i^c}\vec{d}_{i,j}) \times \left(\frac{\partial \mathbf{C_i^c}}{\partial q_{c_m}}\vec{d}_{i,j}\right)\Big]m_{i,j} \\ &+\int_{m_{i,j}}\Big[\mathbf{C_i^c C_{i,j}^i}\vec{\rho}_{i,j} \times \vec{\phi}_{c_m}(o_i) + \mathbf{C_i^c C_{i,j}^i}\vec{\delta}_{i,j} \times \vec{\phi}_{c_m}(o_i) \\ &+\mathbf{C_i^c C_{i,j}^i}\vec{\rho}_{i,j} \times \left(\frac{\partial \mathbf{C_i^c}}{\partial q_{c_m}}\vec{d}_{i,j}\right) + \mathbf{C_i^c C_{i,j}^i}\vec{\delta}_{i,j} \times \left(\frac{\partial \mathbf{C_i^c}}{\partial q_{c_m}}\vec{d}_{i,j}\right)\end{aligned}$$

$$
\begin{aligned}
&+(\vec{d}_i + \mathbf{C}_{\mathbf{i}}^{\mathbf{c}}\vec{d}_{i,j}) \times \left(\frac{\partial \mathbf{C}_{\mathbf{i}}^{\mathbf{c}}}{\partial q_{cm}}\mathbf{C}_{\mathbf{i,j}}^{\mathbf{i}}(\vec{\rho}_{i,j} + \vec{\delta}_{i,j})\right) \\
&+\mathbf{C}_{\mathbf{i}}^{\mathbf{c}}\mathbf{C}_{\mathbf{i,j}}^{\mathbf{i}}\vec{\rho}_{i,j} \times \left(\frac{\partial \mathbf{C}_{\mathbf{i}}^{\mathbf{c}}}{\partial q_{cm}}\mathbf{C}_{\mathbf{i,j}}^{\mathbf{i}}(\vec{\rho}_{i,j} + \vec{\delta}_{i,j})\right) \\
&+\mathbf{C}_{\mathbf{i}}^{\mathbf{c}}\mathbf{C}_{\mathbf{i,j}}^{\mathbf{i}}\vec{\delta}_{i,j} \times \left(\frac{\partial \mathbf{C}_{\mathbf{i}}^{\mathbf{c}}}{\partial q_{cm}}\mathbf{C}_{\mathbf{i,j}}^{\mathbf{i}}(\vec{\rho}_{i,j} + \vec{\delta}_{i,j})\right)\Big] dm_{i,j}\Bigg]\Bigg] \\
&-M\left[\vec{C}_{cm} \times \left(\frac{\partial \vec{C}_{cm}}{\partial q_{cm}}\right)\right]; \qquad \text{(V-4)}
\end{aligned}
$$

$$
\begin{aligned}
&\left[\frac{d}{dt}\left(\frac{\partial \vec{H}}{\partial \dot{q}_{cm}}\right) - \frac{\partial \vec{H}}{\partial q_{cm}}\right] = \\
&2\Bigg\{\int_{m_c} (\dot{\vec{\delta}}_c \times \vec{\phi}_{cm})\, dm_c + \sum_{i=1}^{N}\Bigg[\left[\dot{\vec{d}}_i \times \vec{\phi}_{cm}(o_i)\right] m_i \\
&+\int_{m_i}\Big[\dot{\mathbf{C}}_{\mathbf{i}}^{\mathbf{c}}\vec{\rho}_i \times \vec{\phi}_{cm}(o_i) + \dot{\mathbf{C}}_{\mathbf{i}}^{\mathbf{c}}\vec{\delta}_i \times \vec{\phi}_{cm}(o_i) + \mathbf{C}_{\mathbf{i}}^{\mathbf{c}}\dot{\vec{\delta}}_i \times \vec{\phi}_{cm}(o_i) \\
&+\dot{\vec{d}}_i \times \left(\frac{\partial \mathbf{C}_{\mathbf{i}}^{\mathbf{c}}}{\partial q_{cm}}\vec{\rho}_i\right) + \dot{\vec{d}}_i \times \left(\frac{\partial \mathbf{C}_{\mathbf{i}}^{\mathbf{c}}}{\partial q_{cm}}\vec{\delta}_i\right) + \mathbf{C}_{\mathbf{i}}^{\mathbf{c}}\dot{\vec{\delta}}_i \times \left(\frac{\partial \mathbf{C}_{\mathbf{i}}^{\mathbf{c}}}{\partial q_{cm}}\vec{\rho}_i\right) \\
&+\mathbf{C}_{\mathbf{i}}^{\mathbf{c}}\dot{\vec{\delta}}_i \times \left(\frac{\partial \mathbf{C}_{\mathbf{i}}^{\mathbf{c}}}{\partial q_{cm}}\vec{\delta}_i\right) + \dot{\mathbf{C}}_{\mathbf{i}}^{\mathbf{c}}\vec{\rho}_i \times \left(\frac{\partial \mathbf{C}_{\mathbf{i}}^{\mathbf{c}}}{\partial q_{cm}}\vec{\rho}_i\right) + \dot{\mathbf{C}}_{\mathbf{i}}^{\mathbf{c}}\vec{\rho}_i \times \left(\frac{\partial \mathbf{C}_{\mathbf{i}}^{\mathbf{c}}}{\partial q_{cm}}\vec{\delta}_i\right) \\
&+\dot{\mathbf{C}}_{\mathbf{i}}^{\mathbf{c}}\vec{\delta}_i \times \left(\frac{\partial \mathbf{C}_{\mathbf{i}}^{\mathbf{c}}}{\partial q_{cm}}\vec{\delta}_i\right) + \dot{\mathbf{C}}_{\mathbf{i}}^{\mathbf{c}}\vec{\delta}_i \times \left(\frac{\partial \mathbf{C}_{\mathbf{i}}^{\mathbf{c}}}{\partial q_{cm}}\vec{\rho}_i\right)\Big]\, dm_i \\
&+\sum_{j=1}^{N_i}\Bigg[\Big[(\dot{\vec{d}}_i + \mathbf{C}_{\mathbf{i}}^{\mathbf{c}}\dot{\vec{d}}_{i,j} + \dot{\mathbf{C}}_{\mathbf{i}}^{\mathbf{c}}\vec{d}_{i,j}) \times \vec{\phi}_{cm}(o_i) + (\dot{\vec{d}}_i + \mathbf{C}_{\mathbf{i}}^{\mathbf{c}}\dot{\vec{d}}_{i,j} + \dot{\mathbf{C}}_{\mathbf{i}}^{\mathbf{c}}\vec{d}_{i,j}) \times \\
&\left(\frac{\partial \mathbf{C}_{\mathbf{i}}^{\mathbf{c}}}{\partial q_{cm}}\vec{d}_{i,j}\right)\Big] m_{i,j} + \int_{m_{i,j}}\Big[\Big(\dot{\mathbf{C}}_{\mathbf{i}}^{\mathbf{c}}\mathbf{C}_{\mathbf{i,j}}^{\mathbf{i}}(\vec{\rho}_{i,j} + \vec{\delta}_{i,j}) + \mathbf{C}_{\mathbf{i}}^{\mathbf{c}}\dot{\mathbf{C}}_{\mathbf{i,j}}^{\mathbf{i}}(\vec{\rho}_{i,j} + \vec{\delta}_{i,j}) \\
&+\mathbf{C}_{\mathbf{i}}^{\mathbf{c}}\mathbf{C}_{\mathbf{i,j}}^{\mathbf{i}}\dot{\vec{\delta}}_{i,j}\Big) \times \vec{\phi}_{cm}(o_i) + (\dot{\vec{d}}_i + \mathbf{C}_{\mathbf{i}}^{\mathbf{c}}\dot{\vec{d}}_{i,j} + \dot{\mathbf{C}}_{\mathbf{i}}^{\mathbf{c}}\vec{d}_{i,j}) \times \left(\frac{\partial \mathbf{C}_{\mathbf{i}}^{\mathbf{c}}}{\partial q_{cm}}\mathbf{C}_{\mathbf{i,j}}^{\mathbf{i}}\vec{\rho}_{i,j}\right) \\
&+(\dot{\vec{d}}_i + \mathbf{C}_{\mathbf{i}}^{\mathbf{c}}\dot{\vec{d}}_{i,j} + \dot{\mathbf{C}}_{\mathbf{i}}^{\mathbf{c}}\vec{d}_{i,j}) \times \left(\frac{\partial \mathbf{C}_{\mathbf{i}}^{\mathbf{c}}}{\partial q_{cm}}\mathbf{C}_{\mathbf{i,j}}^{\mathbf{i}}\vec{\delta}_{i,j}\right) \\
&+\left(\dot{\mathbf{C}}_{\mathbf{i}}^{\mathbf{c}}\mathbf{C}_{\mathbf{i,j}}^{\mathbf{i}}(\vec{\rho}_{i,j} + \vec{\delta}_{i,j}) + \mathbf{C}_{\mathbf{i}}^{\mathbf{c}}\dot{\mathbf{C}}_{\mathbf{i,j}}^{\mathbf{i}}(\vec{\rho}_{i,j} + \vec{\delta}_{i,j}) + \mathbf{C}_{\mathbf{i}}^{\mathbf{c}}\mathbf{C}_{\mathbf{i,j}}^{\mathbf{i}}\dot{\vec{\delta}}_{i,j}\right) \times \\
&\left(\frac{\partial \mathbf{C}_{\mathbf{i}}^{\mathbf{c}}}{\partial q_{cm}}\vec{d}_{i,j} + \frac{\partial \mathbf{C}_{\mathbf{i}}^{\mathbf{c}}}{\partial q_{cm}}\mathbf{C}_{\mathbf{i,j}}^{\mathbf{i}}\vec{\delta}_{i,j} + \frac{\partial \mathbf{C}_{\mathbf{i}}^{\mathbf{c}}}{\partial q_{cm}}\mathbf{C}_{\mathbf{i,j}}^{\mathbf{i}}\vec{\rho}_{i,j}\right)\Big] dm_{i,j}\Bigg]\Bigg]\Bigg\}
\end{aligned}
$$

$$-2M\left(\dot{\vec{C}}_{cm}\times\frac{\partial\vec{C}_{cm}}{\partial q_{c_m}}\right); \tag{V-5}$$

$$\begin{aligned}\frac{\partial\vec{H}}{\partial\dot{q}_{i_n}} &= \int_{m_i}\left[\vec{d}_i\times\mathbf{C}_{\mathbf{i}}^{\mathbf{c}}\vec{\phi}_{i_n}+\mathbf{C}_{\mathbf{i}}^{\mathbf{c}}(\vec{\rho}_i\times\vec{\phi}_{i_n})+\mathbf{C}_{\mathbf{i}}^{\mathbf{c}}(\vec{\delta}_i\times\vec{\phi}_{i_n})\right]dm_i\\
&+\sum_{j=1}^{N_i}\left[\left[(\vec{d}_i+\mathbf{C}_{\mathbf{i}}^{\mathbf{c}}\vec{d}_{i,j})\times\mathbf{C}_{\mathbf{i}}^{\mathbf{c}}\vec{\phi}_{i_n}(o_{i,j})\right]m_{i,j}\right.\\
&+\int_{m_{i,j}}\left[\mathbf{C}_{\mathbf{i}}^{\mathbf{c}}\left(\mathbf{C}_{\mathbf{i,j}}^{\mathbf{i}}\vec{\rho}_{i,j}\times\vec{\phi}_{i_n}(o_{i,j})\right)+\mathbf{C}_{\mathbf{i}}^{\mathbf{c}}\left(\mathbf{C}_{\mathbf{i,j}}^{\mathbf{i}}\vec{\delta}_{i,j}\times\vec{\phi}_{i_n}(o_{i,j})\right)\right.\\
&+\mathbf{C}_{\mathbf{i}}^{\mathbf{c}}\left(\mathbf{C}_{\mathbf{i,j}}^{\mathbf{i}}(\vec{\rho}_{i,j}+\vec{\delta}_{i,j})\times\left(\frac{\partial\mathbf{C}_{\mathbf{i,j}}^{\mathbf{i}}}{\partial q_{i_n}}(\vec{\rho}_{i,j}+\vec{\delta}_{i,j})\right)\right)\\
&\left.\left.+(\vec{d}_i+\mathbf{C}_{\mathbf{i}}^{\mathbf{c}}\vec{d}_{i,j})\times\left(\mathbf{C}_{\mathbf{i}}^{\mathbf{c}}\frac{\partial\mathbf{C}_{\mathbf{i,j}}^{\mathbf{i}}}{\partial q_{i_n}}(\vec{\rho}_{i,j}+\vec{\delta}_{i,j})\right)\right]dm_{i,j}\right]\\
&-M\left[\vec{C}_{cm}\times\left(\frac{\partial\vec{C}_{cm}}{\partial q_{i_n}}\right)\right];\end{aligned} \tag{V-6}$$

$$\begin{aligned}&\left[\frac{d}{dt}\left(\frac{\partial\vec{H}}{\partial\dot{q}_{i_n}}\right)-\frac{\partial\vec{H}}{\partial q_{i_n}}\right]=\\
&2\left\{\int_{m_i}\left[\dot{\vec{d}}_i\times\mathbf{C}_{\mathbf{i}}^{\mathbf{c}}\vec{\phi}_{i_n}+\dot{\mathbf{C}}_{\mathbf{i}}^{\mathbf{c}}\vec{\rho}_i\times\mathbf{C}_{\mathbf{i}}^{\mathbf{c}}\vec{\phi}_{i_n}+\dot{\mathbf{C}}_{\mathbf{i}}^{\mathbf{c}}\vec{\delta}_i\times\mathbf{C}_{\mathbf{i}}^{\mathbf{c}}\vec{\phi}_{i_n}+\mathbf{C}_{\mathbf{i}}^{\mathbf{c}}\dot{\vec{\delta}}_i\times\mathbf{C}_{\mathbf{i}}^{\mathbf{c}}\vec{\phi}_{i_n}\right]dm_i\right.\\
&+\sum_{j=1}^{N_i}\left[\left[(\dot{\vec{d}}_i+\mathbf{C}_{\mathbf{i}}^{\mathbf{c}}\dot{\vec{d}}_{i,j}+\dot{\mathbf{C}}_{\mathbf{i}}^{\mathbf{c}}\vec{d}_{i,j})\times\mathbf{C}_{\mathbf{i}}^{\mathbf{c}}\vec{\phi}_{i_n}(o_{i,j})\right]m_{i,j}\right.\\
&+\int_{m_{i,j}}\left[\left(\dot{\mathbf{C}}_{\mathbf{i}}^{\mathbf{c}}\mathbf{C}_{\mathbf{i,j}}^{\mathbf{i}}(\vec{\rho}_{i,j}+\vec{\delta}_{i,j})+\mathbf{C}_{\mathbf{i}}^{\mathbf{c}}\dot{\mathbf{C}}_{\mathbf{i,j}}^{\mathbf{i}}(\vec{\rho}_{i,j}+\vec{\delta}_{i,j})+\mathbf{C}_{\mathbf{i}}^{\mathbf{c}}\mathbf{C}_{\mathbf{i,j}}^{\mathbf{i}}\dot{\vec{\delta}}_{i,j}\right)\times\mathbf{C}_{\mathbf{i}}^{\mathbf{c}}\vec{\phi}_{i_n}(o_{i,j})\right.\\
&+(\dot{\vec{d}}_i+\mathbf{C}_{\mathbf{i}}^{\mathbf{c}}\dot{\vec{d}}_{i,j}+\dot{\mathbf{C}}_{\mathbf{i}}^{\mathbf{c}}\vec{d}_{i,j})\times\left(\mathbf{C}_{\mathbf{i}}^{\mathbf{c}}\frac{\partial\mathbf{C}_{\mathbf{i,j}}^{\mathbf{i}}}{\partial q_{i_n}}(\vec{\rho}_{i,j}+\vec{\delta}_{i,j})\right)\\
&\left.\left.\left.+\left(\dot{\mathbf{C}}_{\mathbf{i}}^{\mathbf{c}}\mathbf{C}_{\mathbf{i,j}}^{\mathbf{i}}(\vec{\rho}_{i,j}+\vec{\delta}_{i,j})+\mathbf{C}_{\mathbf{i}}^{\mathbf{c}}\dot{\mathbf{C}}_{\mathbf{i,j}}^{\mathbf{i}}(\vec{\rho}_{i,j}+\vec{\delta}_{i,j})+\mathbf{C}_{\mathbf{i}}^{\mathbf{c}}\mathbf{C}_{\mathbf{i,j}}^{\mathbf{i}}\dot{\vec{\delta}}_{i,j}\right)\times\right.\right.\right.\\
&\left.\left.\left.\left(\mathbf{C}_{\mathbf{i}}^{\mathbf{c}}\frac{\partial\mathbf{C}_{\mathbf{i,j}}^{\mathbf{i}}}{\partial q_{i_n}}(\vec{\rho}_{i,j}+\vec{\delta}_{i,j})\right)\right]dm_{i,j}\right]\right\}-2M\left(\dot{\vec{C}}_{cm}^{f}\times\frac{\partial\vec{C}_{cm}^{f}}{\partial q_{i_n}}\right);\end{aligned} \tag{V-7}$$

$$\frac{\partial \vec{H}}{\partial \dot{q}_{i,j_p}} = (\vec{d}_i + \mathbf{C}_\mathbf{i}^\mathbf{c}\vec{d}_{i,j}) \times \left(\mathbf{C}_\mathbf{i}^\mathbf{c}\mathbf{C}_\mathbf{i,j}^\mathbf{i} \int_{m_{i,j}} \vec{\phi}_{i,j_p}\, dm_{i,j} \right)$$
$$+\mathbf{C}_\mathbf{i}^\mathbf{c}\mathbf{C}_\mathbf{i,j}^\mathbf{i} \int_{m_{i,j}} (\vec{\rho}_{i,j} \times \vec{\phi}_{i,j_p})\, dm_{i,j}$$
$$+\mathbf{C}_\mathbf{i}^\mathbf{c}\mathbf{C}_\mathbf{i,j}^\mathbf{i} \int_{m_{i,j}} (\vec{\delta}_{i,j} \times \vec{\phi}_{i,j_p})\, dm_{i,j}$$
$$-M\vec{C}_{cm} \times \left(\frac{\partial \vec{C}_{cm}}{\partial q_{i,j_p}} \right); \qquad \text{(V-8)}$$

$$\left[\frac{d}{dt} \left(\frac{\partial \vec{H}}{\partial \dot{q}_{i,j_p}} \right) - \frac{\partial \vec{H}}{\partial q_{i,j_p}} \right] =$$
$$2 \Bigg\{ (\dot{\vec{d}}_i + \mathbf{C}_\mathbf{i}^\mathbf{c}\dot{\vec{d}}_{i,j} + \dot{\mathbf{C}}_\mathbf{i}^\mathbf{c}\vec{d}_{i,j}) \times \left(\mathbf{C}_\mathbf{i}^\mathbf{c}\mathbf{C}_\mathbf{i,j}^\mathbf{i} \int_{m_{i,j}} \vec{\phi}_{i,j_p}\, dm_{i,j} \right)$$
$$+ \int_{m_{i,j}} \Big[\left(\dot{\mathbf{C}}_\mathbf{i}^\mathbf{c}\mathbf{C}_\mathbf{i,j}^\mathbf{i}(\vec{\rho}_{i,j} + \vec{\delta}_{i,j}) + \mathbf{C}_\mathbf{i}^\mathbf{c}\dot{\mathbf{C}}_\mathbf{i,j}^\mathbf{i}(\vec{\rho}_{i,j} + \vec{\delta}_{i,j}) + \mathbf{C}_\mathbf{i}^\mathbf{c}\mathbf{C}_\mathbf{i,j}^\mathbf{i}\dot{\vec{\delta}}_{i,j} \right) \times$$
$$(\mathbf{C}_\mathbf{i}^\mathbf{c}\mathbf{C}_\mathbf{i,j}^\mathbf{i}\vec{\phi}_{i,j_p}) \Big] dm_{i,j} \Bigg\} - 2M \left(\dot{\vec{C}}_{cm} \times \frac{\partial \vec{C}_{cm}}{\partial q_{i,j_p}} \right). \qquad \text{(V-9)}$$

Appendix VI: Derivatives of $\mathbf{I_{sys}}$ and $\vec{H}$ w.r.t. the Joint Generalized Coordinates

The derivative of the moment of inertia matrix with respect to $\alpha^s_{a_i}$, $\frac{\partial \mathbf{I_{sys}}}{\partial \alpha^s_{a_i}}$, can be written as the sum of the different contributions,

$$\frac{\partial \mathbf{I_{sys}}}{\partial \alpha^s_{a_i}} = \frac{\partial \mathbf{I_{cm}}}{\partial \alpha^s_{a_i}} + \frac{\partial \mathbf{I_r}}{\partial \alpha^s_{a_i}} + \frac{\partial \mathbf{I_h}}{\partial \alpha^s_{a_i}} + \frac{\partial \mathbf{I_v}}{\partial \alpha^s_{a_i}} + \frac{\partial \mathbf{I_{h,r}}}{\partial \alpha^s_{a_i}} + \frac{\partial \mathbf{I_{h,v}}}{\partial \alpha^s_{a_i}} + \frac{\partial \mathbf{I_{r,v}}}{\partial \alpha^s_{a_i}},$$

where:

$$\frac{\partial \mathbf{I_{cm}}}{\partial \alpha^s_{a_i}} = -M\left[2\left(\frac{\partial \vec{C}_{cm}}{\partial \alpha^s_{a_i}}\right)^T \vec{C}_{cm}\mathbf{E} - \left(\frac{\partial \vec{C}_{cm}}{\partial \alpha^s_{a_i}}\right)\vec{C}_{cm}{}^T - \vec{C}_{cm}{}^T\left(\frac{\partial \vec{C}_{cm}}{\partial \alpha^s_{a_i}}\right)^T\right];$$

$$\begin{aligned}\frac{\partial \mathbf{I_r}}{\partial \alpha^s_{a_i}} =& -\left(\frac{\partial \mathbf{C^c_i}}{\partial \alpha^s_{a_i}}\right)\mathbf{P^2_i}\mathbf{C^{c\,T}_i} - \mathbf{C^c_i}\mathbf{P^2_i}\left(\frac{\partial \mathbf{C^c_i}}{\partial \alpha^s_{a_i}}\right)^T \\ & -\sum_{j=1}^{N_i}\left[\left(\frac{\partial \mathbf{C^c_i}}{\partial \alpha^s_{a_i}}\right)\mathbf{C^i_{i,j}}\mathbf{P^2_{i,j}}\mathbf{C^{i}_{i,j}}{}^T\mathbf{C^{c\,T}_i} + \mathbf{C^c_i}\mathbf{C^i_{i,j}}\mathbf{P^2_{i,j}}\mathbf{C^{i}_{i,j}}{}^T\left(\frac{\partial \mathbf{C^c_i}}{\partial \alpha^s_{a_i}}\right)^T\right];\end{aligned}$$

$$\begin{aligned}\frac{\partial \mathbf{I_h}}{\partial \alpha^s_{a_i}} =& \sum_{j=1}^{N_i}\left[\left[2\left[\vec{d}_{i,j}{}^T\left(\frac{\partial \mathbf{C^c_i}}{\partial \alpha^s_{a_i}}\right)^T\vec{d}_i\right]\mathbf{E} - \left(\frac{\partial \mathbf{C^c_i}}{\partial \alpha^s_{a_i}}\right)\vec{d}_{i,j}\vec{d}_i{}^T - \vec{d}_i\vec{d}_{i,j}{}^T\left(\frac{\partial \mathbf{C^c_i}}{\partial \alpha^s_{a_i}}\right)^T\right.\right. \\ & \left.\left. - \left(\frac{\partial \mathbf{C^c_i}}{\partial \alpha^s_{a_i}}\right)\vec{d}_{i,j}\vec{d}_{i,j}{}^T\mathbf{C^{c\,T}_i} - \mathbf{C^c_i}\vec{d}_{i,j}\vec{d}_{i,j}{}^T\left(\frac{\partial \mathbf{C^c_i}}{\partial \alpha^s_{a_i}}\right)^T\right]m_{i,j}\right];\end{aligned}$$

$$\begin{aligned}\frac{\partial \mathbf{I_v}}{\partial \alpha^s_{a_i}} =& -\left(\frac{\partial \mathbf{C^c_i}}{\partial \alpha^s_{a_i}}\right)\mathbf{D^2_i}\mathbf{C^{c\,T}_i} - \mathbf{C^c_i}\mathbf{D^2_i}\left(\frac{\partial \mathbf{C^c_i}}{\partial \alpha^s_{a_i}}\right)^T \\ & -\sum_{j=1}^{N_i}\left[\left(\frac{\partial \mathbf{C^c_i}}{\partial \alpha^s_{a_i}}\right)\mathbf{C^i_{i,j}}\mathbf{D^2_{i,j}}\mathbf{C^{i}_{i,j}}{}^T\mathbf{C^{c\,T}_i} + \mathbf{C^c_i}\mathbf{C^i_{i,j}}\mathbf{D^2_{i,j}}\mathbf{C^{i}_{i,j}}{}^T\left(\frac{\partial \mathbf{C^c_i}}{\partial \alpha^s_{a_i}}\right)^T\right];\end{aligned}$$

$$\frac{\partial \mathbf{I_{h,r}}}{\partial \alpha^s_{a_i}} = 2\left[\vec{d}_i{}^T\left(\frac{\partial \mathbf{C^c_i}}{\partial \alpha^s_{a_i}}\right)\vec{P}_i\right]\mathbf{E} - \vec{d}_i\vec{P}_i{}^T\left(\frac{\partial \mathbf{C^c_i}}{\partial \alpha^s_{a_i}}\right)^T - \left(\frac{\partial \mathbf{C^c_i}}{\partial \alpha^s_{a_i}}\right)\vec{P}_i\vec{d}_i{}^T$$

$$
\begin{aligned}
&+\sum_{j=1}^{N_i}\left[2\left[\vec{d}_i^{\,T}\left(\frac{\partial \mathbf{C}_\mathbf{i}^\mathbf{c}}{\partial \alpha_{a_i}^s}\right)\mathbf{C}_{\mathbf{i},\mathbf{j}}^{\mathbf{i}}\vec{P}_{i,j}\right]\mathbf{E}-\left[\vec{d}_i\vec{P}_{i,j}{}^T\mathbf{C}_{\mathbf{i},\mathbf{j}}^{\mathbf{i}}{}^T\left(\frac{\partial \mathbf{C}_\mathbf{i}^\mathbf{c}}{\partial \alpha_{a_i}^s}\right)^T\right.\right.\\
&+\left(\frac{\partial \mathbf{C}_\mathbf{i}^\mathbf{c}}{\partial \alpha_{a_i}^s}\right)\vec{d}_{i,j}\vec{P}_{i,j}{}^T\mathbf{C}_{\mathbf{i},\mathbf{j}}^{\mathbf{i}}{}^T\mathbf{C}_\mathbf{i}^{\mathbf{c}T}+\mathbf{C}_\mathbf{i}^\mathbf{c}\vec{d}_{i,j}\vec{P}_{i,j}{}^T\mathbf{C}_{\mathbf{i},\mathbf{j}}^{\mathbf{i}}{}^T\left(\frac{\partial \mathbf{C}_\mathbf{i}^\mathbf{c}}{\partial \alpha_{a_i}^s}\right)^T\\
&+\left(\frac{\partial \mathbf{C}_\mathbf{i}^\mathbf{c}}{\partial \alpha_{a_i}^s}\right)\mathbf{C}_{\mathbf{i},\mathbf{j}}^{\mathbf{i}}\vec{P}_{i,j}\vec{d}_i^{\,T}+\left(\frac{\partial \mathbf{C}_\mathbf{i}^\mathbf{c}}{\partial \alpha_{a_i}^s}\right)\mathbf{C}_{\mathbf{i},\mathbf{j}}^{\mathbf{i}}\vec{P}_{i,j}\vec{d}_{i,j}{}^T\mathbf{C}_\mathbf{i}^{\mathbf{c}T}\\
&\left.\left.+\mathbf{C}_\mathbf{i}^\mathbf{c}\mathbf{C}_{\mathbf{i},\mathbf{j}}^{\mathbf{i}}\vec{P}_{i,j}\vec{d}_{i,j}{}^T\left(\frac{\partial \mathbf{C}_\mathbf{i}^\mathbf{c}}{\partial \alpha_{a_i}^s}\right)^T\right]\right];
\end{aligned}
$$

$$
\begin{aligned}
\frac{\partial \mathbf{I}_{\mathbf{h},\mathbf{v}}}{\partial \alpha_{a_i}^s}=&2\left[\vec{d}_i^{\,T}\left(\frac{\partial \mathbf{C}_\mathbf{i}^\mathbf{c}}{\partial \alpha_{a_i}^s}\right)\vec{D}_i\right]\mathbf{E}-\vec{d}_i\vec{D}_i^T\left(\frac{\partial \mathbf{C}_\mathbf{i}^\mathbf{c}}{\partial \alpha_{a_i}^s}\right)^T-\left(\frac{\partial \mathbf{C}_\mathbf{i}^\mathbf{c}}{\partial \alpha_{a_i}^s}\right)\vec{D}_i\vec{d}_i^{\,T}\\
&+\sum_{j=1}^{N_i}\left[2\left[\vec{d}_i^{\,T}\left(\frac{\partial \mathbf{C}_\mathbf{i}^\mathbf{c}}{\partial \alpha_{a_i}^s}\right)\mathbf{C}_{\mathbf{i},\mathbf{j}}^{\mathbf{i}}\vec{D}_{i,j}\right]\mathbf{E}-\left[\vec{d}_i\vec{D}_{i,j}{}^T\mathbf{C}_{\mathbf{i},\mathbf{j}}^{\mathbf{i}}{}^T\left(\frac{\partial \mathbf{C}_\mathbf{i}^\mathbf{c}}{\partial \alpha_{a_i}^s}\right)^T\right.\right.\\
&+\left(\frac{\partial \mathbf{C}_\mathbf{i}^\mathbf{c}}{\partial \alpha_{a_i}^s}\right)\vec{d}_{i,j}\vec{D}_{i,j}{}^T\mathbf{C}_{\mathbf{i},\mathbf{j}}^{\mathbf{i}}{}^T\mathbf{C}_\mathbf{i}^{\mathbf{c}T}+\mathbf{C}_\mathbf{i}^\mathbf{c}\vec{d}_{i,j}\vec{D}_{i,j}{}^T\mathbf{C}_{\mathbf{i},\mathbf{j}}^{\mathbf{i}}{}^T\left(\frac{\partial \mathbf{C}_\mathbf{i}^\mathbf{c}}{\partial \alpha_{a_i}^s}\right)^T\\
&+\left(\frac{\partial \mathbf{C}_\mathbf{i}^\mathbf{c}}{\partial \alpha_{a_i}^s}\right)\mathbf{C}_{\mathbf{i},\mathbf{j}}^{\mathbf{i}}\vec{D}_{i,j}\vec{d}_i^{\,T}+\left(\frac{\partial \mathbf{C}_\mathbf{i}^\mathbf{c}}{\partial \alpha_{a_i}^s}\right)\mathbf{C}_{\mathbf{i},\mathbf{j}}^{\mathbf{i}}\vec{D}_{i,j}\vec{d}_{i,j}{}^T\mathbf{C}_\mathbf{i}^{\mathbf{c}T}\\
&\left.\left.+\mathbf{C}_\mathbf{i}^\mathbf{c}\mathbf{C}_{\mathbf{i},\mathbf{j}}^{\mathbf{i}}\vec{D}_{i,j}\vec{d}_{i,j}{}^T\left(\frac{\partial \mathbf{C}_\mathbf{i}^\mathbf{c}}{\partial \alpha_{a_i}^s}\right)^T\right]\right];
\end{aligned}
$$

$$
\begin{aligned}
\frac{\partial \mathbf{I}_{\mathbf{r},\mathbf{v}}}{\partial \alpha_{a_i}^s}=&-\left(\frac{\partial \mathbf{C}_\mathbf{i}^\mathbf{c}}{\partial \alpha_{a_i}^s}\right)\mathbf{D}_\mathbf{i}^{\mathbf{r}T}\mathbf{C}_\mathbf{i}^{\mathbf{c}T}-\mathbf{C}_\mathbf{i}^\mathbf{c}\mathbf{D}_\mathbf{i}^{\mathbf{r}T}\left(\frac{\partial \mathbf{C}_\mathbf{i}^\mathbf{c}}{\partial \alpha_{a_i}^s}\right)^T-\left(\frac{\partial \mathbf{C}_\mathbf{i}^\mathbf{c}}{\partial \alpha_{a_i}^s}\right)\mathbf{D}_\mathbf{i}^\mathbf{r}\mathbf{C}_\mathbf{i}^{\mathbf{c}T}\\
&-\mathbf{C}_\mathbf{i}^\mathbf{c}\mathbf{D}_\mathbf{i}^\mathbf{r}\left(\frac{\partial \mathbf{C}_\mathbf{i}^\mathbf{c}}{\partial \alpha_{a_i}^s}\right)^T-\sum_{j=1}^{N_i}\left[\left(\frac{\partial \mathbf{C}_\mathbf{i}^\mathbf{c}}{\partial \alpha_{a_i}^s}\right)\mathbf{C}_{\mathbf{i},\mathbf{j}}^{\mathbf{i}}\mathbf{D}_{\mathbf{i},\mathbf{j}}^{\mathbf{r}}{}^T\mathbf{C}_{\mathbf{i},\mathbf{j}}^{\mathbf{i}}{}^T\mathbf{C}_\mathbf{i}^{\mathbf{c}T}\right.\\
&+\mathbf{C}_\mathbf{i}^\mathbf{c}\mathbf{C}_{\mathbf{i},\mathbf{j}}^{\mathbf{i}}\mathbf{D}_{\mathbf{i},\mathbf{j}}^{\mathbf{r}}{}^T\mathbf{C}_{\mathbf{i},\mathbf{j}}^{\mathbf{i}}{}^T\left(\frac{\partial \mathbf{C}_\mathbf{i}^\mathbf{c}}{\partial \alpha_{a_i}^s}\right)^T+\left(\frac{\partial \mathbf{C}_\mathbf{i}^\mathbf{c}}{\partial \alpha_{a_i}^s}\right)^T\mathbf{C}_{\mathbf{i},\mathbf{j}}^{\mathbf{i}}\mathbf{D}_{\mathbf{i},\mathbf{j}}^{\mathbf{r}}\mathbf{C}_{\mathbf{i},\mathbf{j}}^{\mathbf{i}}{}^T\mathbf{C}_\mathbf{i}^{\mathbf{c}T}\\
&\left.+\mathbf{C}_\mathbf{i}^\mathbf{c}\mathbf{C}_{\mathbf{i},\mathbf{j}}^{\mathbf{i}}\mathbf{D}_{\mathbf{i},\mathbf{j}}^{\mathbf{r}}\mathbf{C}_{\mathbf{i},\mathbf{j}}^{\mathbf{i}}{}^T\left(\frac{\partial \mathbf{C}_\mathbf{i}^\mathbf{c}}{\partial \alpha_{a_i}^s}\right)^T\right].
\end{aligned}
\tag{VI-1}
$$

Similarly, the derivative of the moment of inertia matrix with respect to $\alpha_{a_{i,j}}^s$,

i.e. $\frac{\partial \mathbf{I_{sys}}}{\partial \alpha^s_{a_{i,j}}}$, can be written as the sum of the different contributions:

$$\frac{\partial \mathbf{I_{sys}}}{\partial \alpha^s_{a_{i,j}}} = \frac{\partial \mathbf{I_{cm}}}{\partial \alpha^s_{a_{i,j}}} + \frac{\partial \mathbf{I_r}}{\partial \alpha^s_{a_{i,j}}} + \frac{\partial \mathbf{I_h}}{\partial \alpha^s_{a_{i,j}}} + \frac{\partial \mathbf{I_v}}{\partial \alpha^s_{a_{i,j}}} + \frac{\partial \mathbf{I_{h,r}}}{\partial \alpha^s_{a_{i,j}}} + \frac{\partial \mathbf{I_{h,v}}}{\partial \alpha^s_{a_{i,j}}} + \frac{\partial \mathbf{I_{r,v}}}{\partial \alpha^s_{a_{i,j}}},$$

where:

$$\frac{\partial \mathbf{I_{cm}}}{\partial \alpha^s_{a_{i,j}}} = -M\left[2\left(\frac{\partial \vec{C}_{cm}}{\partial \alpha^s_{a_{i,j}}}\right)^T \vec{C}_{cm}\mathbf{E} - \left(\frac{\partial \vec{C}_{cm}}{\partial \alpha^s_{a_{i,j}}}\right)\vec{C}_{cm}{}^T - \vec{C}_{cm}\left(\frac{\partial \vec{C}_{cm}}{\partial \alpha^s_{a_{i,j}}}\right)^T\right];$$

$$\frac{\partial \mathbf{I_r}}{\partial \alpha^s_{a_{i,j}}} = -\mathbf{C^c_i}\left(\frac{\partial \mathbf{C^i_{i,j}}}{\partial \alpha^s_{a_{i,j}}}\right)\mathbf{P^2_{i,j}}\mathbf{C^i_{i,j}}{}^T\mathbf{C^{cT}_i} - \mathbf{C^c_i}\mathbf{C^i_{i,j}}\mathbf{P^2_{i,j}}\left(\frac{\partial \mathbf{C^i_{i,j}}}{\partial \alpha^s_{a_{i,j}}}\right)^T\mathbf{C^{cT}_i};$$

$$\frac{\partial \mathbf{I_h}}{\partial \alpha^s_{a_{i,j}}} = 0;$$

$$\frac{\partial \mathbf{I_v}}{\partial \alpha^s_{a_{i,j}}} = -\mathbf{C^c_i}\left(\frac{\partial \mathbf{C^i_{i,j}}}{\partial \alpha^s_{a_{i,j}}}\right)\mathbf{D^2_{i,j}}\mathbf{C^i_{i,j}}{}^T\mathbf{C^{cT}_i} - \mathbf{C^c_i}\mathbf{C^i_{i,j}}\mathbf{D^2_{i,j}}\left(\frac{\partial \mathbf{C^i_{i,j}}}{\partial \alpha^s_{a_{i,j}}}\right)^T\mathbf{C^{cT}_i};$$

$$\begin{aligned}\frac{\partial \mathbf{I_{h,r}}}{\partial \alpha^s_{a_{i,j}}} =& 2\left[\vec{d}_i{}^T\mathbf{C^c_i}\left(\frac{\partial \mathbf{C^i_{i,j}}}{\partial \alpha^s_{a_{i,j}}}\right)\vec{P}_{i,j} + \vec{d}_{i,j}{}^T\left(\frac{\partial \mathbf{C^i_{i,j}}}{\partial \alpha^s_{a_{i,j}}}\right)\vec{P}_{i,j}\right]\mathbf{E} \\ & -\vec{d}_i\vec{P}_{i,j}{}^T\left(\frac{\partial \mathbf{C^i_{i,j}}}{\partial \alpha^s_{a_{i,j}}}\right)^T\mathbf{C^{cT}_i} - \mathbf{C^c_i}\vec{d}_{i,j}\vec{P}_{i,j}{}^T\left(\frac{\partial \mathbf{C^i_{i,j}}}{\partial \alpha^s_{a_{i,j}}}\right)^T\mathbf{C^{cT}_i} \\ & -\mathbf{C^c_i}\left(\frac{\partial \mathbf{C^i_{i,j}}}{\partial \alpha^s_{a_{i,j}}}\right)\vec{P}_{i,j}\vec{d}_i{}^T - \mathbf{C^c_i}\left(\frac{\partial \mathbf{C^i_{i,j}}}{\partial \alpha^s_{a_{i,j}}}\right)\vec{P}_{i,j}\vec{d}_{i,j}{}^T\mathbf{C^{cT}_i};\end{aligned}$$

$$\begin{aligned}\frac{\partial \mathbf{I_{h,v}}}{\partial \alpha^s_{a_{i,j}}} =& 2\left[\vec{d}_i{}^T\mathbf{C^c_i}\left(\frac{\partial \mathbf{C^i_{i,j}}}{\partial \alpha^s_{a_{i,j}}}\right)\vec{D}_{i,j} + \vec{d}_{i,j}{}^T\left(\frac{\partial \mathbf{C^i_{i,j}}}{\partial \alpha^s_{a_{i,j}}}\right)\vec{D}_{i,j}\right]\mathbf{E} \\ & -\vec{d}_i\vec{D}_{i,j}{}^T\left(\frac{\partial \mathbf{C^i_{i,j}}}{\partial \alpha^s_{a_{i,j}}}\right)^T\mathbf{C^{cT}_i} - \mathbf{C^c_i}\vec{d}_{i,j}\vec{D}_{i,j}{}^T\left(\frac{\partial \mathbf{C^i_{i,j}}}{\partial \alpha^s_{a_{i,j}}}\right)^T\mathbf{C^{cT}_i} \\ & -\mathbf{C^c_i}\left(\frac{\partial \mathbf{C^i_{i,j}}}{\partial \alpha^s_{a_{i,j}}}\right)\vec{D}_{i,j}\vec{d}_i{}^T - \mathbf{C^c_i}\left(\frac{\partial \mathbf{C^i_{i,j}}}{\partial \alpha^s_{a_{i,j}}}\right)\vec{D}_{i,j}\vec{d}_{i,j}{}^T\mathbf{C^{cT}_i};\end{aligned}$$

$$\frac{\partial \mathbf{I_{r,v}}}{\partial \alpha^s_{a_{i,j}}} = -\mathbf{C^c_i}\left(\frac{\partial \mathbf{C^i_{i,j}}}{\partial \alpha^s_{a_{i,j}}}\right)\mathbf{D^r_{i,j}}^T\mathbf{C^i_{i,j}}^T\mathbf{C^{c^T}_i} - \mathbf{C^c_i}\mathbf{C^i_{i,j}}\mathbf{D^r_{i,j}}^T\left(\frac{\partial \mathbf{C^i_{i,j}}}{\partial \alpha^s_{a_{i,j}}}\right)^T\mathbf{C^{c^T}_i}$$
$$-\mathbf{C^c_i}\left(\frac{\partial \mathbf{C^i_{i,j}}}{\partial \alpha^s_{a_{i,j}}}\right)\mathbf{D^r_{i,j}}\mathbf{C^i_{i,j}}^T\mathbf{C^{c^T}_i} - \mathbf{C^c_i}\mathbf{C^i_{i,j}}\mathbf{D^r_{i,j}}\left(\frac{\partial \mathbf{C^i_{i,j}}}{\partial \alpha^s_{a_{i,j}}}\right)^T\mathbf{C^{c^T}_i}. \qquad \text{(VI-2)}$$

On simplification, the various expressions have the following form:

$$\frac{\partial \vec{H}}{\partial \dot{\alpha}^s_{a_i}} = \int_{m_i}\left[\left(\vec{d}_i + \mathbf{C^c_i}(\vec{\rho}_i + \vec{\delta}_i)\right) \times \left(\frac{\partial \mathbf{C^c_i}}{\partial \alpha^s_{a_i}}(\vec{\rho}_i + \vec{\delta}_i)\right)\right] dm_i$$
$$+\sum_{j=1}^{N_i}\left[\left[(\vec{d}_i + \mathbf{C^c_i}\vec{d}_{i,j}) \times \left(\frac{\partial \mathbf{C^c_i}}{\partial \alpha^s_{a_i}}\vec{d}_{i,j}\right)\right] m_{i,j}\right.$$
$$+\int_{m_{i,j}}\left[\mathbf{C^c_i}\mathbf{C^i_{i,j}}(\vec{\rho}_{i,j} + \vec{\delta}_{i,j}) \times \left(\frac{\partial \mathbf{C^c_i}}{\partial \alpha^s_{a_i}}\vec{d}_{i,j}\right)\right.$$
$$+(\vec{d}_i + \mathbf{C^c_i}\vec{d}_{i,j}) \times \left(\frac{\partial \mathbf{C^c_i}}{\partial \alpha^s_{a_i}}\mathbf{C^i_{i,j}}(\vec{\rho}_{i,j} + \vec{\delta}_{i,j})\right)$$
$$\left.\left.+\left(\mathbf{C^c_i}\mathbf{C^i_{i,j}}(\vec{\rho}_{i,j} + \vec{\delta}_{i,j})\right) \times \left(\frac{\partial \mathbf{C^c_i}}{\partial \alpha^s_{a_i}}\mathbf{C^i_{i,j}}(\vec{\rho}_{i,j} + \vec{\delta}_{i,j})\right)\right] dm_{i,j}\right]$$
$$-M\left[\vec{C}_{cm} \times \left(\frac{\partial \vec{C}_{cm}}{\partial \alpha^s_{a_i}}\right)\right]; \qquad \text{(VI-3)}$$

$$\left[\frac{d}{dt}\left(\frac{\partial \vec{H}}{\partial \dot{\alpha}^s_{a_i}}\right) - \frac{\partial \vec{H}}{\partial \alpha^s_{a_i}}\right] =$$
$$2\left\{\int_{m_i}\left[\dot{\vec{d}}_i \times \left(\frac{\partial \mathbf{C^c_i}}{\partial \alpha^s_{a_i}}(\vec{\rho}_i + \vec{\delta}_i)\right) + \mathbf{C^c_i}\dot{\vec{\delta}}_i \times \left(\frac{\partial \mathbf{C^c_i}}{\partial \alpha^s_{a_i}}(\vec{\rho}_i + \vec{\delta}_i)\right)\right.\right.$$
$$\left.+\dot{\mathbf{C}}^{\mathbf{c}}_{\mathbf{i}}\vec{\rho}_i \times \left(\frac{\partial \mathbf{C^c_i}}{\partial \alpha^s_{a_i}}(\vec{\rho}_i + \vec{\delta}_i)\right) + \dot{\mathbf{C}}^{\mathbf{c}}_{\mathbf{i}}\vec{\delta}_i \times \left(\frac{\partial \mathbf{C^c_i}}{\partial \alpha^s_{a_i}}(\vec{\rho}_i + \vec{\delta}_i)\right)\right] dm_i$$
$$+\sum_{j=1}^{N_i}\left[\left[(\dot{\vec{d}}_i + \mathbf{C^c_i}\dot{\vec{d}}_{i,j} + \dot{\mathbf{C}}^{\mathbf{c}}_{\mathbf{i}}\vec{d}_{i,j}) \times \left(\frac{\partial \mathbf{C^c_i}}{\partial \alpha^s_{a_i}}\vec{d}_{i,j}\right)\right] m_{i,j}\right.$$
$$+\int_{m_{i,j}}\left[(\dot{\vec{d}}_i + \mathbf{C^c_i}\dot{\vec{d}}_{i,j} + \dot{\mathbf{C}}^{\mathbf{c}}_{\mathbf{i}}\vec{d}_{i,j}) \times \left(\frac{\partial \mathbf{C^c_i}}{\partial \alpha^s_{a_i}}\mathbf{C^i_{i,j}}(\vec{\rho}_{i,j} + \vec{\delta}_{i,j})\right)\right.$$
$$\left.\left.+\left(\dot{\mathbf{C}}^{\mathbf{c}}_{\mathbf{i}}\mathbf{C^i_{i,j}}(\vec{\rho}_{i,j} + \vec{\delta}_{i,j}) + \mathbf{C^c_i}\dot{\mathbf{C}}^{\mathbf{i}}_{\mathbf{i,j}}(\vec{\rho}_{i,j} + \vec{\delta}_{i,j}) + \mathbf{C^c_i}\mathbf{C^i_{i,j}}\dot{\vec{\delta}}_{i,j}\right) \times\right.\right.$$

$$\left(\frac{\partial \mathbf{C_i^c}}{\partial \alpha^s_{a_i}}\left(\vec{d}_{i,j}+\mathbf{C^i_{i,j}}(\vec{\rho}_{i,j}+\vec{\delta}_{i,j})\right)\right]dm_{i,j}\Bigg]\Bigg\}$$
$$-2M\left(\dot{\vec{C}}_{cm}\times\frac{\partial \vec{C}_{cm}}{\partial \alpha^s_{a_i}}\right); \qquad \text{(VI-4)}$$

$$\frac{\partial \vec{H}}{\partial \dot{\alpha}^s_{a_{i,j}}}=\int_{m_{i,j}}\Big[\mathbf{C_i^c}\Big(\Big(\mathbf{C^i_{i,j}}(\vec{\rho}_{i,j}+\vec{\delta}_{i,j})\Big)\times\Big(\frac{\partial \mathbf{C^i_{i,j}}}{\partial \alpha^s_{a_{i,j}}}(\vec{\rho}_{i,j}+\vec{\delta}_{i,j})\Big)\Big)$$
$$+(\vec{d}_i+\mathbf{C_i^c}\vec{d}_{i,j})\times\Big(\mathbf{C_i^c}\frac{\partial \mathbf{C^i_{i,j}}}{\partial \alpha^s_{a_{i,j}}}(\vec{\rho}_{i,j}+\vec{\delta}_{i,j})\Big)\Big]dm_{i,j}$$
$$-M\left(\vec{C}_{cm}\times\frac{\partial \vec{C}_{cm}}{\partial \alpha^s_{a_{i,j}}}\right); \qquad \text{(VI-5)}$$

$$\left[\frac{d}{dt}\left(\frac{\partial \vec{H}}{\partial \dot{\alpha}^s_{a_{i,j}}}\right)-\frac{\partial \vec{H}}{\partial \alpha^s_{a_{i,j}}}\right]=$$
$$2\Bigg\{\int_{m_{i,j}}\Big[(\dot{\vec{d}}_i+\mathbf{C_i^c}\dot{\vec{d}}_{i,j}+\dot{\mathbf{C}}_\mathbf{i}^\mathbf{c}\vec{d}_{i,j})\times\Big(\mathbf{C_i^c}\frac{\partial \mathbf{C^i_{i,j}}}{\partial \alpha^s_{a_{i,j}}}(\vec{\rho}_{i,j}+\vec{\delta}_{i,j})\Big)$$
$$+\Big(\dot{\mathbf{C}}_\mathbf{i}^\mathbf{c}\mathbf{C^i_{i,j}}(\vec{\rho}_{i,j}+\vec{\delta}_{i,j})+\mathbf{C_i^c}\dot{\mathbf{C}}^\mathbf{i}_{\mathbf{i,j}}(\vec{\rho}_{i,j}+\vec{\delta}_{i,j})+\mathbf{C_i^c}\mathbf{C^i_{i,j}}\dot{\vec{\delta}}_{i,j}\Big)\times$$
$$\Big(\mathbf{C_i^c}\frac{\partial \mathbf{C^i_{i,j}}}{\partial \alpha^s_{a_{i,j}}}(\vec{\rho}_{i,j}+\vec{\delta}_{i,j})\Big)\Big]dm_{i,j}\Bigg]\Bigg\}$$
$$-2M\left(\dot{\vec{C}}_{cm}\times\frac{\partial \vec{C}_{cm}}{\partial \alpha^s_{a_{i,j}}}\right). \qquad \text{(VI-6)}$$

Appendix VII: Simplification of the Governing Equations of Motion

Consider the following two components of the system kinetic energy:

$$T_{h,s} = \sum_{i=1}^{N} \left[\int_{m_i} \dot{\vec{d}}_i \cdot \dot{\mathbf{C}}_{\mathbf{i}}^{\mathbf{c}} (\vec{\rho}_i + \vec{\delta}_i)\, dm_i + \sum_{j=1}^{N_i} \left[\int_{m_{i,j}} \left[(\dot{\vec{d}}_i + \mathbf{C}_{\mathbf{i}}^{\mathbf{c}} \dot{\vec{d}}_{i,j}) \cdot \dot{\mathbf{C}}_{\mathbf{i}}^{\mathbf{c}} \mathbf{C}_{\mathbf{i,j}}^{\mathbf{i}} (\vec{\rho}_{i,j} + \vec{\delta}_{i,j}) \right.\right.\right.$$
$$\left. + \dot{\vec{d}}_i \cdot \mathbf{C}_{\mathbf{i}}^{\mathbf{c}} \dot{\mathbf{C}}_{\mathbf{i,j}}^{\mathbf{i}} (\vec{\rho}_{i,j} + \vec{\delta}_{i,j}) + \dot{\vec{d}}_{i,j} \cdot \dot{\mathbf{C}}_{\mathbf{i,j}}^{\mathbf{i}} (\vec{\rho}_{i,j} + \vec{\delta}_{i,j}) \right] dm_{i,j}$$
$$\left.\left. + (\dot{\vec{d}}_i + \mathbf{C}_{\mathbf{i}}^{\mathbf{c}} \dot{\vec{d}}_{i,j}) \cdot (\dot{\mathbf{C}}_{\mathbf{i}}^{\mathbf{c}} \dot{\vec{d}}_{i,j}) m_{i,j} \right] \right]; \qquad \text{(VII-1)}$$

$$T_{h,v} = \sum_{i=1}^{N} \left[\int_{m_i} \dot{\vec{d}}_i \cdot (\mathbf{C}_{\mathbf{i}}^{\mathbf{c}} \dot{\vec{\delta}}_i)\, dm_i + \sum_{j=1}^{N_i} \left[\int_{m_{i,j}} \left[\dot{\vec{d}}_i \cdot (\mathbf{C}_{\mathbf{i}}^{\mathbf{c}} \mathbf{C}_{\mathbf{i,j}}^{\mathbf{i}} \dot{\vec{\delta}}_{i,j}) \right.\right.\right.$$
$$\left.\left. + \dot{\vec{d}}_{i,j} \cdot (\mathbf{C}_{\mathbf{i,j}}^{\mathbf{i}} \dot{\vec{\delta}}_{i,j}) \right] dm_{i,j} \right] \right]. \qquad \text{(VII-2)}$$

Their contribution to the equations of motion are:

$$\frac{d}{dt}\left(\frac{\partial T_{h,s}}{\partial \dot{q}_{i,jp}}\right) - \frac{\partial T_{h,s}}{\partial q_{i,jp}} = -\left\{ \int_{m_{i,j}} \left[\overbrace{\ddot{\vec{d}}_i \cdot (\dot{\mathbf{C}}_{\mathbf{i}}^{\mathbf{c}} \mathbf{C}_{\mathbf{i,j}}^{\mathbf{i}} \vec{\phi}_{i,jp})}^{A} + \mathbf{C}_{\mathbf{i}}^{\mathbf{c}} \ddot{\vec{d}}_{i,j} \cdot (\dot{\mathbf{C}}_{\mathbf{i}}^{\mathbf{c}} \mathbf{C}_{\mathbf{i,j}}^{\mathbf{i}} \vec{\phi}_{i,jp}) \right.\right.$$
$$\left.\left. + \underbrace{\dot{\vec{d}}_i \cdot (\mathbf{C}_{\mathbf{i}}^{\mathbf{c}} \dot{\mathbf{C}}_{\mathbf{i,j}}^{\mathbf{i}} \vec{\phi}_{i,jp})}_{B} + \underbrace{\dot{\vec{d}}_{i,j} \cdot (\dot{\mathbf{C}}_{\mathbf{i,j}}^{\mathbf{i}} \vec{\phi}_{i,jp})}_{C} \right] dm_{i,j} \right\}; \qquad \text{(VII-3)}$$

$$\frac{d}{dt}\left(\frac{\partial T_{h,v}}{\partial \dot{q}_{i,jp}}\right) - \frac{\partial T_{h,v}}{\partial q_{i,jp}} = \int_{m_{i,j}} \left[\ddot{\vec{d}}_i \cdot (\mathbf{C}_{\mathbf{i}}^{\mathbf{c}} \mathbf{C}_{\mathbf{i,j}}^{\mathbf{i}} \vec{\phi}_{i,jp}) + \overbrace{\dot{\vec{d}}_i \cdot (\dot{\mathbf{C}}_{\mathbf{i}}^{\mathbf{c}} \mathbf{C}_{\mathbf{i,j}}^{\mathbf{i}} \vec{\phi}_{i,jp})}^{A} \right.$$
$$\left. + \underbrace{\dot{\vec{d}}_i \cdot (\mathbf{C}_{\mathbf{i}}^{\mathbf{c}} \dot{\mathbf{C}}_{\mathbf{i,j}}^{\mathbf{i}} \vec{\phi}_{i,jp})}_{B} + \ddot{\vec{d}}_{i,j} \cdot (\mathbf{C}_{\mathbf{i,j}}^{\mathbf{i}} \vec{\phi}_{i,jp}) + \underbrace{\dot{\vec{d}}_{i,j} \cdot (\dot{\mathbf{C}}_{\mathbf{i,j}}^{\mathbf{i}} \vec{\phi}_{i,jp})}_{C} \right] dm_{i,j}. \qquad \text{(VII-4)}$$

It is apparent that the terms marked A, B and C in eqs. (VII-3) and (VII-4) cancel each other.

Similar reduction in the expression for $d/dt(\partial\vec{H}/\partial\dot{q}) - \partial\vec{H}/\partial q$ also takes place. Consider, for example:

$$\vec{H}_v = \int_{m_c} (\vec{\delta}_c \times \dot{\vec{\delta}}_c) dm_c + \sum_{i=1}^{N} \left[\int_{m_i} \left[(\mathbf{C_i^c}\vec{\delta}_i) \times (\mathbf{C_i^c}\dot{\vec{\delta}}_i) \right] dm_i \right.$$
$$\left. + \sum_{j=1}^{N_i} \left[\int_{m_{i,j}} \left[(\mathbf{C_i^c C_{i,j}^i}\vec{\delta}_{i,j}) \times (\mathbf{C_i^c C_{i,j}^i}\dot{\vec{\delta}}_{i,j}) \right] dm_{i,j} \right] \right]; \qquad \text{(VII-5)}$$

$$\vec{H}_{v,s} = \sum_{i=1}^{N} \left[\int_{m_i} \left[(\mathbf{C_i^c}\vec{\delta}_i) \times \dot{\mathbf{C}}_\mathbf{i}^\mathbf{c}(\vec{\rho}_i + \vec{\delta}_i) \right] dm_i + \sum_{j=1}^{N_i} \left[\int_{m_{i,j}} \left[(\mathbf{C_i^c C_{i,j}^i}\vec{\delta}_{i,j}) \right. \right. \right.$$
$$\left. \left. \left. \times \left[\dot{\mathbf{C}}_\mathbf{i}^\mathbf{c}\mathbf{C}_\mathbf{i,j}^\mathbf{i}(\vec{\rho}_{i,j} + \vec{\delta}_{i,j}) + \mathbf{C_i^c}\dot{\mathbf{C}}_\mathbf{i,j}^\mathbf{i}(\vec{\rho}_{i,j} + \vec{\delta}_{i,j}) + \dot{\mathbf{C}}_\mathbf{i}^\mathbf{c}\vec{d}_{i,j} \right] \right] dm_{i,j} \right] \right]. \qquad \text{(VII-6)}$$

The contributions of the above terms to the equations of motion are:

$$\frac{d}{dt}\left(\frac{\partial\vec{H}_v}{\partial\dot{q}_{i_n}}\right) - \frac{\partial\vec{H}_v}{\partial q_{i_n}} =$$
$$\int_{m_i} \left[\underbrace{(\dot{\mathbf{C}}_\mathbf{i}^\mathbf{c}\vec{\delta}_i) \times (\mathbf{C_i^c}\vec{\phi}_{i_n})}_{F} + (2\mathbf{C_i^c}\dot{\vec{\delta}}_i) \times (\mathbf{C_i^c}\vec{\phi}_{i_n}) + \overbrace{(\mathbf{C_i^c}\vec{\delta}_i) \times (\dot{\mathbf{C}}_\mathbf{i}^\mathbf{c}\vec{\phi}_{i_n})}^{D} \right] dm_i$$
$$+ \sum_{j=1}^{n_{i,j}} \left[\int_{m_{i,j}} \left[\underbrace{(\mathbf{C_i^c C_{i,j}^i}\dot{\vec{\delta}}_{i,j}) \times (\mathbf{C_i^c}\frac{\partial\mathbf{C}_\mathbf{i,j}^\mathbf{i}}{\partial q_{i_n}}\vec{\delta}_{i,j})}_{G} \right.\right.$$
$$\left.\left. + \underbrace{(\mathbf{C_i^c}\frac{\partial\mathbf{C}_\mathbf{i,j}^\mathbf{i}}{\partial q_{i_n}}\dot{\vec{\delta}}_{i,j}) \times (\mathbf{C_i^c C_{i,j}^i}\vec{\delta}_{i,j})}_{E} \right] dm_{i,j} \right]; \qquad \text{(VII-7)}$$

$$\frac{d}{dt}\left(\frac{\partial\vec{H}_{v,s}}{\partial\dot{q}_{i_n}}\right) - \frac{\partial\vec{H}_{v,s}}{\partial q_{i_n}} =$$
$$\int_{m_i} \left[(\dot{\mathbf{C}}_\mathbf{i}^\mathbf{c}\vec{\rho}_i) \times (\mathbf{C_i^c}\vec{\phi}_{i_n}) + \underbrace{(\dot{\mathbf{C}}_\mathbf{i}^\mathbf{c}\vec{\delta}_i) \times (\mathbf{C_i^c}\vec{\phi}_{i_n})}_{F} + \overbrace{(\dot{\mathbf{C}}_\mathbf{i}^\mathbf{c}\vec{\phi}_{i_n}) \times (\mathbf{C_i^c}\vec{\delta}_i)}^{D} \right] dm_i$$

$$+\sum_{j=1}^{n_{i,j}}\Bigg[\int_{m_{i,j}}\Big[\Big(2\dot{\mathbf{C}}_{\mathbf{i}}^{\mathbf{c}}\mathbf{C}_{\mathbf{i,j}}^{\mathbf{i}}\vec{\delta}_{i,j}+2\mathbf{C}_{\mathbf{i}}^{\mathbf{c}}\dot{\mathbf{C}}_{\mathbf{i,j}}^{\mathbf{i}}\vec{\delta}_{i,j}+\dot{\mathbf{C}}_{\mathbf{i}}^{\mathbf{c}}\mathbf{C}_{\mathbf{i,j}}^{\mathbf{i}}\vec{\rho}_{i,j}+\mathbf{C}_{\mathbf{i}}^{\mathbf{c}}\dot{\mathbf{C}}_{\mathbf{i,j}}^{\mathbf{i}}\vec{\rho}_{i,j}$$

$$+\dot{\mathbf{C}}_{\mathbf{i}}^{\mathbf{c}}\vec{d}_{i,j}\Big)\times\Big(\mathbf{C}_{\mathbf{i}}^{\mathbf{c}}\frac{\partial\mathbf{C}_{\mathbf{i,j}}^{\mathbf{i}}}{\partial q_{i_n}}\vec{\delta}_{i,j}\Big)+\underbrace{(\mathbf{C}_{\mathbf{i}}^{\mathbf{c}}\mathbf{C}_{\mathbf{i,j}}^{\mathbf{i}}\dot{\vec{\delta}}_{i,j})\times\Big(\mathbf{C}_{\mathbf{i}}^{\mathbf{c}}\frac{\partial\mathbf{C}_{\mathbf{i,j}}^{\mathbf{i}}}{\partial q_{i_n}}\vec{\delta}_{i,j}\Big)}_{G}$$

$$+\Big(\dot{\mathbf{C}}_{\mathbf{i}}^{\mathbf{c}}\mathbf{C}_{\mathbf{i,j}}^{\mathbf{i}}\vec{\delta}_{i,j}+\mathbf{C}_{\mathbf{i}}^{\mathbf{c}}\dot{\mathbf{C}}_{\mathbf{i,j}}^{\mathbf{i}}\vec{\delta}_{i,j}+\mathbf{C}_{\mathbf{i}}^{\mathbf{c}}\mathbf{C}_{\mathbf{i,j}}^{\mathbf{i}}\dot{\vec{\delta}}_{i,j}\Big)\times\Big(\mathbf{C}_{\mathbf{i}}^{\mathbf{c}}\frac{\partial\mathbf{C}_{\mathbf{i,j}}^{\mathbf{i}}}{\partial q_{i_n}}\vec{\rho}_{i,j}\Big)$$

$$+\underbrace{(\mathbf{C}_{\mathbf{i}}^{\mathbf{c}}\mathbf{C}_{\mathbf{i,j}}^{\mathbf{i}}\vec{\delta}_{i,j})\times\Big(\mathbf{C}_{\mathbf{i}}^{\mathbf{c}}\frac{\partial\mathbf{C}_{\mathbf{i,j}}^{\mathbf{i}}}{\partial q_{i_n}}\dot{\vec{\delta}}_{i,j}\Big)}_{E}-(\mathbf{C}_{\mathbf{i}}^{\mathbf{c}}\mathbf{C}_{\mathbf{i,j}}^{\mathbf{i}}\vec{\delta}_{i,j})\times\Big(\dot{\mathbf{C}}_{\mathbf{i}}^{\mathbf{c}}\vec{\phi}_{i_n}(o_{i,j})\Big)\Big]dm_{i,j}\Bigg]. \tag{VII-8}$$

In this example, terms D and E in eqs. (VII-7) and (VII-8) cancel, while terms F and G in eqs. (VII-7) and (VII-8) can be combined.

Simplification also occurs with the equations for the joint generalized coordinates. This is illustrated by first examining the terms contributed by T_s and $T_{s,v}$:

$$T_s=\frac{1}{2}\sum_{i=1}^{N}\Bigg[\int_{m_i}\dot{\mathbf{C}}_{\mathbf{i}}^{\mathbf{c}}(\vec{\rho}_i+\vec{\delta}_i)\cdot\dot{\mathbf{C}}_{\mathbf{i}}^{\mathbf{c}}(\vec{\rho}_i+\vec{\delta}_i)\,dm_i+\sum_{j=1}^{N_i}\Bigg[(\dot{\mathbf{C}}_{\mathbf{i}}^{\mathbf{c}}\vec{d}_{i,j})\cdot(\dot{\mathbf{C}}_{\mathbf{i}}^{\mathbf{c}}\vec{d}_{i,j})m_{i,j}$$

$$+\int_{m_{i,j}}\Big[2(\dot{\mathbf{C}}_{\mathbf{i}}^{\mathbf{c}}\vec{d}_{i,j})\cdot\mathbf{C}_{\mathbf{i}}^{\mathbf{c}}\dot{\mathbf{C}}_{\mathbf{i,j}}^{\mathbf{i}}(\vec{\rho}_{i,j}+\vec{\delta}_{i,j})+2(\dot{\mathbf{C}}_{\mathbf{i}}^{\mathbf{c}}\vec{d}_{i,j})\cdot\dot{\mathbf{C}}_{\mathbf{i}}^{\mathbf{c}}\mathbf{C}_{\mathbf{i,j}}^{\mathbf{i}}(\vec{\rho}_{i,j}+\vec{\delta}_{i,j})$$

$$+\dot{\mathbf{C}}_{\mathbf{i,j}}^{\mathbf{i}}(\vec{\rho}_{i,j}+\vec{\delta}_{i,j})\cdot\dot{\mathbf{C}}_{\mathbf{i,j}}^{\mathbf{i}}(\vec{\rho}_{i,j}+\vec{\delta}_{i,j})+\dot{\mathbf{C}}_{\mathbf{i}}^{\mathbf{c}}\mathbf{C}_{\mathbf{i,j}}^{\mathbf{i}}(\vec{\rho}_{i,j}+\vec{\delta}_{i,j})\cdot\dot{\mathbf{C}}_{\mathbf{i}}^{\mathbf{c}}\mathbf{C}_{\mathbf{i,j}}^{\mathbf{i}}(\vec{\rho}_{i,j}+\vec{\delta}_{i,j})$$

$$+2\dot{\mathbf{C}}_{\mathbf{i}}^{\mathbf{c}}\mathbf{C}_{\mathbf{i,j}}^{\mathbf{i}}(\vec{\rho}_{i,j}+\vec{\delta}_{i,j})\cdot\mathbf{C}_{\mathbf{i}}^{\mathbf{c}}\dot{\mathbf{C}}_{\mathbf{i,j}}^{\mathbf{i}}(\vec{\rho}_{i,j}+\vec{\delta}_{i,j})\Big]\,dm_{i,j}\Bigg]\Bigg]; \tag{VII-9}$$

$$T_{s,v}=\sum_{i=1}^{N}\Bigg[\int_{m_i}\dot{\mathbf{C}}_{\mathbf{i}}^{\mathbf{c}}(\vec{\rho}_i+\vec{\delta}_i)\cdot(\mathbf{C}_{\mathbf{i}}^{\mathbf{c}}\dot{\vec{\delta}}_i)\,dm_i+\sum_{j=1}^{N_i}\Bigg[\int_{m_{i,j}}\Big[\dot{\mathbf{C}}_{\mathbf{i,j}}^{\mathbf{i}}(\vec{\rho}_{i,j}+\vec{\delta}_{i,j})\cdot(\mathbf{C}_{\mathbf{i,j}}^{\mathbf{i}}\dot{\vec{\delta}}_{i,j})$$

$$+(\dot{\mathbf{C}}_{\mathbf{i}}^{\mathbf{c}}\vec{d}_{i,j}+\dot{\mathbf{C}}_{\mathbf{i}}^{\mathbf{c}}\mathbf{C}_{\mathbf{i,j}}^{\mathbf{i}}(\vec{\rho}_{i,j}+\vec{\delta}_{i,j}))\cdot(\mathbf{C}_{\mathbf{i}}^{\mathbf{c}}\mathbf{C}_{\mathbf{i,j}}^{\mathbf{i}}\dot{\vec{\delta}}_{i,j})\Big]\,dm_{i,j}\Bigg]\Bigg]. \tag{VII-10}$$

The resulting contributions to the governing equations of motion are:

$$\frac{d}{dt}\left(\frac{\partial T_s}{\partial \dot{\alpha}^s_{a_{i,j}}}\right) - \frac{\partial T_s}{\partial \alpha^s_{a_{i,j}}} =$$

$$\int_{m_{i,j}} \Bigg[\underbrace{\left(\frac{\partial \mathbf{C}^{\mathbf{i}}_{\mathbf{i,j}}}{\partial \alpha^s_{a_{i,j}}}\dot{\vec{\delta}}_{i,j}\right)\cdot \dot{\mathbf{C}}^{\mathbf{i}}_{\mathbf{i,j}}(\vec{\rho}_{i,j}+\vec{\delta}_{i,j})}_{H} + \frac{\partial \mathbf{C}^{\mathbf{i}}_{\mathbf{i,j}}}{\partial \alpha^s_{a_{i,j}}}(\vec{\rho}_{i,j}+\vec{\delta}_{i,j})\cdot \ddot{\mathbf{C}}^{\mathbf{i}}_{\mathbf{i,j}}(\vec{\rho}_{i,j}+\vec{\delta}_{i,j})$$

$$+ \underbrace{\frac{\partial \mathbf{C}^{\mathbf{i}}_{\mathbf{i,j}}}{\partial \alpha^s_{a_{i,j}}}(\vec{\rho}_{i,j}+\vec{\delta}_{i,j})\cdot(\dot{\mathbf{C}}^{\mathbf{i}}_{\mathbf{i,j}}\dot{\vec{\delta}}_{i,j})}_{K} + \mathbf{C}^{\mathbf{c}}_{\mathbf{i}}\frac{\partial \mathbf{C}^{\mathbf{i}}_{\mathbf{i,j}}}{\partial \alpha^s_{a_{i,j}}}(\vec{\rho}_{i,j}+\vec{\delta}_{i,j})\cdot \ddot{\mathbf{C}}^{\mathbf{c}}_{\mathbf{i}}\mathbf{C}^{\mathbf{i}}_{\mathbf{i,j}}(\vec{\rho}_{i,j}+\vec{\delta}_{i,j})$$

$$+\mathbf{C}^{\mathbf{c}}_{\mathbf{i}}\frac{\partial \mathbf{C}^{\mathbf{i}}_{\mathbf{i,j}}}{\partial \alpha^s_{a_{i,j}}}(\vec{\rho}_{i,j}+\vec{\delta}_{i,j})\cdot \dot{\mathbf{C}}^{\mathbf{c}}_{\mathbf{i}}\dot{\mathbf{C}}^{\mathbf{i}}_{\mathbf{i,j}}(\vec{\rho}_{i,j}+\vec{\delta}_{i,j}) + \overbrace{\mathbf{C}^{\mathbf{c}}_{\mathbf{i}}\frac{\partial \mathbf{C}^{\mathbf{i}}_{\mathbf{i,j}}}{\partial \alpha^s_{a_{i,j}}}(\vec{\rho}_{i,j}+\vec{\delta}_{i,j})\cdot(\dot{\mathbf{C}}^{\mathbf{c}}_{\mathbf{i}}\mathbf{C}^{\mathbf{i}}_{\mathbf{i,j}}\dot{\vec{\delta}}_{i,j})}^{L}$$

$$+ \underbrace{\mathbf{C}^{\mathbf{c}}_{\mathbf{i}}\frac{\partial \dot{\mathbf{C}}^{\mathbf{i}}_{\mathbf{i,j}}}{\partial \alpha^s_{a_{i,j}}}(\vec{\rho}_{i,j}+\vec{\delta}_{i,j})\cdot \dot{\mathbf{C}}^{\mathbf{c}}_{\mathbf{i}}\mathbf{C}^{\mathbf{i}}_{\mathbf{i,j}}(\vec{\rho}_{i,j}+\vec{\delta}_{i,j})}_{M} + \underbrace{\left(\mathbf{C}^{\mathbf{c}}_{\mathbf{i}}\frac{\partial \mathbf{C}^{\mathbf{i}}_{\mathbf{i,j}}}{\partial \alpha^s_{a_{i,j}}}\dot{\vec{\delta}}_{i,j}\right)\cdot \dot{\mathbf{C}}^{\mathbf{c}}_{\mathbf{i}}\mathbf{C}^{\mathbf{i}}_{\mathbf{i,j}}(\vec{\rho}_{i,j}+\vec{\delta}_{i,j})}_{I}$$

$$+\mathbf{C}^{\mathbf{c}}_{\mathbf{i}}\frac{\partial \mathbf{C}^{\mathbf{i}}_{\mathbf{i,j}}}{\partial \alpha^s_{a_{i,j}}}(\vec{\rho}_{i,j}+\vec{\delta}_{i,j})\cdot(\ddot{\mathbf{C}}^{\mathbf{c}}_{\mathbf{i}}\vec{d}_{i,j}) + \mathbf{C}^{\mathbf{c}}_{\mathbf{i}}\frac{\partial \mathbf{C}^{\mathbf{i}}_{\mathbf{i,j}}}{\partial \alpha^s_{a_{i,j}}}(\vec{\rho}_{i,j}+\vec{\delta}_{i,j})\cdot(\dot{\mathbf{C}}^{\mathbf{c}}_{\mathbf{i}}\dot{\vec{d}}_{i,j})$$

$$+ \underbrace{\left(\mathbf{C}^{\mathbf{c}}_{\mathbf{i}}\frac{\partial \mathbf{C}^{\mathbf{i}}_{\mathbf{i,j}}}{\partial \alpha^s_{a_{i,j}}}\dot{\vec{\delta}}_{i,j}\right)\cdot(\dot{\mathbf{C}}^{\mathbf{c}}_{\mathbf{i}}\vec{d}_{i,j})}_{J} - \dot{\mathbf{C}}^{\mathbf{c}}_{\mathbf{i}}\frac{\partial \mathbf{C}^{\mathbf{i}}_{\mathbf{i,j}}}{\partial \alpha^s_{a_{i,j}}}(\vec{\rho}_{i,j}+\vec{\delta}_{i,j})\cdot \mathbf{C}^{\mathbf{c}}_{\mathbf{i}}\dot{\mathbf{C}}^{\mathbf{i}}_{\mathbf{i,j}}(\vec{\rho}_{i,j}+\vec{\delta}_{i,j})$$

$$- \underbrace{\mathbf{C}^{\mathbf{c}}_{\mathbf{i}}\frac{\partial \dot{\mathbf{C}}^{\mathbf{i}}_{\mathbf{i,j}}}{\partial \alpha^s_{a_{i,j}}}(\vec{\rho}_{i,j}+\vec{\delta}_{i,j})\cdot \dot{\mathbf{C}}^{\mathbf{c}}_{\mathbf{i}}\mathbf{C}^{\mathbf{i}}_{\mathbf{i,j}}(\vec{\rho}_{i,j}+\vec{\delta}_{i,j})}_{M}\Bigg] dm_{i,j}; \qquad \text{(VII-11)}$$

$$\frac{d}{dt}\left(\frac{\partial T_{s,v}}{\partial \dot{\alpha}^s_{a_{i,j}}}\right) - \frac{\partial T_{s,v}}{\partial \alpha^s_{a_{i,j}}} =$$

$$\int_{m_{i,j}} \Bigg[\overbrace{\frac{\partial \mathbf{C}^{\mathbf{i}}_{\mathbf{i,j}}}{\partial \alpha^s_{a_{i,j}}}(\vec{\rho}_{i,j}+\vec{\delta}_{i,j})\cdot(\dot{\mathbf{C}}^{\mathbf{c}}_{\mathbf{i}}\dot{\vec{\delta}}_{i,j})}^{K} + \frac{\partial \mathbf{C}^{\mathbf{i}}_{\mathbf{i,j}}}{\partial \alpha^s_{a_{i,j}}}(\vec{\rho}_{i,j}+\vec{\delta}_{i,j})\cdot(\mathbf{C}^{\mathbf{c}}_{\mathbf{i}}\ddot{\vec{\delta}}_{i,j})$$

$$\overbrace{-\left(\mathbf{C}_{\mathbf{i}}^{\mathbf{c}}\frac{\partial \mathbf{C}_{\mathbf{i,j}}^{\mathbf{i}}}{\partial \alpha_{a_{i,j}}^{s}}\dot{\vec{\delta}}_{i,j}\right)\cdot(\dot{\mathbf{C}}_{\mathbf{i}}^{\mathbf{c}}\vec{d}_{i,j})}^{J}\overbrace{-\dot{\mathbf{C}}_{\mathbf{i}}^{\mathbf{c}}\frac{\partial \mathbf{C}_{\mathbf{i,j}}^{\mathbf{i}}}{\partial \alpha_{a_{i,j}}^{s}}(\vec{\rho}_{i,j}+\vec{\delta}_{i,j})\cdot(\mathbf{C}_{\mathbf{i}}^{\mathbf{c}}\mathbf{C}_{\mathbf{i,j}}^{\mathbf{i}}\dot{\vec{\delta}}_{i,j})}^{L}$$

$$\Big[\underbrace{-\dot{\mathbf{C}}_{\mathbf{i}}^{\mathbf{c}}\mathbf{C}_{\mathbf{i,j}}^{\mathbf{i}}(\vec{\rho}_{i,j}+\vec{\delta}_{i,j})\cdot\left(\mathbf{C}_{\mathbf{i}}^{\mathbf{c}}\frac{\partial \mathbf{C}_{\mathbf{i,j}}^{\mathbf{i}}}{\partial \alpha_{a_{i,j}}^{s}}\dot{\vec{\delta}}_{i,j}\right)}_{I}\underbrace{-\dot{\mathbf{C}}_{\mathbf{i,j}}^{\mathbf{i}}(\vec{\rho}_{i,j}+\vec{\delta}_{i,j})\cdot\left(\frac{\partial \mathbf{C}_{\mathbf{i,j}}^{\mathbf{i}}}{\partial \alpha_{a_{i,j}}^{s}}\dot{\vec{\delta}}_{i,j}\right)}_{H}\Big]dm_{i,j}. \tag{VII-12}$$

The terms labelled H, I and J from eqs. (VII-11) and (VII-12) cancel one another. In addition, the terms marked M in eq. (VII-11) also cancel. Furthermore, the K and L terms from eqs. (VII-11) and (VII-12) combine.

The terms labelled L do not appear to be alike. However, the fact that they are identical can be illustrated as follows. Consider the homogeneous transformation matrix $\mathbf{C}_{\mathbf{i}}^{\mathbf{c}}$ which transforms a vector in $\mathcal{F}_i$ to $\mathcal{F}_c$. $\mathbf{C}_{\mathbf{i}}^{\mathbf{c}}$ is a unitary or orthogonal, i.e.,

$$\mathbf{C}_{\mathbf{i}}^{\mathbf{c}^T}\mathbf{C}_{\mathbf{i}}^{\mathbf{c}}=\mathbf{I}.$$

Taking the derivative of the above yields

$$\dot{\mathbf{C}}_{\mathbf{i}}^{\mathbf{c}^T}\mathbf{C}_{\mathbf{i}}^{\mathbf{c}}+\mathbf{C}_{\mathbf{i}}^{\mathbf{c}^T}\dot{\mathbf{C}}_{\mathbf{i}}^{\mathbf{c}}=\mathbf{0},$$

or

$$\dot{\mathbf{C}}_{\mathbf{i}}^{\mathbf{c}^T}\mathbf{C}_{\mathbf{i}}^{\mathbf{c}}=-\mathbf{C}_{\mathbf{i}}^{\mathbf{c}^T}\dot{\mathbf{C}}_{\mathbf{i}}^{\mathbf{c}}. \tag{VII-13a}$$

The term labelled L in eq. (VII-11), i.e.,

$$\mathbf{C}_{\mathbf{i}}^{\mathbf{c}}\frac{\partial \mathbf{C}_{\mathbf{i,j}}^{\mathbf{i}}}{\partial \alpha_{a_{i,j}}^{s}}(\vec{\rho}_{i,j}+\vec{\delta}_{i,j})\cdot(\dot{\mathbf{C}}_{\mathbf{i}}^{\mathbf{c}}\mathbf{C}_{\mathbf{i,j}}^{\mathbf{i}}\dot{\vec{\delta}}_{i,j}),$$

can be rewritten as

$$(\vec{\rho}_{i,j} + \vec{\delta}_{i,j})^T \Big(\frac{\partial \mathbf{C}^{\mathbf{i}}_{\mathbf{i,j}}}{\partial \alpha^s_{a_{i,j}}}\Big)^T \mathbf{C}^{\mathbf{c}T}_{\mathbf{i}} \dot{\mathbf{C}}^{\mathbf{c}}_{\mathbf{i}} \mathbf{C}^{\mathbf{i}}_{\mathbf{i,j}} \dot{\vec{\delta}}_{i,j}. \qquad \text{(VII-13b)}$$

Similarly, the term labelled L as it appears in eq. (VII-12), i.e.,

$$-\dot{\mathbf{C}}^{\mathbf{c}}_{\mathbf{i}} \frac{\partial \mathbf{C}^{\mathbf{i}}_{\mathbf{i,j}}}{\partial \alpha^s_{a_{i,j}}} (\vec{\rho}_{i,j} + \vec{\delta}_{i,j}) \cdot (\mathbf{C}^{\mathbf{c}}_{\mathbf{i}} \mathbf{C}^{\mathbf{i}}_{\mathbf{i,j}} \dot{\vec{\delta}}_{i,j}),$$

can be rewritten as

$$-(\vec{\rho}_{i,j} + \vec{\delta}_{i,j})^T \Big(\frac{\partial \mathbf{C}^{\mathbf{i}}_{\mathbf{i,j}}}{\partial \alpha^s_{a_{i,j}}}\Big)^T \dot{\mathbf{C}}^{\mathbf{c}T}_{\mathbf{i}} \mathbf{C}^{\mathbf{c}}_{\mathbf{i}} \mathbf{C}^{\mathbf{i}}_{\mathbf{i,j}} \dot{\vec{\delta}}_{i,j}. \qquad \text{(VII-13c)}$$

Substitution of eq. (VII-13a) into eq. (VII-13c) yields

$$(\vec{\rho}_{i,j} + \vec{\delta}_{i,j})^T \Big(\frac{\partial \mathbf{C}^{\mathbf{i}}_{\mathbf{i,j}}}{\partial \alpha^s_{a_{i,j}}}\Big)^T \mathbf{C}^{\mathbf{c}T}_{\mathbf{i}} \dot{\mathbf{C}}^{\mathbf{c}}_{\mathbf{i}} \mathbf{C}^{\mathbf{i}}_{\mathbf{i,j}} \dot{\vec{\delta}}_{i,j},$$

which is identical to eq. (VII-13b), proving the identity.

The simplification in the $d/dt(\partial \vec{H}/\partial \dot{\alpha}) - \partial \vec{H}/\partial \alpha$ terms can be shown by considering the contributions from $\vec{H}_{h,v}$ and $\vec{H}_{h,s}$:

$$\begin{aligned}\vec{H}_{h,v} = \sum_{i=1}^{N} \Bigg[& \int_{m_i} \big[(\mathbf{C}^{\mathbf{c}}_{\mathbf{i}} \vec{\delta}_i) \times \dot{\vec{d}}_i + \vec{d}_i \times (\mathbf{C}^{\mathbf{c}}_{\mathbf{i}} \dot{\vec{\delta}}_i)\big] dm_i \\ & + \sum_{j=1}^{N_i} \Bigg[\int_{m_{i,j}} \big[(\mathbf{C}^{\mathbf{c}}_{\mathbf{i}} \mathbf{C}^{\mathbf{i}}_{\mathbf{i,j}} \vec{\delta}_{i,j}) \times (\dot{\vec{d}}_i + \mathbf{C}^{\mathbf{c}}_{\mathbf{i}} \dot{\vec{d}}_{i,j}) + (\vec{d}_i + \mathbf{C}^{\mathbf{c}}_{\mathbf{i}} \vec{d}_{i,j}) \times \\ & (\mathbf{C}^{\mathbf{c}}_{\mathbf{i}} \mathbf{C}^{\mathbf{i}}_{\mathbf{i,j}} \dot{\vec{\delta}}_{i,j})\big] dm_{i,j} \Bigg] \Bigg]; \end{aligned} \qquad \text{(VII-14)}$$

$$\begin{aligned}\vec{H}_{h,s} = \sum_{i=1}^{N} \Bigg[& \int_{m_i} \big[\vec{d}_i \times \dot{\mathbf{C}}^{\mathbf{c}}_{\mathbf{i}} (\vec{\rho}_i + \vec{\delta}_i)\big] dm_i + \sum_{j=1}^{N_i} \Bigg[\int_{m_{i,j}} \Big[(\vec{d}_i + \mathbf{C}^{\mathbf{i}}_{\mathbf{c}} \vec{d}_{i,j}) \\ & \times \big[\dot{\mathbf{C}}^{\mathbf{c}}_{\mathbf{i}} \mathbf{C}^{\mathbf{i}}_{\mathbf{i,j}} (\vec{\rho}_{i,j} + \vec{\delta}_{i,j}) + \mathbf{C}^{\mathbf{c}}_{\mathbf{i}} \dot{\mathbf{C}}^{\mathbf{i}}_{\mathbf{i,j}} (\vec{\rho}_{i,j} + \vec{\delta}_{i,j}) + \dot{\mathbf{C}}^{\mathbf{c}}_{\mathbf{i}} \vec{d}_{i,j}\big] \Big] dm_{i,j} \Bigg] \Bigg]. \end{aligned} \qquad \text{(VII-15)}$$

Contributions, in this case, to the equations of motion are:

$$\frac{d}{dt}\left(\frac{\partial \vec{H}_{h,v}}{\partial \dot{\alpha}^s_{a_{i,j}}}\right) - \frac{\partial \vec{H}_{h,v}}{\partial \alpha^s_{a_{i,j}}} = -\left\{ \int_{m_{i,j}} \Big[\underbrace{\left(\mathbf{C}^{\mathbf{c}}_{\mathbf{i}} \frac{\partial \mathbf{C}^{\mathbf{i}}_{\mathbf{i,j}}}{\partial \alpha^s_{a_{i,j}}} \vec{\delta}_{i,j}\right) \times (\dot{\vec{d}}_i + \mathbf{C}^{\mathbf{c}}_{\mathbf{i}} \dot{\vec{d}}_{i,j})}_{O} \right.$$

$$\left. + \underbrace{(\vec{d}_i + \mathbf{C}^{\mathbf{c}}_{\mathbf{i}} \vec{d}_{i,j}) \times \left(\mathbf{C}^{\mathbf{c}}_{\mathbf{i}} \frac{\partial \mathbf{C}^{\mathbf{i}}_{\mathbf{i,j}}}{\partial \alpha^s_{a_{i,j}}} \dot{\vec{\delta}}_{i,j}\right)}_{N} \Big] dm_{i,j} \right\}; \qquad \text{(VII-16)}$$

$$\frac{d}{dt}\left(\frac{\partial \vec{H}_{h,s}}{\partial \dot{\alpha}^s_{a_{i,j}}}\right) - \frac{\partial \vec{H}_{h,s}}{\partial \alpha^s_{a_{i,j}}} = \int_{m_{i,j}} \Big[(\dot{\vec{d}}_i + \dot{\mathbf{C}}^{\mathbf{c}}_{\mathbf{i}} \vec{d}_{i,j} + \mathbf{C}^{\mathbf{c}}_{\mathbf{i}} \dot{\vec{d}}_{i,j}) \times \left(\mathbf{C}^{\mathbf{c}}_{\mathbf{i}} \frac{\partial \mathbf{C}^{\mathbf{i}}_{\mathbf{i,j}}}{\partial \alpha^s_{a_{i,j}}} \vec{\rho}_{i,j}\right)$$

$$+ \underbrace{(\dot{\vec{d}}_i + \mathbf{C}^{\mathbf{c}}_{\mathbf{i}} \dot{\vec{d}}_{i,j}) \times \left(\mathbf{C}^{\mathbf{c}}_{\mathbf{i}} \frac{\partial \mathbf{C}^{\mathbf{i}}_{\mathbf{i,j}}}{\partial \alpha^s_{a_{i,j}}} \vec{\delta}_{i,j}\right)}_{O}$$

$$+ (\dot{\mathbf{C}}^{\mathbf{c}}_{\mathbf{i}} \vec{d}_{i,j}) \times \left(\mathbf{C}^{\mathbf{c}}_{\mathbf{i}} \frac{\partial \mathbf{C}^{\mathbf{i}}_{\mathbf{i,j}}}{\partial \alpha^s_{a_{i,j}}} \vec{\delta}_{i,j}\right)$$

$$+ \underbrace{(\vec{d}_i + \mathbf{C}^{\mathbf{c}}_{\mathbf{i}} \vec{d}_{i,j}) \times \left(\mathbf{C}^{\mathbf{c}}_{\mathbf{i}} \frac{\partial \mathbf{C}^{\mathbf{i}}_{\mathbf{i,j}}}{\partial \alpha^s_{a_{i,j}}} \dot{\vec{\delta}}_{i,j}\right)}_{N} \Big] dm_{i,j}. \qquad \text{(VII-17)}$$

The terms labelled N above cancel, while those marked O combine.

Appendix VIII: An Overview of Linear Optimal Controller Design

VIII.1 Linear Quadratic Regulator (LQR) Design

The Linear Quadratic Regulator (LQR) aims at finding a control signal $\mathbf{u}$ that minimizes the cost functional

$$J = \int_0^\infty \left(\mathbf{z}^T\mathbf{Q}\mathbf{z} + \mathbf{u}^T\mathbf{R}\mathbf{u}\right) dt, \tag{VIII–1}$$

subject to the dynamics:

$$\begin{aligned} \dot{\mathbf{x}} &= \mathbf{A}\mathbf{x} + \mathbf{B}\mathbf{u}; \\ \mathbf{z} &= \mathbf{M}\mathbf{x}. \end{aligned} \tag{VIII–2}$$

$\mathbf{z}$ is referred to as the controlled variable. $\mathbf{Q}$ and $\mathbf{R}$ are positive semi–definite and positive definite symmetric matrices, respectively. They serve as "tuning parameters" for the design procedure, with the principal objective of providing satisfactory principal gains or singular values of the open–loop transfer function. The motivation behind choosing such a performance index is to force the states to zero quickly while penalizing the control effort, both in a weighted sense, to prevent unreasonably large inputs.

The control $\mathbf{u}$ is taken to be a linear function of the state vector $\mathbf{x}$, i.e.

$$\mathbf{u} = -\mathbf{K_c}\mathbf{x}. \tag{VIII–3}$$

The solution to this problem is well known and can be found in many papers and texts. It is described in great detail in [105]. Of particular interest is the steady-state solution when $\mathbf{A}, \mathbf{B}, \mathbf{M}, \mathbf{Q}$ and $\mathbf{R}$ are taken to be time-invariant matrices, and for

cases when the pair [**A**, **B**] is controllable. This solution is given by

$$\mathbf{K_c} = \mathbf{R^{-1}B^T P_c}, \tag{VIII–4}$$

where $\mathbf{P_c}$ satisfies the following algebraic Riccati equation,

$$\mathbf{A^T P_c + P_c A - P_c B R^{-1} B^T P_c + M^T Q M} = 0. \tag{VIII–5}$$

Two desirable features of LQR control is the guarantee of stability and the optimality of the control law [105]. Unfortunately, there are two features of real dynamical systems which tend to limit implementation of the LQR controller: a real system is corrupted by noise and disturbances which tend to drive it away from the steady state; and all the states of the system may not be measurable directly, requiring their estimation. These two caveats can be overcome by employing a modified control design procedure called the Linear Quadratic Gaussian (LQG) method.

VIII.2 Linear Quadratic Gaussian, Loop Transfer Recovery (LQG/LTR)

The Linear Quadratic Gaussian (LQG) problem is similar to the Linear Quadratic Regulator (LQR) problem with two notable exceptions: in addition to the state, the concept of the system output is introduced; and the plant model has a stochastic element in the form of input and measurement noise models, characterized as zero-mean Gaussian or "white noise" processes. They are taken to be uncorrelated in time. The system equations are:

$$\dot{\mathbf{x}} = \mathbf{Ax + Bu + \Gamma w}; \tag{VIII–6}$$

$$\mathbf{y} = \mathbf{Cx + v}; \tag{VIII–7}$$

where $\mathbf{y}$ is the output vector, and $\mathbf{w}$ and $\mathbf{v}$ are the input and measurement noise, respectively. $\mathbf{\Gamma}$ represents the input noise influence matrix. The cost functional to be

minimized is identical to that for the LQR problem, i.e. eq. (VIII-1).

The LQG procedure involves solution of two subproblems. This is referred to as the separation problem and is discussed in detail in Refs. 105 and 117. To begin with, it requires an optimal estimate, $\hat{\mathbf{x}}$, of the state vector $\mathbf{x}$. The estimate is optimal in the sense that $E[(\mathbf{x}-\hat{\mathbf{x}})^T(\mathbf{x}-\hat{\mathbf{x}})]$, i.e. the expected value of $(\mathbf{x}-\hat{\mathbf{x}})^T(\mathbf{x}-\hat{\mathbf{x}})$, is minimized. The estimate of the state is then used as a true measure to solve the LQR problem.

An optimal estimate of the state can be obtained by implementing a Kalman filter as shown in Figure VIII-1.

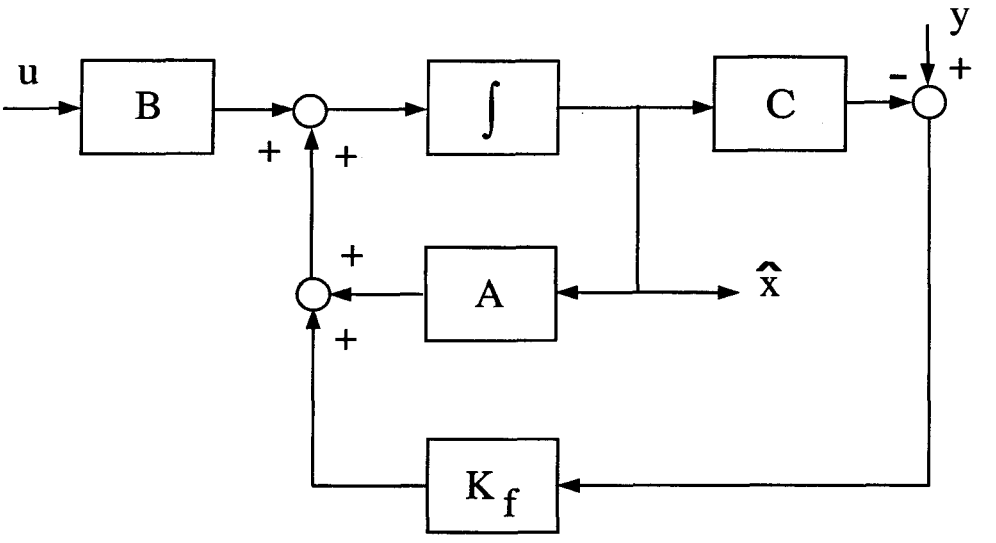

Figure VIII-1 Block diagram for a Kalman filter.

The state equation for the Kalman filter is

$$\dot{\hat{\mathbf{x}}} = (\mathbf{A}-\mathbf{K_f C})\hat{\mathbf{x}} + \mathbf{B}\mathbf{u} + \mathbf{K_f}\mathbf{y}. \qquad \text{(VIII-8)}$$

The Kalman filter gain matrix $\mathbf{K_f}$ is given by

$$\mathbf{K_f} = \mathbf{P_f C}^T \mathbf{V}^{-1}, \qquad \text{(VIII-9)}$$

where: $\mathbf{V} = E[\mathbf{v}\mathbf{v}^T]$; $\mathbf{W} = E[\mathbf{w}\mathbf{w}^T]$; and $\mathbf{P_f}$ satisfies the following algebraic Riccati equation,

$$\mathbf{P_f A}^T + \mathbf{A P_f} - \mathbf{P_f C}^{\mathbf{T}} \mathbf{V}^{-1} \mathbf{C P_f} + \mathbf{\Gamma W \Gamma}^T = 0. \qquad \text{(VIII-10)}$$

The solution to the second part of the problem, namely the optimal regulator problem, is given by equations (VIII-4) and (VIII-5). The matrices $\mathbf{K_f}$ and $\mathbf{K_c}$ exist and the entire closed loop is internally stable if the systems given by $(\mathbf{A}, \mathbf{B}, \mathbf{Q}^{1/2}\mathbf{M})$ and $(\mathbf{A}, \mathbf{\Gamma W}^{1/2}, \mathbf{C})$ are stabilizable and detectable. In other words, all the uncontrollable and unobservable modes are stable.

The two resulting designs, the optimal estimator and the quadratic regulator, have good performance and robustness quality when viewed individually. However, when the LQG design is viewed as a whole, robustness and performance is, in general, not as anticipated. Doyle showed that such designs can exhibit poor stability margins [119]. Even when the conventional wisdom, which requires the observer dynamics to be much faster than the plant dynamics, is followed an improvement in the performance is not always realized [120]. Doyle has outlined a procedure for the adequate design of observer based linear quadratic compensators [120]. In fact, there are two dual approaches. One involves first solving the deterministic linear quadratic regulator problem by adjusting the $\mathbf{Q}$ and $\mathbf{R}$ matrices until a satisfactory loop transfer function

$$\mathbf{K_c}(s\mathbf{I} - \mathbf{A})^{-1}\mathbf{B},$$

is obtained. The next step involves design of a Kalman filter by setting:

$$\mathbf{\Gamma} = \mathbf{B};$$

$$\mathbf{W} = \mathbf{W_o} + q\mathbf{I};$$

$$\mathbf{V} = \mathbf{I}.$$

q is a design parameter which is increased until the combined compensator–plant loop transfer function (broken at the plant input),

$$\mathbf{K_c}(s\mathbf{I} - \mathbf{A} + \mathbf{BK_c} + \mathbf{K_f C})^{-1}\mathbf{K_f C}(s\mathbf{I} - \mathbf{A})^{-1}\mathbf{B},$$

converges to the loop transfer function of the plant, $\mathbf{K_c}(s\mathbf{I} - \mathbf{A})^{-1}\mathbf{B}$, with the LQR controller. The final controller–plant structure is shown in Figure VIII-2.

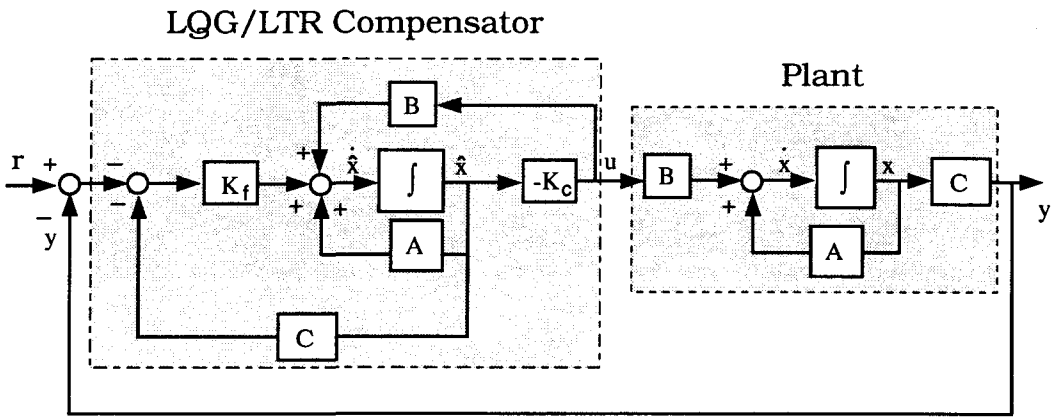

Figure VIII-2 Architecture of plant with LQG/LTR compensator.

Alternately, the procedure can be viewed as the one where the poles of the Kalman filter are chosen to coincide with the finite transmission zeros of the plant. The rest of the poles are taken to be very large. Therefore, this approach can be viewed as the one in which some of the dynamics of the Kalman filter cancels part of the plant

dynamics. An in–depth discussion of this topic is presented by many researchers including Doyle. The procedure is successful for only minimum phase plants (i.e. plants which have no right half plane transmission zeros).

The second part of this procedure is termed Loop Transfer Recovery (LTR). Here the objective is to recover the original LQR properties through a special estimator or filter design. The combined design procedure, called LQG/LTR, provides good stability robustness, and performance characteristics not present either in the LQR or the LQG design. The dual of this entire procedure involves first designing a Kalman filter followed by the state–feedback regulator design. The procedure can be implemented as discussed in Ref. 117.

VIII.3 H_∞ Design

Consider a linear model, consisting of the plant augmented by frequency dependent weighting functions, described by the following dynamics:

$$\begin{aligned} \dot{\mathbf{x}} &= \mathbf{A}\mathbf{x} + \mathbf{B_1}\mathbf{w} + \mathbf{B_2}\mathbf{u}; \\ \mathbf{z} &= \mathbf{C_1}\mathbf{x} + \mathbf{D_{11}}\mathbf{w} + \mathbf{D_{12}}\mathbf{u}; \\ \mathbf{y} &= \mathbf{C_2}\mathbf{x} + \mathbf{D_{21}}\mathbf{w} + \mathbf{D_{22}}\mathbf{u}. \end{aligned} \qquad \text{(VIII–11)}$$

Here, $\mathbf{x} \in \Re^n$, $\mathbf{y} \in \Re^{p2}$, $\mathbf{z} \in \Re^{p1}$, $\mathbf{u} \in \Re^{m2}$ and $\mathbf{w} \in \Re^{m1}$ are the state, observation, error, control input and disturbance vectors, respectively, and $\mathbf{A}$, $\mathbf{B_1}$, $\mathbf{B_2}$, $\mathbf{C_1}$, $\mathbf{C_2}$, $\mathbf{D_{11}}$, $\mathbf{D_{12}}$, $\mathbf{D_{21}}$, and $\mathbf{D_{22}}$ are time–invariant matrices of appropriate dimensions. $\mathbf{P}(s)$ is the transfer function matrix for the standard or augmented plant [122]. It consists of the nominal plant along with frequency dependant weighting functions used to shape the system transfer functions. The standard plant is represented along with the compensator $\mathbf{K}(s)$ in Figure VIII-3.

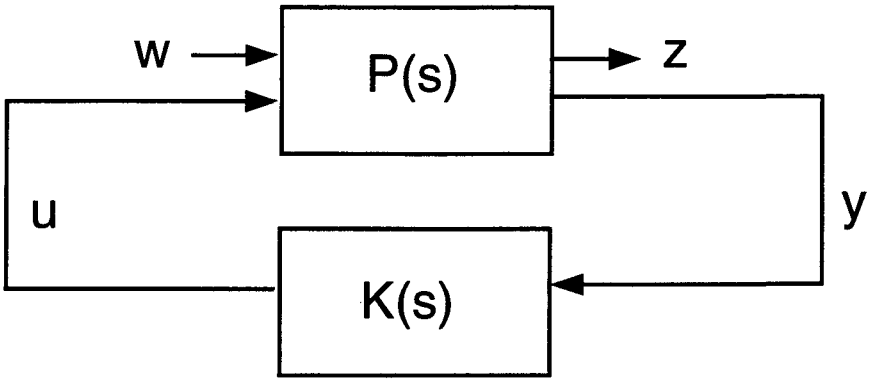

Figure VIII-3 Standard plant/compensator arrangement for H_∞ design.

Considering the control and disturbance input as well as the error and observation output of the plant, the open–loop transfer function, written in the standard form, $\mathbf{C}(s\mathbf{I}-\mathbf{A})^{-1}\mathbf{B}+\mathbf{D})$, is given by

$$\begin{aligned}\mathbf{P}(s) &= \begin{bmatrix}\mathbf{P_{11}}(s) & \mathbf{P_{12}}(s)\\ \mathbf{P_{21}}(s) & \mathbf{P_{22}}(s)\end{bmatrix}\\ &= \begin{bmatrix}\mathbf{D_{11}} & \mathbf{D_{12}}\\ \mathbf{D_{21}} & \mathbf{D_{22}}\end{bmatrix} + \begin{bmatrix}\mathbf{C_1}\\ \mathbf{C_2}\end{bmatrix}(s\mathbf{I}-\mathbf{A})^{-1}\begin{bmatrix}\mathbf{B_1} & \mathbf{B_2}\end{bmatrix}. \qquad \text{(VIII–12)}\end{aligned}$$

With the compensator $\mathbf{K}(s)$, the closed–loop transfer function from $\mathbf{w}$ to $\mathbf{z}$, denoted $\mathcal{F}_l(\mathbf{P},\mathbf{K})$, is given by

$$\mathbf{P_{11}}(s)+\mathbf{P_{12}}(s)\mathbf{K}(s)\left(\mathbf{I}-\mathbf{P_{22}}(s)\mathbf{K}(s)\right)^{-1}\mathbf{P_{21}}(s). \qquad \text{(VIII–13)}$$

It is obvious that the above transfer function should be as small as possible in order to minimize the effects of disturbances on the system. The objective of the H_∞ design problem, then, is to find a controller $\mathbf{K}(s)$, which renders the closed–loop system internally stable and minimizes the ∞ norm of the transfer function matrix $\mathcal{F}_l(\mathbf{P},\mathbf{K})$. A related sub–optimal problem is the one of finding a stabilizing controller

satisfying the relation

$$\|\mathcal{F}_l(\mathbf{P},\mathbf{K})\|_\infty < \gamma. \qquad \text{(VIII-14)}$$

The optimal problem amounts to solving for the smallest value of γ.

There are a number of techniques developed for the solution of the H_∞ problem, including the so-called Model Matching problem [117]. However, this is challenging, both computationally and numerically. A relatively simple alogoritm developed by Glover and Doyle [124], which results in a state space parametrization of stabilizing controllers, is outlined below. The present technique is quite popular and has been implemented in the *Robust Control Toolbox* used in conjunction with the MATLAB software.

VIII.3.1 Glover–Doyle H_∞ Algorithm

Consider a system with its dynamics represented by eq. (VIII-11). The following assumptions are made:

(A1) The realization $(\mathbf{A},\mathbf{B_2},\mathbf{C_2})$ is stabilizable and detectable, which is necessary for a stabilizing $\mathbf{K}(s)$ to exist;

(A2) $\text{rank}(\mathbf{D_{12}}) = m_2$; $\text{rank}(\mathbf{D_{21}}) = p_2$;

(A3) $\mathbf{u}$ and $\mathbf{y}$ are scaled, and unitary transformations of $\mathbf{w}$ and $\mathbf{z}$ are made which allows for the following assumption, without loss of generality,

$$\mathbf{D_{12}} = \begin{bmatrix} \mathbf{0} \\ \mathbf{I} \end{bmatrix}, \qquad \mathbf{D_{21}} = [\mathbf{0} \quad \mathbf{I}], \qquad \mathbf{D_{11}} = \begin{bmatrix} \mathbf{D_{1111}} & \mathbf{D_{1112}} \\ \underbrace{\mathbf{D_{1121}}}_{(m_1-p_2)} & \underbrace{\mathbf{D_{1122}}}_{p_2} \end{bmatrix} \begin{matrix} \} (p_1-m_2) \\ \} \; m_2 \end{matrix};$$

(A4) $\mathbf{D_{22}} = 0$;

(A5) $\text{rank}\begin{bmatrix} \mathbf{A} - j\omega\mathbf{I} & \mathbf{B_2} \\ \mathbf{C_1} & \mathbf{D_{12}} \end{bmatrix} = n + m_2 \quad \forall\omega \in \Re;$

(A6) $\quad \text{rank}\begin{bmatrix} \mathbf{A} - j\omega\mathbf{I} & \mathbf{B_1} \\ \mathbf{C_2} & \mathbf{D_{21}} \end{bmatrix} = n + p_2 \quad \forall\omega \in \Re.$

Furthermore:

$$\mathbf{R} \stackrel{\text{def}}{=} \mathbf{D_{1*}}^T\mathbf{D_{1*}} - \begin{bmatrix} \gamma^2\mathbf{I}_{m_1} & 0 \\ 0 & 0 \end{bmatrix};$$
$$\tilde{\mathbf{R}} \stackrel{\text{def}}{=} \mathbf{D_{*1}}\mathbf{D_{*1}}^T - \begin{bmatrix} \gamma^2\mathbf{I}_{p_1} & 0 \\ 0 & 0 \end{bmatrix};$$

where $\mathbf{D_{1*}} \stackrel{\text{def}}{=} [\mathbf{D_{11}} \quad \mathbf{D_{12}}]$ and $\mathbf{D_{*1}} \stackrel{\text{def}}{=} \begin{bmatrix} \mathbf{D_{11}} \\ \mathbf{D_{21}} \end{bmatrix}$.

The *state feedback*, $\mathbf{F}_I$, and *output injection*, $\mathbf{H}_I$, matrices are defined as:

$$\mathbf{F}_I = -\mathbf{R}^{-1}\left(\mathbf{D_{1*}}^T\mathbf{C_1} + \mathbf{B}^T\mathbf{X}_\infty\right);$$
$$\mathbf{H}_I = -\left(\mathbf{B}_I\mathbf{D_{*1}}^T + \mathbf{Y}_\infty\mathbf{C}^T\right)\tilde{\mathbf{R}}^{-1}.$$

The matrices are partitioned as indicated:

$$\mathbf{F}_I = \begin{bmatrix} \mathbf{F}_{11} \\ \mathbf{F}_{12} \\ \mathbf{F}_2 \end{bmatrix} \begin{matrix} \} \\ \} \\ \} \end{matrix} \begin{matrix} (m_1 - p_2) \\ p_2 \\ m_2 \end{matrix};$$

$$\mathbf{H}_I = [\underbrace{\mathbf{H}_{11}}_{(p_1 - m_2)} \quad \underbrace{\mathbf{H}_{12}}_{m_2} \quad \underbrace{\mathbf{H}_2}_{p_2}].$$

$\mathbf{X}_\infty$ and $\mathbf{Y}_\infty$ are the stabilizing solutions to the following pair of algebraic Riccati equations:

$$\mathbf{X}_\infty\mathbf{U}_1 + \mathbf{U}_1{}^T\mathbf{X}_\infty - \mathbf{X}_\infty\mathbf{B}\mathbf{R}^{-1}\mathbf{B}^T\mathbf{X}_\infty + \mathbf{V}_1 = 0;$$
$$\mathbf{Y}_\infty\mathbf{U}_2{}^T + \mathbf{U}_2\mathbf{Y}_\infty - \mathbf{Y}_\infty\mathbf{C}^T\tilde{\mathbf{R}}^{-1}\mathbf{C}\mathbf{Y}_\infty + \mathbf{V}_2 = 0;$$

where:

$$\mathbf{U}_1 = \mathbf{A} - \mathbf{B}\mathbf{R}^{-1}\mathbf{D_{1*}}^T\mathbf{C}_1;$$
$$\mathbf{V}_1 = \mathbf{C}_1{}^T\left(\mathbf{I} - \mathbf{D_{1*}}\mathbf{R}^{-1}\mathbf{D_{1*}}^T\right)\mathbf{C}_1;$$

$$\mathbf{U}_2 = \mathbf{A} - \mathbf{B}_1\mathbf{D}_{*1}{}^T\tilde{\mathbf{R}}^{-1}\mathbf{C};$$

$$\mathbf{V}_2 = \mathbf{B}_1\left(\mathbf{I} - \mathbf{D}_{*1}{}^T\tilde{\mathbf{R}}^{-1}\mathbf{D}_{*1}\right)\mathbf{B}_1{}^T.$$

Earlier $\mathbf{X}_\infty$ and $\mathbf{Y}_\infty$ were described as being 'stabilizing solutions'. By this, it is meant that the $\mathbf{A}+\mathbf{B}\mathbf{F}_I$ and $\mathbf{A}+\mathbf{H}_I\mathbf{C}$ matrices have all their poles in the open left half plane (OLHP). The main result of the Glover–Doyle algorithm is given by the following theorem:

Theorem VIII-1 (Glover and Doyle, 1988)

(1) A stabilizing controller $\mathbf{K}(s)$ exists, such that $\|\mathcal{F}_l(\mathbf{P},\mathbf{K})\|_\infty < \gamma$, iff

(a) $\gamma > \max\left\{\bar{\sigma}\left[\mathbf{D}_{1111},\mathbf{D}_{1112}\right],\bar{\sigma}\left[\mathbf{D}_{1111}{}^T,\mathbf{D}_{1121}{}^T\right]\right\}$ and,

(b) $\exists\ \mathbf{X}_\infty \geq 0, \mathbf{Y}_\infty \geq 0$ such that $\rho\left(\mathbf{X}_\infty\mathbf{Y}_\infty\right) < \gamma^2$.

(2) If the conditions given in (a) and (b) are satisfied, then all rational stabilizing controllers, $\mathbf{K}(s)$, satisfying $\|\mathcal{F}_l(\mathbf{P},\mathbf{K})\|_\infty < \gamma$ are given by

$$\mathbf{K}(s) = \mathcal{F}_l(\mathbf{K}_a,\mathbf{\Phi})$$

for any rational $\mathbf{\Phi} \in H_\infty$ such that $\|\mathbf{\Phi}\|_\infty < \gamma$. Here $\mathbf{K}_a$ has the realization

$$\mathbf{K}_a \overset{s}{=} \left[\begin{array}{ccccc} \hat{\mathbf{A}} & \vdots & \hat{\mathbf{B}}_1 & \hat{\mathbf{B}}_2 \\ \cdots & \cdots & \cdots & \cdots \\ \hat{\mathbf{C}}_1 & \vdots & \hat{\mathbf{D}}_{11} & \hat{\mathbf{D}}_{12} \\ \hat{\mathbf{C}}_2 & \vdots & \hat{\mathbf{D}}_{21} & 0 \end{array}\right],$$

where

$$\hat{\mathbf{D}}_{11} = -\mathbf{D}_{1121}\mathbf{D}^T{}_{1111}\left(\gamma^2\mathbf{I} - \mathbf{D}_{1111}\mathbf{D}^T{}_{1111}\right)^{-1}\mathbf{D}_{1112} - \mathbf{D}_{1122}.$$

$\hat{\mathbf{D}}_{12} \in \Re^{m2\times m2}$ and $\hat{\mathbf{D}}_{21} \in \Re^{p2\times p2}$ are matrices which satisfy the following relations:

$$\hat{\mathbf{D}}_{12}\hat{\mathbf{D}}^T{}_{12} = \mathbf{I} - \mathbf{D}_{1121}\left(\gamma^2\mathbf{I} - \mathbf{D}^T{}_{1111}\mathbf{D}_{1111}\right)^{-1}\mathbf{D}^T{}_{1121};$$

$$\hat{\mathbf{D}}^T{}_{21}\hat{\mathbf{D}}_{21} = \mathbf{I} - \mathbf{D}^T{}_{1112}\left(\gamma^2\mathbf{I} - \mathbf{D}_{1111}\mathbf{D}^T{}_{1111}\right)^{-1}\mathbf{D}^T{}_{1112};$$

and

$$\begin{aligned}
\hat{\mathbf{B}}_2 &= (\mathbf{B}_2 + \mathbf{H}_{12})\,\hat{\mathbf{D}}_{12};\\
\hat{\mathbf{C}}_2 &= -\hat{\mathbf{D}}_{21}\,(\mathbf{C}_2 + \mathbf{F}_{12})\,\mathbf{Z};\\
\hat{\mathbf{B}}_1 &= -\mathbf{H}_2 + \hat{\mathbf{B}}_2\hat{\mathbf{D}}_{12}^{-1}\hat{\mathbf{D}}_{11};\\
\hat{\mathbf{C}}_1 &= \mathbf{F}_2\mathbf{Z} + \hat{\mathbf{D}}_{11}\hat{\mathbf{D}}_{21}^{-1}\hat{\mathbf{C}}_2;\\
\hat{\mathbf{A}} &= \mathbf{A} + \mathbf{H}\mathbf{C} + \hat{\mathbf{B}}_2\hat{\mathbf{D}}_{12}^{-1}\hat{\mathbf{C}}_1;\\
\mathbf{Z} &= \left(\mathbf{I} - \gamma^{-2}\mathbf{Y}_\infty\mathbf{X}_\infty\right)^{-1}.
\end{aligned}$$ ⋆

In order to minimize $\|\mathcal{F}_l(\mathbf{P},\mathbf{K})\|_\infty$, the above algorithm must be applied iteratively by repeatedly reducing γ until the limiting value $\gamma_\circ$ is reached, which occurs either when $\rho(\mathbf{Y}_\infty\mathbf{X}_\infty) = \gamma_\circ$, or when one of the two Riccati equations fails to return a positive–definite solution for either $\mathbf{Y}_\infty$ or $\mathbf{X}_\infty$.

A common form of the H_∞ problem is the so–called mixed–sensitivity problem whereby $\mathcal{F}_l(\mathbf{P},\mathbf{K})$ is defined as

$$\mathcal{F}_l(\mathbf{P},\mathbf{K}) = \begin{bmatrix} W_1(s)\mathbf{S}(s) \\ W_3(s)\,[\mathbf{I} - \mathbf{S}(s)] \end{bmatrix}, \qquad \text{(VIII–15)}$$

where

$$\mathbf{S}(s) = [\mathbf{I} + \mathbf{G}(s)\mathbf{K}(s)]^{-1}.$$

The significance of such a formulation is that both performance and stability robustness are addressed. With the above weightage, the augmented plant model $\mathbf{P}(s)$ is

given by

$$\mathbf{P}(s) = \begin{bmatrix} \mathbf{P_{11}}(s) & \vdots & \mathbf{P_{12}}(s) \\ \cdots\cdots & \cdots & \cdots\cdots \\ \mathbf{P_{21}}(s) & \vdots & \mathbf{P_{22}}(s) \end{bmatrix} = \begin{bmatrix} W_1(s) & \vdots & -W_1(s)\mathbf{G}(s) \\ 0 & \vdots & W_3(s)\mathbf{G}(s) \\ \cdots\cdots\cdots & \cdots & \cdots\cdots\cdots \\ \mathbf{I} & \vdots & -\mathbf{G}(s) \end{bmatrix}.$$

For the closed loop system to be be stable in the presence of model uncertainty expressed as a multiplicative model error, $\mathbf{E_m}(j\omega)$, the following condition must be satisfied,

$$\bar{\sigma}\left[\mathbf{E_m}(j\omega)\right]\bar{\sigma}\left[\mathbf{I}-\mathbf{S}(j\omega)\right] < 1. \qquad \text{(VIII-16)}$$

Moreover, if $W_3(j\omega)$ is taken to be an upper-bound for $\mathbf{E_m}(j\omega)$, i.e. $|W_3(j\omega)| > \bar{\sigma}\left[\mathbf{E_m}(j\omega)\right]$, then the condition for stability robustness can be rewritten as

$$\bar{\sigma}\left[W_3(j\omega)\left(\mathbf{I}-\mathbf{S}(j\omega)\right)\right] < 1. \qquad \text{(VIII-17)}$$

Therefore, applying eqs. VIII-15 and VIII-17 to eq. VIII-14, and incorporating γ into $W_1(j\omega)$, the design objective for the mixed-sensitivity problem can be written as [71]

$$\|\mathcal{T}_{y_1u_1}\|_\infty \leq 1, \qquad \text{(VIII-18)}$$

where

$$\mathcal{T}_{y_1u_1} = \begin{bmatrix} \frac{1}{\gamma}W_1(s)\mathbf{S}(s) \\ W_3(s)\left[\mathbf{I}-\mathbf{S}(s)\right] \end{bmatrix}. \qquad \text{(VIII-19)}$$

Appendix IX: Linear Control Designs for the FEL Model

The design model for the FEL is given by $(\mathbf{A_r}, \mathbf{B_r}, \mathbf{C_r})$, while the truth model by the $(\mathbf{A_f}, \mathbf{B_f}, \mathbf{C_f})$ matrices. Note, the control input is in kN-m, while the output is measured in 10^{-2} radians (centiradians):

$$\mathbf{A_r} = \begin{bmatrix} 0 & 0 & 0 & 1 & 0 & 0 \\ 0 & 0 & 0 & 0 & 1 & 0 \\ 0 & 0 & 0 & 0 & 0 & 1 \\ -1.131e-6 & 1.799e-11 & 0 & 0 & 0 & -3.976e-9 \\ 1.349e-11 & 4.3102e-6 & 0 & 0 & 0 & -2.084e-3 \\ 0 & 0 & 1.1655e-6 & 6.3720e-9 & 2.1616e-3 & 0 \end{bmatrix};$$

$$\mathbf{B_r} = \begin{bmatrix} 0 & 0 & 0 \\ 0 & 0 & 0 \\ 0 & 0 & 0 \\ 1.5010e-3 & 0 & 1.9472e-5 \\ -2.384e-6 & 0 & 1.8339e-4 \\ 0 & 1.9025e-4 & 0 \end{bmatrix};$$

$$\mathbf{C_r} = \begin{bmatrix} 99.992 & -1.2974 & 0 & 0 & 0 & 0 \\ 0 & 0 & 100 & 0 & 0 & 0 \\ 1.2974 & 99.992 & 0 & 0 & 0 & 0 \end{bmatrix}; \qquad (IX-1)$$

$$\mathbf{A_f} = \begin{bmatrix} \mathbf{0}_{10\times10} & \mathbf{I}_{10\times10} \\ \mathbf{A_{21}} & \mathbf{A_{22}} \end{bmatrix};$$

$$\mathbf{A_{21}} = \begin{bmatrix} 1.6889e-6 & 1.3643e-7 & -1.77e-15 & 6.7830e-1 & -3.83e-15 & \cdots \\ 1.8078e-8 & 4.5454e-6 & -4.71e-16 & 1.2622e+0 & -9.42e-16 & \cdots \\ 1.985e-15 & 1.985e-15 & 1.1969e-6 & 6.594e-12 & 3.7071e-2 & \cdots \\ -1.008e-7 & -2.141e-5 & 1.118e-15 & -1.010e+2 & -1.12e-15 & \cdots \\ 1.588e-14 & 3.706e-14 & 4.8836e-7 & -6.900e-9 & -1.361e+2 & \cdots \\ 3.6647e-5 & 1.0787e-5 & 2.630e-14 & 1.4041e+2 & 8.942e-14 & \cdots \\ 1.694e-12 & 1.355e-12 & 4.2371e-5 & -2.176e-7 & -3.209e+2 & \cdots \\ -1.828e-5 & -7.304e-6 & -2.25e-14 & 1.6156e+1 & -3.63e-14 & \cdots \\ -1.146e-4 & -2.285e-7 & -1.743e-6 & -1.372e+1 & 8.5946e+1 & \cdots \\ 1.1459e-4 & 2.2854e-7 & -1.743e-6 & 1.3720e+1 & 8.5946e+1 & \cdots \end{bmatrix}$$

$$\begin{bmatrix} \cdots & 2.5539e-1 & 1.767e-15 & -8.494e-3 & 2.0569e-2 & -2.057e-2 \\ \cdots & -1.640e-2 & -4.71e-16 & -3.496e-4 & -2.262e-4 & 2.2620e-4 \\ \cdots & -3.06e-12 & -9.073e-3 & 1.022e-13 & -6.168e-4 & -6.168e-4 \\ \cdots & 1.5965e-1 & 8.947e-16 & 1.2246e-3 & -1.028e-3 & 1.0283e-3 \\ \cdots & -4.89e-11 & -3.648e-1 & -1.11e-13 & 6.4418e-3 & 6.4418e-3 \\ \cdots & -1.482e+1 & -4.21e-14 & 1.3959e-1 & -3.492e-1 & 3.4922e-1 \\ \cdots & -5.44e-10 & -1.098e+1 & 2.372e-12 & 4.7694e-3 & 4.7694e-3 \\ \cdots & 2.0939e+0 & 1.384e-14 & -4.786e-1 & 1.7399e-1 & -1.740e-1 \\ \cdots & -5.298e+0 & 7.2350e-2 & 1.7597e-1 & -8.431e-1 & 4.0536e-1 \\ \cdots & 5.2978e+0 & 7.2350e-2 & -1.770e-1 & 4.0536e-1 & -8.431e-1 \end{bmatrix};$$

$$\mathbf{A_{22}} = \begin{bmatrix} 8.836e-16 & 8.836e-16 & -3.015e-5 & 1.1186e-3 & 4.0653e-7 & \cdots \\ -4.71e-16 & -7.07e-16 & -2.136e-3 & 2.0757e-3 & -1.536e-5 & \cdots \\ 1.6578e-6 & 2.1893e-3 & -1.98e-10 & -1.821e-6 & 6.0494e-5 & \cdots \\ 4.473e-16 & 4.473e-16 & 4.7312e-3 & -1.661e-1 & 1.6195e-3 & \cdots \\ -7.452e-4 & 4.3166e-4 & 9.638e-10 & -2.205e-3 & -2.237e-1 & \cdots \\ -2.10e-14 & -2.10e-14 & -2.384e-3 & 2.3084e-1 & 5.0004e-4 & \cdots \\ -1.244e-3 & 3.7451e-2 & -2.277e-7 & -5.206e-3 & -5.276e-1 & \cdots \\ 5.191e-15 & 5.191e-15 & 1.6139e-3 & 2.6746e-2 & -3.296e-4 & \cdots \\ 8.2735e-4 & -1.541e-3 & 5.0501e-5 & -2.282e-2 & 1.4115e-1 & \cdots \\ 8.2735e-4 & -1.541e-3 & -5.050e-5 & 2.2428e-2 & 1.4118e-1 & \cdots \end{bmatrix}$$

$$\begin{bmatrix} \cdots & 1.6264e-3 & 5.9924e-9 & -2.714e-4 & 6.515e-4 & -6.536e-4 \\ \cdots & -1.044e-4 & 2.466e-10 & -1.117e-5 & -4.229e-6 & 1.0124e-5 \\ \cdots & -2.774e-6 & -5.776e-5 & -2.631e-6 & -1.967e-5 & -1.972e-5 \\ \cdots & 1.0163e-3 & -8.64e-10 & 3.9129e-5 & -1.475e-5 & 5.0498e-5 \\ \cdots & -4.259e-5 & -2.323e-3 & 2.7920e-6 & 2.0571e-4 & 2.0571e-4 \\ \cdots & -9.435e-2 & -2.946e-5 & 4.4601e-3 & -1.105e-2 & 1.1106e-2 \\ \cdots & -1.183e-4 & -6.990e-2 & -3.752e-5 & 1.5272e-4 & 1.5188e-4 \\ \cdots & 1.3360e-2 & 3.3764e-7 & -1.529e-2 & 5.5494e-3 & -5.491e-3 \\ \cdots & -3.376e-2 & 4.6082e-4 & 5.5752e-3 & -2.677e-2 & 1.2837e-2 \\ \cdots & 3.3717e-2 & 4.6107e-4 & -5.669e-3 & 1.2792e-2 & -2.682e-2 \end{bmatrix};$$

$$\mathbf{B_f} = \begin{bmatrix} \mathbf{0}_{10\times 3} \\ \mathbf{B_2} \end{bmatrix};$$

$$\mathbf{B_2} = \begin{bmatrix} 5.6492e-3 & 0 & 1.3737e-5 \\ -6.212e-5 & 0 & 1.9744e-4 \\ 0 & 2.0310e-4 & 0 \\ -2.824e-4 & 0 & -5.423e-4 \\ 0 & -1.582e-5 & 0 \\ -9.591e-2 & 0 & 4.9087e-3 \\ 0 & 3.4047e-3 & 0 \\ 4.7785e-2 & 0 & 2.5882e-3 \\ -1.171e-1 & 3.5111e-3 & -2.316e-4 \\ 1.1711e-1 & 3.5111e-3 & 2.3162e-4 \end{bmatrix};$$

$$\mathbf{C_f} = \begin{bmatrix} \mathbf{C_1} & \mathbf{0}_{3\times 10} \end{bmatrix};$$

$$\mathbf{C_1} = \begin{bmatrix} 99.992 & -1.297e+0 & 1.6999e-7 & 4.7261e-10 & 2.3386e-10 & \cdots \\ -1.962e-8 & 0 & 100 & -2.23e-10 & -1.3792e-8 & \cdots \\ 1.2974e+0 & 99.992 & 0 & -1.7175e-9 & 0 & \cdots \end{bmatrix}$$

$$\begin{bmatrix} \cdots & -1.46e-10 & -1.50e-10 & 0 & -3.08e-10 & 0 \\ \cdots & -1.31e-10 & 2.3260e-9 & 1.101e-10 & -3.47e-10 & 1.956e-10 \\ \cdots & 1.838e-10 & 0 & 1.293e-10 & 1.288e-10 & -1.29e-10 \end{bmatrix}.$$

(IX − 2)

LQG/LTR Design

The LQG/LTR compensator obtained with the tuning parameter $q = 10^7$ is repesented by the following model:

$$\dot{\mathbf{x}}_\mathbf{c} = \mathbf{A_c x_c} + \mathbf{B_c}(\mathbf{r} - \mathbf{y})$$

$$\mathbf{u} = \mathbf{C_c x_c}; \qquad (\text{IX} - 3)$$

where:

$$\mathbf{A_c} = \begin{bmatrix} -5.479e+1 & 1.1022e-4 & -6.02e-14 & -1.501e+3 & 4.0753e-3 & -5.077e-8 \\ 1.1022e-4 & -1.915e+1 & -5.96e-11 & 4.0753e-3 & -1.834e+2 & -2.050e-2 \\ -5.93e-14 & -5.96e-11 & -1.951e+1 & 5.0780e-8 & 2.0502e-2 & -1.903e+2 \\ 1 & 0 & 0 & -2.055e-2 & 3.9972e-8 & 6.5842e-9 \\ 0 & 1 & 0 & 4.4661e-8 & -7.649e-3 & 2.2327e-3 \\ 0 & 0 & 1 & -4.248e-9 & -2.018e-3 & -7.349e-3 \end{bmatrix};$$

$$\mathbf{B_c} = \begin{bmatrix} 1.4066e-1 & -1.232e-7 & 1.8251e-3 \\ -2.079e-3 & -4.293e-2 & 1.6027e-1 \\ -5.499e-4 & 1.4118e-1 & 4.2388e-2 \\ 1.3689e+1 & -1.115e-6 & 1.7770e-1 \\ -5.410e-1 & -3.737e-1 & 4.1700e+1 \\ 4.6726e-3 & 3.8629e+1 & -3.602e-1 \end{bmatrix};$$

$$\mathbf{C_c} = \begin{bmatrix} 5.4789e-1 & -2.486e-3 & -7.13e-15 & 1.5010e+1 & -2.384e-2 & -2.661e-6 \\ 5.934e-16 & 5.955e-13 & 1.9507e-1 & -5.08e-10 & -2.051e-4 & 1.9025e+0 \\ 7.1078e-3 & 1.9151e-1 & 5.956e-13 & 1.9472e-1 & 1.8339e+0 & 2.0508e-4 \end{bmatrix}. \qquad (\text{IX} - 4)$$

H_∞ Design

The H_∞ compensator is described by the following model:

$$\dot{\mathbf{x}}_\mathbf{c} = \mathbf{A_c x_c} + \mathbf{B_c}(\mathbf{r} - \mathbf{y});$$

$$\mathbf{u} = \mathbf{C_c x_c}; \qquad (\text{IX} - 5)$$

where:

$$\mathbf{A_c} = \begin{bmatrix} -2.008e-1 & 1.1379e-6 & -6.098e-5 & 1.7534e-3 & 1.8260e-4 & -2.523e-4 & \cdots \\ 1.6447e-6 & -2.009e-1 & 1.9934e-5 & 1.9577e-4 & 5.3346e-4 & 8.1090e-4 & \cdots \\ -1.249e-4 & 2.8237e-5 & -2.004e-1 & -4.828e-3 & 4.9119e-3 & -4.058e-4 & \cdots \\ 6.2740e-3 & 4.8465e-4 & -8.437e-3 & -1.385e-3 & 2.0102e-4 & -1.121e-5 & \cdots \\ 9.6022e-4 & 1.9408e-3 & 1.2615e-2 & 2.9542e-4 & -1.442e-3 & 1.9008e-5 & \cdots \\ -1.738e-3 & 3.8650e-3 & -1.365e-3 & -2.159e-5 & 2.4902e-5 & -1.146e-3 & \cdots \\ -1.877e-5 & 4.2161e-6 & 1.2341e-5 & 3.7715e-6 & -1.306e-5 & -3.735e-5 & \cdots \\ -1.211e-6 & -1.070e-5 & 1.8038e-5 & 2.4160e-6 & -6.465e-5 & -2.241e-5 & \cdots \\ 2.6635e-6 & 1.1877e-5 & 1.2218e-5 & 1.5634e-5 & -4.602e-5 & 4.1254e-5 & \cdots \\ -1.537e-6 & 6.6168e-7 & 7.1782e-6 & -2.138e-5 & 1.1633e-6 & 2.6192e-5 & \cdots \\ -2.254e-7 & -1.021e-6 & 1.3124e-6 & -1.266e-5 & 3.7383e-6 & -2.098e-5 & \cdots \\ 3.8445e-7 & 3.5498e-7 & 1.8042e-6 & 3.1630e-6 & 2.1645e-5 & -3.472e-6 & \cdots \end{bmatrix}$$

$$\begin{bmatrix} \cdots & -5.14e-11 & -1.92e-11 & 1.121e-11 & 2.892e-10 & 3.616e-11 & -4.87e-11 \\ \cdots & 3.054e-11 & -1.29e-11 & 1.391e-11 & -2.28e-10 & 8.039e-11 & -2.58e-11 \\ \cdots & 9.638e-11 & 9.555e-11 & 3.086e-11 & -5.85e-10 & -4.63e-10 & -7.09e-10 \\ \cdots & 1.3961e-9 & 1.468e-11 & 2.569e-10 & 1.1058e-8 & 3.7565e-9 & -3.62e-10 \\ \cdots & -2.48e-10 & -1.437e-9 & -1.273e-9 & -2.730e-9 & -6.667e-9 & -1.696e-8 \\ \cdots & -3.957e-9 & 2.3879e-9 & -1.054e-9 & -3.355e-8 & 7.9166e-9 & 9.5081e-9 \\ \cdots & -4.273e-2 & 1.3826e-2 & -1.138e-2 & -3.463e-1 & 2.5392e-3 & 4.4715e-2 \\ \cdots & -6.838e-3 & -4.151e-2 & -3.685e-4 & -2.806e-2 & -3.147e-1 & -1.798e-1 \\ \cdots & 4.7083e-3 & -4.880e-3 & -4.067e-2 & -1.644e-2 & 1.2022e-1 & -3.660e-1 \\ \cdots & 6.7451e-3 & 1.1028e-3 & 5.2282e-5 & -5.904e-2 & -1.584e-2 & 5.3966e-3 \\ \cdots & -8.595e-4 & 6.5236e-3 & -2.897e-3 & 8.4539e-3 & -6.118e-2 & -3.033e-3 \\ \cdots & -3.340e-4 & 2.0754e-3 & 5.7862e-3 & -1.019e-3 & 4.1729e-3 & -5.860e-2 \end{bmatrix};$$

$$\mathbf{B_c} = \begin{bmatrix} 1.6656e+0 & -6.780e-1 & -7.206e-1 \\ 5.5075e-1 & 2.1508e+0 & -7.368e-1 \\ -1.167e+0 & -5.336e-1 & -2.354e+0 \\ -3.451e+0 & 1.4191e+0 & 2.1193e-1 \\ 5.8784e-1 & 3.5785e-1 & 4.5398e+0 \\ -1.930e+0 & -4.693e+0 & 5.8539e-1 \\ -1.600e-4 & 1.3514e-2 & -1.435e-3 \\ -5.594e-3 & -3.954e-3 & -6.544e-3 \\ -2.828e-4 & -1.413e-3 & -8.539e-3 \\ 2.4422e-3 & -2.839e-3 & -1.322e-4 \\ 2.5187e-3 & 4.3297e-3 & 2.0584e-4 \\ -8.457e-5 & -1.513e-4 & 3.2988e-3 \end{bmatrix};$$

$$\mathbf{C_c} = \begin{bmatrix} 2.4275e-6 & 3.8863e-6 & 1.5229e-6 & 3.1729e-7 & 2.1049e-5 & 3.7170e-5 & \cdots \\ -1.381e-5 & 2.2137e-5 & -7.679e-7 & 3.9344e-5 & 6.9414e-5 & 7.1467e-5 & \cdots \\ -1.333e-5 & -1.204e-5 & 2.3080e-5 & -8.110e-5 & 3.6024e-4 & -1.669e-4 & \cdots \end{bmatrix}$$

$$\begin{bmatrix} \cdots & 3.1630e-2 & 8.1094e-4 & 2.9976e-3 & 2.5303e-1 & 1.0428e-1 & -3.009e-2 \\ \cdots & -7.988e-2 & 1.5278e-1 & -1.184e-1 & -9.031e-1 & 1.2855e+0 & -1.872e-1 \\ \cdots & -3.578e-2 & 1.2867e-1 & 1.8880e-1 & -1.190e-1 & 1.6665e-1 & 2.3416e+0 \end{bmatrix}.$$

(IX − 6)

Appendix X: LQG/LTR Control Design for the PMC Model

Vibration suppression controller design

The 60-state, 2-input, 2-output flexible subsystem is both uncontrollable and unobservable. The Schur model reduction procedure is applied. The resulting 14-state model, which is both controllable and observable is given by the realization $(\mathbf{A_{14}}, \mathbf{B_{14}}, \mathbf{C_{14}})$:

$$\mathbf{A_{14}} = \begin{bmatrix}
3.6303e+0 & -3.014e+0 & 3.7940e-3 & 1.0819e+0 & -1.65e-3 & 2.5834e-4 & \cdots \\
7.8279e+0 & -3.791e+0 & 1.4659e-2 & 2.1779e+0 & -3.426e-3 & 8.9918e-4 & \cdots \\
6.3820e-3 & -2.444e-3 & -3.112e+0 & 3.6163e-2 & 5.1195e-2 & -2.236e-2 & \cdots \\
1.7490e-1 & -1.942e-1 & 4.0680e-2 & 1.7895e+0 & -4.640e-3 & 2.2183e-3 & \cdots \\
4.4098e-4 & 2.3427e-4 & -3.550e-1 & -4.061e-6 & -3.213e-1 & 1.3347e+0 & \cdots \\
-1.105e-3 & 9.9096e-4 & -3.727e-1 & 1.5067e-4 & -1.304e+0 & 3.1848e-1 & \cdots \\
1.5252e-3 & 2.3710e-3 & -4.596e+0 & 2.8827e-2 & -4.733e-1 & 5.7420e-1 & \cdots \\
8.2361e-2 & 7.1988e-3 & 6.1407e-2 & -1.924e+0 & 1.6164e-2 & -2.255e-2 & \cdots \\
6.2355e-4 & -4.796e-3 & 1.0745e+0 & 1.2067e-1 & 2.8799e-1 & -3.032e-1 & \cdots \\
-6.124e-3 & 2.6145e-3 & 3.1569e-1 & 1.3348e-2 & 5.2686e-1 & -5.634e-1 & \cdots \\
-1.136e-1 & 5.0051e-2 & -1.334e-2 & 6.0797e-1 & -2.995e-2 & 3.2401e-2 & \cdots \\
-2.097e-2 & 1.9539e-2 & 6.6842e-3 & -5.380e-2 & 6.0160e-3 & -2.096e-3 & \cdots \\
6.9158e-2 & -1.492e-2 & -7.798e-3 & -6.289e-1 & -1.560e-3 & 4.0784e-3 & \cdots \\
9.8922e-2 & 3.1345e-2 & -1.507e-2 & -2.609e+0 & 4.2740e-3 & 5.5711e-4 & \cdots
\end{bmatrix}$$

$$\begin{bmatrix}
\cdots & 5.9487e-3 & -1.095e-1 & 1.1788e-2 & -1.298e-2 & -3.476e-1 & -5.3182e-1 & \cdots \\
\cdots & 4.9428e-3 & -2.413e-1 & 2.6932e-2 & -3.225e-2 & -6.601e-1 & -1.056e+0 & \cdots \\
\cdots & 4.5824e+0 & -4.344e-3 & 4.4538e-1 & 4.3191e+0 & -2.488e-1 & 1.8045e-2 & \cdots \\
\cdots & -2.659e-2 & -9.029e-2 & 1.1189e-2 & -4.371e-2 & -3.395e-1 & -9.349e-1 & \cdots \\
\cdots & 4.1584e-1 & -2.241e-2 & -2.669e-1 & 5.8809e-1 & -3.385e-2 & 3.4650e-3 & \cdots \\
\cdots & 4.1056e-1 & -2.356e-2 & -2.842e-1 & 5.6115e-1 & -3.630e-2 & 2.4420e-3 & \cdots \\
\cdots & 4.4230e+0 & -1.331e-1 & -1.392e+0 & 4.9284e+0 & -2.990e-1 & 1.8978e-2 & \cdots \\
\cdots & -5.272e-2 & -3.959e-1 & 6.4411e-2 & -3.420e-1 & -2.934e+0 & 5.2489e-1 & \cdots \\
\cdots & -7.459e-1 & 6.8815e-2 & 4.7606e-1 & -2.402e+0 & 3.4010e-1 & -4.581e-2 & \cdots \\
\cdots & -1.495e+0 & 1.9315e-1 & 1.7511e+0 & -1.996e+0 & 1.3211e-1 & -1.413e-2 & \cdots \\
\cdots & 9.2875e-2 & 1.0732e+0 & -1.764e-1 & 1.4429e-1 & 4.3957e-1 & -1.728e-1 & \cdots \\
\cdots & -1.299e-2 & -2.449e-2 & 1.3681e-2 & -1.640e-2 & -1.683e-2 & 3.9652e-3 & \cdots \\
\cdots & 1.0925e-2 & -1.440e-1 & 3.7973e-3 & 6.1331e-5 & -3.364e-1 & -8.108e-1 & \cdots \\
\cdots & -8.034e-3 & 1.1527e-1 & -1.063e-2 & -1.833e-3 & 4.1331e-2 & 2.5258e-1 & \cdots
\end{bmatrix}$$

$$
\begin{bmatrix}
\cdots & -1.342e-1 & 2.8256e+0 \\
\cdots & -2.427e-1 & 5.5411e+0 \\
\cdots & -4.058e-2 & 3.8529e-2 \\
\cdots & -3.764e-1 & 5.4370e+0 \\
\cdots & -2.829e-3 & -8.5280e-3 \\
\cdots & -6.156e-3 & -1.5155e-3 \\
\cdots & -4.102e-2 & -1.415e-2 \\
\cdots & 1.819e-1 & -5.382e+0 \\
\cdots & -1.246e-3 & 3.6916e-1 \\
\cdots & 4.7419e-3 & 3.2447e-2 \\
\cdots & -1.295e-1 & 1.3415e+0 \\
\cdots & 1.2735e+0 & -9.459e-1 \\
\cdots & 1.9702e-1 & -2.049e+0 \\
\cdots & 4.5227e-1 & -2.173e+0
\end{bmatrix};
$$

$$
\mathbf{B_{14}} = \begin{bmatrix}
-2.4601e-7 & 8.6319e-5 \\
-7.0247e-7 & 1.9425e-4 \\
4.1053e-4 & 3.5256e-6 \\
-2.8201e-6 & 4.3392e-4 \\
6.0574e-4 & 1.8436e-6 \\
5.3969e-4 & -2.9529e-6 \\
9.3994e-4 & -2.2825e-6 \\
-2.5127e-5 & -1.5172e-3 \\
-4.2296e-4 & 9.7565e-5 \\
-6.3905e-4 & 1.6763e-6 \\
3.4806e-5 & 2.4982e-4 \\
-4.4235e-6 & 4.0902e-4 \\
2.1108e-6 & -1.4220e-4 \\
-2.5214e-7 & -1.2556e-4
\end{bmatrix};
$$

$$
\mathbf{C_{14}} = \begin{bmatrix}
2.5713e-2 & -1.949e-2 & 4.3400e+1 & -2.624e-1 & 2.7705e+1 & -3.413e+1 & \cdots \\
1.1290e+0 & 6.7704e-1 & -2.038e-1 & -2.765e+1 & -1.269e-1 & -1.728e-1 & \cdots \\
\cdots & -6.207e+1 & -5.757e-1 & -1.608e+1 & -5.531e+1 & 3.1105e+0 & -6.086e-1 & \cdots \\
\cdots & -8.503e-2 & 4.4585e+0 & -4.269e-1 & -9.878e-1 & -8.620e+0 & 2.2803e+1 & \cdots \\
\cdots & 4.1602e-1 & 9.4251e-2 \\
\cdots & -2.797e+1 & -6.288e+1
\end{bmatrix}.
$$

(X – 1)

The process and measurement error covariances matrices, denoted by $\mathbf{Q_f}$ and $\mathbf{R_f}$, respectively, are:

$$
\mathbf{Q_f} = \begin{bmatrix} 1 & 0 \\ 0 & 1 \end{bmatrix};
$$

$$
\mathbf{R_f} = \begin{bmatrix} 0.25 & 0 \\ 0 & 0.25 \end{bmatrix}.
$$

Note, both are used as tuning parameters in the Kalman Filter design. The resulting

filter gain matrix $\mathbf{L_f}$ is

$$\mathbf{L_f} = \begin{bmatrix} 9.8303e-07 & -1.724e-04 \\ 4.2325e-07 & -1.997e-04 \\ 8.8013e-07 & -4.182e-07 \\ 4.6988e-07 & -4.731e-05 \\ 3.1767e-04 & -2.113e-06 \\ -3.726e-04 & -2.142e-06 \\ -9.922e-05 & 3.3252e-07 \\ -1.761e-05 & 1.2435e-04 \\ -2.761e-04 & -1.088e-05 \\ 6.1485e-05 & -9.033e-06 \\ -5.025e-06 & -4.480e-05 \\ -4.906e-06 & 3.0666e-04 \\ -1.743e-06 & -6.130e-04 \\ -4.306e-07 & -3.083e-05 \end{bmatrix}.$$

The optimal state estimator design is recovered by employing an appropriate state feedback matrix $\mathbf{K_{sf}}$. The ficticious measurement noise intensity corresponding to the design is $q_f = 1 \times 10^{10}$. The resulting LQG/LTR vibration suppression controller is given by the following model:

$$\begin{aligned} \dot{\mathbf{x}}_{\mathbf{cf}} &= \mathbf{A_{cf}x_{cf}} + \mathbf{B_{cf}}(\mathbf{r_f} - \mathbf{y_f}) \\ \mathbf{u_f} &= \mathbf{C_{cf}x_{cf}}; \end{aligned} \qquad (\mathrm{X}-2)$$

where:

$$\mathbf{A_{cf}} = \begin{bmatrix} -5.858e+0 & -8.659e+0 & 2.5650e+0 & 2.2846e+2 & 1.6493e+0 & 8.4483e-1 & \cdots \\ -1.352e+1 & -1.649e+1 & 6.4497e+0 & 5.1385e+2 & 4.1316e+0 & 1.3990e+0 & \cdots \\ -1.474e+0 & 6.8009e-1 & -1.854e+3 & 2.0002e+1 & -1.157e+3 & 1.3857e+3 & \cdots \\ -4.752e+1 & -2.857e+1 & 2.0055e+1 & 1.1448e+3 & 1.2759e+1 & -1.097e+0 & \cdots \\ -1.815e+0 & 1.2269e+0 & -2.732e+3 & 2.0613e+1 & -1.708e+3 & 2.0459e+3 & \cdots \\ -1.113e+0 & 1.3944e+0 & -2.434e+3 & 6.2601e+0 & -1.523e+3 & 1.8218e+3 & \cdots \\ -2.250e+0 & 2.2422e+0 & -4.243e+3 & 1.8466e+1 & -2.650e+3 & 3.1731e+3 & \cdots \\ 1.6694e+2 & 9.9157e+1 & 8.7829e+1 & -3.999e+3 & 5.4021e+1 & -1.143e+2 & \cdots \\ -9.599e+0 & -7.325e+0 & 1.9097e+3 & 2.4613e+2 & 1.1937e+3 & -1.426e+3 & \cdots \\ 1.5110e+0 & -1.528e+0 & 2.8817e+3 & -1.219e+1 & 1.8021e+3 & -2.158e+3 & \cdots \\ -2.767e+1 & -1.621e+1 & -1.527e+2 & 6.5960e+2 & -9.538e+1 & 1.2236e+2 & \cdots \\ -4.497e+1 & -2.674e+1 & 2.6832e+1 & 1.0773e+3 & 1.7014e+1 & -6.996e+0 & \cdots \\ 1.5696e+1 & 9.2882e+0 & -1.192e+1 & -3.752e+2 & -7.523e+0 & 4.3692e+0 & \cdots \\ 1.3902e+1 & 8.2405e+0 & -9.904e-1 & -3.334e+2 & -6.777e-1 & -3.287e+0 & \cdots \end{bmatrix}$$

$$
\begin{array}{cccccccc}
\cdots & -4.797e-1 & -3.741e+1 & 3.3247e+0 & 7.4588e+0 & 7.4312e+1 & -2.006e+2 & \cdots \\
\cdots & -2.007e+0 & -8.419e+1 & 7.2436e+0 & 1.5966e+1 & 1.6740e+2 & -4.513e+2 & \cdots \\
\cdots & 2.5402e+3 & 2.2192e+1 & 6.5844e+2 & 2.2556e+3 & -1.239e+2 & 1.7206e+1 & \cdots \\
\cdots & -1.225e+1 & -1.877e+2 & 1.4128e+1 & 2.8835e+1 & 3.7547e+2 & -1.007e+3 & \cdots \\
\cdots & 3.7416e+3 & 3.4179e+1 & 9.7047e+2 & 3.3220e+3 & -1.854e+2 & 3.3148e+1 & \cdots \\
\cdots & 3.3336e+3 & 3.2434e+1 & 8.6441e+2 & 2.9594e+3 & -1.692e+2 & 4.0184e+1 & \cdots \\
\cdots & 5.8097e+3 & 5.5160e+1 & 1.5047e+3 & 5.1584e+3 & -2.924e+2 & 6.3371e+1 & \cdots \\
\cdots & -1.734e+2 & 6.5354e+2 & -1.0536e+2 & -2.932e+2 & -1.306e+3 & 3.5153e+3 & \cdots \\
\cdots & -2.612e+3 & -6.651e+1 & -6.731e+2 & -2.312e+3 & 2.1522e+2 & -2.523e+2 & \cdots \\
\cdots & -3.948e+3 & -3.745e+1 & -1.022e+3 & -3.506e+3 & 1.9886e+2 & -4.337e+1 & \cdots \\
\cdots & 2.1805e+2 & -1.048e+2 & 6.6326e+1 & 2.1651e+2 & 2.0556e+2 & -5.770e+2 & \cdots \\
\cdots & -2.244e+1 & -1.770e+2 & 1.0491e+1 & 1.7526e+1 & 3.5477e+2 & -9.483e+2 & \cdots \\
\cdots & 1.1345e+1 & 6.1407e+1 & -2.721e+0 & -2.958e+0 & -1.239e+2 & 3.2890e+2 & \cdots \\
\cdots & -3.069e+0 & 5.4338e+1 & -5.807e+0 & -1.422e+1 & -1.084e+2 & 2.9123e+2 & \cdots
\end{array}
$$

$$
\begin{array}{cc}
\cdots & 2.4068e+2 \quad 5.4589e+2 \\
\cdots & 5.4169e+2 \quad 1.2277e+3 \\
\cdots & -7.671e+0 \quad 1.6934e+1 \\
\cdots & 1.2103e+3 \quad 2.7355e+3 \\
\cdots & -2.063e+1 \quad 3.7908e+0 \\
\cdots & -3.121e+1 \quad -2.553e+1 \\
\cdots & -4.640e+1 \quad -2.648e+1 \\
\cdots & -4.231e+3 \quad -9.551e+3 \\
\cdots & 2.9018e+2 \quad 6.1964e+2 \\
\cdots & 3.1870e+1 \quad 1.8806e+1 \\
\cdots & 6.9534e+2 \quad 1.5726e+3 \\
\cdots & 1.1425e+3 \quad 2.5724e+3 \\
\cdots & -3.966e+2 \quad -8.968e+2 \\
\cdots & -3.498e+2 \quad -7.921e+2
\end{array}
;
$$

$$
\mathbf{B_{cf}} = \begin{bmatrix}
9.8303e-7 & -1.724e-4 \\
4.2325e-7 & -1.997e-4 \\
8.8013e-7 & -4.182e-7 \\
4.6988e-7 & -4.731e-5 \\
3.1767e-4 & -2.113e-6 \\
-3.726e-4 & -2.142e-6 \\
-9.922e-5 & 3.3252e-7 \\
-1.761e-5 & 1.2435e-4 \\
-2.761e-4 & -1.088e-5 \\
6.1485e-5 & -9.033e-6 \\
-5.025e-6 & -4.480e-5 \\
-4.906e-6 & 3.0666e-4 \\
-1.743e-6 & -6.130e-4 \\
-4.307e-7 & -3.083e-5
\end{bmatrix};
$$

$$
\begin{array}{cccccccc}
\mathbf{C_{cf}} = \begin{bmatrix} 2.6623e+3 & -2.224e+3 & 4.5088e+6 & -2.601e+4 & 2.8191e+6 & -3.375e+6 & \cdots \\ 1.0993e+5 & 6.5387e+4 & -1.682e+4 & -2.634e+6 & -1.109e+4 & -1.940e+4 & \cdots \end{bmatrix} \\
\cdots & -6.176e+6 & -5.775e+4 & -1.602e+6 & -5.483e+6 & 3.0871e+5 & -6.177e+4 & \cdots \\
\cdots & -1.198e+4 & 4.3197e+5 & -4.295e+4 & -1.022e+5 & -8.641e+5 & 2.3176e+6 & \cdots
\end{array}
$$

$$
\begin{array}{cc}
\cdots & 4.2546e+4 \quad 1.2876e+4 \\
\cdots & -2.790e+6 \quad -6.292e+6
\end{array}
\Bigg].
$$

Attitude controller design

The augmented 80-state, 3-input, 3-output system, obtained by employing the vibration controller in feedback with the original PMC plant model. The model used to design the attitude controller is obtained by truncating the non–rigid states of the augmented model. The associated error model is evaluated and used in the robustness test. The 6-state rigid design model, represented by the realization $(\mathbf{A_6}, \mathbf{B_6}, \mathbf{C_6})$ is:

$$\mathbf{A_6} = \begin{bmatrix} 0 & 0 & 0 & 1 & 0 & 0 \\ 0 & 0 & 0 & 0 & 1 & 0 \\ 0 & 0 & 0 & 0 & 0 & 1 \\ 3.3206e-6 & -4.532e-7 & -1.63e-10 & 1.9646e-16 & 1.034e-17 & 1.0115e-4 \\ 2.4713e-8 & 4.7807e-6 & 6.462e-10 & -8.53e-17 & 4.394e-17 & -2.207e-3 \\ 1.737e-15 & -6.46e-10 & 1.1602e-6 & -1.662e-6 & 2.1568e-3 & -5.34e-11 \end{bmatrix};$$

$$\mathbf{B_6} = \begin{bmatrix} 0 & 0 & 0 \\ 0 & 0 & 0 \\ 0 & 0 & 0 \\ 5.8740e-4 & -2.197e-7 & 2.068e-14 \\ -5.1094e-7 & 2.044e-5 & 2.120e-13 \\ 1.489e-12 & 0 & 1.9452e-5 \end{bmatrix};$$

$$\mathbf{C_6} = \begin{bmatrix} 1.0000e+2 & 1.2922e-6 & 6.3621e-6 & 0 & 0 & 0 \\ 2.0187e-7 & 1.0000e+2 & 3.1756e-7 & 0 & 0 & 0 \\ 6.8131e-8 & 1.2062e-6 & 1.0000e+2 & 0 & 0 & 0 \end{bmatrix}.$$

The process and measurement error covariances matrices $\mathbf{Q_r}$ and $\mathbf{R_r}$ are:

$$\mathbf{Q_r} = \begin{bmatrix} 1 & 0 & 0 \\ 0 & 1 & 0 \\ 0 & 0 & 1 \end{bmatrix};$$

$$\mathbf{R_r} = \begin{bmatrix} 4 \times 10^6 & 0 & 0 \\ 0 & 4 \times 10^4 & 0 \\ 0 & 0 & 4 \times 10^4 \end{bmatrix}.$$

The estimator gain matrix is given by

$$\mathbf{L_r} = \begin{bmatrix} 8.1088e-05 & -6.178e-07 & -1.809e-06 \\ -6.180e-09 & 5.2841e-05 & 2.3094e-06 \\ -1.809e-08 & 2.3094e-06 & 4.4861e-05 \\ 3.2877e-07 & -2.218e-08 & -8.952e-09 \\ 1.3485e-10 & 1.3988e-07 & -4.153e-08 \\ -1.398e-10 & 6.4094e-08 & 1.0089e-07 \end{bmatrix}.$$

The estimator design is recovered using a state feedback gain corresponding to a

ficticious measurement noise intensity $q_r = 2000$. The resulting attitude controller has the following model:

$$\dot{\mathbf{x}}_{\mathbf{cr}} = \mathbf{A}_{\mathbf{cr}}\mathbf{x}_{\mathbf{cr}} + \mathbf{B}_{\mathbf{cr}}(\mathbf{r}_{\mathbf{r}} - \mathbf{y}_{\mathbf{r}});$$

$$\mathbf{u}_{\mathbf{r}} = \mathbf{C}_{\mathbf{cr}}\mathbf{x}_{\mathbf{cr}}; \qquad (\mathrm{X}-3)$$

where:

$$\mathbf{A}_{\mathbf{cr}} = \begin{bmatrix} -8.109e-3 & 6.1796e-5 & 1.8092e-4 & 1 & 0 & 0 \\ 6.1797e-7 & -5.284e-3 & -2.309e-4 & 0 & 1 & 0 \\ 1.8092e-6 & -2.309e-4 & -4.486e-3 & 0 & 0 & 1 \\ -2.628e+0 & 2.2433e-3 & 3.8281e-5 & -2.292e+0 & 1.6454e-3 & 1.055e-4 \\ 2.2418e-3 & -9.146e-2 & -4.684e-4 & 1.6483e-3 & -4.277e-1 & -2.238e-3 \\ -8.529e-7 & 4.4321e-4 & -8.703e-2 & -1.686e-6 & 2.1291e-3 & -4.172e-1 \end{bmatrix};$$

$$\mathbf{B}_{\mathbf{cr}} = \begin{bmatrix} 8.1088e-5 & -6.190e-7 & -1.809e-6 \\ -6.1798e-9 & 5.2841e-5 & 2.3094e-6 \\ -1.8092e-8 & 2.3094e-6 & 4.4861e-5 \\ 3.2877e-7 & -2.218e-8 & -8.952e-9 \\ 1.349e-10 & 1.3988e-7 & -4.153e-8 \\ -1.40e-10 & 6.4094e-8 & 1.0089e-7 \end{bmatrix};$$

$$\mathbf{C}_{\mathbf{cr}} = \begin{bmatrix} 4.4733e+3 & -2.143e+0 & -5.500e-2 & 3.9027e+3 & 5.0241e+0 & -6.849e-3 \\ 2.1438e+0 & 4.4734e+3 & 2.3114e+1 & 1.6912e+1 & 2.0920e+4 & 1.4953e+0 \\ 4.4219e-2 & -2.311e+1 & 4.4733e+3 & 9.5681e-4 & 1.4231e+0 & 2.1446e+4 \end{bmatrix}.$$